THE
PHYSICAL REVIEW

A journal of experimental and theoretical physics established by E. L. Nichols in 1893

SECOND SERIES, VOL. 79, NO. 2 JULY 15, 1950

Effect of Assumed Range of Tensor Force on the Neutron-Proton Interaction*

A. A. BROYLES† AND M. H. HULL
Yale University,‡ New Haven, Connecticut
(Received March 29, 1950)

The work of Rarita and Schwinger, while successful in accounting for the experimental value of the quadrupole moment of the deuteron, reduces the central field part of the interaction potential by roughly 30 percent and implies a thorough revision of the nuclear binding energy calculations of Wigner, Feenberg and others. In view of a suggestion by Breit that the experimental deuteron properties might be realized without extreme modification of the central interaction by increasing the range of the tensor interaction, the problem was reinvestigated. The calculations were simplified when it was noticed that closed solutions of the radial wave equations are obtainable if the tensor potential is confined to an infinitely thin spherical shell.

For attractive central and tensor interactions it was found that the quadrupole moment can be accounted for by placing the shell beyond $r_1=0.7(e^2/mc^2)$, and for a central field square well interaction of range either $r_0=e^2/mc^2$ or $r_0=e^2/2mc^2$ if the shell is placed at $r_1=1.5(e^2/mc^2)$ the central field need be reduced by only about two percent. For a repulsive tensor interaction the quadrupole moment can be accounted for with $r_1<0.7(e^2/mc^2)$ but the central interaction had to be increased by a factor of 4 for $r_0=e^2/mc^2$. Investigation of neutron-proton scattering with interaction parameters determined by the deuteron quadrupole moment and binding energy shows that for the case of attractive interaction the zero-energy cross section changes from 4.40 to 4.46 barns as r_1 changes from 1 to $1.5(e^2/mc^2)$ when $r_0=e^2/mc^2$ and from 3.94 to 3.62 barns when $r_0=e^2/2mc^2$. For the case of repulsive tensor force with $r_0=e^2/mc^2$, the zero-energy cross section changes from 4.48 to 2.97 barns as r_1 changes from 0.56 to $0.61(e^2/mc^2)$. It may be noted that this latter range includes the experimental value of the cross section. Extension of the calculations to high energies shows that experimental results for the total cross section are reproduced up to an incident particle energy of 15 Mev and the angular anisotropy is not in disagreement with experiment for the attractive interaction. The theoretical cross section is smaller than experimental values for higher energies except for repulsive tensor force, and the anisotropy is only in qualitative agreement with the recent work at Berkeley.

I. INTRODUCTION

THE experimental quadrupole moment and binding energy of the deuteron have been accounted for theoretically by Rarita and Schwinger[1] using a mixture of tensor and ordinary forces in a square potential well. They find that the ^3S and ^3D radial wave functions, u/r and w/r, respectively, must satisfy the differential equations,

$$\begin{aligned}(d^2/dr^2+E'+J)u&=-8^{\frac{1}{2}}J_t w,\\ (d^2/dr^2-6/r^2+E'+J-2J_t)w&=-8^{\frac{1}{2}}J_t u,\end{aligned}\qquad(1)$$

where energy is expressed in units[2] of mc^2 and length in units of $\hbar/(Mm)^{\frac{1}{2}}c$. Here J and J_t are functions which have the radial dependence of the potentials for the ordinary force and tensor force, respectively. The numerical calculations of Rarita and Schwinger show that the depth of the ordinary well U must be reduced to about two-thirds of the depth required to fit the experimental binding energy when no tensor forces is present if J and J_t both represent square wells of range $r_0=2.8\times10^{-13}$ cm.

The calculations of Wigner,[3] Feenberg and others, based on the deep ordinary well without tensor force, gave theoretical binding energies in agreement with experiment for He[4] and lighter nuclei. However, the work of Gerjuoy and Schwinger[4] indicates that replacement of a portion of the ordinary force by sufficient tensor force of the same range to give the experimental quadrupole moment as well as binding energy for the

* Part of a dissertation presented by A. A. Broyles to the Faculty of the Graduate School of Yale University in candidacy for the degree of Doctor of Philosophy.

† Now at the University of Florida, Gainesville, Florida.

‡ Assisted by the joint program of the ONR and AEC.

[1] W. Rarita and J. Schwinger, Phys. Rev. **59**, 436 (1941).

[2] Except where otherwise indicated, these units will be used throughout the paper. M is approximately the neutron or proton mass, m the electron mass, $\hbar$ Planck's constant divided by 2π, and c is the velocity of light. The conversion factors, mc^2 and $\hbar^2/Mmc^2$ are taken to be, respectively, 0.511 Mev and 0.8120×10^{-24} cm^2.

[3] E. Wigner, Phys. Rev. **43**, 252 (1933); E. Feenberg, Phys. Rev. **47**, 850 (1935); Tyrell, Carroll, and Margenau, Phys. Rev. **55**, 790 (1939); N. Svartholm, "The binding energies of the lightest atomic nuclei," thesis, Lund (1945).

[4] E. Gerjuoy and J. Schwinger, Phys. Rev. **61**, 138 (1942).

deuteron gives insufficient neutron-proton interaction in H^3 and He^4 to account for their binding energies. Current meson theories as well as the work of Breit[5] on approximately relativistically invariant wave equations for nuclear particles have shown that a tensor potential with a radial dependence differing from that of the ordinary potential is not implausible. As a result, Breit[6] has suggested that a tensor potential placed at a greater distance from the origin might require less reduction in the value of the ordinary potential and still give the proper quadrupole moment.

An investigation of tensor square wells of widths different from that of the ordinary well has been made by Guindon.[7] His work is here extended to a wider range of values of potential energy parameters, and approximations in closed form are found for the quadrupole moment formulas.

Additional information about the neutron-proton interaction is obtainable from scattering experiments. The total cross section at zero energy has been measured by several authors[8, 9] who obtained about 20 barns. At higher energies the total cross section has been measured up to a neutron incident energy of 90 Mev[10–14] and the angular distribution of scattering has been found isotropic within experimental error up to 15 Mev[15] and strongly anisotropic at 40 and 90 Mev.[16, 17] The effect of changing the spatial position of the tensor force on the comparison of theoretically expected distributions with these observations is discussed below.

Rarita and Schwinger[1] have also investigated neutron-proton scattering theoretically employing the interaction already described in the first paragraph. They assume that only the state with $J=1$ and of even parity in the incident wave is perturbed by the interaction since this is the only state which contains the S wave and obtain the cross section in terms of δ_0 and δ_2, the phase shifts of the ^3S and ^3D waves, respectively. The same assumption concerning the state perturbed is made here, so that only the phase shifts predicted by the interaction under consideration need be calculated.

Since the spin-orbit-spin (tensor) interaction has the effect of presenting a different potential to incident waves of different magnetic quantum number m, it is expected that the phase shifts will depend on m. Rarita and Schwinger found that four phase shifts must be considered: $\delta_0{}^m$, $\delta_2{}^m$, where the phase shifts are even functions of $m=-1, 0, 1$.

Numerical calculations were carried out for a square ordinary potential well, although many of the formulas used apply equally when a well of any shape is employed. In order to simplify the whole investigation, the tensor force was confined to a shell of infinitesimal thickness, in which case solutions of the wave equations may always be written in closed form.

The following notation is used except where noted:

E' = relative neutron-proton energy. For the bound state, $E'=-4.25\,mc^2$.
$\alpha=(|E'|)^{\frac{1}{2}}$ for a bound state, or $(E')^{\frac{1}{2}}$ for a continuum state.
U = depth of the ordinary well.
r_0 = range of the ordinary well.
J = radial dependence of the ordinary force potential.
$k=(U+E')^{\frac{1}{2}}$.
$\rho=kr$ throughout the range of the ordinary force;
$=i\alpha r$ beyond the range of ordinary force when $E'<0$.
$x=\alpha r$ when $\rho=i\alpha r$.
$z=kr$.
$Y_L(x)=[x^{-2}(x^2+3x+3)]\delta_{2,L}+\delta_{0,L}$, where $\delta_{i,j}$ is the Kroenecker delta.
δr = width of the tensor force potential shell.
U_1 = depth of the tensor force potential shell.
r_1 = position of the tensor shell.
J_t = radial dependence of the tensor force potential.
S = strength of the tensor interaction $=2\lim_{\substack{U_1\to\infty\\ \delta r\to 0}} U_1\delta r$.
Q = quadrupole moment of the deuteron.
Q_{exp} = experimental value of $Q=0.00336\,\hbar/Mmc^2$ or 2.73×10^{-27} cm^2.
M = mass of neutron or proton.
m = mass of electron.
$\hbar$ = Planck's h divided by 2π.
$u=r$ times the radial S function. Normalization of u and w is given by $\int_0^\infty(u^2+w^2)dr=1$.
$w=r$ times the radial D function.
$\mathfrak{R}=w/u$ evaluated at $r=r_1$.
$y_u=du/udr$.
$y_w=dw/wdr$.
Δy_u = difference between values of y_u at the outer and inner edges of the tensor shell.
Δy_w = same for y_w.
$[A, B]=BdA/d\rho-AdB/d\rho$.
$\delta_L{}^m=\kappa_L{}^m+i\zeta_L{}^m$ = phase shift in the wave function for the positive energy state of orbital angular momentum L and magnetic quantum number m.
σ_3 = triplet neutron-proton scattering cross section.

II. SOLUTIONS OF THE DIFFERENTIAL EQUATIONS

Terms involving J_t in Eqs. (1) serve to mix u and w. However, J_t is to be taken as a delta-function which is zero except at $r=r_1$, so that Eqs. (1) may be solved independently as homogeneous equations in u and w, respectively. The effect of J_t is then, along with the logarithmic derivatives of the functions evaluated at the edges of the shell, to determine the ratio of w to u at r_1. The ratio of amplitudes will be called $\mathfrak{R}$; i.e., $\mathfrak{R}=w(r_1)/u(r_1)$.

The character of the solutions of the equations is determined by the radial variation and sign of $(E'+J)$.

[5] G. Breit, Phys. Rev. **51**, 248 (1937).
[6] Private communication.
[7] W. G. Guindon, Phys. Rev. **74**, 145 (1948).
[8] Havens, Rainwater, and Wu, Phys. Rev. **73**, 1265 (1948).
[9] W. B. Jones, Jr., Phys. Rev. **74**, 364 (1948).
[10] Ageno, Amaldi, Boccarelli, and Trabacchi, Phys. Rev. **71**, 20 (1947).
[11] W. Sleator, Phys Rev. **72**, 207 (1947).
[12] R. Scherr, Phys. Rev. **68**, 240 (1945).
[13] Hadley, Kelly, Leith, Segrè, Wiegand, and York, Phys. Rev. **75**, 351 (1948).
[14] Cook, McMillan, Peterson, and Sewell, Phys. Rev. **72**, 1264 (1947).
[15] H. H. Barschall and R. F. Taschek, Phys. Rev. **75**, 1819 (1949).
[16] Brueckner, Hartsough, Hayward, and Powell, Phys. Rev. **75**, 555 (1949).
[17] Yost, Wheeler, and Breit, Bull. Terr. Mag. **40**, 443 (1935).

In particular, if J is a potential well with a sharp range, the solutions will be of different character in the range of r having as boundaries the origin, the edge of the ordinary well, and the position of the tensor shell. In general, u and w are linear combinations of regular and irregular particular solutions of Eqs. (1). The particular solutions for each of the ranges of r mentioned may be defined as if their equations held all the way to the origin. Then the regular function $F_L(\rho)$ is chosen to vanish at $r=0$, and the irregular solution $G_L(\rho)$ is defined so that the Wronskian relation is satisfied as follows:

$$F_L'G_L-G_L'F_L=1,$$

where the prime means differentiation with respect to the argument. The subscript L has the value zero for a solution of the first of Eqs. (1), and the value two for the second.

These general properties define the functions within an arbitrary factor multiplying F_L and dividing G_L. The factor will be chosen to make

$$F_L=(\pi\rho/2)^{\frac{1}{2}}J_{L+\frac{1}{2}}(\rho), \quad G_L=(-1)^L(\pi\rho/2)^{\frac{1}{2}}J_{-L-\frac{1}{2}}(\rho).$$

as in Yost, Wheeler and Breit.[17] The argument ρ incorporates the effect of the value of $(E'+J)$. Thus for a square well, throughout the range of interaction, $\rho=(E'+U)^{\frac{1}{2}}r=kr$, where U is the depth of the well. In the tensor shell, $\rho=(U_1)^{\frac{1}{2}}r$ in the limit that E' and U, are negligible compared to U_1 the depth of the shell. For the bound state, where $E'<0$, beyond the range of the ordinary force $\rho=(E')^{\frac{1}{2}}r=i\alpha r$, where $\alpha=(|E'|)^{\frac{1}{2}}$. For the continuum states in the discussion of scattering, $E'>0$, and $\rho=(E')^{\frac{1}{2}}r$. E' is the relative energy of the neutron-proton system.

For the bound state beyond the range of ordinary interaction, $F_L(i\alpha r)$ and $G_L(i\alpha r)$ involve both $e^{\alpha r}$ and $e^{-\alpha r}$. In order to secure the proper behavior of the wave function at infinity, it is convenient to define

$$F_L^{(e)}(i\alpha r)=G_L(i\alpha r)+iF_L(i\alpha r),$$
$$G_L^{(e)}(i\alpha r)=-\tfrac{1}{2}(F_L(i\alpha r)+iG_L(i\alpha r)).$$

Then $F_L^{(e)}(\rho)$ vanishes exponentially for large r, and $F_L^{(e)}$, $G_L^{(e)}$ satisfy the same Wronskian relations as do F_L and G_L.

The condition on $w(r_1)/u(r_1)$ is obtained as follows. The function J_t is made very large in a small interval δr at $r=r_1$, and its value, U_1, will be set equal to a constant in δr. The quantities J_t and δr are varied together in such a way as to produce finite changes in the logarithmic derivatives $y_u=du/udr$ and $y_w=dw/wdr$ in going across δr from smaller to larger values of r. Inspection of Eqs. (1) shows that du/dr and dw/dr change by finite amounts if the quantity $S=2U_1\delta r$ is kept constant while δr approaches zero. Assuming temporarily that u and w undergo vanishing or finite changes in the interval δr, one sees that the terms in E', J and $6/r^2$ are negligible so that the changes in du/dr and dw/dr are determined by the integrals of U_1u and U_1w across δr. The changes are finite, therefore. Consequently the changes in u and w across δr vanish in the limit of $\delta r=0$. One has, therefore,

$$\Delta(du/dr)=-2^{\frac{1}{2}}Sw(r_1),$$
$$\Delta(dw/dr)=S[w(r_1)-2^{\frac{1}{2}}u(r_1)],$$

where the Δ indicates the difference between the derivative evaluated at the upper boundary of the shell and the derivative evaluated at the lower boundary. It follows from the expressions above that

$$\Delta y_u=-2^{\frac{1}{2}}S\mathfrak{R}, \quad \Delta y_w=-S(2^{\frac{1}{2}}/\mathfrak{R}-1). \tag{2}$$

III. BOUND STATE OF THE DEUTERON

A. Exact Formulas

For the bound state, the ordinary potential and binding energy determine the logarithmic derivatives of u and w at the edges of the shell, so the quantities Δy_u and Δy_w can be determined as properties of solutions which are regular at infinity and zero and, therefore, independently of S. Equation (2) now determines $\mathfrak{R}$ in terms of the known Δy_u and Δy_w as

$$\mathfrak{R}=[-1\pm(1+8\Delta y_w/\Delta y_u)^{\frac{1}{2}}]/(8^{\frac{1}{2}}\Delta y_w/\Delta y_u). \tag{3}$$

This determines the wave functions except for a normalization factor which is common to u and w.

Equation (3) holds equally for any energy, provided the proper functions are used to calculate Δy_u, Δy_w. Equation (2) determines S, and the value thus obtained is a function $S(\epsilon)$ of the energy ϵ used to calculate Δy_u, Δy_w. The eigenvalue problem can be solved by requiring that $S(\epsilon)=S$, where on the right side is meant a preassigned value of the system parameter S. Since in the present work the energy is known in the bound state, it suffices to determine S by means of Eq. (2). In the scattering calculations, the values of S so obtained are used to introduce the effect of the tensor force on the scattering.

For a preassigned value of the energy, Eq. (3) shows that there will, in general, be two values of S and hence two sets of u,w. The two values of S coincide when $\Delta y_w/\Delta y_u=-\frac{1}{8}$. It will be shown subsequently, that physical considerations exclude one of the values of S automatically in some cases. Another limitation on S which will be made is that S be real, since the present investigation is not concerned with the absorption of neutrons by protons. This means that the condition $\Delta y_w/\Delta y_u>-\frac{1}{8}$ must be maintained, which implies a restriction on the choice of r_0, r_1 and U in certain cases.

For cases not interfered with by the above restrictions, the quantities u, w, and S may be calculated from assumed values of r_0, r_1, and U as follows.

Let

$$u=N\mathfrak{F}_0(r), \quad w=N\mathfrak{F}_2(r),$$

where N is the common normalization factor. If the point $r=r_1$ is selected as the pivot point for defining

$\mathfrak{F}_L(r)$, then

$$\mathfrak{F}_L(r)/\mathfrak{F}_L(r_1)=\begin{cases} f_L(r)/f_L(r_1), & r<r_1 \\ h_L(r)/h_L(r_1), & r>r_1. \end{cases} \tag{4}$$

In terms of solutions of Section II, one may write

$$f_L(r)=F_L(\rho), \quad r<r_0, \tag{5}$$
$$f_L(r)=[\![F_L, G_L^{(e)}]\!]_{(0)}F_L^{(e)}(\rho) + [\![F_L^{(e)}, F_L]\!]_{(0)}G_L^{(e)}(\rho), \quad r>r_0;$$

and

$$h_L(r)=F_L^{(e)}(\rho), \quad r>r_0, \tag{6}$$
$$h_L(r)=[\![F_L^{(e)}, G_L]\!]_{(0)}F_L(\rho) + [\![F_L, F_L^{(e)}]\!]_{(0)}G_L(\rho), \quad r<r_0,$$

where $\rho=kr$ when $r<r_0$ and $\rho=i\alpha r$ when $r>r_0$. The special brackets are Wronskian-type expressions with the following meaning in the present case:

$$[\![A, B]\!]=BdA/d\rho-AdB/d\rho=-[\![B, A]\!][\![B, A]\!].$$

The suscript, 0, indicates that the expression is to be evaluated at $r=r_0$. Thus, in order to secure proper continuity at $r=r_0$ it is seen that $d/d\rho=d/d(i\alpha r)$ in Eq. (5) and $d/d\rho=d/d(kr)$ in Eqs. (6).

The logarithmic derivatives appearing in Eqs. (2) and (3) are now readily written down for the two special cases $r_1<r_0$ and $r_1>r_0$:

For $r_1<r_0$, at $r=r_1$,

$$\Delta y/k=h_L'/h_L-F_L'/F_L = [\![F_L^{(e)}, F_L]\!]_{(0)}/F_L(\rho_1)[[\![F_L^{(e)}, G_L]\!]_{(0)}F_L(\rho_1) + [\![F_L, F_L^{(e)}]\!]_{(0)}G_L(\rho_1)]. \tag{7}$$

For $r_1>r_0$, at $r=r_1$,

$$\Delta y/(i\alpha)=F_L^{(e)\prime}/F_L^{(e)}-f_L'/f_L = [\![F_L^{(e)}, F_L]\!]_{(0)}/F_L^{(e)}(\rho_1)[[\![F_L, G_L^{(e)}]\!]_{(0)} \times F_L^{(e)}(\rho_1)+[\![F_L^{(e)}, F_L]\!]_{(0)}G_L^{(e)}(\rho_1)]. \tag{8}$$

In both Eqs. (7) and (8), Δy_u is obtained with $L=0$ and Δy_w is obtained with $L=2$. These formulas suffice for calculation of $\mathfrak{R}$ and hence $\mathfrak{F}_2(r_1)/\mathfrak{F}_0(r_1)$ is determined by them.

The normalization requirement is shown[1] to reduce to

$$\int_0^\infty (u^2+w^2)dr=1.$$

In the present notation, the normalizing factor is determined by the sum of the integrals of $\mathfrak{F}_L^2$ for $L=0$, 2. Equations (4)–(6) show that $\mathfrak{F}_L(r)$ is a linear combination of $F_L(\rho)$. $G_L(\rho)$ or of $F_L^{(e)}(\rho)$, $G_L^{(e)}(\rho)$. When these functions are defined as in Section II, then the following formula holds for the integral:

$$\int_a^b \mathfrak{F}_L^2(r)dr=(r_c/\rho_c)\int_{\rho_a}^{\rho_b} \mathfrak{F}_L^2(\rho)d\rho = (r_c/\rho_c)[(\rho/2)(\mathfrak{F}_L^2-\mathfrak{F}_{L-1}\mathfrak{F}_{L+1})]^{\rho_b}_{\rho_a}, \tag{9}$$

where $r_a<r_c<r_b$. The integration naturally breaks up into three parts: zero to r_1 or r_0, whichever is smaller; this point to r_1 or r_0, whichever is larger; and this point to infinity. $\mathfrak{F}_L(r)$ is defined so that $\mathfrak{F}_L(0)=\mathfrak{F}_L(\infty)=0$.

The quadrupole moment of the deuteron may be computed from the expression

$$Q=(2\tfrac{1}{2}/10)\int_0^\infty r^2[uw-w^2/8^{\frac{1}{2}}]dr.$$

The definitions of u and w are such that $\mathfrak{R}$ will occur as a factor in either $\mathfrak{F}_0$ or $\mathfrak{F}_2$, depending on the form chosen for N in terms of $u(r_1)$ or $w(r_1)$. This indicates that, since experiment shows[18] that Q is positive, $\mathfrak{R}$ must be positive also according to the above formula. As Eq. (3) then shows, when $\Delta y_w/\Delta y_u>0$, the choice of sign before the radical in $\mathfrak{R}$ must be the plus sign. This is the case for attractive tensor force and attractive central force. When repulsive tensor force is allowed it appears that $\Delta y_w/\Delta y_u<0$, and for some choices of the parameters r_1, r_0, U either sign is possible. These restrictions on $\mathfrak{R}$ apply also to S, so that the experimental fact of Q positive may eliminate one of the mathematically possible values of S.

When u and w are expressed in terms of the solutions of Section II for the central interaction represented by a square well, the integrals involved in evaluating Q can be expressed in closed form as trigonometric functions and polynomials in ρ. For ready calculation, however, especially when $\rho=i\alpha r$, the integrals are given below as functions of real arguments or series expansions.

Let $x=\alpha r$, $z=kr$, $R(<)$ the smaller of r_0, r_1 and $R(>)$ the larger of r_0, r_1. Then,

$$\int_{R(>)}^\infty r^2uwdr=(A_0D_0A_2D_2/2\alpha^3)[\xi_0]_{R(>)}, \tag{10}$$
$$\int_{R(>)}^\infty r^2w^2dr=(A_2{}^2D_2{}^2/4\alpha^3)[2x^2+14x+37+36/x]_{R(>)},$$

where $\xi_\beta=x^2+(-1)^\beta 4x+5$. The constants A_0, D_0, etc. appearing in Eqs. (10) and others which will occur later will be defined after all of the integrals are given. In the region $0<r<R(<)$, the integrals are

$$\int_0^{R(<)} r^2uwdr=(A_0A_2/12k^3)[3(z^2-5)\mathbf{SC} + 12z(\mathbf{C}^2-\mathbf{S}^2)-2z^3+18z]_{R(<)}, \tag{11}$$
$$\int_0^{R(<)} r^2w^2dr=(A_2{}^2/12\pi k^4R(<)) \times[-108+36z^2+4z^4+(108-42z^2)(\mathbf{C}^2-\mathbf{S}^2) + (111z-6z^3)\mathbf{CS}]_{R(<)},$$

where $\mathbf{C}=\cos z$, $\mathbf{S}=\sin z$.

[18] A. Nordsieck, Phys. Rev. **58**, 310 (1940); Kellogg, Rabi, Ramsey, and Zaccharias, Phys. Rev. **57**, 677 (1940).

TABLE I. Computed values of Q for $r_0=2.8\times10^{-13}$ cm.[a]

r_1/r_0	U	Q^+	Q^-
0.695	0	0.00336	
0.7	29.25	0.0019	
0.83	27.2	0.00326	
0.9	27.2	0.00410	
1.0	4.25	0.00626	
1.0	29.25	0.00434	
1.0	32.25	0.00387	
1.0	36.25	0.00324	
1.0	40.25	0.00156	
1.5	35.0	0.00723	
1.5	39.75	0.00358	
1.5	40.25	0.00311	
	41.6	0	
0.577	163.3	0.00198	0.00729
0.593	163.3	0.00393	0.00703
0.604	163.3	0.00564	0.00564
0.607	178.8	0.00248	0.00359
0.622	178.8	0.00437	0.00751
0.597	170.9	0.00302	0.00803
0.654	170.9	0.00744	0.00744

[a] Q^+ means that the plus sign has been taken to compute $\mathfrak{R}$, Q^- that the minus sign has been taken. $Q_{\text{exp}}=0.00336\hbar^2/Mmc^2$.

TABLE II. Computed values of Q for $r_0=e^2/2\,mc^2$.

$r_1/2.8\times10^{-13}$ cm	U	Q^+
0.503	4.25	0.001843
0.503	102.65	0.000986
0.695	0	0.00336
1.0	4.25	0.0065
1.0	96.0	0.00401
1.08	118.5	0.00319
1.273	125.2	0.00312
1.5	126.0	0.00363
1.5	128.0	0.00266
	130.0	0

For the intermediate region, $R(<)<r<R(>)$, there are two sets of integrals depending on whether $r_1<r_0$ or $r_0<r_1$. Thus, when $r_0<r_1$,

$$\int_{r_0}^{r_1} r^2uwdr=(A_2A_0/\alpha^3)\{B_0B_2e^{x_0}[\xi_0e^{-2}/4+\eta_1]+B_2C_0e^{-x_0}[\xi_1e^{2x}/4+\eta_0]-B_0C_2e^{x_0}[\xi_0e^{-2x}/4-\eta_1]+C_2C_0e^{-x_0}[\xi_1e^{2x}/4+\eta_0]\}^{x_1}{}_{x_0},$$

$$\int_{r_0}^{r_1} r^2w^2dr=(A_2{}^2/\alpha^3)\{(B_2{}^2x^9/2025)\times(1+9x^2/77+9x^4/2548+\cdots)+(B_2C_2x^4/10)(1-4x^2/63+x^4/168+\cdots)-(9C_2{}^2/x)(1+x^2/3-x^4/108+\cdots)\}^{x_1}{}_{x_0}, \tag{12}$$

where

$$\eta_\beta=(3x/2)[1+(-1)^\beta x/2+x^2/9].$$

When $r_1<r_0$,

$$\int_{r_1}^{r_0} r^2uwdr=(A_0A_2/12k^3)\{(18z-12z^3)b_0+9z^2a_1+[(5-z^2)b_1-4za_0]6\mathbf{SC}+[(-5+z^2)a_0-4zb_1]3(\mathbf{C}^2-\mathbf{S}^2)\}^{z_0}{}_{z_1},$$

$$\int_{r_1}^{r_0} r^2w^2dr=(A_2{}^2/k^3)[(B_2{}^2z^9/2025)\times(1-9z^2/77+4z^4/637+\cdots)+(B_2C_2z^4/10)(1+4z^2/63+z^4/63+\cdots)+(9C_2{}^2/z)(-1+z^2/3+z^4/27+\cdots)]^{z_0}{}_{z_1}, \tag{13}$$

where

$$a_\beta=B_0C_2+(-1)^\beta C_0B_2, \quad \text{and} \quad b_\beta=C_0C_2+(-1)^\beta B_0B_2.$$

The integrals of r^2w^2 in the interval $R(<)<r<R(>)$ are represented by series expansions. Since these integrals are usually small compared to the other integrals in Q, the series as given in Eqs. (12) and (13) have been carried to a sufficient number of terms for most purposes. However, for the case of a repulsive tensor force this is not so, and numerical integration provided the best method of evaluation.

The constants A_0, A_2, etc. which appear in Eqs. (10)–(13) are given as follows: When $r_1<r_0$,

$$\begin{aligned} A_L&=N\mathfrak{F}_L(r_1)/F_L(\rho_1),\\ B_L&=[\![F_L{}^{(e)},G_L]\!]_{(0)}W_L,\\ C_L&=[\![F_L,F_L{}^{(e)}]\!]_{(0)}W_L,\\ Y_L(x_0)D_L&=F_L{}^{(e)}(i\alpha r_0)W_L, \end{aligned} \tag{14}$$

where

$$W_L=F_L(\rho_1)/[[\![F_L{}^{(e)},G_L]\!]_{(0)}F_L(\rho_1)+[\![F_L,F_L{}^{(e)}]\!]_{(0)}G_L(\rho_1)],$$

TABLE III. Interpolated parameters consistent with deuteron binding energy and quadrupole moment, with corresponding triplet zero-energy cross section in barns.

r_0	$r_1/2.8\times10^{-13}$ cm	U	S	$(\sigma_3)_{E'=0}$
I[a]	0.695	0	11.05	3.87
I	0.84	27.2	5.28	4.25
I	1.0	35.6	3.19	4.40
I	1.5	40.0	2.14	4.46
I		41.6	0	4.34
I	0.561	163.3	−12.28	4.478
I	0.584	170.9	−10.72	3.54
I	0.606	178.8	−8.79	2.97
I	0.588	163.3	−41.98	5.19
I	0.603	170.9	−47.54	5.27
I	0.614	178.8	−46.52	
II[b]	0.890	96.7	6.18	3.94
II	1.08	116.5	4.23	3.96
II	1.273	124.0	2.87	3.84
II	1.5	126.7	2.63	3.62
II		130.0	0	3.26

[a] *I* signifies $r_0=2.8\times10^{-13}$ cm.
[b] *II* signifies $r_0=e^2/2mc^2$.

and

$$Y_0(x)=1, \quad Y_2(x)=x^{-2}(x^2+3x+3).$$

Since $r_1<r_0$, the argument $\rho_1=kr_1$ when written explicitly in Eq. (14), and the Wronskian expressions are to be evaluated as in Eq. (6).

When $r_1>r_0$,

$$\begin{aligned}
&A_L=N\mathfrak{F}_L(r_1)/[[\mathfrak{F}_L, G_L^{(e)}]_{(0)}F_L^{(e)}(\rho_1)\\
&\qquad\qquad +[F_L^{(e)}, F_L]_{(0)}G_L^{(e)}(\rho_1)],\\
&B_0=[F_0, G_0^{(e)}]_{(0)}F_0^{(e)}(\rho_0),\\
&B_2=[F_2, G_2^{(e)}]_{(0)}+(i/2)[F_2^{(e)}, F_2]_{(0)},\\
&C_0=[F_0^{(e)}, F_0]_{(0)}G_0^{(e)}(\rho_0),\\
&C_2=-[F_2, G_2^{(e)}]_{(0)}+(i/2)[F_2^{(e)}, F_2]_{(0)},\\
&Y_L(x_1)D_L=[F_L, G_L^{(e)}]_{(0)}F_L^{(e)}(\rho_1)\\
&\qquad\qquad +[F_L^{(e)}, F_L]_{(0)}G_L^{(e)}(\rho_1),
\end{aligned} \tag{15}$$

where $\rho=i\alpha r$ when written explicitly in Eq. (15), and the Wronskian expressions are to be evaluated as in Eq. (5).

Series have been obtained for the integrals involved in the calculation of Q when $U=0$. They are

$$\begin{aligned}
&\int_0^{r_1} r^2[uw-w^2/8^{\frac{1}{2}}]dr\\
&\quad =0.0229x_1^3-0.00995x_1^4+0.00275x_1^5+\cdots,\\
&\int_{r_1}^{0} r^2uwdr=(0.449+0.187x_1\\
&\qquad +0.0204x_1^2+\cdots)Y_2(x_1),\\
&\int_{r_1}^{\infty} r^2w^2dr=(0.617+0.658x_1\\
&\qquad +0.233x_1^2+\cdots)/(x_1Y_2^2(x_1)).
\end{aligned} \tag{16}$$

The formulas (10) through (13) have been used to compute values of Q for square wells with $r_0=2.8\times10^{-13}$ cm and $r_0=e^2/2mc^2$ for various ordinary well depths and shell positions. The range 2.8×10^{-13} cm is used rather than e^2/mc^2 to allow direct comparison with the calculations of Rarita and Schwinger. The values obtained are listed in Tables I and II. Combinations of r_0, U, r_1, and S that give the experimental quadrupole moment[14] of 0.00336 $\hbar^2/Mmc^2$ or $(2.73\pm0.05)\times10^{-27}$ cm^2 have been interpolated and are listed in Table III. Figure 1 is a plot of the values of z_0 against r_1 that give the experimental quadrupole moment.

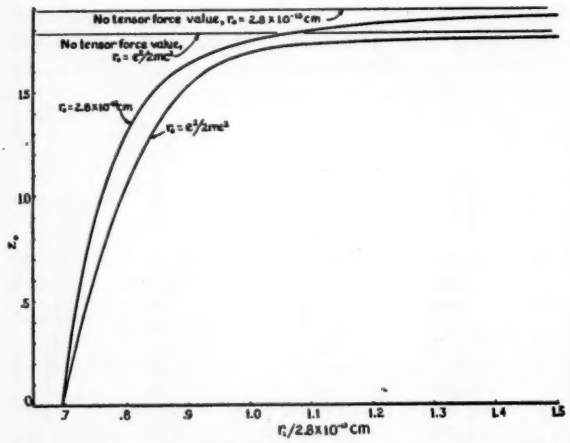

FIG. 1. $z_0=kr_0$ as a function of r_1, the position of the tensor shell, when the deuteron binding energy and quadrupole moment is reproduced theoretically for attractive forces only. The no tensor force parameters were chosen to give the binding energy of the deuteron for the ranges r_0 of the ordinary force shown.

It is interesting to note that, with an attractive ordinary well and tensor force, the shell cannot be placed inside a distance of $0.695\times2.8\times10^{-13}$ cm and give the experimental quadrupole moment.

However, when a repulsive tensor force is allowed while the ordinary force remains attractive, the experimental value of the quadrupole moment can be reproduced theoretically with the shell placed at smaller distances than $0.695\times2.8\times10^{-13}$ cm.

The other possibility of attractive tensor force and repulsive ordinary force was not investigated, although the work of Hu and Massey[19] indicates that parameters can be found with this arrangement to give Q_{exp}. However, since Gerjouy and Schwinger[4] find that a neutron-proton interaction which depends on the tensor force for binding does not explain the binding energies of the light nuclei other than the deuteron, this case was not investigated here.

In Fig. 2 are plotted typical examples of the normalized bound state functions u and w for sets of parameters U and r_1 which give the experimental value of Q when $r_0=2.8\times10^{-13}$ cm. Two cases for attractive and one for repulsive tensor force are given, with the latter case distinguished by a positive value of Δy_u. For comparison, and in support of some arguments for obtaining approximate formulas, the radial S function for the bound state without tensor force is indicated.

B. Approximate Formulas

It is clear from Fig. 2 that w is appreciably smaller than u for $r_0=(2.8)\times10^{-13}$ cm when the potential parameters for attractive forces are adjusted to give the quadrupole moment. It is therefore possible to neglect $\int_0^\infty r^2w^2dr$ as an approximation in the computation of Q for such cases. It is also apparent from Fig. 2 that the no tensor force function may be used as an approximation to u. This eliminates the necessity of normalizing u and w.

It is also possible in all these cases to approximate $\mathfrak{R}$ by $(\Delta y_u/\Delta y_w)^{\frac{1}{2}}$ and w from zero to r_1 by a cubic.

For the shell inside the square well but near to the edge, the effect of the ordinary force on u and w from the shell to the edge of the well may be neglected and the following formula obtained.

$$\begin{aligned}
Q\approx&(u_1^2/2^{\frac{1}{2}}10\alpha^3)x_1^2(x_1^2+4x_1+5)(x_1+z_1\cot z_1)^{\frac{1}{2}}/\\
&[(x_1^2+3x_1+3)(x_1+6x_1^2+15x_1+15)]^{\frac{1}{2}}.
\end{aligned} \tag{17}$$

[19] T. M. Hu and H. S. W. Massey, Proc. Roy. Soc. **A196**, 135 (1949).

Since the no tensor force function is a good approximation to u, the value of the no tensor force function at r_1 may be taken for u_1. This approximation gives a value of 0.67 for $r_1/(2.8)\times10^{-13}$ cm for U equal to zero as compared with 0.695 from Eqs. (16). An ordinary well depth of $41.6mc^2$ was used as the no tensor force value and coefficients of the functions were found to be $A_{00}=1.587$ and $D_{00}=0.947$ where the second of the subscripts, 0, indicates no tensor force. For the shell outside the square well, u from r_0 to r_1 may be approximated by a function of the form A/r^m. An approximate formula for Q is then

$$Q\approx(2\tfrac{1}{2}/10)\mathcal{R}A_{00}^2D_{00}^2\exp[-2(x_1-x_0)]\times\{x_1^2(x_1^2+4x_1+5)/[(x_1^2+3x_1+3)2\alpha^3]+[1-(r_0/r_1)^{6-m}]r_1^3/(6-m)\}. \quad (18)$$

This formula gives Q to within one percent when $r_1=1.5r_0$ for $r_0=(2.8)\times10^{-13}$ cm and for Q close to the experimental value. It gives a value eight percent too small when the shell is moved in to r_0.

IV. NEUTRON-PROTON SCATTERING

A. Formulas for Phase Shifts

1. *Higher Energy Cases*

As with the bound state, there are three scattering cases depending on the relative positions of the tensor shell and the edge of the ordinary well, and a fourth case when the depth of the ordinary well is taken to be zero. For $r<R(>)$, the solutions of the wave equation have the same form as for the bound state with suitable modifications in ρ; i.e., with $E'>0$. When $r>R(>)$, the wave functions can be written

$$u=F_0(\rho)\cos\delta_0+G_0(\rho)\sin\delta_0,\qquad w=\eta[F_2(\rho)\cos\delta_2+G_2(\rho)\sin\delta_2]. \quad (19)$$

Normalization constants and δ_L are determined in terms of η by the requirement that u have unit amplitude at infinity, the continuity of logarithmic derivatives across the boundary of the ordinary well and by use of Eqs. (2) which give the change in the logarithmic derivatives of u and w at the shell position, $r=r_1$. The shell strength S is treated as a known parameter for scattering calculations, and thus introduces the effect of the tensor force. The complete determination of all quantities requires another relation in order to determine η, the ratio of the amplitude of w to u at infinity. Rarita and Schwinger[1] find

$$\eta^m=\beta^m2\sqrt{2}\exp[i(\delta_2{}^m-\delta_0{}^m)],$$

where β^m is proportional to the matrix element of S_{12}, the tensor operator defined in reference 1, between the spin states with magnetic quantum number m, and has the value $-\frac{1}{4}$ for $m=\pm1$ and $\frac{1}{2}$ for $m=0$.

Since η^m is complex, the phase shifts must also be complex. In general they will be written

$$\delta_L{}^m=\kappa_L{}^m+i\zeta_L{}^m.$$

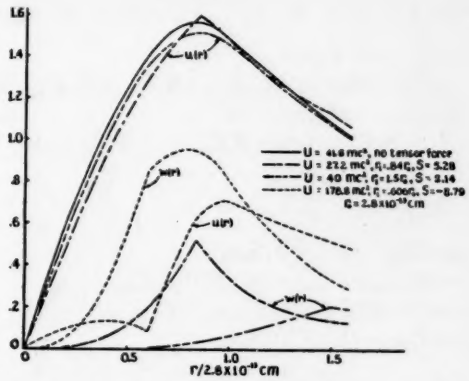

FIG. 2. Normalized bound state wave functions for several sets of parameters which reproduce the deuteron quadrupole moment compared with the no tensor force function. The case for $U=27.2mc^2$ was chosen for direct comparison with the calculations of Rarita and Schwinger.

When all conditions are applied to the wave functions, it is found that the phase shifts may be written in the form:

$$\tan\delta_0{}^m=[v+4\beta^mt+is]/[q+i(-p+4\beta^mt)],\qquad \tan\delta_2{}^m=[t+2\beta^mp+i2\beta^ms]/[2\beta^mq+i(-2\beta^mv+t)], \quad (20)$$

where p, q, s, t, v may be written as

$$v=HK+C_0B_2,\quad t=TCD,\quad s=HP-C_0C_2,\quad q=NK+B_0B_2,\quad p=-NP+B_0C_2,$$

with

$$B_0=\mathbf{S}_0\mathbf{s}_0+(k/(E')^{\frac{1}{2}})\mathbf{C}_0\mathbf{c}_0,\quad C_0=\mathbf{S}_0\mathbf{c}_0-(k/(E')^{\frac{1}{2}})\mathbf{C}_0\mathbf{s}_0,$$
$$B_2=k/(E')^{\frac{1}{2}})F_2'(z_0)G_2(\rho_0)-F_2(z_0)G_2'(\rho_0),$$
$$C_2=F_2(z_0)F_2'(\rho_0)-(k/(E')^{\frac{1}{2}})F_2(\rho_0)F_2'(z_0),\quad T=S/(E')^{\frac{1}{2}},$$

where

$$\mathbf{S}_0=\sin z_0,\quad \mathbf{s}_0=\sin\rho_0,\quad \mathbf{C}_0=\cos z_0,\quad \mathbf{c}_0=\cos\rho_0.$$

It may be noted that $\rho=(E')^{\frac{1}{2}}r$ throughout these equations. When kr is meant, the symbol z is employed as in Sections II and III.

The quantities C, D, H, K, N, P are different for each of the relative positions of shell and well edge. Thus, for $r_1>r_0$,

$$C=B_0\mathbf{s}_1+C_0\mathbf{c}_1,\quad D=B_2F_2(\rho_1)+C_2G_2(\rho_1),\quad H=2T^2CD\mathbf{s}_1+TDC_0,$$
$$K=G_2(\rho_1),\quad N=-2T^2CD\mathbf{c}_1+TDB_0,\quad P=F_2(\rho_1),$$

where

$$\mathbf{s}_1=\sin\rho_1,\quad \mathbf{c}_1=\cos\rho_1.$$

For $r_1<r_0$,

$$C=\sin z_1, \quad D=F_2(z_1),$$
$$H=-2(S/k)^2\mathbf{S}_1F_2(z_1)(C_0\mathbf{C}_1-\lambda\mathbf{S}_1)+(S/k)F_2(z_1)C_0,$$
$$K=B_2G_2(z_1)-\pi F_2(z_1),$$
$$N=(S/k)^2\mathbf{S}_1F_2(z_1)(\epsilon S_1-B_0\mathbf{C}_1)+(S/k)F_2(z_1)B_0,$$
$$P=\tau F_2(z_1)-C_2G_2(z_1),$$

where

$$\epsilon=\mathbf{C}_0\mathbf{s}_0-(k/(E')^{\frac{1}{2}})\mathbf{S}_0\mathbf{c}_0,$$
$$\tau=G_2(z_0)F_2'(\rho_0)-(k/(E')^{\frac{1}{2}})F_2(\rho_0)G_2'(z_0),$$
$$\pi=(k/(E')^{\frac{1}{2}})G_2'(z_0)G_2(\rho_0)-G_2(z_0)G_2'(\rho_0),$$
$$\lambda=\mathbf{C}_0\mathbf{c}_0+(k/(E')^{\frac{1}{2}})\mathbf{S}_0\mathbf{s}_0,$$

and

$$\mathbf{S}_1=\sin z_1, \quad \mathbf{C}_1=\cos z_1.$$

For the remaining cases, $r_1=r_0$ and $U=0$, these quantities are readily obtained from the formulas

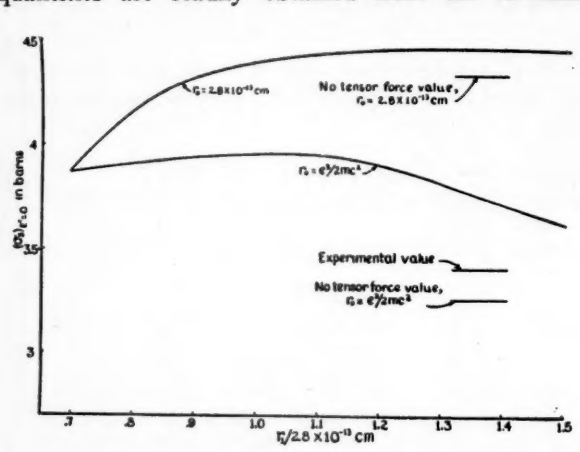

FIG. 3. Triplet zero-energy cross section for neutron-proton scattering as a function of the tensor shell position, r_1. The model parameters were chosen to reproduce the deuteron binding energy and quadrupole moment for attractive forces only. The no tensor force values were calculated from parameters selected as in Fig. 1.

written by taking suitable limits. Thus the formulas for the case of $r_1=r_0$ are obtained from those of either the case $r_1>r_0$ or $r_1<r_0$ by going to the limit $\rho_1=\rho_0$. The case of $U=0$ is most easily obtained from the case of $r_1=r_0$ by going to the limit of $z_0=\rho_0$.

Application of Eqs. (20) with any of the cases above gives the phase shifts in the form:

$$\tan(\kappa+i\zeta)=(e+ih)/(j+ik),$$

where e, h, j, k are combinations of p, q, s, t, v given by Eqs. (20). When real and imaginary parts are separated, there results

$$\tan 2\kappa=2(ej+kh)/[j^2+k^2-e^2-h^2]$$

and

$$\sinh 2\zeta=[(jh-ek)/(ej+kh)]\sin 2\kappa.$$

It is readily shown that the sign of $\sin 2\kappa$ is determined by the sign of $(ej+kh)$. Thus if the denominator of $\tan 2\kappa$ is negative, a phase π must be added to 2κ. The corrected angle is used in computing $\sinh 2\zeta$, since the sign of this function is determined by the sign of $(jh-ek)$.

When κ and ζ are obtained, the results are in a form suitable for direct substitution into the formulas for the cross sections obtained by Rarita and Schwinger.[1]

2. *Zero-Energy Cases*

The zero-energy scattering formulas may be obtained from those listed in Section IV-A.1 in the limit of $\rho=0$. However, an independent derivation brings out the physical relations more clearly.

As E', the relative neutron-proton energy, tends to zero it may be shown that the imaginary parts of δ_0^m and δ_2^m go to zero more rapidly than the real parts, and that the real part of δ_2^m vanishes with a higher power of E' than does the real part of δ_0^m. It further turns out that δ_0^m is independent of β^m and thus of m. These facts are immediately evident in the limiting processes, and follow also from a consideration of the proper solutions of the differential equations in the limit $E'=0$. The zero-energy cross section thus depends only on a single real phase shift δ_0, which may be determined from the Fermi intercept with the result

$$\delta_0=(E')^{\frac{1}{2}}|(1/y_u-r)|_{r=R(>)}, \tag{21}$$

where the bracket containing the logarithmic derivative, y_u, is to be evaluated at the limit of the interaction $R(>)$.

(*a*) *Shell outside the well*: $r_1>r_0$.—When $\mathfrak{R}$ is eliminated from Eqs. (5) there results

$$\Delta y_u=2S^2/(\Delta y_w-S). \tag{22}$$

Since $\Delta y_u=(E')^{\frac{1}{2}}[F_0^{(e)\prime}/F_0^{(e)}-f_0'/f_0]$, application of Eqs. (22) and (21) gives

$$\delta_0=-(E')^{\frac{1}{2}}\{r_1+(S-\Delta y_w)/[2S^2-((E')^{\frac{1}{2}}f_0'/f_0)(S-\Delta y_w)]\}, \tag{23}$$

where

$$\Delta y_w=(-5/r_1)/\{1+3(r_0/r_1)^5[1-z_0F_2'(z_0)/3F_2(z_0)]/[2+z_0F_2'(z_0)/F_2(z_0)]\},$$

and

$$(E')^{\frac{1}{2}}f_0'/f_0=(1/r_1)/[1+(1/r_1)(\delta_{00}/(E')^{\frac{1}{2}})],$$

with

$$\delta_{00}=(E')^{\frac{1}{2}}r_0([F_0(z_0)/z_0F_0'(z_0)]-1).$$

It may be noted that δ_{00} is the phase shift with no tensor force present.

These formulas suffice for the determination of all quantities needed in Eq. (23) to evaluate δ_0.

A convenient approximation results when w is assumed to be a simple cubic in r. Then Δy_w becomes $-5/r_1$, and

$$\delta_0\cong-(E')^{\frac{1}{2}}r_1\{2s^2r_1^2[1+(\delta_{00}/\rho_1)]+Sr_1[\delta_{00}/\rho_1]+5(\delta_{00}/\rho_1)\}/\{2S^2r_1^2[1+(\delta_{00}/\rho_1)]-Sr_1-5\}.$$

(*b*) *Shell inside the well*: $r_1<r_0$.—For this case $y_u(r_0)$ is needed, as Eq. (21) indicates. If $\mathfrak{F}_0(r)$ is taken as

$B_0F_0(z)+C_0G_0(z)$ for $r_1<r<r_0$, then

$$y_u(r_0)=k[(B_0/C_0)F_0'(z_0)+G_0'(z_0)]/[(B_0/C_0)F_0(z_0)+G_0(z_0)].$$

The quantity B_0/C_0 is readily obtained in terms of Δy_u, which is then expressed as a function of S and Δy_w with the aid of Eq. (22). Finally,

$$B_0/C_0=-[k(\Delta y_w-S)+G_0(z_1)F_0(z_1)2S^2]/[2S^2F_0^2(z_0)],$$

where

$$\Delta y_w=k/\{F_2(z_1)[F_2(z_1)[z_0G_2'(z_0)+2G_2(z_0)]/[z_0F_2'(z_0)+2F_2(z_0)]-G_2(z_1)]\},$$

as may be seen by applying the continuity of the logarithmic derivatives at r_0, with Eq. (19) applied in the limit of $E'=0$.

As with the higher energy scattering, the cases for $r_1=r_0$ and $U=0$ may be treated by evaluating the expressions already obtained at the proper limits.

B. Calculations and Comparison with Experiment

1. *Zero-Energy Case*

Calculations employing the formulas of Section IV-A.2 were carried out for the interpolated sets of the parameters r_1, S, and U in Table III which give the deuteron quadrupole moment. The results of these calculations appear in Table III and are plotted in Fig. 3. The experimental cross section for comparison is obtained from two experiments: the total zero-energy cross section[8,9] for neutron-proton scattering and the coherent scattering amplitude[20] at low energies. These data may be expressed as different functions of the singlet and triplet Fermi intercepts,[21] and the triplet cross section which results is

$$\sigma_3=3.41\times10^{-24}\text{ cm}^2.$$

This is smaller than any of the theoretical results when both the ordinary and tensor forces are attractive. However, the trend of the cross section with r_1 in the case of $r_0=e^2/2mc^2$ is promising. For a set of values of U and S extrapolated from Table III the experimental cross section is found to be reproduced for $r_1\sim2.4\times(2.8\times10^{-13})$ cm. This is a large extrapolation, but the validity of the result is supported by the fact that the cross-section variation in this range is almost entirely due to changes in r_1, since U and S have been determined in a region where they vary slowly with r_1.*

For the repulsive tensor force and attractive ordinary

TABLE IV. Theoretical higher energy scattering of neutrons and protons.

E'	r_0	r_1/r_0	$A(10^{-24}\text{ cm}^2)$	B	$\sigma_3(10^{-24}\text{ cm}^2)$
7.5	I[a]	0.587	0.0456	0.4594	0.660
20			0.00704	5.396	0.247
45			0.00292	7.736	0.131
7.5	I	0.695	0.0555	0.0067	0.694
15			0.0236	0.0723	0.304
22.5					0.164
30			0.00763	0.0474	0.0976
7.5	I	0.84	0.0540	0.0212	0.684
15			0.0212	0.0525	0.271
30			0.00575	−0.0582	0.0708
45			0.00218	−0.4278	0.0234
7.5	I	1.0	0.0537	0.0148	0.679
15			0.0209	−0.0082	0.262
30			0.00562	−0.1806	0.0664
7.5	I	1.2	0.0538	0.00256	0.676
15			0.0213	−0.0692	0.262
30			0.00626	0.0815	0.0809
45			0.00292	0.881	0.0475
7.5	I	1.5	0.0544	−0.00945	0.682
15			0.0223	0.0583	0.286
22.5			0.0116	0.4195	0.1663
30			0.00679	0.865	0.110
45			0.00260	0.986	0.0434
7.5	$e^2/2\,mc^2$	3	0.0540	−0.03995	0.669
15			0.0243	0.4278	0.349
30			0.0104	1.250	0.185
45			0.0065	0.9005	0.107

[a] I signifies $r_0=2.8\times10^{-13}$ cm.

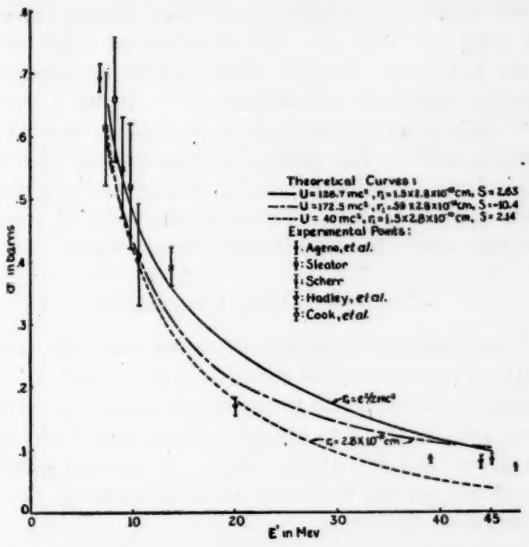

FIG. 4. Total neutron-proton scattering cross section as a function of relative energy. The theoretical cross section is taken as $\sigma=(1/4)\{3\sigma_3+\sigma_1\}$, where σ_3 is the triplet and σ_1 the singlet theoretical cross section. The singlet cross section was obtained by using parameters which reproduced the experimental singlet cross section at zero energy for the two ranges of ordinary force shown. The parameters chosen for the triplet calculation reproduced the deuteron binding energy and quadrupole moment in all cases and reproduced the experimental zero-energy triplet cross section for the repulsive tensor force case.

[20] Shull, Wollan, Mortor, and Davidson, Phys. Rev. **73**, 842 (1948).

[21] J. Schwinger, Phys. Rev. **58**, 1004 (1940).

* *Note added in proof.*—As a result of a suggestion made in the Theoretical Seminar at Yale, preliminary estimates have been made of the effect of varying r_0. It was found that for $r_0=0.532\,e^2/mc^2$, $U=120$ mc² and $r_1=1.5\times2.8\times10^{-13}$ cm, $(\sigma_3)_{E'=0}=2.9$ barns. This set of parameters will also give a theoretical value of Q close to Q_{exp}. It thus appears possible to obtain theoretical agreement with the deuteron properties *and* $(\sigma_3)_{E'=0}$ without employing extreme tensor force ranges.

force, exact calculations have been made only for $r_0=2.8\times10^{-13}$ cm, and the experimental value of the cross section is obtained theoretically for the interpolated values of $r_1/r_0=0.587$, $S=-10.40$, $U=172.5$ mc^2. This value corresponds to the minus sign in the formula for $\mathfrak{R}$. The parallel results for the plus sign imply large negative values for S, and the zero energy cross sections which result are of the order of one and one-half times the experimental cross section.

2. *Higher Energy Calculations*

Computations have been carried out for several relative neutron-proton energies in the range of 7.5 to 45 Mev for most of the same sets of parameters as have been used in the zero energy calculations. The results are given in Table IV in detail. The column headings are based on the following representation of the differential cross section:

$$\sigma_3(\theta)=A(1+B\cos^2\theta),$$

where

$$\sigma_3(\theta)=(1/3)[\sigma_3{}^{m=0}(\theta)+2\sigma_3{}^{|m|=1}(\theta)].$$

The phase shifts $\kappa_L{}^m$ and $\zeta_L{}^m$ are not given in order to save space. The authors will be pleased to supply a more complete table on request. Figure 4 is a plot of the total cross section, including the theoretical contribution from the singlet interaction, with E' for some of the calculations. The experimental cross sections obtained by Amaldi,[10] Sleator,[11] Scherr,[12] Hadley,[13] and Cook[14] are indicated for comparison.

The theoretical cross sections for $r_0=2.8\times10^{-13}$ cm and attractive tensor force consistently fall below the experimental values for $E'>7.5$ Mev, as shown in Fig. 4 and Table IV. The divergence is greater as E' increases. For $r_0=e^2/2mc^2$ and attractive tensor force, the fit is good up to $E'\sim12$ Mev, when the theoretical cross section begins to exceed the experimental values. For the repulsive tensor force, the fit is never very good but the flatness of the theoretical curve at high energies is in agreement with the measurements of Hadley[13] and Cook.[14] This general lack of detailed correspondence of theoretical and experimental results may be attributed in part to the fact that no account is taken of the possibility of exciting the P waves or waves of higher angular momenta in the incident beam. The theoretical curves calculated with the tensor force for $r_0=2.8\times10^{-13}$ cm show better agreement with experimental results than the no tensor force curve for this range. For $r_0=e^2/2mc^2$, the tensor force curve is better only to $E'\sim15$ Mev.

TABLE V. Comparison of theoretical predictions and experimental results for angular distributions of $n-p$ scattering at $E'=20$ and 45 Mev.

E' (Mev)	$\sigma(90°)(10^{-27}$ cm$^2)$ Experimental	$\sigma(90°)(10^{-27}$ cm$^2)$ Theoretical[a]	$\frac{[\sigma(180°)-\sigma(90°)]}{\sigma(90°)}$ Experimental	$\frac{[\sigma(180°)-\sigma(90°)]}{\sigma(90°)}$ Theoretical[a]
45	4	*I*: 2.22 *II*: 6.11 *III*: 2.48	2.6[b]	*I*: 0.871 *II*: 0.718 *III*: 6.90
20	12	*I*: 11.4 *II*: 16.5 *III*: 6.92	0.6	*I*: 0.256 *II*: 0.694 *III*: 4.12

[a] Case *I*: $r_1/r_0=1.5$, $r_0=2.8\times10^{-13}$ cm. *II*: $r_1/r_0=3$, $r_0=e^2/2mc^2$. *III*: $r_1/r_0=0.587$, $r_0=2.8\times10^{-13}$ cm. In all cases, other parameters are adjusted to fit the experimental deuteron properties. The theoretical singlet cross section is included in the theoretical values of $\sigma(90°)$ and $[\sigma(180°)-\sigma(90°)]/\sigma(90°)$.

[b] Since Brueckner found a lack of symmetry about 90°, this represents a mean relative anisotropy.

Hadley *et al.*[13] have measured the angular distribution of $n-p$ scattering at $E'=20$ Mev and $E'=45$ Mev. They were unable to obtain data at scattering angles of less than about 60° for $E'=20$ Mev and 40° for $E'=45$ Mev, but the results indicate a strong anisotropy at these energies, the larger deviation from S-scattering occurring at the higher energy. Since total cross-section measurements were obtained for the same energies, normalization of the differential cross section could be carried out, and thus experimental values of both A and B are available. Brueckner *et al.*[16] also investigated angular distribution at $E'=45$ Mev, and obtained data at smaller angles. Their work indicates a lack of symmetry about 90° and is otherwise in essential agreement with the results of the former group. Table V gives a comparison of these experimental data with three theoretical cases. *I* and *II* are the cases which give the best fit to B at $E'=45$ Mev, when attractive tensor force is used, for $r_0=2.8\times10^{-13}$ cm and $r_0=e^2/2mc^2$, respectively. *III* is the case, when repulsive tensor force is used, which gives theoretical agreement not only with the experimental deuteron properties but also with the zero energy $n-p$ scattering cross section.

As with the comparison of the total cross section, agreement between experiment and theory is here in order of magnitude only. None of the theoretical cases can predict the lack of symmetry of the differential cross section about 90°. Better agreement would doubtless be obtained if scattering of waves of higher angular momenta were considered. Interference between S and P waves would contribute a term in $\cos\theta$, for example, which could produce the observed lack of symmetry about 90°. It is difficult to make a meaningful fit however since, as Kittel and Breit[22] have shown, four P phase shifts must be considered. The interaction for these P waves may be different, so that in order to make a calculation arbitrary assumptions would have to be made which would render the results relatively meaningless. In addition, even if meson theories are taken as a guide to choosing the P interactions, the effect on scattering is sensitive to the range of interaction used. Kittel and Breit[22] have shown, using Bethe's neutral form of the meson theory,[23] that the contribution of the P wave to the total cross section at $E'=8$ Mev is 0.12 barn for a meson mass of $177m$ and is 0.007 barn for a mass of $330m$. Knowledge of the range of the P inter-

[22] C. Kittel and G. Breit, Phys. Rev. **56**, 744 (1939).
[23] H. Bethe, Phys. Rev. **55**, 1261 (1939).

action is not available from experiment, and since it seems possible that there is a difference in the ranges of the ^1S and ^3S interactions,[24] there is little basis on which to choose a range.

The effect of the shape of the interaction on the predicted angular distribution might be considered, but it seems at present that experimental uncertainties in the available data preclude the possibility of deciding between short range potentials of various shapes.

At the lower energies the total cross section is in fair agreement with experiment for all cases. The relative anisotropy for the cases involving an attractive tensor force is two percent or less in agreement with the experiments[15] at these energies which show no anisotropy within experimental uncertainty. With the repulsive tensor force the theoretical relative anisotropy is about ten times as much, and in particular is about nine times the stated uncertainty of Barschall and Taschek.[15] The best over-all agreement with the higher energy scattering experiments is obtained in the theoretical case for $r_0=e^2/2mc^2$, $r_1=1.5\times2.8\times10^{-13}$ cm, as is indicated in Table V and the graphs. The large relative anisotropy at $E'=45$ Mev is not reproduced, and the total theoretical cross section at that energy is higher than the experimental. At $E'=20$ Mev, however, the theoretical and experimental results are in fair agreement, and at lower energies no large anisotropy is predicted for this case. The zero-energy cross section cannot be reproduced exactly with these parameters, as has been previously stated. However, for larger r_1 the zero-energy scattering can be reproduced, and it may be worth while to investigate this case further, especially since the detailed calculations of the variation of the magnitude of the anisotropy with r_1 made for $r_0=2.8\times10^{-13}$ cm indicate that improved agreement with experiment in this respect is possible with r_1 increased.

The calculation of the deuteron magnetic moment has not been considered on the present model. Rarita and Schwinger[1] have shown that a contribution of four percent in the ^3D state will account for the experimental difference $(\mu_p+\mu_n)-\mu_d$ in a non-relativistic calculation. For the cases discussed in preceding paragraphs in connection with scattering, the amount of ^3D state is considerably less than four percent when the tensor force is attractive, and somewhat more than four percent when it is repulsive. The considerations of Breit and Bloch[25] on relativistic corrections to the deuteron moment have indicated that an effect probably no larger than 0.01 nuclear Bohr magneton is to be expected when a Hamiltonian invariant to terms in $(v/c)^2$ is employed. This is essentially independent of the effect considered by Rarita and Schwinger, and may be taken as an indication that a ^3D state between two and six percent is not in disagreement with experiment. Even this range, however, does not include those cases computed on the present model which show the best over-all agreement with measured values.

[24] J. M. Blatt, Phys. Rev. **74**, 92 (1948).

C. Comparison with Results of Rarita and Schwinger

Rarita and Schwinger[1] obtained theoretical agreement with the deuteron binding energy and quadrupole moment by using an ordinary well depth of $27.2mc^2$ and with square wells of range 2.8×10^{-13} cm for both J and J_t. The same parameters for J were examined in this investigation, and it was found that the experimental deuteron properties were reproduced for $r_1=0.84\times2.8\times10^{-13}$ cm. The corresponding zero-energy cross section is 4.25 barns, a value close to the result of 4.21 barns obtained by Rarita and Schwinger. Inspection of their Fig. 1 shows that the maxima of their u and w fall at $r_1/r_0\sim0.8$, resembling strongly the results of the present calculation where the maxima fall at the shell position: $r_1/r_0=0.84$. The corresponding wave functions on the present model are shown as one of the cases for attractive forces in Fig. 2.

It is thus possible to reproduce the important features of the wave functions and therefore of the scattering properties through the use of tensor potentials having very different shapes by employing the same central field potential in the two calculations. The tensor force potential is adjusted in both cases to fit the binding energy and quadrupole moment of the deuteron.

ACKNOWLEDGMENTS

The authors wish to express their thanks to Professor G. Breit for proposing the problem, for his interest and encouragement throughout the course of the work, for pointing out that employment of the Wronskian-type expressions in Section III would simplify the formulas considerably, and particularly for his suggestion that the tensor interaction be confined to an infinitesimal shell in order to reduce the calculational burden.

[25] G. Breit and I. Bloch, Phys. Rev. **72**, 135 (1947).

Disintegration of Li^6 by Deuterons*

WARD WHALING** AND T. W. BONNER
The Rice Institute, Houston, Texas

(Received April 10, 1950)

The cross sections of the $Li^6(d,\alpha)\alpha$ and $Li^6(d,p)Li^7$, $*Li^7$ reactions have been measured up to energies of 1600 kev. Evidence of a resonance level in Be^8 for 347 kev deuterons is presented. The angular distribution of the two proton groups has been observed at 400, 600, 1000, and 1400 kev. The complexity of the angular distribution increases with bombarding energy, requiring a P_6 term in the Legendre polynomial expansion at the highest bombarding energy.

I. INTRODUCTION

THE study of the nuclear reactions that take place when Li^6 is bombarded by deuterons has been hampered in the past by the presence of the much more abundant Li^7 isotope, which takes part in similar reactions under deuteron bombardment. When lithium enriched in the mass six isotope became available through the AEC, it was felt worth while to re-examine the Li^6+H^2 reactions, and this paper reports observations on the following reactions.

$$Li^6+H^2\rightarrow 2He^4+22.23 \text{ Mev}, \quad (1)$$

$$Li^6+H^2\rightarrow Li^7+H^1+4.97 \text{ Mev}, \quad (2)$$

$$Li^6+H^2\rightarrow *Li^7+H^1+4.49 \text{ Mev}. \quad (3)$$

The Q-values above are calculated from Bethe's 1947 values of the nuclear masses.[1] The lithium six targets were prepared from lithium sulfate enriched to 95 percent Li^6, obtained from the Isotopes Branch, Atomic Energy Commission, Oak Ridge, Tennessee.

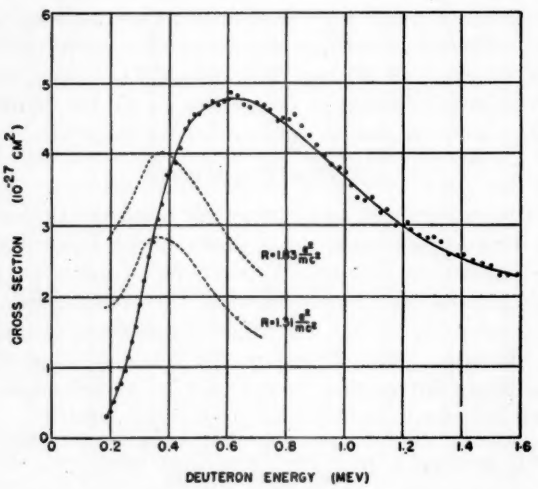

FIG. 1. Cross section for emission of alpha-particles into unit solid angle at 90°. The two dotted curves indicate the excitation function corrected for the penetrability of incident deuteron, assuming two different values of the radius of the Li^6+H^2 system. The units for the dotted curves are arbitrary.

II. ALPHA-PARTICLE EXCITATION FUNCTION

The cross section for the reaction $Li^6+H^2\rightarrow 2He^4+22.23$ Mev has been determined as a function of deuteron energy over the energy range from 190 kev to 1600 kev. The target, a thin layer of $Li_2{}^6SO_4$ (150 micrograms per cm^2), evaporated in vacuum on a thick silver disk, was set at an angle of 45° to the deuteron beam from the Rice Institute pressure Van de Graaff generator. Alpha-particles emitted at an angle of 90° to the beam were detected with a proportional counter, with a window subtending a solid angle of 1.72×10^{-3} steradian. Sufficient aluminum absorber was placed in front of the counter window to stop the shorter range alphas from the $Li^7(d,n)2He^4$ reaction; the long range protons from the $Li^6(d,p)Li^7$, $*Li^7$ reactions were biased out with a discriminating circuit.

The experimental results are shown in the solid curve in Fig. 1. Each point on the curve represents a count of at least 2560 alphas, and the separation between adjacent points on the curve is approximately one-half the target thickness. The energy spread of the deuterons passing through the magnetic analyzer is 10 kev.

The cross section indicated in Fig. 1 is the number of alpha-particles emitted into unit solid angle at 90° per deuteron incident on a target of one Li^6 nucleus per sq. cm, as calculated from the experimental geometry and the target thickness. The target thickness was determined by weighing the target disk before and after evaporation of the Li_2SO_4 upon it. This introduces an uncertainty of 20 percent in the quoted cross section, since it is not known whether the one water of hydration molecule normally present with each Li_2SO_4 molecule appears in a target prepared in this manner and exposed to the atmosphere for periods of from several minutes to several hours before weighing. The cross section has been calculated on the assumption that this water of hydration is not present.

The peak in the alpha-particle excitation curve near 600 kev lies in the energy region in which the increasing penetrability of the incident deuteron through the barrier at the Li^6 nucleus will displace the peak in the experimental excitation curve above the resonant energy. An accurate correction for this penetrability

* This work was assisted by the joint program of the AEC and the ONR.

** Present address: Kellogg Radiation Laboratory, California Institute of Technology, Pasadena, California.

[1] H. A. Bethe, *Elementary Nuclear Theory* (John Wiley & Sons, Inc., New York, 1947).

factor requires a better understanding of the effective radius of the Li^6+H^2 system than is available at present. We have calculated the penetrability correction for two extreme values of the radius, with the expectation that the correct value of the resonant energy will lie somewhere between the two values obtained in this way.

The Gamow penetrability factor $P_l(E)$ for s-deuterons has been calculated after the method given by Bethe.[2] That s-deuterons excite this level in Be^8 seems likely from the angular distribution of the emitted alphas and the magnitude of the cross section.[3] For the larger value of the effective nuclear radius we have taken $1.83\ e^2/mc^2$, as suggested by Resnick and Inglis, which is equivalent to attributing to the deuteron an effective radius equal to that of the Li^6 nucleus determined from the $(e^2/2mc^2)A^{\frac{1}{3}}$ relation. For the smaller value we have taken $1.31e^2/mc^2$, somewhat smaller than the value $1.5\ e^2/mc^2$ proposed for the Li^7+H^1 system.[4,5]

The function $\sigma(90°)/[P_0(E)\lambda^2]$ is plotted in the two dotted curves in Fig. 1 for the two different choices of the nuclear radius; λ is the wave-length of the incident deuteron; $P_0(E)$ is the penetrability factor for s-deuterons incident on the Li^6 nucleus; $\sigma(90°)$ is the cross section for alpha-particle emission into unit solid angle at 90°. These corrected curves show more clearly the behavior of the resonance denominator, with a peak at the resonant energy E_R. For $r=1.31\ e^2/mc^2$, $E_R=380$ kev; and for $r=1.83\ e^2/mc^2$, $E_R=374$ kev. The thickness of the target of 150 micrograms per sq. cm Li_2SO_4 is approximately 60 kev for 380 kev deuterons, calculated from the stopping power of the constituents of the target. Subtracting one-half the target thickness from the mean value of E_R, the resonant energy is 347 kev in the laboratory system, which corresponds to an excitation energy of 22.46 Mev in Be^8.

The use of $\sigma(90°)$ instead of the total cross section is justified by the slight deviation from spherical symmetry in the angular distribution of the alpha-particles at this low bombarding energy. In estimating the width of this level it becomes necessary to consider the shape of the excitation curve at higher energies, where the angular distribution becomes asymmetric, and the total cross section must be used. This total cross section was calculated using our value of $\sigma(90°)$ and the angular distribution data of Heydenburg *et al.* given in reference 3. After making the penetrability correction outlined above, the level width at half maximum appears to be of the order of 520 kev.

III. PROTON EXCITATION FUNCTION

The excitation curves for the two groups of protons from the reactions (2) and (3) have been determined over the energy range from 200 kev to 1800 kev. The $Li_2{}^6SO_4$ target was evaporated on a thin silver foil which was just thick enough to stop the deuteron beam, and protons emitted in the direction of the beam were detected in a proportional counter after passing through the silver target backing. Several targets were used—a thicker one at low bombarding energy where the yield is low, and thinner ones at high energy to improve the resolution of the two groups of protons.

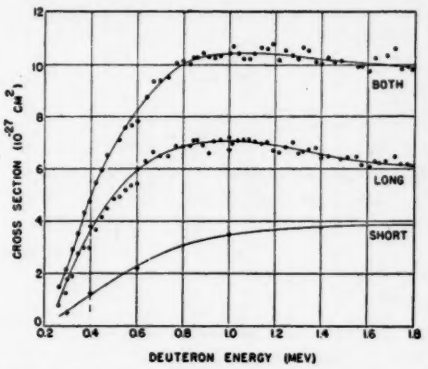

FIG. 2. Cross section for emission of long and short range protons into unit solid angle at 0°.

The two groups were separated by placing in the proton path aluminum absorbers, variable in steps of 3 mm air equivalent. At each bombarding energy the shape of the integral range-numbers curve was determined by observing the counting rate with different amounts of absorber in front of the counter window, and the counting rate for the two groups together and for the longer group alone estimated from the counting rate on the plateaus in the integral range-number curve. The difference in these two counting rates gives the counting rate for the short proton group; no charged particles of range greater than that of the protons in reaction (2) were observed.

The experimental results plotted in Fig. 2 have been corrected for the variation with bombarding energy of the solid angle subtended by the counter in center of mass angle (the solid angle subtended by the counter window at the target is 1.08×10^{-3} steradian). This correction has been calculated from the Q-value 4.97 Mev, and used for both groups of protons; the correction differs from that for $Q=4.49$ Mev by only 3 percent at 1.0 Mev bombarding energy.

At low energies the curves for the individual groups have been drawn through the crossed points, which are

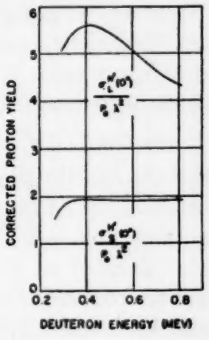

FIG. 3. Excitation curves for long and short range protons corrected for the penetrability of the incident deuteron, assuming a radius for the Li^6+H^2 system of $1.83\ e^2/mc^2$. The units are arbitrary and are different for the two curves.

[2] H. A. Bethe, Rev. Mod. Phys. **9**, 163 (1937).
[3] R. Resnick and D. R. Inglis, Phys. Rev. **76**, 1318 (1949).
[4] D. R. Inglis, Phys. Rev. **74**, 21 (1948).
[5] R. F. Christy and R. Latter, Rev. Mod. Phys. **20**, 185 (1948).

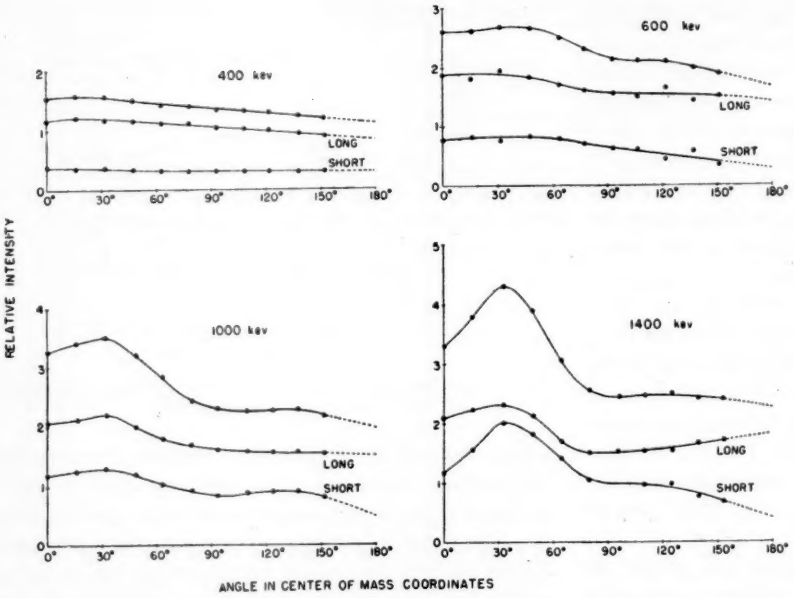

FIG. 4. Angular yield of long and short range proton groups in center of mass coordinates. Proton yield is in arbitrary units but is the same for all curves.

based on the ratio of short to long protons measured with a very thin target mounted on a nickel foil. The cross section indicated in Fig. 2 has been calculated from the weight of the target material as described in the discussion of the alpha-particle excitation curve.

In Fig. 3 are plotted (in arbitrary units) the functions $\sigma^{H^1}(0°)/[P_0(E)\lambda^2]$ obtained by applying the penetrability correction to the experimental excitation functions. The Gamow factor $P_0(E)$ calculated for a nuclear radius of 1.83 e^2/mc^2 for s-deuterons; $\sigma_L{}^{H^1}$ and $\sigma_S{}^{H^1}$ are the cross sections for emission of long range and short range protons respectively into unit solid angle at 0°. It should be noted that the two proton groups differ in range by only $4\frac{1}{2}$ cm out of 35 cm (at 1 Mev bombarding energy) and due to straggling the two groups actually overlap, so that range measurements do not provide a complete separation of the two groups. This experimental error is particularly large for the short proton group at low bombarding energy, where the experimental data is the small difference between two larger experimental counting rates. In view of this uncertainty, the fact that the peak in the corrected excitation curve for the long proton group occurs at 400 kev, instead of 374 kev as in the case of the alpha-particles, is not considered significant. The behavior of the short proton group is more ambiguous. Only at the lowest bombarding energy is there an indication of an approach to a peak in the vicinity of 375 kev, and one is reluctant to draw definite conclusions from these data.

IV. PROTON ANGULAR DISTRIBUTION

The angular distribution of the two groups of protons has been observed for bombarding energies of 400, 600, 1000, and 1400 kev. The scattering chamber used in this experiment is a cylindrical brass pill box with aluminum covered observation ports every 15° between 0° and 150°, and a port at 180° to admit the deuteron beam from the magnetic analyzer. A proportional counter with a window subtending a solid angle of 1.08×10^{-3} steradian can be moved about the perimeter of the cylinder to count protons coming through any of the observation ports. The target, located accurately

TABLE I. Coefficients in the expansion of the proton angular distributions in terms of Legendre polynomials,

$$\sigma(\cos\theta)=\Sigma_l{}^6 A_l P_l(\cos\theta).$$

The units are chosen to make $\sigma(\cos\theta)$ the cross section for emission into unit solid angle.

Bombarding energy		Short proton group	Long proton group	Both groups
		(millibarns)	(millibarns)	(millibarns)
400 kev	A_0	1.14	3.51	4.65
	A_1	<0.01	0.52	0.52
	A_2	0.03	−0.05	−0.01
	A_3	−0.03	0.19	0.16
	A_4	<0.01	−0.14	−0.13
	A_5	−0.03	<0.01	−0.02
	A_6	−0.02	−0.03	−0.05
600 kev	A_0	2.05	5.42	7.46
	A_1	0.83	0.75	1.58
	A_2	−0.25	0.52	0.27
	A_3	<0.01	−0.04	−0.03
	A_4	−0.32	−0.25	−0.57
	A_5	−0.02	−0.19	−0.20
	A_6	<0.01	−0.10	0.10
1000 kev	A_0	2.74	5.67	8.40
	A_1	1.24	1.07	2.31
	A_2	0.59	0.66	1.24
	A_3	0.03	0.08	0.11
	A_4	−0.73	−0.25	−0.99
	A_5	−0.07	−0.23	−0.31
	A_6	0.18	−0.32	−0.14
1400 kev	A_0	3.66	5.45	9.10
	A_1	1.91	0.99	2.92
	A_2	0.58	1.37	1.97
	A_3	−0.06	0.07	0.01
	A_4	−1.21	−0.45	−1.66
	A_5	−0.78	−0.66	−1.44
	A_6	−0.09	−0.45	−0.54

in the center of the chamber, is a thin film of $Li_2{}^6SO_4$ mounted on a thin nickel foil. The thin target, required to give satisfactory resolution of the two proton groups, was not thick enough to stop the deuteron beam at bombarding energies greater than 1500 kev, and our measurements are confined to lower bombarding energies. The target is mounted so that it can be rotated about the axis of the cylinder, perpendicularly to the plane defined by the deuteron beam and the direction of observation.

The following procedure was adopted in determining the angular distributions. At each angle of observation the counting rate was measured with various amounts of aluminum absorber placed in front of the counter window. The counting rate on the plateaus was taken from the integral range-number curve obtained in this way and determines the ratio of long to short protons at the particular angle of observation and bombarding energy used. During these measurements the target was set at the angle which gave the best resolution of the two groups; the consequent variation of target thickness for different angles of observation does not matter, since only the ratio of the two groups is being determined.

The target was next fixed at an angle of 45° with respect to the incident beam, and the total proton counting rate for the two groups together measured over the arc 90° to 150°, counting protons coming from the front surface of the target, and at 0°, counting protons passing through the target backing. The target was then rotated through 90°, so that it presented the same thickness of target material to the incident beam, and the total proton counting rate measured over the arc 0° to 90°, counting protons passing through the target. This procedure was repeated at least twice, taking a count of 2560 protons at each angle. The two sets of data, over the forward and backward angles, were fitted together with the check points at 0° and 90° to give the angular distribution of both groups of protons together. From the ratio of the long group to short group at each angle, the angular distribution of each group alone can be calculated. The observed distribution for both groups and the calculated distribution for each group alone are plotted in Fig. 4 in the center of mass coordinates. Again the correction factor to center of mass coordinates has been calculated for $Q=4.97$ Mev and used for both groups of protons.

In order to gain a quantitative picture of the complexity of these angular distributions the experimental distributions have been expanded in terms of the Legendre polynomials,

$$\sigma(\cos\theta)=\sum_l A_l P_l(\cos\theta)$$

where

$$A_l=\tfrac{1}{2}(2l+1)\int_{-1}^{+1}\sigma(\cos\theta)P_l(\cos\theta)d(\cos\theta).$$

The integration has been carried out numerically by Simpson's method for a second degree polynomial

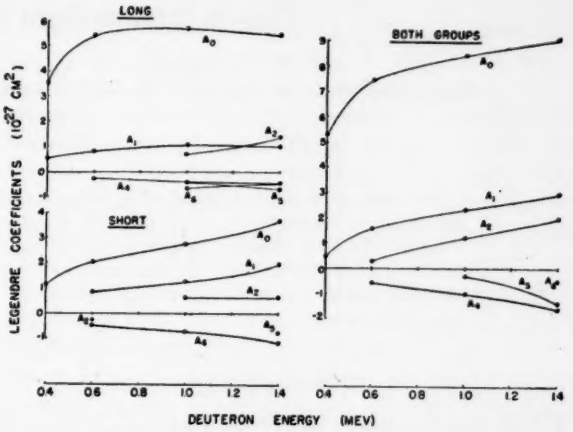

FIG. 5. Coefficients in the expansion of the angular distribution of the proton groups in terms of the Legendre polynomials, plotted as functions of the bombarding energy. The units are chosen so that $\Sigma A_l(E)P_l(\cos\theta)$ is the cross section for proton emission into unit solid angle at the angle Θ. Coefficients not appearing on the graph are less than 0.2×10^{-27} cm^2.

through the experimental points, taking an interval of $\cos\theta=0.05$ between adjacent points to which the second degree polynomial is fitted. This requires that $\sigma(\cos\theta)$ be known at 41 equally spaced intervals between $\cos\theta=-1$ and $\cos\theta=+1$; these values were taken from the smooth curve drawn through the ten experimental points and extended visually from 150° to 180° as is shown by the dotted sections of the curves in Fig. 4. The values of the coefficients obtained in this way are listed in Table I. The functions defined by these coefficients fit the experimental data to within less than the experimental error; for example, the deviation between the experimental distribution for the two groups together at 1.4 Mev, the case of greatest complexity, and the function defined by the calculated coefficients is less than 3 percent. In Fig. 5 these coefficients have been plotted as functions of the bombarding energy. Note that $4\pi A_0$ is the total integrated cross section. For the two groups together, where the experimental accuracy is best, the coefficients show a uniform variation with energy. For the individual proton groups the same general behavior is apparent, with some slight differences that probably indicate the limits of accuracy of these measurements.

Theoretical interpretation of these angular distributions is beyond the scope of this paper. However, it may be noted that the appearance of terms as high as P_4 and P_6 in the expansion may be interpreted to indicate that d and f deuterons take part in the reaction leading to the emission of protons at these bombarding energies. Inglis has already found evidence for the excitation of levels in Be^8 by d-deuterons in this energy range from the angular distribution of the alpha-particles in the $Li(d,\alpha)\alpha$ reaction; f-deuterons do not take part in the alpha-particle reaction.[3]

One of the authors (W.W.) was aided during the course of this work by an AEC fellowship.

Proton Groups from the $B^{11}(d,p)B^{12}$ Reaction *

W. W. Buechner, D. M. Van Patter, E. N. Strait, and A. Sperduto
Physics Department and Laboratory for Nuclear Science and Engineering, Massachusetts Institute of Technology, Cambridge, Massachusetts

(Received April 10, 1950)

Two proton groups observed when boron targets are bombarded with 1.5-Mev deuterons have been identified as arising from the $B^{11}(d,p)B^{12}$ reaction. The Q-values for these groups are 1.136 ± 0.005 and 0.189 ± 0.004 Mev, showing the presence of an excited state in B^{12} at 0.947 ± 0.005 Mev. The reaction energy for the ground-state group is in good agreement with that calculated for the masses and from the B^{12} beta-rays and indicates that the primary mode of decay of B^{12} to C^{12} is between the ground states of these nuclei.

I. INTRODUCTION

THE bombardment of B^{11} with deuterons leads to the formation of radioactive B^{12}. This decays by electron emission to C^{12}, and the beta-ray spectrum has been the subject of several investigations, the most recent of which is that of Hornyak and Lauritsen.[1] These authors find the end point of the B^{12} distribution to be 13.43 ± 0.06 Mev. The shape of the observed distribution is such as to indicate that more than one state of the residual nuclei of B^{12} or C^{12} may be involved in the transformation.

Recently, Hudspeth and Swann[2] have measured, as a function of deuteron energy, the yield of beta-rays from B^{12} formed in the reaction $B^{11}(d,p)B^{12}$. Using photographic plates and range measurements, they have also observed two particle groups which they identify as protons and which they attribute to this reaction. On the basis of this assignment, they have obtained Q-values of 1.25 and 0.15 Mev for the reactions. The relative intensities of these two groups were found to be in the ratio of 1 to 60, the high energy group which is assigned to the reaction leading to the formation of B^{12} in its ground state being the weaker. Hudspeth and Swann conclude that, in the $B^{11}(d,p)B^{12}$ reaction, the B^{12} is usually formed in an excited state at about 1.1 Mev, and that the B^{12} thus formed emits a gamma-ray of this energy before the beta-decay.

We have studied the proton groups emitted from boron targets bombarded by deuterons, using a magnetic spectrometer to analyze the particle groups. We have found two groups of protons that we assign to $B^{11}(d,p)B^{12}$, and the measured Q-values are in approximate agreement with those given by Hudspeth and Swann. However, there is a marked discrepancy between their measurements and ours with regard to the relative intensities of the two groups, our measurements indicating that the ground-state group is about four times as intense as is the one associated with the B^{12} excited state. These measurements and the possible reasons for this disagreement are discussed in the sections that follow.

II. EXPERIMENTAL METHODS AND RESULTS

The apparatus and experimental techniques are essentially the same as those that have been described in a previous paper.[3] The deuteron beam from an electrostatic accelerator and deflecting magnet is directed at a target placed between the pole faces of a large annular magnet. The charged particles emitted at right angles to the incident beam are deflected through 180 degrees and focused in the uniform magnetic field. The particles are recorded on nuclear track plates placed in the focal plane of the magnet so that a series of plates, each exposed at a different field strength, provides a spectrum of the charged particles emitted from the target. As in our previous work, polonium alpha-particles have been used to calibrate the fluxmeter. A similar fluxmeter has been installed in the deflecting magnet used for analyzing the incident deuteron beam, and this is calibrated from measurements on the deuterons elastically scattered from thin foils placed in the target position.

Various measurements and calculations have recently been made that considerably reduce the uncertainties introduced by the conversion from the observed peak positions to the corresponding reaction energies. These new measurements include a precise determination of the angle of observation with respect to the incident beam and will be described in a forthcoming paper on the energies released in a number of nuclear reactions. The results reported here have been treated in the light of these new measurements.

The targets employed in these experiments were prepared by the evaporation of metallic boron onto platinum sheets. Both natural boron and boron in which the proportion of B^{10} was increased 96 percent (obtained from Oak Ridge) were employed. The targets used had effective thickness of approximately 5 kilovolts. With the incident deuteron energy held constant at 1.510 Mev, the various particle groups emitted from both the natural boron and the B^{10} enriched targets have been studied over a wide range of analyzing magnet field strengths, enabling the study of proton groups with energies lying between 1.25 and 10 Mev. Since a 1.5-Mev

* This work has been assisted by the joint program of the ONR and AEC.

[1] W. Hornyak and T. Lauritsen, Phys. Rev. 77, 160 (1950).

[2] E. L. Hudspeth and C. P. Swann, Phys. Rev. 76, 1150 (1949).

[3] Buechner, Strait, Stergiopoulos, and Sperduto, Phys. Rev. 74, 1569 (1948).

deuteron has approximately the same $H\rho$ as a 3-Mev proton (250 kilogauss centimeters), all the plates exposed at field strengths below this value were covered with thin aluminum foil so as to intercept the deuterons that were elastically scattered by the platinum backing of the target. The thickness of these foils was chosen so that, for the particular energy range for which the plates were exposed, the scattered deuterons were completely stopped. This greatly facilitated the counting of the plates in the low energy region. These foils also completely stop any alpha-particles that may be present as, for example, from $B^{10}(d,\alpha)Be^{8}$; since, for a given $H\rho$, alpha-particles have a smaller range than do deuterons. Since, for a given $H\rho$, the deuterons have only approximately half the proton energy, such foils do not seriously shorten the proton tracks.

Large numbers of proton groups were observed in the energy interval investigated. By comparing the yields from the natural boron targets with those enriched in B^{10}, all except two of these proton groups could be identified as arising from either the $B^{10}(d,p)B^{11}$ reaction or from reactions involving various contaminants, such as nitrogen, oxygen, and carbon.

The proton spectrum in the region where these two groups occur is shown in Fig. 1. The upper part of Fig. 1 shows the protons observed from the natural boron targets, while the lower part shows the groups observed from the targets enriched in B^{10}. It can be seen that the groups at 167 and 214 kilogauss centimeters with the natural boron targets are completely missing in the lower curve taken from the targets enriched in B^{10}. This would be expected if these groups are due to B^{11}, since the enriched targets contain only 4 percent B^{11}, as compared with 81 percent for the natural boron. The groups at 171 and 190 kilogauss centimeters are increased in intensity by a factor of approximately 5 when the enriched targets are substituted for the natural boron, as would be expected if they are due to $B^{10}(d,p)B^{11}$, since the B^{10} is only 18 percent in the natural boron but is 96 percent in the enriched material. As indicated on the figure, the other groups observed are identified as arising from reactions involving N^{14} and O^{16}. The very intense peak at 216 kilogauss centimeters has been shown one-half size in the figure and is due to the $O^{16}(d,p)O^{17*}$ reaction, the O^{17} being formed in an excited state. The Q-value for this reaction has been previously measured as 1.049 Mev.[4] This group from oxygen is close to, but clearly resolved from, the group from B^{11}.

As a further check on the assignments of these groups, we have measured the shift in position produced by changes in the energy of the incident deuteron beam. Such measurements provide a sensitive check on the proper assignment of a group to a particular isotope, the change in proton energy being independent of the Q for the reaction and depending only on the ratios of the various masses involved and the change in the deuteron energy. For observations made at 90 degrees, the energy of a proton group from $B^{11}(d,p)B^{12}$ will change by an amount equal to ten-thirteenths of the change in energy of the incident deuteron beam, whereas the fraction will be nine-twelfths in the case of a group from $B^{10}(d,p)B^{11}$. This difference is readily measurable with a magnetic spectrometer of the type employed in these experiments. Studies of this type made on the two groups shown in Fig. 1 at 215 kilogauss centimeters are plotted in Fig. 2. The figure shows the position of these groups for both the natural boron and the B^{10} enriched targets at three different deuteron energies. Since the change in energy of the proton group from $O^{16}(d,p)O^{17*}$ is fifteen-eighteenths the change in the deuteron energy, the energy of this group will decrease more rapidly as the incident energy is lowered than will the energy of a proton group from either of the boron isotopes. This effect can be seen in Fig. 2, the group from oxygen having the higher energy at a bombarding energy of 1.674 Mev and the lower energy for 0.700-Mev deuterons. The change in energy of the group from boron

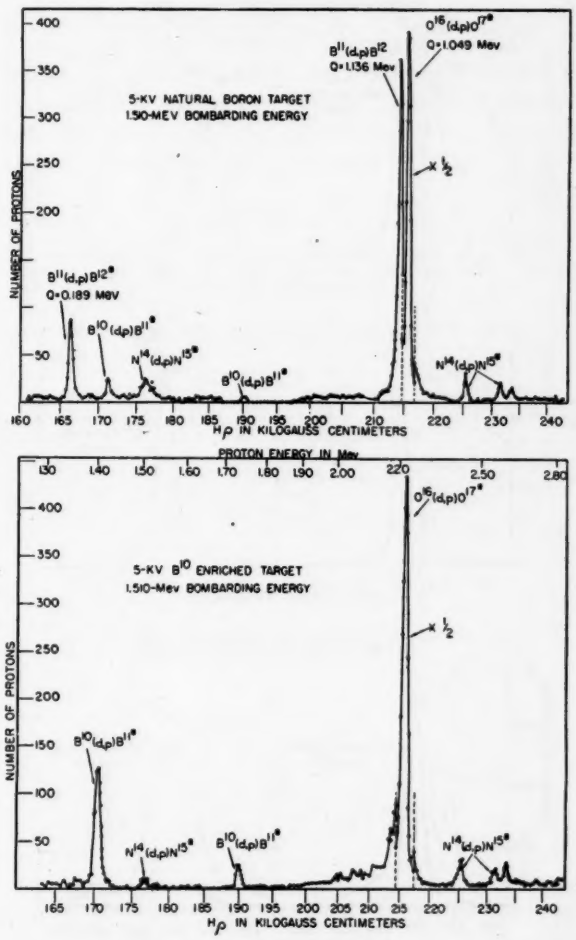

FIG. 1. Proton spectrum from natural boron and B^{10} enriched targets in the energy interval from 1.30 to 2.80 Mev. Incident deuteron energy is 1.510 Mev.

[4] Buechner, Strait, Sperduto, and Malm, Phys. Rev. **76**, 1543 (1949).

shows conclusively that it arises from the $B^{11}(d,p)B^{12}$ reaction; on the basis of this assignment the Q-values calculated for this group, for each of the three bombarding energies, agree to about 1 kilovolt. If the boron group shown on the curve for 1.674-Mev deuterons had been due to $B^{10}(d,p)B^{11}$, it would have appeared at the position shown by the dotted curve in the figure for the natural boron targets at 0.700-Mev deuteron energy. Figure 2 also shows that this peak for boron is absent from the measurements taken on the B^{10} enriched target.

These measurements allow the calculation of the energies released when B^{12} is formed in its ground state and in an excited state. The Q-values obtained are 1.136 ± 0.005 Mev and 0.189 ± 0.004 Mev, respectively. This leads to a value of 0.947 ± 0.005 Mev for the energy of the excited state of B^{12} involved in these reactions. An energy-level diagram of B^{12} is shown in Fig. 3, the excitation curve shown for the $B^{11}(d,p)B^{12}$ reaction being that determined by Hudspeth and Swann for the yield of the disintegration electrons.

The above values for the Q-values have not been corrected for the effect of possible surface contaminants. In general, it is possible to measure the thickness of surface layers, which consist principally of carbon and oxygen, by observations on the intensities of the groups from the $C^{12}(d,p)C^{13}$ and $O^{16}(d,p)O^{17}$ reactions. In the present case, it appears that oxygen is distributed throughout the target; since the boron was evaporated from a graphite crucible, this is also true for carbon. Hence, it is not possible to distinguish the effect of a surface layer in this way. However, the close concordance of results taken over a considerable time interval, together with the good agreement between the Q-values obtained at widely different bombarding energies, indicates that the effect of surface contaminants which would lead to somewhat low Q-values is not serious in these experiments.

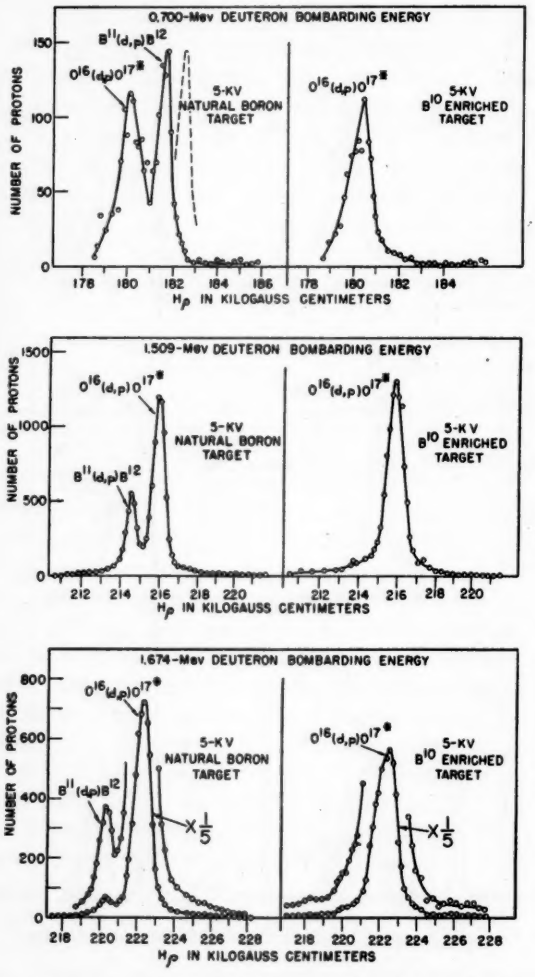

FIG. 2. Proton groups from $B^{11}(d,p)B^{12}$ and $O^{16}(d,p)O^{17*}$ for different incident deuteron energies.

III. DISCUSSION

The curves in Fig. 1 show that the proton group from $B^{11}(d,p)B^{12}$ is about four times an intense as that from $B^{11}(d,p)B^{12*}$ at a bombarding energy of 1.510 Mev. As has been mentioned, Hudspeth and Swann report that, at a deuteron energy of 1.68 Mev, the low energy group is 60 times as intense as the group corresponding to the ground-state reaction. We have not made a detailed study of the variation of yields of these groups as a function of bombarding energy, but the data shown in Fig. 2 indicate that the intensity of the ground-state group is not sensitive to bombarding energy in the range from 1.50 to 1.67 Mev. Such a large change in the relative intensity of the groups would not be expected over such a short energy interval, and it is possible that the discrepancy between the two sets of measurements can be explained as being caused by other factors.

In the measurements of Hudspeth and Swann, the group of particles attributed to the $B^{11}(d,p)B^{12*}$ reaction is more intense than and has a slightly longer range than a group identified as being due to deuterons elastically scattered from a target prepared by the evaporation of boron onto a thin aluminum foil. Their curve indicates that the scattering from the boron is only a small fraction of the scattering from the target. Thus, their interpretation indicates that the protons from $B^{11}(d,p)B^{12*}$ are much more numerous than the deuterons elastically scattered from the boron. We have made measurements on the relative intensities of the protons from $B^{11}(d,p)B^{12*}$ and the elastically scattered deuterons, the targets being formed by the evaporation of boron onto a thin Formvar foil. We find that deuterons elastically scattered from boron are approximately six times as intense as protons from $B^{11}(d,p)B^{12*}$. It appears probable that, in the work of Hudspeth and Swann, the more intense peak having a slightly greater range may be due to a scattering of deuterons from some target contamination of higher atomic number rather than to protons from the boron. It has been suggested by Dr. Hudspeth[5] that such a con-

[5] E. L. Hudspeth, private communication.

taminant might be either wolfram or tantalum from the ribbons used for the boron evaporation, and measurements on the relative ranges of the two groups tend to confirm this interpretation. Since the elastic scattering varies as the square of the atomic number, only a small amount of wolfram or tantalum would be required to produce this group, and we have found that small amounts of these elements are usually deposited on targets prepared by evaporation from such ribbons.

Additional evidence that this peak was probably caused by deuterons scattered by a surface contaminant, rather than by protons from boron, is provided by the fact that it was observed to disappear when a target enriched with B^{10} was bombarded. As can be seen from Fig. 1, the proton group from $B^{11}(d,p)B^{12*}$ is close to a group from $B^{10}(d,p)B^{11*}$. It is unlikely that these two groups would have been resolved in the experiments of Hudspeth and Swann, and it can be seen that the latter group is of considerable intensity when observations are made from a target enriched in B^{10}. These two groups, shown in Fig. 1 for a bombarding energy of 1.51 Mev, would also be somewhat closer together at the higher bombarding energy used in their experiments.

The data in Fig. 2 for a natural boron target at a bombarding energy of 1.674 show the very considerable intensity of the protons from oxygen contamination, as compared with those from $B^{11}(d,p)B^{12}$. It is possible that the measurements of Hudspeth and Swann in this energy region were complicated by the presence of this group from oxygen. That oxygen may have been present in considerable amounts is indicated by the presence of the unidentified higher energy group in their data. This group has approximately the range and relative intensity which would be expected for the protons from $O^{16}(d,p)O^{17}$. The Q-value for this reaction is 1.925 Mev,[4] and we find that, at these bombarding energies, its intensity is approximately half that of the group from $O^{16}(d,p)O^{17*}$.

The measured Q-value for the $B^{11}(d,p)B^{12}$ reaction allows the calculation of the $B^{11}-B^{12}$ mass difference.

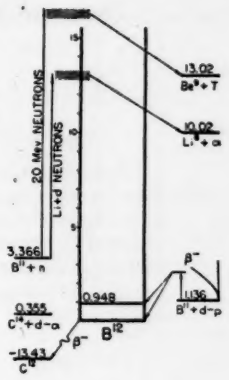

FIG. 3. Energy-level diagram for B^{12}. Energies in Mev.

From this value, together with the mass[6] of B^{11}, and from Hornyak and Lauritsen's value for the end point of the beta-decay from B^{12}, we calculate the mass of C^{12} to be 12.00376. This calculated value agrees with the value otherwise obtained,[6] the difference being within the probable errors of the masses of B^{12} and C^{12}. It thus appears that the primary process in the beta-decay is a direct transition from the ground state of B^{12} to the ground state and, with less probability, to one or more of the excited states of C^{12}.

We are indebted to Dr. E. L. Hudspeth and Mr. C. P. Swann for correspondence regarding their results. We are also indebted to Mr. W. Tripp, Miss C. O'Brien, and Mrs. H. Andrews for their assistance in connection with the reading of the photographic plates.

Note added in proof.—Since the above results were submitted for publication, McMinn, Sampson, and Bullock [Phys. Rev. 78, 296 (1950)] have reported proton groups from the reaction $Be^{9}(\alpha,p)B^{12}$, using 21.94-Mev cyclotron alpha-particles and range measurements. They find proton groups with Q-values of -7.02, -8.06, -8.93, and -11.11 Mev, corresponding to the ground state of B^{12} and excited states at 1.04, 1.91, and 4.09 Mev. Since no probable errors were given for these results, we conclude that the value for the first excited state of B^{12} at 1.04 Mev is in reasonable agreement with our result of 0.947 Mev. No search has been made for a proton group from the $B^{11}(d,p)B^{12}$ reaction corresponding to an excited state in B^{12} at 1.91 Mev.

[6] J. Mattauch and A. Flammersfeld, Isotopic Report, Special Issue, Zeits. f. Naturforsche, 1949.

Note on a Possible Annihilation Process for Negative Protons* †

J. ASHKIN, T. AUERBACH,‡ AND R. MARSHAK
University of Rochester, Rochester, New York

(Received April 5, 1950)

Expressions have been obtained for the annihilation cross sections of proton pairs using weak coupling theory and spin zero mesons. The cross section for annihilation into two charged mesons has a $1/v$ behavior in the limit of very small velocity, v, of the negative proton and dominates over the annihilation into two photons. In the laboratory coordinate system it is possible for one of the emitted mesons to emerge in the *backward* direction with respect to the direction of the incident negative proton even for large incident energies. This may provide a method for distinguishing high energy annihilation events taking place in the cosmic radiation.

I. INTRODUCTION

MESON theoretic calculations on the interaction of nucleons are at present based on the assumption that the "bare" nucleon is an elementary particle obeying the Dirac equation. This assumption, by analogy with electron-positron theory, implies the existence (in real, as well as in virtual, states) of antinucleons. In virtual states the antinucleons are used in higher order meson-nucleon interactions, and indeed recent observations on the supposed decay of a neutral meson into gamma-rays[1,2] offers indirect evidence in favor of the antinucleons. The neutral meson, π^0, presumably decays through the virtual creation of a nucleon-antinucleon pair which annihilates into two gamma-rays, annihilation into π-mesons being energentically impossible in this case.[3,4] In a real state, a proton of negative charge should exist and be capable of undergoing annihilation with a proton or neutron; a similar statement can be made about the antineutron. Since the nucleons are more strongly coupled to the meson field than to the electromagnetic field, it is to be expected that mesons rather than photons will result from real annihilation events.

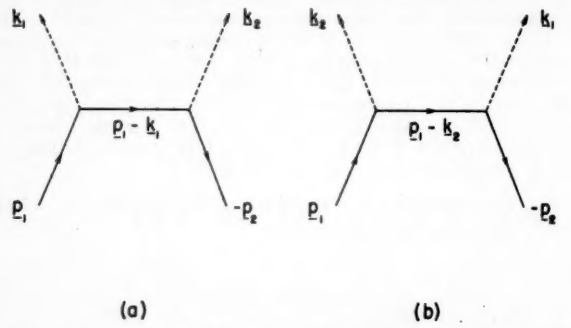

FIG. 1. Feynman diagrams for nucleon annihilations with emission of two mesons k_1 and k_2. For negative proton plus proton, the emission of charged mesons is described by (a); if the emitted mesons are neutral the amplitude contributed by (b) must also be considered.

In the cosmic radiation (until the bevatron is constructed, the only source of particles sufficiently energetic to produce nucleon-antinucleon pairs[5]) there should be very little difference in the behaviors of the nucleon and the antinucleon with respect to collision processes in which the total number of nucleons does not change. The essential difference between the nucleon and the antinucleon from an experimental standpoint should reside in the ability of the antinucleon to initiate an annihilation event. In the present note we have re-examined the annihilation mechanism for antinucleons with a view to underlining those features of the annihilation process which would enable a decision to be made concerning the existence of antinucleons, by observations on the cosmic radiation. Unfortunately, the quantitative conclusions at which we arrive (Section III) are rather equivocal, in the present state of our knowledge.

Earlier work on the production and annihilation of negative protons, using the Heitler theory of radiation damping, has been reported by McConnell.[6] Owing to the discrepancy between his results and our own, and to the sensitive dependence of the results on the strength and character of the meson-nucleon coupling, we have repeated the annihilation calculations. More recent work of Helstrom[7] is in agreement with our results.

All of the cross sections have been calculated by perturbation theory to the lowest order, following the simplified methods introduced by Feynman.[8] It is realized that such a perturbation procedure applied to

* Preliminary results presented to the National Academy of Sciences at its 1949 autumn meeting, Rochester, New York (Science **110**, 438 (1949)).

† This work was supported by the joint program of the ONR and AEC.

‡ Predoctoral AEC fellow.

[1] Bjorklund, Crandall, Moyer, and York, Phys. Rev. **77**, 213 (1950).

[2] Kaplon, Peters, and Bradt, Phys. Rev. **76**, 1735 (1949), Bradt, Kaplon, and Peters, Helv. Phys. Acta **23**, 24 (1950); R. E. Marshak, Phys. Rev. **76**, 1736 (1949).

[3] R. J. Finkelstein, Phys. Rev. **72**, 415 (1947).

[4] J. Steinberger, Phys. Rev. **76**, 1180 (1949).

[5] The threshold kinetic energy for the production of a nucleon-antinucleon pair in the collision of an incident nucleon with a target nucleon at rest is six times the nucleon rest energy, or 5.6 Bev.

[6] J. McConnell, Proc. Roy. Irish Acad. **50A**, 189 (1945); J. McConnell and L. Janossy, Nature **159**, 335 (1947); J. McConnell, Proc. Roy. Irish Acad. **51A**, 173 (1947).

[7] C. W. Helstrom, Phys. Rev. **78**, 88 (1950) and private communication.

[8] R. P. Feynman, Phys. Rev. **76**, 749, 769 (1949).

meson-nucleon problems is extremely crude, but it is thought that the qualitative features will persist in a more correct theory. It is possible that multiple meson emission in higher order annihilation events may have a probability comparable to, or even larger than, the two meson emission. However, for kinetic energies of a few Bev (in which we are mainly interested) the cosmic-ray experiments indicate only a small multiplicity for meson production in proton-nucleon collisions. If this result applies also to annihilations, we may expect that the two-meson emission is not overbalanced by the higher order processes.

II. CROSS SECTIONS FOR VARIOUS ANNIHILATION PROCESSES

Let a free negative proton (energy-momentum four vector $\mathbf{p}_2$) be annihilated with a free positive proton (four vector $\mathbf{p}_1$) resulting in the emission of two charged mesons π^+ and π^- (four vectors $\mathbf{k}_1$ and $\mathbf{k}_2$ respectively). Taking the mesons as pseudoscalar with pseudoscalar coupling, the associated Feynman diagram (Fig. 1(a)) leads to a matrix element proportional to

$$H=g^2\bar{u}_2\gamma_5[1/(\mathbf{p}_1-\mathbf{k}_1-M)]\gamma_5 u_1,$$

where u_1 and u_2 are the Dirac spinors representing proton and negative proton respectively, g is the "mesic" charge of the nucleon, M is the nucleon mass, $\gamma_5=\gamma_1\gamma_2\gamma_3\gamma_4$, $\mathbf{p}=p_\mu\gamma_\mu$, and $\bar{u}_2=u_2^*\gamma_4$. The functions u_1 and u_2 satisfy the Dirac equations $\mathbf{p}_1u_1=Mu_1$ and $\mathbf{p}_2u_2=-Mu_2$. (We use Feynman's notation and choose $\hbar=c=1$.) To obtain the cross section we must average the squared modulus of H over the spins of the nucleons and multiply by the density of final states divided by the incident current. In the center of mass (CM) coordinate system where the energy-momentum relations are simplest, the density of final states is given by $\rho=(\frac{1}{2})kEd\Omega$ and the incident current by $2p/E$, where p and E denote the three-dimensional momentum and energy of each of the approaching nucleons and k the three-dimensional momentum of each of the emerging mesons which are emitted with opposite momenta in the solid angle $d\Omega$. Because of the conservation laws, the energy of each meson is equal to the energy of each of the nucleons: $k^2+\mu^2=p^2+M^2$, μ being the meson mass. After multiplying $|H|^2$ by a factor $2\pi/E$ for each meson and by M/E or $-M/E$ for each nucleon according to the normalization,[9] we obtain finally for the differential cross section for annihilation into mesons with oppositely directed momenta in the solid angle $d\Omega$:

$$d\sigma=d\Omega(g^4k/8pE^2)A(\theta), \tag{1}$$

$$A(\theta)=\frac{[k^2p^2(1-\cos^2\theta)+M^2k^2]}{[p^2+k^2+M^2-2pk\cos\theta]^2}\ \text{(pseudoscalar)}. \tag{1a}$$

θ is the angle between the momentum of the negative proton and the momentum of the negative meson. For scalar mesons with scalar coupling the cross section is expressible in the form (1) with

$$A(\theta)=\frac{k^2p^2(1-\cos^2\theta)+M^2(k^2+4p^2-4kp\cos\theta)}{[p^2+k^2+M^2-2pk\cos\theta]^2}$$

(scalar). (1b)

For the pseudoscalar theory, (1a) is a decreasing function of θ $(0\leq\theta\leq\pi)$ for all energies indicating that the negative meson (π^-) is preferentially emitted in the direction in which the negative proton was originally moving. At very high energies of the negative proton, the π^- is emitted in a narrow forward cone while at very low energies the mesons are emitted (in opposite directions) practically isotropically in the center of mass system (and also in the laboratory system in which the positive proton is initially at rest). For the scalar theory, the angular distribution given by (1b) has the same qualitative features as does the pseudoscalar theory for sufficiently high energies, when p and k are comparable and are large compared with M, but marked differences occur at intermediate nucleon energies. As the energy of the incident negative proton in the laboratory system falls below about 6 Bev, a maximum appears in the scalar angular distribution at some finite angle (>0) and as the incident energy decreases the maximum is is shifted towards π until eventually the differential

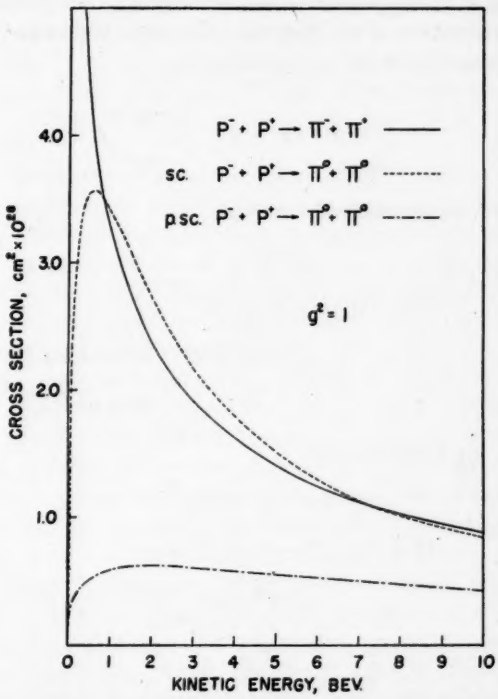

FIG. 2. Total cross sections for the various possible annihilation processes as a function of the kinetic energy of the negative proton in the laboratory system. Normalization is to $g^2=1$. In the annihilation $p^-+p^+\rightarrow\pi^-+\pi^+$ there is no essential difference between scalar or pseudoscalar meson emission but a difference appears in the annihilation into neutral mesons.

[9] R. P. Feynman, I., reference 8, p. 758.

cross section is a monotonically *increasing* function of θ from 0 to π. For an incident kinetic energy of 50 Mev in the laboratory, for example, the differential cross section at 180° is about twice as large as it is at zero degrees in the center of mass system. At this energy, if the emitted mesons were scalar, there would therefore be about twice as many negative mesons emitted backward per unit solid angle in the laboratory as forward, in strong contrast with the pseudoscalar distribution which favors forward emission. At the very low energies the angular distribution becomes isotropic in the directions of the oppositely moving mesons.

Integration of (1) over the solid angle yields the total cross section σ for the annihilation.

$$p^-+p^+\rightarrow\pi^-+\pi^+:\ \sigma=\frac{\pi g^4 k}{4pE^2}J, \tag{2}$$

where, for *pseudoscalar* mesons,

$$J=-1+\frac{2M^2k^2}{M^4+2M^2(k^2+p^2)+(M^2-\mu^2)^2}+\frac{p^2+k^2+M^2}{4kp}\ln\frac{M^2+(k+p)^2}{M^2+(k-p)^2}, \tag{2a}$$

and, for *scalar* mesons,

$$J=-1+\frac{2M^2(2p^2-k^2-2M^2)}{M^4+2M^2(k^2+p^2)+(M^2-\mu^2)^2}+\frac{p^2+k^2+5M^2}{4kp}\ln\frac{M^2+(k+p)^2}{M^2+(k-p)^2}. \tag{2b}$$

Since the total cross section is invariant under Lorentz transformations, we can obtain the dependence on the energy, $M\gamma$, of the incident negative proton in the laboratory (with respect to which the CM system has velocity p/E) by making the substitutions

$$E=M[(\tfrac{1}{2})(\gamma+1)]^{\frac{1}{2}},\quad p=M[(\tfrac{1}{2})(\gamma-1)]^{\frac{1}{2}},\quad k=M[(\tfrac{1}{2})(\gamma+1)-(\mu/M)^2]^{\frac{1}{2}}. \tag{3}$$

In Fig. 2 we have drawn the energy dependence of the cross section for the pseudoscalar case normalized to the value $g^2=1$. In the scalar case the energy dependence is almost identical, being practically indistinguishable from the pseudoscalar on the scale of the drawing. For very low energies, both cross sections behave as $1/v$, where v is the velocity of the negative proton, the quantities J in (2a) and (2b) being identical in the limit of zero p. This $1/v$ behavior is similar to the situation encountered in the electron-positron annihilation with γ-ray emission. If we replace the electron mass by that of the proton in the e^+-e^- annihilation cross section, we may compare the probability for negative proton annihilation with the emission of mesons to the probability for γ-ray emission: (neglect μ^2 compared to M^2).

$$\begin{aligned} &p^-+p^+\rightarrow\pi^-+\pi^+: && \sigma\rightarrow(\pi g^4/4M^2)(1/v),\\ &p^-+p^+\rightarrow\gamma+\gamma: && \sigma\rightarrow(\pi e^4/M^2)(1/v). \end{aligned} \tag{4}$$

Thus the meson emission is more probable by a factor $(\frac{1}{4})(137)^2g^4\approx 10^4$.

McConnell,[6] using the Heitler method of radiation damping and pseudoscalar mesons with pseudovector coupling, has found a different result. He found a constant cross section for annihilation into mesons in the limit $v\rightarrow 0$, and hence a predominance of the γ-ray emission for negative protons annihilating at rest. We have performed an independent perturbation calculation for pseudoscalar mesons with pseudovector coupling *without* radiation damping and have found that $\sigma\rightarrow\pi f^4(M^2/\mu^4)(1/v)$ where f^2 is the appropriate coupling constant. The discrepancy cannot be a consequence of the neglect of radiation damping, which should become unimportant at low energies, and we believe that McConnell's results are incorrect.

It may be of interest to record also the cross section for annihilations in which two *neutral* mesons (π^0) are the final products. In this case there are two interfering amplitudes corresponding to the Feynman diagrams (a) and (b) of Fig. 1. We find for the differential cross section (CM system)

$$p^-+p^+\rightarrow\pi^0+\pi^0,$$

$$d\sigma=d\Omega(g^4k/8pE^2)\{A(\theta)+A(\pi-\theta)-2B(\theta)\}, \tag{5}$$

where $A(\theta)$ is given by (1a) or (1b) and

$$B(\theta)=\frac{k^2p^2(1-\cos^2\theta)+k^2M^2}{(p^2+k^2+M^2)^2-4k^2p^2\cos^2\theta}\ \text{(pseudoscalar)} \tag{5a}$$

or

$$B(\theta)=\frac{k^2p^2(1-\cos^2\theta)+M^2(k^2-4p^2)}{(p^2+k^2+M^2)^2-4k^2p^2\cos^2\theta}\ \text{(scalar)}. \tag{5b}$$

Integration over half the full solid angle (since the emitted mesons are not distinguishable) gives the total cross section:

$$\sigma=(\pi g_0^4k/4pE^2)(J-K), \tag{6}$$

where J is given by (2a) or (2b) and

$$K=\frac{1}{2}\left\{\frac{p^2+k^2+M^2}{8kp}-\frac{k^2(p^2+M^2)}{2kp(p^2+k^2+M^2)}\right\}\times\ln\frac{M^2+(k+p)^2}{M^2+(k-p)^2}\ \text{(pseudoscalar)}, \tag{6a}$$

$$K=\frac{1}{2}\left\{\frac{p^2+k^2+M^2}{8kp}-\frac{k^2p^2+M^2(k^2-4p^2)}{2kp(p^2+k^2+M^2)}\right\}\times\ln\frac{M^2+(k+p)^2}{M^2+(k-p)^2}\ \text{(scalar)}. \tag{6b}$$

In the limit of zero velocity we find readily from (5) or (6) that the interference effects cause the cross section to *vanish*. This is qualitatively in sharp contrast with the charged meson emission. The full energy dependence of the cross section is shown in Fig. 2 for pseudoscalar and scalar mesons. (The normalization is to $g_0^2=1$.)

The g_0 in (6) is the coupling constant of the neutral meson to the nucleons. In the so-called "symmetrical" meson theory of the nuclear forces, the constant g_0 has opposite sign for neutron and proton. Such a possible difference in the sign of g_0 has no effect in (6) but does make a difference if we consider the annihilation of a negative proton with a neutron: $p^-+N \rightarrow \pi^0+\pi^-$. Here also there are two interfering amplitudes and these add or subtract according to whether g_0 remains the same, or changes sign, between neutron and proton. The differential annihilation cross section is

$$d\sigma=d\Omega(g_0^2g^2k/8pE^2)\{A(\theta)+A(\pi-\theta)\mp 2B(\theta)\} \quad (7)$$

and the total is

$$\sigma=(\pi g_0^2g^2k/2pE^2)(J\mp K), \quad (8)$$

where the minus sign is to be used if neutron and proton have the same neutral mesic charge, and the plus sign if the neutral mesic charges are opposite. The difference of 2 in the numerical coefficients for (6) and (8) arises from the fact that in (8) we have *distinguishable* particles, π^0 and π^-, emerging. For zero velocity the cross section approaches zero if the minus sign is valid in (8), and varies like $(\pi g_0^2g^2/M^2v)$ if the plus sign is valid.

We have so far considered annihilation processes in which both nucleons are treated as free. If the negative proton traverses any material except hydrogen however, it will annihilate with a bound nucleon. Under these circumstances it is possible for only one meson to be emitted in the annihilation, with the recoil momentum being distributed among the residual nucleons probably in the form of an energetic star. If the negative proton annihilates with a neutron in some deuteron-like structure in the nucleus, there would result a π^- meson with 1.1 Bev kinetic energy together with a recoil nucleon of kinetic energy about 620 Mev. If the annihilation is with a neutron in an alpha-particle-like structure there would result a 1.35-Bev π^--meson and a 370-Mev recoil He^3. In either case the matrix element would be proportional to a Fourier amplitude of the nuclear wave function corresponding to a large momentum transfer and would therefore be small. An estimate indicates that the "two-meson" annihilation is larger by a factor of at least 1000 for all energies of the negative proton.

III. THE POSSIBILITY FOR OBSERVATION OF ANTINUCLEONS IN THE COSMIC RADIATION

If a nucleon of kinetic energy greater than six times its rest energy (5.6 Bev) strikes a target nucleon at rest, it is energetically possible to produce a nucleon-antinucleon pair. The energetic primary proton component of the cosmic radiation may therefore be expected to give rise to negative protons as secondaries produced in collisions in the topmost layers of the atmosphere. All effects due to the negative protons will therefore be proportional to the cross section for their production as members of nucleon pairs.[10] This cross section has been computed by Helstrom[7] by first making a calculation of the nucleon pair production as a result of meson-nucleon collisions and then applying the Weizsäcker-Williams method. For 30-Bev incident protons the cross section is of the order $0.01\ g^8/M^2$ for the pseudoscalar meson theory (pseudoscalar coupling), and is therefore extremely sensitive to the value of g^2. With $g^2=4$ for pseudoscalar mesons[11] (a value currently suggested on not very clear grounds), Helstrom's formula leads to about 10^{-27} cm^2. For scalar mesons, the production cross section turns out to be much smaller.

A similar sensitive dependence on the value of g^2 is exhibited by the annihilation cross sections, which are proportional to g^4; between pseudoscalar and scalar mesons there is a factor of a hundred. For the pseudoscalar case and a negative proton kinetic energy 2 Bev, the cross section for annihilation with emission of two charged mesons is 3×10^{-27} cm^2. Choosing $g^2=\frac{1}{4}$ for the scalar case, the cross section is $\sim10^{-29}$ cm^2. It is difficult to say which of these annihilation cross sections is the more reasonable. If the annihilation is regarded from a gross point of view as a type of meson production, we may compare it with the experimentally derived cross section for meson production[12] which is of the order 10^{-26} cm^2 or more in the range of 10 Bev. This would make the pseudoscalar value of the annihilation cross section appear the more reasonable. On the other hand, from the point of view of the perturbation theory, the annihilation process in lowest order is closely related to the scattering of a meson by a nucleon. (This is most clearly seen by comparing the Feynman diagrams for the two-processes.) The small observed value of the meson scattering cross section[13,14] would therefore be a reason for preferring a value closer to the scalar value for the annihilation cross section.

In view of these large uncertainties in the cross sections it is not possible to make any quantitative statements on the probability of observing negative protons.[15] Nevertheless it should be possible to make

[10] This leaves out the possibility that there are negative protons in the primary cosmic radiation itself.

[11] H. A. Bethe, Phys. Rev. **76**, 191 (1949). This value of $g^2=4$ is obtained from the nuclear forces predicted in higher order by the pseudoscalar meson theory, the lowest order being small. These forces, however, do not possess the correct exchange or spin dependent properties.

[12] See for example G. Cocconi, Phys. Rev. **75**, 1074 (1949) and **76**, 984 (1949) on the absorption of the hard shower producing component of the cosmic radiation.

[13] W. B. Fretter, Phys. Rev. **76**, 511 (1949).

[14] W. W. Brown and A. S. McKay, Phys. Rev. **77**, 342 (1950).

[15] In spite of the quantitative uncertainties it may be useful to indicate the consequences of different assumptions about the production and annihilation cross section for negative protons. If we are guided by perturbation theory and take g^2 of order 4

use of the fact that the antinucleons are relatively unique among the secondary products of the cosmic radiation since they can be eliminated only in special annihilation events. Negative protons may of course be converted into antineutrons in collision processes in which an excess of one negative meson is produced, and these non-ionizing antineutrons would be difficult to detect. However, if negative protons are produced by the primary radiation, one should expect a comparable production of antineutrons. The antineutrons would be partially converted into negative protons in non-annihilation, meson producing collisions and would compensate for the conversion of negative protons. Therefore we may expect that there should be one annihilation event for every negative proton created. The nature of the predicted annihilation events, that is, whether they occur at high or low energies of the negative proton, depends largely on the magnitudes of g^2 and of g_0^2 if annihilation into neutral mesons or with neutrons is also taken into account from Eqs. (6) to (8). If produced at threshold, the negative proton will have a kinetic energy equal to its rest energy (0.93 Bev). Taking 2 Bev as a typical kinetic energy, the annihilation will have a reasonable chance to occur in flight if the pseudoscalar cross section of 3×10^{-27} cm^2 is correct,[15] but will occur at rest if the scalar value, 10^{-29} cm^2, is nearer the truth.

Many of the annihilations in flight will be indistinguishable from local hard showers in which many mesons and nucleons are involved. There is some possibility, however, that a negative proton entering a nucleus will be annihilated with one of the bound protons *before* making any other collisions and that as a result two relativistic charged mesons will emerge. As a possible means for distinguishing such an event we call attention to the angular distribution of the mesons with respect to the direction of the incident negative proton (forward direction). Since the velocity of the mesons in the CM system, k/E, is greater than the velocity p/E of the CM system with respect to the laboratory system, it is possible to have mesons emitted *backward* in the laboratory. For a negative proton of 2 Bev kinetic energy in the laboratory, about 40 percent of the annihilations yield backward moving mesons in the pseudoscalar case (meson angles of greater than 90° with the incident negative proton direction) compared with 20 percent if the mesons are scalar. In a photographic plate one would see three practically co-planar minimum ionization tracks, two of which would lie in the upper hemisphere. From the observation of a few such events nothing could be concluded, of course, but their frequency might be large enough to overcome the competition afforded by other possible processes.[16]

A slight deviation from coplanarity of the tracks is expected from the "Doppler" effect due to the momentum distribution of the proton bound in the nucleus, but this is found to be less than 5 degrees on the average. The events may also be complicated by the presence of a small evaporation star coming from the excitation of the residual nucleus after the sudden removal of one of its protons. Excitations of ~30 Mev which would be obtained this way would not lead to any sizable stars, however. Finally, the possibility should be added that the mesons produced have an interaction mean free path in the nuclear matter which is small compared to the nuclear radius. It has been argued by Greisen,[17] for example, that there is a large cross section for a meson to produce other mesons in nuclear interactions in spite of the apparently small scattering cross section.[13,14] If this turns out to be correct it will become quite difficult to distinguish annihilations in flight from other events in which several mesons are produced.

The annihilation events that are initiated by very *low* energy negative protons would be much less ambiguous than the events just described. A nuclear process involving 2 Bev would be started by the absorption of a slow heavy charged particle. Two energetic mesons in opposite directions would be expected (or possibly more mesons if their interaction mean free paths are very small). The lifetime, τ, for annihilation in flight at very low energies (considering only annihilation into charged mesons) is given by (4) as $1/\tau=\pi N g^4/4M^2$ where N is the number of protons per unit volume. For an emulsion ($N\approx10^{24}$ cm^{-3}) and $g^2=\frac{1}{4}$, this is 10^{-6} sec.; for $g^2=4$ we find $\frac{1}{2}\times10^{-8}$ sec.[18] In a time of the order 10^{-11} sec., however, the negative proton is slowed down

(pseudoscalar theory), we find a production cross section ~10^{-27} cm^2 at high energies in nucleon-nucleon collisions. This is about 1/20 the cross section for meson production deduced from a nucleon mean free path ~100 g/cm^2 in air. If we assume that the annihilation cross section for negative protons is as large as the meson production cross section and take for the flux of primary protons responsible for the negative proton creation a value ~0.03 proton/cm^2 sec. ster., we estimate that there should be ~10^{-5} annihilation events per cm^3 per sec. in a photographic emulsion at a (total) depth ~50 g/cm^2 below the top of the atmosphere. (This corresponds to 1 in 1000 stars.) With $g^2=4$, however, the pseudoscalar annihilation cross section corresponds to an annihilation mean free path of about 1600 g/cm^2 at 2 Bev and 950 g/cm^2 at 0.5 Bev. While there would thus be some high energy annihilation events, most of the negative protons would annihilate after being brought to rest as a result of energy loss by nuclear collisions and by ionization. The number of annihilations per cm^3 per sec. would depend upon the energy distribution of the negative protons as a function of altitude. This is difficult to estimate but one would guess that after traversing several hundred g/cm^2 of atmosphere (several mean free paths for collision) the negative proton could be stopped by ionization in a convenient absorber.

[16] A similar arrangement of three tracks might be obtained from electron-electron scattering by an upward moving electron (but this is probably distinguishable because of the relatively large multiple scattering of electron tracks in an emulsion even up to a few hundred Mev). Production of one charged meson by a primary proton colliding with a neutron, leaving the nucleus with only a small excitation, will give the appearance of three tracks but there would be no reason to expect these tracks to lie in a single plane. Cases where the angle between each pair of adjacent tracks is greater than 90° may be due to the large angle scattering of a meson by a proton.

[17] K. Greisen, Phys. Rev. **77**, 713 (1950).

[18] If annihilation with a neutron is also taken into account, the lifetime for survival is made somewhat smaller.

from a medium energy (e.g., 5 Mev), passes through the energy zero and is eventually captured in a K orbit around some nucleus. Its lifetime in such an orbit is crudely estimated by taking for N in the above formula the reciprocal volume of a sphere of radius equal to that of the K-shell, multiplied by the number of protons in the nucleus. For carbon, N is about 10^{38} cm^{-3} and the lifetime against annihilation after the negative proton is captured in the K-shell is of the order 10^{-20}–10^{-22} sec. Most of the negative protons reaching low energies would therefore be annihilated after capture in the K-shell, but the general features of the annihilation event as far as the products are concerned, would remain unchanged.

In summary, therefore, we would consider it to be useful to search for high energy annihilation events in material (sensitive emulsions for example) exposed to the cosmic radiation at 50 to 100 g/cm^2 below the top of the atmosphere, and to look for annihilation at rest at several hundred g/cm^2 below the top where the negative protons may be brought to a stop in an absorber.[15]

PHYSICAL REVIEW VOLUME 79, NUMBER 2 JULY 15, 1950

U^{235} Fission Yields in the Rare Earth Region

MARK G. INGHRAM, RICHARD J. HAYDEN, AND DAVID C. HESS
University of Chicago and Argonne National Laboratory, Chicago, Illinois
(Received February 27, 1950)

The U^{235} fission yield curve for uranium fuel rods from mass number 143 to 160 has been measured, utilizing mass spectrometric techniques. Eight percentage yields are assumed in this region, and on the basis of measurements of the neodymium, samarium, europium, and gadolinium fission isotopes, nine other yields are obtained. The resulting yield curve is smooth. Based on the same assumptions which give the smooth yield curve the following cross sections and half-lives are obtained: Cross sections, Sm^{149}, 47,000 barns; Sm^{151}, 7200 barns; Gd^{155}, 41,000 barns; Gd^{157}, 59,500 barns; half-lives, 61^{147}, 2.26 yr.; Sm^{151}, 122 yr.

I. INTRODUCTION

ONE of the problems associated with the fission process is the determination of the fission yield curve for fissionable nuclei at various neutron energies. To date there is no satisfactory explanation of the commonly observed asymmetric fission. On the experimental side a great deal of work has been done in measuring the yields[1] in the fission of U^{235}. Almost all of these yields have been obtained by measuring, with radiochemical methods, the relative number of atoms in the various radioactive chains. To obtain relative yields in this manner the data must be corrected for the half-lives of the isotopes measured and for the relative counter efficiencies for radiations of different energies. In many cases the corrections are difficult or uncertain. An independent and more accurate method has been utilized by Thode and Graham[2] to measure the relative yields of krypton and xenon isotopes in U^{235} fission. They measured the relative abundances of the stable fission products of these elements with a mass spectrometer.

This method is applicable to the entire fission yield curve if necessary corrections are made for neutron absorption in each chain and for long-lived isotopes earlier in that chain. The partial yield curves obtained for various elements can be fitted together by the method of isotopic dilution previously described by the authors.[3] In addition, if the U^{235} depletion is measured, absolute fission yields can be obtained. The mass spectrometer method has been used here to obtain the U^{235} fission yield curve for pile neutrons in the rare earth region. However, because the rare earth samples available to us had been partially depleted of lower atomic number components by resin column extraction, the method of isotopic dilution could not be used to fix the relative positions of the partial curves due to different elements. Thus the yield of one isotope of each element considered was assumed to be consistent with the curve of the previous element. For the first element considered, neodymium, the assumption of absolute yield was made on the basis of chemical data. Thus the relative values obtained, since they depend only on the mass spectrometer measurement, are considerably better than are the absolute values. A further difficulty in the experiment was that certain half-lives and cross sections necessary to deduce the relative yields were not known accurately. Here again certain yields were assumed on the basis of the rest of the curve and the unknown cross sections and half-lives were deduced. Table I gives the final data on fission yields. These data are compared with the fission yields from radio-chemical data in Fig. 1.

[1] Plutonium Project, "Nuclei formed in fission," Rev. Mod. Phys. **18**, 513 (1946).
[2] H. G. Thode and R. L. Graham, Can. J. Research, **A25**, 1 (1947).
[3] Hayden, Reynolds, and Inghram, Phys. Rev. **75**, 1500 (1949).

II. NEODYMIUM

Fission neodymium was obtained from Parker and Lantz of Oak Ridge National Laboratory. It was in a sample of rare earth materials which had been separated from uranium and which had had the lighter rare earths removed by column extraction. The fission product mixture so obtained (neodymium and heavier rare earths) was analyzed by means of a filament source mass spectrometer using techniques previously described.[4] The results of this analysis are given in Table II.

As has been shown by the authors[5] the only appreciable absorber in normal neodymium is Nd^{143} which has an isotopic cross section of 240 barns. Thus the 143-peak here observed was lower, and the 144-peak was higher, than the pure fission yield would predict. The number of atoms of Nd^{143} and Nd^{144} present at time t are

$$N_{143}(t)=\frac{N_u\sigma_u f_{143}\Phi t}{\sigma_{143}\Phi t}[1-\exp(-\sigma_{143}\Phi t)], \quad (1)$$

$$N_{144}(t)=N_u\sigma_u f_{144}\Phi t+\frac{N_u\sigma_u f_{143}\Phi t}{\sigma_{143}\Phi t}\times[\sigma_{143}\Phi t-1+\exp(-\sigma_{143}\Phi t)], \quad (2)$$

where N_u is the number of uranium atoms and σ_u is the fission cross section of uranium. When ratios of the abundance equations are taken these quantities always cancel out. The quantities f are the fractional fission yields, σ_{143} is cross section of Nd^{143} and Φ is the neutron flux. Other yields are given by

$$N_j(t)=N_u\sigma_u f_j\Phi t, \quad j=145, 146, 148, 150. \quad (3)$$

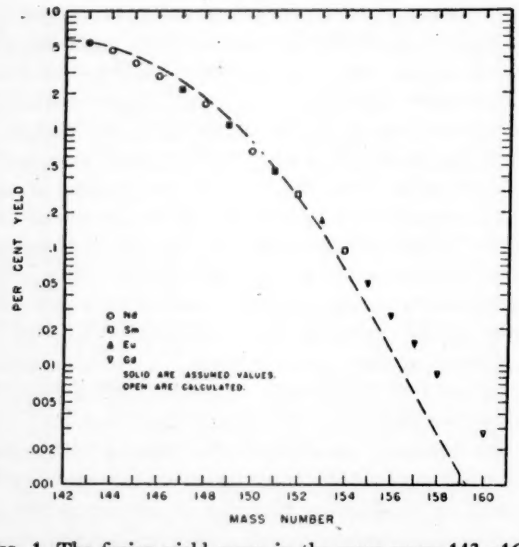

FIG. 1. The fission yield curve in the mass range 143→160 as determined by the mass spectrometer. For comparison the radiochemically determined fission yields (reference 1) are shown as the dashed curve, which is fitted to the data at mass 143.

[4] Inghram, Hayden, and Hess, Phys. Rev. **72**, 967 (1947).
[5] D. C. Hess, Jr. and M. G. Inghram, Phys. Rev. **76**, 300 (1949).

TABLE I. Fission yields in percent (the underlined values are those assumed to be known).

Mass	Nd	Sm	Eu	Gd
143	5.40			
144	4.64			
145	3.62			
146	2.81			
147		2.15		
148	1.64			
149		1.10		
150	0.658			
151		0.445		
152		0.279		
153			0.170	
154		0.0908		
155				0.0500
156				0.0260
157				0.0150
158				0.0084
159				
160				0.0027

From these and the two previous equations the relative values of the fission yields can be obtained, since the $N(t)$'s are proportional to the observed isotopic peak heights. Assuming a value 5.40 for the percentage yield at 143 the values tabulated in Table I and shown in Fig. 1 were obtained. The accuracy of measurement was such that ratios of these values are good to 1 percent.

III. SAMARIUM

The fission samarium and higher rare earths used in this investigation were obtained from Parker and Lantz of the Oak Ridge National Laboratory. The samples consisted of resin column separated heavy rare earths formed from uranium which had been submitted to a flux of 7.45×10^{11} neutrons/cm² sec. for 920 days in the Clinton pile. Three hundred ten days after removal from the pile the lower rare earths (through Pm) were removed from the sample by a resin column extraction. Five hundred five days after removal from the pile the sample was analyzed by a filament source mass spectrometer. The results of this mass analysis are given in Table III.

Several factors complicate the analysis of these data. In the first place the hold-up at mass 147, due to the incomplete decay of Pm^{147} at the time of the column separation, is unknown because of the uncertain half-life[1] of this isotope (2.2 yr. to 4 yr.). Further, although the cross section of Sm^{149} is well known as a function of energy[6] its mean cross section to the neutrons inside a

TABLE II. Fission neodymium, percentage composition.

Mass	143	144	145	146	148	150
Percentage abundance	27.9	25.6	19.3	15.0	8.72	3.51

[6] W. J. Sturm, Phys. Rev. **71**, 757 (1947).

uranium slug in a pile has not been measured. Finally, the cross section of the long-lived Sm^{151} is entirely unknown and its half-life has only been crudely measured.[7]

The equations for the numbers of atoms of the various samarium isotopes are,

$$N_{147}(t_3)=\frac{N_u\sigma_u f_{147}\Phi}{\lambda_{147}^*}[\lambda_{147}^* t_1-\exp[-\lambda_{147}^*(t_2-t_1)]+\exp[-\lambda_{147}^* t_2]], \quad (4)$$

$$N_{149}(t_3)=\frac{N_u\sigma_u f_{149}\Phi}{\sigma_{149}\Phi}[1-\exp[-\sigma_{149}\Phi t_1]], \quad (5)$$

$$N_{150}(t_3)=\frac{N_u\sigma_u f_{149}\Phi}{\sigma_{149}\Phi}[\sigma_{149}\Phi t_1-1+\exp[-\sigma_{149}\Phi t_1]], \quad (6)$$

$$N_{151}(t_3)=\frac{N_u\sigma_u f_{151}\Phi}{\lambda_{151}+\sigma_{151}\Phi}[1-\exp[-(\lambda_{151}+\sigma_{151}\Phi)t_1]]\times\exp[-\lambda_{151}(t_3-t_1)], \quad (7)$$

$$N_{152}(t_3)=N_\mu\sigma_\mu f_{152}t_1+\frac{N_u\sigma_u f_{151}\sigma_{151}\Phi^2}{(\lambda_{151}+\sigma_{151}\Phi)^2}[(\lambda_{151}+\sigma_{151}\Phi)t_1-1+\exp[-(\lambda_{151}+\sigma_{151}\Phi)t_1]], \quad (8)$$

$$N_{154}(t_3)=N_u\sigma_u f_{154}\Phi t_1. \quad (9)$$

In these equations t_1 is the time of neutron irradiation, t_2 is the time from the beginning of neutron irradiation until column separation, t_3 is the time from the beginning of irradiation until isotopic analysis, and λ_{147}^* is the decay constant of Pm^{147}. Division of (5) by (6) yields an equation in σ_{149}, independent of the fission yield, of which a numerical solution then gives for the cross section of Sm^{149}, $\sigma_{149}=47{,}000$ barns. On the basis of the neodymium yield curve, the values 2.15, 1.10, and 0.445 percent are assumed for the yields at 147, 149, and 151 respectively. By combining (4) and (5), λ_{147}^*, and hence the half-life of Pm^{147}, are obtained. Calculation gives $T_{\frac{1}{2}}^{147}=2.26$ years. The assumption is now made that λ_{151} is small relative to $\sigma_{151}\Phi$ and t_3^{-1}. This assumption will later be justified. Then adding (7) and (8) we obtain

$$N_{151}(t_3)+N_{152}(t_3)=N_u\sigma_u\Phi t_1(f_{151}+f_{153}). \quad (10)$$

Division of (10) by (5) yields an equation in f_{152}. Solving this gives $f_{152}=0.279$. Similarly, combining (9) and (10) gives $f_{154}=0.0908$. Solving (7) divided by (9) for σ_{151} gives $\sigma_{151}=7200$ barns. The samarium fission yield data are summarized in Table I and in Fig. 1. The half-life of Sm^{151} cannot be calculated until the europium data are considered.

[7] Inghram, Hayden, and Hess, Phys. Rev. 71, 643 (1947).

TABLE III. Fission samarium, percentage composition.

Mass	147	149	150	151	152	154
Percentage abundance	34.2	12.7	25.2	12.7	12.1	3.11

IV. EUROPIUM

The europium peaks in the first-mentioned fission product sample were also observed. Unfortunately, the amount of fission La^{139} present in the sample, even after column purification, was so large that the mass 155 LaO^+ peak, for which no correction could be made, precluded measurement of the Eu^+ peak at 155. Since europium does not emit appreciably as EuO^+, no measurement of Eu^{155} could be made. Although the Eu^{151} daughter was overlapped by its Sm^{151} parent at the 151 position, utilization of the time fractionation of the emission of these two elements in the manner previously described[3] gave the Eu^{151}/Eu^{153} ratio. Assumption of the fission yield at 153 then allowed the half-life of Sm^{151} to be calculated. The equation which determines λ_{151} is,

$$\frac{N_{151}'(t_3)}{N_{153}'(t_3)}=\frac{f_{151}}{f_{153}}\frac{\lambda_{151}\sigma_{153}'\Phi}{(1-\exp[-\sigma_{153}'\Phi t_1])}\left[\frac{1}{\sigma_{151}'\sigma_{151}\Phi^2}+\frac{\exp[-\sigma_{151}'\Phi t_1]}{\sigma_{151}'(\sigma_{151}'-\sigma_{151})\Phi^2}+\frac{\exp[-\sigma_{151}\Phi t_1]}{\sigma_{151}(\sigma_{151}-\sigma_{151}')\Phi^2}+\frac{(1-\exp[-\sigma_{151}\Phi t_1])(t_3-t_1)}{\sigma_{151}\Phi}\right], \quad (11)$$

where primed quantities refer to isotopes of europium, where unprimed quantities refer to isotopes of samarium, and where, as before, λ_{151} has been assumed small relative to t_3^{-1} and to $\sigma_{151}\Phi$. On the basis of the samarium portion of the yield curve we assume $f_{153}=0.170$. Taking the value of $\sigma_{151}=7200$ barns obtained above, and the values $\sigma_{151}'=5200$ barns and $\sigma_{153}'=240$ barns from previous work,[3] Eq. (11) gives $T_{\frac{1}{2}}^{151}=122$ years. This half-life makes λ_{151} small relative to t_3^{-1} and $\sigma_{151}\Phi$. This new value of $T_{\frac{1}{2}}^{151}$ is certainly more reliable than our previous estimate of 20 years, which was based on photographic darkening.

V. GADOLINIUM

The gadolinium fission products present in the second sample were investigated with the filament source mass spectrometer. The percentage abundances shown in Table IV were obtained.

Owing to the uncertainty in the values of the large cross sections of Gd^{155} and Gd^{157} the fission yields at masses 155, 156, and 157 were assumed. Then the cross sections of Gd^{155} and Gd^{157} and also the fission yields at masses 158 and 160 were computed. The equations used

TABLE IV. Fission gadolinium, percentage abundance.

Mass	155	156	157	158	160
Percentage abundance	26.2	44.8	4.4	22.0	2.5

in the evaluation of these quantities are,

$$N_{155}(t_3)=\lambda_{155}'N_u\sigma_u\Phi f_{155}\Big[\frac{1}{\sigma_{155}\Phi(\lambda_{155}'+\sigma_{155}'\Phi)}+\frac{\exp[-\sigma_{155}\Phi t_1]}{\sigma_{155}\Phi(-\lambda_{155}'-\sigma_{155}'\Phi+\sigma_{155}\Phi)}+\frac{\exp[-(\sigma_{155}'\Phi+\lambda_{155}')t_1]}{(\sigma_{155}'\Phi+\lambda_{155}')(\lambda_{155}'+\sigma_{155}'\Phi-\sigma_{155}\Phi)}\Big]+\frac{N_u\sigma_u f_{155}\Phi}{\lambda_{155}'+\sigma_{155}'\Phi}[1-\exp[-\lambda_{155}'(t_3-t_1)]]\times[1-\exp[-(\lambda_{155}'+\sigma_{155}'\Phi)t_1]], \quad (12)$$

$$N_{156}(t_3)=N_u\sigma_u f_{156}\Phi t+\frac{N_u\sigma_u f_{155}\sigma_{155}'\Phi^2}{(\lambda_{155}'+\sigma_{155}'\Phi)^2}[(\lambda_{155}'+\sigma_{155}'\Phi)t_1-1+\exp[-(\lambda_{155}'+\sigma_{155}'\Phi)t_1]]+N_u\sigma_u f_{155}\sigma_{155}\lambda_{155}'\Phi^2\Big[\frac{t_1}{\sigma_{155}\Phi(\lambda_{155}'+\sigma_{155}'\Phi)}+\frac{1-\exp[-\sigma_{155}\Phi t_1]}{(\sigma_{155}\Phi)^2(\sigma_{156}\Phi-\lambda_{155}'-\sigma_{155}'\Phi)}+\frac{1-\exp[-(\sigma_{155}'\Phi+\lambda_{155}')t_1]}{(\sigma_{155}'\Phi+\lambda_{155}')^2(\lambda_{155}'+\sigma_{155}'\Phi-\sigma_{155}\Phi)}\Big], \quad (13)$$

$$N_{157}(t_3)=\frac{N_u\sigma_u f_{157}\Phi}{\sigma_{157}\Phi}[1-\exp[-\sigma_{157}\Phi t_1]], \quad (14)$$

$$N_{158}(t_3)=N_u\sigma_u f_{158}\Phi t_1+N_u\sigma_u f_{157}\Phi\times\Big[\frac{\sigma_{157}\Phi t_1-1+\exp[-\sigma_{157}\Phi t_1]}{\sigma_{157}\Phi}\Big], \quad (15)$$

$$N_{160}(t_3)=N_u\sigma_u f_{160}\Phi t_1, \quad (16)$$

where primed quantities refer to isotopes of europium, and unprimed quantities refer to isotopes of gadolinium. For the calculation it was assumed that Eu^{155} has a half-life of 1.7 years and a cross section of 7900 barns.[3] Values of f_{155}, f_{156}, and f_{157} of 0.0500, 0.0260, and 0.0150 percent respectively were assumed. Dividing (13) by (12) an equation in σ_{155} was obtained. Numerical solution then gave the value of 41,000 barns for the cross section of Gd^{155}. Then combining (13) and (14) the cross section of Gd^{157} was obtained as 59,500 barns. The variations of these cross sections from those presently accepted are discussed in the conclusion. Finally, (15) and (16) combined with any of the earlier equations give 0.0084 and 0.0027 percent for the fission yields at masses 158 and 160, respectively. These fission yield data are summarized in Table I and in Fig. 1.

VI. CONCLUSIONS AND COMMENTS

Certain of the results here reported differ widely from accepted results, and to a considerably greater extent than would be expected from the uncertainties of measurement or from possible slightly incorrect assumptions for various of the fission yields. The first of these discrepancies is the short half-life obtained for Pm^{147}. Although published values for this half-life vary from 2.2 years to 4 years, a 3.7 year value has been most generally accepted. Another discrepancy is that the cross section of Gd^{157} obtained is considerably lower than the 200,000 barn value reported in the literature.[6,8] We have attempted to explain this result by the assumption that part of the Gd^{157} peak observed is caused by a contamination of the sample with normal gadolinium. However, even if this contamination is assumed to be so large that all the Gd^{160} peak arises from this cause, the effect on the Gd^{157} is not enough to bring its cross section much over 100,000 barns. Thus this explanation of the low cross section appears untenable. Although contamination at the mass 173 position, where the Gd^{157} was measured, due to some other element cannot be entirely ruled out, the low cross section is probably real and due to the high neutron temperature in the uranium. A question might be raised as to the validity of the method of assuming yields to produce a smooth yield curve. In the opinion of the authors this procedure is justified because of the smoothness of the neodymium partial curve and because some simple connection must exist between the yields if the choice of eight yields on a particular smooth curve forces nine other yields to lie on the curve. In conclusion, it should be explicitly pointed out that our fission yields and cross sections are for the neutron energy distribution found in a thick uranium slug. These results would not be expected to be in exact agreement with those obtained by irradiation of thin uranium foils with moderated pile neutrons.

The authors wish to acknowledge their indebtedness to G. W. Parker and P. M. Lantz for the samples used in this investigation and to Professor A. J. Dempster for helpful discussion during the course of the work.

[8] Lapp, Van Horn, and Dempster, Phys. Rev. 71, 745 (1947).

Successive Neutron Capture in Gold*

R. D. HILL AND J. W. MIHELICH
Physics Department, University of Illinois, Urbana, Illinois
(Received March 20, 1950)

Transitions corresponding to 159 and 209 kev have been observed in neutron-activated gold. They have been observed to decay with a half-life of 3.3 days and have been ascribed to Au^{199}, which is formed by a process of successive neutron capture from Au^{197}. The thermal neutron capture cross section of Au^{198} has been estimated to be of the order of 10^4 barns.

THE 2.7-day beta-activity[1] of Au^{198}, produced by neutron capture from the single stable gold isotope Au^{197}, is well known[2] to have a continuous spectrum upper limit at 0.97 Mev and a conversion spectrum[3] from a 0.4112-Mev gamma-ray. Of somewhat disputed existence are two weak gamma-transitions of 0.157 and 0.208 Mev, observed by Levy and Grueling[4] and linked by them with a beta-spectrum having an apparent upper limit at 0.601 Mev. Other evidence in support of these lower energy transitions is reviewed in the paper by Levy and Grueling. However, more recent work by Siegbahn and Hedgran[5] and by Langer[6] indicated that the Au^{198} beta-spectrum was simple and no evidence of the lower energy transitions was found. Peacock and Wilkinson,[7] also, did not observe the transitions in deuteron-bombarded gold, and they believed that in earlier work the lines were due to an impurity of Hg^{197} which has gamma-transitions of 0.170 and 0.230 Mev.

Our experiments with neutron-activated gold were made originally with the aim of calibrating a magnetic beta-ray spectrograph against the 0.411 Mev conversion lines. In the course of these experiments we observed the low energy transition lines. They are difficult to detect, as Levy and Grueling pointed out, situated as they are in the most intense part of the strong continuous spectrum from Au^{198}. As far as photography is concerned, this leads to an optimum exposure of the film for visibility of the lines. Best contrast is also obtained when the source is thin, of the order of 0.2 mg/cm^2 or less. The sources were prepared by evaporation of gold on to thin aluminum backing before neutron bombardment in the pile.

A reproduction of the low energy part of the conversion spectrum, taken with a spectrograph using secondary electrostatic focusing,[8] is shown in Fig. 1. Although only the more intense lines are visible in the reproduction, there are at least fourteen lines visible on the best films. Of these lines, one of 63 kev was found to decay with a half-life of approximately 24 hours, and was attributed to W^{187} which undoubtedly arose as a contaminant from the tungsten heater from which the gold was evaporated in preparation. Two low energy lines of 33 and 35 kev were very weak and their existence was only observed on one exposure. They may arise from a 48 kev transition converted in the L_I, L_{III} sub-shells. The other lines can be ascribed to two transitions: one of 159 kev which is converted in the K, L_I, L_{III}, M and N shells of mercury; the other of 209 kev which shows only one line, presumably the K shell conversion.

Since it was previously claimed[4] that the low energy transitions decayed with a half-life of 2.7 day, we made an effort to determine a significant lifetime. By following the relative decays of the 411 and 159 lines over a period of many weeks, we have observed that the 159 lines decay more slowly than do the 411 lines. Decay plots for the 411-M and 159-L lines (which are of comparable intensity) are shown in Fig. 2. Their decays are consistent with half-lives of 2.7 day and 3.3 day, respectively. A 3.3-day decay is known to be associated with Au^{199} and recently Beach, Peacock and Wilkinson[9] have observed transitions of 24, 51, 70, 156, 207 and 230 kev from Au^{199} produced as a disintegration product from 31-minute Pt^{199}. We therefore assign our 159 and 209 kev transitions in neutron-activated gold to Au^{199}.

We have also observed that the low energy transitions are suppressed by enclosing the gold source in a cadmium box during neutron activation. In order to

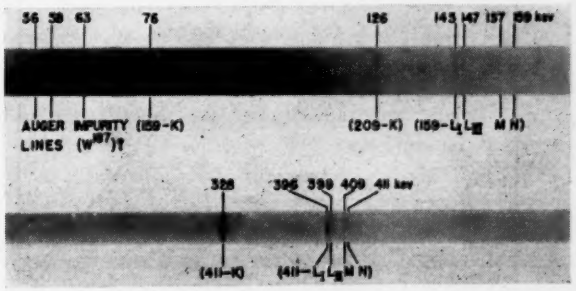

FIG. 1. Conversion electron spectra. Upper spectrum taken with $B=100$ gauss instrument and secondary electrostatic focusing. Lower spectrum taken with $B=200$ gauss instrument.

* This work was supported in part by the joint program of the AEC and the ONR.

[1] E. Fermi *et al.*, Proc. Roy. Soc. **A146**, 483 (1934).
[2] D. Saxon, Phys. Rev. **73**, 811 (1948).
[3] DuMond, Lind, and Watson, Phys. Rev. **73**, 1392 (1948).
[4] P. W. Levy and E. Grueling, Phys. Rev. **75**, 819 (1949).
[5] K. Siegbahn and A. Hedgran, Phys. Rev. **75**, 523 (1949).
[6] L. Langer and H. C. Price, Phys. Rev. **76**, 641 (1949).
[7] C. L. Peacock and R. G. Wilkinson, Phys. Rev. **74**, 297 (1948).
[8] Hill, Mihelich, and Pigott, Rev. Sci. Inst. **21**, 498 (1950).
[9] Beach, Peacock, and Wilkinson, Phys. Rev. **76**, 1585 (1949).

make quantitative measurements of this effect, we obtained two identical sources and had them irradiated under the same conditions, except that one source was enclosed in $\frac{1}{16}$ inch cadmium. It was found that the 159 and 209 kev transition lines were absent, and certainly reduced in intensity by a factor of 10, in the cadmium shielded source; whereas the 411 kev lines were reduced in intensity only by a factor of approximately two. As will be shown later, these results cannot be accounted for by the presence of a platinum impurity in the gold, but can be attributed to the production of Au^{199} through a very large thermal neutron capture cross-section of Au^{198}. The remainder of the discussion will be concerned with obtaining an estimate of this cross section.

The intensity of the 411-K line relative to the 159-K line, for a particular gold source bombarded 8 days in the pile, was determined as 31 to 1, at a time immediately after removal from the pile. This figure does not represent the relative populations of the 411 and 159 kev excited states, but must be corrected for the magnitudes of the conversions. Although the latter have not been directly determined, we may obtain some idea of them from the conversion line intensities within a particular transition group. The experimental observations of these intensities are given in Table I.

The value of $N_K/N_L=2.1$ for the 411 transition is in reasonable agreement with Siegbahn and Hedgran's[5] value of 3. The theoretical value of N_K/N_L for a 2^2-electric transition of 411 kev in mercury is 3.8 and the K-conversion coefficient is 0.033. Siegbahn and Hedgran[5] obtain $\alpha_K=0.031$, Peacock and Wilkinson[7] a value $\alpha_K=0.025$ and Plesset[10] a value $\alpha_K=0.04$.

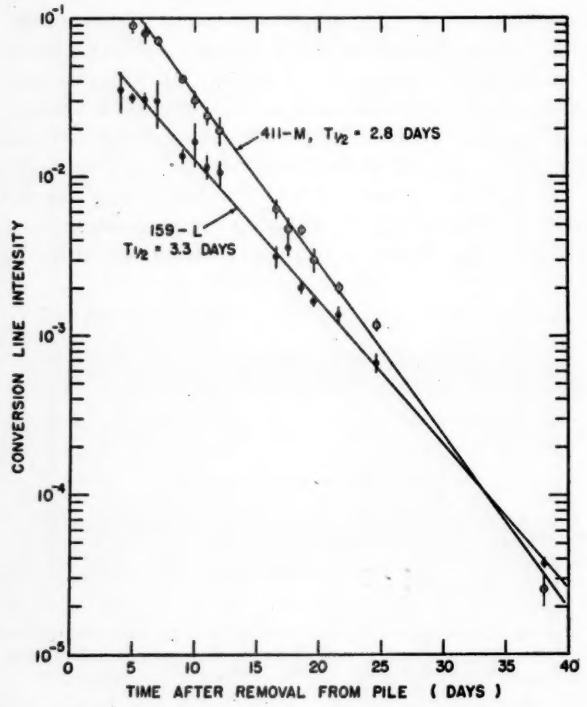

FIG. 2. Decay of conversion lines from neutron-activated gold.

TABLE I. Relative intensities of conversion lines.

Conversion line	411-K	411-L_I	411-L_{III}	411-M	411-N
Relative intensity	1.0	0.335	0.135	0.099	0.026
Conversion line	159-K	159-L_I	159-L_{III}	209-K	
Relative intensity	1.0	0.685	0.43	0.65	

The value of $N_K/N_L=0.87$ for the 159 transition agrees excellently with one of 0.8 obtainable from the Au^{199} spectrum published by Beach, Peacock, and Wilkinson.[9] The theoretical values of N_K/N_L lying closest to the experimental ones are: 0.5 for electric 2^3, 2 for electric 2^2 and 3 for magnetic 2^3 transitions. Thus, if electric 2^3 is the most probable assignment for the 159 transition, the theoretical K-conversion coefficient $\alpha_K=0.8$.

Thus a very tentative estimate of the 411 to 159 gamma-ray intensity ratio is

$$(N\gamma)_{411}/(N\gamma)_{159}=750.$$

Then, if we assume with Beach, Peacock, and Wilkinson[9] that the 159 kev transition occurs in 30 percent of the Au^{199} decays, and also that the 411 kev transition occurs in 100 percent of the Au^{198} decays, the population ratio of Au^{198} to Au^{199} is

$$(Au^{198})/(Au^{199})=95.$$

It is now clear that the Au^{199} cannot be produced from a Pt^{198} impurity in the gold sample. The isotopic thermal capture cross section of Pt^{198} for the formation of 31-minute Pt^{199} is known[11] to be 25 times less than that of Au^{197} for the formation of 2.7-day Au^{198}. Thus an isotopic impurity of 25/95, or approximately 26 percent, of Pt^{198} in Au^{197} would be required to produce the observed ratio of Au^{199} to Au^{198}. Since Pt^{198} is present only to the extent 7.2 percent in ordinary platinum that is clearly impossible; moreover chemical analysis of the gold showed no platinum present to within 10 parts in 10^6. This conclusion is also supported by the fact[12] that cadmium shielding reduces the 31-minute Pt^{199} activity to 75 percent, whereas our experiments indicated that the 159 and 209 kev transitions were certainly reduced to less than 10 percent, of their unshielded intensities.

The most likely process for the production of Au^{199} in neutron-irradiated gold is by neutron capture in radioactive Au^{198}. If we consider the following successive reactions:

$$Au^{197}+n=Au^{198}\xrightarrow{\beta^-}Hg^{198}+\gamma(411\text{ kev})$$

$$Au^{198}+n=Au^{199}\xrightarrow{\beta^-}Hg^{199}+\gamma(159,\ 209\text{ kev}),$$

[10] E. H. Plesset, Phys. Rev. **62**, 181 (1942).
[11] Seren, Friedlander and Turkel, Phys. Rev. **72**, 888 (1947).
[12] A. W. Sunyar and M. Goldhaber, Phys. Rev. **76**, 189 (1949).

the relative populations of Au^{198} and Au^{199}, immediately after activation for a time T, are:

$$\frac{(Au^{199})}{(Au^{198})}=\frac{F\sigma}{\lambda_2-\lambda_1}\left\{1-\frac{\lambda_1(1-\exp-\lambda_2 T)}{\lambda_2(1-\exp-\lambda_1 T)}\right\},$$

where F is the activating neutron flux, σ is the total capture cross section of Au^{198}, and λ_1 and λ_2 are the decay constants of Au^{198} and Au^{199}, respectively. For a thermal flux of 10^{12} neutrons cm^2-sec., σ is evaluated to be about 3.5×10^4 barns.

It is well known that the $Au^{197}(n,\gamma)Au^{198}$ reaction has been used[13] to produce Hg^{198} in centigram amounts for use in discharge tubes as a source of light. Bradt and Mohler[14] found mass-spectrographically that one particular sample contained 0.16 percent of Hg^{199}, which they noted may well have come from a secondary nuclear reaction. Kessler[15] has also found the presence of forbidden Hg^{199} lines in the spectrum of mercury obtained from the neutron bombardment of gold. The amounts of Hg^{199} contaminant in the two samples prepared in this way were stated to be 3.6 and 0.3 percent respectively. Since the anticipated Hg^{199}/Hg^{198} ratio in a successive reaction process is $F\sigma/\lambda_1$, our values of σ and F would lead to a 1.2 percent Hg^{199} contaminant. It seems probable that the variation of Hg^{199} yield is due to different values of F, and thus the purest Hg^{198} can be obtained by using the lowest admissible neutron flux.

The gold sources were prepared at the Argonne National Laboratory, Chicago, Illinois. We wish to acknowledge our indebtedness to Dr. C. O. Muehlhouse for arranging for the source preparation, and to Dr. M. Goldhaber for helpful criticism of this work.

[13] J. H. Wiens and L. W. Alvarez, Phys. Rev. **58**, 11, 1005 (1940); **65**, 58 (1944).
[14] P. Bradt and F. L. Mohler, Phys. Rev. **73**, 925 (1948).
[15] K. G. Kessler, Phys. Rev. **77**, 559 (1950).

PHYSICAL REVIEW VOLUME 79, NUMBER 2 JULY 15, 1950

Neutron Capture Gamma-Ray Multiplicity

C. O. MUEHLHAUSE
Argonne National Laboratory, Chicago, Illinois
(Received March 31, 1950)

The average number of γ-rays, $\bar{\nu}_\gamma$, per neutron capture has been measured for about thirty isotopes. Correlations of $\bar{\nu}_\gamma$ with atomic weight and nuclear type are presented.

I. INTRODUCTION

WHEN a nucleus of atomic weight A absorbs a neutron, a compound nucleus of atomic weight $A+1$ is formed in a highly excited state (6 to 9 Mev). This excess energy may be released in the form of cascade γ-rays[1,2] involving many[3,4] levels of the compound nucleus. In any particular cascade process only a few of the total number of available levels are excited. Unless one or more of these levels is metastable, the total decay time is $\sim10^{-13}$ sec. The many levels immediately below the capture state (i.e., for ~1 Mev) are most likely not involved in the cascade process, since the probability for γ-ray emission is proportional to $E^{2(l-1)}$ (E is the transition energy, and l is the transition angular momentum change). This leaves a total number of levels, L, between which γ-ray transitions have a significant cascade probability. Also the number of γ-rays, ν_γ for any given capture process is such that $1\leq\nu_\gamma\leq L$. For example, let us take an oversimplified view of this process. If one allows all transitions from any given energy state to all lower energy states to have the same probability, then $\bar{\nu}_\gamma{}^2\simeq L$. Here $\bar{\nu}_\gamma$ is the average number of γ-rays per capture.

It is the purpose of this paper to present measurements of $\bar{\nu}_\gamma$ for various nuclei and to attempt to reveal the dependence of $\bar{\nu}_\gamma$ on atomic weight and nuclear type.

II. METHOD

Measurements of $\bar{\nu}_\gamma$ can be made in a number of ways. For example, with one γ-ray counter, a collimated neutron beam of flux, f, and n atoms/cm^2 of absorption cross section, σ_a, in the neutron beam, a γ-ray counting rate, s, results which is given by:

$$s=\epsilon f n\sigma_a a\bar{\nu}_\gamma.$$

Here ϵ is the over-all counting efficiency and a is the area of the neutron beam. Determination of $\bar{\nu}_\gamma$ by this method, however, depends on a knowledge of σ_a and f.

It is preferable to employ a method which is independent of uncertain nuclear data and difficult flux measurements. If two γ-ray counters in coincidence are used and both single, s, and coincidence, c, counting rates are recorded, then:

$$s_1=\epsilon_1 f n\sigma_a a\bar{\nu}_\gamma,\quad s_2=\epsilon_2 f n\sigma_a a\bar{\nu}_\gamma,$$

and

$$c=\epsilon_1\epsilon_2 f n\sigma_a a\bar{\nu}_\gamma(\bar{\nu}_\gamma-1).$$

[1] Amaldi *et al.*, Proc. Roy. Soc. (A)**149**, 522 (1935).
[2] J. Griffiths and L. Szilard, Nature **139**, 323 (1937).
[3] B. Hamermesh, Phys. Rev. **76**, 182A (1949).
[4] Kinsey, Bartholomew, and Walker, Phys. Rev. **77**, 723 (1950).

Therefore:

$$c/\bar{s}=[2\epsilon_1\epsilon_2(\bar{\nu}_\gamma-1)]/(\epsilon_1+\epsilon_2).$$

The ratio of the coincidence to the average single counting rate is proportional to $\bar{\nu}_\gamma-1$. Such a measurement is independent of cross section and of neutron flux. Furthermore, since at least one γ-ray is always emitted in every cascade event, this minimum of one γ-ray is, in effect, deducted from the average number, $\bar{\nu}_\gamma$. The measurement is more sensitive to the value of $\bar{\nu}_\gamma$.

One can, of course, continue along these lines and employ three or more counters in higher order coincidences. With three counters, the ratio of threefold to twofold coincidences is proportional to $\bar{\nu}_\gamma-2$. Such a measurement is most sensitive to the value of $\bar{\nu}_\gamma$ in the case of a material which emits a minimum of two γ-rays in *each* cascade process.

The method employed in this work is that of making simple twofold coincidence measurements; i.e., one step beyond the zero-order measurement which depends on nuclear constants.

It should be remarked in passing that this method can be used to measure neutron absorption cross sections.[2] $\bar{\nu}_\gamma(1)$ and $\bar{\nu}_\gamma(2)$ are first measured for substances (1) and (2) respectively. If substance (1) has a known cross section, $\sigma(1)$, the unknown cross section, $\sigma(2)$ of substance (2) can be determined via the single counting rates $\bar{s}(1)$ and $\bar{s}(2)$:

$$\sigma(2)=\sigma(1)[\bar{s}(2)/\bar{s}(1)]\cdot[\bar{\nu}_\gamma(1)/\bar{\nu}_\gamma(2)].$$

III. APPARATUS

A collimated beam of neutrons from the Argonne heavy water reactor passes between two γ-ray scintillation counters in coincidence and through a thin neutron absorbing foil as shown in Fig. 1. Coincidence, c, and single, s_1 and s_2, counting rates from the capture γ-ray bursts are recorded. Anthracene crystals having about 6 percent detection efficiency are cemented to each of the 5819 photo-multiplier tube windows. The counters are partially shielded by bismuth from pile γ-rays, and operate at room temperature with a one-electron sensitivity. The mixer circuit is of a simple pulse addition type and has a resolving time of 0.15μsec.

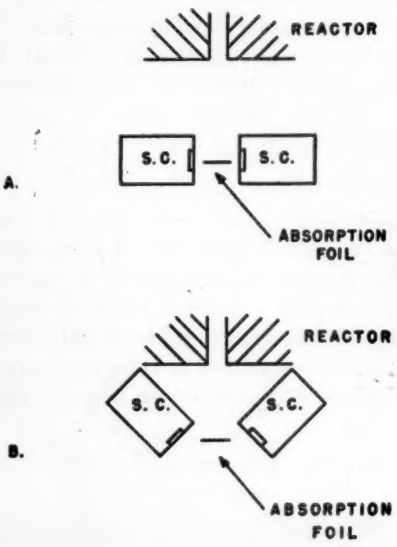

FIG. 1. Schematic diagram of counter and foil arrangement for measurement of capture γ-ray coincidences. (A) 180° apart. (B) 90° apart.

IV. COUNTING TECHNIQUE

Measurements were taken for two different counter positions as illustrated in A and B of Fig. 1. This was done to indicate possible γ-ray angular correlations.

Foils were of such a thickness that γ-ray source strengths of $\sim 10^4$/sec. resulted. The natural backgrounds of the counters were negligible. Other sources of background which were significant were as follows:

(a) pile γ-rays independent of pile power,
(b) pile γ-rays proportional to pile power,
(c) capture γ-rays from scattered neutrons,
(d) fortuitous coincidences resulting from single γ-ray scattering,
(e) chance coincidences.

Expressions for the single and coincidence background counting rates contained terms proportional to time, monitor counts, and the scattering cross section of the material being studied. In addition, the coincidence background contained terms proportional to the average single counting rates (scattering) and the product of the single counting rates (chance). Single background counting rates ranged from 5 to 50 percent of the total effect. Calibration was effected with active 5-yr. Co^{60} ($\nu_\gamma=2$) and active 12.8-hr. Na^{24} ($\nu_\gamma=2$). Foils of these materials having the same area as the neutron beam were placed between the counters with the pile inoperative. The net ratio, $c/\bar{s}$, of coincidence to average single counting rate was measured, and "k" in the following expression was determined:

$$c/\bar{s}=k(\bar{\nu}_\gamma-1)=k \text{ for } \nu_\gamma=2.$$

Though the average γ-ray energy, $\bar{E}_\gamma$, is different for Co^{60} (1.2 Mev) and Na^{24} (2.1 Mev), the same value of k ($\sim$0.002) was obtained for each. This was fortunate since it indicated that the counters had approximately constant sensitivity in the energy range from 1 Mev to 2 Mev. As will be shown later $\bar{\nu}_\gamma\sim 3$ to 4 for most substances, and this gives $\bar{E}_\gamma\sim 1.5$ to 2.5 Mev. That is, most capture γ-rays fall in or near the energy range over which the counters have nearly constant sensitivity.

In all cases measurements were made with either thermal plus resonance neutrons (i.e., open pile beam) or resonance neutrons only (cadmium and boron filtered pile beam). This was done to investigate a possible dependence of $\bar{\nu}_\gamma$ on neutron energy.

In several instances a short-lived activity was induced in the sample by the neutron bombardment. Measurements were made after equilibrium had been reached. To illustrate how this situation was analyzed consider the case of $V^{51}+n\rightarrow V^{52}$ (3.7 min. β^- with one γ-ray). The extra delayed γ-ray could not coincide with the capture γ-rays thereby making the ratio $c/\bar{s}$

too small. That is:

$$(c/\bar{s})\cdot(\bar{\nu}_\gamma+1)/\bar{\nu}_\gamma=k(\bar{\nu}_\gamma-1)$$

from which one can solve for the proper value of $\bar{\nu}_\gamma$. Dividing $\bar{s}$ by $\bar{\nu}_\gamma+1$ yielded the single counting rate per γ-ray. This figure was checked by turning the pile off and allowing the 3.7-min. γ-ray activity to decay. The total single γ-ray counts were recorded and the single counting rate per γ-ray was again computed. The two figures agreed to within 1 percent.

V. RESULTS

Results on the measurements of $\bar{\nu}_\gamma$ for twenty-seven isotope sets are given in Table I. Several important features should be noted:

(a) $\bar{\nu}_\gamma$ increases on the average with increasing atomic weight. This is to be expected for approximately constant binding energy and increasing level density.

(b) In the light element region, $\bar{\nu}_\gamma$ is approximately the same ($\sim$2.5) for odd Z-even N and even Z-odd N nuclei. In this same region, $\bar{\nu}_\gamma$ is less ($\sim$1.7) for even Z-even N nuclei. This observation is in agreement with the fact that neutron resonance levels are much more widely separated in the compound nucleus resulting from even Z-even N neutron capture than in compound nuclei resulting from odd Z or odd N neutron capture.[5]

(c) $\bar{\nu}_\gamma$ is low for a closed shell nucleus[6] (such as La^{139} with 82 neutrons). This observation is in agreement with the fact that the neutron level spacing of compound nuclei resulting from closed shell nuclear neutron capture is large.[5]

(d) The isotope with the largest value of $\bar{\nu}_\gamma$($_{62}Sm^{149}$ for which $\bar{\nu}_\gamma=5.6$) is of the even Z-odd N type. It has one and a half more γ-rays than the isotope ($_{48}Cd^{113}$ for which also Z is even and N is odd) having the next largest number of γ-rays.

Other important observations made in this work are as follows:

(e) No angular γ-ray correlations were observed. That is $\bar{\nu}_\gamma$ (position A)$=\bar{\nu}_\gamma$ (position B). This result is not surprising since a typical value of $\bar{\nu}_\gamma$ is $\sim$3. This implies about 10 important levels (i.e., $\bar{\nu}_\gamma^2$) leading to many different modes of cascade. Such a complex decay scheme is likely to average all individual correlations to about zero.

(*f*) $\bar{\nu}_\gamma$ measured with and without cadmium plus boron filtering (see conclusion of Section IV) was observed to be equal for the three cases studied. These were $_{25}Mn^{55}$, $_{33}As^{75}$, and $_{79}Au^{197}$. With some uncertainty in the case of manganese, the thermal absorption cross section can be calculated from the resonance parameters of the principal resonance level[7] at 345 ev. However, one might suspect that the thermal absorption cross section is compounded of a different proportion of spin states ($J=2$ or 3) than is the resonance absorption cross section (principally $J=3$). This, in turn, might lead to different $\bar{\nu}_\gamma$ values for thermal and resonance absorption. In the case of gold no such difference in $\bar{\nu}_\gamma$ is to be expected, since the principal resonance level[8] at 4.8 ev does yield the proper thermal absorption cross section. That is, thermal energies lie in the wing of the 4.8 ev state. In none of the three cases was $\bar{\nu}_\gamma$ found to depend on neutron energy. Doubtless neutron absorption at energies of around 1 Mev would result in a different value of $\bar{\nu}_\gamma$ from that at thermal or at low energy resonance absorption, since an extra 1 Mev is carried into the nucleus.

TABLE I. Values of $\bar{\nu}_\gamma$.

Nuclear types (odd, even) →(odd, odd)		(even, odd) →(even, even)		(even, even) →(even, odd)		Comment
$_{11}Na^{23}$	<2	——		——		——
$_{13}Al^{27}$	~2	——		——		——
$_{17}Cl^{35}$	3.1	——		——		for KCl
$_{23}V^{51}$	2.5	——		——		——
——		$_{24}Cr^{53}$	2.3	$_{24}Cr$	<2	——
$_{25}Mn^{55}$	2.6	——		——		therm. and res.
——		——		$_{26}Fe$	1.7	——
$_{29}Cu$	2.6	——		——		——
——		$_{32}Ge^{73}$	~4	$_{32}Ge$	2.0	73 impure?
$_{33}As^{75}$	2.7	——		——		therm. and res.
$_{35}Br$	3.4	——		——		large res. abs.
$_{41}Cb^{93}$	2.6	——		——		——
$_{47}Ag$	2.9	——		——		——
——		$_{48}Cd^{113}$	4.1	——		——
$_{49}In^{115}$	3.3	——		——		——
$_{57}La^{139}$	2.7	——		——		82 neutrons
——		$_{62}Sm^{149}$	5.6	——		maximum
$_{63}Eu$	3.8	——		——		——
——		$_{64}Gd$	3.9	——		——
——		——		$_{66}Dy^{164}$	3.7	——
——		——		$_{72}Hf$	3.8	even-N abs.
$_{75}Re$	3.2	——		——		——
$_{77}Ir$	3.6	——		——		——
$_{79}Au$	3.5	——		——		therm. and res.
——		$_{80}Hg$	3.3	——		——

The author is indebted to Mr. R. Swank for both the construction of the electronic equipment and for the production of the anthracene crystals used in this work.

[5] Harris, Muehlhause, and Thomas, Phys. Rev. **79**, 11 (1950).
[6] M. Mayer, Phys. Rev. **75**, 1969 (1949).
[7] High speed Argonne resonance region time-of-flight data by W. Selove.
[8] Havens, Wu, Rainwater, and Meaker, Phys. Rev. **71**, 165 (1947).

Half-Life of Pa^{232} *

ARTHUR H. JAFFEY AND EARL K. HYDE†
Argonne National Laboratory, Chicago, Illinois
(Received April 10, 1950)

The half-life of Pa^{232} from two methods of preparation ($Pa^{231}+n$, and $Th^{232}+d$) has been measured and found to be 1.32 days.

I. INTRODUCTION

THE half-life[1] of Pa^{232} has been measured on samples of Pa^{232} prepared by two different reactions: (1) by $Th^{232}(d,2n)Pa^{232}$ and (2) by $Pa^{231}(n,\gamma)Pa^{232}$. The half-lives were determined only incidentally in the course of other experiments and are of but limited accuracy. However, they are being reported here because values of greater accuracy have not as yet been published.

Both samples of Pa^{232} had long-lived contaminants, whose activities had to be subtracted in order to get the desired half-life. In the bombardment of Th^{232}, Pa^{233} was also formed by the reaction

$$Th^{232}(d,p)Th^{233} \xrightarrow{\beta^-} Pa^{233} \quad \text{and} \quad Th^{232}(d,n)Pa^{233}.$$

Although the 17-day beta-emitter[2] Pa^{230} was also formed by the reaction $Th^{232}(d,4n)$, its concentration was much lower than that of the Pa^{233}, because of the relatively low energy of the deuteron beam (about 19 Mev). Its activity, therefore, had no measurable effect on the tail of the decay curve. The long-lived activity in the Pa^{232} formed by the $Pa^{231}(n,\gamma)$ reaction was due to the Pa^{231} itself. Because Pa^{231} has several alpha-particles with energies differing by several hundred kev,[3] the differences in energy are released in the form of gamma-rays, which are partially converted. Thus, Pa^{231} gives a rather sizeable amount of Geiger activity.

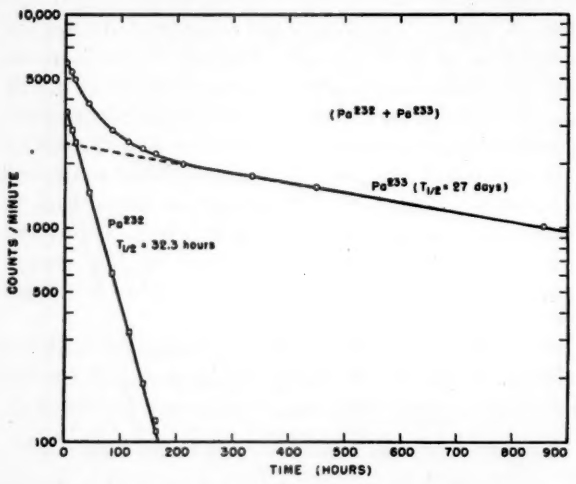

FIG. 1. Decay curve of Pa^{232} prepared from $Th^{232}+d$.

II. EXPERIMENTAL

In the first experiment, thorium metal was bombarded with approximately 100μa hr. of 19-Mev deuterons in the 60-in. cyclotron at Berkeley. The protactinium was isolated from the thorium and from the fission products and other interfering activities by a multiple stage solvent extraction procedure based on the work by Hyde and Wolf[4] This method employed diisopropyl ketone to extract the protactinium from an aqueous phase. The decay of samples taken at the end of this procedure and at the end of two repetitions of it was followed with a mica-window G-M counter supported in a standard shelf arrangement.[5]

TABLE I. Half-life values from Pa^{232} formed by $Th^{232}(d,2n)$.

Number of purification cycles involving diisopropyl ketone extraction	Half-life values for various samples	Relative precision[a] of decay curve	Average value for half-life
	32.0 hr.	Good	
1	31.5	Fair	32.4±0.5
	33.3	Good	
	32.3	Good	
	32.3	Good	
2	33.4	Fair	32.4±0.3
	32.3	Good	
	32.0	Fair	
3	31.8	Good	31.8
			32.3±0.4[b]

[a] Represents the closeness of fit of the points to the decay curve. Curves labeled "Good" are arbitrarily given twice the weight of those labeled "Fair."
[b] Direct average taken for all the decay curves without regard to purification cycles.

* This paper, which will appear as Paper No. 9.20 of the National Nuclear Energy Series, Division IV, Vol. 17B, is based on work done in 1945.

† Present address: Radiation Laboratory, University of California.

[1] J. W. Gofman and G. T. Seaborg, "Production and properties of U^{232} and Pa^{232}," Paper No. 19.14, *The Transuranium Elements* (McGraw-Hill Book Company, Inc., New York, 1949), National Nuclear Energy Series, Division IV, Vol. 14B.

[2] M. H. Studier and E. K. Hyde, Phys. Rev. **74**, 591 (1948).

[3] Tsien San-Tsiang, Bachelet, and Boulssieres, Phys. Rev. **69**, 39 (1946). Clark, Spencer-Palmer, and Woodward, "Alpha-ray analysis of uranium isotopes," British Report 522 (October 10, 1944). S. Rosenblum and E. Cotton, Comptes Rendus **226**, 171 (1948). G. T. Seaborg and I. Perlman, Rev. Mod. Phys. **20**, 585 (1948).

[4] K. Hyde and M. J. Wolf, Paper No. 3.12, National Nuclear Energy Series, Division IV, Vol. 17B, Argonne National Laboratory Report CB-3810 (April 30, 1947).

[5] Jaffey, Kohman, and Crawford, "A manual on the measurement of radioactivity," Report M-CC-1602 (January, 1944), declassified as MDDC-388.

The second experiment involved the bombardment of Pa^{231} with neutrons in the center of the Argonne heavy-water pile, in order to determine the $Pa^{231}(n,\gamma)$ cross section.[6] In this case, the cross section was so large that the amount of extraneous activity due to the slight fission of Pa^{231} was considered negligible and no purification was carried out. Aliquots were prepared and the decay followed with a mica-window G-M counter. Toward the end of the decay of the Pa^{232}, the G-M tube started to fail and the decay curve was continued with a new mica-window G-M tube. It was possible to count the samples on both tubes several times before the first tube finally failed. The ratio of these counts was used to correct the data subsequently taken with the second tube. The tails of the decay curves consist of data taken with the second tube corrected to what they presumably would have been had the first tube been used. This procedure may have been slightly in error, due to the difference in window thickness (3.4 and 2.7 mg/cm², respectively) and other possible differences. However, since the Pa^{231} contributed only a small fraction of the initial count, a slight error in the measurement of its Geiger activity would hardly affect the half-life determination.

Because of their high initial disintegration rate, the samples were at first counted on the second shelf of the standard G-M tube support,[5] and later, as they decayed further, they were counted on the first shelf. The second-shelf counts were normalized to the first shelf by taking several ratios between the counts at the first- and second-shelf positions at times when the counting rates were suitable.

In both experiments, the resolution losses were corrected for, the split-pair technique described by Kohman[7] being used to evaluate the properties of the G-M tubes. The G-M tubes used were the brass-walled, mica-window type described elsewhere,[5] which were quenched by Neher-Harper circuits. These were used with the Cyclotron Specialties scaler.[8]

III. RESULTS

For the Pa^{232} samples coming from the thorium plus deuteron bombardment, the half-life values determined were somewhat less precise than those determined from the decay of pile-produced Pa^{232}, i.e., the deviation of the points from the straight line was greater. Table I shows the half-life values for various samples, while Fig. 1 shows the decay of a typical sample.

There is no evidence that more than one purification cycle was necessary for isolating the protactinium fraction.

For the samples of Pa^{232} formed by $Pa^{231}(n,\gamma)$, Table II shows the half-life values for various samples and Fig. 2 shows the decay of a typical sample.

The deviations shown in Tables I and II represent the mean deviation of the individual values from the average. The two values for the half-life are 32.3±0.4 hr. (from $Th^{232}+d$) and 31.2±0.2 hr. (from $Pa^{231}+n$). Although the data in Table II are the more precise, both half-life values are averaged, since there is the possibility of consistent errors in either measurement.

We may take the half-life from these experiments to be 31.7 hr. or 1.32 days.

TABLE II. Half-life values from Pa^{232} formed by $Pa^{231}(n,\gamma)$.

Half-life values for various samples	Average
31.4	
31.3	
31.3	
30.8	
31.3	31.2±0.2 hr.

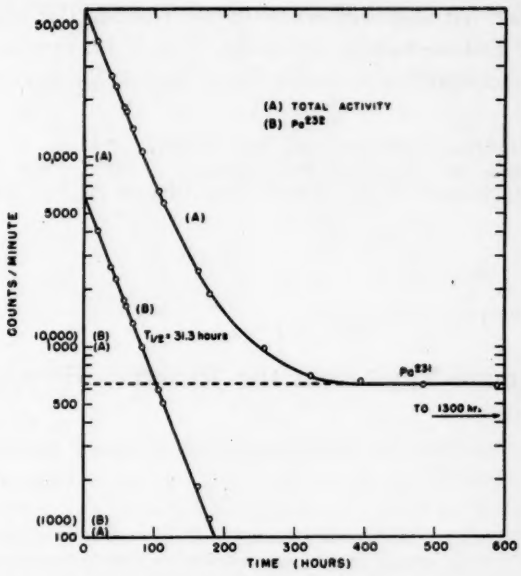

FIG. 2. Decay curve of Pa^{232} prepared from $Pa^{231}(n,\gamma)$.

IV. RESULTS OF OTHER EXPERIMENTS

Pa^{232} was first reported by Gofman and Seaborg to be 1.6 days. Their Pa^{232} was formed[1] by deuteron bombardment of Th^{232} in the Berkeley cyclotron, and was purified by two complete cycles, each cycle involving precipitation with zirconium phosphate, solution in HF and low temperature precipitation with zirconium hydroxide. The protactinium was finally electrolyzed onto a copper cathode. The longer half-life found in this experiment may have been due to incomplete separation from fission products or activities formed from impurities in the thorium. It has been found in this laboratory that purification with diisopropyl ketone is more effective in purifying protactinium from such radioactive impurities than is precipitation with zirconium carriers.

[6] A. H. Jaffey and Q. Van Winkle, "Radiations of Pa^{232}," Argonne National Laboratory Report ANL-4193 (1948) and "Thermal neutron capture cross section of Pa^{231}," Argonne National Laboratory Report ANL-4283 (1948), National Nuclear Energy Series, Division IV, Vol. 17B.

[7] T. P. Kohman, "A general method for determining coincidence corrections of counting instruments," Paper No. 22.50, National Nuclear Energy Series, Division IV, Vol. 14B.

[8] Cyclotron Specialties Company, Morago, California.

Pa^{232} has also been made[9] by the reaction $Pa^{231}(d,p)Pa^{232}$ and the half-life was found to be 33 hr. In view of the fact that this determination of the half-life was complicated by the presence of considerable amounts of the two long-lived impurities Pa^{230} (17 days) and Pa^{231}, the agreement with the measurements presented here is quite satisfactory.

The advice and assistance of W. M. Manning and G. T. Seaborg under whose general supervision this work was done are gratefully acknowledged.

[9] Osborne, Thompson, and Van Winkle, "Products of the deuteron and helium-ion bombardments of Pa^{231}," Paper No. 19.11, National Nuclear Energy Series, Division IV, Vol. 14B.

PHYSICAL REVIEW VOLUME 79, NUMBER 2 JULY 15, 1950

Gamma-Rays from the Reaction $H^1(n,\gamma)D^2$ and the Binding Energy of the Deuteron

R. E. BELL AND L. G. ELLIOTT
Atomic Energy Project, National Research Council of Canada, Chalk River, Ontario, Canada
(Received March 20, 1950)

The binding energy of the deuteron has been determined directly as 2.230±0.007 Mev by measuring the energy of the gamma-radiation from the reaction $H^1(n,\gamma)D^2$. The energy of this gamma-radiation was compared with that of the 2.615-Mev gamma-ray of ThC″ by a spectrometer study of the photo-electrons ejected from a thin uranium radiator. The probable error of 0.007 Mev includes a probable error of 0.004 Mev in the energy of the ThC″ gamma-ray.

I. INTRODUCTION

THE present paper describes a direct determination of the binding energy of the deuteron, BE(D), by measuring the energy of the gamma-radiation from the reaction $H^1(n,\gamma)D^2$ in a beta-ray spectrometer. A preliminary value of BE(D) measured in this way has been published previously.[1]

The experiments designed to measure BE(D) directly may be classified as follows: (a) photo-disintegration of the deuteron and measurement either of the energy of the emitted particles, or of the gamma-ray threshold energy for photo-disintegration; (b) synthesis of the deuteron by the reaction $H^1(n,\gamma)D^2$ and measurement of the energy of the gamma-radiation emitted at the instant of neutron capture. Many measurements have been made by method (a) and all have given values consistent with an average value of 2.187±0.011 Mev, as is given in a review by Stephens.[2] The probable error quoted for this average is low, but each of the individual experiments contains uncertainties such as an imperfect knowledge of the proton range-energy and ionization-energy relations, or an imperfect voltage calibration of high voltage generators. Method (b) is very direct but has not been used in the past for an accurate determination because of the lack of a sufficiently intense neutron source. The early attempts[3] to measure the energy of the neutron-proton recombination gamma-radiation used absorption methods and merely succeeded in showing that the energy was of the expected order of magnitude. In the present work the energy of this gamma-radiation was compared with that of the 2.615-Mev gamma-ray of ThC″ by a spectrometer study of the photo-electrons ejected from a thin uranium radiator. The result for BE(D) obtained in this experiment, 2.230±0.007 Mev, is much higher than the previously accepted value.

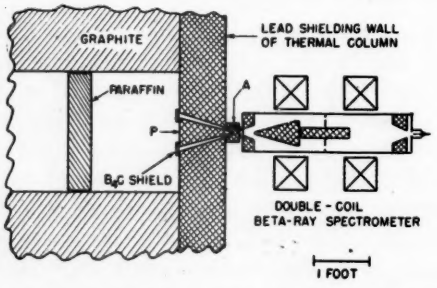

FIG. 1. Schematic diagram of the experimental arrangement used in run 1. The graphite thermal column extends to the left beyond the diagram to the reacting core of the pile.

II. EXPERIMENTAL PROCEDURE

The gamma-radiation from the reaction $H^1(n,\gamma)D^2$ was produced in paraffin irradiated with thermal neutrons. The energy of the gamma-radiation from the paraffin was measured in a beta-ray spectrometer by comparing the momenta of the photo-electrons ejected from a thin uranium radiator by this radiation and those ejected by the 2.615-Mev gamma-ray of ThC″. The ThC″ gamma-ray was chosen as a standard since its energy has been well studied and is close to that of the paraffin gamma-radiation. Two separate determinations (referred to hereafter as run 1 and run 2) were made using two slightly different experimental arrangements. In a third experiment the paraffin

[1] R. E. Bell and L. G. Elliott, Phys. Rev. **74**, 1552 (1948).
[2] W. E. Stephens, Rev. Mod. Phys. **19**, 19 (1947).
[3] R. Fleischmann, Zeits. f. Physik **103**, 113 (1936); Kikuchi, Aoki, and Husimi, Nature **137**, 186 (1936).

gamma-radiation was compared with the 2.208-Mev gamma-ray of RaC.

The experimental arrangement used in run 1 is shown schematically in Fig. 1. The spectrometer was situated outside the shielding wall of the graphite thermal column of the NRX pile. Part of the graphite was removed to admit the paraffin sample in the form of a slab of dimensions 25×25×5 in. Neutrons were prevented from escaping from the pile by the B_4C shield. The gamma-radiation from the paraffin was collimated by the lead plug P situated in a conical hole in the thermal column shield, into a thin conical shell of 15° half-angle converging on a uranium photo-electron radiator at the source position of the beta-ray spectrometer. The small hole A allowed the insertion of the ThC″ gamma-ray source behind the radiator without any mechanical motion of the experimental arrangement.

Figure 2 shows the collimating hole used in run 2 and the spectrometer arrangement common to runs 1 and 2. This collimating hole was a cone of half-angle 2.3°. The cup C was made of brass in run 1 and of Lucite in run 2, and had a post B on which the uranium radiator was mounted. The radiator was a disk of uranium metal of diameter 6 mm and superficial density 142 mg/cm², and could be removed for background runs. The difference between run 1 and run 2 lay mainly in the manner of collimating the gamma-rays as described above. In run 1 the paraffin gamma-radiation converged on the radiator at an angle of 15°, while in run 2 it struck it in an approximately parallel beam. In both runs the ThC″ gamma-rays struck the radiator in an approximately parallel beam.

The beta-ray spectrometer was of the magnetic lens type using two coils as shown in Fig. 1 and having baffles arranged to select negatrons with a line width at half-maximum about 2.3 percent in momentum. The detector at the focus of the spectrometer was a small end-window Geiger-Müller counter. The two lens coils were connected in series to an electronic current stabilizer supplied by a motor-generator. The current was stabilized to 1 part in 10^4 and was measured by the voltage drop across a standard resistor. A potentiometer and standard cell were used to make relative measurements of this voltage with an accuracy of 2 parts in 10^4. The shape of the secondary electron spectrum in a given momentum interval was measured by an automatic current-switching and counting device which recorded the time for a predetermined number of counts at 25 preselected successive values of the current, and repeated the process until stopped.

In each of the determinations of the energy of the paraffin gamma-radiation (i.e., in run 1 as well as in run 2) the sequence of events was as follows: A survey of 25 points separated by 1.2 percent in momentum was first made of the momentum region containing the K and L photo-electron peaks of the paraffin gamma-radiation. In order to study the peaks in detail, 25 points

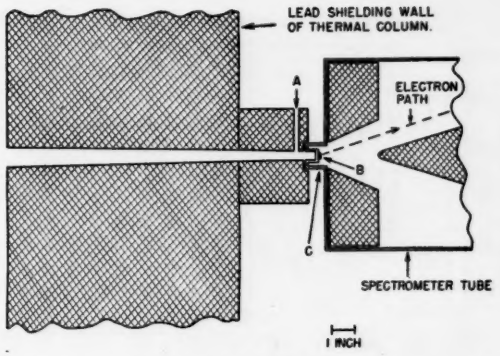

FIG. 2. Schematic diagram of the collimator arrangement of run 2 and the spectrometer arrangement common to runs 1 and 2.

spaced at intervals of 0.4 percent in momentum were measured by the automatic device about 75 times in succession, recording 1000 counts per point each time. The pile was then shut down and the ThC″ source was inserted into the hole A, shown in Figs. 1 and 2. The K and L photo-electron peaks of the 2.615-Mev gamma-ray were then measured both automatically and manually to a statistical accuracy comparable with that obtained for the paraffin radiation. A return was then made to the paraffin radiation and another long recording of the counts was made as before. This gave a total of about 150,000 counts at each of the 25 points of the detailed study of the paraffin radiation. During this procedure the spectrometer was not moved mechanically. Finally the U radiator was removed and background runs were made. The same general procedure was used for the comparison of the paraffin gamma-radiation with the RaC 2.208-Mev gamma-ray, using the experimental arrangement of run 2.

Between the two determinations, run 1 and run 2, the paraffin was removed from the thermal column of the pile and the secondary electron spectrum was checked to show that the gamma-radiation studied above was no longer present.

III. EXPERIMENTAL RESULTS

The experimental results of run 1 have been given previously[1] and will not be repeated in detail. The data obtained in run 2 will be given in full in order to show the method of analysis used in both runs.

Figure 3 shows the secondary electron spectrum observed in run 2 in the region of the photo-electron lines from the paraffin gamma-radiation. The main curve consists of Compton recoil electrons and K and L photo-electron peaks from the U radiator, all on a background sloping upward to the right, caused by higher energy gamma-rays from the thermal column of the pile. The shape of the background under the photo-electron peaks was measured after removing the U radiator, leaving a thick Lucite radiator. The background curve shown in Fig. 3 was obtained by normalizing these results to fit the main curve at point A.

A similar pair of curves for the ThC″ gamma-ray is

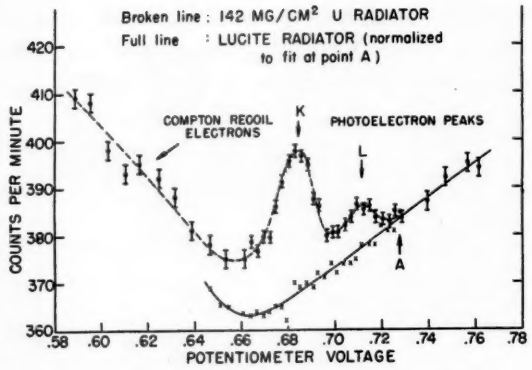

FIG. 3. Secondary electron spectrum observed in run 2 in the region of the photo-electron lines from the paraffin gamma-radiation. On the upper curve the standard deviation of each of the points is indicated by a vertical bar, and on the lower curve it is about two counts per minute.

shown in Fig. 4. The general background in this figure is much lower than that for Fig. 3 because the pile was shut off during these measurements.

In Fig. 5 both the ThC″ and paraffin photo-electron peaks are shown with their backgrounds subtracted and with the K photo-electron peaks normalized to equal heights. The potentiometer voltage scales have been adjusted in the figure to make the two K photo-electron peaks coincide on the high energy side. Any relative shift of the photo-electron peaks due to the effect of finite radiator thickness is small because the paraffin gamma-radiation is close to the standard gamma-ray in energy. We believe that any error in the relative positions of the peaks due to uncertainties in the background subtraction procedure is small because the subtraction has been done in the same manner for both curves. The horizontal bar at A in Fig. 5 indicates the magnitude of the estimated probable error in bringing the two K peaks into coincidence.

The two potentiometer voltage scales in Fig. 5 are related by the factor 1.1530, so that the ratio of the $H\rho$-values of the two photo-electron lines is 1.1530 $\pm$0.0023. Using a value of 116 kev for the K-electron

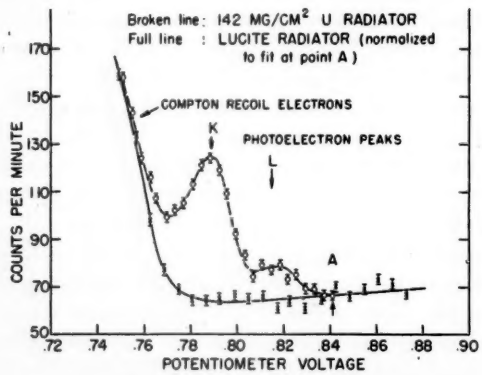

FIG. 4. Secondary electron spectrum observed in run 2 in the region of the photo-electron lines from the ThC″ gamma-ray. The standard deviations of the points on the curves are indicated by vertical bars.

binding energy of U, and Wolfson's value[4] of 2.615 $\pm$0.004 Mev for the energy of the ThC″ gamma-ray, we obtain 2.228$\pm$0.007 Mev for the energy of the paraffin gamma-radiation. Adding 1.3 kev for the recoil of the deuterium nucleus, we obtain from this run BE(D)=2.229$\pm$0.007 Mev.

The results of run 1 have been given previously[1] as BE(D)=2.237$\pm$0.005 Mev, relative to an assumed energy for the ThC″ gamma-ray of 2.620 Mev. Taking Wolfson's value 2.615$\pm$0.004 Mev, this becomes BE(D)=2.233$\pm$0.007 Mev.

The experimental results of the comparison of the paraffin gamma-radiation with the 2.208-Mev gamma-ray of RaC are shown in Fig. 6. These results cannot be used for a determination of BE(D) to an accuracy comparable with those just mentioned, mainly because the 2.208-Mev gamma-ray of RaC is weak and is badly situated in the RaC gamma-ray spectrum. The background for the RaC curve in Fig. 6 was determined at a number of points with the U radiator removed, and is indicated as a broken line. The photo-electron peaks of the 2.208-Mev gamma-ray are situated on the rise of the Compton recoil electrons from the 2.452-Mev line[4] of RaC, whose K photo-electron peak would lie at potentiometer voltage 0.744 in Fig. 6. Taking Wolfson's value of 2.208$\pm$0.006 Mev for the RaC gamma-ray, Fig. 6 yields a value BE(D)=2.232$\pm$0.013 Mev, in agreement with the results above. Figure 6 shows definitely that the 2.208-Mev gamma-ray of RaC is not capable of disintegrating the deuteron.

IV. DISCUSSION

In averaging the results of run 1 and run 2 to obtain the most probable value of BE(D), run 2 will be given double weight for two reasons: (1) in the experimental arrangement of run 2 the degree of collimation is closely the same for the paraffin gamma-radiation and the

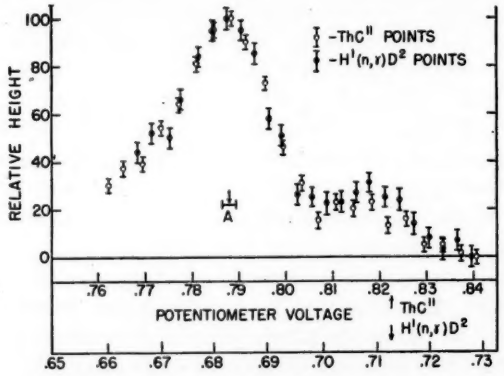

FIG. 5. The ThC″ and paraffin photo-electron peaks with backgrounds subtracted. The K photo-electron peaks have been normalized to the same height. The potentiometer voltage scales have been adjusted so as to make the two K photo-electron peaks coincide on the high energy side. The horizontal bar at A indicates the magnitude of the estimated probable error in bringing the two peaks into coincidence.

[4] J. L. Wolfson, Phys. Rev. **78**, 176 (1950).

ThC″ gamma-rays, and (2) the photo-electron peaks from the paraffin gamma-radiation stand out from the background more prominently in run 2 than in run 1. The probable errors given for runs 1 and 2 are mainly estimates of systematic errors which are not reduced by the averaging process. The average obtained in this way for the binding energy of the deuteron is

$$BE(D)=2.230\pm0.007 \text{ Mev}.$$

This value is determined assuming an energy of 2.615 ± 0.004 Mev for the standard ThC″ gamma-ray. If a very much more accurate value for this latter energy should become available, a value of BE(D) with a probable error of 0.005 Mev could be computed from the above experimental data.

A value of the $(n-H^1)$ energy difference can be obtained by using the above result in the equation

$$(n-H^1)=BE(D)-(H^1H^1-D^2),$$

where the $(H^1H^1-D^2)$ difference is a mass spectrometric measurement converted to energy units. The value 1.432 ± 0.002 Mev given for $(H^1H^1-D^2)$ by Cohen and Hornyak[5] yields $(n-H^1)=0.798\pm0.007$ Mev. Roberts and Nier[6] have recently published the value 1.442 Mev for $(H^1H^1-D^2)$ with a probable error given as a few kilovolts. This yields the value $(n-H^1)=0.788$ Mev, having a probable error exceeding 0.007 Mev by an amount depending on Roberts and Nier's error. The agreement of the latter value of $(n-H^1)$ with recent determinations of this quantity by other methods[7,8] lends weight to Roberts and Nier's value for $(H^1H^1-D^2)$.

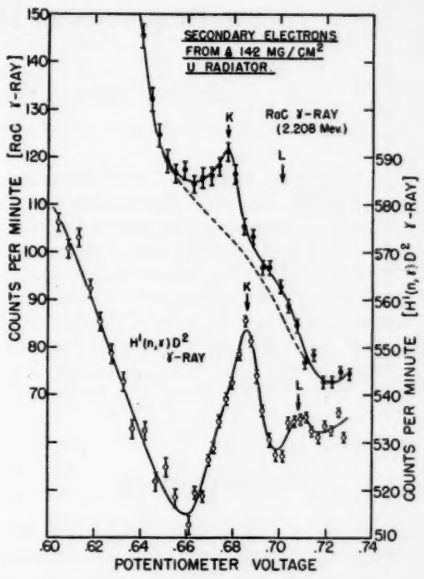

FIG. 6. Secondary electron spectra representing the comparison of the paraffin gamma-radiation with the 2.208-Mev gamma-ray of RaC. The standard deviations of the points on the curves are indicated by vertical bars.

The authors wish to express their thanks to Drs. W. B. Lewis and B. W. Sargent for interesting discussions concerning this investigation. We also wish to thank the NRX pile crew for their kind cooperation during this experiment.

[5] R. Cohen and W. R. Hornyak, Phy. Rev. **72**, 1127 (1947).
[6] T. R. Roberts and A. O. Nier, Phys. Rev. **77**, 746 (1950).
[7] Tollestrup, Jenkins, Fowler, and Lauritsen, Phys. Rev. **75**, 1947 (1949).
[8] Taschek, Argo, Hemmendinger, and Jarvis, Phys. Rev. **76**, 325 (1949).

Some Properties of High Resistivity P-Type Germanium

W. C. DUNLAP
Research Laboratory, General Electric Company, Schenectady, New York
(Received October 10, 1949)

A summary is given of some characteristics of single crystals of high resistivity, homogeneous, *P*-type germanium. The Hall effect, resistivity, and rectification characteristics of this material were studied with respect to changes of temperature and magnetic field. A very high mobility figure at 25°C (~2730 cm²/volt-sec. for a field of 3600 gauss) was obtained by calculating $10^8R/\rho$. An effect of type of contact at the Hall probes on Hall effect measurements is pointed out. The resistivity of the material was 18.8 ohm-cm average, the Hall coefficient 5.14×10^{-4} volt-cm/amp.-gauss. The magneto-resistance of this germanium amounted to about 22 percent in a field of 13,750 gauss. The Hall coefficient decreased by about 22 percent between 3600 and 13,750 gauss. The band separation for one sample was 0.82 volts from Hall effect data, 0.75 from the resistivity. The mobility was found to obey a $T^{-2.0}$ law in the temperature range 78 to 400°K. This *P*-type material exhibited only slight rectification.

I. INTRODUCTION

THE purpose of the present paper is to present results of an experimental study of several single crystals of high resistivity *P*-type germanium. We shall also discuss several points at which these results appear to bear upon existing theory. The results are a more complete report of work partially reported earlier.[1]

The work dealt mainly with measurements of resistivity, Hall coefficient, and rectification characteristics. Magnetic field strength and temperature were used as independent variables. Results will be given following a discussion of experimental methods.

II. PREPARATION OF THE GERMANIUM

The germanium used in the present work was obtained during the course of a study of the preparation of germanium for high voltage diodes.

Germanium oxide (GeO_2) obtained from the Eagle-Pitcher Company (Lot AC 409) was reduced by Mr. F. C. Kelley for 16 hr. at 650°C in a hydrogen furnace. The reduced powder was then heated to 900°C for 3 hr. and cooled in the furnace.

The reduced powder was melted at a pressure that was less than 10^{-3} mm during the entire melting operation. A graphite crucible previously fired four hours at 1700°C in an Arsem furnace was used for this melting. The ingot was cooled to room temperature within several hours. No attempt was made at directional cooling. Annealing for 2 hr. at 650°C was carried out. Subsequent annealing at 500°C did not change the characteristics appreciably. This ingot was designated H114.

It was observed upon cutting it into slices that the entire ingot appeared to be a single crystal. Subsequent microscopic examination of most of the cut surfaces was made, and the conclusion was drawn that the ingot was a single crystal. The surfaces tested in this way were etched both by electrolytic etching (10 percent KOH) and by chemical etching (conc. HF mixed with conc. HNO_3 in the proportion 2:1). Subsequent tests were also made on several plates of this germanium by the back-reflection x-ray technique. These tests also confirmed the conclusion of the single crystalline nature of the crystals.

Some tests were made on several of the sample plates to determine the homogeneity of the material. A thermoelectric test utilizing a hot platinum point and a galvanometer indicated uniform *P*-type character over all the surfaces tested. Tests were also made of the uniformity of the resistivity. A plot of this characteristic for sample 103 is shown in Fig. 1. It is seen that the potential follows a linear relationship over a distance of about 1 cm. This behavior can be contrasted to the extremely non-linear potential characteristic often

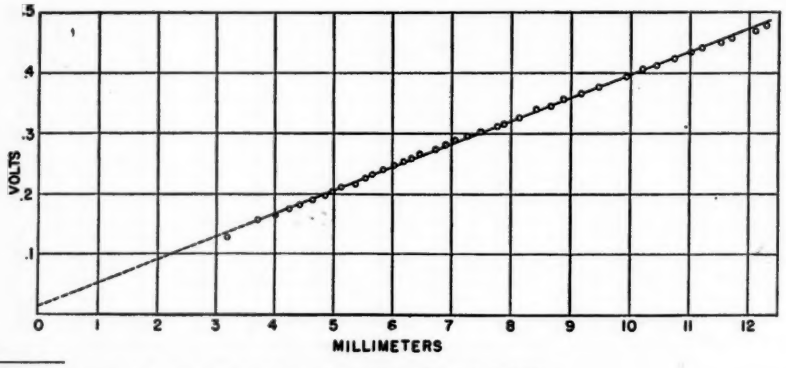

FIG. 1. Potential distribution along the length of a single crystal of high resistivity *P*-type germanium. (No. 103, 25°C.)

[1] W. C. Dunlap and E. F. Hennelly, Phys. Rev. 74, 976 (1948).

found in other samples of high resistivity germanium. Failure of the potential line to pass through the origin (the location of the fixed probe) is probably due to non-uniformity of the current flow pattern near the electrode.

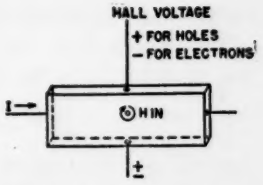

FIG. 2. Schematic diagram of electrode arrangement on samples of germanium for measurement of conduction properties. All measurements are made with potentiometer methods.

III. EXPERIMENTAL METHODS

A simplified diagram of the connections to a sample for measurement of the conduction properties is shown in Fig. 2. All significant potential measurements were made with potentiometer methods.

Preliminary measurements were made on several samples from ingot H114 by simply clamping the sample in a holder, using stainless steel points for the Hall and probe contacts. Results of these measurements are given in Table I together with some results on N-type material for comparison. Subsequent tests were made with silver-plated and tin-soldered contacts. The latter methods were used for the data in Fig. 3. A somewhat lower value of mobility results from the use of contacts having an appreciable area of contact. This effect may simply involve shorting some of the primary current through the contact. Thus we consider the higher values, obtained with pressure point contact, more reliable than those obtained with tin-soldered or plated contacts. A list of conduction properties, their units and significance, follows.

(1) Resistivity, ρ, is measured in ohm cm

$$\rho = VA/Il,$$

where V is the voltage drop, I the current in amperes, A the cross section along which current flows, and l is the distance between probes.

(2) *Hall coefficient*, R, is measured in terms of the voltage produced across the Hall probes, per unit magnetic field and current. $R = Vt/HI$, where V is the Hall voltage, t the thickness of the plate along the magnetic field, H the magnetic field in gauss, I the current through the sample in amperes. R can be measured in volt-cm/amp. gauss, or in e.m.u. To obtain a result in the latter unit, we multiply by 10^9 the result obtained in the former. In this paper we use R in volt-cm/amp.-gauss. The magnetic field in the present work was obtained with a calibrated electromagnet. The calibration of the magnetic field was carried out by flip-coil-fluxmeter methods. The magnetic field is considered known with an error of less than two percent. A field strength of 3600 gauss was used for most of the measurements. Results generally are averaged with respect to reversal of the magnetic field, and were also checked for dependence upon direction of current flow through the samples. The latter effect was not found in the present work.

(3) The "mobility figure," μ is determined, according to the free electron theory, by the ratio R/ρ. (We neglect here the factor $8/3\pi$ that R/ρ must be multiplied by, according to this theory, to give the true mobility.) The mobility is physically the drift velocity attained by an electron in unit electric field. In practical units,

$$\mu = (R/\rho) \times 10^8 (\text{cm}^2/\text{volt-sec.})$$

(4) The *magneto-resistance*, namely the change in resistivity in a magnetic field is denoted simply as $(100\Delta\rho)/\rho_0$, the percentage change in resistivity measured with respect to the zero-field resistivity.[2] The magneto-resistance appears to be related to the distribution of electron velocities in the germanium. That is, when equilibrium has been established in the magnetic field the Hall field tends to exactly offset the deflecting force of the magnetic field, but only for electrons of the average velocity. These electrons continue through the sample with unchanged paths. Electrons of higher and lower velocity than the average will be either overcompensated for or undercompensated for by the Hall field, and they will acquire new, curved trajectories that lead to a higher resistance. This picture gives a simple explanation of the nature of magneto-resistance.

(5) By measurement of the temperature dependence of the Hall coefficient one can get an approximate value

TABLE I. Room temperature conduction properties for a number of germanium samples prepared by melting in vacuum (10^{-3} mm Hg). Temperature effects were studied only for 104. The band separation was 0.75 ev, and the intercept N_0 from the Hall effect $6\times10^{21}/\text{cm}^3$. The mobility varied roughly as $T^{-2.0}$. The magneto-resistance varied as $H^{+1.56}$ at room temperature, and as $H^{0.75}$ at −195°C.

	25°C							−195°C
Sample No.	48	93	94	95	103	104	105	104
Melt No.	H90	H107	H107	H107	H114	H114	H114	H114
Type of conduction	*N*	*N*	*N*	*N*	*P*	*P*	*P*	*P*
Resistivity ohm-cm	2.2	8.9	9.9	8.5	19.9	19.1	17.4	2.35
Hall coeff. ($\times10^5$)(volt-cm/amp.-gauss)	8.4	21.2	29.4	20.4	53.5	51.6	49.0	42.0
Mobility figure ($\times10^{-3}$)(cm^2/volt-sec.)	3.8	2.4	3.0	2.4	2.7	2.7	2.8	18.0
$\Delta\rho/\rho_0$ at 13,750 g ($\times100$)	17.1	13.0	15.7	14.1	22.5	22.0	22.0	85
$\Delta R/R$ ($\times100$)	6.3	5.7	5.6	—	23	24	21	4

[2] W. C. Dunlap, Phys. Rev. **71**, 471A (1947).

for the band separation $\Delta\epsilon$. For the one sample studied in the present work, $\Delta\epsilon = 0.82$ ev. One can also obtain the quantity N_0 in the relation:[3]

$$N = N_0 e - (\Delta\epsilon/2kT).$$

According to the free electron theory, for carriers of only one sign the electron density $N = 1/Re$ (e.m.u.) so that $1/N_0$ is determined by the intercept of R on the $1/T$ axis, whereas $\Delta\epsilon$ is determined by the slope of the curve $\log R$ plotted against $1/T$. For one sample (104) N_0 was found to be $6\times10^{21}/\text{cm}^3$.

For the temperature variation of the resistivity ρ, one can also get a value for $\Delta\epsilon$, assuming $\rho = \rho_0 \exp(\Delta\epsilon/2kT)$. For two separate runs on 104, the values of $\Delta\epsilon$ obtained by this method were 0.740 and 0.755 ev. These values agree well with the value of 0.75 previously given by Lark-Horovitz *et al.*[4] The difference between the Hall effect value and the resistivity value may be accounted for by the fact that the theory of intrinsic conduction as stated by Fröhlich gives the following temperature dependence for R:

$$N \propto 1/R = \text{const } (T)^{\frac{3}{2}} \exp(-\Delta\epsilon/2kT)$$

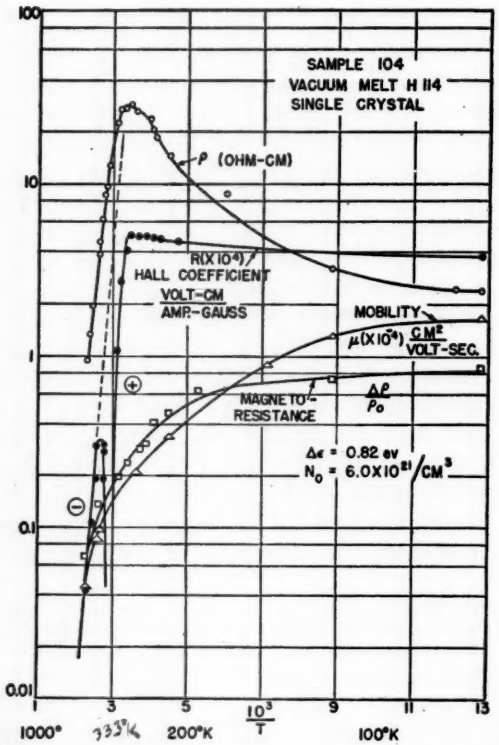

FIG. 3. Summary of conduction properties of sample 104, a single crystal of high resistivity P-type germanium. The crystal reversed from P- to N-type at 70°C. Tin-soldered contacts were used for this set of measurements.

and

$$1/\rho = Ne\mu = \text{const} \exp(-\Delta\epsilon/2kT),$$

if we use the relation that μ varies as $T^{-\frac{3}{2}}$ in the region where lattice vibrations determine the mobility. Thus the Hall coefficient is expected to vary more rapidly in the intrinsic range than the resistivity, and thus is expected to lead to a larger value of band separation than the resistivity value.

(6) The variation of the Hall coefficient with magnetic field was found for the samples studied. Measurements were made at 3600 and 13,750 gauss, and the percentage difference between these values, relative to the low field value, was tabulated. This is the quantity $(\Delta R/R)$ referred to in Table I.

IV. RESULTS

In Table I is shown a summary of the conduction properties of several samples of high resistivity germanium, including both P- and N-types. The samples from melt H114 and sample 48 were single crystals. The reproducibility of the results on samples from H114 is seen to be good. The average resistivity was 18.8 ohm-cm, the average Hall coefficient 5.14×10^{-4} volt-cm/amp.-gauss and the average $R/\rho = 2730$ cm²/volt-sec. In other data presented in the paper these properties may be given somewhat different values because of slightly different electrode arrangements, such as may be required for obtaining results as a function of temperature. It is found, for example, that pressure contacts are too high in resistance at low temperatures (<-100°C) to yield reliable results.

It has been found during the course of a study of Hall effect and magneto-resistance in germanium, that measurements with pressure contacts lead to higher values of Hall effect and mobility than measurements with broad contacts such as those obtained by silver-plating and soldering. It has further been found that reduction of the area of the plated or soldered contact increases the apparent mobility of the sample almost to the value obtained with point contacts.

These results lead us to believe that the values of mobility are correct when obtained with pressure point-contacts. The effect of contact area is to reduce the value of the Hall coefficient by as much as a factor of three, when contacts are increased in diameter to 70 mils, but there is little effect on the resistivity, as long as the contacts are not greater than 25 mils in diameter. (See Fig. 5.)

The value of the mobility figure, 2730 cm²/volt-sec. (or 2330, if the factor $8/3\pi$ is included) obtained in the present work is much greater than that obtained by other workers. Pearson[5] has recently given a value of 1700 cm²/volt-sec. for the mobility of holes in P-type single crystals of germanium. Earlier estimates of the mobility of holes, given by Lark-Horovitz *et al.*[4] were in the neighborhood of 1000.

[3] The free electron theory for semi-conductors is summarized in Chapter IV of Seitz' "Modern Theory of Solids" (New York, McGraw-Hill, 1939), and in Fröhlich's "Electron Theory of Metals" (Berlin, Springer, 1936).

[4] Lark-Horovitz, Middleton, Miller, and Walerstein, Phys. Rev. **69**, 258(A) (1946).

[5] G. L. Pearson, Phys. Rev. **76**, 179(A) (1949).

We should perhaps also mention here that our R/ρ mobility values for N-type germanium obtained with pressure contacts range up to $\sim$3800 cm²/volt-sec. This value is, like the values obtained for P-type germanium, considerably higher than that reported by others.[4,5]

From Table I it is seen that the Hall coefficient varies with magnetic field. The quantity $\Delta R/R$ between 3600 and 13,750 gauss is about 22 percent for the high resistivity P-type material, but only about six percent for the lower resistivity N-type samples. In general, both the magneto-resistance and the variation of the Hall effect with magnetic field for germanium seem to increase with increasing resistivity of the sample, and to be larger for P-type than N-type material of comparable resistivity. The value of 2730 for μ was obtained at 3600 gauss. If we use the Hall coefficient at 1000 gauss, we obtain an even higher value of mobility figure, about 3000 cm²/volt-sec.

We present in Fig. 3 a summary of the temperature-dependence of the conduction properties of a single crystal of P-type germanium. At room temperature the mobility figure for this ample, with tin-soldered lead connections, was only 2100 cm²/volt-sec., in distinction to the higher value obtained with pressure contacts. The resistivity value is also somewhat different because of the different electrode arrangement. The mobility figure reached the very high value of about 18,000 cm²/volt-sec. at liquid air temperature for this crystal. This effect appeared from the large drop in resistivity between room temperature and liquid air temperature, coupled with a nearly constant value of Hall coefficient. This drop in ρ is the largest yet observed by the author in any sample of germanium and appears to confirm the existence of high purity and good homogeneity in this germanium.

It will be noticed that the Hall coefficient reverses from positive to negative at about $10^3/T=2.9$. The temperature of reversal was 70°C. At this temperature the effectively N-type intrinsic conduction overbalances the P-type impurity conduction.

The forbidden energy gap $\Delta\epsilon$ was found from the slope of the "intrinsic line" of the resistivity to be 0.75 ev. The value of N_0 was found to be 6.0×10^{21}/cm³. By extrapolating the "intrinsic line" for ρ to room temperature (25°C) one finds also the so-called intrinsic resistivity at room temperature. Extrapolation for two independent runs on 104 yielded results of 71 and 84 ohm-cm, for the intrinsic resistivity. The average value is about 78 ohm-cm, but may be in error by 10 to 15 percent because of the tin-soldered resistivity probes. The magneto-resistance was found to be very large in this high resistance P-type material. At liquid air temperature the magneto-resistance $\Delta\rho/\rho_0$ amounted to about 85 percent, at 13,750 gauss, whereas at room temperature the effect amounted to about 22 percent.

Figure 4 shows the variation of resistivity with magnetic field. At 25°C the variation, for small fields was approximately according to the relation $\Delta\rho/\rho_0=C_1H^{1.56}$, at −196°C the relation was $\Delta\rho/\rho_0=C_2H^{0.75}$. The above relation at 25°C applies only to about 10 kilogauss.

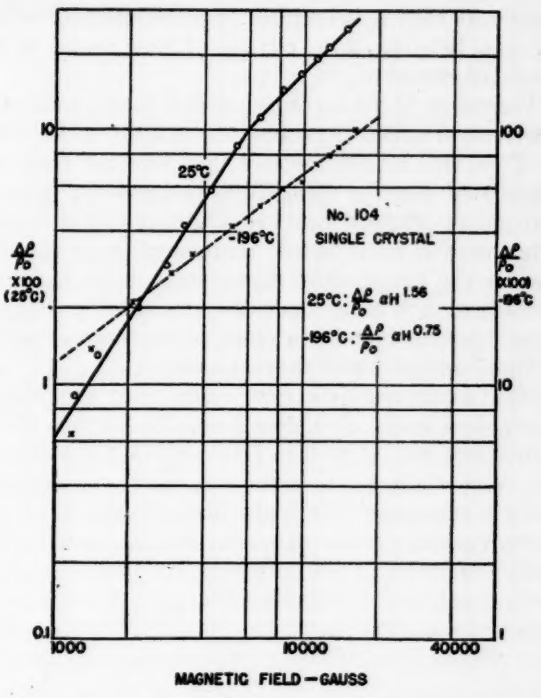

FIG. 4. Variation of magneto-resistance with magnetic field for a single crystal of P-type germanium.

Figure 5 shows the variation of the Hall coefficient for sample 104 as a function of magnetic field strength. The drop in the Hall coefficient between 1000 and 15,000 gauss amounted to about 38 percent of the value at 1000 gauss. On the other hand, at liquid air temperatures, the Hall coefficient was practically constant with varying magnetic field.

Because of the apparently high degree of purity and homogeneity in the sample tested, it was thought that the temperature dependence of the mobility figure $10^8R/\rho$ might be of significance. A plot of this characteristic for several high resistivity P-type samples, together with one of $\Delta\rho/\rho_0$ at 13,750 gauss, is shown on a log-log scale in Fig. 6. The mobility for sample 104 follows a law $\mu=CT^{-2.0}$ fairly accurately between 120 and 400°K, but appears to depart from this rule at higher and lower temperatures. For one other P-type sample, 43 ohm cm, the exponent was −2.3. It is of interest to note the large mobility of holes, 18,000, at −196°C. It is to be expected that, because of impurity scattering,[6] the mobility will reach a maximum somewhat below the temperature of liquid nitrogen. The magneto-resistance of the sample did not obey a power law relationship, and varies more slowly with temperature than the mobility at low temperature, but more

[6] E. Conwell and V. F. Weisskopf, Phys. Rev. 77, 388 (1950).

rapidly at high temperatures. A more detailed report will soon be given of the relation of these results to the theory of electrons.

The theory of conductivity predicts that if scattering is a result of lattice vibrations, the mobility should vary as $T^{-1.5}$. Our results indicate that this law does not adequately describe the behavior of positive holes in germanium. Measurements on single crystals of N-type germanium indicate better approximation to the $T^{-\frac{3}{2}}$ law for the temperature dependence of the mobility. Investigation is being made of the possibility that the large exponent found is a result of the large variation of Hall coefficient with magnetic field.

Point-plane rectifiers were made from the P-type germanium under discussion here. The surface of the germanium was etched in $2HF-HNO_3$ for about 15 sec. Very little rectification was observed, and the contact resistance was quite high, several thousand ohms. Various whisker materials have been used for this study, including Pt-10 percent Ru, brass, stainless steel, dural, and aluminum. The highest rectification obtained was from aluminum, with a rectification ratio at 5 volts of about 6. One expects that a metal such as aluminum, having a low work function, should give the best rectification possible.[7] Recently Pfann and Scaff[8] have shown that a.c. pulsing of the contact at the P-type germanium surface can be made to yield better P-type rectification.

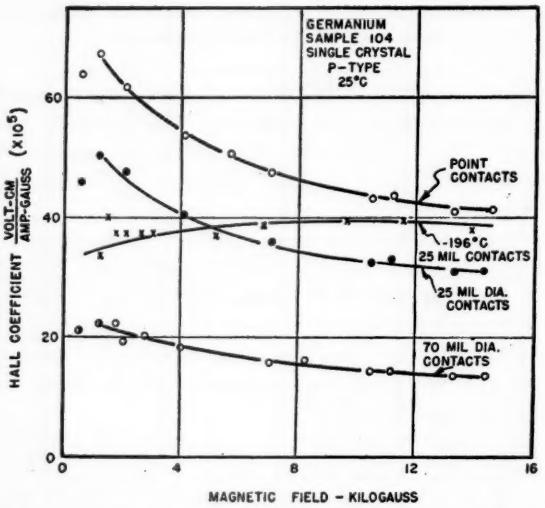

FIG. 5. Variation of Hall coefficient of a single crystal of P-type germanium. The 25° curve differs in absolute value from the results in Fig. 3, because of a somewhat different contact connection. Such differences, however, move the curve vertically without altering its shape.

V. DISCUSSION

From the results obtained we draw the following conclusions: (1) The mobility figure of holes is, according to the present Hall effect data and the theory of electrons, in the neighborhood of 3000 cm²/volt-sec. or higher. Similarly it appears that the mobility figure of electrons is in the region of 4000 cm²/volt-sec. or higher. (2) High resistivity P-type germanium has a large dependence of Hall coefficient and resistivity on magnetic field strength. (3) High resistivity P-type germanium of the type discussed here has a dependence of mobility on temperature considerably greater than does N-type germanium, and a dependence considerably greater than that predicted by the $T^{\frac{3}{2}}$ law for lattice scattering. These measurements, of course, involve use of a given magnetic field for all temperatures, and it is possible that the effects involved in (2) and (3) are related.

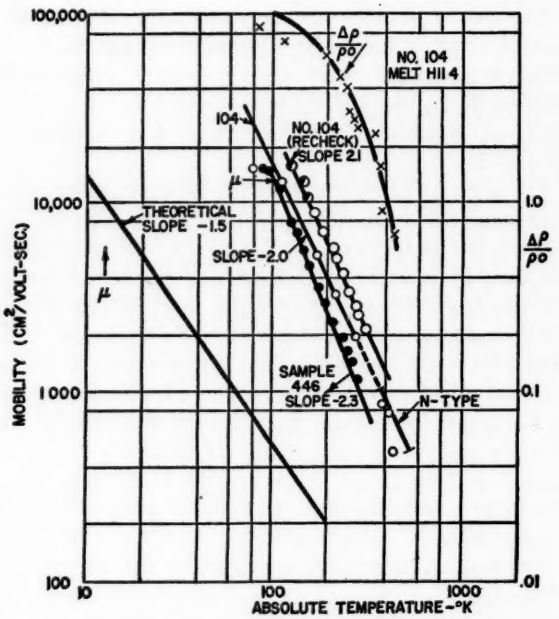

FIG. 6. Mobility figure (R/ρ) for single crystal (sample 104) as a function of temperature. The mobility follows a $T^{-2.0}$ relation quite closely over the range 78 to 300°K. Additional curves shown include a recheck of 104 with different electrodes, and results on another high resistivity P-type sample, 446. Also shown is the line representing the theoretical slope of -1.5. A curve showing $\Delta\rho/\rho_0$, the magneto-resistance, as a function of temperature, is also given.

A factor that has not been introduced as yet into discussion of the present results is the influence of the intrinsic conductivity on the characteristics. P-type germanium of 20 ohm-cm resistivity at room temperature possesses an appreciable number of carriers thermally excited from the filled band, apart from the "impurity" carriers excited from the impurity levels. Some of these carriers are electrons and some are holes. The actual density of holes and electrons is determined by a law similar to the law of mass action for chemical equilibrium of dilute solutions;[9] $N_eN_h=\text{const.}=1.93\times10^{26}$ for 25°C. The value 1.93×10^{26} is obtained from the assumption that $\mu_e=4500$, $\mu_h=3000$, intrinsic resistivity at 25°C = 60 ohm cm. Because of the effec-

[7] W. E. Meyerhof, Phys. Rev. **71**, 727 (1947).
[8] W. Pfann and J. H. Scaff, Phys. Rev. **76**, 459(A) (1949).
[9] G. L. Pearson and J. Bardeen, Phys. Rev. **75**, 865 (1949).

tively opposite charges on electrons and holes, the measured mobility is less than the true hole mobility. That is, the electrons present tend to counterbalance the net P-type Hall effect and thus reduce the mobility value as measured.

In Fig. 7 we show a curve for the apparent mobility* of high resistivity germanium as a function of resistivity. For one set of calculations we assume a hole mobility figure of 3000, and an electron mobility figure of 4500. For the other, we assume $\mu_e=2600$, $\mu_n=1700$, as found by Pearson. The theory of mixed conduction by holes and electrons can be expressed in the following form:**

$$R=-\frac{1}{e}\frac{N_e\mu_e^2-N_h\mu_h^2}{(N_e\mu_e+N_h\mu_h)^2}\times 10^{-8} \quad (e \text{ in coulombs}).$$

This can be expressed in the form

$$R=-\frac{1}{e}\frac{-N_eC^2+N_h}{(N_eC+N_h)^2}\times 10^{-8},$$

where C is the ratio μ_e/μ_h, here assumed to be 1.5.

Also the conductivity σ is given by

$$\sigma=e(N_e\mu_e+N_h\mu_h)=eN_h\mu_h[(N_e/N_h)C+1] \text{ ohm}^{-1}\text{-cm}^{-1}.$$

Hence the apparent mobility $\mu=R/\rho\times 10^8$ is given by

$$\mu/\mu_h=[-(N_e/N_h)C^2+1]/[(N_e/N_h)C+1].$$

From these equations one can get a curve for $\mu=f(\rho)$.

The curve representing the "apparent mobility" $\mu=(10^8R/\rho)$ as a function of resistivity is an ellipse with the following equation,

$$\frac{[\frac{1}{2}(\mu_e-\mu_h)+\mu]^2}{(\mu_e+\mu_h)^2/4}+\frac{\rho^2}{\left(\frac{1}{4e^2\mu_h\mu_eK(T)}\right)}=1,$$

where μ_e is electron mobility, μ_h is hole mobility, μ=apparent mobility$=10^8R/\rho$, $K(T)=N_hN_e$, a function of temperature.

The ellipse has the following properties when we assume $\mu_e=4500$ cm^2/volt-sec., $\mu_h=3000$, $K(T)=1.93\times 10^{26}$ at 25°C; the center is at (0, −750); the semi-major axis is 61.7 ohm-cm, the semiminor axis 3750 cm^2/volt-sec. The intercept on the ρ-axis is 60. This is the resistivity of zero Hall effect, assuming homogeneity throughout the sample. In Fig. 7 is shown part of the ellipse, corresponding to P-type samples.

It is of interest in connection with the present work, that at 20 ohm-cm P-type germanium is already influenced by the intrinsic conductivity to the extent that the apparent mobility should be raised by about three percent to obtain the true hole mobility figure. At 40 ohm-cm the apparent mobility should be increased by 44 percent. Preliminary experiments were made on especially purified P-type samples kindly furnished by R. N. Hall. Also shown in Fig. 7 are results of mobility measurements on these samples (crosses). Although considerable scatter is found, several values were as high as expected from the author's presumed values for the electron and hole mobility and for the intrinsic resistivity.

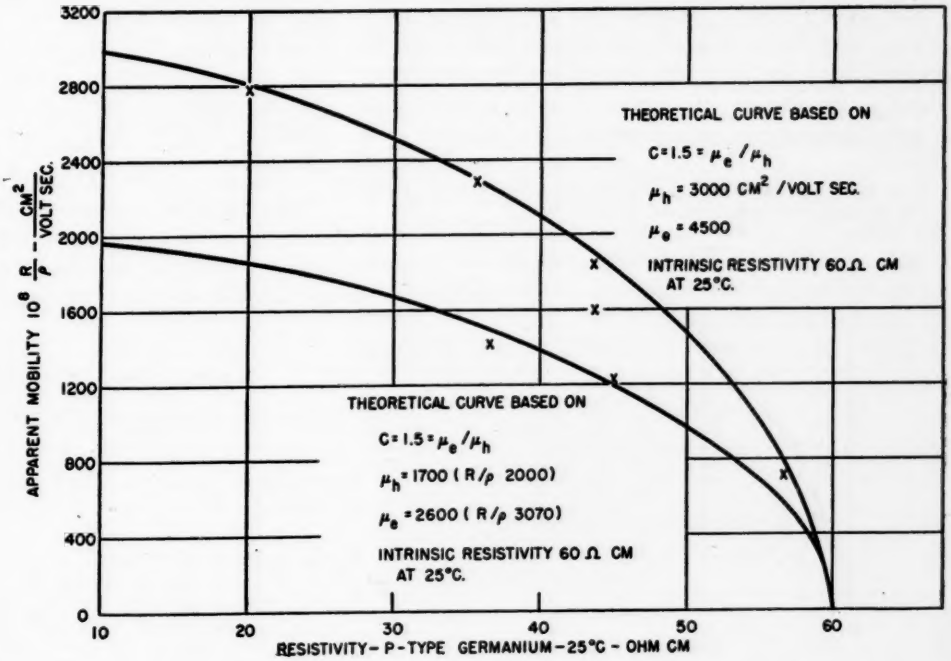

FIG. 7. Comparison between experimental values of mobility for high resistivity P-type samples with theoretical curves based on two sets of assumptions regarding mobility of holes and electrons. The crosses represent measured mobilities of P-type crystals ($10^8R/\rho$). The upper curve is based on mobilities indicated by present results. The lower is based on mobility values of Pearson.

* In what follows we use the term "apparent mobility" to mean the mobility figure $10^8R/\rho$ for a sample in which both hole and electron conduction must be considered.

** Again we neglect the factor $8/3\pi$ often included in this equation.

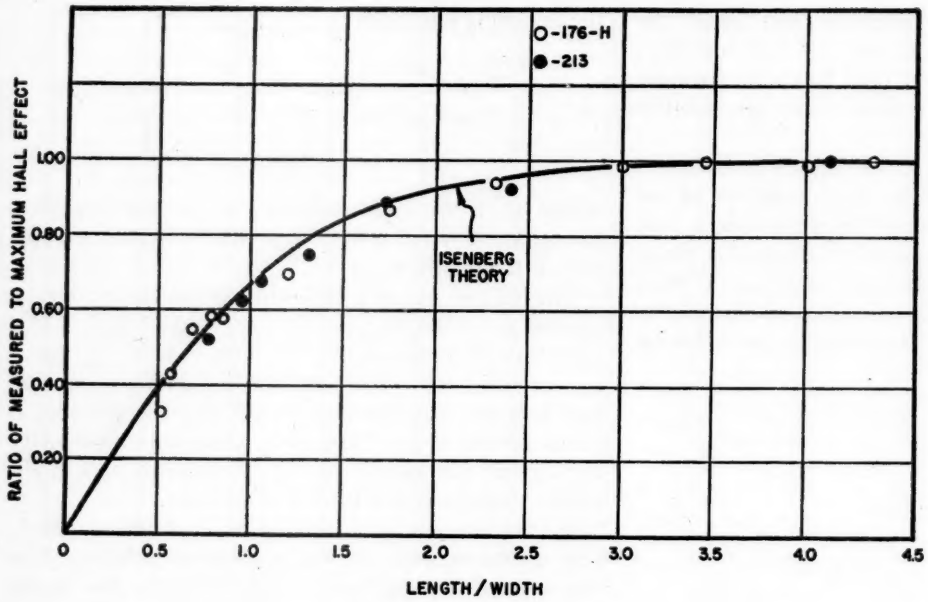

FIG. 8. Comparison of Isenberg's theory for end-effect in Hall effect measurements with experimental values obtained with *P*-type germanium samples. The samples were approximately square and were progressively cut away until the sample was long and narrow. The experimental points are seen to fit the theoretical curve quite well.

An effect that is sometimes encountered in working with small samples is the so-called end-effect on Hall coefficient measurements. This effect has been studied theoretically by Isenberg.[10] Although the samples studied in the present work were long enough so that no corrections were needed, within the accuracy of these measurements, it may be of interest to present some data taken on *P*-type samples to study this effect. Figure 8 shows these results. The experimental points for two *P*-type samples are seen to be well fitted by the theoretical curve.

The recent work of Haynes[11] on the drift mobility of holes and electrons is of considerable interest in the present discussion. The drift method involves measuring directly the velocity of a pulse of holes injected into *N*-type germanium, or conversely, the velocity of a pulse of electrons injected into *P*-type germanium. The most recent values of Haynes for the mobilities are:

$$\mu_e = 3500 \text{ cm}^2/\text{volt-sec.}$$
$$\mu_h = 1700 \text{ cm}^2/\text{volt-sec.}$$

It appears that the value for electrons is in good agreement to the value assigned by the author[12] on the basis of a large number of samples of both *N*- and *P*-type germanium; namely, $\mu = R/\rho \times 10^8 = 4000$ for electrons. There remains a considerable discrepancy between Haynes' value of 1700 for the hole mobility and the present author's results of 3000 cm²/volt-sec. Also, although Haynes' results for holes agree well with the value of Pearson, obtained by the Hall effect, Haynes' value of 3500 for electrons still remains considerably higher than Pearson's value of 2600 for electrons.

[10] Isenberg, Russell, and Greene, Phys. Rev. **74**, 1255(A) (1948).
[11] J. R. Haynes, Phys. Rev. **77**, 739(A) (1949).
[12] W. C. Dunlap, Jr., Phys. Rev. **77**, 759(A) (1950).

The Penetration of Particles Associated with Cosmic-Ray Stars*

C. G. MONTGOMERY, D. D. MONTGOMERY, AND J. A. NORTHROP
*Sloane Physics Laboratory, Yale University,** New Haven, Connecticut*
(Received April 10, 1950)

A survey was made at Climax, Colorado (elevation 3510 meters) of the particles associated with nuclear explosions, of stars, which were capable of emerging from the thin-walled ionization chamber in which the stars were recorded, and of penetrating various thicknesses of lead absorber. The experiment was so designed as to distinguish between electrons and penetrating particles. It was found that in a small fraction of the nuclear events (1 to 2 percent) there were associated electrons. In some of these events there were pairs of associated rays capable of penetrating 8 inches of lead placed below the chamber. The absorption in lead was found to be exponential with a mean free path of 107 ± 30 g/cm^2.

I. INTRODUCTION

MANY cloud-chamber photographs have been published[1] in which a nuclear disintegration occurs together with the production of penetrating particles and with copious numbers of electrons and photons. It is difficult, however, to obtain from such pictures any absolute values for the rates of occurrence of such processes. Some triggering device is required to actuate the chamber and the efficiency of triggering is difficult to estimate. These high energy nuclear events can be detected also with ionization chambers, but they must be selected from nuclear events of low energy (stars) and from extensive showers. Analyses of the number of bursts of ionization caused by extensive showers have been carried out previously.[2] Bridge and Rossi[3] have selected events in which there were large numbers of electrons by using a thick lead shield above an ionization chamber. Nuclear events produced within a lead shield were detected by the resultant cascade radiation crossing the chamber. Extensive showers were recorded by counters in coincidence with the chamber. Thus the bursts of ionization measured were not caused, in most cases, by the heavily ionizing particles from the nucleus and the rate of occurrence of stars within the lead shield was not measured. The present experiment was designed to measure both stars and high energy nuclear events which occurred in the thin walls of an ionization chamber, events of the two kinds being separated by the discharges of counters below the chamber.

II. ARRANGEMENT OF APPARATUS

Figure 1 shows a sketch of the apparatus to scale. Stars were produced in the 30-mil wall of the brass ionization chamber A which was 3 inches in diameter and 10 inches long. The chamber was filled with tank argon to 60 lb./in.^{2} gauge pressure. Potential changes caused by bursts of ionization occurring within the chamber were amplified and passed through a discriminator so that pulses larger than a given size were recorded. As in the previous experiments,[2] the low collecting field near the chamber wall was insufficient to produce saturation from short-range heavily ionizing rays such as contamination alpha-particles from the wall, and these were not recorded. Particles crossing the chamber near the central electrode encountered high fields and were recorded. The discriminator level and amplifier gain were set so that approximately 100 bursts per hour were counted, corresponding to sizes greater than 1.6×10^5 ion pairs. Variations in the rates observed were caused by changes in the amplifier gain and in the condition of purity of the gas. Since relative rates only were considered important, no special attempt was made to secure absolutely constant conditions. Because of these changes in the purity of the gas, some contamination alpha-particles may have been counted as stars. The observed coincidences with the counters, however, could not have been the result of alpha-particles.

Bursts in the chamber A were recorded in coincidence with the discharges of three arrays of counters.

(a) A row of 6 counters B, each 16 inches long and 1 inch in diameter, was placed 3.3 inches below the chamber axis. Between the chamber and the counters B small thicknesses of lead, up to 1 inch, could be inserted. The B counters were utilized in two ways. In some runs alternate counters were connected together

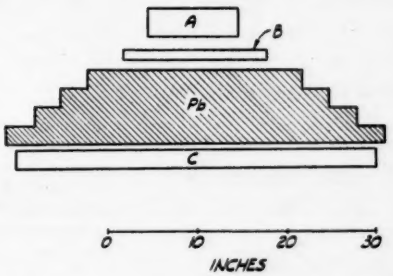

FIG. 1. Scale diagram of apparatus. The ionization chamber is A, B represents the active area of a tray of 7 counters, and C a tray of 6 counters.

* Part of a dissertation to be presented by J. A. Northrop for the degree of Doctor of Philosophy, Yale University.
** Assisted by the joint program of the ONR and the AEC.
[1] For example, W. B. Fretter, Phys. Rev. **76**, 511 (1949); C. Y. Chao, Phys. Rev. **75**, 581 (1949).
[2] C. G. Montgomery and D. D. Montgomery, Phys. Rev. **72**, 131 (1947), **76**, 1482 (1949); Bridge, Hazen, Rossi, and Williams, Phys. Rev. **74**, 1083 (1948).
[3] H. S. Bridge and B. Rossi, Phys. Rev. **75**, 810 (1949).

and twofold coincidences between the two groups were recorded. In other runs, the B counters were connected in three groups and threefold coincidences were recorded.

(b) A second row of 6 counters C, each 40 inches long and 2 inches in diameter, was placed 14.8 inches below the chamber axis. Between the chamber A and the C counters lead blocks up to a thickness of 8 inches could be inserted. Alternate C counters were connected together and twofold coincidences were recorded.

(c) A set of 8 counters D, each 8 inches long and $1\frac{5}{8}$ inches in diameter, was placed about 50 cm from the center of the chamber in a horizontal array. These counters were connected in three groups, two groups of three counters and one of two, and triple coincidences were measured among the groups.

Pulses from these arrays of counters were combined, by a set of adding diodes, with pulses from the ion chamber and the following coincidences were recorded: A, AB, ABC, ABD, $ABCD$, BC, and BD. Since the rise-times of the chamber pulses were limited by the amplifiers to about 100 μsec., the counter pulses were lengthened by means of multivibrators to 250 μsec. This period represents the resolving time of the equipment. Accidental coincidences in the AB rate were not negligible and the necessary corrections have been made. No corrections for accidental coincidences in the other rates were necessary.

III. OBSERVATIONS WITH SMALL THICKNESSES OF LEAD

The coincidence of a shower recorded by the D counters and a burst of ionization in the chamber A was taken to indicate that the event observed was associated with an extensive shower. Such a shower could result in a sufficient number of electrons (about 30) crossing the chamber to be recorded. The B counters would then also be discharged. Extensive showers of this kind were measured in the same chamber at Climax in the summer of 1948. The ABD and $ABCD$ rates

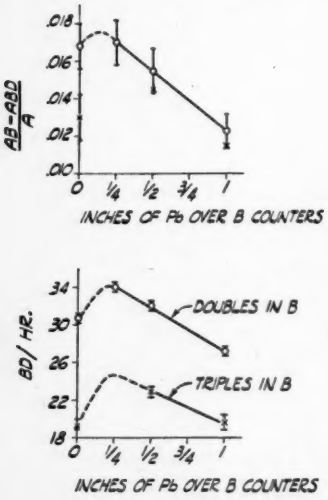

FIG. 2. (a) Fraction of stars containing particles emerging from the chamber as a function of lead over B counters. The circles represent twofold coincidences, the crosses threefold coincidences. (b) The transition curve for extensive showers as measured by BD coincidences.

TABLE I. Rates of occurrence of coincidences of the ion chamber A with the counter tray B.

Lead over B counters	Doubles in B			Triples in B		
	$\frac{AB}{A}$	$\frac{ABD}{A}$	$\frac{AB-ABD}{A}$	$\frac{AB}{A}$	$\frac{ABD}{A}$	$\frac{AB-ABD}{A}$
0	0.0201 ±0.0012	0.0033 ±0.0005	0.0168 ±0.0012	0.0216 ±0.0015	0.0086 ±0.0010	0.0130 ±0.0012
$\frac{1}{4}$	0.0199 ±0.0013	0.0029 ±0.0005	0.0170 ±0.0012	—	—	—
$\frac{1}{2}$	0.0188 ±0.0012	0.0032 ±0.0005	0.0155 ±0.0012	0.0184 ±0.0021	0.0039 ±0.0008	0.0145 ±0.0014
1	0.0159 ±0.0010	0.0036 ±0.0005	0.0123 ±0.0009	0.0170 ±0.0023	0.0055 ±0.0013	0.0115 ±0.0018

measured in the present experiment, which were approximately equal with no absorber present, agree well with the extensive showers measured previously.

Coincidences AB which were not accompanied by a discharge of the D counters (AB–ABD) could be caused by, (1) stars with particles emerging from the chamber and passing through the absorber over B, with or without multiplication, and discharging the B counters, or (2) stars in A accompanied by groups of a small number of particles, probably electrons, arriving with the star-producing radiation and passing through the B counters.

The observations are summarized in Table I. Corrections of the AB rates have been made. Figure 2a shows the variation in the AB rate corrected for extensive showers as the amount of absorber over B was changed. Because the rate was low, the data for all thicknesses of lead over the C counters have been combined in plotting this curve, although there may be a small effect of this lead because of particles produced in it traveling in an upward direction into the B tray. As ordinate is plotted the quantity $(AB-ABD)/A$, the fraction of stars accompanied by the discharge of two counters in B, corrected for extensive showers. The abscissa gives the thickness of lead over B. The statistical errors shown are standard deviations. The points indicated by dots and crosses indicate, respectively, two- or threefold coincidences in the B tray. That the particles tripping the B counters are electrons is indicated by the shape of the transition curve. For com-

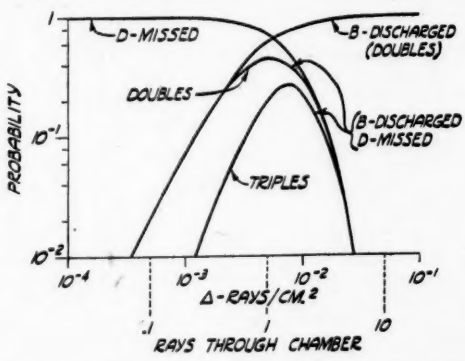

FIG. 3. Calculated probabilities for the discharges of the B and D counter trays.

parison, the observed rates BD are plotted in Fig. 2b. These events are extensive showers of the usual kind consisting of electrons and photons falling on the counters with small density.

It is to be noted that, at the maximum, only about 2 percent of the stars are accompanied by discharges of two B counters. It is difficult to assess the accuracy of this fraction. As already mentioned, it has been assumed that the ionization produced by alpha-particles from radioactive contamination in the ion-chamber walls was suppressed by negative-ion formation in the weak field near the walls. This electron capture was aided by the presence of impurities which accumulated from the chamber. Since fresh gas was added from time to time, it is possible that the alpha-particle ionization was not sufficiently reduced at times and that the alpha-particles may have contributed to the A rate. That this effect was small is indicated by a comparison of the present experiment with measurements made during the previous summer. The same ionization chamber was used, but slow amplifiers and positive-ion collection was employed. A convenient check is provided by the ratio of the rates of occurrence of extensive showers to the total burst rates in the chamber, the numbers for the present experiment being recorded in the third column of Table I. The average A rate for these data was 121 per hour. In the 1948 experiments the occurrence of coincidences between two chambers was the criterion for selection of extensive showers, a different one than employed here. The ratio corresponding to the present A rate was earlier found to be 0.0031, in close agreement with the present measurements. It therefore seems probable that the effects of alpha-particles were small.

It is instructive to consider the counter efficiencies involved in these experiments. The efficiency of the D counters for recording extensive showers depends, of course, on the density of particles in the shower. The probability that a shower with Δ rays per unit area does not discharge the D counters is given by

$$1-(1-e^{-D\Delta})^n,$$

where D is the area of each group of D counters and n the order of coincidence. For the present experiment, this probability is plotted in Fig. 3. As an auxiliary scale of abscissas is shown the number of rays crossing the chamber A corresponding to each value of Δ. Since, over the separations involved, the density is nearly constant, it is evident that all showers dense enough to be recorded in A also set off the D counters.

The probability that the B counters discharge can be calculated in a similar fashion as a function of Δ. Also the probability that a shower misses the D counters but discharges the B counters is easily found, and these curves are shown also in Fig. 3. A range of densities is seen to exist, corresponding to from 4 to 0.4 ray through the chamber, over which this probability is appreciable. Thus star-producing radiation accompanied by a few electrons could be responsible for some of the AB–ABD coincidences.

TABLE II. Rates of occurrence of coincidences with the C counters.

Lead over C counters	Doubles in B			Triples in B		
	$\frac{ABC}{AB}$	$\frac{ABCD}{AB}$	$\frac{ABC-ABCD}{AB}$	$\frac{ABC}{AB}$	$\frac{ABCD}{AB}$	$\frac{ABC-ABCD}{AB}$
0	0.515 ±0.046	0.172 ±0.023	0.344 ±0.035	0.450 ±0.085	0.135 ±0.041	0.315 ±0.068
2	0.395 ±0.046	0.199 ±0.030	0.196 ±0.030	0.469 ±0.092	0.296 ±0.069	0.173 ±0.050
4	0.275 ±0.037	0.153 ±0.026	0.122 ±0.023	0.420 ±0.062	0.336 ±0.054	0.084 ±0.024
8	0.238 ±0.053	0.200 ±0.054	0.038 ±0.019	0.180 ±0.032	0.142 ±0.028	0.038 ±0.014

To test the possibility of electrons accompanying star-producing radiation a short run was taken with the ionization chamber beside the B counters, connected for triple coincidences, instead of over them. The ratio $(AB-ABD)/A$ observed was 0.008 ± 0.002. Unfortunately the observations are too meager to allow a complete answer; accompanying electrons appear to exist A further indication of this possibility is afforded by data of Bridge and Rossi,[3] who found that a set of counters placed over a thick lead plate above an ion chamber often had several counters discharged in coincidence with the chamber even though the lead was thick enough to absorb completely any cascade radiation. An experiment designed to clarify this point is under way.

IV. OBSERVATIONS WITH LARGE THICKNESSES OF LEAD

The observations of coincidences between the chamber and the C counters can also be accounted for by two possibilities. The coincidences ABC–$ABCD$ could be caused by (1) stars in A from which emerge at least two rays capable of traversing the lead over B and C, or (2) the production of stars in A simultaneously with the appearance of associated rays that trip the B and C counters. The observations with C coincidences are given in Table II. Figure 4a shows the effect of lead placed over the C counters. The data have been averaged over all the (small) thicknesses of B lead so that each point corresponds to a total thickness of lead between zero and one inch greater than the value of the abscissa. To minimize the effects of the B lead in increasing the AB rates (transition effect), the quantity plotted as ordinate is $(ABC-ABCD)/AB$. It was necessary to combine the data in this way to obtain as satisfactory statistics as possible, since the counting rates were very low indeed, one per hour or less.

Under 8 inches of lead the number of stars associated with penetrating particles corrected for extensive showers is about 3.5 percent of the AB rate. Thus, at most, only 0.02 percent of the stars have at least two emerging particles capable of penetrating 8 inches of lead. Two sets of data are shown on the curve. The dots represent data taken with twofold coincidences in B

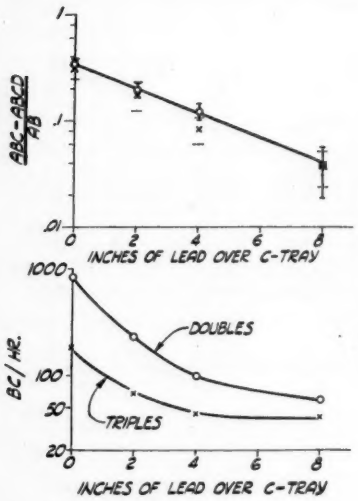

FIG. 4. (a) The absorption of penetrating rays in the lead over the *C* counters. The circles and crosses represent two- and threefold coincidences, respectively, in the *B* tray. (b) The absorption of shower rays not associated with bursts in the ionization chamber.

and with the *C* counters shielded on the sides by 4 inches of lead at all times, the crosses represent data taken with threefold coincidences in *B* and without the lead shield at the sides of *C*. The two sets of points fit one straight line on the semilogarithmic plot within the statistical errors shown. This agreement may indicate either, (1) that a relatively large number of rays cross the tray of *B* counters and the number of side showers is relatively unimportant, or (2) that there is compensation between these two effects. In any event, it is not profitable to discuss probability relations involving discharges of the *C* counters since we do not know enough about the angular distributions of the shower rays and other geometrical factors.

The slope of the line in Fig. 4 corresponds to a mean free path for absorption of 107 ± 30 g/cm^2. If the particles are protons, the mean energy must be at least 310 Mev. If μ-mesons are involved, the corresponding energy is 150 Mev; for π-mesons, the value is somewhat larger. Thus all these energies are of the same order of magnitude. Electrons would, of course, have to have much higher energies.

For comparison, in Fig. 4b is plotted the absorption curve obtained from the *BC* coincidences in the present experiment with no lead over the *B* counters. These coincidences presumably represent narrow showers[4] made up of a soft component, presumably electrons, and a hard one which is evident from the flatter portion of the curve from 4 to 8 inches of lead. The absorption curve of the events represented by the *ABC* coincidences has quite a different shape.

The exponential shape of the burst absorption curve does not allow a distinction between protons and mesons as the penetrating particles in a burst. Moreover, since star production is often a cascade process,[1] the mean free path is not directly related to the range of the penetrating particles. The mean free path corresponding to the geometrical cross section of the lead nucleus is about 160 g/cm^2.

The authors wish to express their appreciation to Professor Marcel Schein of the University of Chicago for the use of the facilities of the University of Chicago High Altitude Laboratory, and to Mr. C. J. Abrams of the Climax Molybdenum Company for his cooperation and hospitality.

[4] J. Wei and C. G. Montgomery, Phys. Rev. **76**, 1488 (1949); J. P. N. Wei (to be published).

Asymptotic Expression for the Stopping Power of K-Electrons

L. M. BROWN
Laboratory of Nuclear Studies, Cornell University, Ithaca, New York
(Received March 13, 1950)

An asymptotic form for the high energy stopping number of K-electrons (for any element) is determined by using the Born approximation expressions for the excitation and ionization probabilities of the K shell. The stopping number takes the form $B_K(\theta,\eta)=A(\theta)\ln\eta+B(\theta)+C(\theta)(1/\eta)+\cdots$, where η is a dimensionless quantity proportional to the energy of the incident particle and θ is proportional to the observed ionization energy of the K shell. Other results include the stopping number for hydrogen, obtained by sum-rule methods, to order $(1/\eta)$, and results of M. C. Walske, obtained by numerical methods, for the low energy stopping number of K-electrons.

I. INTRODUCTION

THE stopping power formula of Bethe[1] is valid without correction only if $E\gg(M/m)E_{el}$ for each electron in the atom; here E_{el} is the ionization potential of an electron in the atom, m the electronic mass, E and M the energy and mass of the incident particle. For many important cases this condition is not well fulfilled, particularly for the K-electrons of the heavier elements, and it is useful therefore to obtain separately the contribution of the K-electrons, in order that the formula can be corrected.[2]

Curves for the stopping number, B_K, of the K-electrons have already been published in reference 1, and this new calculation of an asymptotic expression for large incident energies is undertaken to provide more accurate results in this energy region and to extend the former results to heavier elements.

II. GENERAL THEORY

If we measure all energies in units of the "ideal ionization potential" of the K shell, Z_{eff}^2Ry, the contribution to the stopping number due to excitation of K-electrons is[1]

$$B_K=\int_\theta^{\epsilon_{max}}\epsilon d\epsilon\int_{Q_{min}}^{Q_{max}}\frac{dQ}{Q^2}|F_n(Q)|^2, \qquad (1)$$

where $\epsilon=E_n-E_1$ is the energy given to the atomic electron, $Q=(\mathbf{p}-\mathbf{p}')^2/2m$, $\mathbf{p}$ and $\mathbf{p}'$ being the momenta of the incident particle before and after the collision, $Q_{min}=\epsilon^2/4\eta$ is the smallest possible value of Q for a given ϵ, $Q_{max}=4\eta$, with $\eta=mv^2/2$, v being the velocity of the incident particle. The minimum energy transferable to a K-electron, θ, is the observed ionization energy of the K shell.

If we use hydrogenic wave functions for the evaluation of the form factor $F_n(Q)$, the contribution which arises from the continuum states $\epsilon>1$ will be the same (in our units) as the continuum contribution in the case of hydrogen. The integral over ϵ from θ to 1 will be evaluated using the excitation functions for hydrogen; however, the principal quantum number, n, of the excited state must be allowed to vary continuously.

The asymptotic expression for B_K will be obtained as an expansion in η which will take the form

$$B_K(\theta,\eta)=A(\theta)\ln\eta+B(\theta)+C(\theta)(1/\eta)+\cdots \qquad (2)$$

and we shall obtain A, B, and C.

The work will consist of several parts: (a) The excitation function

$$\Phi_n=\kappa\int_{Q_{min}}^{Q_{max}}\frac{dQ}{Q^2}|F_n(Q)|^2, \quad \kappa=\frac{2\pi e^4z^2}{mv^2}, \qquad (3)$$

will first be evaluated for discrete, non-integral, values of n. It will be shown that the η-dependence arising from the upper limit occurs first in $O(1/\eta^5)$ and that the integral may therefore be extended to ∞ and the η-dependence, $A(\theta)$ and $C(\theta)$ in Eq. (2), obtained from a small Q approximation. (b) An asymptotic expansion of Φ_n for large n will be obtained, which will be useful for $n>5$. (c) The integration over ϵ will be performed to obtain the contribution of the states $\theta\leqq\epsilon\leqq1$ to B_K. (d) The total stopping power of hydrogen will be found, by sum-rule methods, to order $1/\eta$. (e) The contribution of the discrete states to B_K for hydrogen will be found. This will be subtracted from the total B_K for hydrogen, obtained by sum-rule methods, and the continuum contribution will thus be obtained. This will be added to the result of Section V for several values of θ, and will constitute our final result.

III. EXCITATION FUNCTION

The excitation function for a hydrogen-like atom is[3]

$$\Phi_n=\frac{2^8\kappa}{n^3}\int_{Q_{min}}^{Q_{max}}\frac{dQ}{Q}[\tfrac{1}{3}(1-1/n^2)+Q]\times\frac{[(1-1/n)^2+Q]^{n-3}}{[(1+1/n)^2+Q]^{n+3}}. \qquad (4)$$

[1] For a general discussion of the stopping power theory to which this paper is a supplement, see M. S. Livingston and H. A. Bethe, Rev. Mod. Phys. 9, 263–265 (1937).

[2] J. O. Hirschfelder and J. L. Magee, Phys. Rev. 73, 207 (1948) have used the previously published (reference 1) stopping power for K-electrons, modifying it for the L, M, etc. shells, to construct directly, shell by shell, the stopping power of a number of substances for low energy protons.

[3] H. A. Bethe, *Handbuch der Physik* (1933), Vol. 24, p. 507.

We shall write this as

$$\Phi_n = A_n\psi_1 + B_n\psi_2 \tag{5}$$

with

$$\psi_1 = \int_{Q_{\min}}^{Q_{\max}} \frac{dQ}{Q}\frac{(a+Q)^{n-3}}{(b+Q)^{n+3}},$$

$$\psi_2 = \int_{Q_{\min}}^{Q_{\max}} dQ\frac{(a+Q)^{n-3}}{(b+Q)^{n+3}}, \tag{5a}$$

$$A_n = (2^8\kappa/3n^3)(1-1/n^2), \quad B_n = 2^8\kappa/n^3,$$

$$a = (1-1/n)^2, \quad b = (1+1/n)^2. \tag{5b}$$

We now examine the limits of integration. For a fixed value of $\epsilon = E_n - E_1$,

$$2M\epsilon = \mathbf{p}^2 - \mathbf{p}'^2 = (\mathbf{p}-\mathbf{p}')\cdot(\mathbf{p}+\mathbf{p}').$$

If we let $q_{\min} = p - p'$, with $p = |\mathbf{p}|$, then

$$q_{\min} = \frac{p^2-p'^2}{p+p'} = \frac{2M\epsilon}{2p-q_{\min}} \approx \frac{\epsilon}{v}\left(1+\frac{q_{\min}}{2p}\right) = \frac{\epsilon}{v}(1+\epsilon/2pv).$$

Thus $Q_{\min} = q_{\min}^2/2m = \epsilon^2/4\eta$; the next term, being of relative order $\epsilon(m/M)(1/\eta)$, has been neglected. For the upper limit, $Q_{\max}$, we may take the maximum energy which a heavy particle can transfer to a free electron, namely, $2mv^2 = 4\eta$. We may note, however, that if we take $Q_{\max}$ to be infinite we make an error in ψ_2 of

$$\int_{4\eta}^{\infty} \frac{dQ}{Q^6}\frac{(1+a/Q)^{n-3}}{(1+b/Q)^{n+3}} = \int_{4\eta}^{\infty}\frac{dQ}{Q^6}[1+O(1/Q)] = O(1/\eta^5).$$

Similarly, the error in ψ_1 is $O(1/\eta^6)$. Since we wish to compute only to order $1/\eta$, we may take $Q_{\max} = \infty$.

For the above reason, assuming η to be large, we can obtain the η-dependence of Φ_n by expanding the integrand for small Q.

$$\psi_2 = \int_{Q_{\min}} dQ\frac{(a+Q)^{n-3}}{(b+Q)^{n+3}}$$

$$= \frac{a^{n-3}}{b^{n+3}}\int_{Q_{\min}} dQ\frac{(1+Q/a)^{n-3}}{(1+Q/b)^{n+3}}$$

$$= \frac{a^{n-3}}{b^{n+3}}\int_{Q_{\min}} dQ\left\{1+Q\left[n\left(\frac{1}{a}-\frac{1}{b}\right)-3\left(\frac{1}{a}+\frac{1}{b}\right)\right]+\cdots\right\},$$

$$B_n\psi_2/\kappa = \frac{2^8}{n^3}\frac{a^{n-3}}{b^{n+3}}[\text{const.} - Q_{\min}]$$

$$= |x_{0n}|^2\{\text{const.} - 3(1-1/n^2)/4\eta\} \tag{6}$$

where x_{0n} is the dipole moment,[3]

$$|x_{0n}|^2 = [2^8n^7(n-1)^{2n-5}]/[3(n+1)^{2n+5}]. \tag{7}$$

Similarly,

$$\psi_1 = \int_{Q_{\min}} \frac{dQ}{Q}\frac{(a+Q)^{n-3}}{(b+Q)^{n+3}}$$

$$= \frac{a^{n-3}}{b^{n+3}}\{\text{const.} - \ln Q_{\min} + 2Q_{\min}n^2(n^2+3)/(n^2-1)^2\},$$

$$A_n\psi_1/\kappa = |x_{0n}|^2\{\text{const.} + \ln\eta + 2(1+3/n^2)/4\eta\}. \tag{8}$$

Combining (6) and (8), according to (5), and denoting the constant by $G(n)$, we obtain the result

$$\Phi_n/\kappa = |x_{0n}|^2\{G(n) + \ln\eta - (1-9/n^2)/4\eta\}. \tag{9}$$

Expression (9) is valid for any value of n, and there remains the evaluation of the part independent of η, $|x_{0n}|^2G(n)$. This is somewhat lengthy as no approximations can be made concerning Q in the integrand. We can, however, set $Q_{\max} = \infty$.

Introduce the variable

$$z = Q/\gamma(b+Q),$$

with

$$\gamma = (n-1)^2/4n.$$

$$dQ = \gamma b\,dz/(1-\gamma z)^2, \quad dQ/Q = dz/z(1-\gamma z),$$
$$1+Q/b = 1/(1-\gamma z), \quad 1+Q/a = (1+z)/(1-\gamma z).$$

Equation (4) becomes

$$\Phi_n/\kappa = |x_{0n}|^2\int_{Q_{\min}}^{\infty}\frac{dQ}{Q}[1+3Q/(ab)^{\frac{1}{2}}]\frac{(1+Q/a)^{n-3}}{(1+Q/b)^{n+3}}$$

$$= |x_{0n}|^2\left\{\int_{z_0}^{1/\gamma}\frac{dz}{z}(1-\gamma z)^5(1+z)^{n-3} + 3[\gamma(\gamma+1)]^{\frac{1}{2}}\int_{z_0}^{1/\gamma} dz(1-\gamma z)^4(1+z)^{n-3}\right\}, \tag{10}$$

with $z_0 = Q_{\min}/\gamma(b+Q_{\min}) \ll 1$.

Let

$$L_k(n) = \int_{z_0}^{1/\gamma} dz(1-\gamma z)^k(1+z)^{n-3},$$

$$M_n = \int_{z_0}^{1/\gamma}(1+z)^{n-3}dz/z. \tag{11}$$

Then, as

$$(1-\gamma z)^5 - 1 = -\gamma z\sum_{k=0}^{4}(1-\gamma z)^k,$$

$$\int_{z_0}^{1/\gamma}(1-\gamma z)^5(1+z)^{n-3}dz/z = M_n - \gamma\sum_{k=0}^{4}L_k(n),$$

and

$$\Phi_n/\kappa = |x_{0n}|^2\{M_n + 3[\gamma(\gamma+1)]^{\frac{1}{2}}L_4(n) - \gamma\sum_{k=0}^{4}L_k(n)\}. \tag{12}$$

In $L_k(n)$, the lower limit can now be replaced by zero. Integrating repeatedly by parts we obtain,

$$L_k(n)=\frac{(1+z)^{n-2}}{(n-2)}\Big\{(1-\gamma z)^k + \frac{\gamma k}{(n-1)}(1-\gamma z)^{k-1}(1+z)+\cdots + \frac{\gamma^k k!(1+z)^k}{(n-1)n\cdots(n-2+k)}\Big\}\Big|_0^{1/\gamma}$$

$$-L_k(n)=\frac{1}{(n-2)}+\frac{k\gamma}{(n-2)(n-1)}+\cdots + \frac{k!\gamma^k[1-(1+1/\gamma)^{n-2+k}]}{(n-2)(n-1)\cdots(n-2+k)}.$$

Thus the result for Φ_n/κ, apart from the η-dependence, is

$$\Phi_n/\kappa=|x_{0n}|^2\{M_n-3[\gamma(\gamma+1)]^{\frac{1}{2}}f_1(n) +5\gamma f_2(n)-\gamma(1+1/\gamma)^{n-2}f_3(n)] \quad (13)$$

where

$$f_1(n)=-L_4(n)=\frac{1}{n-2}\Big\{1+\frac{4\gamma}{(n-1)}+\frac{12\gamma^2}{(n-1)n} +\frac{24\gamma^3}{(n-1)n(n+1)}+\frac{24\gamma^4[1-(1+1/\gamma)^{n+2}]}{(n-1)n(n+1)(n+2)}\Big\}, \quad (13a)$$

$$f_2(n)=\frac{1}{n-1}\Big\{1+\frac{2\gamma}{(n-1)}+\frac{4\gamma^2}{(n-1)n} +\frac{6\gamma^3}{(n-1)n(n+1)}+\frac{24}{5}\frac{\gamma^4}{(n-1)n(n+1)(n+2)}\Big\}, \quad (13b)$$

$$f_3(n)=\frac{1}{n-2}\Big\{1+\frac{(1+\gamma)}{(n-1)}+\frac{2(1+\gamma)^2}{(n-1)n} +\frac{6(1+\gamma)^3}{(n-1)n(n+1)}+\frac{24(1+\gamma)^4}{(n-1)n(n+1)(n+2)}\Big\}. \quad (13c)$$

Unfortunately, the integral M_n can be calculated exactly only for certain discrete values of n. A tabulation of the numerical value of the part of M_n which is independent of η is given in Table I for those values of n for which M_n was integrated in closed form.

Bethe[3] gives expressions for Φ_n for $n=2$, 3, 4, 5. These have been evaluated and the numerical results for $|x_{0n}|^2$, and for the part of Φ_n which is independent of η, are given also in Table I.

The constant part of Φ_n/κ (the term independent of η) may be represented within 0.1 percent in the range $1.75\leqq n\leqq 5$ by the expression

$$|x_{0n}|^2G(n)=2.31197(1/n^3)+3.17662(1/n^5) +0.75111(1/n^7)+7.3743(1/n^9)-54.117(1/n^{11}) \quad (14)$$

IV. ASYMPTOTIC EXPANSION OF Φ_n

Expression (9) for Φ_n is valid for any bound excited state, and $G(n)$ has been determined for $n\leqq 5$. In this part of the work we will get an asymptotic expression for $G(n)$ which will be useful for $n>5$.

We write Eq. (4) in the form

$$\Phi_n/\kappa=\frac{2^8}{n^3}\int_{Q_{\min}}^{Q_{\max}}\frac{dQ}{Q}\frac{(1-1/n^2)/3+Q}{[(1-1/n)^2+Q]^3[(1+1/n)^2+Q]^3} \times\Big[\frac{(1-1/n)^2+Q}{(1+1/n)^2+Q}\Big]^n. \quad (15)$$

The last factor in the integral of (15) can be expanded for large values of n as

$$[1+4(Q-\tfrac{1}{3})/n^2(1+Q)^3]e^{-4/(1+Q)}.$$

Expanding also the remaining factors of the integrand we obtain

$$\Phi_n/\kappa=\frac{2^8}{n^3}\int_{Q_{\min}}^{Q_{\max}}\frac{dQ}{Q}\frac{Q+\frac{1}{3}}{(1+Q)^6}e^{-4/(1+Q)} +\frac{2^8}{3n^5}\int_{Q_{\min}}^{Q_{\max}}\frac{dQ}{Q} \times\frac{-19Q^3+3Q^2+15Q+11/3}{(1+Q)^9}e^{-4/(1+Q)}. \quad (16)$$

If we now make the substitutions $y=1/(1+Q)$, $y_0=1/(1+Q_{\min})$, $y_1=1/(1+Q_{\max})$, we get, after some simplification:

$$\Phi_n/\kappa=\frac{2^8}{3n^3}\int_{y_1}^{y_0}y^4e^{-4y}dy[2+1/(1-y)] +\frac{2^8}{9n^5}\int_{y_1}^{y_0}y^5e^{-4y}dy \times[-32y^2+112y-68+11/(1-y)]. \quad (17)$$

TABLE I. Calculated values of several quantities.

n	M_n	$\lvert x_{0n}\rvert^2$	$G(n)$	$\lvert x_{0n}\rvert^2G(n)$
1.75	0.177425	1.217489	0.470380	0.572682
2.00		0.554929	0.689255	0.382488
2.25	0.979248	0.305527	0.845516	0.258328
2.50	1.38629	0.188806	0.960383	0.181326
3.00		0.088989	1.113891	0.099124
3.50	2.98629	0.049766	1.208570	0.060145
4.00		0.030924	1.270918	0.039302
4.50	4.44946	0.020644	1.314077	0.027128
5.00		0.014519	1.345081	0.019529

Letting

$$I_k=\int_{y_1}^{y_0} y^k e^{-4y}dy \quad \text{and} \quad R=\int_{y_1}^{y_0} e^{-4y}dy/(1-y),$$

we note that

$$\int_{y_1}^{y_0} y^k e^{-4y}dy/(1-y)=\int_{y_1}^{y_0} (y^k-1)e^{-4y}dy/(1-y)+R,$$

and

$$(y^k-1)/(1-y)=-\sum_{l=0}^{k-1} y^l.$$

Thus

$$\int_{y_1}^{y_0} y^k e^{-4y}dy/(1-y)=R-\sum_{l=0}^{k-1} I_l,$$

and

$$\Phi_n/\kappa=\frac{2^8}{3n^3}\{2I_4-\sum_{l=0}^{3} I_l+R\}$$

$$+\frac{2^8}{9n^5}\{-32I_7+112I_6-68I_5-11\sum_{l=0}^{4} I_l+11R\}. \quad (18)$$

The integrals I_k are elementary, and the integral R can be evaluated, giving

$$R=-e^{-4}[Ei(4(1-y_0))-Ei(4(1-y_1))].$$

Keeping terms to relative order $1/n^2$, the final expression for n large becomes:

$$|x_{0n}|^2n^3G(n)=2.31197+3.17662(1/n^2). \quad (19)$$

This agrees with the results obtained in Section III, Eq. (14) to order $1/n^2$ and agrees with the exact result, given in Table I, for $n=5$ within 0.1 percent.

V. CONTINUOUS SPECTRUM CONTRIBUTION TO B_K

We will now obtain the contribution to B_K of the part of the continuous spectrum between θ and 1. This is given by

$$D_K(\theta)=\frac{1}{\kappa}\int_{\theta}^{1} \epsilon d\epsilon\Phi_n(\epsilon)=\frac{1}{\kappa}\int_{(1-\theta)^{-\frac{1}{2}}}^{\infty} (1-1/n^2)\Phi_n dn. \quad (20)$$

Φ_n is given by (9) with $|x_{0n}|^2$ defined by (7); $G(n)$ is given by (14) for $1.75\leqq n\leqq 5$, and by the first two terms of (14) for $n>5$. To perform the integration for the $\ln\eta$ and the $1/\eta$-terms it is convenient to expand $|x_{0n}|^2$ to order $1/n^{10}$ as follows:

$$n^3|x_{0n}|^2=1.56294+5.73076(1/n^2)+13.1634(1/n^4)$$
$$+24.2952(1/n^6)+39.4260(1/n^8)+58.8077(1/n^{10}). \quad (21)$$

We obtain, finally,

$$\begin{aligned}D_K(\theta)=&[1.15599(1-\theta)+1.37215(1-\theta)^2\\&+0.654622(1-\theta)^3+1.01568(1-\theta)^4\\&-4.67429(1-\theta)^5+4.50977(1-\theta)^6]\\&+\ln\eta[0.781468(1-\theta)+1.04196(1-\theta)^2\\&+1.23877(1-\theta)^3+1.39148(1-\theta)^4\\&+1.51307(1-\theta)^5+1.61515(1-\theta)^6]\\&-(1/\eta)[0.195367(1-\theta)-0.618662(1-\theta)^2\\&-1.25324(1-\theta)^3-1.74256(1-\theta)^4\\&-2.12640(1-\theta)^5-2.43323(1-\theta)^6], \quad (22)\end{aligned}$$

from which

$$\begin{aligned}D_K(0.7)&=0.377789\ln\eta+0.488121+0.051963(1/\eta)\\D_K(0.75)&=0.287153\ln\eta+0.385488+0.018884(1/\eta)\\D_K(0.8)&=0.210696\ln\eta+0.291738-0.000677(1/\eta)\\D_K(0.9)&=0.089961\ln\eta+0.130034-0.011899(1/\eta).\end{aligned} \quad (23)$$

VI. TOTAL STOPPING POWER OF HYDROGEN

We now obtain the total stopping number of hydrogen to order $1/\eta$. Following the method of Bethe,[4] we break the stopping number

$$B_H=\sum_{\substack{\text{all}\\\text{states}}} (E_n-E_1)\int_{q_{\min}}^{q_{\max}}\frac{dQ}{Q^2}|F_n(Q)|^2 \quad (24)$$

into two parts (introducing $q^2=Q$) as follows:

$$B_H=2\int_{q_0}^{q_{\max}}\frac{dq}{q^3}\sum_n|F_n(q)|^2(E_n-E_1)$$
$$-2\sum_n\int_{q_0}^{q_{\min(n)}}\frac{dq}{q^3}|F_n(q)|^2(E_n-E_1) \quad (25)$$

where q_0 may be chosen arbitrarily, and will be taken to be small. In the first term, integration and summation have been interchanged, as q_0 and $q_{\max}$ are independent of n. Bethe[5] has shown that

$$\sum_n|F_n(q)|^2(E_n-E_1)=q^2,$$

so that the first term can be integrated directly giving $2\ln(q_{\max}/q_0)$.

To evaluate the second term in (25), expand $\varphi_n(q^2)=(E_n-E_1)|F_n(q)|^2/q^2$ about zero in Taylor's series, getting

$$\varphi_n(q^2)\approx\varphi_n(0)+q^2(d/dq^2)\varphi_n(q^2)|_{q^2=0}. \quad (26)$$

The second term in (25) then becomes

$$-2\sum_n\varphi_n(0)\ln(q_{\min}/q_0)-\sum_n q_{\min}{}^2(d\varphi_n/dq^2)|_{q^2=0}.$$

[4] Reference 3, p. 520.
[5] H. A. Bethe, Ann. d. Physik 5, 325 (1930).

As $q_{\min}^2=(E_n-E_1)^2/4\eta$, we must evaluate the sum

$$\sum_n(E_n-E_1)^3\frac{d}{dq^2}\frac{|F_n(q)|^2}{q^2}=\sum_n(E_n-E_1)^3\frac{d}{dq^2}\frac{|(e^{iqx})_{1n}|^2}{q^2}. \tag{27}$$

With Hamiltonian H and wave functions ψ_n,

$$(E_n-E_1)\int e^{iqx}\psi_n^*\psi_1 d\tau=(He^{iqx}-e^{iqx}H)_{1n}=\{e^{iqx}[q^2-2iq(\partial/\partial x)]\}_{1n}=K_{1n},$$

(using atomic units throughout), and

$$(E_n-E_1)^2\int e^{iqx}\psi_n^*\psi_1 d\tau=(HK-KH)_{1n},$$

$$HK-KH=[H, e^{iqx}][q^2-2iq(\partial/\partial x)]+e^{iqx}[H, q^2-2iq(\partial/\partial x)]=e^{iqx}[q^2-2iq(\partial/\partial x)]^2+2iqe^{iqx}(\partial V/\partial x).$$

Thus,

$$(E_n-E_1)^3\left|\int e^{iqx}\psi_n^*\psi_1 d\tau\right|^2=\left\{\int\psi_1^*[q^2-2iq(\partial/\partial x)]e^{-iqx}\psi_n d\tau\right\}\left\{\int\psi_n^*e^{iqx}\{[q^2-2iq(\partial/\partial x)]^2+2iq(\partial V/\partial x)\}\psi_1 d\tau\right\}.$$

Making use of closure,

$$\sum_n(E_n-E_1)^3|(e^{iqx})_{1n}|^2=\int\psi_1^*[q^2-2iq(\partial/\partial x)]\{[q^2-2iq(\partial/\partial x)]^2+2iq(\partial V/\partial x)\}\psi_1 d\tau.$$

We obtain, finally,

$$-\sum_n(E_n-E_1)^3|(e^{iqx})_{1n}|^2=-q^6+4q^4\langle\nabla^2\rangle_{11}-2iq^3\langle\partial V/\partial x\rangle_{11}-(4/3)q^2\langle\nabla^2V\rangle_{11}-4q^2\langle(\partial V/\partial x)(\partial/\partial x)\rangle_{11}. \tag{28}$$

These expectation values can be obtained easily, giving,

$$\langle\nabla^2\rangle_{11}=-1,\quad\langle\nabla^2V\rangle_{11}=8,\quad\left\langle\frac{\partial V}{\partial x}\frac{\partial}{\partial x}\right\rangle_{11}=-\frac{4}{3},\quad\left\langle\frac{\partial V}{\partial x}\right\rangle_{11}=0,$$

and thus

$$(1/q^2)\sum_n(E_n-E_1)^3|(e^{iqx})_{1n}|^2=+q^4+4q^2+16/3, \tag{29}$$

$$\sum_n q_{\min}^2(d\varphi_n/dq^2)|_{q^2=0}=1/\eta, \tag{30}$$

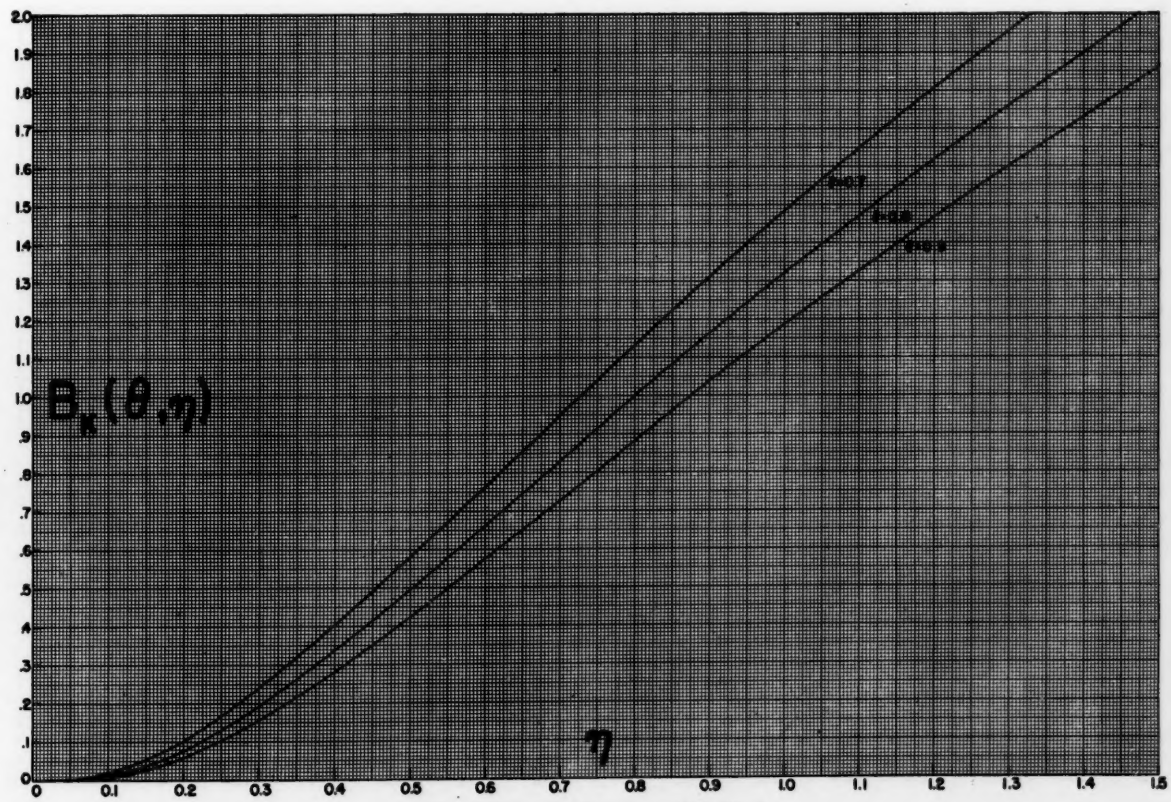

FIG. 1. Parametric curves of $B_K(\theta, \eta)$.

and

$$B_H=2\ln(4\eta)^{\frac{1}{2}}q_{\max}-1/\eta-2\textstyle\sum_n\varphi_n(0)\ln(1-1/n^2). \tag{31}$$

The last sum in (31) has been evaluated numerically (observe that $\varphi_n(0)=|x_{0n}|^2(1-1/n^2)$) and is equal to 0.096990. We set $q_{\max}=(4\eta)^{\frac{1}{2}}$ in (31), and obtain, finally,

$$B_H=2\ln\eta+2.57861-1/\eta. \tag{32}$$

VII. CONTRIBUTION OF DISCRETE STATES TO B_K FOR HYDROGEN

We next obtain the contribution of the discrete states to the asymptotic stopping number of hydrogen; this is given by $\sum_{\substack{\text{discrete}\\ \text{states}}}(1-1/n^2)\Phi_n/\kappa$. Bethe[3] gives formulas for Φ_n for $n=2, 3, 4, 5$ which we have evaluated, and which agree with (9). These give

$$\begin{aligned}\Phi_2/\kappa&=0.554929\ln\eta+0.382488+0.173415(1/\eta),\\ \Phi_3/\kappa&=0.0889893\ln\eta+0.0991244,\\ \Phi_4/\kappa&=0.0309238\ln\eta+0.0393016-0.0033823(1/\eta),\\ \Phi_5/\kappa&=0.0145191\ln\eta+0.0195294-0.0023231(1/\eta),\end{aligned} \tag{33}$$

$$\sum_{n=2}^{5}(1-1/n^2)\Phi_n/\kappa=0.538228\ln\eta+0.430570+0.124661(1/\eta). \tag{34}$$

For $n>5$ we approximate the sum over discrete states by an integral. For Φ_n we use the asymptotic form of (9), $|x_{0n}|^2G(n)$ being given by (19) and $|x_{0n}|^2$ by (21). The expression used

$$\begin{aligned}n^3\Phi_n/\kappa=&2.31197+3.17662(1/n^2)\\&+[1.56294+5.73076(1/n^2)+13.1634(1/n^4)]\\&\times[\ln\eta-(1-9/n^2)/4\eta]\end{aligned} \tag{35}$$

gives agreement with the exact value at $n=5$ to within 0.1 percent. The Euler-Maclaurin summation formula,

$$\sum_{n=6}^{\infty}f(n)=\int_6^{\infty}f(n)dn+f(6)/2+\Delta^1/12-\Delta^3/720+\cdots \tag{36}$$

with $f(n)=(1-1/n^2)\Phi_n/\kappa$, $\Delta^r=-f^{(r)}(6)$, gives

$$\sum_{6}^{\infty}(1-1/n^2)\Phi_n/\kappa=0.026778\ln\eta+0.038120-0.0057038(1/\eta). \tag{37}$$

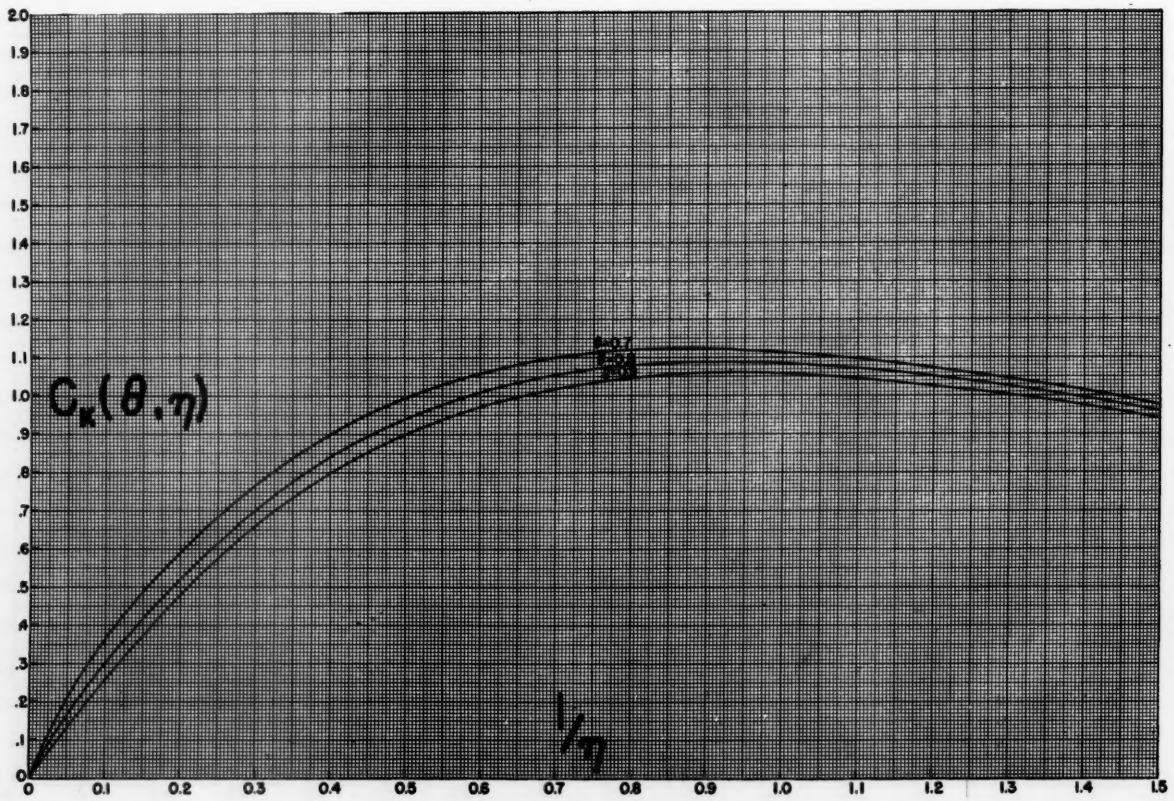

FIG. 2. Parametric curves of $C_K(\theta, \eta)$.

The error in approximating the sum by (36) is better than 0.01 percent.

The contribution of the discrete states to the hydrogen stopping number is thus, adding (34) and (37),

$$\sum_{2}^{\infty}(1-1/n^2)\Phi_n/\kappa=0.565006\ln\eta +0.468690+0.118957(1/\eta). \quad (38)$$

Subtracting this from the total stopping number (32), we obtain the continuum contribution

$$E_K=\sum_{\text{continuum}}(1-1/n^2)\Phi_n/\kappa=1.43499\ln\eta +2.10992-1.11896(1/\eta). \quad (39)$$

When (39) is added to Eq. (23), we obtain the asymptotic expression for the stopping power of K-electrons of any element, $B_K(\theta,\eta)$:

$$\begin{aligned} B_K(0.7,\eta) &= 1.81278\ln\eta+2.59804-1.06699(1/\eta),\\ B_K(0.75,\eta) &= 1.72215\ln\eta+2.49540-1.10007(1/\eta),\\ B_K(0.8,\eta) &= 1.64569\ln\eta+2.40165-1.11963(1/\eta),\\ B_K(0.9,\eta) &= 1.52495\ln\eta+2.23995-1.13085(1/\eta). \end{aligned} \quad (40)$$

VIII. RESULTS

In Fig. 1 we give the results of M. C. Walske[6] for $B_K(\theta,\eta)$ for $\theta=0.7$, 0.8, 0.9, and for $0\leqq\eta\leqq1.5$, for which, of course, the expressions (40) are not valid. These curves, having an absolute accuracy of 0.01 in B_K, were obtained from a numerical evaluation of (1), using for $|F_n(Q)|^2/Q$ expression (755) of reference 1. Walske has carried his calculations up to $\eta=10$, and for $\eta>1$ his values lie below those given by (40). As a guide to the energy region where (40) may be applied, we give in Table II the error in (40) for several values of η.

TABLE II. Percentage difference between Eq. (40) and the results of Walske.

	$\theta=0.7$	0.8	0.9
$\eta=2.5$	13.9	12.5	12.0
5	7.5	6.4	5.8
10	4.0	3.0	2.6

For large values of η it is convenient to write $B_K(\theta,\eta)$ in the form

$$B_K(\theta,\eta)=A(\theta)\ln\eta+B(\theta)-C_K(\theta,\eta), \quad (41)$$

where $-C_K(\theta,\eta)$ approaches the $1/\eta$-term in (40) as η increases. In Fig. 2 we plot $C_K(\theta,\eta)$ as a function of $(1/\eta)$.

The author wishes to thank Professor H. A. Bethe, under whose direction this work was carried out, for continued assistance and encouragement.

[6] We wish to thank Mr. Walske for making available to us his results, which have not previously been published.

PHYSICAL REVIEW VOLUME 79, NUMBER 2 JULY 15, 1950

Photo-Disintegration of Deuterium by 4.5 to 20.3 Mev X-Rays*†‡

E. G. FULLER
Physics Research Laboratory, University of Illinois, Champaign, Illinois

(Received March 31, 1950)

A study is made of the angular distributions and the distribution in energy of the photo-protons arising from the photo-disintegration of deuterium by the continuous x-ray spectrum produced when electrons accelerated in the betatron to a kinetic energy of 20.3 Mev impinged on a 0.005 in. Pt target. The collimated x-ray beam passed through a deuterium gas-filled reaction chamber in which nuclear emulsions were placed to detect the resulting photo-protons. The angular distributions for six photon energy intervals are consistent with a differential cross section in the center of mass system of the form: $\sigma(\theta)\approx a+\sin^2\theta(1+\alpha\cos\theta)$. Assuming an intensity spectrum for the betatron radiation of the shape determined by Koch and Carter a curve for the relative cross section for the photo-disintegration of deuterium as a function photon energy was determined. This curve falls off more slowly than does the Bethe-Peierls expression. The discrepancy, however, is within the experimental errors and the uncertainties in the spectrum of the betatron radiation.

I. INTRODUCTION

THE photo-disintegration process in deuterium, i.e., the process $D(\hbar\omega, n)P$, has been the subject of considerable experimental study during the last few years. Most of this work has been done with photons having energies below 3 Mev. Both the photo-neutrons[1] and the photo-protons[2] have been observed and their angular distributions studied. At these low energies both the observed angular distributions and the total cross sections[3] seem to be in general agreement with the theoretically predicted values.

* Assisted by the joint program of the ONR and the AEC.

† Part of a thesis submitted in partial fulfillment of the requirement for the degree of Doctor of Philosophy in Physics in the Graduate College of the University of Illinois.

‡ Deuterium gas obtained on allocation from the U. S. Atomic Energy Commission.

[1] B. Hammermesh and A. Wattenberg, Phys. Rev. **75**, 1290 (1949); E. P. Meiners, Phys. Rev. **76**, 259 (1949); J. Genevese, Phys. Rev. **76**, 1288 (1949).

[2] N. O. Lassen, Phys. Rev. **74**, 1533 (1948), Phys. Rev. **75**, 1099 (1949); W. M. Woodward and I. Halpern, Phys. Rev. **76**, 107 (1949).

[3] Wilson, Collie, and Haban, Nature **163**, 245 (1949); Russell, Sachs, Wattenberg, and Fields, Phys. Rev. **73**, 545 (1948); Snell, Barker, and Sternberg, Phys. Rev. **75**, 1290 (1949).

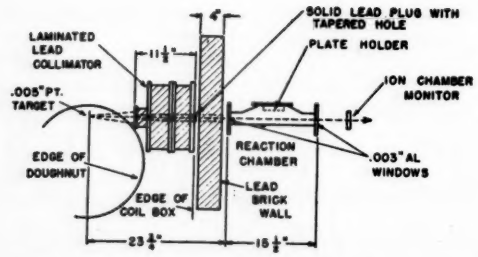

FIG. 1. Experimental arrangement. The limiting aperture for the x-ray beam was the entrance end (0.14 in. in diameter) of the tapered hold in the solid lead plug 5 in. long in the final section of the collimator. The angle of the cone of which this hole was a section was 48 minutes of arc. The full angular width of the x-ray beam was 36 minutes of arc.

Little experimental work has been done with photons having energies above three Mev. Van Allen and Smith[4] have obtained a value of 11.6×10^{-28} cm^2 for the total cross section at 6.2 Mev. As they point out, this value is considerably below any of the theoretically predicted values except that given by the Bethe-Periels expression for zero range. At this same energy Gibson, Green, and Livesy[5] have observed sixty proton tracks in deuterium-loaded emulsions. The angular distribution of these sixty tracks was compatible with a $\sin^2\theta$ distribution.[6]

Recently Wäffler and Younis[7] have reported preliminary results of a photo-disintegration of deuterium experiment using as a photon source the $Li^7(p,\gamma)Be^8$ reaction. No attempt was made to separate the effects of the two photon lines at 14.8 and 17.6 Mev. They obtained a value for the mean cross section corresponding to this radiation of $8\pm3\times10^{-28}$ cm^2. Assuming a differential cross section of the form, $\sigma(\theta)\approx a+\sin^2\theta$, they obtained the value $a=0.05\pm0.15$.

TABLE I. Exposure conditions.

Run	Plates	Mean distance plate to beam (cm)	Height of plate above beam (cm)	Gas	Pressure
1	1	4.26	0.58	H_2+	3 Atmos.
	2	4.34	1.01	H_2O	8 mm Hg
2	3	4.26	0.58	D_2+	3 Atmos.
	4	4.34	1.01	H_2O	7 mm Hg
3	5	3.69	0.58		
	6	3.69	1.01	H_2O	8 mm Hg
4	7	2.66	0.65	H_2+	1 Atmos.
	8	2.66	0.94	H_2O	6 mm Hg
5	9	2.66	0.94	D_2+	1 Atmos.
	10	2.66	0.65	H_2O	6 mm Hg

[4] J. Van Allen and N. Smith, Phys. Rev. **59**, 618 (1941).
[5] Gibson, Green, and Livesy, Nature **160**, 534 (1947).
[6] At the Chicago meeting of the American Physical Society [Phys. Rev. **77**, 753 (1950)] Gerson Goldhaber reported preliminary results using the $F^{19}+H^1$ radiation. The angular distribution obtained was fitted by an expression of the form: $a+\sin^2\theta+\alpha1(\cos\theta)$.
[7] H. Wäffler and S. Younis, Helv. Phys. Acta **22**, 414 (1949).

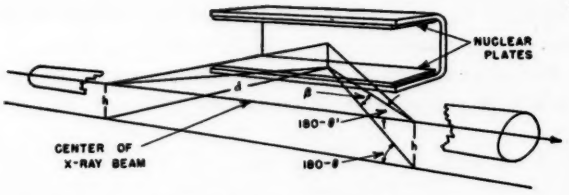

FIG. 2. Exposure geometry.

The present experiment is an attempt to determine the relative cross section for the photo-disintegration of deuterium as a function of photon energy between about 5 and 20 Mev and, in addition, to obtain mean angular distributions for a number of photon energy intervals between these two limits.

II. THE EXPERIMENTAL ARRANGEMENT AND PROCEDURE

The photon source used in this experiment was the continuous x-ray spectrum produced when electrons, accelerated to a kinetic energy of 20.3 Mev in the betatron, impinged on a platinum target 0.005 inch thick. The experimental arrangement is indicated in Fig. 1. The x-rays from the betatron target were collimated into a beam having a full angular width of thirty-six minutes of arc by means of a laminated lead collimator placed between the coil boxes of the betatron. This collimator was lined up such that the center of the tapered hole running through the collimator was along a central ray of the x-ray beam coming from the target of the betatron. After leaving the collimator the beam passed through a small hole in the lead brick wall erected immediately in front of the betatron, then through the reaction chamber, and finally through an ion chamber monitor. The diameter of the beam at the center of the reaction chamber was 0.85 centimeter. The line up of the x-ray beam with respect to the scattering chamber was checked before each run by means of pictures taken of the beam on dental x-ray plates in holders which positioned the plates accurately with respect to the scattering chamber.

The exposure geometry is indicated in Fig. 2. Two Ilford type C-2, one-hundred micron nuclear plates were exposed simultaneously in the scattering chamber in a plate holder which positioned the plates parallel to, and to one side of, the x-ray beam. These two plates were held parallel to each other, one being slightly above and the other below the x-ray beam. A total of five runs were made under the conditions listed in Table I.

The plates were developed using standard development techniques. After drying, all plates were given a coat of polyvinyl alcohol which, when dry, formed a thin hard transparent film over the surface of the emulsion. This film served to both protect the surface of the emulsion and to keep the emulsion from peeling.

The observations were made with a Bausch and Lomb binocular microscope using the 1.8 mm oil

emersion objective (97×) and the 5× oculars. This gave a field of view that was approximately two hundred microns in diameter. Plates were searched by taking six centimeter swaths along the long dimension of the plates. Successive swaths were taken parallel to and antiparallel to the direction of the x-ray beam. In searching the plates only those tracks were measured which started in the field of view and which entered the emulsions in directions such that they could have come from the x-ray beam. The following measurements were made on each track entering the surface of the emulsion:

(1) The angle, projected in the plane of the plate, which the first few microns of each track made with the leading edge of the plate. This is the angle θ in Fig. 2. This angle was measured by means of a protractor eye piece fitted to one of the oculars. Precision: ±2°.

(2) The range of the track projected into the plane of the plate. This was measured by means of a calibrated reticule in one of the oculars. This reticule also served as the pointer used in measuring the track angle. Precision: for a total range under 87 microns ±0.5 microns, and for a total range over 87 microns ±1.2 microns.

(3) The final depth reached by the track. This was measured using the micron scale on the final focus adjustment of the microscope. Precision: ±1.1 micron.

The figures for the precision of the measurements indicated above are the mean deviations of the various quantities measured obtained by having two swaths (about 250 tracks) re-measured both by the observer, who had originally made the observations, and by the second observer.

III. TREATMENT OF THE DATA

From the above measurements the following quantities were determined:

(a) The range in the emulsion corrected for the vertical shrinkage.

(b) The angle with respect to the normal to the surface of the emulsion each track made as it entered the emulsion. (Only tracks entering the surface with angles such that they could have come from the x-ray beam were kept in the final data.)

(c) The angle each track made with respect to the direction of the x-ray beam.

The energy of each track as it entered the emulsion was determined from the range-energy relation for protons in the Ilford emulsions.[8] Using the stopping number data of Hirschfelder and Magee[9] the energy of each proton was corrected for its range in the gas of the chamber before it reached the emulsion.

Owing to the finite diameter of the x-ray beam there was an uncertainty in the range of each proton in the gas of the chamber. In the case of the lowest energy proton used in the distribution the resultant uncertainty in the energy was ±0.1 Mev or ±10 percent for θ equal to 20 or to 160 degrees. For $40° \leq \theta \leq 140°$ this uncertainty was ±0.06 Mev or less. The photon energy corresponding to each proton was determined from a family of curves representing, for various values of the quantum energy, the function:

$$E_{LAB}=\frac{\hbar\omega-\epsilon}{2}+\frac{\hbar\omega}{4Mc^2}$$
$$\times[\cos\theta_l[4Mc^2(\hbar\omega-\epsilon)-(\hbar\omega)^2(\sin^2\theta_l+1)]^{\frac{1}{2}}-\hbar\omega\sin^2\theta_l],$$

where $\hbar\omega$ is the energy of the incident photon, Mc^2 the mass energy of the proton, ϵ the binding energy of the deuteron, and θ_l the angle the ejected proton makes with respect to the direction of the photon in the laboratory system.

A distribution of photo-protons as a function of photon energy was obtained by normalizing the data taken from the "high energy" plates (i.e., run 2 of Table I) to that taken from the "low energy" plates (run 5). This was accomplished by normalizing to the same total number of tracks above 10 Mev. After correcting for the neutron background, the observed angular distributions between 20 and 160 degrees were extrapolated to zero and 180 degrees to obtain the corrections for the tracks missed in the extreme wings of the angular distributions. A correction was also made for the tracks which were either scattered out of the emulsion or went through the emulsion into the glass before reaching the ends of their ranges. These tracks amounted to about 7 percent of the tracks corresponding to the photons above 13 Mev.

In order to plot angular distributions, the data were grouped into six photon energy intervals and the tracks in each energy interval grouped into seven 20-degree angular intervals according to the angle they made with the direction of the x-ray beam in the laboratory system.

The mean differential cross section over the 20-degree laboratory angular interval was then given by:

$$\bar{\sigma}=\frac{\text{No. tracks in } \Delta\theta}{\text{const.}\int_{\Delta V}(Pz/R)(\Delta A/R^2)dV}=\frac{\text{No. tracks in } \Delta\theta}{f(\theta)}$$

where z is the height of a volume element, dV, of the x-ray beam above the surface of the plate, R is the distance of the volume element from an element of area ΔA of the plate surface, and P is the pressure of the gas in the chamber. The integration is taken over the volume, ΔV, of the x-ray beam defined by the section of the beam between two planes which intersect along the normal to ΔA in an angle of 20 degrees. The function $f(\theta)$ was normalized to unity for the angular interval about ninety degrees. In the first approximation $f(\theta)$was given by the average value of $\sin\theta$ over the 20 degree angular interval.

IV. THE NEUTRON BACKGROUND

The number of tracks observed entering the surface of the plates exposed with the chamber filled with 8 mm of water vapor was of the order of 0.3 tracks per square

[8] Lattes, Fowler, and Cuer, Nature **159**, 301 (1947).
[9] J. O. Hirschfelder and J. L. Magee, Phys. Rev. **73**, 207 (1948).

millimeter. On the plates exposed with the chamber filled with one atmosphere of hydrogen and 8 mm of vapor, the number of tracks was of the order of 3.0 tracks per square millimeter. There was then a definite background due to the gas in the chamber.

This background was caused by the neutron flux passing through the chamber. The flux was studied by observing the recoil protons produced in neutron-proton scattering events which took place both within the emulsions themselves and in the hydrogen-filled chamber. These data could be explained by assuming the flux to be made up of an isotropic component superimposed upon which there was a broad diverging beam of neutrons coming from the general direction of the lead collimator and shielding. The magnitude of the flux through the emulsions was of the order of 2 to 6×10^3 neutrons/mm²-sec. This was calculated using a mean neutron energy of about 1 Mev.

On the basis of this study it was assumed that the principle background effect would arise from the $n-d$ scattering taking place when the chamber was filled with deuterium. The correction for this scattering was made by making exposures with the chamber filled with hydrogen and observing the $n-p$ scattering taking place in the gas of the chamber. The observed

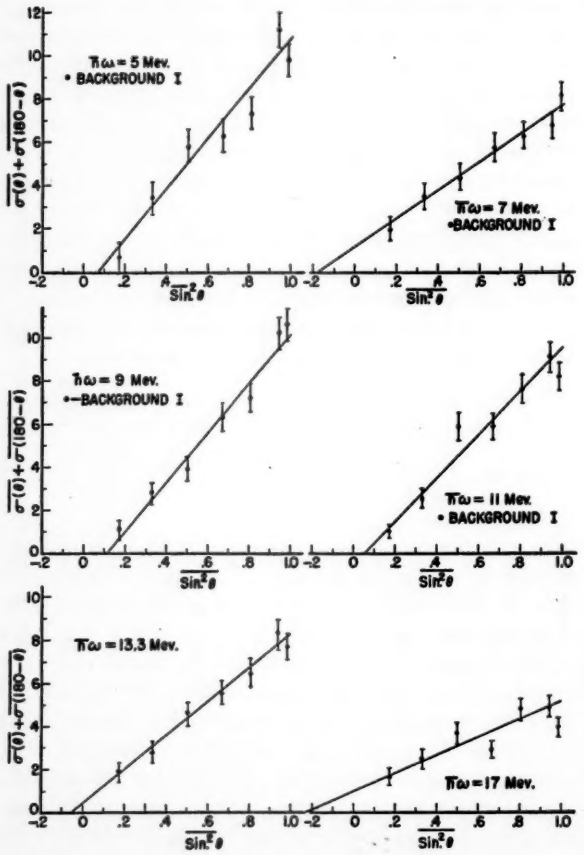

FIG. 3. The isotropic component. The ordinates represent the sum of the numbers of tracks per mean solid angle observed in a ten degree angular interval about the angle θ plus the corresponding quantity for $(180°-\theta)$. The abscissas represent the mean value of $\sin^2\theta$ over the corresponding ten degree angular interval. θ is the angle in the laboratory system the ejected photo-proton makes with respect to the direction of the incident photon.

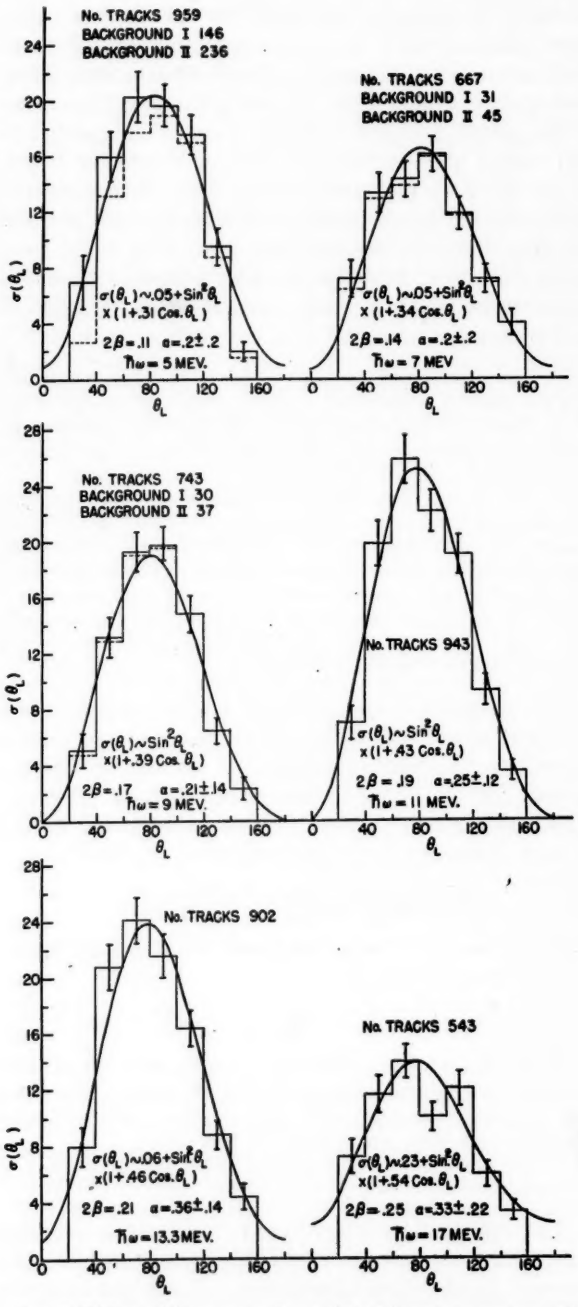

FIG. 4. Differential cross sections in the laboratory system. The energy indicated is the mean photon energy for each interval. Theoretical differential cross section in the laboratory system is of the form:

$$\sigma(\theta_l)\sim a+\sin^2\theta_l\left(1+\left[\alpha+\frac{2\beta\hbar\omega}{\hbar\omega-W}\right]\cos\theta_l\right).$$

In each case above, 2β is the value of α given by the theory of Marshall and Guth while the values for α are those determined experimentally. The smooth curve, whose equation is given in each histogram, is the theoretical curve given by the theory of Marshall and Guth. Solid histograms were obtained using background *I*, dashed histograms using background *II*.

$n-p$ scattering was then converted to the expected energy and angular distributions for $n-d$ scattering. In making this conversion two assumptions were made: First, it was assumed that the neutron flux through the chamber was completely random. The conversion was then made using the ratio of the total $n-d$ to $n-p$ scattering cross sections. Second, it was assumed that all the recoil particles were scattered into a twenty degree cone about the direction of the incident neutron. In this case the conversion was made using the ratio of the mean differential cross sections corresponding to a back scattering of the neutron in the center of mass system.[10]

These background corrections were important only at low energies. For photons with energies above 8 Mev the corrections were negligible.

V. RESULTS AND CONCLUSIONS

The results of this work are presented in the graphs of Figs. 3 through 6. The errors indicated are the mean statistical errors.

(A) The Angular Distributions

In the case of the photo-disintegration of deuterium by photons having energies greater than 50 Mev, the theoretical calculations of Rose and Goertzel[11] have indicated that a forward asymmetry is to be expected in the angular distribution of the resulting photo-protons. The recent work of Marshall and Guth[12] indicates that this asymmetry should also be expected at energies below 20 Mev. The expression obtained by the latter for the differential cross section in the center of mass system is of the form:

$$\sigma(\theta_{cm})\sim a+\sin^2\theta_{cm}(1+\alpha\cos\theta_{cm}),$$

where α is a constant depending on the energy of the incident photon and the type of interaction assumed for the neutron-proton force. Making the conversion to the laboratory system the differential cross section is given approximately by:

$$\sigma(\theta_l)\sim a+\sin^2\theta_l\left(1+\left[\alpha+\frac{2\beta\hbar\omega}{\hbar\omega-W}\right]\cos\theta_l\right),$$

where $\beta=[(\hbar\omega-W)/Mc^2]^{\frac{1}{2}}$ and W is the threshold for the photo-disintegration of deuterium. For an equal mixture of exchange and ordinary forces Marshall and Guth find that α is equal to 2β.

In Fig. 3 the angular distribution histograms have been folded about ninety degrees and plotted as a function of $\sin^2\theta_1$. The data using the first background correction were used. Assuming a differential cross section in the laboratory system of the form given above, these plots should result in straight lines, the negative intercepts of which at the $\sin^2\theta_1$ axis give the values of the isotropic terms, a, in the angular distributions. Due to the large and rather uncertain background corrections that have to be applied in the case of the distributions at 5 and at 7 Mev, it is felt that no definite statements can be made about the magnitude of the isotropic term at these energies. These data do, however, indicate a trend, i.e., an isotropic term that is small at 5 and 7 Mev, dropping to near zero between 9 and 11 Mev, increasing to about 0.05 at 13.3 Mev and to something of the order of 0.2 at 17 Mev.

The differential cross-section histograms in the laboratory system are given in Fig. 4. The smooth curve in each case is the differential cross-section curve in the laboratory system as given by the theory of

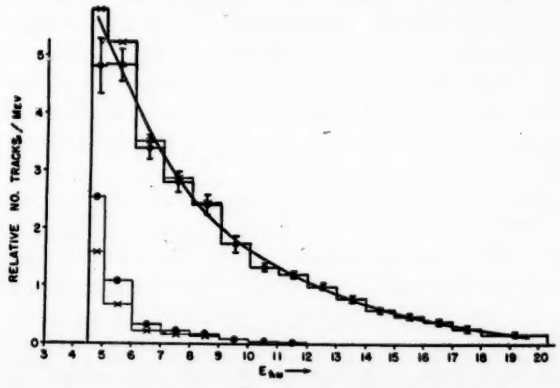

FIG. 5. Relative number of photo-protons per Mev as a function of photon energy. Light histogram indicates background that was subtracted. Crosses indicate background *I*. Circles indicate background *II*.

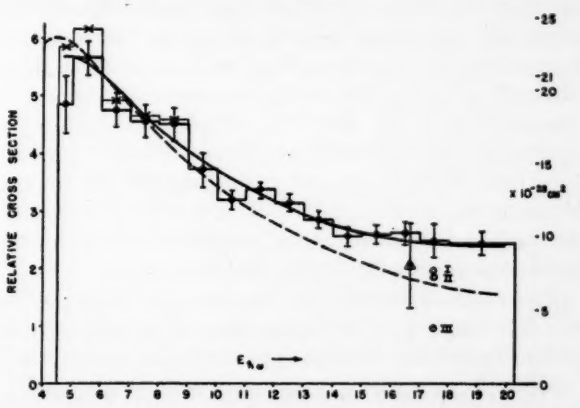

FIG. 6. Relative cross section for the photo-disintegration of deuterium. Scale on right fitted to give a cross section of 21×10^{-28} cm² at 6.0 Mev. Dashed curve has the energy dependence of the Bethe-Peierls expression. Points calculated by Rarita and Schwinger; I symmetrical theory, II charged theory, III neutral theory. Point obtained by Wäffler and Younis; Δ. Crosses indicate points obtained using background I, circles those obtained using background II.

[10] The angular distribution data for $n-d$ scattering given by the calculations of Buckingham and Massey [Proc. Roy. Soc., **A179**, 123 (1941)] were used in obtaining the mean differential cross section corresponding to a forward scattering of the deuteron.

[11] M. E. Rose and G. Goertzel, Phys. Rev. **72**, 749 (1947).

[12] J. F. Marshall and E. Guth, Phys. Rev. **76**, 1879 (1949). The author wishes to express his gratitude for being sent the results of this work before publication.

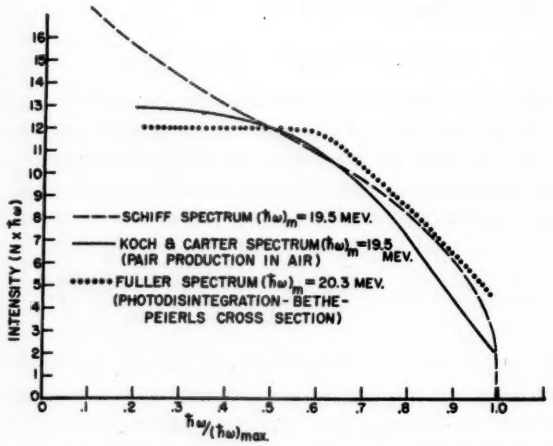
INTENSITY (N x ħω)
SCHIFF SPECTRUM (ħω)m = 19.5 MEV.
KOCH & CARTER SPECTRUM (ħω)m = 19.5 MEV.
(PAIR PRODUCTION IN AIR)
FULLER SPECTRUM (ħω)m = 20.3 MEV.
(PHOTODISINTEGRATION - BETHE-PEIERLS CROSS SECTION)
ħω/(ħω)max.

FIG. 7. Comparison of intensity spectra for betatron radiation.

Marshall and Guth for the mean energy of each interval. On each histogram the corresponding value of 2β is indicated, as well as the value of α calculated from the experimental data. While agreeing within large experimental errors with the value 2β, the value of α determined experimentally is larger than 2β in each case.

(B) The Energy Distribution

Figure 5 gives the distribution of the photo-protons as a function of photon energy after correction for the neutron background and for the tracks missed in the wings of the angular distributions. Also indicated is the background that was subtracted. Figure 6 gives the relative cross section for the photo-disintegration of deuterium as a function of the photon energy determined by dividing the energy distribution of Fig. 5 by the photon spectrum of thin target betatron radiation determined by Koch and Carter.[13] The smooth solid curve is the curve obtained by dividing the smooth curve in Fig. 5 by the photon spectrum.[14]. The dashed curve has the energy dependence of the Bethe-Peierls expression. The two curves have been fitted at 6.0 Mev. The sale on the right has been normalized to give a cross section of 21×10^{-28} cm^2 at 6.0 Mev. This is the theoretical value given by the Bethe-Peierls expression with the correction for the finite range of the nuclear forces in the ground state.[15] On the basis of this scale the various experimental and theoretical values for the total cross section have been plotted.

The curve obtained here for the total cross section as a function of photon energy falls off less rapidly with increasing photon energy than does the Bethe-Peierls expression. For energies above 13 Mev a curve falling off as $1/E^{\frac{1}{2}}$, where E is the photon energy, fits the data well. All of the theoretical calculations that have been made to date give a cross section which falls off at least as rapidly as the Bethe-Peierls expression; i.e., roughly as $1/E^{\frac{1}{2}}$ for high energies.

The shape of the curve obtained for the relative cross section as a function of energy is strongly dependent on the shape of the curve used to give the relative photon spectrum. Using the Schiff intensity spectrum to determine a distribution of photons and the distribution of photo-protons given in Fig. 5, a curve can be obtained for the relative cross section as a function of energy which above 10 Mev is in good agreement with the Bethe-Peierls expression. Below 10 Mev, however, the curve thus obtained falls considerably below the Bethe-Peierls expression.

At these energies the Bethe-Peierls expression seems to be a good approximation for the energy dependence of the photo-disintegration cross section.[12,16] Assuming the cross section to have this energy dependence a curve for the intensity spectrum of the betatron radiation was determined. This is given in Fig. 7. Also plotted for comparison is the spectrum determined by Koch and Carter and that calculated by Schiff as given in Koch and Carter's paper. The discrepancy between the Schiff spectrum and that indicated by the present work is essentially the same as that recently found by Wang and Weiner[17] using a 10 Mev betatron.

Due to the large uncertainties in the spectrum of the betatron radiation and those in the distribution of the photo-protons as a function of photon energy, it is not felt that the results of this experiment have established a discrepancy with a theoretical cross section having the energy dependence of the Bethe-Peierls expression between 6 and 20 Mev. It is felt, however, that these data would be inconsistent with a theoretical cross section falling off any more rapidly with increasing photon energy than does the Bethe-Peierls expression.

The results of this experiment indicate the need for more work on this problem at these energies. Except for the photo-magnetic effect, there have been no theoretical calculations to date that give the magnitude of the isotropic term in the angular distribution as a function of photon energy. The large isotropic term at high energies is explicable on the basis of a tensor force interaction.[18] Experimentally the magnitude of this term seems to increase extremely rapidly with increasing photon energy above 11 Mev. Further experimental work using both monoenergetic photons and higher energy betatrons would be of considerable value in establishing the features of cross section dependence on

[13] H. W. Koch and R. E. Carter, Phys. Rev. **77**, 165 (1950).

[14] In using the photon energy spectrum it was necessary to expand the energy scale slightly since the maximum x-ray energy in this work was 20.3 Mev, while Koch and Carter used a maximum x-ray energy of 19.5 Mev.

[15] In a previous preliminary report of this work [E. G. Fuller, Phys. Rev. **76**, 576 (1949)] a scale was given that was normalized to give a cross section of 11.7 $(10)^{-28}$ cm^2 at 7 Mev. This is the cross section given by the Bethe-Peierls expression for zero range. The present normalization is considered to be more reasonable.

[16] J. S. Levinger, Phys. Rev. **76**, 699 (1949).

[17] P. K. S. Wang and M. Weiner, Phys. Rev. **76**, 1724 (1949).

[18] W. Rarita and J. Schwinger, Phys. Rev. **59**, 436, 556 (1941); Tsi-Ming Hu and H. S. W. Massey, Proc. Roy. Soc. **A196**, 135 (1949).

energy and the angular distributions which seem to be indicated by this work.

The author wishes to gratefully acknowledge the encouragement and advice of Professor A. O. Hanson, who initiated and directed this work. He also wishes to acknowledge the helpful discussions of the work held with Professor S. M. Dancoff and Mr. J. S. Blair.

The task of lining up the collimator and of making the exposures was accomplished with the able assistance of Mr. B. C. Diven and Mr. D. Riesen.

The analysis of the low energy plates was greatly facilitated by the careful and accurate work of Wilna D. Johnston, who helped in the reading of these plates and in the analysis of the data.

PHYSICAL REVIEW VOLUME 79, NUMBER 2 JULY 15, 1950

Liquid Helium II: The Hydrodynamics of the Two-Fluid Model*

P. R. ZILSEL
The University of Connecticut, Storrs, Connecticut
(Received March 10, 1950)

Exact non-linear equations of motion for reversible processes in the two-fluid model of liquid He II are obtained from a variational principle of the type first introduced by Eckart in a different connection. Transitions between the two fluids are taken into account. Except for a term giving the effect of these transitions the equations obtained are substantially identical with those given by Landau. In the limit of very small velocities they reduce to the linear equations obtained by Tisza. The momentum and energy theorems are shown to be satisfied.

I. INTRODUCTION

THE two-fluid model of liquid He II developed by Tisza[1–3] and, from a different point of view, by Landau,[4] is based on these fundamental assumptions.

(a) At temperatures below the λ-transition liquid helium can be regarded as a homogeneous mixture of two fluids, the "superfluid," with density ρ_s, and the "normal fluid," with density ρ_n. The total density of the liquid is then given by

$$\rho=\rho_s+\rho_n. \tag{1.1}$$

In thermodynamic equilibrium the ratio

$$x=\rho_n/\rho \tag{1.2}$$

is a function of temperature and pressure, being unity for $T\geqslant T_\lambda$, and zero for $T=0$. The quantity x can thus be interpreted as a disorder parameter associated with the λ-transition. Experimentally it is found[3] that

$$x\simeq(T/T_\lambda)^{5.5}\ (T\leqslant T_\lambda). \tag{1.3}$$

The two fluids can move relative to each other, each having its own hydrodynamic velocity field, $\mathbf{v}_s$, and $\mathbf{v}_n$, respectively. The motion of the liquid as a whole is then given by

$$\rho\mathbf{V}=\rho_s\mathbf{v}_s+\rho_n\mathbf{v}_n, \tag{1.4}$$

and the relative velocity of the two fluids by

$$\mathbf{v}=\mathbf{v}_n-\mathbf{v}_s. \tag{1.5}$$

(b) The superfluid has zero entropy. Thus, if S=entropy per gram of liquid He II, S_n=specific entropy of the normal fluid,

$$S=xS_n. \tag{1.6}$$

For reversible processes inside the bulk liquid the law of conservation of entropy accordingly takes the form

$$\partial\rho S/\partial t=-\operatorname{div}(\rho S\mathbf{v}_n)=-\operatorname{div}(\rho_n S_n\mathbf{v}_n). \tag{1.7}$$

Tisza considers Eqs. (1.6) and (1.7) to be approximations valid only for temperatures $T\gtrsim 1°$K, where the phonon contribution to the entropy is a negligible fraction of the whole, whereas Landau considers these equations to be exact.

From the latter point of view the superfluid constitutes at all times a single macroscopic quantum state with properties varying adiabatically with the macroscopic boundary conditions and with the properties of the normal fluid with which the superfluid is in contact. The normal fluid, on the other hand, is a statistical mixture with the distribution in momentum space depending on temperature and pressure. The basic ideas underlying this picture are perhaps best expressed by writing down the kind of distribution in velocity space to which it corresponds:

$$\rho(\mathbf{r})=\int\{\rho_n(\mathbf{r},\mathbf{u})+\rho_s(\mathbf{r})\delta[\mathbf{u}-\mathbf{v}_s(\mathbf{r})]\}d\mathbf{u},$$

$$\rho_n(\mathbf{r})=\int\rho_n(\mathbf{r},\mathbf{u})d\mathbf{u},\quad \rho_n\mathbf{v}_n=\int\rho_n(\mathbf{r},\mathbf{u})\mathbf{u}d\mathbf{u}. \tag{1.8}$$

All the quantities in Eq. (1.8) are, in general, also functions of the time.

---

* Part of the work reported here was done at Duke University under Contract N7onr-455 with the ONR.

[1] L. Tisza, Comptes Rendus **207**, 1035 and 1186 (1938).
[2] L. Tisza, J. de phys. et rad. **1**, 165 and 350 (1940).
[3] L. Tisza, Phys. Rev. **72**, 838 (1947).
[4] L. Landau, J. Phys. U.S.S.R. **5**, 71 (1941); **8**, 1 (1944).

For what follows it is not essential which of the two points of view outlined is adopted. In the one case the equations we shall obtain can be regarded as approximations valid even for reversible processes only at temperatures above $\sim 1°K$; in the other case they can be regarded as exact for reversible processes.

Tisza[3] makes the additional assumption that for reversible processes ρ_n and ρ_s obey separate conservation laws, no transitions between the two fluids taking place in the bulk liquid. This, together with Eq. (1.7), implies that the specific entropy of the normal fluid, S_n, is a constant independent of temperature and pressure, so that in the diagram of state of liquid He II lines of constant x would also be lines of constant entropy. While this assumption may be approximately correct, it is certainly not exactly fulfilled. Thus, for example, along the λ-line, which is the line $x=1$, the entropy varies[5] between -0.45 and -0.55 Clausius/g. In any case Tisza's assumption is unnecessarily restrictive; we shall see that transitions between the normal and the superfluid have an effect on the hydrodynamic equations of motion.

(c) The viscosity of liquid He II as observed in oscillating disk experiments,[6] for example, is due entirely to the normal fluid. The superfluid moves without internal friction.

The model based on the assumptions (a, b, c) accounts rather well for the peculiar properties of liquid He II, at least in the limit of small velocities of the two fluids.

In his 1947 paper Tisza[3] gives a derivation of hydrodynamic equations of motion of the two fluids based on the Hamilton principle of particle mechanics. In applying this principle to hydrodynamics one is using the *substantial* description of the motion since Hamilton's principle describes the motion of individual particles, which means the motion of individual fluid elements in the application to hydrodynamics. Consequently the Lagrangian density must be summed over the fluid elements, which means that it must be integrated over a volume *moving with the fluid*. However this treatment cannot be carried through consistently in the present case of two distinct velocity fields since one obviously cannot integrate the Lagrangian density over a volume moving with both fluids at the same time. Tisza does not, in fact, distinguish clearly between local and substantial derivatives and his equations are valid only in the limit of small velocities when the difference between local and substantial derivatives can be neglected. As was pointed out by Landau,[7] Tisza's equations fail to satisfy the law of conservation of momentum.

Recent work[8,9] on heat conduction and second sound propagation data in liquid He II has called attention to the importance of non-linear terms in the equations of motion. In particular, Gorter and Mellink[10] have shown that the heat conduction data in narrow slits can be accounted for by the *ad hoc* assumption of a mutual friction between the normal and the superfluid proportional to the cube of the relative velocity.

Without entering into the question of the ultimate validity of the two-fluid model, it is the purpose of the present paper to obtain from the basic assumptions of the model exact non-linear equations of motion, at least for stationary and quasi-stationary processes. In this paper we shall confine ourselves to reversible effects, neglecting the viscosity of the normal fluid. The effect of irreversible entropy production on the equations of motion will be considered in detail in a later paper.

The equations of motion will be obtained from a variational principle of the type first introduced by Eckart[11] in classical electrodynamics. The Lagrangian density

$$L = \text{kinetic energy density of matter—potential energy density,} \quad (1.9)$$

is here associated not with a definite element of matter but with a volume element fixed in space and is integrated over a stationary volume. All derivatives are, then, local derivatives and one is dealing with a *local* description of the motion. In the two-fluid case this approach obviates the difficulties of a substantial description connected with the fact that parts of a given element of fluid move with different hydrodynamic velocities.

In the local description of the motion the hydrodynamic velocities are not the time derivatives of true coordinates of the system; consequently, in Eckart's variational principle, they are varied independently and not as the time derivatives of coordinates. As a result of this feature of the treatment one obtains, beside the equations of motion, certain subsidiary conditions on the velocities. In the case of the hydrodynamics of an ideal fluid these conditions amount to a restriction to potential flow. It may be argued that these subsidiary restrictions are exactly what is required to give a correct description of the motion of a "superfluid" as distinguished from the infinitely many possible solutions of the hydrodynamic equations with given boundary conditions if arbitrary turbulence is admitted. In fact Eckart's method was used by Cook[12] to obtain the London equations[13] for superconductivity without additional assumptions. In the present case the restriction obtained for the superfluid velocity field $\mathbf{v}_s$, (Eq. (2.10)), is exactly the condition stated by Landau[4]

[5] W. H. Keesom, *Helium* (Elsevier Publishing Company, Inc., Amsterdam, 1942), p. 246.
[6] W. H. Keesom and G. E. McWood, Physica **5**, 737 (1938).
[7] L. Landau, Phys. Rev. **75**, 884 (1949).
[8] W. Band and L. Meyer, Phys. Rev. **73**, 226; **74**, 386 and 394 (1948).
[9] F. London and P. R. Zilsel, Phys. Rev. **74**, 1148 (1948).
[10] C. J. Gorter and J. H. Mellink, Physica **15**, 285 (1949).
[11] C. Eckart, Phys. Rev. **54**, 920 (1938).
[12] E. Cook, Phys. Rev. **58**, 357 (1940).
[13] F. and H. London, Proc. Roy. Soc. **A149**, 71 (1935); F. London, *Une Nouvelle Conception de la Supraconductivité* (Hermann et Cie, Paris, 1937).

and by F. London[14] as characteristic of superfluid flow. This restriction is in line with the point of view which considers the state of motion of the superfluid as determined uniquely by the macroscopic conditions.

It should be pointed out, however, that whether or not the subsidiary restrictions obtained from the variational principle are considered to be relevant to a correct description of the states of motion of the two-fluid model, the validity of the equations of motion obtained is unaffected. The subsidiary conditions only restrict the class of admissible solutions of the equations of motion. They do not affect the equations themselves.

In the present case the potential energy density used in the Lagrangian (1.9) is the internal energy density, ρU, where U is the internal energy per gram of liquid He II.

The point of view adopted will be that of considering the actual system to be approximated by a collection of small volume elements each of which is in thermodynamic equilibrium with definite values of the temperature, T, the pressure, P, and x. Then T, P, and x are, in general, functions of both the time, t, and the position, $\mathbf{r}$, of the volume element. As was pointed out by Callen,[15] who used this method of "local equilibrium" in a discussion of the thermoelectric effects, the approximation involved corresponds to the approximate solution of Boltzmann's kinetic equation in statistical mechanics, when one assumes that the statistical distribution is given by a local-equilibrium distribution, with the parameters being functions of t and $\mathbf{r}$, plus a small correction term. The latter is neglected in calculating "flow terms," but it becomes important when irreversible processes associated with collisions are considered.

The assumptions involved in this "local equilibrium" approach are correct if the processes considered are slow compared to the relaxation time for the establishment of local equilibrium; that is, for stationary and quasi-stationary processes. Thus we should not expect our equations to be applicable exactly to such processes as second sound propagation at high frequencies.

In the case of local equilibrium the local value of x is determined by the local values of S and ρ. If the two fluids were at rest with respect to each other this equilibrium value would be determined by the condition

$$(\partial U/\partial x)_{S,\rho}=0.$$

In the general case of relative motion of the two fluids the equilibrium value of $\partial U/\partial x$ depends on the kinetic energy of relative motion.

[14] F. London, Phys. Soc. Cambridge Conference Report, p. 1 (1947).

[15] H. B. Callen, Phys. Rev. **73**, 1349 (1948).

II. THE EQUATIONS OF MOTION

The Lagrangian density (1.9) is in the present case

$$L=\tfrac{1}{2}\rho_s v_s^2+\tfrac{1}{2}\rho_n v_n^2-\rho U$$
$$=\rho[\tfrac{1}{2}(1-x)v_s^2+\tfrac{1}{2}xv_n^2-U], \quad (2.1)$$

where the specific internal energy is taken as a function of ρ, S, x:

$$U=U(\rho, S, x). \quad (2.2)$$

The equation of conservation of total mass[16]

$$\partial\rho/\partial t=-\operatorname{div}(\rho_s\mathbf{v}_s+\rho_n\mathbf{v}_n)$$
$$=-\operatorname{div}\{\rho[(1-x)\mathbf{v}_s+x\mathbf{v}_n]\} \quad (2.3)$$

and of entropy, Eq. (1.7), are introduced as subsidiary conditions.

The variational principle then states that

$$\delta\int_{t_0}^{t_1}\int_V\{\rho[\tfrac{1}{2}(1-x)v_s^2+\tfrac{1}{2}xv_n^2-U]$$
$$-\alpha\{\partial\rho/\partial t+\operatorname{div}\rho[(1-x)\mathbf{v}_s+x\mathbf{v}_n]\}$$
$$-\beta[\partial\rho S/\partial t+\operatorname{div}(\rho S\mathbf{v}_n)]\}d\tau dt=0. \quad (2.4)$$

The quantities to be varied are ρ, S, x, $\mathbf{v}_n$, and $\mathbf{v}_s$. The volume of integration V is fixed in space.

The Euler variational equations of (2.4) are

$$\delta\rho:\ \tfrac{1}{2}(1-x)v_s^2+\tfrac{1}{2}xv_n^2-U-\rho\partial U/\partial\rho$$
$$+\partial\alpha/\partial t+[(1-x)\mathbf{v}_s+x\mathbf{v}_n]\cdot\operatorname{grad}\alpha$$
$$+S\partial\beta/\partial t+S\mathbf{v}_n\cdot\operatorname{grad}\beta=0; \quad (2.5)$$

$$\delta x:\ -\tfrac{1}{2}v_s^2+\tfrac{1}{2}v_n^2-\partial U/\partial x+(\mathbf{v}_n-\mathbf{v}_s)\cdot\operatorname{grad}\alpha=0; \quad (2.6)$$

$$\delta S:\ -\partial U/\partial S+\partial\beta/\partial t+\mathbf{v}_n\cdot\operatorname{grad}\beta=0; \quad (2.7)$$

$$\delta\mathbf{v}_n:\ x\mathbf{v}_n+x\operatorname{grad}\alpha+S\operatorname{grad}\beta=0; \quad (2.8)$$

$$\delta\mathbf{v}_s:\ \mathbf{v}_s+\operatorname{grad}\alpha=0. \quad (2.9)$$

From (2.9) it follows immediately that

$$\operatorname{curl}\mathbf{v}_s=0, \quad (2.10)$$

which is the condition posited by Landau[4] and by F. London.[14]

The equations of motion are obtained by eliminating the Lagrangian multipliers α and β from Eqs. (2.5) to (2.9). By straightforward substitution one obtains

$$\operatorname{grad}\beta=(\mathbf{v}_s-\mathbf{v}_n)x/S, \quad (2.11)$$

and

$$\partial U/\partial x=\tfrac{1}{2}(\mathbf{v}_n-\mathbf{v}_s)^2. \quad (2.12)$$

Using the thermodynamic identities

$$\partial U/\partial S=T;\quad \partial U/\partial\rho=P/\rho^2 \quad (2.13)$$

one has

$$\partial\beta/\partial t=T+\mathbf{v}_n\cdot(\mathbf{v}_n-\mathbf{v}_s)x/S \quad (2.14)$$

and

$$\partial\alpha/\partial t=\tfrac{1}{2}v_s^2-\tfrac{1}{2}x(\mathbf{v}_n-\mathbf{v}_s)^2+U-ST+P/\rho. \quad (2.15)$$

[16] We are dealing here with local derivatives.

Defining the substantial derivatives

$$\begin{aligned} D_s/Dt &\equiv \partial/\partial t + \mathbf{v}_s\cdot\text{grad} \\ D_n/Dt &\equiv \partial/\partial t + \mathbf{v}_n\cdot\text{grad} \end{aligned} \tag{2.16}$$

we obtain the equation of motion of the superfluid:

$$\begin{aligned} D_s\mathbf{v}_s/Dt &= \partial\mathbf{v}_s/\partial t + \tfrac{1}{2}\,\text{grad}v_s^2 \\ &= -\text{grad}[G - \tfrac{1}{2}x(\mathbf{v}_n-\mathbf{v}_s)^2], \end{aligned} \tag{2.17}$$

where the thermodynamic potential G is

$$G = U - ST + P/\rho.$$

Thus, remembering (2.12),

$$\begin{aligned} D_s\mathbf{v}_s/DT &= S\,\text{grad}T \\ &\quad -(1/\rho)\,\text{grad}P + (\rho_n/2\rho)\,\text{grad}v^2, \end{aligned} \tag{2.18}$$

where $\mathbf{v}$ is the hydrodynamic velocity of relative motion defined by Eq. (1.5).

Similarly, from the relation

$$D_n\mathbf{v}_n/Dt = \partial\mathbf{v}_n/\partial t + \tfrac{1}{2}\,\text{grad}v_n^2 - \mathbf{v}_n\times\text{curl}\mathbf{v}_n, \tag{2.19}$$

the equation of motion of the normal fluid is found to be

$$\begin{aligned} D_n\mathbf{v}_n/Dt &= -\frac{\rho_s}{\rho_n}S\,\text{grad}T - \frac{1}{\rho}\text{grad}P \\ &\quad -\frac{1}{2}\frac{\rho_s}{\rho}\text{grad}v^2 + \mathbf{v}D_nS_n/S_nDt, \end{aligned} \tag{2.20}$$

where S_n is the specific entropy of the normal fluid given by Eq. (1.6).

The significance of the last term in Eq. (2.20) can be clarified by introducing explicitly transitions between the normal and the superfluid. We rewrite the continuity Eq. (2.3) in the form of separate equations for the two fluids:

$$\left.\begin{aligned} \partial\rho_n/\partial t + \text{div}(\rho_n\mathbf{v}_n) &= \Gamma, \\ \partial\rho_s/\partial t + \text{div}(\rho_s\mathbf{v}_s) &= -\Gamma. \end{aligned}\right\} \tag{2.21}$$

Γ then represents a source density of the normal fluid and a corresponding sink density of the superfluid. Using Eqs. (2.21) and the definitions (2.16) of the substantial derivatives one obtains the following identities for any function f:

$$\left.\begin{aligned} \partial\rho_n f/\partial t &= \rho_n D_n f/Dt - \text{div}(\rho_n f\mathbf{v}_n) + f\Gamma, \\ \partial\rho_s f/\partial t &= \rho_s D_s f/Dt - \text{div}(\rho_s f\mathbf{v}_s) - f\Gamma. \end{aligned}\right\} \tag{2.22}$$

The conservation of entropy, Eq. (1.7), then gives

$$\rho_n D_n S_n/Dt = -S_n\Gamma. \tag{2.23}$$

We can thus rewrite the equation of motion (2.20) in the form

$$\begin{aligned} D_n\mathbf{v}_n/Dt &= -\frac{\rho_s}{\rho_n}S\,\text{grad}T - \frac{1}{\rho}\text{grad}P \\ &\quad -\frac{1}{2}\frac{\rho_s}{\rho}\text{grad}v^2 - \mathbf{v}\Gamma/\rho_n. \end{aligned} \tag{2.20'}$$

III. THE MOMENTUM AND ENERGY THEOREMS

The momentum theorem is obtained most easily by use of Eqs. (2.22). One has

$$\left.\begin{aligned} \partial\rho_n\mathbf{v}_n/\partial t &= \rho_n D_n\mathbf{v}_n/Dt - \text{div}(\rho_n\mathbf{v}_n\mathbf{v}_n) + \mathbf{v}_n\Gamma, \\ \partial\rho_s\mathbf{v}_s/\partial t &= \rho_s D_s\mathbf{v}_s/Dt - \text{div}(\rho_s\mathbf{v}_s\mathbf{v}_s) - \mathbf{v}_s\Gamma. \end{aligned}\right\} \tag{3.1}$$

Using Eqs. (2.18) and (2.20'), and adding Eqs. (3.1) one obtains for the rate of change of the total momentum density $\rho\mathbf{V}$, defined by Eq. (1.4)

$$\partial\rho\mathbf{V}/\partial t = -\text{grad}P - \text{div}(\rho_n\mathbf{v}_n\mathbf{v}_n + \rho_s\mathbf{v}_s\mathbf{v}_s). \tag{3.2}$$

The energy theorem is obtained in a similar manner. Equations (2.22) yield

$$\left.\begin{aligned} \partial(\tfrac{1}{2}\rho_n v_n^2)/\partial t &= \rho_n\mathbf{v}_n\cdot D_n\mathbf{v}_n/Dt \\ &\quad -\text{div}(\tfrac{1}{2}\rho_n v_n^2\mathbf{v}_n) + \tfrac{1}{2}v_n^2\Gamma, \\ \partial(\tfrac{1}{2}\rho_s v_s^2)/\partial t &= \rho_s\mathbf{v}_s\cdot D_s\mathbf{v}_s/Dt \\ &\quad -\text{div}(\tfrac{1}{2}\rho_s v_s^2\mathbf{v}_s) - \tfrac{1}{2}v_s^2\Gamma. \end{aligned}\right\} \tag{3.3}$$

Hence, using the equations of motion, (2.18), (2.20'), the rate of change of the kinetic energy density is found to be

$$\begin{aligned} &\frac{\partial}{\partial t}(\tfrac{1}{2}\rho_s v_s^2 + \tfrac{1}{2}\rho_n v_n^2) \\ &\quad = -\mathbf{V}\cdot\text{grad}P - \rho_s S\mathbf{v}\cdot\text{grad}T - \tfrac{1}{2}v^2\Gamma \\ &\quad -\frac{1}{2}\frac{\rho_s\rho_n}{\rho}\mathbf{v}\cdot\text{grad}v^2 - \text{div}(\tfrac{1}{2}\rho_s v_s^2\mathbf{v}_s + \tfrac{1}{2}\rho_n v_n^2\mathbf{v}_n). \end{aligned} \tag{3.4}$$

Defining the substantial derivative moving with the center of mass velocity $\mathbf{V}$

$$D/Dt \equiv \partial/\partial t + \mathbf{V}\cdot\text{grad}, \tag{3.5}$$

and using the conservation of total mass, Eq. (2.3), one has

$$\partial\rho U/\partial t = \rho DU/Dt - \text{div}(\rho U\mathbf{V}). \tag{3.6}$$

Now

$$\begin{aligned} \rho DU/Dt &= \rho\partial U/\partial\rho D\rho/Dt \\ &\quad + \rho\partial U/\partial S DS/Dt + \rho\partial U/\partial x Dx/Dt \\ &= PD\rho/\rho Dt + \rho T DS/Dt + \tfrac{1}{2}\rho v^2 Dx/Dt. \end{aligned} \tag{3.7}$$

From Eq. (2.3)

$$D\rho/Dt = -\rho\,\text{div}\mathbf{V}; \tag{3.8}$$

by Eq. (1.7)

$$\rho DS/Dt = \partial\rho S/\partial t + \text{div}(\rho S\mathbf{V}) = -\text{div}(\rho_s S\mathbf{v}); \tag{3.9}$$

and by Eq. (2.21)

$$\rho Dx/Dt = \partial\rho x/\partial t + \text{div}(\rho x\mathbf{V}) = \Gamma - \text{div}(\rho_s\rho_n\mathbf{v}/\rho). \tag{3.10}$$

Thus one obtains for the rate of change of the internal energy density

$$\begin{aligned} \partial\rho U/\partial t &= -P\,\text{div}\mathbf{V} - T\,\text{div}(\rho_s S\mathbf{v}) + \tfrac{1}{2}v^2\Gamma \\ &\quad -\tfrac{1}{2}v^2\,\text{div}(\rho_s\rho_n\mathbf{v}/\rho) - \text{div}(\rho U\mathbf{V}). \end{aligned} \tag{3.11}$$

Adding Eqs. (3.4) and (3.11) yields the energy theorem

$$\frac{\partial}{\partial t}(\tfrac{1}{2}\rho_s v_s^2+\tfrac{1}{2}\rho_n v_n^2+\rho U)$$
$$=-\operatorname{div}\{P\mathbf{V}+\rho_s S T\mathbf{v}+\tfrac{1}{2}\rho_s\rho_n\mathbf{v}^2\mathbf{v}/\rho$$
$$+\tfrac{1}{2}\rho_n v_n^2\mathbf{v}_n+\tfrac{1}{2}\rho_s v_s^2\mathbf{v}_s+\rho U\mathbf{V}\}. \quad (3.12)$$

IV. DISCUSSION

The equations of motion (2.18) and (2.20′) are essentially identical with those given by Landau[4] except for the last term in the equation of motion of the normal fluid, which gives the effect of transitions between the two fluids. This term is new. In the limit of very small velocities the variational principle employed here becomes identical with Hamilton's principle of particle mechanics, and our equations reduce to the linear ones obtained by Tisza.[3]

It is interesting to note that in reversible processes only the velocity of the normal fluid is affected by transitions between the two fluids. This is closely connected with the basic assumption that the superfluid has zero entropy. Using the interpretation expressed in Eqs. (1.8), whereby the local hydrodynamic velocity of the normal fluid, $\mathbf{v}_n$, is an *average* over a statistical distribution, whereas $\mathbf{v}_s$ is the *exact* local velocity of *all* the particles constituting the superfluid fraction of the mixture, we may exemplify the situation by a simple kinetic model: Consider transitions between the two fluids to occur through two-particle collisions of the type

$$\mathbf{u}_1+\mathbf{u}_2\rightleftarrows\mathbf{u}_3+\mathbf{v}_s, \quad (4.1)$$

where $\mathbf{u}_1$, $\mathbf{u}_2$, and $\mathbf{u}_3$ are velocities different from $\mathbf{v}_s$, and the particles having these velocities are thus part of the normal fluid. Such a collision proceeding from left to right of Eq. (4.1) constitutes the transition of one particle from the normal to the superfluid; proceeding from right to left it represents an elementary transition from the superfluid to the normal fluid.

Consider δN such transitions from the superfluid to the normal fluid taking place in a small volume element of the liquid, resulting in a change in the mass of normal fluid

$$\delta M_n=-\delta M_s=m\delta N; \quad (4.2)$$

m is the mass of the single particle of the liquid. There is no change in the velocity of the superfluid due to such collisions:

$$\delta\mathbf{v}_s=0. \quad (4.3)$$

However there is a change in the momentum of the superfluid due to the change in the number of particles constituting the superfluid,

$$\delta\mathbf{P}_s=\mathbf{v}_s\delta M_s=-\mathbf{v}_s\delta M_n. \quad (4.4)$$

Since the total momentum is conserved in these collisions we have for the change of momentum of the normal fluid

$$-\delta\mathbf{P}_s=\delta\mathbf{P}_n=M_n\delta\mathbf{v}_n+\mathbf{v}_n\delta M_n. \quad (4.5)$$

Thus one obtains for the change in the velocity of the normal fluid

$$\delta\mathbf{v}_n=(\mathbf{v}_s-\mathbf{v}_n)\delta M_n/M_n, \quad (4.6)$$

which is just the last term in the equation of motion (2.20′) of the normal fluid.†

Throughout the present paper we have confined ourselves to a consideration of reversible effects, the method of derivation from a variational principle not being suitable for the treatment of dissipative processes. Thus we have neglected the viscosity of the normal fluid. If the viscosity were to be taken into account there would appear, in particular, a dissipative term proportional to the square of the velocity of the normal fluid in Eq. (1.7) giving the rate of change of the entropy density. A similar term would then appear in Eq. (2.23) relating the source density Γ of the normal fluid to the rate of change of the entropy. Thus the term

$$-\mathbf{v}\Gamma/\rho_n$$

in the equation of motion (2.20′) would be modified by a correction term cubic in the velocities, which is the type of term shown by Gorter[10] to be required for a correct description of the heat conduction data. Irreversible effects will be considered in detail in a later paper.

The author is indebted to Professor F. London of Duke University for suggesting the problem and for a number of stimulating discussions.

† *Note added in proof.*—By considering the conservation of total energy

$$E=\tfrac{1}{2}M_n v_n^2+\tfrac{1}{2}M_s v_s^2+(M_s+M_n)U$$

in these collisions one can obtain directly the equilibrium condition (2.12):

$$0=\delta E=\tfrac{1}{2}v^2\delta M_n+M_n\mathbf{v}_n\cdot\delta\mathbf{v}_n+(M_s+M_n)(\partial U/\partial M_n)\delta M_n.$$

Using Eq. (4.6) this yields immediately

$$(M_s+M_n)\partial U/\partial M_n=\tfrac{1}{2}v^2.$$

The Radiofrequency Spectrum of $Rb^{85}F$ and $Rb^{87}F$ by the Electric Resonance Method*

VERNON HUGHES** AND LUDWIG GRABNER
Columbia University, New York, New York

(Received February 24, 1950)

The radiofrequency spectrum of the two molecular species $Rb^{85}F$ and $Rb^{87}F$ was studied by the molecular beam electric resonance method. The electrical quadrupole interaction constant, eq_1Q_1/h, of Rb in RbF was determined for $Rb^{87}F$ in rotational states $J=1$ and $J=2$ for the first few vibrational states, and for $Rb^{85}F$ in rotational state $J=1$ for the first few vibrational states. The interaction constants are unusually large for an alkali halide molecule; for the zeroth vibrational state of $Rb^{85}F$, $eq_1Q_1/h = -70.31\pm0.10$ Mc/sec. and for the zeroth vibrational state of $Rb^{87}F$, $eq_1Q_1/h = -34.00\pm0.06$ Mc/sec. The absolute value of the interaction constant decreases about 1.1 percent from one vibrational state to the next higher one; the values of the interaction constants for rotational states $J=1$ and $J=2$ are the same within the limit of error. The ratio of the electric quadrupole moment of Rb^{85} to that of Rb^{87} is $+2.07\pm0.01$.

Results are reported on the spin-orbit coupling $c_2(\mathbf{I}_2\cdot\mathbf{J})$, between the spin of the fluorine nucleus and the molecular rotational angular momentum. For the zeroth vibrational state of $Rb^{85}F$, $|c_2/h| = 11\pm3$ kc/sec. and for the zeroth vibrational state of $Rb^{87}F$, $|c_2/h| = 14\pm4$ kc/sec. No variation in $|c_2/h|$, with vibrational state was observed.

Finally, an unpredicted line group was observed in the spectrum at one-half the frequency of one of the line groups in the $Rb^{85}F$ spectrum. Possible origins of this line group are discussed, including that of a double quantum transition.

The vibrational frequency, ω_0, of $Rb^{85}F$ is 340 ± 68 cm^{-1}.

I. INTRODUCTION

THE radiofrequency spectrum of the two isotopic species of RbF—$Rb^{87}F$ and $Rb^{85}F$—have been studied by the molecular beam electric resonance method.[1,2] This technique permits the study of the energy levels in a static electric field of polar diatomic molecules which are in the $^1\Sigma$ electronic state, in a low vibrational state, and in the rotational state $J=1$. Sometimes molecules in the rotational state $J=2$ can also be studied. The research reported in this paper is a continuation of the studies of the internal interactions of the alkali fluoride molecules.[2,3] The apparatus used was the one described in references 1 and 2, and further details on the experimental technique are given in reference 3.

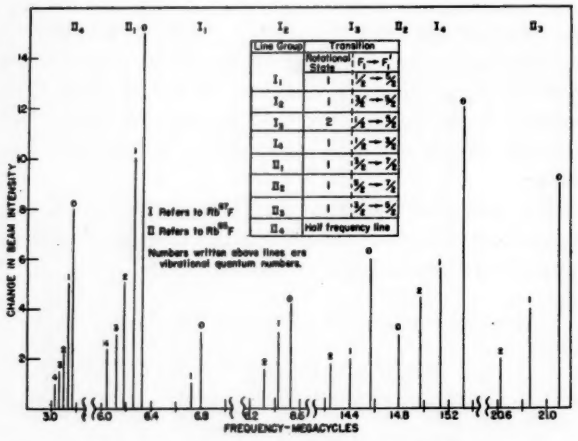

FIG. 1. Spectrum observed for $Rb^{85}F$ and $Rb^{87}F$ under low electric field conditions (i.e., $\mu^2E^2/h^2/2A \ll |eq_1Q_1|$). Change in beam intensity is expressed in cm of deflection on a galvanometer scale. All the lines were not taken under comparable conditions so line intensities cannot be compared indiscriminately. Fine structure of the lines is not indicated.

Under low field conditions the frequencies of the transitions induced are determined primarily by the internal molecular interactions. The largest of these is the electrical quadrupole interaction associated with the Rb nucleus, and it was determined for each molecular species for several vibrational states. The interaction constants for the RbF molecules are very much larger than those for CsF[2] or $K^{39}F$[3] or, indeed, than those for any other alkali halide molecule yet studied.

A splitting of the spectral lines of both $Rb^{87}F$ and $Rb^{85}F$ was observed. This is caused primarily by a spin-orbit interaction between the fluorine nucleus and the molecular rotational angular momentum. The magnetic dipole-dipole interaction between the two nuclei also contributes slightly to this splitting.

The appearance of an unpredicted line group at exactly one-half the frequency of a line group in the weak field spectrum of $Rb^{85}F$ is reported. Possible explanations for these lines are discussed, including the one that they are double quantum transitions in which two one-half frequency quanta provide the energy for the transitions. However, none of these explanations seems to account for all the observations.

II. EXPERIMENTAL DATA

The spectra for the two isotopic species $Rb^{87}F$ and $Rb^{85}F$, were observed simultaneously[4] under conditions of low electric field intensity, i.e., the interaction energy of the external electric field with the molecule was small compared to the electrical quadrupole interaction energy associated with the Rb nucleus. The spectrum (see Fig. 1) consists of some 26 lines occurring in the

* This research has been supported in part by the ONR.

** Submitted by Vernon Hughes in partial fulfillment of the requirements for the degree of Doctor of Philosophy in Physics at Columbia University.

[1] H. K. Hughes, Phys. Rev. 72, 614 (1947).
[2] J. W. Trischka, Phys. Rev. 74, 718 (1948).
[3] L. Grabner and V. Hughes (to be published).

[4] Simultaneous observation of the spectra of both isotopic species was possible because the A and B field voltages which refocus one molecular isotope refocus the other molecular isotope as well. All the data were taken using the $(1, \pm1)_A - (1, 0)_B$ refocused beam as described in reference 3.

frequency range from about 3 Mc/sec. to 21 Mc/sec.; a search was made over the more extended range from 1 Mc/sec. to 45 Mc/sec. but no lines were found other than those shown. These lines are analyzed into line groups which are designated by Roman numerals with subscripts. The lines within a group correspond to the same transition for different vibrational states, and they are distinguished by the vibrational quantum numbers which are written directly above the lines. It will be shown that with the exception of the line group near 3 Mc/sec., the spectrum can be understood as due to transitions of molecules with rotational states $J=1$ and $J=2$.

III. THEORY

The following Hamiltonian is assumed for the diatomic molecule in a static electric field.[2]

$$\mathcal{H}=\frac{\hbar^2}{2A}\mathbf{J}^2-\boldsymbol{\mu}\cdot\mathbf{E}-\frac{eq_1Q_1}{2I_1(2I_1-1)(2J-1)(2J+3)}\times\{3(\mathbf{I}_1\cdot\mathbf{J})^2+\tfrac{3}{2}(\mathbf{I}_1\cdot\mathbf{J})-\mathbf{I}_1^2\mathbf{J}^2\}+c_2(\mathbf{I}_2\cdot\mathbf{J})+\frac{g_1g_2\mu_N^2}{r^3}\left\{\mathbf{I}_1\cdot\mathbf{I}_2-3\frac{(\mathbf{I}_1\cdot\mathbf{r})(\mathbf{I}_2\cdot\mathbf{r})}{r^2}\right\}. \quad (1)$$

The first term in which $\mathbf{J}$ is the rotational angular momentum and A is the moment of inertia is the rotational energy term. The second term gives the interaction of the external electric field $\mathbf{E}$ with the permanent electric dipole moment $\boldsymbol{\mu}$ of the molecule. The third term is the electrical quadrupole interaction between the electric quadrupole moment of the Rb nucleus, Q_1, and a second derivative of the electric potential at the position of the Rb nucleus, q_1, produced by those charges in the molecule which are exterior to the nucleus.[5] (The subscript $_1$ refers to the Rb nucleus.) $\mathbf{I}_1$ is the spin of the Rb nucleus. There is no electrical quadrupole interaction with the F nucleus because its spin is $\frac{1}{2}$. The fourth term is a cosine coupling between the spin of F designated by $\mathbf{I}_2$ and the rotational angular momentum of the molecule.[6,7] The last term is the magnetic dipole-dipole interaction between the Rb and F nuclei, in which $\mathbf{r}$ is the internuclear distance, g_1 and g_2 are the gyromagnetic ratios for the Rb and F nuclei respectively, and μ_N is one nuclear magneton.[8]

Several vibrational states and two rotational states are expected to be present in the refocused beam, so the observed spectrum will be a superposition of lines from molecules in these different rotational and vibrational states. Hence we shall observe the variation of the terms appearing in the Hamiltonian with vibrational and rotational state.

TABLE I. Quadrupole interactions of Rb^{85} in $Rb^{85}F$ and of Rb^{87} in $Rb^{87}F$.

	Line	Rotational state	Transition $F_1\rightarrow F_1'$	Vibrational state	Line frequency (center of line*) in Mc./sec.	Quadrupole interaction $-(eq_1Q_1/h)$ in Mc./sec.
$Rb^{85}F$	${}^0II_1$	1	3/2→7/2	0	6.328	70.312
	${}^1II_1$	1	$0.09(eq_1Q_1/h)$	1	6.259	69.544
	${}^2II_1$	1		2	6.184	68.712
	${}^3II_1$	1		3	6.119	67.988
	${}^4II_1$	1		4	6.048	67.200
	${}^0II_2$	1	5/2→7/2 $0.21(eq_1Q_1/h)$	0	14.800	70.476
	${}^0II_3$	1	3/2→5/2	0	21.103	70.344
	${}^1II_3$	1	$0.3(eq_1Q_1/h)$	1	20.863	69.544
	${}^2II_3$	1		2	20.632	68.774
$Rb^{87}F$	${}^0I_1$	1	1/2→5/2	0	6.800	34.000
	${}^1I_1$	1	$0.2(eq_1Q_1/h)$	1	6.725	33.626
	${}^2I_1$	1		2	6.640	33.200
	${}^0I_2$	1	3/2→5/2	0	8.520	34.080
	${}^1I_2$	1	$0.25(eq_1Q_1/h)$	1	8.425	33.700
	${}^2I_2$	1		2	8.330	33.320
	${}^0I_3$	2	1/2→5/2	0	14.570	33.996
	${}^1I_3$	2	$3/7(eq_1Q_1/h)$	1	14.418	33.642
	${}^2I_3$	2		2	14.250	33.250
	${}^0I_4$	1	1/2→3/2	0	15.319	34.042
	${}^1I_4$	1	$0.45(eq_1Q_1/h)$	1	15.143	33.552
	${}^2I_4$	1		2	14.971	33.268

* See text for further discussion of how the "centers" of the lines are chosen.

In the application of the perturbation theory to the calculation of the eigenvalues of (1), it is important to know that $|eq_1Q_1|\gg|c_2|$ and $(g_1g_2\mu_N^2/r^3)$. Furthermore, the electric field intensity is such in our experiments that either:

$$\mu^2E^2/(\hbar^2/2A)\ll|c_2| \quad (\text{"very weak" field}) \quad (a)$$

or

$$|eq_1Q_1|\gg\mu^2E^2/(\hbar^2/2A)\gg|c_2| \quad (\text{"weak" field}). \quad (b)$$

In both cases there is a strong coupling of $\mathbf{I}_1$ and $\mathbf{J}$, which is the electrical quadrupole interaction associated with Rb; hence there is a well-defined $\mathbf{F}_1=\mathbf{I}_1+\mathbf{J}$ vector. We regard the zeroth order part of our Hamiltonian as:

$$\mathcal{H}_0=\frac{\hbar^2}{2A}\mathbf{J}^2-\frac{eq_1Q_1}{2I_1(2I_1-1)(2J-1)(2J+3)}\times\{3(\mathbf{I}_1\cdot\mathbf{J})^2+\tfrac{3}{2}(\mathbf{I}_1\cdot\mathbf{J})-\mathbf{I}_1^2\mathbf{J}^2\} \quad (2)$$

$\mathcal{H}_0$ has only diagonal matrix elements in a representation (I_1, J, F_1, m_{F_1}), in which m_{F_1} is the projection of F_1 in the field direction. These energy values depend upon F_1 but are degenerate in m_{F_1}. In case (a) $\mathbf{F}_1$ and $\mathbf{I}_2$ are coupled by the internal interactions involving $\mathbf{I}_2$ (4th and 5th terms in (1)) to form a total angular momentum $\mathbf{F}=\mathbf{F}_1+\mathbf{I}_2$. In a representation (I_1, J, F_1, I_2, F, M), in which M is the projection of $\mathbf{F}$ in the field direction, the first and third terms in the Hamiltonian (1) are diagonal. The diagonal matrix elements of the fourth

[5] J. Bardeen and C. H. Townes, Phys. Rev. **73**, 97 (1948). Note that in the initial report of this research in the abstracts of the June, 1949, American Physical Society meeting at Cambridge, q' rather than q_1 was used. ($q'=q_1/2e$ in which e is the proton charge.) Since our first report it has been agreed in this laboratory, in the interests of uniformity, to use q as defined by Bardeen and Townes.

[6] H. Foley, Phys. Rev. **72**, 504 (1947).

[7] G. C. Wick, Phys. Rev. **73**, 51 (1948).

[8] Kellogg, Rabi, and Ramsey, Phys. Rev. **72**, 1075 (1947).

and fifth terms of (1) depend on F but not on M. There are off-diagonal elements of the fourth and fifth terms in (1) which connect different F_1 states, but these are neglected in our computations. The $-\boldsymbol{\mu}\cdot\mathbf{E}$ interaction has no diagonal matrix elements in this representation, and its effect is computed by second-order perturbation theory. The degeneracy for different M values is partially removed by the field interaction, but states differing only in the sign of M still remain degenerate. In case (b) we use a representation (I_1, J, F_1, m_{F_1}, I_2, m_2) in which m_2 is the projection of $\mathbf{I}_2$ in the field direction. The first and third terms in (1) have only diagonal matrix elements and are considered first. The interaction with the field, $-\boldsymbol{\mu}\cdot\mathbf{E}$, is computed by second-order perturbation theory and finally the effects of the $c_2(\mathbf{I}_2\cdot\mathbf{J})$ interaction and of the nuclear dipole-dipole interaction are considered as smaller perturbations which couple $\mathbf{F}_1$ and $\mathbf{I}_2$. The field interaction is the same for states with $+m_{F_1}$ and $-m_{F_1}$ and the interactions involving $\mathbf{I}_2$ are the same for states with the same value of the product $m_{F_1}m_2$. Hence some degeneracy remains even after all interactions have been considered. The eigenvalues and eigenfunctions for the two cases are given in detail elsewhere.[9,10]

IV. ANALYSIS OF SPECTRUM

(A) Spectrum of $Rb^{85}F$

The lines assigned to the more abundant (73 percent) molecular species $Rb^{85}F$, in which the Rb nucleus has a spin of 5/2, are shown in Fig. 1. The three line groups, designated II_1, II_2, and II_3, are assigned to rotational state $J=1$. The uniqueness of this assignment rests on the facts that: (1) Only a few of the lower rotational states can be present in the refocused beam because only these are deflected sufficiently to get around the wire stop. Indeed only rotational states $J=1$ and $J=2$ are known to have been refocused as yet in electrical resonance experiments. (2) The spectral pattern is different for different rotational states.

The lines within a group are assigned to different vibrational states as indicated by numbers written directly above the lines. There is a fine structure for the lines which is not indicated in Fig. 1. This structure is due to the $-(\boldsymbol{\mu}\cdot\mathbf{E})$ interaction and to the fourth and fifth terms in the Hamiltonian (1), and will be discussed in the next paragraphs.

The positions of the lines are determined primarily by the change in the electrical quadrupole interaction-energy of Rb-term (3) in Hamiltonian (1). This change can be designated by the two F_1 values involved and in Table I the transition to which each line corresponds is indicated. The line frequency is taken at the center of the fine structure and on this basis the electrical quadrupole interaction constant is calculated. The reliability of the values shown for the interaction constants can only be evaluated after we have discussed the fine structure of the lines; however, it can be remarked that the equality of the quadrupole interaction constants evaluated from the different line groups is the proof that the identification of the observed lines with certain transitions is correct.

That the quadrupole interaction constant, eq_1Q_1/h, must be negative will now be shown with the aid of Fig. 2. It is to be remembered that transitions between states at low fields will be observed only if the two states involved correspond to states with different $|m_J|$ at high fields.[3] It is seen from Fig. 2, which is drawn for $eq_1Q_1/h<0$, that transitions from the levels $F_1=3/2$ to $F_1=7/2$ will be observable. If a diagram similar to Fig. 2 is drawn for the case in which $eq_1Q_1/h>0$, then it will be seen that a transition from a state with $F_1=3/2$ to a state with $F_1=7/2$ would be between two states which at high fields had $|m_J|=1$, and hence

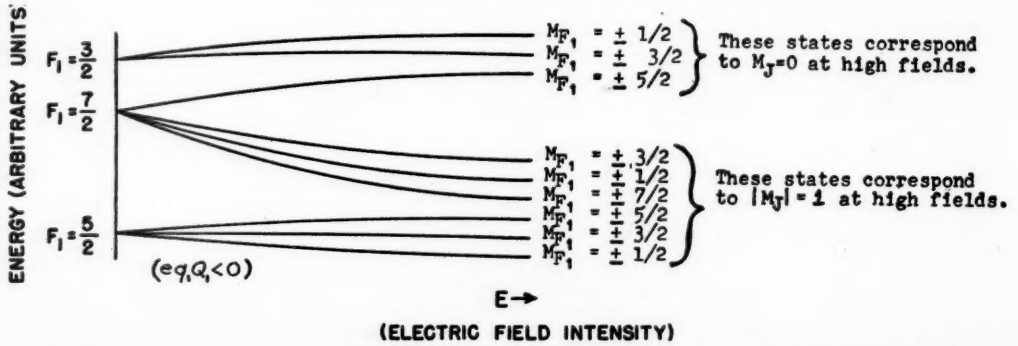

FIG. 2. A diagram indicating which low field states of $Rb^{85}F$ go into states with $M_J=0$ at high fields and which go into states with $|M_J|=1$. (M_J is the projection of $\mathbf{J}$ in the field direction—M_{F1} is the projection of $\mathbf{F}_1$ in the field direction.) States with $J=1$ and $I_1=5/2$ are shown. An adiabatic change in the field parameter is assumed. The level spacings are not drawn to scale and there may be some crossing of levels with different MF_1 values, but these matters are not important to the discussion for which this figure is used. The correct ordering of the levels at high and low fields is shown. See reference 10 for the method of establishing the correspondence between low and high field states.

[9] Nierenberg, Rabi, and Slotnick, Phys. Rev. **73**, 1430 (1948).
[10] V. Hughes and L. Grabner (to be published).

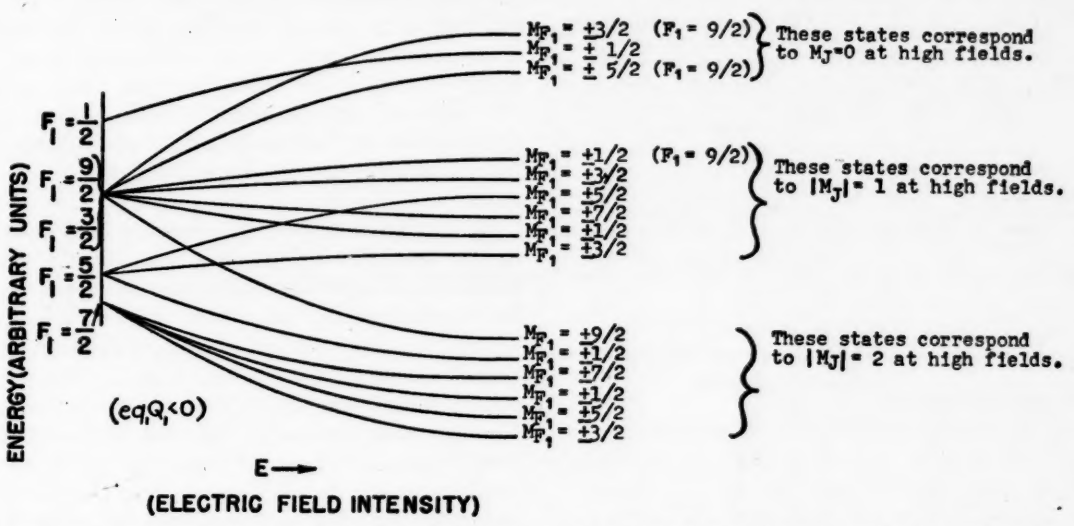
These states correspond to $M_J=0$ at high fields.
These states correspond to $|M_J|=1$ at high fields.
These states correspond to $|M_J|=2$ at high fields.
ENERGY (ARBITRARY UNITS)
$(eq_1Q_1<0)$
E→
(ELECTRIC FIELD INTENSITY)

FIG. 3. A diagram indicating the correspondence between low and high field states for $Rb^{85}F$ ($I_1=5/2$, $J=2$). Other remarks apply as given in Fig. 2.

would not be observed. Since this transition was observed experimentally, eq_1Q_1/h must be negative.[11]

The number of line groups observed will now be considered in view of the selection rules and with the assumption of the observability criterion.[12] For the rotational state $J=1$ three transitions are allowed and all three were observed. It can be noted from Fig. 2 that the transition $F_1=5/2$ to $F_1=7/2$ is expected to be weak because most of the component lines are non-observable; it is indeed true that this line is of weak intensity. The non-appearance of any $J=2$ lines for $Rb^{85}F$ can be made plausible with the aid of Fig. 3. It is pointed out in reference 3 that because of the nature of the refocusing process if the observability criterion holds a transition at low fields will be observed only if it is between two states which at high fields correspond to $m_J=0$ and $|m_J|=2$. Of the seven lines allowed by the selection rule $\Delta F_1=\pm1, \pm2$ four will not be observed because they do not satisfy the above condition. Three transitions—($F_1=1/2$, to $F_1=5/2$), ($F_1=9/2$ to $F_1=7/2$), and $F_1=9/2$ to $F_1=5/2$)—satisfy the observability requirement but they would be expected to be weak lines for the following reasons:

(a) Only a few of the component lines for these F_1 transitions fulfil the observability requirement.

(b) The fraction of the total number of $J=2$ state molecules issuing from the oven that appear in the refocused beam is smaller than the analogous fraction for $J=1$ state molecules, because a larger fraction of $J=2$ state molecules impinge on the wire stop. Hence it is expected that these lines would be weak, and they were not observed at all.

Fine Structure

For a study of the fine structure we consider the line group II_1 (Fig. 4) which was taken under "very weak" field conditions. Five lines were observed corresponding to vibrational states $v=0$ to $v=4$; each line is a doublet with a separation between the two components of about 20 kc/sec. The interaction of the electric field with the molecule is less than 1 kc/sec., and hence is negligible.[13]

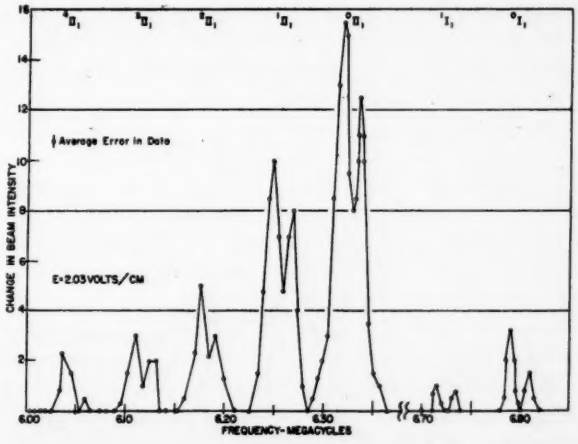

FIG. 4. Detailed spectrum of line groups II_1 and I_1 (see Table I). For line group I_1 radiofrequency field, $E_{rf}\sim4$ volts/cm: for line group II_1, $E_{rf}\sim8$ volts/cm. Change in beam intensity is expressed in cm of deflection on a galvanometer scale.

[11] The correspondence between states at low fields and at high fields which must be known in order to draw a figure such as figure 2 is established by the requirements that a state has the same m_{F_1} value at all fields and that states with the same m_{F_1} values cannot cross. See reference 10.

[12] See reference 10. The selection rule is $\Delta F_1=0, \pm1, \pm2$. The transitions with $\Delta F_1=0$ would involve frequencies of the order of the fine structure of our lines; such transitions were not studied. The observability criterion is that transitions will be observed only if they occur between states which can be adiabatically transformed into states at high fields with the proper $|m_J|$ values for the refocussing process. The existence of the refocused beam $(1, \pm1)_A-(1, 0)_B$ indicates the occurrence of nonadiabatic transitions in the interfield, regions and hence it may be that the observability criterion is not strictly applicable. For further discussion see references 3 and 10.

[13] This interaction is calculated using a value for μ of 10.6 debye.

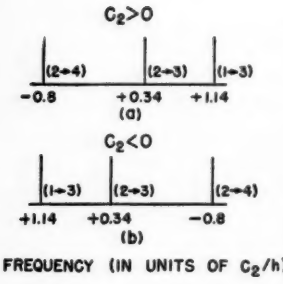

FIG. 5. Line splitting predicted from interaction $c_2(\mathbf{I}_2\cdot\mathbf{J})$ for transition $F_1=3/2$ to $F_1=7/2$ of $Rb^{85}F$ ($J=1$). The transition in F value is indicated in parentheses. Figure (a) applies when $c_2>0$ and figure (b) applies when $c_2<0$. No attempt is made to indicate relative line intensities. Zero value for the abscissa refers to the line position due to the quadrupole interaction alone.¶

TABLE II. Internal interactions of $Rb^{85}F$ and $Rb^{87}F$.

	Rotational state	Vibrational state	Quadrupole interaction $-eq_1Q_1/h$ in Mc./sec.	$\lvert c_2/h\rvert$ kc/sec.
	1	0	70.31±0.10	11±3
	1	1	69.54±0.10	13±3
$Rb^{85}F$	1	2	68.71±0.10	10±3
	1	3	67.99±0.10	10±3
	1	4	67.20±0.10	14±4
	1	0	34.00±0.06	14±4
	1	1	33.63±0.06	14±4
$Rb^{87}F$	1	2	33.20±0.06	—
	2	0	34.00±0.06	—
	2	1	33.62±0.06	—
	2	2	33.25±0.06	—

It is natural to assume that the doublet should arise from an interaction involving the fluorine nucleus. Two such interactions are given in the fourth and fifth terms of the Hamiltonian of Eq. (1). Using the known values of g_1 and g_2[14] and a calculated value of the internuclear distance,[15] it is found that the maximum splitting that the nuclear dipole-dipole interaction can produce is about 1 kc/sec. Hence the major portion of the splitting must be assigned to the spin-orbit interaction between the F nucleus and the molecular rotational angular momentum.

Since this line group was taken under "very weak" field conditions, an appropriate representation for the states involved is (I_1, J, F_1, I_2, F, M); the energy depends on M only because of the field interaction. The transition is $F_1=3/2$ to $F_1=7/2$ so the states involved are (5/2, 1, 3/2, 1/2, 1, M), (5/2, 1, 3/2, 1/2, 2, M) and (5/2, 1, 7/2, 1/2, 3, M), (5/2, 1, 7/2, 1/2, 4, M). The general selection rule allows $\Delta F=0, \pm1, \pm2$ but not[12] $\Delta F=\pm3$, so three components are allowed for the line of each vibrational state. Actually, the lines are split into two components with the larger intensity component appearing at the lower frequency.

The line splitting expected for the $c_2(\mathbf{I}_2\cdot\mathbf{J})$ interaction is shown in Fig. 5 for the cases of c_2 negative and positive. The positions of the three component lines were computed from the weak field formula given in reference 9. A half-width of about 10 kc/sec is predicted for our lines from the relationship $\Delta\nu\Delta t\sim1$ in which $\Delta\nu$ is the half width in c.p.s. and Δt is the time spent by the molecule in the C-field.[2] Thus in view of the magnitude of the observed line splitting (~20 kc/sec) we would not expect to resolve the two closer-lying component lines ($F=3\rightarrow F=1$) and ($F=3\rightarrow F=2$). One of the lines of the observed doublet must therefore be regarded as the superposition of the two line components ($F=3\rightarrow F=1$) and ($F=3\rightarrow F=2$).

To say which of the two observed lines corresponds to the transition ($F=4\rightarrow F=2$) requires a theory of relative line intensities. It does not seem, however, that experimental conditions are sufficiently well known to allow such a theory. Thus non-adiabatic transitions are known to occur in the absence of an applied radiofrequency field as the molecule traverses the apparatus, and such transitions could affect relative line intensities. It is believed that these transitions occur in the interfield region between the A and C fields, but little is known of their exact character. Furthermore, the amplitude of the radiofrequency field at the position of the beam is adjusted so that the transition probability is believed to be rather high. But the r-f amplitude is not sufficiently well known so that relative transition probabilities can be calculated. Several simplifying assumptions have been tried, but none of them explained the relative intensity data for the $c_2(\mathbf{I}_2\cdot\mathbf{J})$ splitting in both the $Rb^{85}F$ and $Rb^{87}F$ spectra. A further discussion of relative line intensities is given in reference 10.

The inability to say which of the two observed lines corresponds to the transition ($F=2$ to $F=4$) means that only the absolute value of c_2/h can be determined. If we assume that either one of the observed lines appears midway between the predicted positions of the transitions ($F=3\rightarrow F=1$) and ($F=3\rightarrow F=2$)—i.e. at $0.74\ c_2/h$—and that the other observed line appears at the position of the transition ($F=4\rightarrow F=2$)—i.e. at $-0.8c_2/h$—we easily compute that $\lvert c_2/h\rvert=(11\pm3)$ kc/sec. for vibrational state $v=0$. The results for the other vibrational states as well are given in Table II. The limiting error of ±3 kc/sec. is assigned because of

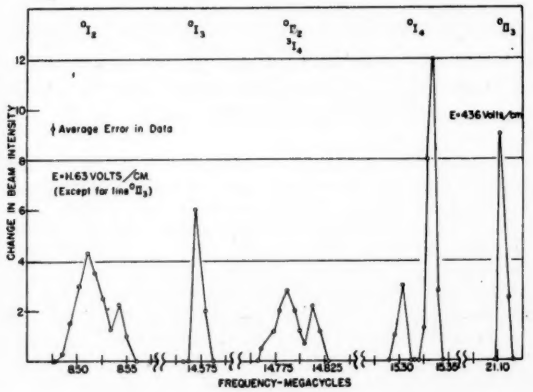

FIG. 6. Detailed spectrum of zeroth vibrational state lines for several line groups (see Table I). $E_{rf}\sim4$ volts/cm. Change in beam intensity is expressed in cm of deflection on a galvanometer scale.

[14] J. B. M. Kellogg and S. Millman, Rev. Mod. Phys. **18**, 323 (1946).
[15] Schomaker and Stevenson, J. Am. Chem. Soc. **63**, 37 (1941).

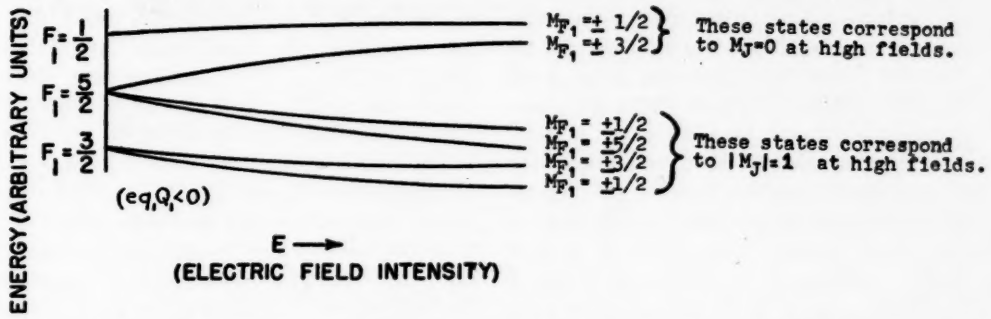

FIG. 7. A diagram indicating the correspondence between low and high field states for $Rb^{87}F$ ($I_1=3/2$, $J=1$). Other remarks apply as given in Fig. 2.

the uncertainty in the peak positions of the observed lines and because of the uncertainty as to whether the observed line which corresponds to the transitions ($F=3\rightarrow F=1$) and ($F=3\rightarrow F=2$) appears exactly at the midpoint between the predicted positions of these two transitions.

We can now discuss the accuracy with which the determination of the quadrupole interaction constant is made. Our understanding of the fine structure splitting of the $F_1=7/2$ to $F_1=3/2$ line allows us to specify the position at which this line would appear in the absence of the $c_2(\mathbf{I}_2\cdot\mathbf{J})$ interaction. These frequencies are given in Table I for the line group II_1 and are called the positions of the "centers" of the lines. Because of the experimental uncertainty in the determination of the peaks of the lines, these positions can only be given to ± 5 kc/sec. This implies that the quadrupole interaction constant can be given to about ± 0.1 percent. Another source of error arises from the theory used, which neglected off-diagonal matrix elements of the quadrupole operator connecting different J states.[16] The percentage error thus introduced is of the order of the quadrupole interaction energy divided by the energy difference between rotational states J and $J+2$ and for our case is about 0.1 percent. The correction of the theory has not been made because the error introduced is of the order of the error in the experimental data.

Little can be learned from the fine structure of the other $Rb^{85}F$ lines, because both lines were obtained under electric field conditions such that the $(\boldsymbol{\mu}\cdot\mathbf{E})$ term as well as the small internal interactions (terms (4) and (5) in Hamiltonian (1)) contribute significantly to the fine structure. The zeroth vibrational states of the two other line groups (II_2 and II_3) assigned to $Rb^{85}F$ are shown in Fig. 6. Line ${}^0II_3$ was obtained for a field condition intermediate between "very weak" and "weak." It is a superposition of some 10 unresolved components which are produced by a splitting due to the field interaction of 10 kc/sec. and by a splitting due to the $c_2(\mathbf{I}_2\cdot\mathbf{J})$ interaction of 8 kc/sec. Line ${}^0II_2$ was obtained under "weak" field conditions and is composed of 4 components with a total width of about 40 kc/sec.

[16] See U. Fano, J. Research Nat. Bur. Stand. 40, 215 (1948).

In the observed structure there also occurs the vibrational state $v=3$ for line group I_4 of $Rb^{87}F$. Line ${}^0II_2$ appears with low intensity and the higher vibrational states were not observed. The positions of the centers of the lines in line groups II_2 and II_3 (defined as the centers of the observed structures) provide confirmation for the values of the quadrupole interaction constants determined from line group II_1 (See Table I).

(B) Spectrum of $Rb^{87}F$

We consider those lines in the spectrum which are assigned to the less abundant (27 percent) molecular species $Rb^{87}F$ (see lines designated by I in Fig. 1). The nucleus Rb^{87} has a spin of 3/2; hence we expect the spectrum of $Rb^{87}F$ to be similar to that of $K^{39}F$ which is reported upon in detail in another paper.[3] Indeed, four line groups were observed under low electric field conditions as was also the case for $K^{39}F$. Three of these groups, designated I_1, I_2, and I_4, are assigned to rotational state $J=1$; and line group I_3 is assigned to rotational state $J=2$.

The transition in F_1 value to which each line corresponds is indicated in Table I. The quadrupole interaction constants are calculated by taking as the line positions the centers of the fine structure of the lines. The sign of the quadrupole interaction constant, eq_1Q_1, is determined to be negative by the existence of the line group $F_1=1/2$ to $F_1=5/2$, as explained in reference 3 (see Fig. 7). The argument is similar to that used earlier in this paper to prove that the quadrupole interaction constant for $Rb^{85}F$ is negative.

The number of line groups expected on the basis of

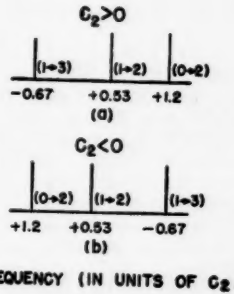

FIG. 8. Line splitting predicted from interaction $c_2(\mathbf{I}_2\cdot\mathbf{J})$ for transition $F_1=1/2$ to $F_1=5/2$ of $Rb^{87}F$ ($J=1$). The transition in F value is indicated in parentheses. Figure (a) applies when $c_2>0$ and figure (b) applies when $c_2<0$. No attempt is made to indicate relative line intensities. Zero value for the abscissa refers to the line position due to the quadrupole interaction alone.

the observability criterion were observed. For the rotational state $J=1$ three transitions are allowed and all three were observed.[12] For the rotational state $J=2$ five transitions are allowed;[12] two of these are coincident with transitions for the $J=1$ state and a third is observed.[17] The other two allowed transitions for the $J=2$ state were not observed because they occur between states which experience the same deflection in the B field; i.e., have the same value of $|m_J|$ at high fields. This matter is discussed in detail in reference 3 for the exactly similar case of $K^{39}F$, and an analogous discussion has been given earlier in this paper for the isotopic species $Rb^{85}F$.

Fine Structure

The fine structure of $Rb^{87}F$ is similar to that of $Rb^{85}F$. Line group I_1, shown in Fig. 4, was taken under "very weak" field conditions for which the effect of the field term is negligible. Two lines were observed corresponding to vibrational states $v=0$ and $v=1$.[18] The doublet character of the lines is due primarily to the interaction $c_2(\mathbf{I}_2\cdot\mathbf{J})$. The contribution to the splitting caused by the nuclear spin-spin interaction is less than 1 kc/sec.

The line splitting expected for the $c_2(\mathbf{I}_2\cdot\mathbf{J})$ interaction is shown in Fig. 8 for the cases of c_2 negative and positive. The two component lines ($F=2\rightarrow F=0$) and ($F=2\rightarrow F=1$) of Fig. 8 will be unresolved, so the doublet which is observed is expected.

As in the analogous case for $Rb^{85}F$ it is not possible to say which of the two observed lines corresponds to the transition ($F=3\rightarrow F=1$) because of the lack of understanding of line intensities. Thus only the absolute value and not the sign of c_2/h can be determined. By a comparison of the observed doublet with the line pattern of Fig. 8 it is found by reasoning similar to that used for $Rb^{85}F$ that $|c_2/h|=(14\pm4)$ kc/sec. for both the $v=0$ and $v=1$ vibrational states. This value is the same within experimental error as the value of $|c_2/h|$ obtained for $Rb^{85}F$. This agreement is expected since by its nature the $c_2(\mathbf{I}_2\cdot\mathbf{J})$ interaction depends only on the fluorine nucleus and the molecular electronic configuration, and so should be substantially the same for the two isotopic species.

As for the case of $Rb^{85}F$ we use this knowledge of c_2 to specify the positions at which the lines $F_1=5/2$ to $F_1=1/2$ would appear in the absence of the $c_2(\mathbf{I}_2\cdot\mathbf{J})$ interaction. These positions are given as the "centers" of the lines in line group I_1 in Table I, and from them are computed the quadrupole interaction constants given in Table II. The accuracy with which the quadrupole interaction constants can be stated is limited in exactly the same way as for $Rb^{85}F$.

The zeroth vibrational state lines of the other $Rb^{87}F$ line groups are shown in Fig. 6 and the transitions to which they correspond are indicated in Fig. 1. They were obtained under "weak" field conditions so that the $-(\boldsymbol{\mu}\cdot\mathbf{E})$ interaction contributes significantly to the fine structure. It is predicted that line ${}^0I_2$ will be split into five components by the field interaction and the $c_2(\mathbf{I}_2\cdot\mathbf{J})$ interaction, with a separation of about 60 kc/sec. between the outermost components. This is in agreement with the observed line width, but the resolution was not sufficient to distinguish all this structure. For line ${}^0I_4$ a splitting due to the field interaction into two components of about the observed separation is predicted. Each of these components will in principle be further split by the interactions with the F nucleus; the magnitude of this splitting is below the resolution of the experiment. Finally, the internal structure of line ${}^0I_3$, which is assigned to rotational state $J=2$, caused by the field interaction and by the interactions with the F nucleus is less than the resolution width.

The positions of the centers of lines I_2, I_3, and I_4 (defined as the centers of the observed structures) confirm the values of the quadrupole constants determined from line I_1 (see Table I).

V. THE EXTRA LINE

An extra line group shown in Fig. 9 was observed in the neighborhood of 3 Mc/sec. This line group appears in all detail at one half the frequency of line group II_1 which was shown in Fig. 4. This extra line group is not predicted from the Hamiltonian (1) for either molecular species for rotational states $J=0$ to $J=3$, and no higher rotational states are deflected sufficiently by the inhomogeneous electric fields to pass by the wire stop.

The possibility that the half frequency line could arise because of harmonics in the oscillator which provides the radiofrequency field is believed to be ruled out by the following studies. The intensity of the 6 Mc/sec. line was studied as a function of the r-f amplitude applied to the C field plates and it was found that the line was of zero intensity when the r-f amplitude was a factor of ten less than that used for the data of Fig. 4. Then a low pass filter, which attenuated the amplitude of signals near 6 Mc/sec. by a factor of about 30 relative to those near 3 Mc/sec., was inserted between the oscillator and the C field plates, but this had no effect on the intensity of the extra line group. Furthermore, the extra line was observed to be exactly the same when taken using two different oscillators—a GR signal generator 805C, and a home-made oscillator. A study of the harmonic output of these two oscillators was made; using a GR 724—A Precision Wavemeter it was found that the second harmonic output from the

[17] It is to be remarked that the reasons mentioned earlier in the analysis of the $Rb^{85}F$ spectrum for expecting the line intensities associated with $J=2$ state transitions to be weak are applicable to $Rb^{87}F$ as well. However, a $J=2$ state transition was observed for $Rb^{87}F$ whereas none was observed for $Rb^{85}F$. It is felt that the relative line intensity problem is not well enough understood so that the non-appearance of several presumably weak lines for the $J=2$ state of $Rb^{85}F$ should be regarded as surprising.

[18] The line for vibrational state $v=2$ (Fig. 1) is not shown in Fig. 4 because this very weak line was only observed when the radiofrequency field was larger than it was for the lines shown and no fine structure was resolved.

home-made oscillator was about 1 percent, and by a measurement technique involving a radio receiver it was found that the second harmonic output from the GR 805*C* oscillator was as high as 10 percent. Both the 6 Mc/sec. and the 3 Mc/sec. lines were taken with approximately the same amplitude of the radiofrequency field as is indicated in the captions to Figs. 4 and 9. Hence, the harmonic of the 3 Mc/sec. signal could not have caused the extra line, because the 6 Mc/sec. harmonic of the 3 Mc/sec. signal would have been too low to cause a 6 Mc/sec. line of appreciable intensity. Thus it seems clear that harmonics generated by the oscillator cannot account for the extra line. And there is no other place in our circuit at which harmonics of the required amplitude would be expected to be generated, since the circuit consists simply in the connection of the output from the oscillator to the two gold-plated plates of the *C*-field.

A chemical analysis[19] of the RbF was undertaken to determine whether there were appreciable amounts of other alkali halides in the sample used. By a spectrographic analysis it was found that no other alkali was present in a concentration of greater than 1 percent, and by a precipitation test the same conclusion was reached as to the presence of other halides. Such concentrations are too small to give rise to an observable line in our spectrum. Furthermore, of course, the refocussing procedure would in general eliminate the effects of any impurities.

It was suggested by Professor I. I. Rabi that this half-frequency line might arise as a double quantum transition in which two half frequency quanta supply the energy for the transition. Transitions occur normally only because there is a perturbation of the field free state and the matrix element for a transition is proportional to $EE_{rf}\sin\omega t$ in which E is the intensity of the static field and E_{rf} is the maximum intensity of the radiofrequency field. If we regard the radiofrequency field as causing the perturbation of the field-free state as well as the transition, then the matrix element will be proportional to $E_{rf}^2\sin^2\omega t$, and hence there will be a resonance at $\omega/2$ whereas in the normal case there was a resonance at ω. A more detailed theory of this process is found in reference 10. It is clear that this process will be important when E_{rf} and E are of comparable magnitude; this is indeed the case for our experiment in which computation indicated that both the static field and the radio-frequency field are of several volts/cm intensity.

The extra line was found to disappear at a somewhat higher value of E ($\sim$55 volts/cm which is still a weak field condition, since the field interaction amounts only to about 750 kc/sec.), whereas the upper frequency line is present and split up in the predicted manner at this same value of E. The theory of the double quantum process does not predict the complete disappearance of the half-frequency line at such a low static field intensity. We were not able to determine whether the extra line was present at $E=0$ as would be expected from the theory of the double quantum transition. It should be remarked that it is often impossible to study resonance effects when the *C*-field voltage is near zero.[3]

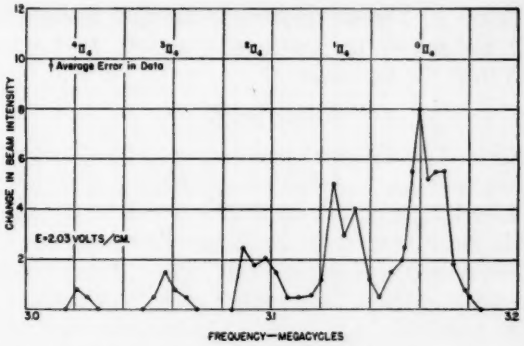

FIG. 9. Detailed spectrum of "extra" line group II_4. Radiofrequency field, $E_{rf}\sim 5$ volts/cm. Change in beam is expressed in cm of deflection on a galvanometer scale.

An observation which is in apparent conflict with the double quantum theory of the line origin is that the intensities of both line groups were found to vary in about the same way with the amplitude of the radiofrequency field. This observation was made with amplitudes of the radiofrequency field from $\sim$1 to 8 volts/cm for which the corresponding line intensities (in arbitrary units) varied from $\frac{1}{2}$ (which is the minimum value observable) to 12. It would be expected that the lower frequency line, for which the transition matrix element is proportional to E_{rf}^2, would vary more rapidly in intensity with the amplitude of the radio-frequency field than would the upper frequency line, for which the transition matrix element is proportional to E_{rf}. Still it should be mentioned that the transition probability is high in these experiments, so that it is not true that the transition probability is simply proportional to the square of the connecting matrix element; indeed, a near unity transition probability may obtain for the higher amplitudes of radio-frequency fields used. A much more conclusive test should be made under conditions for which the transition probability is known to be very small, but such a test will necessitate a considerable improvement in sensitivity.

Nor is it clear from the theory of the double quantum transition why only one half-frequency line group is observed rather than one for each of the seven primary line groups.

VI. RESULTS

Table II shows the results for the internal interaction constants. The values of the quadrupole interaction constants and of $|c_2/h|$ for rotational state $J=1$ are taken from line groups II_1 and I_1 for which the field interaction is negligible. The quadrupole interaction constants for rotational state $J=2$ are obtained from

[19] We are indebted to Professor T. I. Taylor and Mr. Robert Anderson of the Columbia Chemistry Department for performing this analysis.

line group I_3. The effective magnetic field produced at the F nucleus by the molecular rotation can be computed from the formula:

$$H=c_2/(\mu_N g_2)$$

in which H is the field per unit rotational quantum number and μ_N is 1 nuclear magneton. For $Rb^{87}F$, $H=4.5\pm1.2$ gauss and for $Rb^{85}F$, $H=3.8\pm0.9$ gauss. Within our experimental error there is no variation of H with vibrational state. The errors stated for the quadrupole interaction constant and $|c_2/h|$ arise primarily from the experimental inaccuracies in the determination of line positions.

The vibrational constant, ω_0, of the molecule can be determined from measured values of the relative intensities of the different vibrational lines of a line group.[2] The value obtained for $Rb^{85}F$ from a consideration of line groups II_1 and II_3 is:

$$\omega_0=(340\pm68)\ \text{cm}^{-1}.$$

The electric dipole moment, μ, of the molecule and the moment of inertia, A, can also be determined in principle by the electric resonance method, but the electrical quadrupole interactions for RbF are so large that the electric fields required for such a determination become very high. This results in a considerable decrease in line resolution, so that the accuracy of the determination would be quite poor.[3]

VII. DISCUSSION

A primary result of these studies is the determination of the electrical quadrupole interaction constant for Rb in RbF. This constant is determined for both molecular species for rotational state $J=1$ for several vibrational states, and for $Rb^{87}F$ also for rotational state $J=2$ for several vibrational states. These interaction constants are at least an order of magnitude larger than any other quadrupole interaction constant yet reported for an alkali halide molecule, and, incidentally, for this reason have not been determined by the magnetic resonance method. The absolute value of the quadrupole interaction constant is found to decrease by about 1.1 percent from one vibrational state to the next higher one. Within the experimental accuracy no difference was observed between the quadrupole interaction constants for rotational states $J=1$ and $J=2$ for $Rb^{87}F$.

It is expected that the ratio of the quadrupole interaction constants for the two molecular species $Rb^{85}F$ and $Rb^{87}F$ is largely independent of the molecular constants, q. Thus the perturbation treatment of the diatomic molecule yields for the molecular wave function $\psi=\psi_{\text{electronic}}(x_i, R)\cdot\psi_{\text{vibrational}}(R)\cdot\psi_{\text{rotational}}(\theta, \phi)$ in which x_i are the electron coordinates, R is the internuclear distance, and θ, ϕ are the spherical coordinate angles specifying the direction of the internuclear axis with respect to a fixed coordinate system. $\psi_{\text{electronic}}$ is independent of the reduced mass of the two nuclei. $\psi_{\text{vibrational}}$ and $\psi_{\text{rotational}}$ depend on the reduced mass of the system. The variation of q from one isotopic species to the other will be caused by the variation of $\psi_{\text{vibrational}}$ and $\psi_{\text{rotational}}$. The variation of q for a single molecular species has been found to be only about 1 percent from one vibrational state to another and no variation of q from rotational states $J=1$ to $J=2$ was found for $Rb^{87}F$. However, the variation of $\psi_{\text{vibrational}}$ and $\psi_{\text{rotational}}$ from one vibrational or rotational state to another is much larger than the variation of these functions from one molecular species to the other. Hence it seems to be a conservative estimate that q can vary by no more than 1 percent from one molecular species to the other. Thus we state $Q(Rb^{85})/Q(Rb^{87})=2.07\pm0.02$. In support of this argument there is evidence that the values of the field gradient, q, evaluated at the positions of the chlorine nuclei in the molecules $TlCl^{35}$ and $TlCl^{37}$ are the same.[20] For within the error of the experiment the ratio of the quadrupole interaction constants for chlorine in $TlCl^{35}$ and $TlCl^{37}$ is equal to the ratio of the electric quadrupole moments of the nuclei Cl^{35} and Cl^{37}, which have been measured by the method of atomic beams.[21] It is interesting to note that $\mu(Rb^{85})/\mu(Rb^{87})=0.492$ where μ is the nuclear magnetic dipole moment so that $(\mu Q)Rb^{85}\simeq(\mu Q)Rb^{87}\sim1$. This is a further example of an empirical rule suggested by Gordy[22] and would indicate that the sign of the nuclear quadrupole moments of Rb is positive.

The constant $|c_2/h|$ characterizes the spin-orbit interaction between the spin of the fluorine nucleus and the rotational angular momentum of the molecule. Such an interaction in an alkali halide molecule was first reported by Nierenberg and Ramsey for LiF.[23] From their data we compute $|c_2/h|=14$ kc/sec. Trischka found c_2/h to be $+16\pm2$ kc/sec for CsF. Our values for $|c_2/h|$ are 11 ± 3 kc/sec. for $Rb^{85}F$ and 14 ± 4 kc/sec. for $Rb^{87}F$. The magnitudes of c_2/h for the RbF molecules are close to the values reported for LiF and CsF; unfortunately, the sign of c_2/h was not determined in our experiment. The theory of H. M. Foley[6] attributes this $c_2(\mathbf{I}_2\cdot\mathbf{J})$ interaction to the effect of the bonding p electron of the halogen atom. This theory predicts an order of magnitude for the constants $|c_2/h|$ which is in agreement with the experimental results. The magnitudes of $|c_2/h|$ for the different alkali fluorides depend upon the moment of inertia of the molecules and upon the exact molecular wave functions, and have not been computed.

We are deeply indebted to our research director, Professor I. I. Rabi, for encouragement and for many enlightening discussions. We also wish to thank Professor H. M. Foley for several helpful discussions. One of the authors (VH) is indebted to the National Research Council for the grant of a predoctoral fellowship (1946–1949).

[20] H. Zeiger *et al.*, Bull. Am. Phys. Soc. **25**, No. 1, 35 (1950).
[21] L. Davis *et al.*, Phys. Rev. **76**, 1076 (1949).
[22] W. Gordy, Phys. Rev. **76**, 139 (1948).
[23] W. A. Nierenberg and N. F. Ramsey, Phys. Rev. **72**, 1075 (1947).

On the Directional Correlation of Successive Nuclear Radiations*

DAVID L. FALKOFF**
University of Notre Dame, Notre Dame, Indiana

AND

G. E. UHLENBECK
University of Michigan, Ann Arbor, Michigan

(Received March 27, 1950)

The theory of angular correlation is given in a form applicable to the successive emissions of any nuclear radiations. It is shown that the theoretical specification of angular correlation requires two kinds of information; namely, the angular momenta of the nuclear states and emitted radiations, and the Hamiltonian interaction between the outgoing particles and nucleus. The former information enters in the same way in all angular correlations while the latter, differing with the kind of particles emitted, is needed to obtain the angular distributions associated with each component of a line. The structure of such angular distributions is studied in relation to isotropy requirements and an explicit construction to exhibit them is given. Systematic simplifications in the calculation of angular correlation functions $W(\vartheta)$ are shown to result from several theorems relating to the combinations of transformation coefficients occurring in $W(\vartheta)$. These make possible a complete tabulation of $W(\vartheta)$ in canonical forms applicable, on proper specialization, to any angular correlation in which the angular momentum of the decay products in either transition is 1 or $2\hbar$. The specializations for α- and γ-emission are given.

I. INTRODUCTION

THE theory of the directional correlation between gamma-quanta emitted in successive nuclear transitions as given by Hamilton[1] has proved to be a valuable tool in nuclear spectroscopy. In many cases, comparison of experiment[2] with theory has yielded consistent assignments of the angular momentum quantum numbers for the nuclear states involved and the multipole orders for the successive gamma-radiations. These successes have stimulated further work on the angular correlations of successive nuclear radiations. Thus far, most of the detailed extensions[3–6] of the angular correlation theory have been concerned only[7] with the $\gamma-\gamma$-angular correlation. However, experiments on other types of angular correlations, e.g., $\beta-\gamma$,[8] internal-conversion[9]-γ and[10] $\alpha-\gamma$, have now also been reported.

We have developed the theory of angular correlation in a form applicable to the successive emissions of any nuclear particles. It will be shown that the theoretical specification of the angular correlation requires two kinds of information: (a) information associated with the rotationally invariant description of the nuclear states and the successive decay products, as for example, their angular momenta, parities and the polarizations and direction of emission of the emitted radiations; (b) the specific interaction Hamiltonian giving the coupling between outgoing particles and the nucleus. The use of information of type (a) is of quite general validity, being based solely on rotational invariance arguments, and is common to all angular correlations. On the other hand the information of type (b) will vary with the kinds of particles emitted and will, therefore, be different, say, for a $\beta-\gamma$-correlation than for a $\gamma-\gamma$-correlation.

Our program for this article is to carry through the *explicit* calculation of angular correlation functions using only "rotational" information of type (a). There are several advantages in such a procedure. In the first place, we are then able to tabulate the angular correlation functions in "canonical" (or parametric) forms which are applicable, on proper specialization of the parameters, to any cascade emissions in which the angular momenta of the successive decay products is 1 or $2\hbar$. In this way one can eliminate completely the duplication of rather formidable[11] calculations which would otherwise be necessary if, say, the $\gamma-\gamma$, $\beta-\gamma$ and internal conversion $-\gamma$-correlations were treated

* Part of a Doctoral Dissertation by D. L. Falkoff submitted to the Graduate School of the University of Michigan, April, 1948.

** National Research Council Predoctoral Fellow (1945–1948).

[1] D. R. Hamilton, Phys. Rev. **58**, 122 (1940).

[2] E. L. Brady and M. Deutsch, Phys. Rev. **72**, 870 (1947); **74**, 1541 (1948); **78**, 558 (1950). M. Deutsch and F. Metzger, Phys. Rev. **74**, 1542 (1948); **78**, 551 (1950).

[3] G. Goertzel, Phys. Rev. **70**, 897 (1946).

[4] D. L. Falkoff, Phys. Rev. **73**, 518 (1948).

[5] D. R. Hamilton, Phys. Rev. **74**, 782 (1948), Astrophys. J. **106**, 457 (1947).

[6] D. S. Ling, Jr. and D. L. Falkoff, Phys. Rev. **76**, 1639 (1949).

[7] Exceptions: The $\beta-\gamma$-angular correlation has been treated by D. L. Falkoff, Thesis, University of Michigan (1948). See also the succeeding article in this issue of The Physical Review. The internal conversion $-\gamma$-angular correlation has been treated by D. S. Ling, Jr., Thesis, University of Michigan (1948). Also V. B. Berestetski, J. Exp. Theor. Phys. U.S.S.R. **18**, 1057 (1948), (in Russian), and J. W. Gardner, Proc. Phys. Soc. London **62**, 763 (1949).

[8] Grace, Allen, and Halban, Nature **164**, 538 (1949); S. Frankel, Phys. Rev. **77**, 747 (1950). R. Garwin, Phys. Rev. **76**, 1876 (1949), T. B. Novey, **78**, 66 (1950), D. T. Stevenson and M. Deutsch, **78**, 640 (1950).

[9] A. H. Ward, and D. Walker, Nature **163**, 168 (1949), H. Frauenfelder, M. Walter, and W. Zünti, Phys. Rev. **77**, 557 (1950).

[10] B. T. Feld, Phys. Rev. **75**, 1618 (1949). Also R. Garwin and W. Arnold, private communication, B. Rose and A. R. W. Wilson, Phys. Rev. **78**, 68 (1950).

[11] Thus M. Fierz, Helv. Phys. Acta **XXII**, 489 (1949) gives general expressions for $\gamma-\gamma$ and internal conversion $-\gamma$-angular correlations, but his results cannot be compared with experiment since none of the required sums are evaluated.

separately *ab initio*. Secondly, one obtains a certain insight into the physical reasons for angular correlation and the structure of the correlation function by considering the general case. In particular, one can establish which properties of angular correlation are independent of the choice of interaction Hamiltonian.[12] This is of especial interest for β-emission where the choice of interaction is far from unique.

The results of most interest to experimentalists are the discussion and tables of Section IV. In order to get numerical values for the correlation functions, $W(\vartheta)$, one has only to insert the appropriate values of the parameters for the particle emissions of interest. The necessary specializations of the parameters for correlations involving α-particles and γ-rays are given as illustrations in Section III; the $\beta-\gamma$-correlation is discussed in a subsequent article.

II. THE ANGULAR CORRELATION FUNCTION, $W(\vartheta)$

Consider the successive emissions of particles, say, 1 and 2, in directions $\mathbf{k}_1$ and $\mathbf{k}_2$ respectively during transitions $A\rightarrow B$, $B\rightarrow C$ between states A, B and C of a nucleus. (The nuclear states, each having definite total angular momentum will be degenerate with respect to their magnetic quantum numbers l, m, p respectively.) The problem is to find $W(\vartheta)=W(\mathbf{k}_1\cdot\mathbf{k}_2)$, the probability that particle 2 is emitted at an angle ϑ with respect to the direction of emission of particle 1.

Hamilton[1] gave a rigorous quantum mechanical derivation of $W(\vartheta)$ for the $\gamma-\gamma$-correlation by applying second-order time dependent perturbation theory to an initial system of excited nucleus and quantized radiation field. With minor notational changes, his derivation is equally valid for more general correlations, and the final form may be written:

$$W(\vartheta)=S_1\,S_2\sum_{l,p}\Big|\sum_m(A_l|H_1(\mathbf{k}_1)|B_m)\times(B_m|H_2(\mathbf{k}_2)|C_p)^*\Big|^2, \quad (1)$$

where A_l, B_m, C_p represent wave functions for the degenerate sublevels of initial, intermediate and final nuclear state.

$H_1(\mathbf{k}_1)$ is the interaction Hamiltonian for emission of the first particle in direction $\mathbf{k}_1$; $H_2(\mathbf{k}_2)$ for emission of particle 2 in direction $\mathbf{k}_2$. Either H factor may also be a function of other arguments as, for example, the spin or polarization of the emitted particle as well as the direction and energy of any other simultaneously emitted particle (e.g., the neutrino in β-decay).

The symbol S_1 denotes an average over-all directional information (such as spins, polarizations or directions of emission of other particles) associated with the first transition, *except* for the direction of $\mathbf{k}_1$ of particle 1, with a similar meaning for S_2 and the second transition.

[12] This was done by C. N. Yang, Phys. Rev. **74**, 764 (1948), who treated angular correlations using solely rotational invariance arguments. By purely group theoretic methods he proved theorems about the *forms* of the angular distributions without actually exhibiting them. See also R. D. Myers, Phys. Rev. **54**, 361 (1938) and G. Goertzel, reference 3.

The matrix elements $(A_1|H|B_m)$ are probability amplitudes for the various possible transitions between degenerate sublevels.

Equation (1) is seen to differ from what one would expect from conventional second-order perturbation theory only in that the degeneracy of the nuclear states has been taken into account and non-angular dependent factors such as common energy denominators have been discarded. It is not, however, in a form which is easy to use because the products of probability amplitudes in (1) are summed over intermediate sublevels m before, rather than after, squaring, which gives rise to interference between the various ways in which a transition can occur from a given initial sublevel A_l to a final sublevel C_p via different intermediate sublevels B_m. This interference can be removed[13] by simply taking the z-axis of quantization along the direction of emission of one of the decay particles. Thus, with $\angle(\mathbf{k}_1,z)=0$, $\angle(\mathbf{k}_2,z)=\vartheta$, Eq. (1) reduces to:

$$W(\vartheta)=\sum_m\{\sum_l[S_1|(A_l|H_1(0)|B_m)|^2]\times\sum_p[S_2|(B_m|H_2(\vartheta)|C_p)|^2]\}. \quad (2)$$

This equation is the most convenient starting point for all explicit calculations of correlation functions. Moreover, in this form involving only squares of matrix elements, the summands in (2) have a particularly simple physical interpretation, namely

$$S_1|(A_l|H_1(0)|B_m)|^2\equiv P_{lm}(0)$$

is the (relative) probability for the emission of the first particle along the $\vartheta=0$ direction during a nuclear transition between sublevels A_1 and B_m. Similarly

$$S_2|(B_m|H_2(\vartheta)|C_p)|^2\equiv P_{mp}(\vartheta)$$

gives the (relative) probability for particle 2 to be emitted at angle ϑ in the particular transition $B_m\rightarrow C_p$. And the over-all correlation function is, therefore, of the form

$$W(\vartheta)=\sum_{lmp}P_{lm}(0)P_{mp}(\vartheta). \quad (2a)$$

Since the probabilities for each transition now appear independently in (2a), it is natural to begin the analysis of $W(\vartheta)$ by studying the structure of $P_{mm'}(\vartheta)$ for a single transition.

III. THE STRUCTURE OF A SINGLE TRANSITION BETWEEN DEGENERATE LEVELS

We now treat the angular distribution and intensity of the radiation associated with each component of a line.[14] First Section III(A) we state some general proper-

[13] Hamilton (reference 1) has proved this in detail for the $\gamma-\gamma$ case, and we have verified it for all the interactions of interest to us. (See the Theses of D. S. Ling, Jr. and D. L. Falkoff, reference 7.) Although it seems almost intuitively obvious to us that the removal of the interference in this way must hold whatever the interaction H, we have not been able to give a convincing general proof for it.

[14] Following the terminology of atomic spectra (see E. U. Condon and G. H. Shortley, *Theory of Atomic Spectra* (Cambridge University Press, London, 1935), Chapter IV) we define a *line* as

ties of the $P_{mm'}(\vartheta)$ sufficient to guarantee the isotropy requirements for a line. This discussion generalizes to transitions involving the emission of arbitrary particles of angular momentum L the properties which are familiar in atomic dipole radiation.[14] At the same time it leads to additional insight on the reasons for angular correlation. Then in Section III(B) we give a constructive procedure for obtaining the angular distributions and (relative) intensities for each component of a line from the Hamiltonian interaction describing the emission of the given radiation. These exhibit the properties assumed in Section III(A). Finally, in Section III(C), the angular distributions are put in a particularly simple parametric form which is convenient for use in angular correlations.

(A) Isotropy Considerations

It will be shown in Section III(B) that the relative probability for the component of a line corresponding to a transition between states with total and z-component angular momentum quantum numbers J, m and J', m' respectively with emission of a particle with total and z-component of angular momentum of L, M in the direction ϑ (with respect to the z-axis) must have the form:

$$P_{mm'}(\vartheta)=G^{JLJ'}_{m,m'}F_L{}^M(\vartheta) \text{ with } m'=m+M. \qquad (3)$$

Here $G^{JLJ'}_{m,m'}$ is an intensity factor depending only on the angular momentum quantum numbers JLJ', mMm', and $F_L{}^M(\vartheta)$ gives the angular dependence of the radiation associated with the $m\rightarrow m'$ component. Moreover, these have the following properties:

$$F_L{}^M(\vartheta)=F_L{}^{-M}(\vartheta), \qquad (4a)$$

$$\int F_L{}^M(\vartheta)d\Omega \text{ is independent of } M, \qquad (4b)$$

$$\sum_{M=-L}^{L} F_L{}^M(\vartheta) \text{ is independent of } \vartheta, \qquad (4c)$$

$$\sum_{m=-J}^{J} G^{JLJ'}_{m,m+M} \text{ is independent of } M, \qquad (5a)$$

$$\sum_{m=-L}^{L} G^{JLJ'}_{m,m+M} \text{ is independent of } m. \qquad (5b)$$

We now make the physical assumption[15] that all initial magnetic sublevels for a line are equally populated, as will be the case if the nuclei are randomly oriented. Then the following theorems are direct consequences of the properties (4b), (4c), (5a), (5b).

Theorem 1: *The total probability for transitions from each magnetic sublevel, m, of the initial level is independent of m.*

Proof: This probability is proportional to

$$\sum_{m'}\int d\Omega P_{mm'}(\vartheta).$$

Since $m'=m+M$, for fixed m one can replace $\sum_{m'}$ by $\sum_M$. Then

$$\sum_{m'}\int d\Omega P_{mm'}(\vartheta)=\left[\sum_M G^{JLJ'}_{m,m+M}\int F_L{}^M(\vartheta)d\Omega\right]$$

which by (4b) and (5b) is independent of m.

In virtue of the relationship of the lifetime of a state to the probability for spontaneous transition from it this shows that the lifetime of each initial sublevel is the same.

In a similar way one gets:

Theorem 2: *The total probability for transition to each final sublevel m' is the same independent of m'.*

Theorem 3: *The total intensity of all components of a line with the same $M=m'-m$ is independent of M.*

(The equal intensities for the normal Zeeman triplets are a familiar example of this theorem in atomic spectra.)

Finally, suppose one does not average over all directions of emission, but considers instead the sum of the radiations due to all components for fixed ϑ. Then using (4c) and (5a) one obtains:

Theorem 4: *The sum of the radiations from all components of a line is isotropic, i.e., is independent of ϑ.*

Let us now apply these isotropy results to the case of two successive emissions. Assuming equal populations for the initial magnetic sublevels, Theorem 4 guarantees that the radiation in the first emission will be isotropic. Moreover, the radiation from the second transition will also be isotropic since the initial sublevels for it are the final sublevels for the first emission, and by Theorem 2, these are all equally excited! How then does an angular correlation occur? It is the crux of the angular correlation theory to note that the equal population for the (intermediate) sublevels is obtained (Theorems 1 and 2) only *after* averaging over all directions, ϑ. If one specifies the direction of emission, ϑ, for the first transition, then the relative populations for the terminating sublevels of this transition will *not* be the same; they are in fact given by

$$\sum_M G^{JLJ'}_{m'-M,m'}F_L{}^M(\vartheta)$$

which is not independent of m'.

---

the total radiation associated with all possible transitions between two degenerate levels consistent with the angular momentum selection rules. A *component of a line* refers to the radiation arising from a transition between a particular pair of sublevels. Thus, $P_{mm'}(\vartheta)$ refers to the component $B_m\rightarrow C_{m'}$ of the line $B\rightarrow C$.

[15] This assumption of "natural excitation" is also made in the derivation of $W(\vartheta)$, Eq. (2). It could be violated if the nuclei were anisotropically excited, as by unidirectional radiation.

It is this unequal weighting of the intermediate sublevels when the direction of the first emission is specified which gives rise to the angular correlation.

(B) Angular Distributions and Intensities of Components

We now exhibit the reduction of

$$P_{mm'}(\vartheta)=S|(B_m|H|C_{m'})|^2 \tag{6}$$

to the form (3). The matrix element is taken with respect to the initial and final nuclear wave functions. These are in general not known, but they can be designated by their associated quantum numbers. Denoting all other quantum numbers than the total angular momentum and its z-component by α, we can write:

$$(B_m|H|C_{m'})\equiv(\alpha Jm|H|\alpha' J'm').$$

Two requirements are now imposed on the interaction Hamiltonian H: First, H should be invariant under any rotation of space coordinates. Second, it should correspond to the emission of a particle (or particles) with total angular momentum L.[16]

The rotational invariance of H can be guaranteed if it can be written as an inner product of two tensors of the same order. Such tensors must of course be constructed from the various argument vectors (and spinors)[17] on which H depends. These argument vectors will be of two kinds: those, denoted by $\mathbf{X}_i$, which are nucleonic operators and with respect to which the nuclear matrix elements are taken, and vectors, denoted by $\mathbf{A}_i$ which are associated with the description of the emitted particles, such as propagation vector $\mathbf{k}$, polarizations $\mathbf{e}$, etc. The $\mathbf{A}_i$, being independent of the nuclear coordinates, can be taken outside of the matrix elements. We choose one tensor to be a function of the $\mathbf{X}_i$, say $T(\mathbf{X}_i)$, and the other a function of the $\mathbf{A}_i$: $T(\mathbf{A}_i)$.

To make these tensors unique, we use the requirement that the matrix element is to correspond to the emission of a particle with angular momentum L. Group theoretically, this means that under a 3-dimensional rotation of coordinates the tensor $T(\mathbf{X}_i)$ should transform irreducibly according to the $(2L+1)$ dimensional irreducible representation $\mathfrak{D}^L$ of the 3-dimensional rotation group.[18] The construction of the required irreducible tensor of order L is given in Appendix I. Denoting the irreducible tensor by its components $T_{i_1 i_2 \cdots i_L}$, where each $i_1, i_2, \cdots, i_L=1, 2, 3$, one has then:

$$H(\mathbf{A}_i, \mathbf{X}_i)=\sum_{i_1, \cdots i_L} T_{i_1 \cdots i_L}(\mathbf{A}_i)T_{i_1 \cdots i_L}(\mathbf{X}_i). \tag{7}$$

In this form H is rotationally invariant and corresponds to a definite value of L. But to get the angular distributions associated with each component, one needs a decomposition of H according to the $(2L+1)$ possible M values. This decomposition is provided by the identity (proved in Appendix I):

$$\sum_{M=-L}^{L} \mathcal{Y}_{LM}(\mathbf{A}_i)^*\mathcal{Y}_{LM}(\mathbf{X}_i) \equiv \sum_{i_1, \cdots, i_L} T_{i_1 \cdots i_L}(\mathbf{A}_i)T_{i_1 \cdots i_L}(\mathbf{X}_i) \tag{8}$$

where the $\mathcal{Y}_{LM}$ are suitably *polarized*[19] and normalized *solid* harmonics. For then one gets for the nuclear matrix element:

$$(\alpha Jm|H|\alpha' J'm') = \sum_{M=-L}^{L} \mathcal{Y}_{LM}(\mathbf{A}_i)^*(\alpha Jm|\mathcal{Y}_{LM}(\mathbf{X}_i)|\alpha' J'm').$$

Since the $\mathcal{Y}_{LM}$ are eigenfunctions of L_z, one has

$$(\alpha Jm|\mathcal{Y}_{LM}(\mathbf{X}_i)|\alpha' J'm')=0, \text{ unless } m'=m+M,$$

which is just the magnetic selection rule. In virtue of this, the indicated sum reduces to a single term:

$$(\alpha Jm|H|\alpha' J'm')=\mathcal{Y}_{LM}(\mathbf{A}_i)^*(\alpha Jm|\mathcal{Y}_{LM}(\mathbf{X}_i)|\alpha' J'm'), \tag{9}$$

with $M=m'+m$.

The matrix element on the right can always be factored in the form[20]

$$(\alpha Jm|\mathcal{Y}_{LM}(\mathbf{X}_i)|\alpha' J'm') = f(\alpha, \alpha', J, J', \mathbf{X}_i)(JLJ'm'|JLmM), \tag{10}$$

where the first factor being independent of m, m', M, is the same (albeit unknown!) for each component of the line, while the second factor is completely determined by the indicated angular momentum quantum numbers, and is just the well-known (real) transformation coefficient for the vector addition of angular momenta.[21]

On substituting (7), (8), (9), and (10) into the general expression (6) for $P_{mm'}(\vartheta)$, and dropping the factor common to all components one gets explicitly the de-

[16] The case of more than one value of L in a single transition is treated in reference 6.

[17] We do not consider spinors separately since in most applications they occur quadratically and in this form the various covariants are tensors. W. Pauli, Ann. Inst. Henri Poincaré **6**, 109 (1936).

[18] E. Wigner, *Gruppentheorie* (Friedrich Vieweg and Sohn, Braunschweig, 1931), Chapters 14 and 15. H. Weyl, *The Theory of Groups and Quantum Mechanics* (Dover Publications, New York, 1948), Chapters 3 and 4. B. L. v. d. Waerden, *Die Gruppentheoretische Methode in der Quantenmechanik* (Verlag. Julius Springer, Berlin, 1931), Chapter III.

[19] The term *polarize* is used here in the technical sense of invariant theory. See. H. Weyl, *The Classical Groups* (Princeton University Press, Princeton, 1939), p. 5. Also Appendix I.

[20] E. Wigner, reference 18, p. 264. C. Eckart, Rev. Mod. Phys. **2**, 305 (1930).

[21] Condon and Shortley, reference 14, pp. 73–78. E. Wigner, reference 18, p. 206.

composition (3) assumed in Section III(A), with:

$$G_{m,m'}^{JLJ'} = (JLJ'm'|JLmM)^2 \tag{11}$$

and

$$F_L{}^M(\vartheta) = S_{\mathbf{A}_i}|\,\mathcal{Y}_{LM}(\mathbf{A}_i)\,|^2, \tag{12}$$

where $S_{\mathbf{A}_i}$ denotes an average over all $\mathbf{A}_i$, except the particular vector specifying the direction of emission.

The properties (4*a*, *b*, *c*) for the $F_L{}^M(\vartheta)$ can be established from (12) by noting that they are satisfied by the ordinary spherical harmonic angular distributions $|\,Y_{LM}(\vartheta,\varphi)\,|^2$ (see Example (*a*) below) and these formal properties are not affected by the subsequent polarization and averaging processes indicated in (12). The properties (5*a*, *b*) can be proved for (11) by group theoretical methods.[22] The $G_{m,m'}^{JLJ'}$ yield the familiar selection rules for the vector addition of angular momenta $\mathbf{J}+\mathbf{L}=\mathbf{J}'$, $m+M=m'$, and are the same for any particle emission characterized by these angular momenta. For the distinction between the different kinds of particle emissions, one must look to the angular distributions $F_L{}^M(\vartheta)$ of Eq. (12).

EXAMPLES.

(a) *Spherical Harmonic Distributions.* The simplest example of (12) is that in which there is only one argument vector: $\mathbf{A}_i=\mathbf{k}$; namely, that one specifying the direction of emission of the particle. Then there is no need for a summation, S, over any other directional information, and (12) yields:

$$F_L{}^M(\vartheta) = |\,\mathcal{Y}_{LM}(\mathbf{k})\,|^2 = k^{2L}|\,Y_{LM}(\vartheta,\varphi)\,|^2, \tag{13}$$

where the $Y_{LM}(\vartheta,\varphi)$ are the usual spherical harmonics; ϑ, φ, the polar angles of $\mathbf{k}$.

These "spherical harmonic distributions" are appropriate for the emission of any spin zero particle, in particular, α-particles or scalar mesons with orbital angular momentum L. Dropping common factors, these $F_L{}^M(\vartheta)$ are for $L=1$ and 2:

$$\begin{aligned} L=1:\quad & |Y_{1,0}|^2 = 2\cos^2\vartheta, \\ & |Y_{1,\pm1}|^2 = 1-\cos^2\vartheta, \end{aligned} \tag{14}$$

$$\begin{aligned} L=2:\quad & |Y_{2,0}|^2 = 1-6\cos^2\vartheta+9\cos^4\vartheta, \\ & |Y_{2,\pm1}|^2 = 6\cos^2\vartheta-6\cos^4\vartheta, \\ & |Y_{2,\pm2}|^2 = \tfrac{3}{2}-3\cos^2\vartheta+\tfrac{3}{2}\cos^4\vartheta. \end{aligned} \tag{15}$$

(b) *Gamma-angular distributions.* The various electromagnetic multipoles can be obtained by expanding the exponential in the interaction Hamiltonian, $H\sim\mathbf{p}\cdot\mathbf{A}=\mathbf{p}\cdot\mathbf{e}e^{i\mathbf{k}\cdot\mathbf{r}}$. Thus for electric dipole, $H=\mathbf{p}\cdot\mathbf{e}$. In this case the irreducible tensors are just the vectors $\mathbf{p}$, the nuclear momentum operator, and $\mathbf{e}$, the polarization vector for the emitted quantum, these vectors transforming according $\mathfrak{D}^L$ with $L=1$. Using the solid harmonics $\mathcal{Y}_{1,0}(\mathbf{r})=z$, $\mathcal{Y}_{1,\pm1}(\mathbf{r})=\mp[(x\pm iy)/2^{\frac{1}{2}}]$, the identity corresponding to (8) is

$$\mathbf{p}\cdot\mathbf{e} = \sum_{M=-1}^{1} \mathcal{Y}_{1M}(\mathbf{p})^*\mathcal{Y}_{1M}(\mathbf{e})$$

whence applying (12) with S now denoting an average over the two polarizations $\mathbf{e}_1$ and $\mathbf{e}_2$ perpendicular to $\mathbf{k}$, one gets for the electric dipole angular distributions

$$\begin{aligned} F_1{}^0(\vartheta) &= \Sigma_{\mathbf{e}}|\,\mathcal{Y}_{1,0}(\mathbf{e})\,|^2 = e_{1z}{}^2+e_{2z}{}^2 = 1-k_z{}^2 = 1-\cos^2\vartheta, \\ F_1{}^{\pm1}(\vartheta) &= \Sigma_{\mathbf{e}}|\,\mathcal{Y}_{1,\pm1}(\mathbf{e})\,|^2 = \tfrac{1}{2}(1+\cos^2\vartheta). \end{aligned} \tag{16}$$

[22] See for example, G. Breit and B. T. Darling, Phys. Rev. **71**, 465 (1947).

If one retains only the second term in the exponential, then

$$H\sim(\mathbf{p}\cdot\mathbf{e})(\mathbf{k}\cdot\mathbf{r}) = \Sigma_{i,j}\, e_i k_j p_i x_j, \quad i,j=1,2,3.$$

Here H is rotationally invariant, but the tensors e_ik_j and p_ix_j are not irreducible. In fact, p_ix_j can be decomposed into the following irreducible tensors:

(i) a symmetric tensor with spin zero:

$$T_{ij}(\mathbf{p},\mathbf{r}) = p_ix_j+p_jx_i-\tfrac{2}{3}(\mathbf{p}\cdot\mathbf{r})\delta_{ij}.$$

(ii) axial vector:

$$p_ix_j-p_jx_i = -(\mathbf{r}\times\mathbf{p}).$$

(iii) scalar: $\mathbf{p}\cdot\mathbf{r}$

which transform irreducibly according to $\mathfrak{D}^L$ with $L=2$, 1, 0, respectively. The first gives rise to electric quadrupole radiation, the second to magnetic dipole, while the third, the electric "unipole" [23] does not give rise to any radiation. Thus the interaction for pure electric quadrupole radiation can be written:

$$H = \Sigma_{ij}\, T_{ij}(\mathbf{p},\mathbf{r})T_{ij}(\mathbf{e},\mathbf{k}) = \sum_{M=-2}^{2} \mathcal{Y}_{2M}(\mathbf{e},\mathbf{k})^*\mathcal{Y}_{2M}(\mathbf{p},\mathbf{r}),$$

where $T_{ij}(\mathbf{e},\mathbf{k})$ is of the same form as $T_{ij}(\mathbf{p},\mathbf{r})$ in (i) and the polarized solid harmonics are given in Appendix I. The angular distributions obtained using (12) are:

$$\begin{aligned} F_2{}^0 &= 6\cos^2\vartheta-6\cos^4\vartheta, \\ F_2{}^{\pm1}(\vartheta) &= 1-3\cos^2\vartheta+4\cos^4\vartheta, \\ F_2{}^{\pm2}(\vartheta) &= 1-\cos^4\vartheta. \end{aligned} \tag{17}$$

These particular distributions can be derived by other methods;[24] in fact, using only classical electromagnetic theory. However, our formalism is particularly well suited to the β-decay theory for which there is no classical analog.

(C) Parametric Forms of $F_L{}^M(\vartheta)$

The general expression (12) for the $F_L{}^M(\vartheta)$ not only yields the "isotropy conditions" (4b, c) used in Section III(A), but also strongly restricts the form of $F_L{}^M(\vartheta)$. Indeed, from the invariance of (12) under reflection of coordinates: $F_L{}^M(\vartheta)=F_L{}^M(-\vartheta)=F_L{}^M(\pi-\vartheta)$, it follows that $F_L{}^M(\vartheta)$ must be a function of $\cos^2\vartheta$. And since the $|\,\mathcal{Y}_{LM}(\mathbf{A}_i)\,|^2$, like the spherical harmonic distributions (13), transform under rotation of coordinates according to $\mathfrak{D}^L\times\mathfrak{D}^{L*}$, each $F_L{}^M(\vartheta)$ can be at most[12] a polynomial of degree L in $\cos^2\vartheta$. Therefore one can write in general

$$F_L{}^M(\vartheta) = \sum_{i=0}^{L} C_i{}^{(M)}\cos^{2i}\vartheta, \quad M=0,\ \pm1,\ \cdots,\ \pm L. \tag{18}$$

The $(2L+1)(L+1)$ coefficients $C_i{}^{(M)}$ cannot all be independent since the conditions (4a, b, c) must be satisfied. However, even with these constraints imposed on the $F_L{}^M(\vartheta)$, there could still remain L^2+1 possible independent coefficient among the $C_i{}^{(M)}$. It is, therefore, noteworthy that the *maximum number of independent coefficients in the most general set of $F_L{}^M(\vartheta)$ is $L+1$ and not L^2+1.* This can be seen as follows: Consider any $F_L{}^M(\vartheta)$ for any fixed $M\neq0$, the $C_i{}^{(M)}$ being left arbitrary. Physically, $F_L{}^M(\vartheta)$ is associated with radiation having a z-component of angular momentum M about

[23] H. C. Brinkman, *Zur Quantenmechanik der Multipolstrahlung* (Proefschrift, Utrecht, 1932), p. 29.

[24] The angular distribution for electromagnetic multipoles have been given in a closed form, which is easy to evaluate, for arbitrary L in reference 6.

some arbitrary z-axis. Suppose one chooses a new z'-axis so that the z'-component for this *same* radiation becomes $M'=0$. Then one will have $F_L{}^M(\vartheta)=F_L{}^0(\vartheta')$ where ϑ' is measured with respect to the z'-axis. If one now expresses ϑ' in $F_L{}^0(\vartheta')$ in terms of ϑ, then on equating the coefficients of linearly independent powers of $\cos^2\vartheta$ in the resulting equality, one will get the $C_i{}^{(M)}$ expressed (linearly) in terms of the $(L+1)C_i{}^{(0)}$. It follows, moreover, that the $(L+1)$ linearly independent coefficients may be taken as the $(L+1)$ coefficients, $C_i{}^{(M)}$, for any fixed M. The normalization of the $F_L{}^M(\vartheta)$ being arbitrary, one can divide through the set of $F_L{}^M(\vartheta)$ by any one of the $C_i{}^{(M)}$. Then the maximum number of independent "homogeneous parameters" required to parametrize the set of $F_L{}^M(\vartheta)$ is L. We illustrate the use of such parametrizations for $L=1$ and 2.

For $L=1$, the most general set $F_1{}^M(\vartheta)$ can be taken in the form:

$$\begin{aligned} F_1{}^0(\vartheta)&=(1+\lambda)-2\lambda\cos^2\vartheta,\\ F_1{}^{\pm1}(\vartheta)&=1+\lambda\cos^2\vartheta, \end{aligned} \tag{19}$$

where λ is the one arbitrary homogeneous parameter.

Several special cases of λ are noteworthy:

(a) $\lambda=1$ yields the dipole γ-distributions (16),

(b) $\lambda=-1$ yields the spherical harmonic distributions (14),

(c) When $\lambda=0$, both $F_1{}^0(\vartheta)$ and $F_1{}^{\pm1}(\vartheta)$ are independent of ϑ, even though $L=1$. Examples of this in the β-theory are the tensor and axial vector allowed transitions.

For $L=2$, a convenient parametrization for the general set of $F_2{}^M(\vartheta)$ is:

$$\begin{aligned} F_2{}^0(\vartheta)&=\mu_1+\cos^2\vartheta+\mu_2\cos^4\vartheta,\\ F_2{}^{\pm1}(\vartheta)&=(\mu_1+\tfrac{1}{6})+(\mu_2+\tfrac{1}{2})\cos^2\vartheta-\tfrac{2}{3}\mu_2\cos^4\vartheta,\\ F_2{}^{\pm2}(\vartheta)&=(\mu_1+\tfrac{1}{2}\mu_2+\tfrac{2}{3})-(\mu_1+1)\cos^2\vartheta+\tfrac{1}{6}\mu_2\cos^4\vartheta. \end{aligned} \tag{20}$$

Another equivalent set with different choice of the two independent homogeneous parameters is

$$\begin{aligned} F_2{}^0(\vartheta)&=(k_1+k_2)+(3k_2-1)\cos^2\vartheta+\cos^4\vartheta,\\ F_2{}^{\pm1}(\vartheta)&=(k_1+\tfrac{3}{2}k_2-\tfrac{1}{6})+(\tfrac{3}{2}k_2+\tfrac{1}{2})\cos^2\vartheta-\tfrac{2}{3}\cos^4\vartheta,\\ F_2{}^{\pm2}(\vartheta)&=(k_1+3k_2-\tfrac{1}{6})-3k_2\cos^2\vartheta+\tfrac{1}{6}\cos^4\vartheta. \end{aligned} \tag{21}$$

For γ-quadrupole, (17), $k_1=k_2=0$, while for the internal conversion $F_2{}^M(\vartheta)$ Ling[7] has shown that $k_1=F_2{}^2(0)=0$.

The advantage of such parametrizations is that they reduce the problem of finding the set of $F_L{}^M(\vartheta)$ associated with a given particle emission to that of evaluating the L parameters which uniquely determine the $F_L{}^M(\vartheta)$. In particular it is only necessary to find $F_L{}^M(\vartheta)$ for one particular M; the other $F_L{}^M(\vartheta)$ can then be written down at once from the parametric forms.

We have chosen to express the $F_L{}^M(\vartheta)$ in powers of $\cos^2\vartheta$, since this form is most useful in tabulating angular correlations for comparison with experiment. Had we chosen an expansion in terms of the spherical harmonic distributions the form of the parametrization would have been neater. Thus for $L=2$, the corresponding expansion equivalent to (20) or (21) is:

$$\begin{aligned} F_2{}^0(\vartheta)&=A|Y_{2,0}|^2+\tfrac{1}{3}B[4|Y_{1,0}|^2+2|Y_{1,\pm1}|^2]+C,\\ F_2{}^{\pm1}(\vartheta)&=A|Y_{2,\pm1}|^2+B[|Y_{1,0}|^2+|Y_{1,\pm1}|^2]+C,\\ F_2{}^{\pm2}(\vartheta)&=A|Y_{2,\pm2}|^2+B[2|Y_{1,\pm1}|^2]+C, \end{aligned} \tag{22}$$

with the $|Y_{LM}|^2$ given by (14) and (15) and A, B, C arbitrary scalar parameters. Formally, one sees that the effect of averaging over spins, polarizations, etc. in (12) is to introduce linear combinations of spherical harmonic distributions for $l<L$. For each l, these linear combinations must be such as to satisfy (4b, c).

IV. REDUCTION AND TABULATION OF CORRELATION FUNCTIONS

The general expression (2) for $W(\vartheta)$ becomes, using (11) and (12):

$$\begin{aligned} W(\vartheta)=\sum_m\{&[\textstyle\sum_{m'}(J'm'|L_1M_1|Jm)^2F_{L_1}{}^{M_1}(0)]\\ &\times[\textstyle\sum_{m''}(Jm|L_2M_2|J''m'')F_{L_2}{}^{M_2}(\vartheta)]\}. \end{aligned} \tag{23}$$

Without carrying out any of the indicated summations, one can make some general statements concerning the form[12] of $W(\vartheta)$. Thus, since the $F_L{}^M(\vartheta)$ are polynomials of degree at most L in $\cos^2\vartheta$, and since one may choose the z-axis along the direction of emission for either the first or second transition, it follows from (2) that $W(\vartheta)$ *is a polynomial in* $\cos^2\vartheta$ *of degree at most* L, *where* L *is the minimum of* L_2 *and* L_2. Another more obvious consequence is that *if the angular distributions* $F_L{}^M(\vartheta)$ *for each component of one of the emissions are isotropic (even when* $L>0$*) then there can be no angular correlation.*

To obtain the coefficients of the powers of $\cos^2\vartheta$ in $W(\vartheta)$, the $F_L{}^M(\vartheta)$ must be exhibited and the indicated sums in (23) must be carried out. Having given a pro-

TABLE I. R/Q for $L_1=L_2=1$. $\phi=\phi(\lambda,\Delta)$ is given by Eq. (28).

	$\Delta J=1$	$\Delta J=0$	$\Delta J=-1$
$\Delta j=1$	$\dfrac{1}{10\phi+3}$	$\dfrac{-(2J+3)}{[10J]\phi+(4J+1)}$	$\dfrac{(J+1)(2J+3)}{[10J(2J-1)]\phi+[6J^2-5J-1]}$
$\Delta j=0$	$\dfrac{-(2J-1)}{[10(J+1)]\phi+(4J+3)}$	$\dfrac{(2J-1)(2J+3)}{[10J(J+1)]\phi+[2J^2+2J+1]}$	
$\Delta j=-1$	$\dfrac{J(2J-1)}{10(J+1)(2J+3)\phi+(6J^2+17J+10)}$		

TABLE II. R/Q for $L_1=1$, $L_2=2$ or $L_1=2$, $L_2=1$. For $L_1=1$, $L_2=2$, ϕ denotes ϕ_{12}, Eq. (30). This same table may be used for $L_1=2$, $L_2=1$ provided one takes $\phi=\phi_{21}$ and ΔJ and Δj are taken to refer to the first and second transition respectively, as per Eq. (25).

	$\Delta j=1$	$\Delta j=0$	$\Delta j=-1$
$\Delta J=2$	$\dfrac{-3}{21\phi+8}$	$\dfrac{3(2J-1)}{[21(J+1)]\phi+(5J+8)}$	$\dfrac{-3(2J-1)J}{[21(J+1)(2J+3)]\phi+[16J^2+34J+21]}$
$\Delta J=1$	$\dfrac{3(J+6)}{[42J]\phi+(13J-6)}$	$\dfrac{-3(2J-1)(J+6)}{[42J(J+1)]\phi+(16J^2+25J-6)}$	$\dfrac{3(2J-1)(J+6)}{[42(J+1)(2J+3)]\phi+(26J^2+59J+48)}$
$\Delta J=0$	$\dfrac{(2J-3)(2J+5)}{[14J(2J-1)]\phi+[8J^2-6J+5]}$	$\dfrac{-(2J-3)(2J+5)}{[14J(J+1)]\phi+[6J^2+6J-5]}$	$\dfrac{(2J-3)(2J+5)}{[14(J+1)(2J+3)]\phi+[8J^2+22J+19]}$
$\Delta J=-1$	$\dfrac{3(2J+3)(J-5)}{[42J(2J-1)]\phi+[26J^2-7J+15]}$	$\dfrac{-3(2J+3)(J-5)}{[42J(J+1)]\phi+[16J^2+7J-15]}$	$\dfrac{3(J-5)}{[42(J+1)]\phi+[13J+19]}$
$\Delta J=-2$	$\dfrac{-3(J+1)(2J+3)}{[21J(2J-1)]\phi+[16J^2-2J+3]}$	$\dfrac{3(2J+3)}{[21J]\phi+[5J-3]}$	$\dfrac{-3}{21\phi+8}$

cedure for the former we next show how this latter task can be considerably simplified.

(A) Relations between Sums

Following Hamilton's notation,[1] let $J'=J-\Delta j$, $J''=J+\Delta J$ and define

$$g^{\Delta j,\,L}_{m-M,\,m}=(J-\Delta j,\,m-M\,|\,LM\,|\,Jm)^2$$
$$\equiv(J-\Delta j,\,L,\,J,\,m\,|\,J-\Delta j,\,L,\,m-M,\,M)^2,$$
$$G^{\Delta J,\,L}_{m,\,m+M}=(Jm\,|\,LM\,|\,J+\Delta J,\,m+M)^2,$$
$$d_m^{\Delta j,\,L}=g^{\Delta j,\,L}_{m-1,\,m}+g^{\Delta j,\,L}_{m+1,\,m};\quad D_m^{\Delta J,\,L}=G^{\Delta J,\,L}_{m,\,m-1}+G^{\Delta J,\,L}_{m,\,m+1},$$
$$e_m^{\Delta j,\,L}=g^{\Delta j,\,L}_{m-2,\,m}+g^{\Delta j,\,L}_{m+2,\,m};\quad E_m^{\Delta J,\,L}=G^{\Delta J,\,L}_{m,\,m+2}+G^{\Delta J,\,L}_{m,\,m-2}.$$

et simile.

Then using (4a), Eq. (23) becomes

$$W(\vartheta)=\sum_m\{[g_{mm}F_{L_1}{}^0(0)+d_mF_{L_1}{}^1(0)+\cdots]$$
$$\times|G_{mm}F_{L_2}{}^0(\vartheta)+D_mF_{L_2}{}^1(\vartheta)+\cdots]\},\quad(23a)$$

where we have dropped superscripts, the g_{mm}, d_m, of the first bracket being associated with the Δj, L_1 of the first transition and G_{mm}, D_m with the ΔJ, L_2 of the second. For given L_1 and L_2 there are $(L_1+1)(L_2+1)$ indicated sums of products of squares of transformation coefficients occurring in (23a) which are to be evaluated for all possible J, $\Delta j=0,\pm1,\cdots\pm L_1$, $\Delta J=0,\pm1,\cdots\pm L_2$. Fortunately, these sums are not all independent. Namely, we can prove[25] that *all the* $(L_1+1)(L_2+1)$ *sums* $(\sum_m g_{mm}G_{mm}, \sum_m d_mG_{mm}$, *etc.) occurring in* $W(\vartheta)$ *can be expressed as linear combinations of* $(L+1)$ *linearly independent sums, where* L *is the minimum of* L_1 *and* L_2, *these relations holding for all* J, Δj *and* ΔJ. *Moreover, the* $(L+1)$ *independent sums may be taken to be the* $(L+1)$ *sums occurring in the* $2^{L_1}-2^{L_2}\gamma-\gamma$ *correlation.*[26]

The explicit relations between these sums for L_1, $L_2=1$ or 2 are listed below with the notation $\sum_m d_m{}^{\Delta j,\,L_1}G_{mm}{}^{\Delta J,\,L_2}$ abbreviated still further to dG. In each case, the sums which are underlined represent a convenient choice of the linearly independent ones.

(a) $L_1=L_2=1$.

Sums: $\underline{gG}\quad\underline{gD}$; $\underline{dG}\quad\underline{dD}$

Relations: $dG=gD$; $gG=\frac{1}{2}[dD-dG]$

(b) $L_1=1$, $L_2=2$.

Sum: $gG\quad\underline{gD}\quad gE$; $dG\quad\underline{dD}\quad dE$

Relations: $dE=2gD$; $gE=dD-gD$; $dG=\frac{1}{3}[2dD-gD]$; $gG=\frac{1}{6}[5gD-dD]$

(c) $L_1=L_2=2$.

Sums: $\underline{gG}\quad\underline{gD}\quad\underline{gE}$; $\underline{dG}\quad\underline{dD}\quad\underline{dE}$; $\underline{eG}\quad\underline{eD}\quad\underline{eE}$

Relations: $dG=gD$; $eG=gE$; $eD=dE$; $gG=\frac{1}{4}[2dD-dE]$; $eG=\frac{1}{4}[-2dG+3dE]$; $eE=\frac{1}{4}[6dG+4dD-3dE]$

[25] A constructive method of proof, outlined in the thesis of D. L. Falkoff (reference 7) is to make use of the fact that $W(\vartheta)$ must be the same whether evaluated by taking the z-axis along the direction of emission of the first or second particle. By varying the choice of the arbitrary parameters in the $F_L{}^M(\vartheta)$ and equating the two different formal expressions for $W(\vartheta)$ obtained in this way, one can get all the relations between these sums of products of matrix elements. See also Appendix II. The work of Gardner (reference 7) suggests the possibility of a more direct proof using methods developed by G. Racah, Phys. Rev. **62**, 438 (1942), for dealing with multiple products of transformation coefficients.

[26] That only $(L+1)$ such sums occur in $W(\vartheta)$ for the $\gamma-\gamma$-correlations follows from the fact (references 1, 3, 6) that for the γ-angular distributions $F_L{}^M(0)=0$ except for $M=\pm1$.

TABLE III. The linearly independent sums, dG, dD, dE for $L_1=L_1=2$. (Common factors for each Δj, ΔJ are dropped.)

$\Delta j=2$, $\Delta J=2$ or $\Delta j=-2$, $\Delta J=-2$	$(dG)=5/2$ $(dD)=14/3$ $(dE)=10/3$
$\Delta j=2$, $\Delta J=1$ or $\Delta j=-1$, $\Delta J=-2$	$(dG)=(2J-1)$ $(dD)=1/6(23J-10)$ $(dE)=2/3(7J+4)$
$\Delta j=2$, $\Delta J=0$ or $\Delta j=0$, $\Delta J=-2$	$(dG)=(2J-1)(J-1)$ $(dD)=1/3(16J^2-6J+11)$ $(dE)=2/3(J-1)(10J+7)$
$\Delta j=2$, $\Delta J=-1$ or $\Delta j=1$, $\Delta J=-2$	$(dG)=1/2(4J-1)(2J^2-J+3)$ $(dD)=1/6(46J^3-75J^2+14J-33)$ $(dE)=1/3(28J^3-48J^2+5J+21)$
$\Delta j=2$, $\Delta J=-2$	$(dG)=1/2(20J^4-52J^3+31J^2-17J+6)$ $(dD)=1/3(56J^4-148J^3+130J^2-29J+15)$ $(dE)=2/3(20J^4-76J^3+85J^2-20J-12)$
$\Delta j=1$, $\Delta J=2$ or $\Delta j=-2$, $\Delta J=-1$	$(dG)=(2J+3)$ $(dD)=1/6(23J+33)$ $(dE)=2/3(7J+3)$
$\Delta j=1$, $\Delta J=1$ or $\Delta j=-1$, $\Delta J=-1$	$(dG)=1/8(7J^3+7J-6)$ $(dD)=1/24(59J^2+59J-66)$ $(dE)=1/12(23J^2+23J+42)$
$\Delta j=1$, $\Delta J=0$ or $\Delta j=0$, $\Delta J=-1$	$(dG)=1/2(J-1)(2J+3)(4J+1)$ $(dD)=1/6(28J^3-12J^2-19J+87)$ $(dE)=1/3(J-1)(16J^2+34J+39)$
$\Delta j=1$, $\Delta J=-1$	$(dG)=1/8(14J^4-33J^3-11J^2+69J+9)$ $(dD)=1/24(118J^4-9J^3-13J^2-27J-261)$ $(dE)=1/12(46J^4-9J^3-103J^2-27J+117)$
$\Delta j=0$, $\Delta J=2$ or $\Delta j=-2$, $\Delta J=0$	$(dG)=(J+2)(2J+3)$ $(dD)=1/3(16J^2+38J+33)$ $(dE)=2/3(J+2)(10J+3)$
$\Delta j=0$, $\Delta J=1$ or $\Delta j=-1$, $\Delta J=0$	$(dG)=1/2(J+2)(2J-1)(4J+3)$ $(dD)=1/6(28J^3+96J^2+89J-66)$ $(dE)=1/3(J+2)(16J^2-2J+21)$
$\Delta j=0$, $\Delta J=0$	$(dG)=1/3(2J-1)(2J+3)(2J^2+2J+3)$ $(dD)=1/3(32J^4+64J^3-44J^2-76J+87)$ $(dE)=2/3(8J^4+16J^3+22J^2+14J-39)$
$\Delta j=-1$, $\Delta J=2$ or $\Delta j=-2$, $\Delta J=1$	$(dG)=1/2(4J+5)(2J^2+5J+6)$ $(dD)=1/6(46J^3+213J^2+302J+168)$ $(dE)=1/3(28J^3+132J^2+185J+60)$
$\Delta j=-1$, $\Delta J=1$	$(dG)=1/8(14J^4+89J^3+172J^2+64J-24)$ $(dD)=1/24(118J^4+481J^3$ $+722J^2+500J-120)$ $(dE)=1/12(46J^4+193J^3+200J^2+32J+96)$
$\Delta j=-2$, $\Delta J=2$	$(dG)=1/2(20J^4+132J^3+307J^2+315J+126)$ $(dD)=1/3(56J^4+372J^3+910J^2+957J+378)$ $(dE)=2/3(20J^4+156J^3+433J^2+498J+189)$

Since Hamilton[1] has evaluated the linearly independent sums for the $\gamma-\gamma$-correlations with L_1, $L_2=1$ or 2, these relations give directly all the necessary sums for any other correlation with these same values of L_1, L_2.

For the cases in which $L_1=L_2=L$, a rather interesting property of correlation functions can be proved based on the symmetry of the sums; e.g., $dG=gD$, $eG=gE$, etc. as is illustrated in (a) and (c). Namely, for the successive emission of particles ρ and σ, each with angular momentum L, $W(\vartheta)$ *is the same for the sequences of states*

TABLE IV. Linear combinations of the sums dG, dD, dE occurring in Canonical correlation functions for $L_1=L_1=2$.

For brevity, the following combinations are denoted by their order of appearance in the table, thus:

(1): $dG+dD+dE$
(2): $dD+4dE$
(3): $dD-dE$
(4): $dG+1/2dD-dE$
(5): $-6dG+4dD-dE$
(6): $3dG+13/2dD+17dE$
(7): $1/3dG+1/2dD+dE$
(8): $dD+dE$
(9): $2dG-dD$

$\Delta j=2$, $\Delta J=2$ or $\Delta j=-2$, $\Delta J=-2$	(1)	21/2
	(2)	18
	(3)	4/3
	(4)	3/2
	(5)	1/3
	(6)	189/2
	(7)	13/2
	(8)	8
	(9)	1/3
$\Delta j=2$, $\Delta J=1$ or $\Delta j=-1$, $\Delta J=-2$	(1)	$21/2J$
	(2)	$9/2(5J+2)$
	(3)	$-1/6(5J+26)$
	(4)	$-3/4(J+6)$
	(5)	$-2/3(2J+5)$
	(6)	$63/4(7J+2)$
	(7)	$1/4(29J+6)$
	(8)	$1/2(17J+2)$
	(9)	$1/6(J-2)$
$\Delta j=2$, $\Delta J=0$ or $\Delta j=0$, $\Delta J=-2$	(1)	$7J(2J-1)$
	(2)	$(32J^2-10J-15)$
	(3)	$-1/3(2J-5)(2J+5)$
	(4)	$-1/2(2J-3)(2J+5)$
	(5)	$4/3(J+2)(2J+5)$
	(6)	$1/2(308J^2-112J-105)$
	(7)	$1/2(20J^2-8J-5)$
	(8)	$(2J-1)(6J+1)$
	(9)	$-1/3(2J+1)(2J+5)$
$\Delta j=2$, $\Delta J=-1$ or $\Delta j=1$, $\Delta J=-2$	(1)	$21/2J(2J-1)(J-1)$
	(2)	$9/2(10J^3-17J^2+2J+5)$
	(3)	$-1/6(2J+3)(5J^2-18J+25)$
	(4)	$-3/4(J-1)(J-5)(2J+3)$
	(5)	$-2/3(2J+3)(J+2)(2J+5)$
	(6)	$63/4(J-1)(J-1)(14J+5)$
	(7)	$1/4(58J^3-93J^2+20J+15)$
	(8)	$1/2(34J^3-57J^2+8J+3)$
	(9)	$1/6(2J+3)(J^2+18J+5)$
$\Delta j=2$, $\Delta J=-2$	(1)	$21/2J(J-1)(2J-1)(2J-3)$
	(2)	$9(8J^4-28J^3+30J^2-7J-3)$
	(3)	$1/3(J+1)(2J+3)(8J^2-18J+13)$
	(4)	$3/2(J+1)(J-1)(2J-3)(2J+3)$
	(5)	$1/3(J+1)(2J+3)(J+2)(2J+5)$
	(6)	$63/2(J-1)(J-1)(6J+1)(2J-3)$
	(7)	$1/2(J-1)(2J-3)(26J^2-19J-3)$
	(8)	$(2J-1)(16J^3-42J^2+29J+3)$
	(9)	$1/3(J+1)(2J+3)(2J^2-9J+1)$
$\Delta j=1$, $\Delta J=2$ or $\Delta j=-2$, $\Delta J=-1$	(1)	$21/2(J+1)$
	(2)	$9/2(5J+3)$
	(3)	$-1/6(5J-21)$
	(4)	$-3/4(J-5)$
	(5)	$-2/3(2J-3)$
	(6)	$63/4(7J+5)$
	(7)	$1/4(29J+23)$
	(8)	$1/2(17J+15)$
	(9)	$1/6(J+3)$

TABLE IV.—*Continued.*

$\Delta j=1, \Delta J=1$ or $\Delta j=-1, \Delta J=-1$	(1)	$21/4J(J+1)$
	(2)	$9/8(9J^3+9J+10)$
	(3)	$1/24(13J^2+13J-150)$
	(4)	$3/16(J-5)(J+6)$
	(5)	$2/3(2J-3)(2J+5)$
	(6)	$63/16(13J^2+13J+10)$
	(7)	$5/16(11J^2+11J+6)$
	(8)	$1/8(35J^2+35J+6)$
	(9)	$-1/24(17J^2+17J-30)$
$\Delta j=1, \Delta J-0$ or $\Delta j=0, \Delta J=-1$	(1)	$7J(J+1)(2J-1)$
	(2)	$1/2(52J^3+44J^2+7J-75)$
	(3)	$-1/6(2J-3)(2J+5)(J+11)$
	(4)	$1/4(J-5)(2J-3)(2J+5)$
	(5)	$-8/3(J+2)(2J-3)(2J+5)$
	(6)	$7/4(76J^3+56J^2-5J-75)$
	(7)	$1/4(36J^3+24J^2-7J-25)$
	(8)	$1/2(20J^3+8J^2-3J+3)$
	(9)	$1/6(2J-3)(2J+5)(5J+7)$
$\Delta j=1, \Delta J=-1$	(1)	$21/4J(J+1)(J-1)(2J-1)$
	(2)	$9/8(18J^4-3J^3-31J^2-9J+25)$
	(3)	$1/24(2J+3)(13J^3-15J^2+119J-165)$
	(4)	$3/16(J-1)(2J+3)(J-5)(J-5)$
	(5)	$2/3(2J+3)(2J-3)(2J+5)(J+2)$
	(6)	$63/16(J-1)(J-1)(26J^2+45J+25)$
	(7)	$1/16(J-1)(110J^2+73J^2-76J-75)$
	(8)	$1/8(70J^4-9J^3-73J^2-27J-9)$
	(9)	$-1/24(2J+3)(17J^3+69J^2-77J-105)$
$\Delta j=0, \Delta J=2$ or $\Delta j=-2, \Delta J=0$	(1)	$7(J+1)(2J+3)$
	(2)	$(32J^3+74J+27)$
	(3)	$-1/3(2J-3)(2J+7)$
	(4)	$-1/2(2J-3)(2J+5)$
	(5)	$4/3(J-1)(2J-3)$
	(6)	$7/2(44J^2+104J+45)$
	(7)	$1/2(20J^2+48J+23)$
	(8)	$(2J+3)(6J+5)$
	(9)	$-1/3(2J-3)(2J+1)$
$\Delta j=0, \Delta J=1$ or $\Delta j=-1, \Delta J=0$	(1)	$7J(J+1)(2J+3)$
	(2)	$1/2(52J^3+112J^2+75J+90)$
	(3)	$-1/6(2J-3)(2J+5)(J-10)$
	(4)	$1/4(J+6)(2J+5)(2J-3)$
	(5)	$-8/3(2J-3)(2J+5)(J-1)$
	(6)	$7/4(76J^3+172J^2+111J+90)$
	(7)	$1/4(36J^3+84J^2+53J+30)$
	(8)	$1/2(20J^3+52J^2+41J+6)$
	(9)	$1/6(2J-3)(2J+5)(5J-2)$
$\Delta j=0, \Delta J=0$	(1)	$14/3J(J+1)(2J-1)(2J+3)$
	(2)	$(32J^4+64J^3+44J^2+12J-75)$
	(3)	$1/3(2J-3)(2J+5)(4J^2+4J-11)$
	(4)	$1/6(2J-3)(2J+5)(2J-3)(2J+5)$
	(5)	$16/3(2J-3)(2J+5)(J-1)(J+2)$
	(6)	$21/2(16J^4+32J^3+16J^2-25)$
	(7)	$1/18(208J^4+416J^3+160J^2-48J-225)$
	(8)	$(2J-1)(2J+3)(4J^2+4J-1)$
	(9)	$-1/3(2J-3)(2J+5)(4J^2+4J-7)$
$\Delta j=-1, \Delta J=2$ or $\Delta j=-2, \Delta J=1$	(1)	$21/2(J+1)(J+2)(2J+3)$
	(2)	$9/2(10J^3+47J^2+66J+24)$
	(3)	$-1/6(2J-1)(5J^2+28J+48)$
	(4)	$-3/4(J+2)(J+6)(2J-1)$
	(5)	$-2/3(J-1)(2J-1)(2J-3)$
	(6)	$63/4(14J^3+65J^2+92J+36)$
	(7)	$1/4(58J^3+267J^2+380J+156)$
	(8)	$1/2(34J^3+159J^2+224J+96)$
	(9)	$1/6(2J-1)(J^2-16J-12)$

$J-\Delta j\rightarrow J\rightarrow J+\Delta J$ *as for* $J+\Delta J\rightarrow J\rightarrow J-\Delta j$. Thus

$$W_{\rho,\sigma}^{\Delta j,\Delta J}(\vartheta)=W_{\rho,\sigma}^{-\Delta J,-\Delta j}(\vartheta). \tag{24}$$

TABLE IV.—(*Continued*).

$\Delta j=-1, \Delta J=1$	(1)	$21/4J(J+1)(J+2)(2J+3)$
	(2)	$9/8(18J^4+75J^3+86J^2+28J+24)$
	(3)	$1/24(2J-1)(13J^3+54J^2+188J+312)$
	(4)	$3/16(J+2)(2J-1)(J+6)(J+6)$
	(5)	$2/3(J-1)(2J-1)(2J-3)(2J+5)$
	(6)	$63/16(J+2)(J+2)(26J^2+7J+6)$
	(7)	$1/16(J+2)(110J^3+257J^2+108J+36)$
	(8)	$1/8(70J^4+289J^3+374J^2+188J+24)$
	(9)	$-1/24(2J-1)(17J^3-18J^2-164J-24)$
$\Delta j=-2, \Delta J=2$	(1)	$21/2(J+1)(J+2)(2J+3)(2J+5)$
	(2)	$9(8J^4+60J^3+162J^2+183J+70)$
	(3)	$1/3J(2J-1)(8J^2-34J+39)$
	(4)	$3/2J(J+2)(2J+5)(2J-1)$
	(5)	$1/3J(J-1)(2J-1)(2J-3)$
	(6)	$63/2(J+2)(J+2)(6J+5)(2J+5)$
	(7)	$1/2(J+2)(2J+5)(26J^2+71J+42)$
	(8)	$(2J+3)(16J^3+90J^2+161J+84)$
	(9)	$1/3J(2J-1)(2J^2+13J+12)$

When both particles are the same, as in $\gamma-\gamma$-correlations, this relation asserts no more than would follow from the equality of the correlation function for direct and inverse processes as is implied by the hermiticity of all matrix elements in $W(\vartheta)$. Indeed, hermiticity yields quite generally

$$W_{\rho,\sigma}^{\Delta j,\Delta J}{}_{L_1,L_2}(\vartheta)=W_{\sigma,\rho}^{-\Delta J,-\Delta J}{}_{L_2,L_1}(\vartheta). \tag{25}$$

However, for *unlike* particle emissions and same L, (24) is a stronger relation since it equates two *direct* processes. The proof of (24) follows directly by expanding both sides of (24) and using the symmetry of the sums (proved for any value of L in Appendix II) and the hermiticity property of the squares of the transformation coefficients:

$$g_{m'm}^{\Delta j,L}=G_{mm'}^{-\Delta j,L}.$$

(B) Canonical Forms for Correlation Functions

We now combine all the preceding reductions of the angular distributions $F_L{}^M(\vartheta)$ and sums $(\cdots\sum d_m{}^{\Delta j_1 L_1}\times G_{mm}{}^{\Delta J_1 L_2})$ occurring in $W(\vartheta)$ to obtain "canonical forms" for the correlation functions with L_1, $L_2=1$ or 2 which will be both general and easy to evaluate. The only indeterminateness remaining in the $W(\vartheta)$ which we tabulate is the specification of the parameters for the $F_L{}^M(\vartheta)$; these will vary with the particles involved in the angular correlation.

(a) $L_1=L_2=1$.

Inserting the parametric forms (19) for the $F_1{}^M(\vartheta)$ in $W(\vartheta)$, Eq. (23a), one gets for the most general $L_1=L_2=1$ angular correlation:

$$W(\vartheta)=1+R/Q\cos^2\vartheta \tag{26}$$

with

$$R/Q=\frac{dD-2dG}{\phi(\lambda,\Lambda)[dD+dG]+dG} \tag{27}$$

where

$$\phi(\lambda, \Lambda)=\frac{4-(\lambda-1)(\Lambda-1)}{4\lambda\Lambda}, \tag{28}$$

λ and Λ being the arbitrary parameters for the first and second transitions, respectively.

The ratio R/Q in the form (27) is tabulated for all J, $\Delta j=0, \pm1$, $\Delta J=0, \pm1$ in Table I.

If the second transition is dipole $-\gamma$, then $\Lambda=1$ and ϕ reduces to $1/\lambda$. For $\alpha-\gamma$- or $\gamma-\gamma$-correlations, $\lambda=-1$ and $+1$ respectively.

(b) $L_1=1$, $L_2=2$.

One obtains in a similar way:

$$W(\vartheta)=1+R/Q\cos^2\vartheta$$

with

$$R/Q=\frac{dD-2gD}{\phi_{12}[dD+gD]+gD}. \tag{29}$$

Here $\phi_{12}(\lambda; \Lambda_1, \Lambda_2)$ is a definite function of the parameters λ for the $F_1{}^M(\vartheta)$ and Λ_1 and Λ_2 for the $F_2{}^M(\vartheta)$. Its value for given $F_1{}^M(\vartheta)$ and $F_2{}^M(\vartheta)$ is of course independent of how (or whether) one chooses to parametrize the latter. If, in particular, one chooses Λ_1 and Λ_2 as K_1 and K_2, Eq. (21), one gets

$$\phi_{12}(\lambda; K_1, K_2)$$

$$=\frac{1}{(21K_2-1)}\left[\frac{15(K_1+2K_2)+5\lambda K_1-2-4\lambda K_2}{2\lambda}\right]. \tag{30}$$

This is applicable to any correlation with $L_1=1$, $L_2=2$, but is especially convenient when the $L=2$ transition is γ or internal conversion since for both of these $K_1=0$. For the γ-quadrupole, Eq. (17) $K_2=0$ also, so that

$$\phi_{12}(\lambda; 0, 0)=1/\lambda.$$

The ratio R/Q in the form (29) is tabulated for all J, $\Delta j=0, \pm1$ and $\Delta J=0, \pm1, \pm2$ in Table II.

(b′) $L_1=2$, $L_2=1$.

By using relation (25) one can obtain any correlation for $L_1=2$, $L_1=1$ involving successive nuclear states $J+\Delta J\to J\to J-\Delta j$ from its inverse in Table II, which is set up for $L_1=1$, $L_2=2$ and successive states $J-\Delta j\to J\to J+\Delta J$.

For some β-interactions, the choice of parameters μ_1 and μ_2, Eq. (20), for the $F_2{}^M(\vartheta)$ is convenient, since $\mu_2=0$. Then the appropriate $\phi_{21}(\mu_1, \mu_2; \Lambda)$ to insert in (29) becomes:

$$\phi_{21}(\mu_1, \mu_2; \Lambda)=\frac{5(3\mu_1+1)+3\mu_2+\Lambda(5\mu_1-3\mu_2-3)}{2\Lambda(6\mu_2+7)}, \tag{31}$$

where Λ is the parameter for the $L=1$, $F_1{}^M(\vartheta)$, (19). If the second transition is γ-dipole, $\Lambda=1$, this reduces to

$$\phi_{21}(\mu_1, \mu_2; 1)=\frac{10\mu_1+1}{6\mu_2+7} \tag{32}$$

(c) $L_1=L_2=2$.

Taking k_1, k_2 and K_1, K_2, Eq. (21), as parameters for the $F_2{}^M(\vartheta)$ for the first and second transitions respectively, and expressing all sums occurring in $W(\vartheta)$, Eq. (23a), in terms of the linearly independent ones, dG, dD, and dE, one obtains

$$W(\vartheta)=1+(R/Q)\cos^2\vartheta+(S/Q)\cos^4\vartheta, \tag{33}$$

with

$$\begin{aligned}Q=&[\tfrac{5}{2}k_1K_1-\tfrac{1}{3}(k_1+K_1)+5(k_1K_2+k_2K_1)]\\&\times[dG+dD+dE]+k_2K_2[3dG+(13/2)dD+17dE]\\&-(K_2+k_2)[\tfrac{1}{3}dG+\tfrac{1}{2}dD+dE]+(1/18)[dD+dE],\\R=&[21k_2K_2-k_2-K_2][dG+\tfrac{1}{2}dD-dE]\\&+\tfrac{1}{6}[2dG-dD],\\S=&-\tfrac{1}{3}[dG-\tfrac{2}{3}dD+\tfrac{1}{6}dE].\end{aligned} \tag{34}$$

These general expressions simplify considerably if one of the transitions, say the second, is γ-quadrupole. Then $K_1=K_2=0$, and one gets:

$$\begin{aligned}Q=&-6k_1[dG+dD+dE]\\&-6k_2[dG+\tfrac{3}{2}dD+3dE]+[dD+dE],\\R=&-18k_2[dG+\tfrac{1}{2}dD-dE]+3[2dG-dD],\\S=&-[6dG-4dD+dE].\end{aligned} \tag{35}$$

Equivalent expressions for Q, R, and S when the parameters for the first transitions are μ_1, μ_2 are:

$$\begin{aligned}Q=&6\mu_1[dG+dD+dE]+3\mu_2dE+[dD+4dE],\\R=&6\mu_2[dD-dE]+6[dG+\tfrac{1}{2}dD-dE],\\S=&\mu_2[6dG-4dD+dE].\end{aligned} \tag{36}$$

When $\mu_2=0$, $S=0$.

To facilitate the use of these formulae, the linearly independent sums dG, dD, dG as well as all of the linear combinations of them occurring in (34), (35), (36) are tabulated for all J, $\Delta j=0, \pm1, \pm2$ and $\Delta J=0, \pm1, \pm2$ in Tables III and IV.

In all tables, common factors have been dropped. In particular, the normalization factors in the transformation coefficients were discarded. Where no entry is given in a table, the $W(\vartheta)$ for that choice of L_1, L_2, Δj, ΔJ, J, may be obtained from one equal to it in virtue of the relations (25) or (24).

As regards the conditions for the valid use of these tables our assumptions are the same as Hamilton's in his $\gamma-\gamma$-correlation tabulations. In particular, we have assumed that only one L is associated with each transition. If either transition is mixed, i.e., has two L values associated with the outgoing particles, then, as shown in reference 6, the resulting $W(\vartheta)$ is not simply the weighted sum of the $W(\vartheta)$'s found from each L considered separately: major interference effects can also occur. It would not be very difficult to tabulate "canonical" correlations functions which include this

interference, since the necessary sums have already been evaluated in reference 6. However, it hardly seems desirable to introduce this complication into the theory until experiment demands it.

We should like to acknowledge the kind cooperation of Professor D. R. Hamilton in making available to us unpublished computations of his which greatly simplified the preparation of the tables. We have also benefitted from many discussions with Dr. D. S. Ling, Jr. concerning his related work on internal conversion angular correlations. The preparation for publication was supported in part by the joint program of the ONR and AEC at the University of Notre Dame.

APPENDIX I. IRREDUCIBLE TENSORS AND SOLID HARMONICS

Weyl (reference 19, p. 149 et seq.) has shown that if a tensor of order L satisfies the conditions

(a) $T_{i_1 i_2 \cdots i_L}$ is symmetric with respect to the interchange of any two indices,

(b) $\Sigma_{i_1} T_{i_1 i_1 i_3 \cdots i_L}=0$: all spurs vanish,

then it is irreducible under the n-dimensional orthogonal group. For the 3-dimensional rotation group these conditions can also be shown to characterize all the irreducible tensors. In this case, for each L there is, to within an equivalence, but one irreducible tensor having $(2L+1)$ independent components which transform irreducibly according to $\mathfrak{D}^L$.

Let $T_{i_1 i_2 \cdots i_L}(\mathbf{r})$ be the irreducible tensor constructed from the reducible tensor with components $x_{i_1} x_{i_2} \cdots x_{i_L}$ by imposing the conditions (a) and (b). Since the solid harmonics $\mathcal{Y}_{LM}(\mathbf{r}) = r^L Y_{LM}(\vartheta, \varphi)$ are also a set of $(2L+1)$ linearly independent functions homogeneous of degree L in r which transform irreducibly according to $\mathfrak{D}^L$, these must be linear combinations of the $(2L+1)$ linearly independent components of the irreducible tensor $T_{i_1 i_2 \cdots i_L}(\mathbf{r})$. Moreover, since the only invariants which can be constructed with each of these sets individually are

$$\sum_{M=-L}^{L} |\mathcal{Y}_{LM}(\mathbf{r})|^2 \quad \text{and} \quad \sum_{i_1 \cdots i_L} T_{i_1 \cdots i_L}(\mathbf{r}) T_{i_1 \cdots i_L}(\mathbf{r}),$$

by suitable adjustment of their normalization, these must be equal:

$$\sum_{M=-L}^{L} |\mathcal{Y}_{LM}(\mathbf{r})|^2 = \sum_{i_1 \cdots i_L} T_{i_1 i_2 \cdots i_L}(\mathbf{r}) T_{i_1 i_2 \cdots i_L}(\mathbf{r}). \tag{37}$$

This identity can be extended to the case in which there are as many as L distinct argument vectors $\mathbf{A}, \mathbf{B}, \cdots \mathbf{H}$ by making use of the process of *polarization*, defined by the operation:

$$\frac{1}{L!} \sum_{i_1 \cdots i_L} A_{i_1} B_{i_2} \cdots H_{i_L} \frac{\partial}{\partial x_{i_1}} \frac{\partial}{\partial x_{i_2}} \cdots \frac{\partial}{\partial x_{i_L}}$$

applied to any homogeneous monomial of degree L. In particular, this gives a unique prescription for defining irreducible tensors and solid harmonics of as many as L distinct argument vectors. Thus

$$\mathcal{Y}_{LM}(\mathbf{A}, \mathbf{B}, \cdots, \mathbf{H}) = (1/L!) \sum_{i_1 \cdots i_L} A_{i_1} B_{i_2} \cdots \times H_{i_L} \frac{\partial}{\partial x_{i_1}} \frac{\partial}{\partial x_{i_2}} \cdots \frac{\partial}{\partial x_{i_L}} \mathcal{Y}_{LM}(\mathbf{r}).$$

Polarization leaves invariant the transformation properties since it replaces vectors by other vectors. The generalization of Eq. (37) which follows by polarization is Eq. (8).

Example: Taking

$$\begin{aligned} \mathcal{Y}_{2,0}(\mathbf{r}) &= (\tfrac{5}{8})^{\frac{1}{2}}(3z^2-r^2), \quad \mathcal{Y}_{2,\pm 1}(\mathbf{r}) = \mp 2z(x \pm iy), \\ \mathcal{Y}_{2,\pm 2}(\mathbf{r}) &= (x \pm iy)^2, \end{aligned} \tag{38}$$

the completely polarized solid harmonics are

$$\begin{aligned} \mathcal{Y}_{2,0}(\mathbf{A}, \mathbf{B}) &= (\tfrac{5}{8})^{\frac{1}{2}}[3A_z B_z - \mathbf{A} \cdot \mathbf{B}], \\ \mathcal{Y}_{2,\pm 1}(\mathbf{A}, \mathbf{B}) &= \mp[A_z(B_x \pm iB_y) + B_z(A_x \pm iA_y)], \\ \mathcal{Y}_{2,\pm 2}(\mathbf{A}, \mathbf{B}) &= (A_x \pm iA_y)(B_x \pm iB_y). \end{aligned} \tag{39}$$

The irreducible tensor $T_{ij}(\mathbf{r}) = x_i x_j - \frac{1}{3} r^2 \delta_{ij}$ when polarized becomes:

$$T_{ij}(\mathbf{A}, \mathbf{B}) = A_i B_j + A_j B_i - \tfrac{2}{3}(\mathbf{A} \cdot \mathbf{B}) \delta_{ij}$$

and for any four vectors **A**, **B**, **C**, **D**, one gets then

$$\sum_{M=-2}^{2} \mathcal{Y}_{2M}(\mathbf{A}, \mathbf{B}) \mathcal{Y}_{2M}(\mathbf{C}, \mathbf{D})^* = \sum_{i,j} T_{ij}(\mathbf{A}, \mathbf{B}) T_{ij}(\mathbf{C}, \mathbf{D}).$$

APPENDIX II. THE SYMMETRY OF THE SUMS

The symmetry relations between sums of products of squares of transformation coefficients (e.g. $gD = dG$, etc. in the abbreviated notation of Section IV) which hold when $L_1 = L_2 = L$ can be proved by using the properties of the parametrized $F_L{}^M(\vartheta)$, $M = 0, \pm 1, \cdots, \pm L$. Namely the set of $F_L{}^M(\vartheta)$ as given by (12) will in general be $(L+1)$ linearly independent functions of $\cos^2\vartheta$ because they are obtained by applying the same linear operations (S) to the set of $(L+1)$ linearly independent $|Y_{LM}(\vartheta, \varphi)|^2$. Moreover, it follows that one can then always choose the $L+1$ arbitrary parameters so that all $F_L{}^M(0) = 0$ except for one M, say $M = 1$, for which $F_L{}^1(0) = 1$. Inserting such a set of $F_L{}^M(\vartheta)$ for both the first and second transition in $W(\vartheta)$, (23a) and equating the two $W(\vartheta)$'s obtained by taking the z-axis to be the direction of emission of the first or second particle emitted respectively, one gets

$$\begin{aligned} \Sigma_m d_m{}^{\Delta j}[G_{m,m}{}^{\Delta J} F_L{}^0(\vartheta) + D_m{}^{\Delta J} F_L{}^1(\vartheta) + \cdots] \\ = S_m[g_{m,m}{}^{\Delta j} F_L{}^0(\vartheta) + d_m{}^{\Delta j} F_L{}^1(\vartheta) + \cdots] D_m{}^{\Delta J}. \end{aligned}$$

Equating the coefficients of the linearly independent $F_L{}^M(\vartheta)$ gives the symmetry relations for all sums containing $d_m{}^{\Delta j}$ and $D_m{}^{\Delta J}$. Similarly, by taking different $F_L{}^M(0) \neq 0$ in turn, one gets all the other symmetry relations.

In the same way one can also obtain all the relations between sums for any L_1 and L_2.

On the Beta-Gamma-Angular Correlation*

DAVID L. FALKOFF
University of Notre Dame, Notre Dame, Indiana

AND

G. E. UHLENBECK
University of Michigan, Ann Arbor, Michigan

(Received March 27, 1950)

The angular distributions for the components of a line in a β-transition are exhibited for use in obtaining numerical values for the angular correlation between successive nuclear beta- and gamma-radiations. The calculations are made with each of the five linearly independent electron-neutrino interactions (assuming $Z=0$) for allowed, first and second forbidden β-transitions. In general, the theory yields an angular correlation for forbidden β-transitions which will vary with the interaction and the degree of forbiddenness, and thus affords a means of disintinguishing between these. It is shown that no angular correlation is to be expected whenever, (*a*) the β-transition is allowed, (*b*) the transition is classified as forbidden but has an allowed energy spectrum, (*c*) only the low energy β-particles are counted.

I. INTRODUCTION

WHEN any two particles are emitted in successive nuclear transitions, theory[1,2] shows that there can, in general, be an angular correlation between their directions of emission. The form of such a correlation function, $W(\vartheta)$, depends only on the angular momenta of the nuclear states involved and of the outgoing particles. However, the determination of the coefficients of the powers of $\cos^2\vartheta$ in $W(\vartheta)$ requires more detailed information concerning the interactions describing the respective emissions.

The $\beta-\gamma$-angular correlation is of particular interest in this respect, for we shall show that it can be used both to determine the degree of forbiddenness for the β-transition and to distinguish between the different electron-neutrino interactions which are possible according to the Fermi[3-5] theory of β-decay.

In reference 1 we have reduced the problem of calculating the angular correlation to that of obtaining, for both the β- and γ-transitions, the angular distributions $F_L{}^M(\vartheta)$ which are associated with each component of a line. The required angular distributions for the electromagnetic multipoles have been derived elsewhere.[6-8]

It thus remains to obtain the angular distributions $F_L{}^M(\vartheta)$ associated with transitions between the different magnetic sublevels of the nuclear states involved in the β-transition. This is done in Section II, using the solid harmonic decomposition of irreducible tensors exhibited in reference 1, Section III(B). The applications to, and discussion of, the $\beta-\gamma$-correlation are given in Section III.

All of our calculations are with the Fermi theory of β-decay in the $Z=0$ approximation. In order to apply the "canonical correlation functions" tabulated in Section IV of reference 1, we must further make the same two assumptions which underlie Hamilton's tabulations for the $\gamma-\gamma$-correlation, namely (*a*) that the natural line-width of the intermediate nuclear state be much larger than the hyperfine splitting of that state—or in other words that the lifetime of the intermediate state be short enough—and (*b*) that only one angular momentum be carried off by the outgoing particles (i.e., β-particle and neutrino) for a given β-transition, and similarly for the γ-transition. The second assumption as applied to the γ-transition requires the γ-radiation to be a pure multipole field and not a mixture of multipoles.[8] Applied to the β-theory, it means that we consider only one matrix element at a time, rather than the mixtures of unknown matrix elements which occur in the usual "forbidden"[4,5] β-transitions. This policy has the advantage that the predicted $\beta-\gamma$-correlations can then be made completely definite and do not involve any unknown ratio of matrix elements. One could, of course, extend the $\beta-\gamma$-correlation theory to take into account mixtures of matrix elements as was done for the $\gamma-\gamma$-correlation in reference 8, but the present status of the experiments on β-emitters does not yet warrant such an additional complication.[9]

---

* Part of a Doctoral Thesis by D. L. Falkoff submitted to the Graduate School, University of Michigan, April, 1948. Preparation for publication has been aided in part by the joint program of the AEC and ONR at the University of Notre Dame.

[1] D. L. Falkoff and G. E. Uhlenbeck, Phys. Rev. (preceding paper).
[2] C. N. Yang, Phys. Rev. **74**, 764 (1948).
[3] E. Fermi, Zeits. F. Physik **88**, 161 (1934).
[4] E. J. Konopinski and G. E. Uhlenbeck, Phys. Rev. **60**, 308 (1941).
[5] E. J. Konopinski, Rev. Mod. Phys. **15**, 209 (1943).
[6] D. R. Hamilton, Phys. Rev. **38**, 122 (1940).
[7] G. Goertzel, Phys. Rev. **70**, 897 (1946).
[8] D. S. Ling, Jr. and D. L. Falkoff, Phys. Rev. **76**, 1639 (1949).

[9] If sufficient experimental evidence were available, then the angular correlation could yield information not obtainable by the usual β-lifetime or β-spectrum measurement. Namely, while these latter can in principle determine the relative magnitudes of the nuclear matrix elements, the angular correlation with mixtures also is sensitive to the relative *phases* of the matrix elements. See reference 8 for a detailed discussion of this point as applied to $\gamma-\gamma$-correlations.

II. THE β-ANGULAR DISTRIBUTIONS

The probability per unit time for emission of a β-particle with energy W and momentum $\mathbf{p}$ in the solid angle $d\Omega_e$ and simultaneous emission of neutrino with momentum $\mathbf{q}$ and energy $K=W_0-W$ in the solid angle $d\Omega_\nu$ can be written[3,5] as

$$P(W)dWd\Omega_e d\Omega_\nu = G^2/(2\pi)^5 pWK^2 S_{e,\nu} \times |(\psi_i|H|\psi_f)|^2 d\Omega_e d\Omega_\nu dW, \quad (1)$$

where H is the electron-neutrino interaction, ψ_i, and ψ_f, initial and final nuclear wave functions, and $S_{e,\nu}$ denotes an average over the two possible spin orientations for electron and neutrino. A detailed treatment of the matrix elements occurring in (1) for allowed and forbidden β-transitions with each of the five linearly independent electron-neutrino interactions, H, has been given by Konopinski and Uhlenbeck.[4] We shall assume familiarity with the methods and notations of their paper, and shall consider here the extensions of it necessary for the treatment of angular correlations with β-particles.

The usual β-theory, insofar as it is concerned only with obtaining β-lifetimes or the shapes of the energy spectra, has no need to take into account the angular momentum degeneracy of the nuclear states. However, as shown in reference 1, Section III(A), for the angular correlations it is necessary to obtain the angular distributions $F_L{}^M(\vartheta)$ associated with each component $m\to m'=m+M$ of a line, and to specify the angular momentum quantum numbers for initial and final nuclear states. Thus, in the notation of Section III of reference 1, we denote initial and final nuclear states by the quantum numbers αJm and $\alpha' J'm'$ respectively. Then from (1), the (relative) probability for β-emission with energy W in the direction ϑ during the transition $\alpha Jm\to\alpha' J'm'$, irrespective of the spin polarizations of β-particle or neutrino, or direction of emission of the neutrino, is given by:

$$P_{mm'}(\vartheta;W)=\int d\Omega_\nu S_{e,\nu}|(\alpha Jm|H|\alpha' J'm')|^2, \quad (2)$$

where factors in (1) common to each component are dropped. Konopinski and Uhlenbeck[4] have already obtained the various interactions, H, in irreducible tensor form. Hence one can directly apply the solid harmonic decomposition, reference 1, Eq. (8), to obtain the required angular distributions for each component $m\to m'$. In particular, if the interaction H involves only one irreducible matrix element corresponding to angular momentum L, then the analysis of Section III(B) of reference 1 shows that (2) can be written in the form

$$P_{mm'}(\vartheta;W)=|\mathfrak{M}|^2 G_{mm'}^{JLJ'} F_L{}^M(\vartheta;W), \quad m'=m+M \quad (3)$$

Here $\mathfrak{M}$ represents the unknown nuclear matrix element $f(\alpha,\alpha',J,J',\mathbf{X}_i)$ of reference 1, Eq. (10), which is independent of m, m', M and, therefore, common to each component. It can be, for example, any one of the irreducible tensor matrix elements for $L=0, 1, 2, 3$ listed in Table I of reference 4. The $G_{m,m'}^{JLJ'}$ are the squares of the transformation coefficients for vector addition of angular momenta [reference 1, Eq. (11)]. The $F_L{}^M(\vartheta)$ are given explicitly by reference 1, Eq. (12) with S replaced by $\int d\Omega_\nu S_{e,\nu}$. Thus

$$F_L{}^M(\vartheta;W)=\int d\Omega_\nu S_{e,\nu}|\mathcal{Y}_{LM}(\mathbf{A}_i)|^2, \quad (4)$$

the argument vectors $\mathbf{A}_i$ depending on the interaction. These will be called *differential* angular distributions, since they apply to β-particles with energy between W and $W+dW$. One can also obtain angular distributions for a component irrespective of the β-energy:

$$F_L{}^M(\vartheta;W_0)=\int_1^{W_0} pW(W_0-W)^2 F_L{}^M(\vartheta;W)dW. \quad (5)$$

These will be called *integrated* angular distributions. Had we not assumed $Z=0$, both the differential and integrated $F_L{}^M(\vartheta)$ would also have depended on Z.

We illustrate the use of (4) with the polar vector interaction, and then enumerate the results, similarly obtained, with the other interactions.

(A) Polar Vector Interaction

(i) *Allowed Transitions*

The matrix element for allowed transitions is:

$$(\psi_i|H|\psi_f)=(A^*B)(\psi_i,\psi_f),$$

where A and B are 4-component Dirac spinors for the electron and antineutrino respectively. The scalar nuclear matrix element, (ψ_i,ψ_f) corresponding to $L=0$ is denoted by $\int 1$ in reference 4. The associated angular distribution, given by[10]

$$F_0{}^0(\vartheta)=\int d\Omega_\nu S_{e,\nu}|(A^*B)|^2 = \int d\Omega_\nu(1-\mathbf{p}\cdot\mathbf{q}/WK)\simeq 1 \quad (6)$$

is isotropic, as one would expect physically for a scalar operator.

(ii) *First Forbidden Transitions*

The interaction is here

$$H=-i(A^*B)(\mathbf{P}\cdot\mathbf{r})-(A^*\boldsymbol{\alpha}B)\cdot\boldsymbol{\alpha}_H, \quad (7)$$

where $\mathbf{P}=\mathbf{p}+\mathbf{q}$; $\boldsymbol{\alpha}$ and $\boldsymbol{\alpha}_H$ are Dirac operators on light and heavy particles (nucleons), respectively. Applying the solid harmonic decomposition to each of the vectors $\mathbf{P}$, $\mathbf{r}$, $\boldsymbol{\alpha}$, $\boldsymbol{\alpha}_H$ this becomes

$$H=-[i(A^*B)\sum_{M=-1}^{1}\mathcal{Y}_{1M}(\mathbf{P})^*\mathcal{Y}_{1M}(\mathbf{r}) + \sum_{M=-1}^{1}(A^*\mathcal{Y}_{1M}(\boldsymbol{\alpha})^*B)\mathcal{Y}_{1M}(\boldsymbol{\alpha}_H)]. \quad (8)$$

[10] All constant factors are dropped.

From (2) and (3), denoting the nuclear matrix elements by $\int \boldsymbol{\alpha}$, $\int \mathbf{r}$,

$$P_{mm'}(\vartheta;W)=G^{J1J'}_{mm'}\left[\int d\Omega_{\nu}S_{e,\nu}\left[|\mathcal{Y}_{1M}(\mathbf{P})|^2\right.\right.$$
$$\times|(A^*B)|^2\left|\int \mathbf{r}\right|^2+|(A^*\mathcal{Y}_{1M}(\boldsymbol{\alpha})^*B)|^2\left|\int \boldsymbol{\alpha}\right|^2$$
$$\left.\left.+\left\{i(A^*B)(A^*\mathcal{Y}_{1M}(\boldsymbol{\alpha})B)^*\int \mathbf{r}\cdot\int \boldsymbol{\alpha}^*+\text{c.c.}\right\}\right]\right]. \quad (9)$$

The resultant angular distribution in square brackets is seen to involve the weighted sum of the angular distributions associated with each of the matrix elements $\int \boldsymbol{\alpha}$ and $\int \mathbf{r}$ *plus* an interference term with coefficients $i(\int \boldsymbol{\alpha}\cdot\int \mathbf{r}^*-\int \boldsymbol{\alpha}^*\cdot\int \mathbf{r})$. If only one unknown matrix element were present, then being common to all components it could be dropped since only the angular distributions and not absolute transition probabilities are needed for the angular correlation. However, when two matrix elements are retained, one can divide through by the squared magnitude of one of them, but the resultant expression (e.g., Eq. (9)) will still depend on the unknown *relative phase* and *relative magnitude* of the two matrix elements. In this case, since $\int \boldsymbol{\alpha}$, $\int \mathbf{r}$ are both vector operators, $L=1$, the transformation coefficients enter in the same way in (9) for both their squares and the interference cross term, and hence the resultant $P_{mm'}(\vartheta;W)$ is still suitable for use with the canonical correlation functions tabulated in reference 1. This would not be so if the matrix elements belonged to different values of L (see "second forbidden transitions" below).

The angular distributions associated with the respective matrix elements in (9) are:

(a) $\left|\int \mathbf{r}\right|^2$

$$F_1{}^0(\vartheta;W)=\tfrac{1}{3}q^2+p^2(1+2q^2/3WK)\cos^2\vartheta, \quad (10)$$
$$F_1{}^{\pm1}(\vartheta;W)=\tfrac{1}{3}q^2+\tfrac{1}{2}p^2(1+2q^2/3WK)$$
$$-\tfrac{1}{2}p^2(1+2q^2/3WK)\cos^2\vartheta,$$

(b) $\left|\int \boldsymbol{\alpha}\right|^2$

$$F_1{}^0(\vartheta;W)=F_1{}^{\pm1}(\vartheta;W)=1, \quad (11)$$

(c) $i\int \boldsymbol{\alpha}\cdot\int \mathbf{r}^*+\text{c.c.}$

$$F_1{}^0(\vartheta;W)=q^2/3K+(p^2/W)\cos^2\vartheta, \quad (12)$$
$$F_1(\vartheta;W)=(p^2/2W+q^2/3K)-(p^2/2W)\cos^2\vartheta.$$

These $F_L{}^M(\vartheta)$, like all those that we shall obtain, satisfy the "isotropy conditions" of reference 1, Section III, namely, that $\int F_L{}^M(\vartheta)d\Omega$ is independent of M, and $\sum_{M=-L}^{L} F_L{}^M(\vartheta)$ is independent of ϑ. Moreover, they will also satisfy the parametrizations for the $F_L{}^M(\vartheta)$ exhibited in Section III(C) of reference 1 for $L=1$ and $L=2$.

Thus for $|\int \mathbf{r}|^2$ the one "homogeneous" parameter λ of Eq. (19) of reference 1 for the differential angular distributions (10) is[11]

$$\lambda(p)=\frac{-p^2/2(1+2q^2/3WK)}{q^2/3+p^2/2(1+2q^2/3WK)}. \quad (13)$$

The corresponding parameter $\lambda(W_0)$, for the integrated distributions is obtained from (13) by weighting both numerator and denominator by the "statistical factor," $(W_0-W)^2(W^2-1)^{\frac{1}{2}}WdW$, and integrating over the β-energy spectrum. This, and all subsequently obtained integrated parameters associated with matrix elements corresponding to $L=1$ or 2 in the various β-interactions, will not be listed explicitly, but are plotted in Figs. 2 and 3 respectively as functions of W_0.

For $\int \boldsymbol{\alpha}$, both $\lambda(p)$ and $\lambda(W_0)$ are zero. For the interference angular distributions (12):

$$\lambda(p)=\frac{-p^2/2W}{p^2/2W+q^2/3K}. \quad (14)$$

As shown in reference 1, Section III(C) the parametrization of the $F_L{}^M(\vartheta)$ is but the formal expression of the fact that it is sufficient to obtain any $F_L{}^M(\vartheta)$ for fixed M and then the remaining $F_L{}^M(\vartheta)$ are uniquely determined. They may then be obtained explicitly from the parametric representation. Accordingly we shall henceforth exhibit only one of the $F_L{}^M(\vartheta)$, say $F_L{}^0(\vartheta)$, from which can be read off the values of the differential and integrated parameters for obtaining the remainder of the set. These parameters are all that are needed to make the tabulated correlation functions of reference 1, Section IV completely definite.

It is rather interesting that the angular distributions (11) associated with $\int \boldsymbol{\alpha}$ are isotropic, notwithstanding the fact that $\boldsymbol{\alpha}$ is a vector operator, $L=1$. Physically this is understandable since the angular momentum of the outgoing β-particle and neutrino due to the $\boldsymbol{\alpha}$ term in the first forbidden interaction is wholly spin angular momentum. (This is because one has set $e^{i\mathbf{P}\cdot\mathbf{r}}=1$ in this term, which is equivalent to assuming that the electron and neutrino are emitted in s-states). But since one has averaged over all spin orientations one should not expect any net angular dependence from this term. On the other hand, $\int \mathbf{r}$ comes from the $(\mathbf{P}\cdot\mathbf{r})$ term in the expansion of the exponential, and this is

[11] We use relativistic units $\hbar=m=c=1$, throughout; since the neutrino rest mass is zero, $K=q$. We have not canceled the q/K, for purely didactic purposes: (*a*) the factor $1/WK$ identifies terms due to spurs in taking spin averages (*b*) to show the connection with the corresponding formulas of reference 4.

associated with the total *orbital* angular momentum of the emitted particles. In spite of this distinction we classify both matrix elements as $L=1$, since it is this value of L which determines the selection rules for the matrix elements and the transformation coefficients $(JLJ'M'|JLmM)$ which enter into the explicit calculation of angular correlations (reference 1, Section IV).

(iii) Second Forbidden Transitions

Konopinski and Uhlenbeck[4] have shown that the following irreducible tensor matrix elements occur in the interaction for second forbidden transitions: the scalars $\int r^2$ and $\int \boldsymbol{\alpha}\cdot\mathbf{r}$, the axial vector $\int \boldsymbol{\alpha}\times\mathbf{r}$, and two second order tensors with spin zero:

$$R_{ij}=\int x_i x_j-\tfrac{1}{3}r^2\delta_{ij}$$

and

$$A_{ij}=\int \alpha_i x_j+\alpha_j x_i-\tfrac{2}{3}(\boldsymbol{\alpha}\cdot\mathbf{r})\delta_{ij}.$$

Of these, the scalars are discarded as having the same selection rules as the allowed transition and representing only a small correction to it. The axial vector ($L=1$) and the two second-order tensors ($L=2$) are retained since they yield different selection rules than either allowed or first forbidden transitions. On retaining these latter three matrix elements, one gets not only the angular distributions associated with each one individually, but also additional interference angular distributions associated with each pair. These interference terms are of two kinds. First there is the term with coefficients $\sum_{ij} A_{ij}R_{ij}^*$ which is similar to the $\int\boldsymbol{\alpha}\cdot\int\mathbf{r}^*$ cross term in (9) in that both irreducible tensors belong to the *same* L. Therefore, no new products of transformation coefficients are introduced: the same $G_{mm'}{}^{JLJ'}$ is common to squares of these matrix elements and their cross terms. Hence the canonical correlation function tabulations of reference 1, Section IV are applicable to such mixtures even though one still carries along the unknown relative magnitudes and phases of nuclear matrix elements. The second type of cross term is that involving the axial vector and either A_{ij} or R_{ij}. For such cross products of operators transforming according to *different* values of L, the interference term can be shown to vanish if one considers only a single transition.[8] (Thus, contributions from this kind of cross term do not occur in the "energy correction factors" obtained in reference 4.) However, they can be shown to contribute to the angular correlation.[8] The occurrence of products of transformation coefficients with different L makes inapplicable the canonical correlation functions tabulated in Section IV of reference 1.

In accordance with the policy stated in the introduction, we shall consider only the angular distributions associated with each matrix element individually for then the theoretical angular correlations can be made completely definite.

Thus

(a) $\int\boldsymbol{\alpha}\times\mathbf{r}$

$$F_1{}^0(\vartheta;W)=\{p^2[1-(4q^2/3WK)]+\tfrac{2}{3}q^2\}+p^2[(4q^2/3WK)-1]\cos^2\vartheta, \quad (15)$$

whence

$$\lambda(p)=\frac{\frac{p^2}{2}[1-(4q^2/3WK)]}{\frac{p^2}{2}[1-(4q^2/3WK)]+\frac{2}{3}q^2}. \quad (16)$$

(b) R_{ij}

$$F_2{}^0(\vartheta;W)=\left[\frac{2}{15}q^4+\frac{2}{9}p^2q^2+\frac{1}{6}p^4+\frac{2p^2q^2}{9WK}\left(p^2+\frac{2q^2}{5}\right)\right]+\left[\frac{2}{3}p^2q^2-p^4+\frac{4p^2q^2}{3WK}(\tfrac{1}{5}q^2-p^2)\right]\cos^2\vartheta+\left[\frac{3}{2}p^4+\frac{2p^4q^2}{WK}\right]\cos^4\vartheta. \quad (17)$$

Taking the homogeneous parameters for the $L=2$, $F_2{}^M(\vartheta)$ as μ_1 and μ_2 of reference 1, Eq. (20), these differential parameters are here:

$$\mu_1(p)=\frac{\frac{2}{15}q^4+\frac{2}{9}p^2q^2+\frac{1}{6}p^4+\frac{2p^2q^2}{9WK}(p^2+2q^2/5)}{\frac{2}{3}p^2q^2-p^4+\frac{4p^2q^2}{3WK}(\frac{1}{5}q^2-p^2)}. \quad (18a)$$

$$\mu_2(p)=\frac{\frac{3}{2}p^4+\frac{2p^4q^2}{WK}}{\frac{2}{3}p^2q^2-p^4+\frac{4p^2q^2}{3WK}(\frac{1}{5}q^2-p^2)}. \quad (18b)$$

(c) A_{ij}

$$F_2{}^0(\vartheta;W)=\tfrac{1}{3}(2p^2+4q^2)+2p^2\cos^2\vartheta \quad (19)$$

whence

$$\mu_1(p)=(p^2+2q^2)/3p^2 \quad (20a)$$

and

$$\mu_2(p)=0. \quad (20b)$$

Note that although A_{ij} has selection rules for $L=2$, $\cos^2\vartheta$ rather than $\cos^4\vartheta$ is the highest power occurring in the $F_2{}^M(\vartheta)$, (19). This can be understood by the same argument which applied to $\int\boldsymbol{\alpha}$ above.

(B) Scalar and Pseudoscalar Interactions

The nuclear matrix elements for allowed, first and second forbidden scalar interaction are almost the same

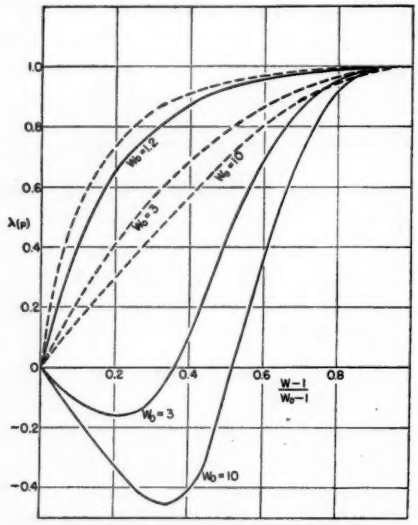

FIG. 1. The differential parameter $\lambda(p)$ *versus* $(W-1)/(W_0-1)$ for the matrix elements $\int\boldsymbol{\sigma}\times\mathbf{r}$ and $\int\beta\boldsymbol{\sigma}\times\mathbf{r}$ occurring in the axial-vector and tensor interactions respectively. The solid line denotes $\int\boldsymbol{\sigma}\times\mathbf{r}$, the broken line $\int\beta\boldsymbol{\sigma}\times\mathbf{r}$.

as the $\int 1$, $\int\mathbf{r}$ and R_{ij} of the polar vector except that the scalar Dirac operator β replaces 1. The only effect of this is to change the signs of all terms in $1/WK$ in the corresponding angular distributions for the matrix elements $\int\beta$, $\int\beta\mathbf{r}$ and $R_{ij}{}^{\beta}$. The pseudoscalar interaction differs from the scalar only in that $\beta\gamma_5$ replaces β throughout. But since these operators affect the $F_L{}^M(\vartheta)$ only through the spurs (from $S_{e,\nu}$) and these are the same for both β and $\beta\gamma_5$, it follows that *for all degrees of forbiddenness the pseudoscalar angular distributions are exactly the same as the corresponding scalar* $F_L{}^M(\vartheta)$.

(i) Allowed Transitions: $\int\beta$, $\int\beta\gamma_5$

$$F_0{}^0(\vartheta)=1. \tag{21}$$

(ii) First Forbidden Transitions: $\int\beta\mathbf{r}$, $\int\beta\gamma_5\mathbf{r}$

$$F_1{}^0(\vartheta;W)=\tfrac{1}{3}q^2+\tfrac{1}{2}p^2(1-2q^2/3WK)\cos^2\vartheta, \tag{22}$$

whence

$$\lambda(p)=\frac{-\frac{1}{2}p^2[1-(2q^2/3WK)]}{\frac{1}{2}p^2[1-(2q^2/3WK)]+\frac{1}{3}q^2}. \tag{23}$$

(iii) Second Forbidden Transitions: R_{ij}, $R_{ij}{}^{\beta\gamma_5}$

Changing the sign of the $1/WK$ terms in (17), (18a) and (18b), one gets:

$$\mu_1(p)=\frac{\frac{2}{15}q^4+\frac{2}{9}p^2q^2+\frac{1}{6}p^4-\frac{2p^2q^2}{9WK}(p^2+\frac{2}{5}q^2)}{\frac{3}{2}p^2q^2-p^4-\frac{4p^2q^2}{3WK}(\frac{1}{5}q^2-q^2)}, \tag{24a}$$

$$\mu_2(p)=\frac{\frac{3}{2}p^4-\frac{2p^4q^2}{WK}}{\frac{2}{3}p^2q^2-p^4-\frac{4p^2q^2}{3WK}(\frac{1}{5}q^2-p^2)}. \tag{24b}$$

(C) Axial Vector Interaction

(i) Allowed Transitions

The nuclear matrix element occurring here is $\int\boldsymbol{\sigma}$ corresponding to $L=1$, but the associated angular distributions are isotropic:

$$F_1{}^0(\vartheta)=F_1{}^{\pm1}(\vartheta)=1.$$

Physically, the reason for this is the same as the isotropy of the $F_1{}^M(\vartheta;W)$ for $\int\boldsymbol{\alpha}$. Formally, all spurs in $\boldsymbol{\sigma}$ are the same as the corresponding spurs in $\boldsymbol{\alpha}$, and these spurs yield terms linear in the neutrino and electron momentum which vanish when averaged over all directions.

(ii) First Forbidden Transitions

The matrix elements effective here (reference 4, Table I) are $\int\boldsymbol{\sigma}\cdot\mathbf{r}$, $\int\gamma_5$, $\int\boldsymbol{\sigma}\times\mathbf{r}$ and

$$B_{ij}=\int\sigma_ix_j+\sigma_jx_i-\tfrac{2}{3}(\boldsymbol{\sigma}\cdot\mathbf{r})\delta_{ij}.$$

The first two being scalars yield isotropic distributions $F_0{}^0(\vartheta)=1$. The member $\int\boldsymbol{\sigma}\times\mathbf{r}$ yields the same $F_1{}^M(\vartheta)$ as $\int\boldsymbol{\alpha}\times\mathbf{r}$ of the polar-vector second forbidden transitions, (15) and (16), while B_{ij} gives exactly the same $F_2{}^M(\vartheta)$ as A_{ij}: (19), (20a, b). Note that no term of higher power than $\cos^2\vartheta$ occurs in any of these angular distributions.

(iii) Second Forbidden Transitions

The $F_2{}^M(\vartheta;W)$ associated with

$$T_{ij}=\int(\boldsymbol{\sigma}\times\mathbf{r})_ix_j+(\boldsymbol{\sigma}\times\mathbf{r})_jx_i$$

are obtained from the relation

$$F_2{}^M(\vartheta;W)=\int d\Omega_{\nu}S_{e,\nu}|(A^*\mathcal{Y}_{2M}(\boldsymbol{\sigma}\times\mathbf{P},\mathbf{P})B)|^2$$

which gives

$$F_2{}^0(\vartheta;W)=\left[\frac{2q^4}{15}+\frac{p^2q^2}{3}-\frac{4}{15}\frac{p^2q^4}{WK}\right]+\left[p^4+\frac{p^2q^2}{3}-\frac{2p^4q^2}{WK}\right]\cos^2\vartheta+\left[-p^4+\frac{2p^4q^2}{WK}\right]\cos^4\vartheta. \tag{25}$$

The corresponding parameters are

$$\mu_1(p)=\frac{(2q^4/15)+(p^2q^2/3)-(4/15)(p^2q^4/WK)}{p^4+(p^2q^2/3)-(2p^4q^2/WK)}, \quad (26a)$$

$$\mu_2(p)=\frac{-p^4+(2p^4q^2/WK)}{p^4+(p^2q^2/3)-(2p^4q^2/WK)}. \quad (26b)$$

We do not exhibit the $F_3^M(\vartheta)$ associated with S_{ijk} since it corresponds to $L=3$ and the canonical correlation functions of reference 1 are given only for $L=1$ or 2. One can easily show, however, that $\cos^4\vartheta$ is the highest power of $\cos\vartheta$ occurring in these $F_3^M(\vartheta)$.

(D) Tensor Interaction

All the $F_L^M(\vartheta)$ for the matrix elements in the tensor interaction may be found from those already obtained. Namely, the nuclear matrix elements here differ from those for the axial vector and vector interactions only in that $\boldsymbol{\sigma}$ or $\boldsymbol{\alpha}$ are replaced by $\beta\boldsymbol{\sigma}$. The sole effect of this is to change the signs of the $1/WK$ terms wherever these occur in the associated $F_L^M(\vartheta)$.

(i) *Allowed Transitions*

The $F_1^M(\vartheta)$ associated with $\int\beta\boldsymbol{\sigma}$ are isotropic.

(ii) *First Forbidden Transitions*

$\int\beta\boldsymbol{\sigma}\cdot\mathbf{r}$ is a scalar with $F_0^0(\vartheta)=1$. $\int\beta\boldsymbol{\alpha}$ is isotropic just as is $\int\boldsymbol{\alpha}$, (11).

$$B_{ij}^{\beta}=\int\beta[\sigma_i x_j+\sigma_j x_i-\tfrac{2}{3}(\boldsymbol{\sigma}\cdot\mathbf{r})\delta_{ij}]$$

yields the same $F_2^M(\vartheta)$ as B_{ij} and A_{ij} (19) since no $1/WK$ terms are present.

However, the $F_1^M(\vartheta)$ for $\int\beta\boldsymbol{\sigma}\times\mathbf{r}$ differ by the sign of the $1/WK$ term from the $F_1^M(\vartheta)$ for $\int\boldsymbol{\alpha}\times\mathbf{r}$ (15), whence:

$$\lambda(p)=\frac{\frac{1}{2}p^2[1+(4q^2/3WK)]}{\frac{1}{2}p^2[1+(4q^2/3WK)]+2q^2/3}. \quad (27)$$

(iii) *Second Forbidden Transitions*

Changing the signs of the $1/WK$ terms in (25), (26a, b), the parameters for

$$T_{ij}^{\beta}=\int\beta[(\boldsymbol{\sigma}\times\mathbf{r})_i x_j+(\boldsymbol{\sigma}\times\mathbf{r})_j x_i]$$

are

$$\mu_1(p)=\frac{(2q^4/15)+(p^2q^2/3)+(4/15)(p^2q^4/WK)}{p^4+(p^2q^2/3)+(2p^4q^2/WK)}, \quad (28a)$$

$$\mu_2(p)=\frac{-p^4-(2p^4q^2/WK)}{p^4+(p^2q^2/3)+(2p^4q^2/WK)}. \quad (28b)$$

The application of these results to angular correlations are considered in Section III.

Before leaving the angular distributions, we state several other applications of the methods used here to obtain the $F_L^M(\vartheta;W)$. First the solid harmonic decomposition of irreducible tensors may be used to show generally that the maximum power of $\cos\vartheta$ in any Nth forbidden β-transition is $\cos^{2N}\vartheta$, notwithstanding that irreducible tensor matrix elements corresponding to $L=(N+1)$ do occur in the axial-vector and tensor interactions (e.g., B_{ij} for $N=1$, etc.). Second, by averaging the $F_L^M(\vartheta;W)$ over ϑ, the resulting expression (which is independent of M) gives precisely the "energy correction factors" to the allowed energy spectrum obtained in reference 4 for the respective forbidden matrix elements. Moreover, one can exhibit[12] the energy correction factors in closed form for arbitrary Nth degree of forbiddenness and can show generally these are at most of degree $2N$ in the energy, W. Indeed, the degree of the energy correction factor cannot be less than the maximum power of $\cos\vartheta$ for any given interaction. It follows that *if a forbidden β-transition has an allowed spectrum shape, then the associated $F_L^M(\vartheta)$ are isotropic.* The converse is not true in general (e.g., $\int\boldsymbol{\sigma}\cdot\mathbf{r}$). Finally, we remark that by not carrying out the averaging over neutrino directions or over β-particle spin orientations, our formalism would yield the angular distributions needed for angular correlations in which both the directions of neutrino and of β-particle are specified or in which both the direction and spin polarization of the β-particle are given.

III. THE $\beta-\gamma$ ANGULAR CORRELATION

We now combine the preceding information about the β-angular distributions with the properties of cor-

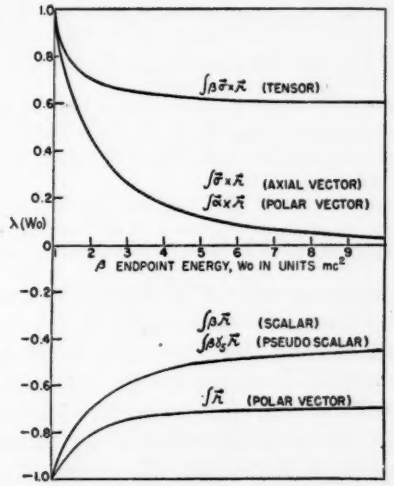

FIG. 2. The integrated parameters, $\lambda(W_0)$, *versus* W_0 for matrix elements with $L=1$ occurring in the various interactions. The matrix elements $\int\boldsymbol{\alpha}$, $\int\boldsymbol{\sigma}$, $\int\beta\boldsymbol{\sigma}$ having $\lambda=0$ (no correlation) are not shown.

[12] See the thesis of D. L. Falkoff, University of Michigan, April, 1948 for details. E. Greuling, Phys. Rev. **61**, 568 (1942) obtained by induction more general formulas for the Nth forbidden energy correction factors which are valid also for $Z\neq 0$.

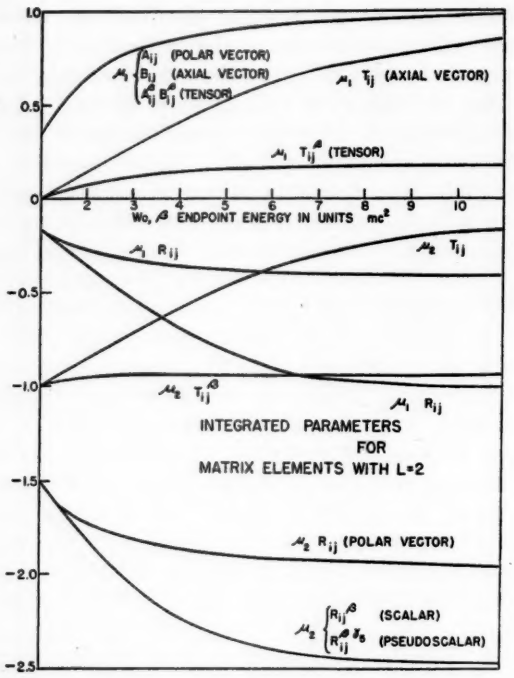

FIG. 3. The integrated parameters $\mu_1(W_0)$ and $\mu_2(W_0)$ *versus* W_0 for matrix elements with $L=2$. $\mu_2=0$ (no $\cos^4\vartheta$ term) for A_{ij}, B_{ij}, B_{ij}^{β} and A_{ij}^{β}.

relation functions established in reference 1 to draw conclusions[13] about the $\beta-\gamma$-correlation.

Conclusions which hold irrespective of the particular β-interaction are:

(1) For allowed β-transitions followed by any other radiation, there can be no angular correlation.

(2) For any forbidden β-transition having an allowed spectrum shape followed by any other radiation there can be no angular correlation.

(3) For all first forbidden β-transitions followed by any γ-multipole, $W(\vartheta)$ is of the form $A+B\cos^2\vartheta$.

(4) For all second forbidden β-transitions followed by γ-quadrupole or higher multipole, $W(\vartheta)$ is of the form $A+B\cos^2\vartheta+C\cos^4\vartheta$. However, if the γ-transition is dipole, $W(\vartheta)$ reduces to the form $A+B\cos^2\vartheta$.

(5) For β-particles near the low energy end of the β-spectrum there is no $\beta-\gamma$-angular correlation: β-particles having energy near the maximum, W_0, will yield the strongest correlation.

More detailed results can be deduced by examination of the behavior of the parameters for the $F_L{}^M(\vartheta)$ for each matrix element (see Figs. 1, 2, 3). In particular, to obtain numerical values for the coefficients of the powers of $\cos^2\vartheta$ in $W(\vartheta)$ for any proposed decay scheme, one has only to insert the values of the parameters for the interaction of interest into the canonical correlation functions tabulated in reference 1, Section IV. Since these can differ markedly from matrix element to matrix element, it follows that *the $\beta-\gamma$-angular correlation can distinguish between the different interactions.* (The scalar and pseudoscalar interactions are exceptions, yielding identical correlations in all degrees of forbiddenness.) In this respect it should be noted that although the angular correlation will be strongest for electrons near the upper limit of the β-spectrum, this is not always the optimum energy region for distinguishing between interactions. For example, the matrix elements $\int\beta\boldsymbol{\sigma}\times\mathbf{r}$ and $\int\boldsymbol{\sigma}\times\mathbf{r}$, occurring in the tensor and axial-vector interactions respectively, yield the same correlation for the high energy β-particles, but differ appreciably for intermediate energies.[14] This can be seen from the behavior of their associated differential parameters, $\lambda(p)$, plotted *versus* $(W-1)/(W_0-1)$ for different values of W_0 in Fig. 1.

In Figs. 2 and 3 the integrated parameters occurring in the different forbidden transitions are plotted as functions of W_0. These are grouped according to values of L; i.e., $\lambda(W_0)$ for $L=1$ in Fig. 2 and $\mu_1(W_0)$ and $\mu_2(W_0)$ for matrix elements with $L=2$ in Fig. 3.

With two possible exceptions[15] the experiments thus far reported on $\beta-\gamma$-angular correlations have given mostly negative results.[16] In most cases the experiments were done with β-emitters which would be classified as first or second forbidden according to their ft values, so that in general one would expect some angular correlation. However, in no case was the shape of the β-energy spectrum measured in conjunction with the correlation experiment. Since, as we have seen, one can get no correlation for forbidden transitions if the β-spectrum has the allowed shape, one can always account for a negative result by assuming that suitable matrix elements (e.g., $\int\boldsymbol{\alpha}$, $\int\boldsymbol{\sigma}\cdot\mathbf{r}$) are dominant even when the transition is first forbidden. This is no longer possible with second forbidden transitions where all matrix elements (except $\int\boldsymbol{\alpha}\cdot\mathbf{r}$ ($0\rightarrow0$ only) in the tensor interaction) would yield a correlation. However, it is known that the classification based on ft values alone is not very dependable, so that perhaps all investigated cases were only first forbidden. Therefore, it seems to us to be of great importance that the shape of the β-spectrum should confirm the degree of forbiddenness. For it is only if the shape agrees with a forbidden transition while no correlation is present that one will have a clear cut contradiction with theory.

[13] D. R. Hamilton, Phys. Rev. **60**, 168 (1941). D. L. Falkoff and G. E. Uhlenbeck, Phys. Rev. **73**, 649 (1948). C. N. Yang, reference 2.

[14] The reason for this is that the associated $F_1{}^M(\vartheta)$ differ only in the signs of the $1/WK$ terms arising from the relativistic spin averaging, and these terms do not contribute at either end of the energy spectrum.

[15] S. Frankel, Phys. Rev. **77**, 747 (1950); D. T. Stevenson and M. Deutsch, Phys. Rev. **78**, 640 (1950), report a $\beta-\gamma$-correlation in Rb^{86}. T. B. Novey, Phys. Rev. **78**, 66 (1950) reports a $\beta-\gamma$-correlation in Tm^{170}.

[16] M. A. Grace, R. A. Allen, H. Halban, Nature **164**, 538 (1949). R. Garwin, Phys. Rev. **76**, 1876 (1949). M. Wiedenbeck and J. R. Beyster, private communications.

The Equilibrium between *F*-Centers and Higher Aggregates in KCl*

ALLEN B. SCOTT AND LAMAR P. BUPP
Department of Chemistry, Oregon State College, Corvallis, Oregon
(Received March 24, 1950)

The conversion of *F*-centers to centers giving a broad absorption band at about 700 mμ has been found to be primarily thermal rather than optical. Evidence is presented to show that these centers are higher aggregates of *F*-centers and lattice vacancies, but are not colloidal. At temperatures between 300 and 500°C the *F*-centers are in equilibrium with the higher aggregates; the equilibrium was studied as a function of temperature and concentration. Absorption measurements at −195°C show that several species contribute to absorption in the band; some suggestions as to the likely nature of the centers are given.

I. INTRODUCTION

THE presence in alkali halides, colored by stoichiometric excess of alkali metal or by high energy radiation, of absorbing centers other than *F*- or *F'*-centers has been noted by several workers.[1–4] Except for the work of Glaser and Molnar, no experimental studies of the formation of the centers or of their possible structure have been reported. It has commonly been assumed that bands occurring at longer wave-lengths than the *F*-band are due to colloidal metal formed when additively colored crystals are cooled too slowly, and are thus undesirable from a theoretical standpoint, though the presence of a second metallic phase has not been demonstrated except in extreme cases.[5]

Molnar observed the development of a band (the *M*-band) at about 820 mμ in addition to the *F*-band and the *U*-band when KCl was colored by *x*-rays. This band and the *F*-band were interconvertible by irradiation with light of the wave-length absorbed by the respective bands, but during the interconversion some of the intensity of the *F*- and *M*-bands appeared as two new bands at about 675 and 730 mμ, called the *R*-bands.

Glaser studied the destruction of *F*-centers by irradiation with white light from an arc to obtain some type of aggregation of the centers, the assumption being that the process was made possible by the absorption of radiation in the visible region. Seitz suggests that the *M*-centers of Molnar are among the first products and may be an *F*-center attached to a pair of lattice vacancies; further that the *R*-centers may be first aggregates of *F*-centers such as F_2- or F_2^+-centers.

In the course of preparing KCl colored with stoichiometrically excess K for studies on the paramagnetism of color centers, it was found in this laboratory that at high concentrations of alkali metal (10^{18} to 10^{19} atoms/cc) in large crystals the formation of bands at wave-lengths greater than the *F*-bands could not be avoided even with the most rapid quenching experimentally possible. In the lower range of concentration, particularly when the crystals were smaller and thus more rapidly quenched, the bands were identical with the *R*- and *M*-bands. At concentrations around 10^{19}/cc the bands merged and increased to a prominence of the order of the *F*-band, having a maximum from 800 to 900 mμ. It was also desired to find a means of destroying *F*-centers by some process which could be conducted with the crystal in place upon a sensitive magnetic balance, and it was noted that irradiation with an arc light for a few minutes converted the *F*-band into the broad band.

The experiments reported here were undertaken to obtain information regarding the nature of the centers responsible for the broad band and their relationship with the *F*-, *M*-, and *R*-centers. For purposes of brevity the band will be referred to as the *R'*-band, and the centers as *R'*-centers, because of their absorption in the red. KCl colored with additional K was used in all cases

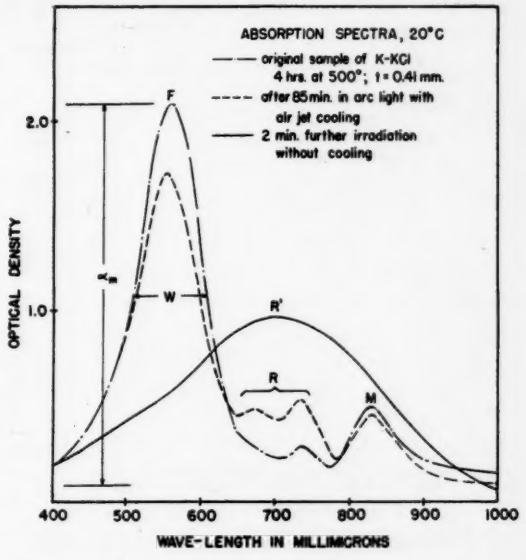

FIG. 1. Optical and thermal conversion of *F*-centers in KCl.

* This work has been supported by the ONR. Published with the approval of the Oregon State College Monographs Committee as Research Paper No. 157, Department of Chemistry, School of Science.

[1] R. Ottmer, Zeits. f. Physik **46**, 798 (1928).
[2] G. Glaser, Göttinger Nachrichten **3**, 31 (1937).
[3] J. P. Molnar, unpublished work described in reference 4; Phys. Rev. **59**(A), 944 (1941).
[4] F. Seitz, Rev. Mod. Phys. **18**, 384 (1946), reviews recent work on color centers in alkali halides, particularly the work of Molnar and Glaser.
[5] R. W. Pohl, *Optik* (Frederick Ungar, New York, 1943).

because more data is available on this system than on other alkali-halides; further high concentrations of color centers are more readily obtainable in well-formed crystals than in others investigated.

II. EXPERIMENTAL

(A) Preparation of Additively Colored Crystals

Single crystals of KCl, prepared commercially for optical use, were cleaved to the desired size, generally about 2.7×0.4×0.3 cm for use in magnetic studies. These were heated in closed bombs of $\frac{3}{8}$ in. copper pipe, with a small pellet of metallic K. The concentration of absorbed K depends upon the temperature.[6] Diffusion is quite slow, and at the lower temperatures several days were required to achieve a uniform color in large crystals. To obtain 10^{19} color centers/cc the bombs were heated at 675°C for 3 hours and for 5×10^{17}/cc, at 475°C for 72 hours. Following heating, the bombs were quenched in cold water; rapidity of quenching, as well as preservation of accurate dimensions of the crystals, was assisted by wrapping the crystals in thin copper foil, leaving the ends open, prior to placing in the bomb.

(B) Analytical Methods

The concentration of F-centers in crystals having less than 10^{18}/cc was obtained from absorption data,

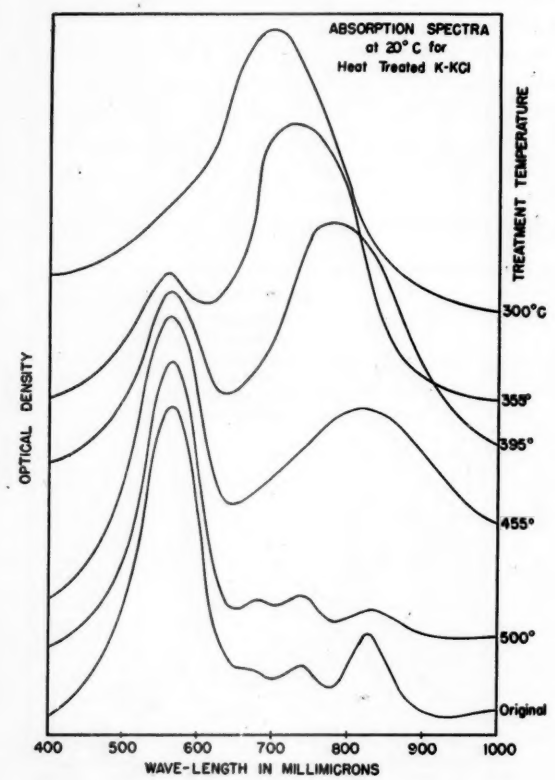

FIG. 2. Thermal equilibrium between F- and R'-centers.

[6] R. W. Pohl, Proc. Phys. Soc. 49 (extra part), 3 (1937).

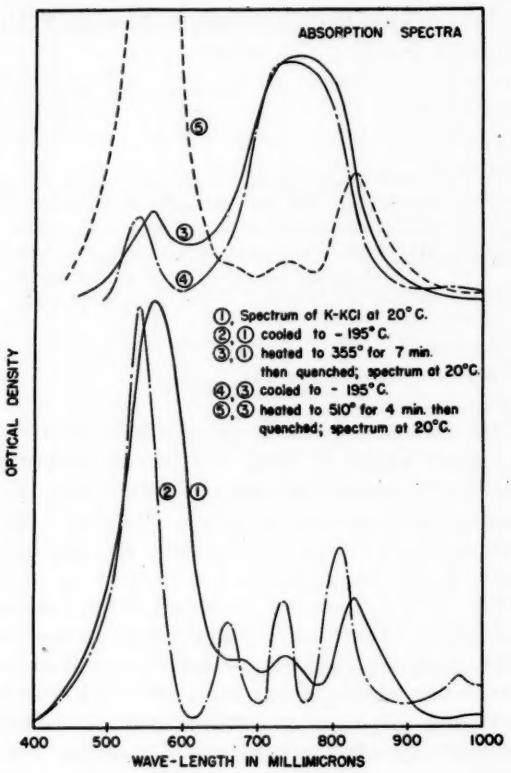
ABSORPTION SPECTRA
①, Spectrum of K-KCl at 20° C.
②, ① cooled to - 195° C.
③, ① heated to 355° for 7 min. then quenched; spectrum at 20°C.
④, ③ cooled to - 195° C.
⑤, ④ heated to 510° for 4 min. then quenched; spectrum at 20°C.
OPTICAL DENSITY
400
500
600
700
800
900
1000
WAVE-LENGTH IN MILLIMICRONS

FIG. 3. Effect of low temperature on R'-, R-, and M-bands; thermal conversion of R'- to F-bands.

using the dispersion formula developed by Smakula[7]

$$n=(1.31\times10^{17}n')/[f(n'^2+2)^2]W_M W,$$

where n is the number of F-centers/cc, n' is the refractive index of the pure salt, α_M is the extinction coefficient at the center of the band in cm^{-1}, W is the width of the absorption curve, at half-maximum, in electron volts, and f is the oscillator strength for F-centers. In KCl, Kleinschrod[8] found $f=0.81$. A typical curve showing the F-band appears in Fig. 1.

At higher concentrations, the absorption becomes so great in the F-band that it becomes impossible to cleave thin sections of accurately known thickness, and, though spectra were obtained for crystals having as high as 1.7×10^{19} centers/cc, by careful grinding or cutting of mounted crystals, it was necessary to use chemical analytical methods to determine concentration.

The chemical method consisted of measuring the change in pH occurring in 3 ml of boiled, slightly acidified water when a colored crystal weighing about 60 mg was dissolved. A Beckmann pH meter, having "micro" electrodes, was used. The probable error in concentrations measured in this way was about 10 percent, the error being due principally to variations within a given large crystal, and to some absorption of

[7] A. Smakula, Zeits. f. Physik 59, 603 (1930).
[8] F. G. Kleinschrod, Ann. d. Physik 27, 97 (1936).

CO_2 during solution of the crystal. There is an uncertainty of at least this magnitude in the optical determination of the lower concentrations, so that in general the lack of exact analytical methods presents a serious obstacle to accurate quantitative studies upon color centers.

It must also be noted that while the optical method yields the concentration of F-centers as such, the chemical method yields the concentration of K in stoichiometric excess, whether in F- or in other centers. At concentrations around 10^{19}/cc, it was found that a considerable proportion of the K was present as R'-centers.

(C) Thermal and Optical Measurements

Absorption measurements were made by the Beckmann Spectrophotometer, Model DU. A special Dewar flask was designed for measurements at −195°C having a bottom section small enough to fit into the usual cell holder and silvered except for two small areas to permit passage of light. The top of the flask projected five inches above the cell compartment and was covered by a light-proof box so that the flask was free to move laterally. Room temperature measurements were made prior to addition of liquid N_2 with the crystal in place in the Dewar, then the measurements in liquid N_2 and finally the absorption of the N_2 and cell were measured in the range 400–1100 mμ. In every case the latter was negligible throughout the range.

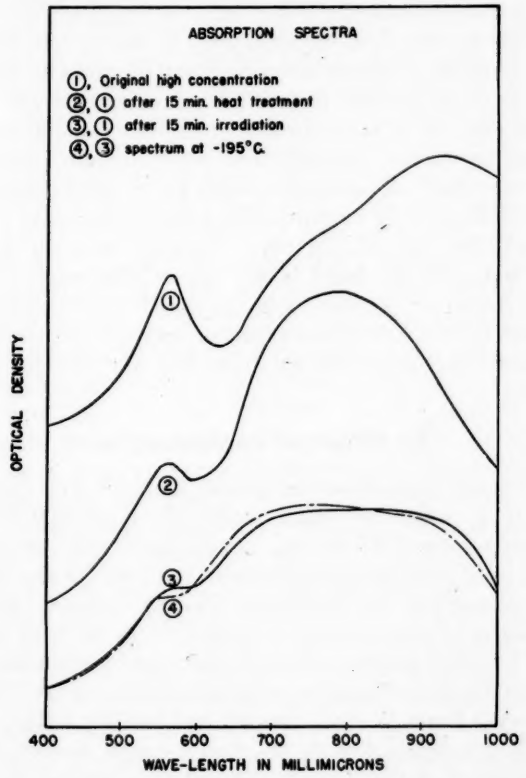

FIG. 5. Effects of concentration of the $F-R'$ equilibrium. Ordinates for curves 3 and 4 displaced downward one unit.

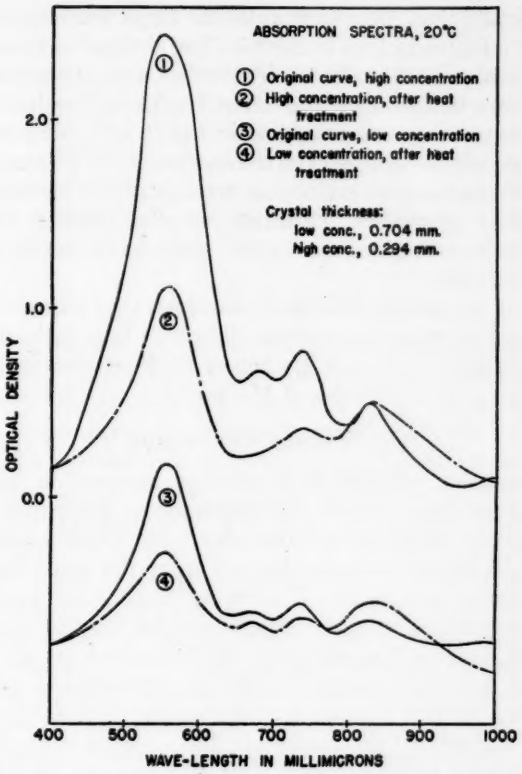

FIG. 4. Absorption spectra in densely colored crystals.

Heat treatments were carried out in air in a muffle furnace with automatic temperature control. Treatments carried out in vacuum as a check gave identical results. For these experiments it was not necessary to achieve very accurate control or measurement of temperature. Temperatures reported are accurate within about 5° below 400°C and about 10° above 400°C. Relative errors in absolute temperature are thus negligible compared to analytical errors.

III. DISCUSSION OF RESULTS

(A) Conversion of F- to R'-Centers by Irradiation

Glaser found that 20 minutes of arc light irradiation at room temperature was sufficient to destroy all F-centers in a particular sample of colored KCl. This effect could have been either optical or due to local increase in temperature, but the assumption has been that the mechanism has been dependent upon F-center ionization by irradiation, and Seitz[4] has offered an explanation of the conversion of F-centers into aggregates on this basis. An experiment was performed to determine whether the process is primarily thermal or optical. A small additively colored crystal containing about 6×10^{17} F-centers/cc was illuminated strongly with light from a carbon arc, but kept at about room temperature by means of a jet of air. The absorption spectrum was measured initially and at intervals during

the irradiation. After 85 minutes the air jet was removed for 2 minutes further treatment. The absorption curves obtained after 85 minutes irradiation with the crystal at room temperature and after 2 minutes irradiation without cooling are compared in Fig. 1 with the curve for the original sample. The change from F- to R'-centers must occur almost entirely as a result of the increased mobility of centers, vacancies, or other defects with increasing temperature rather than as a result of illumination.

It is interesting to observe, however, that absorption of light at room temperature did result in a noticeable conversion of F- and M-centers to R-centers, in accordance with the work of Molnar.[8]

(B) Thermal Conversion

In order to determine whether increase in temperature alone, without the simultaneous absorption of light, was sufficient to bring about the $F-R'$ conversion, a number of samples, all from the same large crystal containing 5×10^{17} color centers/cc, were heated in the dark at several temperatures for varying times. After heating the samples were quenched on an Al block and their absorption spectra measured. Crystals heated at 125° showed a slow decrease in the F-band and corresponding increase in the R'-band, complete conversion being attained after 40 hours. At 300° the conversion was complete after 15 minutes. At still higher temperatures the conversion became very rapid but less complete; for example, at 455°, all crystals heated more than 2 minutes showed the same equilibrium curve for which conversion was about 40 percent complete, while at 500° there was little change in the original spectrum, except for a decrease in the M-band, for a crystal heated as long as 15 minutes. Equilibrium curves are shown in Fig. 2, in which the ordinates are displaced for clarity. The left intercept in each case represents about the same optical density; however, since the thicknesses of the crystals were not identical, the vertical location of the curves has no significance. It is evident that at this concentration R'-centers are the more stable form at temperatures below 300°C and F-centers above 500°C, while at intermediate temperatures they are clearly in thermal equilibrium. A pronounced shift of the maximum of the R'-band toward longer wave-lengths for higher treatment temperatures, indicates a change in the nature of, or relative abundance of, the absorbing centers.

It is doubtful if any existing analytical means will make possible a calculation of the equilibrium constant at the various temperatures, since the dispersion formula of Smakula[7] can be applied only to bands arising from a single absorbing species, and it will be shown presently that the R'-band arises from several species. It is also evident that as the nature of the R'-band is complex and variable with temperature, no single constant could describe numerically the state of equilibrium. However, it is of interest to note that in the case of the 300° sample of Fig. 2, the application of the dispersion formula, though not justified on theoretical grounds, yields the same concentration of absorbing centers, within 10 percent, as was found for F-centers in the original crystal. This result was confirmed in all similar cases where the formula was applied, and leads to some confidence in its use to estimate the concentration of excess K responsible for each type of band if not the concentration of centers as such.

The reversibility of the conversion was established by heating a crystal in which the R'-band was well developed (curve 3, Fig. 3) to 510° for 4 minutes and then quenching rapidly. Curve 5, Fig. 3, shows the reestablishment of the F- and M-bands and the marked reduction of the R'-band to the two R-bands.

(C) Low Temperature Absorption

Measurements of the absorption spectrum of several colored crystals at −195°C were made to determine whether a resolution of the R'-band into two or more bands occurred. Typical results are presented in Fig. 3. All data were obtained using the same crystal, whose original spectrum is given by curve 1. From the sharpening and displacement of the bands, shown in curve 2, with reduced temperature, it is apparent that the R- and M-bands of additively colored crystals, as well as F-bands,[6] are due to single absorbing species. Molnar[3] has observed this temperature effect on bands produced by x-rays. The definite appearance of a band at 980 mμ, which was occasionally observed as a broad low band at 1000 mμ at room temperature, is worthy of note. This band has been reported by Burstein and Oberly,[9] who have designated it the N-band. Curves 3 and 4 prove that the R'-band consists of a number of different absorbing species, probably not less than four or five and very likely several more, since at low temperature only a slight shift toward shorter wave-lengths is observed, the top of the curve remains more or less rounded, and the band is not appreciably narrowed. Such behavior is also to be expected of a colloidal system so that additional experiments were carried out to show whether or not the band was due to colloidal metal.

(D) Effects of Concentration

Although present experimental methods are insufficient to allow an exact study of the equilibrium between F- and R'-centers, a semiquantitative experiment was undertaken to establish the order of size (on the average) of the R'-centers. Two KCl crystals were prepared having F-center concentrations of 6.0×10^{17} and 7.8×10^{16} respectively as determined by application of the dispersion formula to the absorption curves (Fig. 4, curves 1 and 3). Both crystals had initially an appreciable development of R-, M-, and N-bands, though the appearance of the R-bands differed considerably. Both

[9] E. Burstein and J. J. Oberly, Phys. Rev. **76**, 1254 (1949).

crystals were heated simultaneously at about 450°C for 12 minutes and quenched. Curves 2 and 4, Fig. 4, show the absorption following heating. The concentrations of F-centers were reduced to 2.6×10^{17} and 5.3×10^{16}/cc.

The effect of a concentration increase of approximately eightfold upon the number and distribution of the centers formed thermally is very pronounced. The relative decrease upon heating was much greater in the sample having the higher concentration, which shows that on the average more than one F-center is used in producing one R'-center. It is apparent also that centers absorbing at wave-lengths above 800 mμ are favored by increasing concentration.

An approximate calculation of the average size of the R'-centers, in terms of the number of F-centers contained, may be made by assuming the thermal equilibrium between F- and R'-centers to be expressed by the equation

$$nF=(F)_n,$$

where $(F)_n$ is that part of the R'-center composed of negative ion vacancies and an equivalent number of electrons. Leaving out of consideration the presence, either initially or at equilibrium, of R- and M-centers, the equilibrium concentrations of R'-centers for the two cases are $(1/n)(3.4\times10^{17})$ and $(1/n)(2.5\times10^{16})$. Since, at equilibrium, the concentration of R'-centers varies as the nth power of the concentration of F-centers, n may be evaluated from the two sets of equilibrium concentrations and turns out to be 1.7. The significance of this number is severely limited by the simplifying assumptions noted but indicates that R'-centers in this concentration range contain few (certainly less than 5) F-centers. At present no indication of the number of lattice vacancies also contained can be deduced, so that a large variety of R'-centers is possible.

Even without detailed calculation the absence of colloidal aggregates may be seen from these data. If they are colloidal, their equilibrium with the F-centers is heterogeneous, and the concentration of F-centers which may be in equilibrium is then dependent upon the temperature and the coexistence of the two phases, and independent of total concentration. Since at equilibrium at 450°, the F-center concentration of one sample was about 5 times that of the other, the possibility of a second phase and hence the existence of colloidal particles, at least for the lower concentration, is excluded. Observations made with the ultramicroscope also failed to show the presence of colloidal material.

Experiments at higher concentrations are severely limited by the difficulty of obtaining thin crystals of accurately known thickness. An inspection of curve 1 in Fig. 5, however, shows the marked increase in the R'-band in very thin section of crystal having an excess K concentration of 1.3×10^{19}/cc and rapidly quenched from 675°C. The effect of concentration in favoring the higher aggregates has reduced the F-band to a minor role, though the concentration of F-centers is still much higher than in the previous experiments. Also shown, curve 2, is the spectrum of the same crystal after heating 15 minutes at 300°. Complete equilibrium probably was not attained because of the extreme concentration, but the temperature shift of the maximum is apparent. Curve 3 shows the effect of arc-irradiation for 15 minutes and curve 4 illustrates the lack of resolution of the spectrum, even for this very broad band, at liquid N_2 temperature.

IV. CONCLUSION

We are now in a position to draw some tentative conclusions regarding the products of the thermal and optical destruction of F-centers in KCl, and to review the suggestions of Seitz[4] in view of the present experiments. It is immediately apparent that several processes are occurring simultaneously during either thermal, optical, or combined treatments, and that an isolation of effects by more refined experiments will be necessary before the properties and structure of the variety of centers produced may be known in the same way as those of the F-centers are known. Certain of these refinements are now being undertaken in this laboratory.

(a) Under irradiation with white light alone, the temperature remaining low, both F- and M-bands are somewhat unstable and R-bands are increased. This process may take place by ionization of F-centers and migration of electrons thus raised to the conduction level or by migration of positive vacancies which have sufficient mobility at room temperature to move several atomic spacings during the few minutes consumed in the process. If, as Seitz suggests, an M-center consists of a F-center combined with a pair of vacancies, and R-centers are F_2- or F_2^+-centers, the process could occur along these lines: an electron produced upon ionization of F-centers is trapped by a quartet of vacancies, and the weakening of the electrostatic bond between vacancies results in the loss of one or both of the positive ion vacancies. The loss of one would result in the center identified above as an M-center; if it were photoelectrically active, further illumination might result in its ionization and the reestablishment of a F-center. The loss of a second positive-ion vacancy would result in a F_2^+-center. Trapping of an electron by a F_2^+-center would result in a F_2-center; these latter two should be stable in the first excited level and thus not destroyed by irradiation. No migration of pairs is necessary for these occurrences if the initial presence of quartets of vacancies be assumed.

(b) With increasing temperature, even in the dark, the formation of the R'-centers becomes rapid, which strongly suggests that the process depends not on ionization but on migration of groups of vacancies (probably pairs at the lower temperatures). A pair combining with a F-center would yield the centers of the type produced by irradiation; however, because of the great variety of centers which now may result from

the mobility of the negative vacancies (as members of pairs) the overlapping of absorption bands would lead to a broad band exhibiting the behavior of the R'-band. Among the R'-centers, particularly during early stages, will undoubtedly be found the R- and M-centers. There is no certainty that the R'-centers formed thermally are precisely the same as those formed by heating combined with irradiation; indeed Fig. 5 shows considerable difference in the R'-band formed thermally and that formed by irradiation of samples of the same colored crystal. The size of the R'-centers is probably not great, certainly not of colloidal size, and at temperatures above 300°C noticeable dissociation into F-centers and vacancies becomes apparent. At 510°, dissociation into F- and M-centers is virtually complete.

(c) The shift of maximum in the R'-band with variation in equilibrium temperature is undoubtedly related to the increasing mobility of negative-ion vacancies with temperature which should lead to the rapid formation of aggregates containing several F-centers by direct diffusion and combination.

Further experiments are being undertaken in this laboratory to establish more fully the structure and physical properties of the R-, M- and R'-centers.

PHYSICAL REVIEW VOLUME 79, NUMBER 2 JULY 15, 1950

The Paramagnetism of Color Centers in KCl*

ALLEN B. SCOTT, HENRY J. HROSTOWSKI,† AND LAMAR P. BUPP
Department of Chemistry, Oregon State College, Corvallis, Oregon

(Received March 24, 1950)

Two methods for studying susceptibility changes occurring during thermal and optical alterations in color centers in KCl are described. The magnetic changes accompanying formation of R'-centers from F-centers, and upon completely destroying both F- and R'-centers, indicate that the moment of a F-center is that calculated for an s-electron, that R'-centers have a variable moment depending on the distribution of centers, but generally very nearly that of F-centers, and that irradiation during R'-center formation results in a destruction of paramagnetism.

I. INTRODUCTION

THE theory of color centers in alkali halides has been reviewed by Mott and Gurney[1] and by Seitz.[2] The interpretation of a variety of experiments on the optical and electrical properties of crystals colored both by radiation and by the addition of a stoichiometric excess of alkali metal has led to some quite definite ideas regarding the nature of the absorbing centers. A F-center is considered to consist of an electron trapped in a halide ion vacancy. Such trapped electrons behave optically very much as s-electrons, and since they are unpaired, the presence of F-centers should impart a small paramagnetic susceptibility to the over-all diamagnetism of the salt, given by

$$\kappa = n\beta^2/kT,$$

where n is the concentration of F-centers/cc, β is the Bohr magneton, and k is Boltzmann's constant. Jensen[3] succeeded in measuring the decrease in diamagnetism of a KBr crystal containing a small amount of KH when F-centers were produced by ultraviolet illumination; the agreement with the decrease calculated from this equation, was very good in view of the experimental difficulties involved. His experimental moment for a F-center was about 10 percent below that for an unpaired s-electron in a free atom but it is doubtful whether the difference is significant.

In order to provide further confirmation of the theory of F-centers and to permit a study of the magnetic changes accompanying the formation and destruction of other color centers in alkali halides,[4] methods have been developed for the measurement of the small susceptibility changes occurring in additively colored crystals when subjected to thermal and optical treatments.

The expected change in volume susceptibility as a densely colored alkali halide, containing for example 10^{19} F-centers/cc, is de-colorized completely by prolonged heating in vacuum is about 2×10^{-8} c.g.s. unit; in the case of KCl this represents a 2 percent increase in diamagnetism. Although this change can be conveniently detected for samples which may remain in place during a magnetic transformation, for samples requiring removal from the magnetic balance for extended thermal treatment and later replacement upon the balance, the errors due to positioning in the field

* This work has been supported by the ONR. Published with the approval of the Oregon State College Monographs Committee as Research Paper No. 158, Department of Chemistry, School of Science.

† Present address, Department of Chemistry, University of California, Berkeley, California.

[1] Mott and Gurney, *Electronic Processes in Ionic Crystals* (Oxford University Press, New York, 1940).

[2] F. Seitz, Rev. Mod. Phys. 18, 384 (1946).

[3] P. Jensen, Ann. d. Physik 34, 161 (1939).

[4] Such as R-, M-, and R'-centers, discussed by Scott and Bupp, Phys. Rev. 79, 341 (1950), preceding paper.

are sufficient to mask a 2 percent change occurring during the treatment. To overcome positional errors, a differential magnetic balance has been designed which detects the change, due to susceptibility changes, in the equilibrium position of a sample in the field of a small magnet. A second magnetic balance utilizing a strongly non-homogeneous field, and referred to hereafter as the Faraday balance, was designed to observe magnetic changes in colored crystals upon arc-light illumination of the crystal *in situ*.

A group of experiments on the susceptibility changes accompanying the complete destruction of *F*- and *R'*-centers in KCl, and the thermal conversion of *F*- to *R'*-centers was carried out by means of the differential balance; changes accompanying the conversion of *F*- to *R'*-centers by arc light irradiation were studied by means of the Faraday balance. KCl colored with excess K was used in all cases for the reasons given in reference 4.

II. EXPERIMENTAL

(A) Differential Magnetic Balance

Figure 1A illustrates schematically the principle of the differential balance. The balance beam of fine glass tubing was suspended by a 10μ quartz fiber from an adjustable brass mounting. At one end of the beam, between the poles of an Alnico permanent magnet, was rigidly suspended a V-shaped glass trough in which was cemented a plain KCl crystal (*D*) of length 2.7 cm and cross section about 0.13 cm^2. The sample under investigation (*C*), of about the same dimensions, was laid in the trough and butted up against *D*. In this way its position in the carrier could be reproduced, upon removing and replacing, with accuracy. Beneath the glass trough was suspended a 4-mm o.d. glass tube filled with a mixture of MgO and $NiCO_3$, in such proportions that the entire assembly, including the two crystals, was very slightly paramagnetic. The adjustment of this proportion and the cross section of the crystals was done by trial-and-error until the assembly came to rest with the inner end of *D* at about the center of the homogeneous portion of the field. The restoring force for small displacements from the equilibrium position depended on the field-strength gradients at the outer ends of the crystals, trough and tube, on variations of cross section and susceptibility and corresponding field-strength gradients along the axis of the assembly, and on the torsional constant of the quartz fiber. This force could be made as small as desired by reduction in the proportion of $NiCO_3$ in the mixture. The rotational period of the balance at optimum sensitivity was about 20 seconds.

Variations in equilibrium position were followed by scale readings in the micrometer eyepiece of the traveling microscope *M*. The force necessary to give a particular displacement was obtained from the current through the solenoid *S*, which acted upon a tube of $NiCO_3$ of known susceptibility. For these experiments the sensitivity was about 7×10^{-5} dyne/μ. The change in volume susceptibility of *C* during a thermal treatment was related to the change in equilibrium position of the assembly before and after by the equation

$$\Delta\kappa = 2dS/[A(H_1^2 - H_2^2)],$$

where d is the displacement of equilibrium position in μ, S is the sensitivity in dynes/μ, A is the cross-sectional area of C, H_1 is the field at the inner end, and H_2 at the outer end of C.

The entire balance was mounted upon a heavy marble slab resting on rubber cushions, and was surrounded by a draft-proof case and a second larger curtained enclosure to reduce thermal variations. The crystal carrier was illuminated through a double glass window by fluorescent light.

Magnetic field determinations were in all cases made by means of a small flip-coil and ballistic galvanometer which were calibrated in the field of a large electromagnet which had been accurately measured by means of its force on a $NiCl_2$ solution of known susceptibility.[5] The susceptibility of the $NiCO_3$ tube (in the solenoid) was measured in terms of κA for the tube plus contents at field strengths of 4650 and 1740 oersteds, as a test for ferromagnetic impurities. Values at the two field strengths agreed within the small experimental error and justified the extrapolation to the much smaller field in the solenoid. The field of the permanent magnet of the balance was measured before and after the data were obtained, and as the strength varied only 0.2 percent during a period of three months, the final value, 4560 oersteds, was used for H_1. The value of H_2 was 1310 oersteds. The current through the solenoid, of

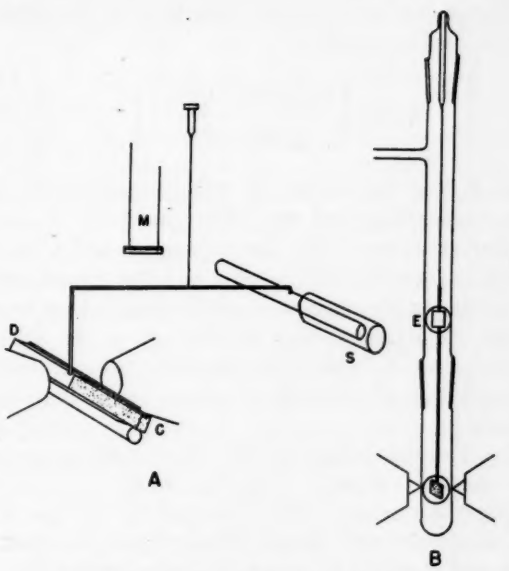

FIG. 1. A. Differential magnetic balance. B. Faraday magnetic balance.

[5] P. W. Selwood, *Magnetochemistry* (Interscience Publishers, Inc., New York, 1943), pp. 26, 46.

109.2 turns/cm, was measured by a calibrated ammeter. Errors in electrical and magnetic field measurements were in general negligible as compared with analytical errors and errors in measuring balance displacements.

Susceptibility changes were determined by observing the average rest position of the outer end of sample crystal as it was repeatedly removed and replaced in the carrier trough and the average rest position after it was subjected to a particular thermal treatment. The purpose of obtaining average values based on removing and replacing the crystal was to reduce the observational error due to variation in the position of the crystal in the trough as it was removed from and replaced on the balance. Actually it was found that there was a slow periodic drift of rest position, and to avoid error from this source the position of the sample crystal was measured in terms of a reference crystal of the same dimensions which was placed on the balance alternately with the sample. The average positional difference between sample and reference before treatment was subtracted from the average difference after treatment to obtain the displacement corresponding to the magnetic change produced. Sufficiently many observations were made, usually about 16 before and 16 after treatment, to reduce the probable observational error of the displacement to 6μ or less. The relative observational error, in the case of a volume susceptibility change of 2×10^{-8} c.g.s. unit in a crystal of cross section 0.13 cm^2, was 1.5 percent. The current through the solenoid required to give an equal displacement in the opposite direction was then measured by repeated observations with the current on and off.

The change in atomic susceptibility of the stoichiometrically excess K occurring during a particular treatment can be computed directly from the solenoid current by the equation

$$\Delta\chi_M=\left[\frac{\kappa_1 A_1(0.4\pi N_S)^2 l_1 N}{l_2(H_1^2-H_2^2)}\right]\frac{I^2}{An},$$

where $\kappa_1 A_1$ is the product of volume susceptibility and cross-sectional area of the $NiCO_3$ and tube, N_S is the number of turns/cm for the solenoid, l_1 and l_2 are the distances from the $NiCO_3$ tube and the crystal carrier to the quartz fiber suspension (11.9 and 17.4 cm respectively), N is Avogadro's number, I is the solenoid current, and A is the cross-sectional area and n the concentration of excess K, in atoms/cc, of the sample crystal.

The Faraday balance, Fig. 1B, served to measure susceptibility changes occurring when crystals containing color centers are irradiated by the arc light. The sample crystal, about $10\times5\times2$ mm, mounted on a 0.1-mm glass rod by means of a glass spring clip, was suspended by a 5μ-quartz fiber approximately 50 cm long. The crystal could be rotated by a vacuum-tight torsion head, and its position followed by means of the mirror E, together with a lamp and scale. The field of an Alnico permanent magnet was rendered strongly non-homogeneous by two cone-shaped pole tips and the position of the magnet and torsion head so adjusted that the long axis of the crystal lay quite nearly along the axis of the poles. This was found to be the position of maximum sensitivity.

TABLE I. Change in molar susceptibility of color centers in KCl during certain processes.

Differential balance				
$n\times10^{-19}$	A(cm^2)	I(amp)	Process	$\Delta\chi_M\times10^3$
0.66	0.130	0.67	$F, R'\rightarrow$decol.	1.2
1.1	0.127	1.06	$F, R'\rightarrow$decol.	1.8
1.1	0.135	0.78	$F, R'\rightarrow$decol.	0.96
		Average	$F, R'\rightarrow$decol.	1.3±0.3
1.7	0.130	0.00	$F, R'\rightarrow R'$	0.00
1.3	0.130	0.48	$F, R'\rightarrow R'$	0.32
1.1	0.135	0.63	$F, R'\rightarrow R'$	0.62
		Average	$F, R'\rightarrow R'$	(0.3)
1.7	0.130	0.56	$R'\rightarrow$decol.	0.33
1.3	0.126	0.84	$R'\rightarrow$decol.	1.0
		Average	$R'\rightarrow$decol.	(0.7)
Faraday balance				
$n\times10^{-19}$	P_{air}(mm)	$\kappa\times10^8$	Process	$\Delta\chi_M\times10^3$
1.1	630	2.4	$F, R'\rightarrow R'$	1.3
1.3	570	2.2	$F, R'\rightarrow R'$	1.0
1.3	750	2.9	$F, R'\rightarrow R'$	1.3
		Average	$F, R'\rightarrow R'$	1.2±0.2

The apparatus was calibrated by evacuating and observing the change of position of the crystal at several pressures as air was readmitted. From the known volume susceptibility of air the lamp-and-scale reading was then known as a function of the change in volume susceptibility of the sample. The calibration was repeated using oxygen and CO_2 to establish that there was no rotational effect associated with the buoyancy exerted by the gases; the rotation per cm oxygen was about five times that of air and for CO_2 was about 10 percent of that of air and in the opposite direction, which is to be expected from the relative susceptibilities. The air calibration was repeated for each sample studied, as it was strongly dependent upon crystal size and position in the field.

Susceptibility changes were measured by determining the rest position of the sample colored crystal, the apparatus being evacuated, and again after about 15 minutes of strong illumination, through a quartz window, with an arc lamp. The change in molar susceptibility for the color centers was computed from the relation

$$\Delta\chi_M=(PN\kappa_a)/760,$$

where P is the pressure of air in mm giving an equivalent positional change and κ_a is the volume susceptibility of air at 760 mm and 20°C (assumed to be 2.90×10^{-8} c.g.s. unit).

The thermal changes occurring in the apparatus during illumination caused a large temporary positional change, but when a sample of pure KCl was used for repeated measurements, it was found to return to its

initial position after the treatment, with a probable error of 1.6 cm, measured on the scale. Since the magnetic displacements were between 6 and 13 cm, this represents an observational error of from 12 to 25 percent.

The preparation of colored crystals, analytical methods, and thermal and optical processes of altering color centers have been discussed in reference 4. All concentrations were determined by the *p*H-change method.

III. RESULTS

The changes in susceptibility during the following processes were measured by means of the differential balance.

(a) Crystals containing a high concentration of *F*- and *R'*-centers were heated at 300° for 15 minutes to convert all, or nearly all, centers to *R'*-centers. Absorption curves for densely colored crystals before and after this treatment were all similar to curves 1 and 2, Fig. 5, of reference 4. This process is referred to as *F*, *R'*→*R'*.

(b) Crystals containing a high concentration of *F*- and *R'*-centers were heated in vacuum at 500–600°C until they appeared to be colorless. Absorption measurements after the process showed no absorption in the visible region, but considerable in the near ultraviolet which was probably due to a residue of K_2O in the lattice. This process is referred to as *F*, *R'*→decol.

(c) Crystals treated as in (a) were decolorized as in (b). This process is referred to as *R'*→decol.

The change in molar susceptibility, calculated on the basis of the excess K as determined from *p*H measurements, for these processes is tabulated in Table I.

It will be noted that the average decrease in molar susceptibility as a crystal containing a mixture of *F*- and *R'*-centers is completely decolorized is $(1.3\pm0.3)\times10^{-3}$ c.g.s unit. The estimate of error is based on the observed deviations and the estimated analytical error. The theoretical molar susceptibility for free atoms having one *s*-electron each is 1.28×10^{-3} unit at 25°C. The decrease in susceptibility as *F*-centers are converted to *R'*-centers thermally was non-reproducible but was small, on the average; similarly, the decolorization of crystals containing only *R'*-centers gave a non-reproducible susceptibility change, on the average less than that expected for the same amount of K in the form of free atoms.

These data may be interpreted, in view of the suggestions made in reference 4, in the following way: since *R'*-centers are a variety of small aggregates containing one or more *F*-centers and lattice-vacancies, a considerable paramagnetism should arise from centers having an odd number of electrons, such as the F_2^+-center or the combination of an *F*-center and a pair of vacancies. Centers containing 3*F*-centers would contribute one-third of the paramagnetism of an equal number of *F*-centers, and so on. Thus we expect that as the concentration and temperature at which the *R'*-centers are established varies there would be a range of paramagnetism due to the variation in distribution of the types of *R'*-centers; it would approach the paramagnetism of *F*-centers under condition favoring the formation of aggregates containing only one *F*-center. This conclusion is borne out by the variations in $\Delta\chi_M$ for different crystals undergoing heat treatment to form *R'*-centers or decolorization of crystals containing *R'*-centers. It is evident that, on the average, *R'*-centers have a paramagnetism not much less than *F*-centers.

The value of $\Delta\chi_M$ accompanying irradiation of color centers by arc-light, as measured upon the Faraday balance, is also given in Table I. The estimated error was obtained as above. It is surprising to note that during arc-light irradiation a decrease in paramagnetism very nearly equal to that produced by complete decolorizing is observed.

Comparison of curve 3 with curve 2, Fig. 5, of reference 4, indicates that *R'*-centers produced by irradiation do not absorb exactly as do *R'*-centers produced thermally, at least in densely colored crystals. It is likely that during excitation most or all of the centers will be ionized and that electrons may move through the conduction levels from trap to trap until a very stable set of centers is produced. Centers having an even number of electrons in the form of pairs would be a probable result, and the paramagnetism of the original *F*- and *R'*-centers would be destroyed. Additional experiments to show whether there are any other observable differences between *R'*-centers produced thermally and those produced by a combination of illumination and heating would be very desirable.

It must be emphasized that the foregoing results cannot be interpreted in a precise way, particularly due to lack of information on the concentration of *R'*-centers as such. It is significant, however, that the magnetic data is in general consistent with the suggestions made in reference 4 in regard to the structure of *R'*-centers. It may also be concluded that the moment of the *F*-centers is adequately predicted by theory, if allowance be made for the paramagnetism of the accompanying *R'*-centers.

Antiferromagnetism. Theory of Superexchange Interaction

P. W. ANDERSON
Bell Telephone Laboratories, Murray Hill, New Jersey
(Received January 9, 1950)

In this paper the general formalism of Kramers indicating the existence of superexchange interaction has been reduced, under simplifying assumptions, to the point where actual formulas for the interaction can be written down directly in terms of spin operators, with certain exchange and transition integrals as parameters. Two results of physical interest are the following: (a) superexchange must be expected to show the directional properties (as far as directional relations of interacting magnetic ions are concerned) of the orbitals in the outer shell of the non-magnetic connecting ions; and (b) the sign of the effective exchange integral depends upon the sign of the internal exchange coupling of an added electron on the magnetic ion.

I. INTRODUCTION

IN the course of a general study of the phenomenon of antiferromagnetism[1] it became clear that in many substances the atoms which strongly interact magnetically are quite definitely separated from each other by intervening non-magnetic ions. In such substances as MnSe and MnTe this can be verified simply by drawing spheres of ionic radii about the anions, which then separate practically completely even nearest neighbor cations. However, the best illustration of this fact is the substance MnO, in which, by means of neutron diffraction,[2] Shull has been able to actually identify the pattern of magnetic spins below the antiferromagnetic Curie point. This pattern was at first baffling, since it showed that the 12 nearest neighbor spins (MnO is an NaCl structure; the Mn^{++} ions are thus in a face-centered cubic lattice) to a given spin are uncorrelated with this spin; instead, the four separate simple cubic lattices of which the f.c.c. lattice is made up are each lined up in a perfect antiferromagnetic pattern, but entirely uncorrelated one with the other.[3] The pattern is indicated in Fig. 1.[4]

This pattern means that the strongly coupled Mn^{++} ions are separated by a supposedly non-magnetic O^{--} ion directly between them, as we can see from Fig. 1. The Curie point of MnO is 122°K; this means that the exchange coupling between these separated ions is more than a tenth of ordinary exchange integrals (for instance in Fe), and it seems inconceivable that this large magnitude can come from "ordinary" or "direct" exchange. Thus we are led to believe that the primary interaction in MnO, and to a lesser certainty in other similar antiferromagnets (FeO, MnS, etc.) is a superexchange interaction operating through the intermediary of the O^{--} ions.

II. A SIMPLE CASE

Kramers[5] first pointed out that it is possible to have an exchange spin-coupling through the agency of intermediate non-magnetic atoms. The resolution of this paradox lies in Kramers' mechanism: his assumption that "excited states" of the intermediate atoms are present is equivalent to assigning a weight in the total wave function to configurations in which the intermediate atoms have some paramagnetism. As an example we may take such a crystal as MnO; in addition to the totally ionic state $Mn^{++}O^{--}$ it is reasonable from all available evidence to allow a considerable admixture of the state in which at least one p-electron from the oxygen has gone into an s or d-state on Mn^{++}, and thus the oxygen is paramagnetic and can enter into "magnetic" interactions.

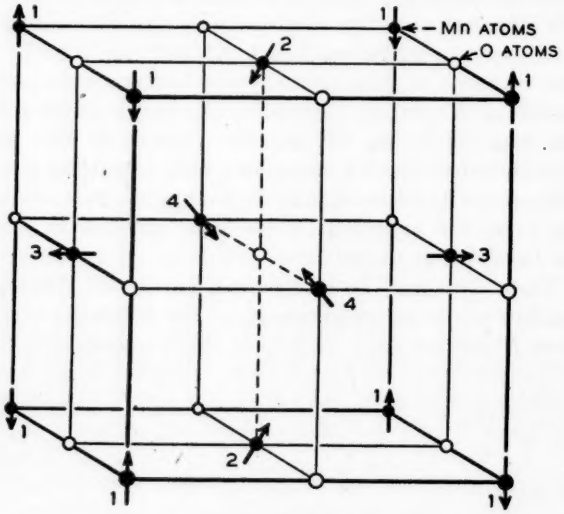

FIG. 1. Pattern for the MnO structure.

[1] To be published in a series of papers by G. H. Wannier and the author.

[2] C. G. Shull and J. S. Smart, Phys. Rev. **76**, 1256 (1949). Dr. Shull has kindly given us more recent results as to the most probable actual pattern present.

[3] Dr. Shull informs us that the data are not inconsistent with a pattern suggested by Neél, which has the sublattices not uncorrelated but arranged (presumably by weaker forces of some kind) in such a way as to make all spins parallel in 111 planes, and these planes antiparallel in succession. Such a pattern is not different in essentials from Fig. 1, and still requires strong next nearest neighbor interaction.

[4] In a later paper of this series we shall show that there is theoretical as well as experimental evidence for the pattern found by Dr. Shull. A modified Weiss molecular field treatment indicates that, if T_c is the Curie point and θ the constant in $\chi=c/(T+\theta)$, a value of $\theta/T_c=5$, as in MnO, indicates that the next-nearest neighbor interaction is high and that the pattern is probably that of Fig. 1. Also, quantum mechanical considerations seem to indicate that possibly no *nearest neighbor* antiferromagnetism can exist in the f.c.c. lattice.

[5] H. A. Kramers, Physica **1**, 182 (1934).

Let us, to fix our ideas, think of the system of two magnetic ions, such as Mn^{++}, separated by an O^{--} ion. We shall, for simplicity, consider only two of the electrons on the O^{--} ion, assuming them to be in the same p-state; in addition we shall consider the magnetic ions as possessing one electron each, in (for example) a d-state. (We always ignore orbital moments, however, assuming them to be quenched). By hypothesis there is no direct overlap between the two d wave functions; also by hypothesis there is a finite probability that an electron will jump from the O^{--} ion into (perhaps) an s-state on one of the magnetic ions. We must think (as Kramers did not point out) of this s-state as coupled by some strong spin dependent interaction with the d-electron already on the magnetic ion; otherwise there is no superexchange.

Qualitatively it is now easy to see the process involved in superexchange. To the ground state only two spin-states are available, since the p-state spins are necessarily antiparallel: a singlet and a triplet. If, for simplicity, we assume that in the "excited" state the two electrons, which here occupy one magnetic ion, are coupled strongly antiparallel by internal interactions there are in this state also a singlet and a triplet only. The situation is shown schematically in Table I. We see that in the *excited* state there is a triplet-singlet splitting because there can be an appreciable exchange integral between the remaining p-electron on the negative ion and the magnetic electron on the magnetic ion to which an electron has not been transferred. Now, we assume that the true wave function is given by

$$\psi^{s,t}=a\psi^{s,t}{}_{\text{ground}}+b\psi^{s,t}{}_{\text{excited}}. \tag{1}$$

The part of the Hamiltonian causing the ground-excited transition is not such as to mix singlet and triplet states. Thus one or the other superscript in (1) holds and there is a singlet-triplet splitting for the true wave function of approximately

$$\Delta E_{s-t\,(\text{apparent})}=b^2(\Delta E)_{s-t\,(\text{excited})}. \tag{2}$$

This is equivalent to a normal exchange coupling, reduced by the quantity b^2. Note that the total number of spins has not changed, and thus that the effective magneton number will not be altered greatly by superexchange coupling.

III. THE KRAMERS FORMULA

In his original paper, Kramers gives a perturbation treatment of the superexchange problem. His ideas are applicable to a system for which we define a "ground" state in which: (a) the electron wave-functions are orthogonal, (b) all "non-magnetic" ions contain only filled shells, (c) the effect of exchange between atoms is neglected, although exchange internal to the ions is included.[6] The unperturbed Hamiltonian H_0 is that

[6] The assumption (c) will be justified later simply on the grounds that the internal exchange splittings are as large as the ground-excited orbital splittings.

TABLE I. Interaction scheme in superexchange.

Ground Orbital State	Electron number		1	2	3	4
	Electron is on ion		magnetic$_1$	O^{--}	O^{--}	magnetic$_2$
	in orbital state		d_1	p	p	d_2
	Magnetic State	singlet	spin up	(antiparallel) (no splitting because no 1–4 interaction)		spin down
		triplet	spin up	(antiparallel)		spin up
Excited Orbital State	Electron is on ion		magnetic$_1$	magnetic$_1$	O^{--}	magnetic$_2$
	in state		d_1	s_1	p	d_2
	Magnetic State	singlet	(antiparallel)		spin up	spin down
		triplet	(antiparallel)	(splitting if 3–4 interact)	spin up	spin up

which this ground state satisfies. He then shows that one lifts the permutation degeneracy of this ground state neither by including the exchange terms H^{ex} (violating (c)) nor by the transition terms H^{tr} (violating (b)) separately, but that the first terms entering are of third order in these interactions, containing H^{tr} twice and H^{ex} once.[7]

We shall take Kramers' final expression for the superexchange interaction matrix $H_{tt'}$ as given; it is simply the third-order perturbation under these conditions:

$$H_{tt'}=\sum_{u,u'}\frac{(t|H^{tr}|u)(u|H^{ex}|u')(u'|H^{tr}|t')}{(E_u-E_t)(E_{u'}-E_t)}. \tag{3}$$

Here t and t' refer to the various initially degenerate spin states of the ground state, while u and u' are various spin states of the excited orbital state. We have implicitly included the strong internal exchange couplings, such as that postulated in our simple model between the d and s-electrons on Mn^{+}, in the unperturbed Hamiltonian, so that E_u and $E_{u'}$ are not necessarily equal. $H_{tt'}$ is then an effective Hamiltonian due to the third-order perturbation, acting on the unperturbed states.

So far we have been presenting essentially the ideas of Kramers. The purpose of this paper is to find a method of evaluating the sum (3) in such a way that even in complicated cases we can immediately write down $H_{tt'}$ in terms of spin operators referring to the ground state. These can then be evaluated to give the spin-dependence of the superexchange coupling.

[7] For some applications it is of interest to point out that H^{tr} contains, besides obvious terms giving the non-ionicity of the compound (thus violating assumption (b)), some other terms which result from the physical fact of violation of assumption (a). If, in the simple model of Table I, the wave-functions "d" and "p" are not orthogonal, there is a splitting in the *ground* state. Since we have artificially excluded this possibility by orthogonalizing, there must be terms in H^{tr} restoring the actual physical state of affairs. These terms will have the order of magnitude, (exchange integral)×(overlap integral),[2] which is generally much smaller than the interactions involved in the antiferromagnets. However, such terms might go far in explaining the observed magnitudes of exchange interactions in more magnetically dilute substances.

IV. EVALUATION OF THE KRAMERS EXPRESSION

A short introductory note on the method to be used is in order. The basic idea is similar to one Serber[8] used in a study of configuration interactions in atomic spectra: we shall extend the Dirac vector model of spin-coupling by exchange forces to the problem of the interaction of two configurations, which we shall call the ground (ionic) state and the excited state. If this interaction can be assumed small Kramers' matrix element (3) is the correct form for it, written as a perturbation on the levels of the ground configuration. There is a second-order effect, but this is necessarily the same for all parts of the ground configuration and merely changes the average total energy of the ground state.

We shall treat at first only the four-electron system with the ground configuration (A) consisting of one electron on each of two magnetic ions, (orbitals d_1 and d_2) and two electrons in one orbital (p) of the intervening ion. The excited configuration (B) is that in which one electron from a p-orbital has gone into an orbital on one of the magnetic ions (say "s_1"). Later work will indicate the essentially easy extension to more complicated systems. The Kramers expression (3) involves three matrix elements, two of which connect A with B (M_{AB}) and one of which involves only the excited configuration (M_{BB}). In order to couple the d_1 and d_2 spins, it is necessary to have *two* spin-dependent factors in this expression. One of these is always furnished by M_{BB}, which gives a coupling of p and d_2, but in order also to couple d_1 with p and "complete the chain" between d_1 and d_2 there must be a second spin dependence either in M_{AB} or hidden in the expression (3). There are three ways in which this spin-dependence can be achieved: (a) M_{AB} may be an exchange matrix element causing the transition. We treat this case in Appendix I, although we believe it to be secondary. In the other possibilities we allow M_{AB} to be spin-independent, but assume that the energy or the very existence of the separate multiplets of the configuration B are so spin-dependent that the denominator terms in (3) provide the second spin-dependence, either (b) due to strong internal exchange coupling between s_1 and d_1, or (c) due to the operation of the exclusion principle if s_1 and d_1 happen to be the same orbital, which would give a result like our "simple example."

Cases (b) and (c) may be treated together. To treat these two cases we shall, for the time being, assume that the forces causing the actual orbital transition are of a one-electron type; we might use a Hartree field caused by the unperturbed orbitals to determine the transition probabilities. Since one-electron Hamiltonians are spin-independent we shall show that $(t|H^{tr}|u)$ can be thrown into a very simple form. For example, we may choose as our basic wave-functions for orbitals a, b, c, d, etc. the functions

$$\psi(s_1s_2s_3s_4\cdots)=\psi(s)$$
$$=A[a(1)\chi_{s_1}(1)b(2)\chi_{s_2}(2)\cdots\text{etc.}] \quad (4)$$

where the χ's are the basic spin-function α and β, and A is an operator antisymmetrizing these products in electrons, 1, 2, 3$\cdots$. Then if the orbital states are

$$\psi_t=a(1)b(2)c(3)d(4),\cdots, \quad (5)$$
$$\psi_u=a'(1)b(2)c(3)d(4),\cdots,$$

$$(t|H^{tr}|u)=(a|H^{tr}|a')\delta_{tu}, \quad H^{tr}\simeq H_{\text{1-electron}}, \quad (6)$$

where t and u are taken to represent the sets of spins s_1, $s_2\cdots$ belonging to the various orbits. One difficulty is here apparent: if some of the sets $abcd\cdots$, or $a'bcd\cdots$, of orbitals are identical, some of the wave-functions (4) will vanish identically or become linearly dependent. For the time being we shall use Serber's trick of pretending that the orbitals are not identical, and will later remove the non-existent wave-functions by a simple strategem.

In our further development it will be necessary to choose for our upper states, u, not the basic functions (4) but linear combinations of these chosen in such a way that part or all of the spin-dependent exchange Hamiltonian is diagonalized. In this case the new states are obtainable by means of a unitary (canonical) transformation from the old states (4) (which we shall call "s"):

$$\psi_u=\sum_s(u|s)\psi(s). \quad (7)$$

Similarly, it will be necessary to pick definite linear combinations, t, for the lower states (here primarily in order to choose states which are allowed by the symmetries in the orbital function); again there is a unitary transforming matrix $(t|s)$. Now we can write down a new form for the transition matrix $(t|H^{tr}|u)$, in terms of any such linear combinations:

$$(t|H^{tr}|u)=(a|H^{tr}|a')\sum_{s,s'}(t|s)(\delta_{ss'})(s'|u)$$
$$=(a|H^{tr}|a')(t|u). \quad (8)$$

Thus the matrix causing transitions between the two sets of orbitals is simply a constant times the appropriate canonical transformation of the spin functions. The step of starting always from (4) means that we have a 1−1 correspondence among spin functions for the two states, in spite of the difference in orbitals; thus the canonical transformation $(t|u)$ exists.

Now it is necessary to consider the spin-dependent, or exchange, part of the Hamiltonian. The part of the perturbation $(u|H^{ex}|u')$ is such a spin-dependent Hamiltonian. In addition, before superexchange can occur we showed that it is necessary that the problem contain a strong spin-dependent coupling (included, as we pointed out, really in the unperturbed Hamiltonian) sufficient to affect appreciably the energy levels E_u. Among such "strong" couplings we include the infinitely strong coupling involved in the use of the same orbital for two electrons.

The spin-dependent part of the Hamiltonian, referred exclusively to upper states u, can be written down[9] in terms of operators referring to the spins of

[8] R. Serber, Phys. Rev. 45, 461 (1934)

[9] P. A. M. Dirac, *Quantum Mechanics* (Clarendon Press, Oxford, 1930), first edition, p. 216.

electrons in the various orbitals. If we have orbitals i, j, etc. the Hamiltonian is

$$V=-\sum_{i<j}\tfrac{1}{2}V_{ij}(1+\boldsymbol{\sigma}_i\cdot\boldsymbol{\sigma}_j)+\text{const.} \tag{9}$$

V_{ij} is the matrix element referring to interchange of orbitals i and j. We divide (9) artificially into two parts

$$V=V_1+V_2 \tag{10}$$

where V_1 contains all the terms which are included in E_u. In our simple case of Table I, we would have:

$$V=-\tfrac{1}{2}[V_{d_1s_1}(1+\boldsymbol{\sigma}_{d_1}\cdot\boldsymbol{\sigma}_{s_1})+V_{pd_2}(1+\boldsymbol{\sigma}_p\cdot\boldsymbol{\sigma}_{d_2})], \tag{11}$$

where

$$V_1=\tfrac{1}{2}V_{d_1s_1}(1+\boldsymbol{\sigma}_{d_1}\cdot\boldsymbol{\sigma}_{s_1})$$
$$V_2=\tfrac{1}{2}V_{pd}(1+\boldsymbol{\sigma}_p\cdot\boldsymbol{\sigma}_{d_2}).$$

Suppose that we choose our upper spin-states u in such a way as to diagonalize the operator V. Then the basic Eq. (3) for the coupling becomes, with (8) (upper and lower states differ only in the choice of orbital a or a' for one electron):

$$H_{tt'}=|(a|H|a')|^2\sum\frac{(t|u)(u|V_2|u)(u|t')}{(E_u-E_t)^2}. \tag{12}$$

If V_1 is sufficiently strong that we may say that only those states belonging to the lowest eigenvalue E_u in (12) can occur, the others being completely absent because of large denominators, it is open to us to modify V_2 in such a way as to leave out entirely the high states. Then we are permitted to "pretend" that E_u-E_t is constant for all states.

The method of modifying V_2 in such a way as to eliminate the states belonging to higher values of E_u is well known. We simply multiply by the appropriate projective operator which "projects" V_2 on the subspace belonging only to the lowest eigenvalue of V_1.

$$V_2'=PV_2,$$

or

$$(V_2')_{uu'}=\sum_{u''}P_{uu''}(V_2)_{u''u'}. \tag{13}$$

At this point it is possible also to take into account the effect of having pairs of identical orbitals in either upper or lower states. In the upper states we simply use a slight modification of the above procedure. That is, we ignore the states which are not allowed—states which contain the same pair of orbitals with parallel spins—by applying the appropriate projective operator (such as (16′) below) to eliminate such states. However, we shall show in Appendix II that this is not quite enough to take care of the linear dependences between states when pairs of orbitals are identical (for example, the states $A[a(1)\alpha(1)a(2)\beta(2)]$ and $A[a(1)\beta(1)a(2)\beta(2)]$ are identical but for sign.) There we show that, because the unitary transformation (7) acting on such an "incomplete" set of states can lead to non-normalized wave functions, we must multiply the projective operator by a factor 2 to take care of a re-normalizing factor whenever a pair of orbitals are equal.

If pairs of orbitals in the lower state are identical, we can take care of this fact simply by ignoring such states in our final result. We shall, later, actually take advantage of the fact that there is a basic limitation on the permissible lower states. Again, however, for every pair of identical orbitals we must multiply our final interaction by 2 to renormalize the wave functions, as will be shown in Appendix II. Now that we have a constant denominator in (12), we can apply the rules of matrix multiplication and obtain simply:

$$H_{tt'}=\frac{|(a|H^{tr}|a')|^2}{[(E_u-E_t)_{\text{(lowest)}}]^2}$$
$$\times\sum_u(t|u)(u|V_2'|u)(u|t')=b^2(t|V_2'|t') \tag{14}$$

where

$$b=\frac{(a|H^{tr}|a')}{(E_u-E_t)_{\text{(lowest)}}}. \tag{15}$$

We see that we have now written down the superexchange interaction operator $H_{tt'}$ in terms of V_2', which is in general easily obtainable for a particular case. As it stands in (13), V_2' is an operator working only on spin states of the "excited" state; however, it is just the idea of our calculation, and of the simplification (8), that we can establish a precise correspondence among states t and u, and, in the end, simply write V_2' as though it pertained to electrons in the lower states. Physically, this means that since the transition probability is spin-independent, the electrons retain their spins on making the transition.

Our example of Eq. (11) will make this clearer. There are two cases, depending on the sign of the "internal" exchange integral V_{d_1s}:

(A). V_{d_1s} large, >0. Then parallel spins $\boldsymbol{\sigma}_{d_1}$, $\boldsymbol{\sigma}_s$ are favored, and we want to write for P an operator which eliminates all states for which $\boldsymbol{\sigma}_{d_1}$ and $\boldsymbol{\sigma}_s$ are antiparallel. Such an operator is

$$P_1=\tfrac{1}{4}(3+\boldsymbol{\sigma}_{d_1}\cdot\boldsymbol{\sigma}_s). \tag{16}$$

Then in this case (inserting the extra factor 2):

$$H_{tt'}=b^2(t|\tfrac{1}{4}(3+\boldsymbol{\sigma}_{d_1}\cdot\boldsymbol{\sigma}_{p_1})V_{p_2d_2}(1+\boldsymbol{\sigma}_{p_2}\cdot\boldsymbol{\sigma}_{d_2})|t'). \tag{17}$$

We have simply read $\boldsymbol{\sigma}_{d_1}$ for $\boldsymbol{\sigma}_s$, this being the electron making the transition.

(B). V_{ds} large, <0 (or d and s are same orbital). Parallel spins for the d and s orbitals are to be eliminated in this case, and the proper projective operator is[10]

$$P_2=\tfrac{1}{4}(1-\boldsymbol{\sigma}_{d_1}\cdot\boldsymbol{\sigma}_{s_1}) \tag{16′}$$

$$H_{tt'}=\tfrac{1}{4}b^2(t|V_{pd}(1-\boldsymbol{\sigma}_{d_1}\cdot\boldsymbol{\sigma}_{p_1})(1+\boldsymbol{\sigma}_{p_2}\cdot\boldsymbol{\sigma}_{d_2})|t'), \tag{17′}$$

[10] We shall hereafter simply understand the factor 2 when P_2 is due to a Pauli principle limitation, i.e. d and s are the same orbital. Since b^2 is unknown anyway, this leads to no important change in the theory.

TABLE II. Sign of the interaction.

	If internal coupling favors spin of added electron	and exchange coupling of p-electron and other atom is	then coupling is
1	parallel	ferromagnetic	antiferromagnetic
2	parallel	antiferromagnetic	ferromagnetic
3	antiparallel	ferromagnetic	ferromagnetic
4	antiparallel	antiferromagnetic	antiferromagnetic

where in both cases

$$b=\frac{(s|H_{\text{1-electron}}|p)}{E_{\text{(bonding)}}-E_{\text{(ionic)}}}. \tag{18}$$

To compute the effective coupling we observe that $\boldsymbol{\sigma}_d\cdot\boldsymbol{\sigma}_p$ acting on wave-functions in which $\boldsymbol{\sigma}_p$ is the spin of one of a pair of electrons in the p-orbital gives an identically zero result, as it must always make an $S=1$ state out of an $S=0$ state, and the $S=1$ wave functions vanish identically. Then the true coupling is proportional to

$$(\boldsymbol{\sigma}_{d_1}\cdot\boldsymbol{\sigma}_p(1))(\boldsymbol{\sigma}_{d_2}\cdot\boldsymbol{\sigma}_p(2))$$

$\boldsymbol{\sigma}_p(1)+\boldsymbol{\sigma}_p(2)=0$; thus the coupling is, by a simple expansion into components,

$$\begin{aligned}(\boldsymbol{\sigma}_{d_1}\cdot\boldsymbol{\sigma}_p(1))(\boldsymbol{\sigma}_{d_2}\cdot\boldsymbol{\sigma}_p(2))&=-(\boldsymbol{\sigma}_{d_1}\cdot\boldsymbol{\sigma}_p)(\boldsymbol{\sigma}_{d_2}\cdot\boldsymbol{\sigma}_p)\\&=-(\boldsymbol{\sigma}_{d_1}\cdot\boldsymbol{\sigma}_{d_2}),\end{aligned} \tag{19}$$

where the cross-product term $i\boldsymbol{\sigma}_p\cdot(\boldsymbol{\sigma}_{d_1}\times\boldsymbol{\sigma}_{d_2})$ has vanished, again because $\boldsymbol{\sigma}_p$ vanishes identically.

The effective coupling is thus

$$\mp\tfrac{1}{4}b^2V_{pd}(\boldsymbol{\sigma}_{d_1}\cdot\boldsymbol{\sigma}_{d_2})\begin{bmatrix}-\text{Case } A\\+\text{Case } B\end{bmatrix}.$$

There is an equal term also present due to transitions to atom 2 and exchange with atom 1. Note that (17) is correctly isotropic in respect to lattice rotations.

V. GENERALIZATIONS

Various generalizations of this method from the simple case come immediately to mind. The most apparent is the generalization to the case in which V_1 is not infinitely strong, but instead leads simply to a finite splitting of the levels E_u, sufficient for the energy denominators in (12) to be somewhat different. For example, suppose that in Case A

$$\frac{(\Delta E)_{\text{parallel}}}{(\Delta E)_{\text{anti-parallel}}}=x,\ x<1.$$

Then it is necessary to leave in the sum (12) an amount of the antiparallel states proportional to x^2. A "partial projective operator" which will do just this is

$$\begin{aligned}P'&=\tfrac{1}{4}(3+\boldsymbol{\sigma}_d\cdot\boldsymbol{\sigma}_s)+\tfrac{1}{4}x^2(1-\boldsymbol{\sigma}_d\cdot\boldsymbol{\sigma}_s)\\&=\tfrac{1}{4}[(3+x^2)+(1-x^2)\boldsymbol{\sigma}_d\cdot\boldsymbol{\sigma}_s],\end{aligned} \tag{20}$$

then

$$\begin{aligned}H=\tfrac{1}{4}b^2V_{pd}[(3+x^2)+(1-x^2)(\boldsymbol{\sigma}_{d_1}\cdot\boldsymbol{\sigma}_{p_1})]\\\times[1+\boldsymbol{\sigma}_{d_2}\cdot\boldsymbol{\sigma}_{p_2}]\end{aligned} \tag{21}$$

note that if $x^2=1$, or $V_{\text{strong}}=0$, there is no coupling, since the singlet and triplet averages of H are not then different.

The reader may object that the splittings caused by Hund's rule that internal exchange favors parallel spins are, in general, quite small (of the order of 2 to 3 ev) compared to normal orbital splittings, and thus that x should be nearly equal to unity, and the internal exchange should also be a small perturbation. Then the terms considered in the main body of the paper would be fourth-order, and thus small compared to those due to exchange transitions, which are considered in Appendix I. These latter are easily worked out but do not lead to such simply interpretable results as the ones we are considering. However, it must be remembered that the very fact that superexchange is so strong indicates that the energy level representing ionization of the anion is very low in the antiferromagnetic crystals, as one could also conclude by noting that O^-, Te^-, etc., have large negative electron affinities. BaO, a compound similar to those considered, has its first exciton level at roughly 3.8 ev which is certainly *not* large compared to the 2 to 3 ev exchange splittings. We therefore believe that the terms here considered are probably the dominant ones.

A second trivial generalization is to the case in which the ions have spins of greater than one-half. In this case we must again guess the direction of coupling of an added electron (perhaps by Hund's rule) and proceed essentially as in the simple case. The projective operators are derived as follows:

$$(\mathbf{S}\cdot\boldsymbol{\sigma})_{(S+\frac{1}{2}\boldsymbol{\sigma})=S+\frac{1}{2}}=S \tag{22}$$

$$(\mathbf{S}\cdot\boldsymbol{\sigma})_{(S+\frac{1}{2}\boldsymbol{\sigma})=S-\frac{1}{2}}=-(S+1) \tag{22'}$$

so that in case we wish to eliminate parallel spin $-\mathbf{S}$ cases we use

$$P_{S\text{(anti-parallel)}}=\left(1-\frac{\mathbf{S}\cdot\boldsymbol{\sigma}}{S}\right)\cdot\frac{S}{2S+1} \tag{23}$$

and in the opposite case

$$P_{S\text{(parallel)}}=\left(1+\frac{\mathbf{S}\cdot\boldsymbol{\sigma}}{S+1}\right)\cdot\frac{S+1}{2S+1}. \tag{23'}$$

Here again it is possible to apply the argument of equation (19) and thus the coupling is always proportional to $\mathbf{S}_1\cdot\mathbf{S}_2$.

Table II expresses the available information on the sign of the interaction.

The dependence of the coupling on the sign of the internal coupling can be verified in some actual cases, since by Hund's rule we know that an electron will be

added most easily with parallel spin for ions with less than half-filled shells (Cr^{++} for instance) and antiparallel for ions with more than half-filled shells (Mn^{++}). Indeed, it is observed that chromium telluride is ferromagnetic, although manganese telluride, analagous in structure and very similar in many ways, is antiferromagnetic. The dichlorides of these two ions, and also of V and Fe, show, again, this sign change although here the crystal structures are not known.[11] Many other compound pairs could easily be investigated for this feature.

It is easily seen that the presence of other electrons in the same shell as that occupied by the "p" (or transition-making) electron does not change the mathematics. So long as only one electron leaves O^{--} at a time, the electrons in the shell other than the one associated with the absent one are represented in V_1 by infinite terms; thus the wave functions in which they are not antiparallel by pairs are absent. However, these wave functions are not considered in the ground state either; thus these electrons have no effect, since the related projection operator does not enter the true Hamiltonian. This reasoning has an interesting consequence: if superexchange occurs through p-electrons it has a p-type of directionality. That is, if the electron making the transitions is primarily the p-electron, as one suspects, the remaining p-electron in *the same state* will provide the exchange coupling. However, this p-state can only couple with the magnetic ion diametrically opposite to the ion to which the transition is made, and the strongest coupling will thus "look like" a p wave-function, with maxima at 180° from the O^{--} ion. One must realize, however, that the s-electrons of the outer shell will contribute a smaller direction-independent coupling.

This conclusion is interesting in view of the quoted results of Shull[12] on MnO, in which he finds a strong coupling of next nearest neighboring Mn ions rather than of nearest neighbors; this indicates that the superexchange directly through the O^{--} ion may be more powerful than that between locations making angles of 90° with the O^{--} ions.[12] This directionality property is simply a result of the superexchange mechanism, and it should be emphasized as being more general than any of the special assumptions of the theory such as the perturbation treatment or one-electron transitions.

It can be shown that the general form of the superexchange interaction is much the same when the electronic structure of the entire solid is taken into consideration. The easiest procedure in this case is to use the full Hamiltonian for the unperturbed energy for all but a few atoms surrounding a pair of chosen magnetic ions; then the exchange and "state-mixing" Hamiltonians are introduced as simultaneous perturbations on the ground state so defined. This is legitimate as long as there is only a small probability of two electrons "jumping" to or from the same ion at the same time; i.e., as long as the perturbation treatment is valid.

This paper incorporates the results of many helpful discussions with several of my colleagues, particularly Drs. G. H. Wannier, C. Kittel, and W. Shockley. Professor J. H. Van Vleck made several very useful suggestions.

APPENDIX I

Consideration of Transitions Involving Exchange

In the text we have always assumed that the potential causing the transition between orbitals was of the form $\Sigma V(r_i)$ involving only one-electron forces. In case the potential contains important terms of the form $\Sigma V(r_{ij})$ one can carry through the same kind of analysis, but the results are somewhat more complicated and lead to less clarification of the problem.

Let us confine ourselves to the simple case worked out in the text. Then the type of exchange integral which is important is

$$V_{12}=\int s_1(1)d_1(2)p_2(3)d_2(4)V(r_{12})d_1(1)p_1(2)p_2(3)d_2(4). \quad (24)$$

The essential idea is that the proof of Dirac[9] for formula (9) does not break down in this case;[13] the actual transition matrix elements are matrix elements of the operator

$$V=\tfrac{1}{2}V_{12}(1+\sigma_1\cdot\sigma_2), \quad (25)$$

where we have made the same identification of orbitals in ground and excited states as before:

$$\begin{cases}\sigma_1=\text{spin matrix of electron in } \begin{bmatrix}d_1 \text{ (ground)}\\ d_1 \text{ (excited)}\end{bmatrix} \text{ orbital}\\ \sigma_2=\text{spin matrix of electron in } \begin{bmatrix}p_1 \text{ (excited)}\\ s_1 \text{ (ground)}\end{bmatrix}\end{cases} . \quad (26)$$

The proof merely follows the lines of Dirac's proof. First: as an operator acting on products of spin+electron wave functions, $V(r_{ij})$ is equivalent to

$$V_{ij}P_0(ij), \quad (27)$$

where V_{ij} is simply an orbital exchange matrix element of the type (24), while $P_0(ij)$ is the permutation operator interchanging orbitals i and j. Then $P_0(ij)$ on wave-functions forced by the Pauli principle to be antisymmetric is just equivalent to the same permutation acting on the spin wave-functions corresponding to the two orbitals, by the usual argument:

$$P_0\psi(S)=\pm P^{-1}P_0\psi(S)=\pm P_S\psi(S),$$

where P^{-1} is the permutation operator acting on both spins and orbitals. Thus the result of operating with $P_0(ij)$ on our basic wave-functions (4) is the same as that of multiplying by an

[11] Foex, *Le Magnetisme* III, (Strasbourg, 1939) p. 222. Also, one should note that the theory is not here as well founded, since the main coupling may not be superexchange.

[12] Still a further experimental confirmation of our general ideas can be found in the Weiss molecular field theory mentioned in a previous footnote applied to a series of compounds MnO, MnS, MnSe, MnTe. Since the electronegativity of the anion decreases along this series, one would expect a decrease in ionic character, and thus an increase in the constant b of Eq. (15). At the same time, the molecular field theory leads us to expect that the θ/T_c ratio should decrease with increasing superexchange coupling of the Mn^{++} ions and thus should decrease along this series. This seems to be the case; the values are (Bizette, *Thesis*, Paris 1946): MnO: 5.0; MnS: 3.2; MnSe: ~3.0.

[13] R. Serber, reference 8, has also proved the theorem used here, that (25) is true (except for factors $\sqrt{2}$) even for configuration transitions.

operator $P_S(ij)$. $P_S(ij)$ can then be proved to be:

$$P_S(ij)=\tfrac{1}{2}(1+\sigma_i\cdot\sigma_j). \tag{28}$$

Now the steps by which we made it possible to ignore the energy denominators in (3) can be carried through as before, leaving us with simple matrix multiplication of the three types of matrix elements. The transition matrices $(t|H|u)$ here are simply

$$\tfrac{1}{2}V_{12}(1+\sigma_1\cdot\sigma_2),$$

which multiply the "modified" exchange matrix $(u|V_2'|u)$.

Let us do an actual example. Suppose that the energy denominators do not enter, and thus that

$$V_2'=\tfrac{1}{2}V_{34}(1+\sigma_3\cdot\sigma_4).$$

Both exchange and one-electron transitions are assumed to be important, and thus the matrix element causing transitions is

$$\tfrac{1}{2}V_{12}(1+\sigma_1\cdot\sigma_2)+(a|H^{tr}|a').$$

Then Kramers' expression (3) is

$$H_{tt'}=\left\{t\left|\left[b+\frac{V_{12}}{E_u-E_t}\left(\frac{1+\sigma_1\cdot\sigma_2}{2}\right)(V_{34})\left(\frac{1+\sigma_3\cdot\sigma_4}{2}\right)\right]\right.\right.$$
$$\left.\left.\times\left[b+\frac{V_{12}}{E_u-E_t}\left(\frac{1+\sigma_1\cdot\sigma_2}{2}\right)\right]|t'\right\}.$$

The square of $\frac{1}{2}(1+\sigma_1\cdot\sigma_2)$ is unity, since this is the representative of a simple permutation operator, and thus, since it commutes with $(1+\sigma_3\cdot\sigma_4)$, the part of this expression involving V_{12}^2 has no spin-dependence. Similarly the b^2 part has no spin-dependence since we have left out the spin-dependence due to the denominator. Only cross-terms between the one-electron and spin transitions remain:

$$H_{tt'}=\frac{bV_{12}V_{34}}{E_u-E_t}\times\tfrac{1}{2}(t|(1+\sigma_1\cdot\sigma_2)(1+\sigma_3\cdot\sigma_4)1(t')$$
$$=-\frac{bV_{12}V_{34}}{E_u-E_t}\times\tfrac{1}{4}(\sigma_1\cdot\sigma_4).$$

We see that here the sign of the coupling cannot be predicted by Hund's rule, although our other conclusions are still valid, and in particular the coupling is still roughly proportional to the square of the non-ionicity, and is still a $(\sigma_1\cdot\sigma_4)$ coupling. One might expect that this type of coupling, which would be roughly the same for more than half-filled and less than half-filled shells, in some cases might predominate over the one-electron coupling, and as a result in some cases the sign of the coupling might not change between the two cases, although its magnitude could vary greatly.

APPENDIX II

Justification of the Factor 2 Due to Pairs of Identical Orbitals

In this appendix we shall try to indicate the two sources which lead to an error of a factor of $\sqrt{2}$ in our transition matrix elements computed according to the prescription (8) as compared with the true transition matrix element when identical orbitals are present. The rigorous proof has been given by Serber (reference 8, pp. 463–464).

First we shall compute the transition probability for a very simple case. Suppose our configurations are of two orbitals, and one (A) has two different orbitals (ab), while the second has two identical ones (a^2). Then transitions will only be possible between the singlet states

$$\left.\begin{aligned}\psi_A^S&=\tfrac{1}{2}[a(1)b(2)+a(2)b(1)][\alpha(1)\beta(2)-\alpha(2)\beta(1)]\\ \psi_B^S&=\tfrac{1}{2}\sqrt{2}a(1)a(2)[\alpha(1)\beta(2)-\alpha(2)\beta(1)].\end{aligned}\right\} \tag{29}$$

These are the rigorous nomalized states, and it is easy to see that if $H=H'(1)+H'(2)$

$$(\psi_A^S|H|\psi_B^S)=\tfrac{1}{4}\sqrt{2}[\alpha(1)\beta(2)-\alpha(2)\beta(1)]^2$$
$$\times[(a(1)b(2)+a(2)b(1))|H'(1)+H'(2)|a(1)a(2)]$$
$$=\sqrt{2}(a|H'|b) \tag{30}$$

The result of our prescription (8), however, is perfectly obvious since both states are singlets, obtained by the same process from the basic wave-functions (4), and thus

$$(t|u)=1 \tag{31}$$

and the matrix element is

$$(a|H'|b). \tag{32}$$

The first source of error is fairly obvious. The basic wave functions (4) in the case of configuration B are not orthogonal; one is

$$(1/\sqrt{2})a(1)a(2)[\alpha(1)\beta(2)-\alpha(2)\beta(1)],$$

and the other is

$$(1/\sqrt{2})a(1)a(2)[\alpha(2)\beta(1)-\alpha(1)\beta(2)],$$

and so the result of the unitary transformation (7) (in this case simply antisymmetrizing) is

$$a(1)a(2)[\alpha(1)\beta(2)-\alpha(2)\beta(1)], \tag{33}$$

which is not normalized, and in fact is too large by a factor of $\sqrt{2}$. Thus we predict that the matrix element (32) is too *large* by a factor $\sqrt{2}$ since it is computed on the basis of a non-normalized wave function. The existence of further orbitals in the configuration does not change this result, and we get the general rule: "For every pair of orbitals in either configuration which are identical in one but not in the other, our transition matrix element must be divided by $\sqrt{2}$ caused by the linear dependence of the basic wave functions."

This factor, unfortunately, is in the wrong direction and makes the error in (32) now 2 rather than $\sqrt{2}$.

The other factor of 2 we can find by looking at the steps in Eq. (30). We notice that the Hamiltonian depends symmetrically on the coordinates of electrons (1) and (2), and in fact is the sum of a term for each electron. Thus it happened that $a(1)a(2)$ combined with *both* $a(1)b(2)$ and $a(2)b(1)$. This is the source of the missing factor 2. What this means is that Eq. (6) of the text is in error when orbitals are identical. Actually, there are cases in which the basic wave-functions combine in case a pair of orbitals are equal. The wave-function

$$A[a(1)\chi_1(1)a(2)\chi_2(2)\cdots] \tag{34}$$

combines (if χ_1 and χ_2 are different, as they must be), both with

$$A[a(1)\chi_1(1)b(2)\chi_2(2)\cdots], \tag{35}$$

and, except for a changed sign,

$$(A7\text{-}b)\quad A[a(1)\chi_2(1)b(2)\chi_1(2)\cdots]. \tag{35'}$$

This is due to the fact that (34) is actually identical with the wave-function with χ_1 and χ_2 interchanged.

Fortunately, since only the singlet wave-function in these two orbitals can enter due to the fact that there are identical orbitals in one of the configurations, (35) and (35′) will always enter as an antisymmetrized linear combination, and the only result of the failure of formula (6) of the text is the missing factor of 2, due to the fact that the wave-function with identical orbitals combines with twice too many wave-functions in the other configuration.

Thus, to take account of these two effects the transition matrix element must be multiplied by $2/\sqrt{2}=\sqrt{2}$ for each pair of identical orbitals in either configuration which do not also appear in the other configuration. We can equally well simply multiply the total interaction, or if we like the projective operator, by 2.

The separate matrix elements referring only to upper or to lower configurations are not modified by the presence of identical orbitals, as was shown by Dirac.[9] The procedure of the text is thus shown to be correct.

Antiferromagnetism. The Triangular Ising Net

G. H. WANNIER
Bell Telephone Laboratories, Murray Hill, New Jersey
(Received February 11, 1950)

In this paper the statistical mechanics of a two-dimensionally infinite set of Ising spins is worked out for the case in which they form either a triangular or a honeycomb arrangement. Results for the honeycomb and the ferromagnetic triangular net differ little from the published ones for the square net (Curie point with logarithmically infinite specific heat). The triangular net with antiferromagnetic interaction is a sample case of antiferromagnetism in a non-fitting lattice. The binding energy comes out to be only one-third of what it is in the ferromagnetic case. The entropy at absolute zero is finite; it equals

$$S(0)=R\frac{2}{\pi}\int_0^{\pi/3}\ln(2\cos\omega)d\omega=0.3383R.$$

The system is disordered at all temperatures and possesses no Curie point.

I. INTRODUCTION

THANKS to the work of Kaufman and Onsager[1–3] we are now in possession of a method of solving exactly a certain number of cooperative problems in physics. We can obtain the thermal properties and some order-parameters for a two-dimensional periodic structure whose members are "spins" capable of existing in two states; these spins interact with their nearest neighbors only, according to the mode put forward by Ising.[4] In addition to the general theory, the papers quoted contain also its application to the rectangular Ising net which is shown in Fig. 1. The main feature of their results is the temperature singularity. The singularity is mainly known at this time through its manifestation in the specific heat curve. For a complete study of this "Curie point" transition one would like to know also the magnetic properties. These quantities are not available in the literature at this time although the spontaneous magnetization has been calculated.[5]

In the original calculations the Ising model was thought of as ferromagnetic. Within recent years, however, antiferromagnetism has received considerable attention, and one might wish to think of the model in terms of this new application. The salient features of antiferromagnetism are described in an article of Bizette.[6] The specific heat resembles that of ferromagnetic materials; the susceptibility curves resemble the specific heat curves somewhat, having a pronounced maximum at the Curie point. Both these features can be accounted for qualitatively on the basis of nearest neighbor interaction. The specific heat calculation of Onsager[1] actually does not distinguish at all between ferromagnetism and antiferromagnetism, owing to the well-known symmetry property which applies to all lattices having α- and β-sites with all α-sites surrounded by β-sites and vice versa.

A closer study of antiferromagnetism removes to a great extent this superficial similarity. It may be seen from the work of Hulthén[7] that the difference between the quantum and Ising interactions is much more drastic in the antiferromagnetic than the ferromagnetic case. Specifically, a linear chain of quantum spins whose interaction is $J\Sigma\boldsymbol{\sigma}_i\cdot\boldsymbol{\sigma}_{i+1}$ has a lowest energy which is 1.775 times that of a corresponding set of Ising spins. This situation is in contrast to the ferromagnetic case and by itself removes any hope of a simple analogy. In addition, the antiferromagnetic materials MnO, MnS, MnTe, FeO crystallize in the NaCl structure; this gives the paramagnetic metal ions a face-centered cubic arrangement. Such an arrangement of sites does not divide into α- and β-sites in the manner described above. In consequence, even for an Ising antiferromagnet the thermal properties are not trivally related to some "equivalent" ferromagnetic arrangement.

This paper is one in a series of related studies on these non-trivial aspects of antiferromagnetism. We will derive in it the properties of an antiferromagnetic triangular Ising net (Fig. 2). This arrangement is a two-dimensional analog of the face-centered cubic structure, in that it is also a lattice into which antiferromagnetism does not fit. The Kaufman-Onsager calculation can be carried out for it and full results obtained. We shall

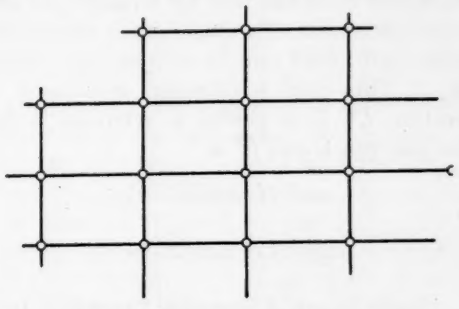

FIG. 1. Rectangular Ising net. The circles indicate the location of the spins and the straight lines the interactions.

[1] L. Onsager, Phys. Rev. **65**, 117 (1944).
[2] Kaufman, Phys. Rev. **76**, 1232 (1949).
[3] B. Kaufman and L. Onsager, Phys. Rev. **76**, 1244 (1949).
[4] E. Ising, Zeits. f. Physik **31**, 253 (1925).
[5] B. Kaufman (private communication).
[6] H. Bizette, thesis, Paris, Masson et Cie, pp. 62–96.
[7] L. Hulthén, Arkiv f. Mat. Astr. o. Fys. **26A**, No. 11 (1938).

find that the lowest energy state of the model is disordered and actually possesses a finite entropy; there is no discontinuity in the specific heat and probably no maximum in the susceptibility. Results for the ferromagnetic triangular net and the honeycomb net will be obtained as a by-product of the work; they do not differ essentially from the results obtained for the square net.[1-3]

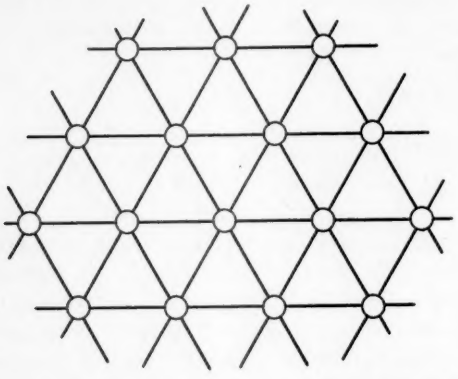

FIG. 2. Triangular Ising net. No perfectly regular antiferromagnetic arrangement can be fitted into this structure.

II. QUALITATIVE DISCUSSION

It is convenient to discuss by simpler methods two salient features of the triangular net; namely, the ferromagnetic Curie point and the antiferromagnetic zero-point entropy.

The derivation which locates the Curie point and establishes the symmetry property about that point may be found elsewhere in the literature.[8] We will not return to this derivation, but make use of the results.

The calculations involve one parameter L only, which is defined as

$$L=J/(2kT), \tag{1}$$

where J is the coupling energy (energy required to turn over one pair of spins from the parallel to the antiparallel position), k is Boltzmann's constant, and T is the temperature. It is shown in reference 8 how the partition function for any two-dimensional net is linked with the partition function for the "dual" which is constructed from the first by replacing all areas by points and vice versa. The dual for the triangular net is the honeycomb; their mutual relationship is illustrated in Fig. 3. This dual relationship involves a "dual" temperature L^*. It is shown in reference 8 that the relation between L and L^* is

$$\sinh 2L \sinh 2L^*=1, \tag{2a}$$

or

$$\tanh^2 2L+\tanh^2 2L^*=1, \tag{2b}$$

or

$$\cosh 2L \tanh 2L^*=\cosh 2L^* \tanh 2L=1. \tag{2c}$$

The dual relationship for the partition functions is given in reference 8, Eq. (23). For infinite systems we may suppress a negligible factor $\sinh 2L$ and write it in the form

$$f(L)/(2\sinh 2L)^{N/2}=f^*(L^*)/(2\sinh 2L^*)^{N^*/2}. \tag{3}$$

Although this dual relation is a reversible one, we shall use it in the following in a one-sided way and preferably associate the star with the honeycomb.

It is possible to return from $f^*(L^*)$ to f by a second algebraically independent transformation, the so-called star-triangle transformation.[8] The transformation is illustrated in Fig. 4. In the state sum, f^*, the summation is carried out over all spins, μ. In executing this sum, one can, however, divide them into two classes which are marked, respectively, by full and open circles in Fig. 4. The sum over the open circles is carried out first; this is relatively simple because the summation over μ_0 in Fig. 4 involves only the three spins μ_1, μ_2, and μ_3.

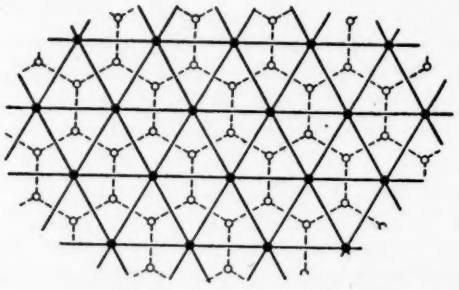

FIG. 3. Dual relationship between the triangular and the honeycomb net. Areas replace corners in a reciprocal fashion, sides replace sides.

The result of the summation can be expressed by a fictitious interaction J^+ between μ_1, μ_2, and μ_3 which is shown in heavy dotted outline. These dotted interactions, when continued throughout the lattice produce again a triangular net, but with a new interaction J^+. Apart from certain factors, the partition function for the triangle net at the "temperature" L is thus equivalent to the same partition function at the "temperature" L^+ where L^+ is derived from J^+ by Eq. (1). The relation between L and L^+ is found to be[8] expressible in the forms

$$[\exp(4L)-1][\exp(4L^+)-1]=4, \tag{4a}$$

$$(\coth 2L-1)(\coth 2L^+-1)=1, \tag{4b}$$

$$\tanh 2L+\tanh 2L^+=1, \tag{4c}$$

and the symmetry relationship for f reads

$$f(L)/(2\sinh 2L)^{N/2}=f(L^+)/(2\sinh 2L^+)^{N/2}. \tag{5}$$

We shall refer to the temperature defined by (4) and (5) as the "inverted" temperature and to the process as temperature inversion. The dual temperature is thus the "inverted" temperature for the square net.

It may be noted that relationships (3) and (5) completely specify the temperature inversion for the honey-

[8] G. H. Wannier, Rev. Mod. Phys. 17, 50 (1945), Part IV.

comb. We find that

$$f^*(L^*)/(2\sinh 2L^*)^{N^*/2}=f^*(L^{*+})/(2\sinh 2L^{*+})^{N^*/2}. \quad (6)$$

The relation between L^* and L^{*+} follows from (2c) and (4) as

$$\sinh L^* \sinh L^{*+}=\tfrac{1}{2}, \quad (7a)$$

or

$$\operatorname{sech} 2L^*+\operatorname{sech} 2L^{*+}=1. \quad (7b)$$

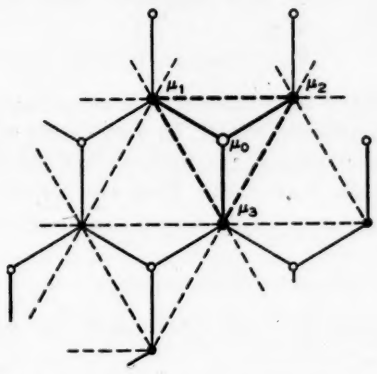

FIG. 4. Star-triangular transformation: Removal by summation of the open-circled spins from the honeycomb state sum (full lines) leaves a triangular net (dotted lines).

It is curious that the quantity entering into (3) is also the one entering into (5) and (6). At this time, this is not obvious from any previous reasoning.

The relationships (2), (4), and (7) locate the Curie point of the material as the point at which the temperature equals its inverse.

From the partition function, f, the internal energies are obtained by differentation

$$U=-\tfrac{1}{2}Jd(\ln f)/dL. \quad (8)$$

Thus each of the relations (3), (5), and (6) has a corrollary involving the energies U. We shall restrict outselves to (3) which yields

$$\frac{U(L)}{-\frac{1}{2}J\coth 2L}+\frac{U^*(L^*)}{-\frac{1}{2}J\coth 2L^*}=N+N^*=S, \quad (9)$$

where S is the number of sides of either one of the dual nets.

The second part of this qualitative discussion will be concerned with the antiferromagnetic triangular net.

It was mentioned that the thermal properties of the rectangular and honeycomb net are independent of the sign of the interaction J; this symmetry is also apparent in the relations (2) and (7). For the triangular net, however, we must expect entirely different results in the two cases.

The fact that antiferromagnetism does not fit into the triangular pattern modifies particularly the low temperature behavior because of a different type of ground state. The energy of this state is quite easily perceived to be only one-third of the corresponding ferromagnetic value. We prove this in two steps: first, we show that it cannot possibly be lower; second, we actually construct states of this energy.[9] For the first point we decompose the net into triangles as shown in Fig. 5. Each triangle contains three interactions, and the best we can achieve within each is to have two spins of one sign and one of the other. Thus the final arrangement contains at least one-third of the wrong interactions.

There are actually states in which the number of wrong interactions is just one-third which have therefore the energy minimum

$$U(0)=-\tfrac{1}{6}SJ=-\tfrac{1}{2}NJ. \quad (10)$$

An example of such an arrangement is shown in Fig. 6. It consists of rows of positive spins alternating with rows of negative spins. It is not likely to be ever realized because there are arrangements of much higher weight.

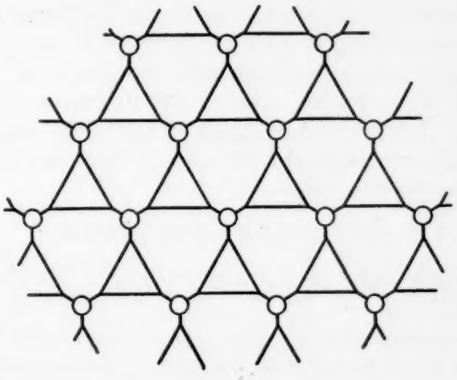

FIG. 5. Decomposition of the triangular net into individual triangles. Each interaction forms part of one and only one triangle. At least two neighbors must be equal in each triangle.

Figure 7 shows one which consists of rows of alternate spins. Each row may be laid independently; i.e., we may commit a large number of "stacking errors" and still stay in the ground state. The entropy of the arrangement is still zero because the weight is proportional to N^1 only. In Fig. 8, on the other hand, we have an arrangement of finite entropy.[10] We see that in this arrangement the correct energy is obtained by an unbalance; around a (+) spin the ratio of right and wrong interactions is 6:0, while for the more numeous (−) spins it is 3:3. From this latter ratio it follows that we can reverse any one of the negative spins without changing the energy. We may even perform this operation independently for each one of the encircled negative spins and thus gain a weight of $2^{N/3}$. This is not yet the full weight because there is a large amount of contingent freedom. Since the encircled spins can be varied independently, it will occur quite often that three encircled spins forming a triangle have equal sign. In the overwhelming majority of cases (by the arguments of fluctuation theory) each of the arrangements

[9] The following proof is due to W. Shockley.

[10] The following considerations are due to P. W. Anderson.

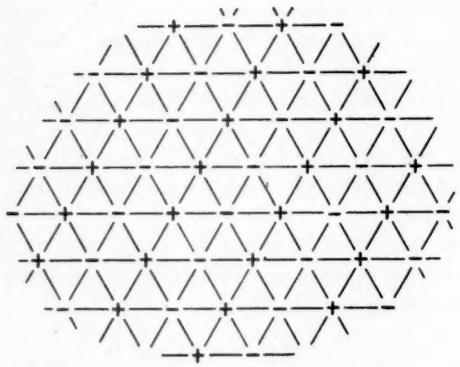

FIG. 6. A simple arrangement of minimum energy: Rows of positive spins placed in alteration with rows of negative spins.

of Fig. 9 will prevail at least at one out of eight positions. It now happens for the center spin of this tripod that its interactions are in the ratio 3:3. Hence it may be reversed also and there are another $(N/24)+(N/24)$ free spins added to the original number of $N/3$. The weight of the ground state thus is pushed to $2^{5N/12}$; it is clear that it may be pushed up further by consideration of more involved contingencies. We thus have for the zero-point entropy

$$S(0)>(5/12)R\ln 2=0.288811R. \tag{11}$$

The exact value of this entropy will be derived later (Eq. (37)).

Long-range order is incompatible with a ground state of this type. As an example, there is shown in Fig. 10, an arrangement in which two ordered sections of the type shown in Fig. 8 adjoin. Long-range order in each ordered section is different and a transition region results. This region has, however, the same low energy as do the ordered regions themselves. We conclude therefore that long-range order offers no energy advantage for this structure.

It has been mentioned earlier that we are not able, at this time, to compute the paramagnetic susceptibility. We can, however, draw qualitative conclusions easily. The situation exemplified by Fig. 10 clearly implies an infinite susceptibility at absolute zero. After that, the susceptibility must drop and there is no physical reason to expect that magnetization will ever become easier as the temperature rises. Thus we would expect a paramagnetic sort of a curve which is at variance with experimental observations.[6]

III. CALCULATION OF THE THERMAL PROPERTIES

We shall, in this section, supplement the considerations of Section II by calculating explicitly the thermal properties of the triangular net; these can be obtained by applying the methods of Kaufman and Onsager.[1-3] The reader is assumed to be familiar with this earlier work and we shall only note the necessary modifications.

The honeycomb may be deformed topologically to take the appearance of a "brick" net (Fig. 11). This rectangular arrangement differs from the one studied in reference 1 only in that certain interactions are missing. This means some minor modification in the basic operations.

We shall assume that the brick net is being built up sideways rather than upward. No interaction is then missing in the direction of the build-up and the operator V_1 can be taken over unaltered from reference 1, Eq. (21) as

$$V_1=(2\sinh 2L^*)^{n/2}e^{LB}. \tag{12}$$

The reversal of the dual star is in accordance with the convention adopted earlier. In place of the operator V_2 defined in reference 1, Eq. (28), we have two operators V_3 and V_4 which alternate. They are, respectively,

$$V_3=\exp H^*(s_1s_2+s_3s_4+\cdots), \tag{13}$$

$$V_4=\exp H^*(s_ns_1+s_2s_3+\cdots). \tag{14}$$

The partition function is obtained by using these

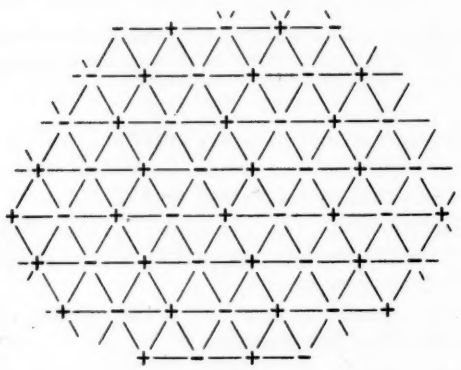

FIG. 7. An arrangement of minimum energy having medium-high weight: Rows of alternating spins stacked at random.

operators in the arrangement

$$\cdots V_1V_3V_1V_4V_1V_3V_1V_4V_1\cdots.$$

Two rows of spins will have to be laid down before the cycle repeats. Consequently, Eq. (29) of reference 1 is replaced by

$$\lambda\psi=(V_3V_1V_4V_1)\psi. \tag{15}$$

Among the various steps which follow (15), the passage to operators P_i, Q_i defined in reference 2 requires some discussion. This necessary transition introduces unsymmetric end terms, such as the one in reference 2, Eq. (14). The author feels that it is not generally worth while to pay too much attention to such terms. Bulk properties and even short-range order should be unaffected by a modification of the "seam." Long-range order is probably affected because such a modification of operators may remove the degeneracy. It is known that degeneracy is essential for the study of long-range order.[11] Apart from such special require-

[11] J. Ashkin and W. E. Lamb, Phys. Rev. 64, 159 (1943).

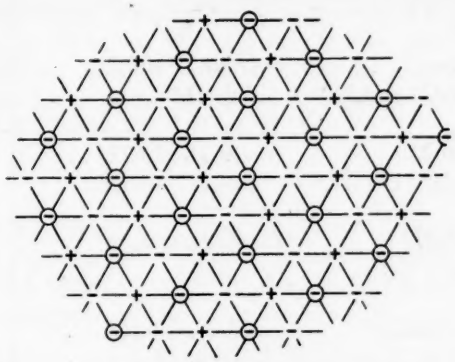

FIG. 8. An arrangement of minimum energy having finite entropy: Two sublattices have spins of fixed sign, but in the third, each sign individually may be picked at random.

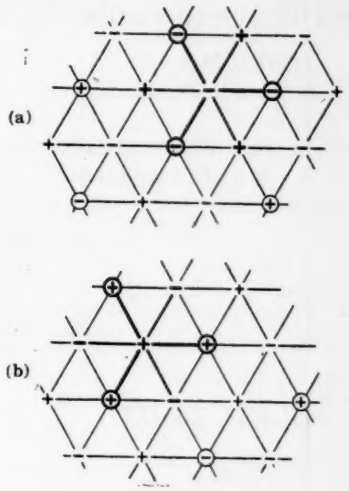

FIG. 9. Two arrangements (a, b) of contingent freedom. If three neighboring ringed spins of Fig. 8 happen to have equal sign, their center may be chosen at random. Such considerations make the entropy larger than $\frac{1}{3}R\ln 2$.

ments we may disregard this refinement and consider Eq. (41) of reference 2 as the matrix of the rectangular Ising problem (apart from a factor dropped in passing from Eqs. (4) to (8) of reference 2). Its analog for the brick lattice is obvious; it contains three rather than two types of factors, each of which represents a set of commuting plane rotations. We write the rotation represented by V_1 in the form

$$\begin{pmatrix} \cosh 2L & & & & & & -i\sinh 2L \\ & \cosh 2L & i\sinh 2L & & & & \\ & -i\sinh 2L & \cosh 2L & & & & \\ & & & \cosh 2L & i\sinh 2L & & \\ & & & -i\sinh 2L & \cosh 2L & & \\ & & & & & \ddots & \\ i\sinh 2L & & & & & & \cosh 2L \end{pmatrix}. \tag{16}$$

Similarly V_3 represents the matrix

$$\begin{pmatrix} \cosh 2L^* & i\sinh 2L^* & & & & \\ -i\sinh 2L^* & \cosh 2L^* & & & & \\ & & 1 & & & \\ & & & 1 & & \\ & & & & \cosh 2L^* & i\sinh 2L^* \\ & & & & -i\sinh 2L^* & \cosh 2L^* \\ & & & & & \ddots \end{pmatrix}. \tag{17}$$

Finally, V_4 represents the matrix

$$\begin{pmatrix} 1 & & & & & & \\ & 1 & & & & & \\ & & \cosh 2L^* & i\sinh 2L^* & & & \\ & & -i\sinh 2L^* & \cosh 2L^* & & & \\ & & & & 1 & & \\ & & & & & 1 & \\ & & & & & & \cosh 2L^* \\ & & & & & & \ddots \end{pmatrix}. \tag{18}$$

The analysis following Eq. (43) of reference 2 applies to the present case except that $f=4$. The resultant matrix

has the same form as their Eq. (50) with

$$a=\begin{bmatrix} \cosh 2L^*(\cosh^2 2L+\sinh^2 2L\cosh 2L^*) & i\sinh 2L^*(\cosh^2 2L+\sinh^2 2L\cosh 2L^*) & -\cosh 2L\sinh 2L(1+\cosh 2L^*)\sinh 2L^* & -i\cosh 2L\sinh 2L\sinh^2 2L^* \\ -i\sinh 2L^*(\cosh^2 2L+\sinh^2 2L\cosh 2L^*) & \cosh 2L^*(\cosh^2 2L+\sinh^2 2L\cosh 2L^*) & i\cosh 2L\sinh 2L(1+\cosh 2L^*)\cosh 2L^* & -\cosh 2L\sinh 2L\cosh 2L^*\sinh 2L^* \\ 0 & -i\cosh 2L\sinh 2L(1+\cosh 2L^*) & \cosh^2 2L\cosh 2L^*+\sinh^2 2L & i\cosh^2 2L\sinh 2L^* \\ 0 & -\cosh 2L\sinh 2L\sinh 2L^* & -i\cosh^2 2L\sinh 2L^* & \cosh^2 2L\cosh 2L^*+\sinh^2 2L \end{bmatrix} \tag{19}$$

$$b=\begin{bmatrix} \sinh^2 2L\sinh^2 2L^* & 0 & 0 & 0 \\ -i\sinh^2 2L\cosh 2L^*\sinh 2L^* & 0 & 0 & 0 \\ -\cosh 2L\sinh 2L\sinh 2L^* & 0 & 0 & 0 \\ i\cosh 2L\sinh 2L(1+\cosh 2L^*) & 0 & 0 & 0 \end{bmatrix} \tag{20}$$

$$c=\begin{bmatrix} 0 & i\sinh^2 2L\cosh 2L^*\sinh 2L^* & \cosh 2L\sinh 2L\cosh 2L^*\sinh 2L^* & -i\cosh 2L\sinh 2L(\cosh 2L^*+1)\cosh 2L^* \\ 0 & \sinh^2 2L\sinh^2 2L^* & i\cosh 2L\sinh 2L\sinh^2 2L^* & -\cosh 2L\sinh 2L(\cosh 2L^*+1)\sinh 2L^* \\ 0 & 0 & 0 & 0 \\ 0 & 0 & 0 & 0 \end{bmatrix}. \tag{21}$$

The secular equation of this matrix has the form

$$x^4-Ax^3+Bx^2-Ax+1=0. \tag{22}$$

The roots are therefore pairs of reciprocals and the substitution

$$x=e^{\gamma} \tag{23}$$

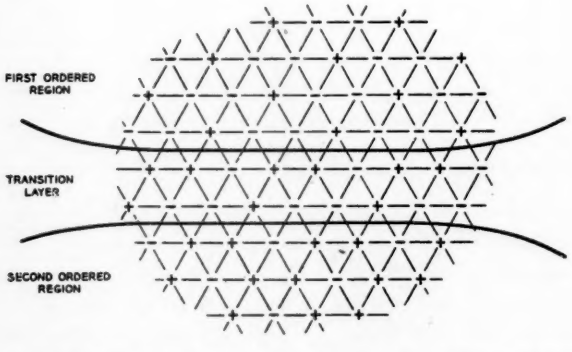

FIG. 10. Two adjoining regions having different types of long-range order. The energy of the transition layer may be made just as low as that of the ordered regions.

yields a quadratic equation in $\cosh\gamma$. This equation is

$$\cosh^2\gamma-(\kappa^{-1}-1+\cos\omega)\cosh\gamma+\tfrac{1}{4}\kappa^{-2}-\kappa^{-1}-\cos\omega=0, \tag{24}$$

where

$$\epsilon^2+\epsilon^{-2}=2\cos\omega \tag{25}$$

and

$$\kappa=(e^{4L}-1)/(e^{4L}+1)^2. \tag{26}$$

κ is a symmetric parameter similar to that defined in reference 1, Eq. (114). It is zero for high or low temperatures and reaches a maximum of $\frac{1}{8}$ at the Curie point; for antiferromagnetic interactions it is negative. In view of this symmetry, the roots of (24) are invariant with respect to temperature inversion and the only asymmetric factor entering into the partition function is the scalar factor evident in (12). We thus get the analog of reference 2, Eq. (71), as

$$f^*(L^*)=(2\sinh 2L^*)^n\Pi^{\frac{1}{2}n}_{m=1}\exp[\tfrac{1}{2}\gamma_1^{(m)}+\tfrac{1}{2}\gamma_2^{(m)}], \tag{27}$$

where γ_1 and γ_2 are the two roots of (24) with $\omega=\omega^{(m)}$ and

$$\omega^{(m)}=4\pi m/n. \tag{28}$$

The expression obtained is for two rows of n spins in the arrangement of Fig. 11; i.e., for $2n$ spins in the honeycomb. Thus $N^*=2n$, and the factor in (27) is just the asymmetric factor to be expected from (3). An inspection of Fig. 3 shows that

$$N=\tfrac{1}{2}N^*=n.$$

The expression (27) becomes thus the partition function for n triangular spins; altering factors according to (3) we arrive thus at the partition function $\lambda(L)$ per spin of the triangular net as

$$\lambda^n=(2\sinh 2L)^{n/2}\Pi^{\frac{1}{2}n}_{m=1}\exp[\tfrac{1}{2}\gamma_1{}^{(m)}+\tfrac{1}{2}\gamma_2{}^{(m)}] \quad (29)$$

or, passing to the limit of infinite n and using Eq. (28), we find

$$\ln\lambda=\tfrac{1}{2}\ln(2\sinh 2L)+\frac{1}{8\pi}\int_0^{2\pi}[\gamma_1(\omega)+\gamma_2(\omega)]d\omega. \quad (30)$$

We use the solution of (24) in the form

$$\cosh\tfrac{1}{2}\gamma=\tfrac{1}{2}[\kappa^{-1}+\cos^2\tfrac{1}{2}\omega]^{\frac{1}{2}}\pm\tfrac{1}{2}\cos\tfrac{1}{2}\omega. \quad (31)$$

This gives

$$\ln\lambda=\frac{1}{2}\ln(2\sinh 2L)+\frac{1}{4\pi}\int_0^{2\pi}\operatorname{arc\,cosh}\left[\frac{1}{2}\left(\frac{1}{\kappa}+\cos^2\frac{1}{2}\omega\right)^{\frac{1}{2}}+\frac{1}{2}\cos\frac{1}{2}\omega\right]d\omega+\frac{1}{4\pi}\int_0^{2\pi}\operatorname{arc\,cosh}\left[\frac{1}{2}\left(\frac{1}{\kappa}+\cos^2\frac{1}{2}\omega\right)^{\frac{1}{2}}-\frac{1}{2}\cos\frac{1}{2}\omega\right]d\omega.$$

We apply the identity (107) of reference 1 to the integrals and observe that the sign of the cos term occurring there is immaterial; thus we get

$$\ln\lambda=\frac{1}{2}\ln(2\sinh 2L)+\frac{1}{8\pi^2}\int_0^{2\pi}\int_0^{2\pi}\ln\left[\left(\frac{1}{\kappa}+\cos^2\frac{1}{2}\omega\right)^{\frac{1}{2}}+\cos\frac{1}{2}\omega-2\cos\omega'\right]d\omega d\omega'+\frac{1}{8\pi^2}\int_0^{2\pi}\int_0^{2\pi}\ln\left[\left(\frac{1}{\kappa}+\cos^2\frac{1}{2}\omega\right)^{\frac{1}{2}}-\cos\frac{1}{2}\omega+2\cos\omega'\right]d\omega d\omega'.$$

Combining the integrals and using (26) we reduce this

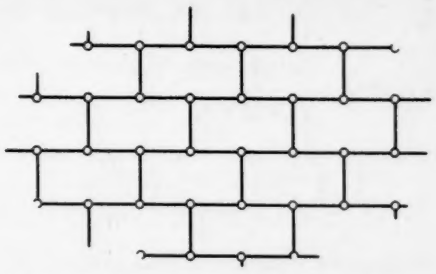

FIG. 11. The "brick" net. When all interactions are taken to be equal the net is equivalent to the "honeycomb" of Fig. 3. However, it suggests a way of applying the method of Kaufman and Onsager which is basically rectangular.

to the form

$$\ln\lambda=\ln(e^{3L}+e^{-L})+\frac{1}{8\pi^2}\int_0^{2\pi}\int_0^{2\pi}\ln[1+4\kappa\cos\omega\cos\omega'-4\kappa\cos^2\omega']d\omega d\omega'. \quad (32)$$

Employing the substitution

$$\omega'=\tfrac{1}{2}(\omega_1+\omega_2),\quad \omega=\tfrac{1}{2}(\omega_1-\omega_2),$$

we obtain

$$\ln\lambda=\ln(e^{3L}+e^{-L})+\frac{1}{8\pi^2}\int_0^{2\pi}\int_0^{2\pi}\ln[1-2\kappa+2\kappa\cos\omega_1+2\kappa\cos\omega_2+2\kappa\cos(\pi-\omega_1-\omega_2)]d\omega_1 d\omega_2. \quad (33)$$

The form (33) is of the type first suspected by Kac and Berlin.[12] The number of cos terms equals the number of linkages and the number of integrations equals the number of dimensions.

Applying formula (8) to Eq. (32), we find for the

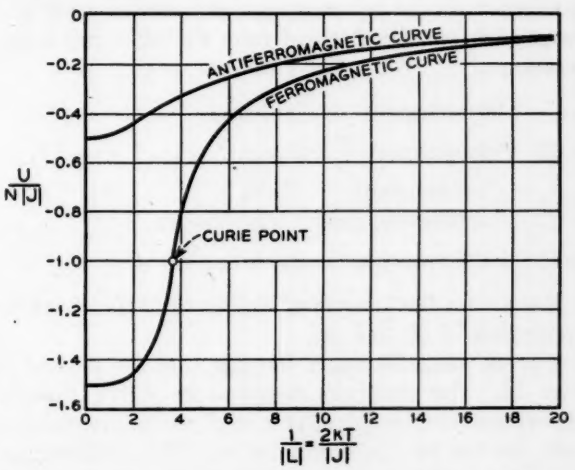

FIG. 12. Energy-*vs.*-temperature plot for the triangular Ising net. Ferromagnetic and antiferromagnetic coupling.

[12] M. Kac and T. Berlin (private communication).

energy U

$$\frac{U}{-\frac{1}{2}NJ}=\coth 2L-\frac{2e^{4L}(3-e^{4L})}{\pi(e^{4L}+1)^3\kappa}\cdot\int_{-1}^{+1}\frac{dx}{[(1-x^2)((1-2\kappa)^2-4\kappa x-4\kappa^2x^2)]^{\frac{1}{2}}}.$$

The integral is a complete elliptic integral of the first kind. Because of Landen's identity, its reduction to the standard integral $K(k)$ is not a complete determinate process. The most convenient reduction happens to differ from the one found in handbooks. It is

$$\int_\gamma^\beta\frac{dx}{[(\alpha-x)(\beta-x)(x-\gamma)(x-\delta)]^{\frac{1}{2}}}=\frac{2K\left\{\frac{[(\alpha-\gamma)(\beta-\delta)]^{\frac{1}{2}}-[(\alpha-\beta)(\gamma-\delta)]^{\frac{1}{2}}}{[(\alpha-\gamma)(\beta-\delta)]^{\frac{1}{2}}+[(\alpha-\beta)(\gamma-\delta)]^{\frac{1}{2}}}\right\}}{[(\alpha-\gamma)(\beta-\delta)]^{\frac{1}{2}}+[(\alpha-\beta)(\gamma-\delta)]^{\frac{1}{2}}}.$$

This gives in our case

$$\frac{U}{-\frac{1}{2}NJ}=\frac{2}{1-\mu}\left\{1-\frac{\mu(3-\mu)}{1+|\mu|}\frac{(2/\pi)K(k)}{[1+\frac{1}{4}(1-|\mu|)^2]^{\frac{1}{2}}}\right\}\quad(34)$$

where

$$k=\frac{1-|\mu|}{1+|\mu|}\left\{\frac{1+\frac{1}{4}(1+|\mu|)^2}{1+\frac{1}{4}(1-|\mu|)^2}\right\}^{\frac{1}{2}},\quad(35)$$

and

$$\mu=1-2\tanh 2L.\quad(36)$$

The parameter μ defined here is a very convenient one with which to express the results. It is not itself invariant against temperature inversion, but its square is, as may be seen from (4c). When μ varies from -1 to $+3$ it covers both the ferromagnetic and antiferromagnetic range; this can be observed from the following juxtaposition

$\mu=-1$ ferromagnetic absolute zero, $U=-\frac{3}{2}NJ$,

$\mu=0$ ferromagnetic Curie point, $U=-NJ$,

$\mu=1$ {ferromagnetic / antiferromagnetic} high temperature, $U=0$,

$\mu=3$ antiferromagnetic absolute zero, $U=-\frac{1}{2}N|J|$.

Results for the honeycomb follow from the above by application of (2) and (9).

Curves which illustrate formula (34) are plotted in Fig. 12. The energy-*vs.*-temperature curve for the ferromagnetic triangular net is in all essentials identical with the one for the square lattice. The antiferromagnetic one is new. It shows no singular point. The value of U at the absolute zero is only one-third of the ferromagnetic value.

To obtain the entropy at absolute zero, we return to Eq. (32) and set $\kappa=-1$, $L\to-\infty$. We get

$$\ln\lambda\cong|L|+\frac{1}{8\pi^2}\int_0^{2\pi}\int_0^{2\pi}\ln[1-4\cos\omega\cos\omega'+4\cos^2\omega']d\omega d\omega'.$$

Remembering that

$$\lambda=e^{-U/RT}e^{+S/R},$$

we see that the first term just re-establishes the energy value (11):

$$-U(0)/RT=|L|=|J|/2kT.$$

The second term is therefore the entropy

$$S(0)=\frac{R}{8\pi^2}\int_0^{2\pi}\int_0^{2\pi}\ln[1-4\cos\omega\cos\omega'+4\cos^2\omega']d\omega d\omega'.$$

The integral over ω can be found in tables.[13] It equals

$$4\pi\ln 12\cos\omega'1[1-D(2\cos\omega')]$$

where D is the Dirichlet function, $D(x)=1$ if $|x|<1$, $D(x)=0$ if $|x|>1$. Thus we get for the zero-point entropy

$$S(0)=\frac{2R}{\pi}\int_0^{\pi/3}\ln(2\cos\omega')d\omega'.\quad(37a)$$

The integral must be computed by numerical methods. By elementary considerations we can get the alternate expression

$$\frac{S(0)}{R}=\frac{3}{\pi}\int_0^{\pi/6}\ln(2\cos\omega)d\omega.\quad(37b)$$

The small interval suggests a power series in ω. We get from it

$$\frac{S(0)}{R}=\frac{1}{2}\ln 2-\frac{1}{12}\left(\frac{\pi}{6}\right)^2-\frac{1}{120}\left(\frac{\pi}{6}\right)^4-\frac{1}{630}\left(\frac{\pi}{6}\right)^6-\frac{17}{45360}\left(\frac{\pi}{6}\right)^8-\cdots=0.338314\quad(37c)$$

in agreement with the inequality (11).

In conclusion the author wishes to express his thanks to his colleagues of the Bell Laboratories, particularly Dr. C. Kittel who first brought antiferromagnetism to his attention, and to Dr. P. W. Anderson and Dr. William Shockley who made the contributions mentioned in the text.

[13] Bierens de Hahn, *Nouvelles Tables d'Integrales Definies*, Table 330, integral 5.

Magnetoresistance of Germanium Samples between 20° and 300°K*

I. ESTERMANN AND A. FONER†
Department of Physics, Carnegie Institute of Technology, Pittsburgh, Pennsylvania

(Received April 6, 1950)

The resistivity of "pure" germanium samples and of samples with small additions of aluminum, antimony, and indium was measured at various temperatures and at various orientations in external magnetic fields. The samples chosen had sufficiently low carrier densities to remain within the limits of classical statistics. The results were compared with those following from the theoretical investigation of a classical electron gas in combined electric and magnetic fields in an isotropic medium and in a medium possessing cubic symmetry. In the transverse orientation, the relative change of the electrical conductivity was found to be proportional to the square of the magnetic field strength at low fields. The effect tends to become linear as the field strength increases. The magnitude of the effect was found to increase with the purity of the material. In the longitudinal orientation, the change of conductivity is of the expected order of magnitude in p-type samples, but is much larger than the theoretical results indicate in n-type samples. The angular dependence of the effect is as expected. Carrier mobilities calculated from magnetoresistance measurements in pure samples agree reasonably well with those calculated from Hall effect and conductivity of single crystals. In the case of samples with additions, there is fair agreement between the values of mobilities calculated from measurements of magnetoresistance and of the Hall effect on the same samples.

I. INTRODUCTION

IT has been pointed out by several authors that the theoretical treatment of the effect of magnetic fields on the electrical resistance of conductors involves considerable difficulties.[1,2] It has also been pointed out that these difficulties are much more easily resolved in the case of semiconductors than for metals. This is due to the fact that the concentration of the free electrons in electronic semiconductors may be so low that the electron gas is no longer degenerate as it is in metals, but obeys Maxwell-Boltzmann statistics.[3] It therefore seems to be of interest to compare the results of the theory of the magnetoresistance of semiconductors based on the classical theory of electric conductance with experimental measurements.

II. THEORETICAL DISCUSSION

The first theoretical investigation of the behavior of a classical electron gas in combined electric and magnetic fields is due to Gans.[4] He considered the electron gas in an isotropic medium, and carried the solution to terms in the current which depend on the first power of the electric field strength and on arbitrary powers of the magnetic field strength. He obtained a solution in closed form for the transverse Hall effect and for the conductivity as functions of the magnetic field. These calculations have been extended by Harding, Sengupta, and Davis[5] to include the case of an anisotropic medium. Equations in a closed form have recently been obtained by Seitz[6] for a system possessing cubic symmetry. They include quadratic terms in the dependence of the conductivity on the magnetic field, but neglect higher terms. Within the limits of this approximation, and neglecting the anisotropic terms, Seitz' work leads to the following vector equation for the current density $\mathbf{I}$

$$\mathbf{I}=\sigma_0\mathbf{E}+\alpha\mathbf{E}\times\mathbf{H}+\beta\mathbf{E}H^2+\gamma\mathbf{H}(\mathbf{E}\cdot\mathbf{H}), \qquad (2.1)$$

where $\mathbf{E}$ and $\mathbf{H}$ are the electric and magnetic fields, σ_0 is the conductivity in the absence of a magnetic field, α is the Hall coefficient, and β and γ are constants of the material.

We shall now discuss the effect of the relative orientation of $\mathbf{E}$ and $\mathbf{H}$ on the resistivity.

For the longitudinal position, in which $\mathbf{E}$ is parallel to $\mathbf{H}$, the vector equation (2.1) reduces to

$$I_x=[\sigma_0+(\beta+\gamma)H^2]E_x. \qquad (2.2)$$

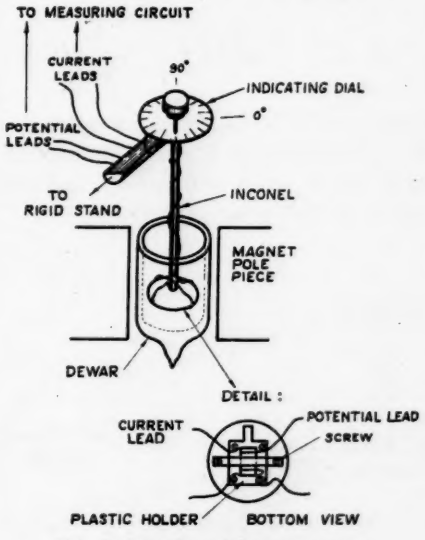

FIG. 1. Experimental arrangement.

* Assisted by the ONR. Results were presented at the Chicago Meeting of the American Physical Society, November, 1949; Phys. Rev. 77, 759 (1950).

† Abstract of thesis submitted by Anna Foner in partial fulfillment of the requirements for the degree of Doctor of Science at Carnegie Institute of Technology.

[1] J. W. Harding, Proc. Roy. Soc. 140, 205 (1933).
[2] M. Sengupta, Ind. J. Phys. 11, 319 (1937).
[3] A. H. Wilson, Proc. Roy. Soc. 133, 458 and 134, 277 (1931).
[4] R. Gans, Ann. d. Physik 20, 293 (1906).
[5] L. Davis, Phys. Rev. 56, 93 (1939); see also A. Sommerfeld and N. H. Frank, Rev. Mod. Phys. 3, 1 (1931); and A. Sommerfeld and H. A. Bethe, *Handbuch der Physik* (1934), Vol. 24, p. 2.
[6] F. Seitz, Phys. Rev. 79, 372 (1950), following paper.

TABLE I. Characteristic properties of the germanium samples.

T °K	ohm-cm	Hall const. cm³/coulomb	n carrier/cm³
	Sample 35P, p-type, 0.006 atomic percent Al added		
300	0.032	26	2.8×10^{17}
77	0.027	40	1.8×10^{17}
20	0.064	13.1	5.6×10^{17}
	Sample 501, p-type, 0.001 atomic percent In added		
292	0.063	69	1.07×10^{17}
77	0.043	100	7.37×10^{16}
20	0.212	86	8.6×10^{16}
	Sample 33E, n-type, 0.04 atomic percent Sb added		
295	0.044	67	1.1×10^{17}
77	0.057	173	4.3×10^{16}
20	0.20	354	2.1×10^{16}
	Sample 481, n-type, no additions		
300	10.8	2.6×10^{4}	2.8×10^{14}
77	2.42	3.5×10^{4}	2.1×10^{14}
20	8.1	8.3×10^{4}	8.4×10^{14}
	Sample 491, n-type, no addition, apparently single crystal		
295	2.4	5.5×10^{3}	1.3×10^{15}
77	0.49	6.7×10^{3}	1.06×10^{15}
20	0.72	3.3×10^{4}	2.15×10^{14}

For the transverse position ($\mathbf{E}=E_x$, $\mathbf{H}=H_z$) Eq. (2.1) yields the following pair of equations

$$I_x=\sigma_0E_x+\alpha E_yH_z+\beta E_xH^2,$$
$$0=\sigma_0E_y-\alpha E_xH_z+\beta E_yH^2. \tag{2.3}$$

Solving for E_y, we obtain

$$E_y=\alpha E_xH_z/(\sigma_0+\beta H^2),$$

and

$$I_x=[\sigma_0+\alpha^2H^2/(\sigma_0+\beta H^2)+\beta H^2]E_x, \tag{2.4}$$

and, neglecting terms with a higher power of H than the second we get

$$I_x=\left[\sigma_0+\left(\frac{\alpha^2}{\sigma_0}+\beta\right)H^2\right]E_x$$
$$=\sigma_0\left[1+\left(\frac{\alpha^2}{\sigma_0^2}+\frac{\beta}{\sigma_0}\right)H^2\right]E_x. \tag{2.5}$$

The parameters α, β, γ, and σ_0 for an isotropic medium under the assumptions of Maxwell-Boltzmann energy distribution and a mean free path λ independent of velocity have the following values:

$$\sigma_0=ne\mu, \tag{2.6}$$

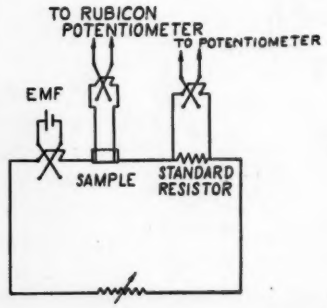

FIG. 2. Measuring circuit.

$$\alpha=-3\pi ne\mu^2/8c=-3\pi\mu\sigma_0/8c, \tag{2.7}$$

$$\beta=-9\pi\mu^3ne/16c^2=-9\pi\mu^2\sigma_0/16c^2, \tag{2.8}$$

$$\gamma=-\beta, \tag{2.9}$$

where n is the number of conducting particles (electrons or holes) per cm³, e their charge, c the velocity of light, and μ the mobility in electrostatic units defined by

$$\mu=(8e\lambda/3\pi m\bar{v}). \tag{2.10}$$

Here m is the effective mass, and $\bar{v}$ is the average velocity of the conduction electrons,

$$\bar{v}=4(kT/2\pi m)^{\frac{1}{2}}. \tag{2.11}$$

From these equations, we obtain for the conductivity σ_H in a magnetic field H for the longitudinal orientation

$$\sigma_H{}^l=(I_z/E_z)^l=\sigma_0, \tag{2.12}$$

and in the transverse orientation

$$\sigma_H{}^t=(I_z/E_z)^t=\sigma_0[1-(9\pi\mu^2/16c^2)(1-\tfrac{1}{4}\pi)]H^2. \tag{2.13}$$

For orientations other than those discussed above, σ_H will also be a function of the angle θ between $\mathbf{I}$ and $\mathbf{H}$. From Eq. (2.1) we obtain

$$\sigma_H=\sigma_0\left[1+\left(\frac{\beta}{\sigma_0}+\frac{\gamma\cos^2\theta}{\sigma_0}+\frac{\alpha^2\sin^2\theta}{\sigma_0^2}\right)H^2\right]$$
$$=\sigma_0\left[1=\left(\frac{9\pi\mu^2}{16c^2}(1-\tfrac{1}{4}\pi)H^2\sin^2\theta\right)\right] \tag{2.14}$$

or

$$(\sigma_0-\sigma_H)/\sigma_0=(9\pi\mu^2/16c^2)(1-\tfrac{1}{4}\pi)H^2\sin^2\theta. \tag{2.15}$$

For an anisotropic system possessing cubic symmetry, Seitz chooses a Cartesian coordinate system with axes x, y, z coinciding with the axes of the crystal. Equation (2.1) has then to be replaced by the three component equations

$$\left.\begin{aligned} I_x&=\sigma_0E_x+\alpha(E_yH_z-E_zH_y)+\beta E_xH^2\\ &\quad+\gamma H_x(\mathbf{E}\cdot\mathbf{H})+\delta E_xH_x^2,\\ I_y&=\sigma_0E_y+\alpha(E_zH_x-E_xH_z)+\beta E_yH^2\\ &\quad+\gamma H_y(\mathbf{E}\cdot\mathbf{H})+\delta E_yH_y^2,\\ I_z&=\sigma_0E_z+\alpha(E_xH_y-E_yH_x)+\beta E_zH^2\\ &\quad+\gamma H_z(\mathbf{E}\cdot\mathbf{H})+\delta E_zH_z^2,\end{aligned}\right\} \tag{2.16}$$

where δ accounts for the anisotropic terms, vanishing for an isotropic medium. For the longitudinal position, this results in

$$I_x=[\sigma_0+(\beta+\gamma+\delta)H^2]E_x, \tag{2.17}$$

or

$$\sigma_H{}^l-\sigma_0=(\beta+\gamma+\delta)H^2. \tag{2.18}$$

The most pertinent results of the theory are that for the isotropic case, there is no change in the conductivity if $\mathbf{I}\parallel\mathbf{H}$, and that if the angle between $\mathbf{I}$ and $\mathbf{H}$ is θ, the relative change in conductivity is proportional to $H^2\sin^2\theta$, as long as higher terms in H are neglected. For

a cubic system, there is also a change of couductivity proportional to H^2 for the longitudinal case, as shown in Eq. (2.18).

III. SURVEY OF PREVIOUS EXPERIMENTS

Most of the measurements of magnetoresistance reported in the literature[7] were carried out with metals, and are, therefore, outside the range of the assumptions in the preceding paragraphs. Kapitza's measurements on semiconductors are restricted to germanium, silicon, tellurium, and graphite. It appears that germanium should be a good system for the test of the theory, since it is a typical electronic semiconductor with a cubic lattice. The results obtained by Kapitza with germanium are very similar to those obtained with metals (except bismuth, which shows a much larger effect[8]). At low fields, the relative change of resistance $\Delta R/R_0$ obeys a quadratic law, and at high fields, the dependence on H is linear. Kapitza defines a "critical field" H_K at which the quadratic law changes into the linear law; it is about 45 kilogauss at room temperature and 55 kilogauss at liquid nitrogen temperature. The highest values of $\Delta R/R_0$ observed at a magnetic field of 300 kilogauss were 0.5 at room temperature and 1.28 at liquid nitrogen temperature. All measurements were taken for $\mathbf{E} \perp \mathbf{H}$.

A closer investigation of the data supplied by Kapitza shows, however, that the germanium samples which he used cannot be treated as semiconductors in which the electron gas obeys Maxwell-Boltzmann statistics. The resistivity of his material was 2.6×10^{-3}

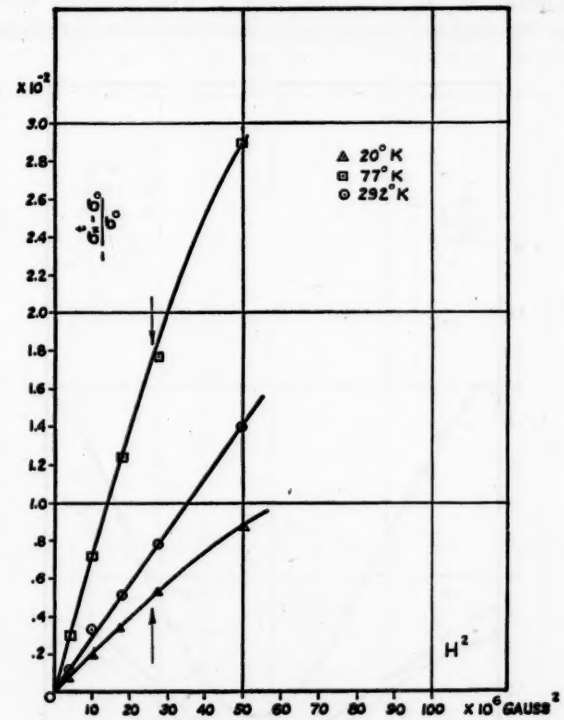

FIG. 3. Relative change of conductivity *vs.* H^2, transverse orientation, sample 501.

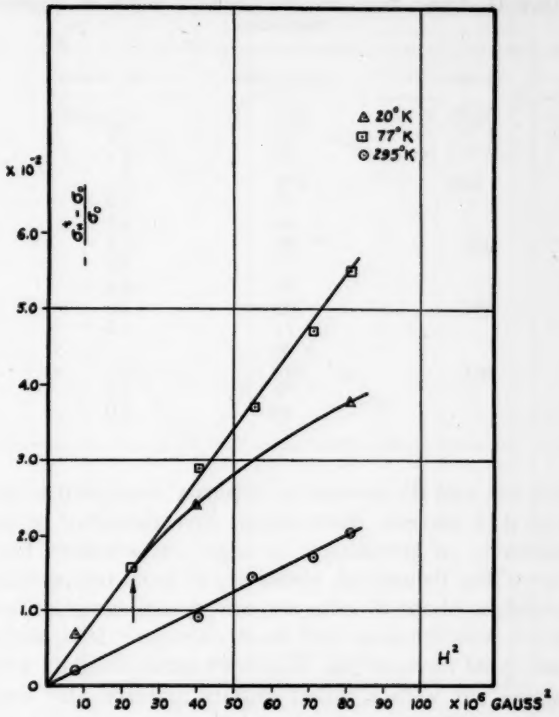

FIG. 4. Relative change of conductivity *vs.* H^2, transverse orientation, sample 33E.

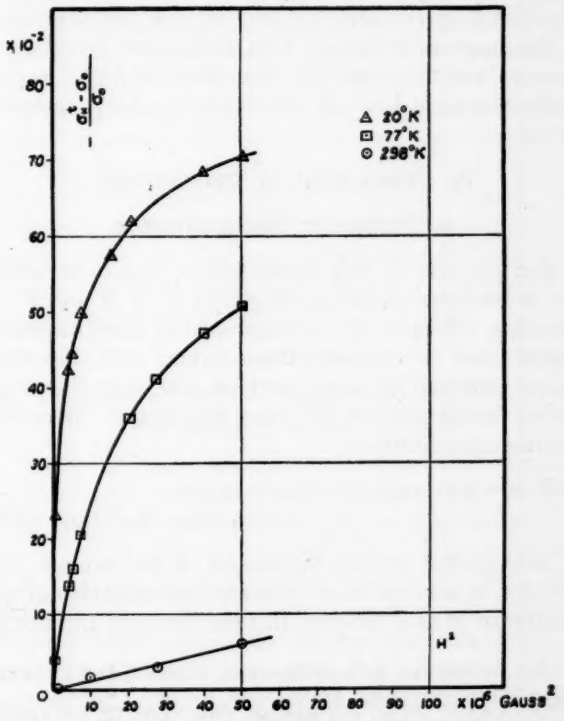

FIG. 5. Relative change of conductivity *vs.* H^2, transverse orientation, sample 481.

[7] P. Kapitza, Proc. Roy. Soc. **123**, 292 (1929). A bibliography of the earlier literature is given in this reference.
[8] P. Kapitza, Proc. Roy. Soc. **119**, 387 (1928).

TABLE II. Upper limits for the quadratic region of magneto-resistance.

Sample	Temp. (°K)	H_K (Gauss)
35P	301	8.5×10^3
	77	9.0
	20	4.5
33E	295	9.0
	77	9.0
	20	4.7
481	298	7.0
	77	1.6
	20	0.85
491	295	7.0
	77	1.4
	20	
501	292	7.0
	77	5.0
	20	5.0

ohm-cm, and the amount of impurity was given as less than 0.01 percent. More recent investigations[9] of the resistivity of germanium at high temperatures have shown that its intrinsic resistivity at room temperature should be about 60 ohm-cm, and actual samples have shown resistivities as high as 30 ohm-cm.[10] It is, therefore, quite obvious that Kapitza's measurements were carried out with a rather impure material. By comparison with other samples of similar resistivity, for which the Hall effect has been measured, one can conclude that the electron gas in Kapitza's samples had a density of about 3×10^{18} electrons per cm^3, and consequently a degeneracy temperature of $\sim$120°K, which means that even at room temperature the assumption of classical statistics is not too good. In view of this situation it was decided to carry out new measurements of the magneto-resistance with much purer germanium samples, and to include the dependence of $\Delta R/R$ on the angle θ between **I** and **H**, which had not been reported before.

IV. EXPERIMENTAL PROCEDURE

A. Method of Measurements

The purpose of this investigation was to measure the dependence of the conductivity σ on H and θ, to calculate values of the mobility μ from these measurements, and to compare these values with mobility values obtained by other methods and with the theoretical results given in the preceding section. Since the interesting quantity Q,

$$Q(H,\theta)=(\sigma_0-\sigma_H)/\sigma_0=-(\rho_H-\rho_0)/\rho_H$$
$$=-(R_H-R_0)/R_H, \quad (4.1)$$

is independent of the dimensions of the sample, the problem is reduced to an accurate determination of the resistance R as a function of field strength and angle.

[9] See, for instance, K. Lark-Horovitz, Report N.D.R.C.-14-585 (March, 1942–November, 1945).

[10] Estermann, Foner, and Randall, Phys. Rev. **72**, 530 (1947); G. L. Pearson, Phys. Rev. **76**, 179 (1949); K. Lark-Horovitz, reference 9.

Within the region of validity of the quadratic approximation in H, the magnetic fields are rather small and the quantity Q is frequently less than one percent. The dependence of Q on the angle θ is even smaller. Consequently, the resistance measurements had to be carried out with extreme care. Since the resistivity of the germanium samples is strongly temperature-dependent, small variations of the temperature of the samples may obscure the effect of the variation of the angle θ completely. Consequently, the measurements were carried out only at temperatures where good temperature baths were available. These baths were contained in a special Dewar vessel and consisted of a kerosene bath for room temperature, and baths of liquefied methane, nitrogen, and hydrogen boiling at constant pressure for the other temperatures.

Measurements were made in magnetic fields from 260 to 9300 gauss and through a total angle of 240°, usually in steps of 15° or 30° with check points at 0° (longitudinal position) and 90° (transverse position). In some instances experiments at certain temperatures were repeated on different days, and the reproducibility was always very good. Figure 1 shows the experimental arrangement for mounting and turning the sample in a Dewar vessel in the magnetic field.

The resistance measurements were made by measuring the potential drops through the sample and through a standard resistance in series with the sample with a Rubicon Model B potentiometer. The samples were thin rectangular parallelopipeds with current electrodes

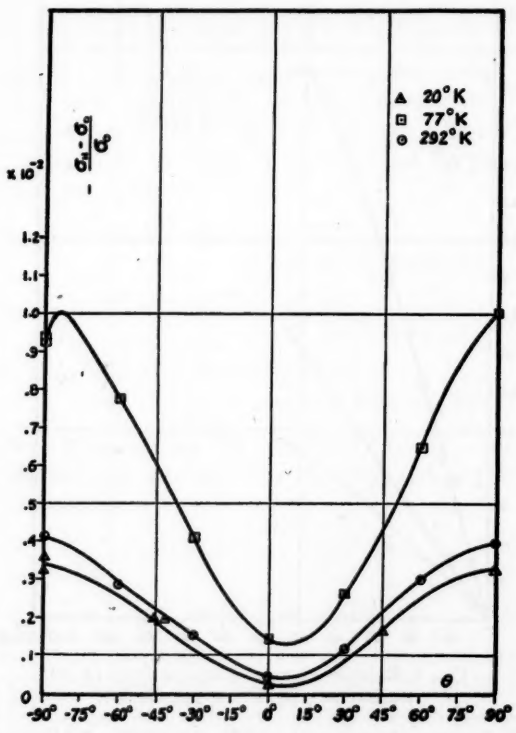

FIG. 6. Relative change of conductivity as function of orientation, sample 501, $H=3900$ gauss. 0° is longitudinal orientation.

attached to the end surfaces and potential electrodes to the top surface. The long dimension of the rectangles was taken as the direction of the applied electric field (x direction), and the sample was rotated about a vertical axis (y direction) between the pole pieces of an electromagnet. The field of the magnet was calibrated against a standard solenoid. The circuit is shown schematically in Fig. 2.

In some germanium samples, particularly at very low temperatures, it was found that the current was not proportional to the applied voltage even in the absence of a magnetic field. In all the measurements used below, it was made certain that Ohm's law was obeyed, which means that the current was proportional to the applied electromotive force.

Each measurement of the resistance at a given angle θ required six potential measurements across the potential probes for a given constant current and magnetic field. These were two potential drop measurements in zero field with current in forward and reversed directions, two similar measurements with the magnetic field on in one direction, and two with the magnetic field reversed.

The dependence of Q as function of H was obtained from a similar set of six potential measurements, but with θ always 90°, that is with the sample in the transverse orientation.

B. Choice of Samples

The applicability of the Maxwell-Boltzmann statistics to the electron gas in a semiconductor depends on the density of the conducting particles. Previous work has shown that below room temperature this density is determined even in the purest samples by the number of impurity centers. The electron density (or hole density) in all samples was determined from Hall effect measurements over the whole temperature range concerned. Only those for which the Fermi energy was small compared to kT at all temperatures and for which, therefore, Maxwell-Boltzmann statistics is applicable, are considered in the following sections. Their important characteristics are given in Table I. The samples include "pure" material from different sources, and n- and p-type material with small additions of Al, In, and Sb, all of which remained non-degenerate at all temperatures, except where otherwise noted.

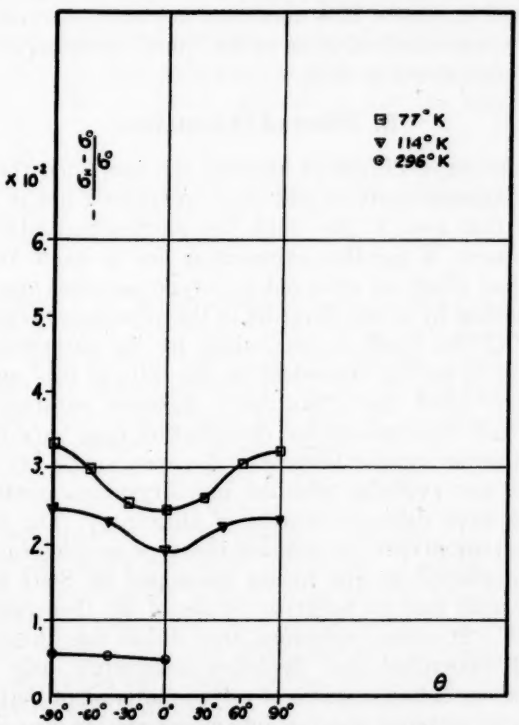

FIG. 7. Relative change of conductivity as function of orientation, sample 33E, $H=4700$ gauss.

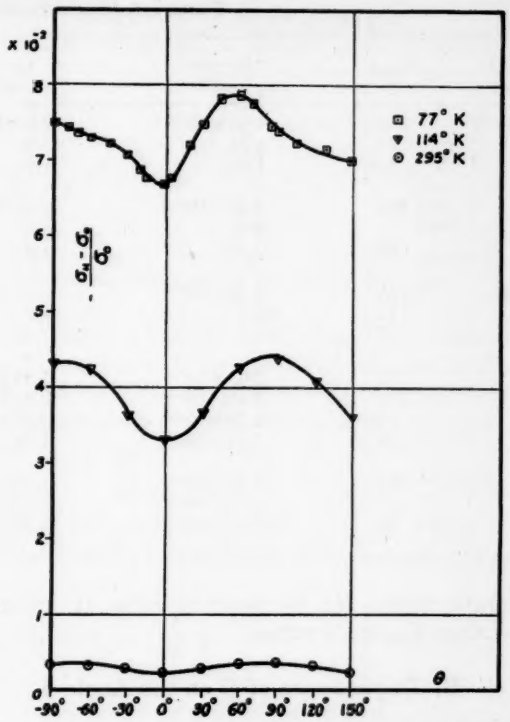

FIG. 8. Relative change of conductivity as function of orientation, sample 481, $H=1280$ gauss.

V. RESULTS

A. Dependence of the Electrical Conductivity on the Magnetic Field Strength

For these measurements the samples were mounted in the transverse orientation. As the results given in Figs. 3–5 show, the relative change of the conductivity $\Delta\sigma/\sigma_0$ at low fields is proportional to H^2, changing into a more nearly linear dependence at higher fields. This behavior is in general agreement with Kapitza's observations. The magnitude of the observed effect is, however, quite different, and varies from sample to sample with the purity of the sample. In all cases, $\Delta\sigma/\sigma_0$ is much larger than the values reported by Kapitza. On the other hand, the upper limits of the

TABLE III. Mobilities calculated by various methods.

Sample	Temp. °K	$\frac{\sigma_0-\sigma H^2}{\sigma_0 H^2}$	$\frac{\sigma_0-\sigma H^4}{\sigma_0 H^2}$	Mobility, μ, in cm²/volt-sec. from Eq. (6.1)	Eq. (6.4)	Eq. (6.5)	Eq. (6.6)
35P	292	1.64×10^{-10}	2.0×10^{-11}	2.07×10^{3}	1.9×10^{3}	0.69×10^{3}	0.91×10^{3}
	77	3.74	3.8	3.12	2.9	1.16	0.74
	20	1.28	7.9	1.83	1.1	0.21	
501	292	2.84×10^{-10}	2.6×10^{-11}	2.72×10^{3}	2.6×10^{3}	0.92×10^{3}	1.7×10^{3}
	77	6.78	8.6	4.20	3.9	2.00	1.7
	20	2.16	1.3	2.38	2.3	0.34	1.8
33E	296	2.36×10^{-10}	2.2×10^{-10}	2.49×10^{3}	0.604×10^{3}	1.23×10^{3}	
	114	11.1	8.7	5.39	2.51		
	77	14.7	11.2	6.20	3.02	2.61	
481	295	2.05×10^{-9}	1.39×10^{-9}	7.32×10^{3}	4.15×10^{3}	1.64×10^{3}	
	114	2.64×10^{-8}	2.01×10^{-8}	26.3	12.81	7.12	
	77	4.78×10^{-8}	4.07×10^{-8}	35.3	13.5	11.8	
	20	1.19×10^{-6}	1.04×10^{-6}	176.1	62.6		
491	295	2.48×10^{-8}	1.54×10^{-9}	8.05×10^{3}	5.37×10^{3}	1.78×10^{3}	
	77	4.74×10^{-8}	3.58×10^{-8}	35.2	17.2	11.4	
	20	4.84×10^{-7}	4.26×10^{-7}	111.2	42.1	40.6	

quadratic region, H_K, as shown in Table II, are much lower than Kapitza's values.

B. Dependence of Q on the Angle θ

In order to remain within the region of validity of the quadratic approximation in H, these measurements were carried out at fields $H<H_K$. Typical results are plotted in Figs. 6–8, and show a periodic change of Q with θ, depending in magnitude on the character of the sample and on the temperature.

VI. DISCUSSION OF THE RESULTS

A. General Observations

Within the region of the validity of the quadratic dependence of Q on H and the assumption of isotropy, the magnitude of $(Q/H^2)^{\frac{1}{2}}$ should be proportional to the square of the carrier mobility, μ^2. At high temperatures, this mobility is determined principally by the lattice vibrations and is, therefore, about the same for all relatively pure germanium samples. At lower temperatures, even room temperature, the mobility is in part determined by impurity scattering,[11] and at very low temperatures the impurity scattering becomes the predominant factor. In this temperature region, therefore, the effect should vary widely from sample to sample, and should have its largest magnitude in the case of the purest samples. Since the lattice scattering decreases with decreasing temperature, the mobility and the magneto-resistance should increase as the temperature is lowered, until the impurity scattering becomes dominant. We shall, therefore, expect $\Delta\sigma/\sigma_0$ to have a maximum at a certain temperature, this maximum shifting to lower temperatures as the purity of the sample increases. This maximum has been observed in the p-type samples, while in the "pure" samples, $\Delta\sigma/\sigma_0$ increases down to 20°K.

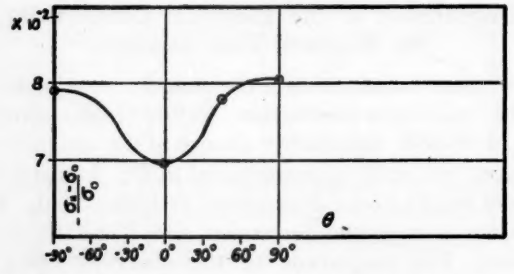

FIG. 9. Relative change of conductivity as function of orientation, sample 481, $H=260$ gauss, $T=20$°K.

[11] E. Conwell and V. F. Weisskopf, Phys. Rev. **77**, 388 (1950). (Earlier references are given in this paper.)

B. Effect of Orientation

The major difference between the simplified theory for isotropic systems and the experiments lies in the fact that even at low fields the longitudinal effect is not zero. A possible explanation for a small longitudinal effect, as observed in p-type samples, may be furnished by a consideration of the anisotropic term in Eq. (2.18), which is determined by the parameter δ, which in turn is dependent on the ratio of the "anisotropic" and the "isotropic" collision parameters[12] $(\tau_1/\tau_0)^2$. The anisotropic contribution may vary from sample to sample because well-grown single crystals were not available and the multicrystalline material may have different degrees of anisotropy. The large longitudinal effect as observed in n-type samples, cannot be explained by the theory developed by Seitz since it would lead to negative values of μ^2. (See Section VI-C.) It seems, therefore, that either this theory is still incomplete and describes adequately only the behavior of holes, that is of p-type material, or that the n-type material was too inhomogeneous to provide a

[12] See F. Seitz, reference 6, Eq. (20e).

fair test for the theory. It is known that holes can pass much more easily through internal barriers than electrons, and consequently it may be expected that inhomogeneities are less effective in p-type than in n-type semiconductors.

C. Calculation of the Mobility

Introducing numerical values into Eq. (2.13) and changing from e.s.u. to practical units, and neglecting the anisotropic terms in Eq. (2.16), we obtain

$$\mu=1.616\times10^8\times[(\sigma_0-\sigma_H{}^t)/\sigma_0]^{\frac{1}{2}}\times H^{-1}\ \text{cm}^2/\text{volt-sec.} \quad (6.1)$$

Values for μ for the different samples and temperatures are given in Table III, column 5.

One can attempt to make a correction for the anisotropic terms by subtracting the longitudinal effect from the effect measured at other angles. This means that one considers the contribution from the anisotropic term to be independent of θ for any given value of H. The experimental curves showing Q as function of θ can actually be represented quite well by an equation of the form

$$Q=f(H)+g(H)\sin^2\theta, \quad (6.2)$$

where from Eq. (2.15)

$$g(H)=(9\pi\mu^2/16c^2)(1-\tfrac{1}{4}\pi)H^2. \quad (6.3)$$

Under this assumption, μ can be calculated from the formula

$$\mu=1.616\times10^8\times[(\sigma_H{}^l-\sigma_H{}^t)/\sigma_0]^{\frac{1}{2}}\times H^{-1}\ \text{cm}^2/\text{volt-sec.} \quad (6.4)$$

Values so calculated are given in Table III, column 6 and are, of course, somewhat smaller than those calculated from Eq. (6.1), particularly for the n-type samples.

Finally, Table III contains in column 7 values for μ calculated from the Hall constant C and the electrical conductivity σ_0 according to the equation

$$\mu=0.85\times C\times\sigma_0. \quad (6.5)$$

These values are again somewhat smaller than those calculated from Eq. (6.4), but the discrepancy is usually less than a factor of two, while previous attempts to obtain numerical values for magnetoresistance on a theoretical basis lead to an incorrect order of magnitude. Moreover, values calculated according to Eq. (6.5) are likely to be too small since the directly measured values of σ_0 may easily be influenced by internal barriers in the samples. Measurements on germanium single crystals published recently by Pearson[13] have shown larger values for electron and hole mobilities than those reported for microcrystalline material, namely 2600 and 1700 cm²/volt-sec., respectively, which are even closer to our results from magneto-resistance measurements.

[13] G. L. Pearson, Phys. Rev. **76**, 179 (1949). See also W. C. Dunlap, Jr., Phys. Rev. **77**, 759 (1950).

TABLE IV. τ_1/τ_0 for p-type samples.

Sample	Temperature °K	τ_1/τ_0
35P	292	0.24
	77	0.40
501	292	0.14
	77	0.26
	20[a]	0.10

[a] At this temperature, the sample is near the degeneracy point.

A more rigorous analysis of the anisotropic contribution in a medium of cubic symmetry can be obtained from Eq. (2.16), using the evaluation of the parameters α, β, γ, and δ given by Seitz. This analysis leads to the equation

$$\left(\frac{\sigma_0-\sigma_H{}^t}{\sigma_0H^2}\right)-\left(\frac{532}{80}\right)\left(\frac{\sigma_0-\sigma_H{}^t}{\sigma_0H^2}\right)=\frac{9\pi}{16c^2}\left(1-\frac{\pi}{4}\right)\mu^2 \quad (6.6)$$

or

$$\mu^2=2.62\times10^{16}\left(\frac{\sigma_0-\sigma_H{}^t}{\sigma_0H^2}\right)-6.65\left(\frac{\sigma_0-\sigma_H{}^l}{\sigma_0H^2}\right)(\text{cm}^3/\text{coulomb})^2$$

from which μ can be calculated. Values obtained in this way for samples 35P and 501 are also given in Table III, column 8 and agree reasonably well with those from Hall effect and conductivity, except at $T=20°$K where these samples are near the degeneracy temperature. It is obvious that Eq. (6.6) will lead to negative values for

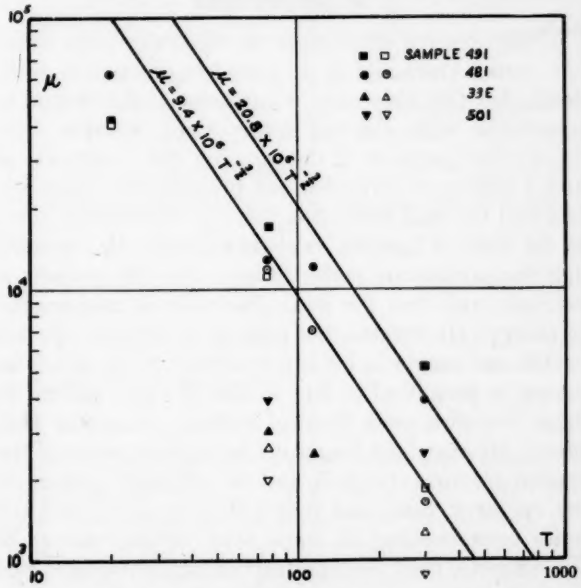

FIG. 10. Mobilities calculated from Hall effect (open symbols) and magnetoresistance according to Eq. (6.4) (filled symbols). The straight lines are adjusted to give mobilities of 1800 cm²/volt-sec. at room temperature (our Hall effect measurements on pure samples) and 4000 cm²/volt-sec. (measurements by Dunlap on n-type single crystals).

μ^2 if $(\sigma_0-\sigma_H{}^l)/\sigma_0H^2$ is larger than 6.65 $(\sigma_0-\sigma_H{}^t)/\sigma_0H^2$. This is unfortunately the case in our n-type samples. We feel, therefore, that the rather crude way of correcting for the anisotropic contribution used in Eq. (6.4) is a workable compromise and that mobility values computed in this way are at least of the right order of magnitude.

An estimate of the relative magnitude of the collision parameters τ_1 and τ_0 can also be obtained from our measurements. Using again the evaluation of β, γ, and δ given by Seitz, we obtain from Eq. (2.18)

$$\sigma_H{}^l-\sigma_0=(\beta+\gamma+\delta)H^2 = -(80/32)(\tau_1/\tau_0)^2(9\pi/16c^2)\sigma_0\mu^2H^2 \quad (6.7)$$

or

$$(\tau_1/\tau_0)^2=(\sigma_0-\sigma_H{}^l)/(\sigma_0H^2)(32/80)(16c^2)(9\pi\mu^2) = 2.26\times10^{15}(\sigma_0-\sigma_H{}^l)/(\sigma_0H^2\mu^2).$$

Values for τ_1/τ_0 computed from this equation are given in Table IV.

According to the theory of lattice scattering, the temperature dependence of the mobility should go with $T^{-\frac{3}{2}}$. As is shown in Fig. 10, this holds in the purest cases down to liquid oxygen temperature, but at lower temperatures there is a systematic deviation toward smaller mobilities due to the effect of impurity scattering. The same deviation is, of course, also present in the case of samples with added impurities where it reduces the mobility even at room temperature.

We are indebted to Professor F. Seitz for many helpful discussions of the theoretical aspects of this work. We also wish to thank Professor Lark-Horovitz for samples 35P and 33E, and the Research Corporation for a grant from which part of the equipment used in this work was purchased.

PHYSICAL REVIEW VOLUME 79, NUMBER 2 JULY 15, 1950

Note on the Theory of Resistance of a Cubic Semiconductor in a Magnetic Field

FREDERICK SEITZ
University of Illinois, Urbana, Illinois
(Received April 6, 1950)

The theory of the behavior of a classical electron gas in combined electric and magnetic fields, developed by Gans and extended by Sommerfeld and Davis, is applied to a system possessing cubic symmetry. The problem is limited to that case in which terms involving the magnetic field to higher than the second power are neglected.

I. INTRODUCTION

THE density of carriers in relatively pure semiconductors and in all photo-conductors is sufficiently low that they may be treated as if distributed in accordance with classical rather than quantum statistics. The problem of determining the resistance of such a system of carriers in the presence of a magnetic field and the Hall coefficient was first treated by Gans[1] on the basis of Lorentz' transport theory. He assumed that the carriers are perfectly free, that the medium is isotropic, and that the mean free path is independent of energy. He treated the case in which the applied electric and magnetic fields are normal and in which no current is permitted to flow in the direction normal to these two directions (case of normal transverse Hall effect). He examined his results to the first power of the applied electrostatic field and to arbitrary powers of the magnetic field, and found that he could add the series corresponding to sums over various powers of the magnetic field. Sommerfeld[2] subsequently obtained the same results more concisely by use of an appropriate assumption concerning the initial form of the distribution function in the presence of a magnetic field. Harding[3] has also applied more modern techniques to the problem and has noted an error in Gans' paper. Sengupta,[4] in turn has criticized Harding's analysis of measurements of Kapitza on germanium.

More recently Davis[5] generalized Gans' treatment of the problem for the case in which the electric and magnetic fields are arbitrarily oriented relative to one another, the electrons are not perfectly free, the medium is not necessarily isotropic, the mean free path is an arbitrary function of the wave number of the conduction electrons, and the distribution function is degenerate. Naturally, Davis' treatment is sufficiently general that the results are not given in closed form, but are expressed instead in terms of series in powers of the magnetic field, the coefficients being integrals which must be evaluated in particular cases.

We shall discuss here the solution of Davis' equations in the particular case in which the following assumptions are valid. (1) The electrons behave as if perfectly free, although their effective mass may be different from the true electron mass. (2) The collision frequency is not perfectly isotropic, but contains terms

[1] R. Gans, Ann. d. Physik **20**, 293 (1906).
[2] A. Sommerfeld and N. H. Frank, Rev. Mod. Phys. **3**, 1 (1931).
[3] J. W. Harding, Proc. Roy. Soc. **140**, 205 (1933).
[4] M. Sengupta, Ind. J. Phys. **11**, 319 (1937).
[5] L. Davis, Phys. Rev. **56**, 93 (1939).

of cubic symmetry when expressed in terms of the electron wave number. (3) For given direction of travel, the mean free path is independent of energy. (4) The electrons are distributed classically. (5) The magnetic field is sufficiently weak that only quadratic terms in the resistance need be considered. These five assumptions appear to fit fairly closely the conditions which should be met for moderately strong magnetic fields in relatively pure homogeneous n-type silicon or germanium or in a cubic photo-conductor, such as the photo-conducting diamond investigated by Maurer and Klick in which the current is carried by electrons rather than holes. It is not evident that the results should be immediately applicable to p-type semiconductors or photo-conductors since the holes are associated with a band derived from three overlapping zones and it is possible that the levels of highest energy in this band are the triply degenerate set associated with zero wave number. Of the five assumptions, the second is the most difficult to treat precisely. We shall find it convenient to make somewhat simplifying assumptions concerning the form of the deviations from isotropy.

II. PHENOMENOLOGICAL FORMULATION

We shall be interested in the approximation in which the current varies linearly with the electrostatic field, whose components are designated by E_1, E_2, and E_3 and in which it varies with magnetic field to terms quadratic in the components H_1, H_2, and H_3. This approximation is adequate for a discussion of the dependence of resistivity upon magnetic field strength to quadratic terms. Moreover, we shall deal with the case in which the material has cubic symmetry, the cubic axes being chosen coincident with a Cartesian set. The permissible form for the current vector, whose components are designated as I_1, I_2, and I_3, is

$$\begin{aligned}
I_1&=\sigma_0E_1+\alpha(E_2H_3-E_3H_2)\\
&\quad+\beta E_1H^2+\gamma H_1(\mathbf{E}\cdot\mathbf{H})+\delta E_1H_1^2\\
I_2&=\sigma_0E_2+\alpha(E_3H_1-E_1H_3)\\
&\quad+\beta E_2H^2+\gamma H_2(\mathbf{E}\cdot\mathbf{H})+\delta E_2H_2^2\\
I_3&=\sigma_0E_3+\alpha(E_1H_2-E_2H_1)\\
&\quad+\beta E_3H^2+\gamma H_3(\mathbf{E}\cdot\mathbf{H})+\delta E_3H_3^2. \qquad (1)
\end{aligned}$$

Here σ_0, α, β, γ, and δ are constants of the material being investigated. σ_0 is the electrical conductivity and α is the normal Hall coefficient in the approximation in which the current varies linearly with the magnetic field. The parameter δ would vanish in an isotropic medium. Its presence marks the only distinction between a cubic and an isotropic medium. Evidently in the isotropic case (1) may be written in the abbreviated form

$$\mathbf{I}=\sigma_0E+\alpha\mathbf{E}\times\mathbf{H}+\beta\mathbf{E}H^2+\gamma\mathbf{H}(\mathbf{E}\cdot\mathbf{H}). \qquad (2)$$

If it were desired to discuss the dependence of the Hall coefficient to terms quadratic in the magnetic field it would be necessary to add to the first of Eqs. (1) three terms of the form

$$\begin{aligned}
&\epsilon'(E_2H_3^3-E_3H_2^3)+\lambda'H_1^2(E_2H_3-E_3H_2)\\
&\qquad+\eta'H_2H_3(E_2H_2-E_3H_3). \qquad (3)
\end{aligned}$$

Symmetrically equivalent terms are to be added to the other two equations in (1). The parameters ϵ', λ', and η' satisfy the following relations in the isotropic case

$$\epsilon'=\lambda'=\eta', \qquad (4)$$

so that (3) becomes the first component of the vector

$$H^2\mathbf{E}\times\mathbf{H}. \qquad (5)$$

We shall now examine the connection between the phenomenological relations (1) and those given by Davis' treatment of the problem.

III. EVALUATION OF PHENOMENOLOGICAL COEFFICIENTS

As mentioned in Section I, Davis has generalized Gans' solution by considering a case in which the medium is anisotropic. Using Davis' notation, we shall assume that the number of electrons per unit volume whose wave vectors lie in the range (dk_1, dk_2, dk_3) is

$$(\tfrac{1}{4}\pi^3)f(k)dk_1dk_2dk_3. \qquad (6)$$

The absolute value of the wave number vector k is 2π times the reciprocal of the wave-length.

Davis obtains a solution of Boltzmann's equation in the form

$$f=f_0-\Phi(k)\partial f_0/\partial\epsilon, \qquad (7)$$

where $f_0(k)$ is the distribution function in the absence of a field (a Boltzmann distribution in the case of a non-degenerate semiconductor) and $\epsilon(k)$ is the energy of the electrons as a function of wave number. The function $\Phi(k)$, which depends upon the components of field vectors, is given by

$$\begin{aligned}
\Phi(k)&=-(e/\hbar)\{(\tau\mathbf{E}\cdot\mathrm{grad}\epsilon+(e/\hbar^2c)\tau\mathbf{H}\cdot\boldsymbol{\Omega}(\tau\mathbf{E}\cdot\mathrm{grad}\epsilon)\\
&\quad+(e/\hbar^2c)^2\tau\mathbf{H}\cdot\boldsymbol{\Omega}[\tau\mathbf{H}\cdot\boldsymbol{\Omega}(\tau\mathbf{E}\cdot\mathrm{grad}\epsilon)]+\cdots\}. \qquad (8)
\end{aligned}$$

Here τ is the collision frequency, which depends upon the wave number vector, and $\boldsymbol{\Omega}$ is the vector operator.

$$\boldsymbol{\Omega}=\mathrm{grad}\epsilon\times\mathrm{grad}. \qquad (9)$$

The solution (8) may be expressed in the operational form

$$\Phi(k)=-(e/\hbar)(1/1-0)\cdot(\tau\mathbf{E}\cdot\mathrm{grad}\epsilon), \qquad (10)$$

in which 0 is the operator

$$0=(e/\hbar^2c)\tau\mathbf{H}\cdot\boldsymbol{\Omega}. \qquad (11)$$

Gans' solution for the isotropic case was obtained by summing the series (8). The series (8) is much more difficult to sum in the anisotropic case so we shall restrict attention to the terms quadratic in the magnetic field.

The current associated with the distribution function (7) is

$$I=-(e/4\pi^3\hbar)\int\mathrm{grad}(\partial f_0/\partial\epsilon)\Phi dV, \qquad (12)$$

in which dV is an element of volume in wave number space. Although Davis investigated this integral in the anisotropic case, he did so under the assumption that the magnetic field is along one of the cubic axes. This treatment of the problem represents a relatively specialized one since it does not permit a direct determination of all of the constants in (1). It is necessary to investigate the value of the integral when the magnetic field lies off the cubic axis to obtain explicit values for all constants.

A straightforward comparison of the components of (1) with those of (12) leads to the following relationships:

$$\sigma_0=-\frac{e^2}{4\pi^3\hbar^2}\int\tau\left(\frac{\partial\epsilon}{\partial k_1}\right)^2\frac{\partial f_0}{\partial\epsilon}dV, \tag{13a}$$

$$\alpha=-\frac{e^3}{4\pi^3\hbar^4c}\int\frac{\partial\epsilon}{\partial k_1}\frac{\partial f_0}{\partial\epsilon}\tau\Omega_3\left(\tau\frac{\partial\epsilon}{\partial k_2}\right)dV, \tag{13b}$$

$$\beta=-\frac{e^4}{4\pi^3\hbar^6c^2}\int\frac{\partial\epsilon}{\partial k_1}\frac{\partial f_0}{\partial\epsilon}\tau\Omega_3\left[\tau\Omega_3\left(\tau\frac{\partial\epsilon}{\partial k_1}\right)\right]dV, \tag{13c}$$

$$\gamma=-\frac{e^4}{4\pi^3\hbar^6c^2}\int\frac{\partial\epsilon}{\partial k_1}\frac{\partial f_0}{\partial\epsilon}\tau\left\{\Omega_1\left[\tau\Omega_2\left(\tau\frac{\partial\epsilon}{\partial k_2}\right)\right]+\Omega_2\left[\tau\Omega_1\left(\tau\frac{\partial\epsilon}{\partial k_2}\right)\right]\right\}dV, \tag{13d}$$

$$\beta+\gamma+\delta=-\frac{e^4}{4\pi^3\hbar^6c^2}\int\frac{\partial\epsilon}{\partial k_3}\frac{\partial f_0}{\partial\epsilon}\tau\Omega_3\times\left[\tau\Omega_3\left(\tau\frac{\partial\epsilon}{\partial k_3}\right)\right]dV. \tag{13e}$$

Here $\Omega_i(i=1, 2, 3)$ are the three components of the vector $\boldsymbol{\Omega}$ given by Eq. (9).

The integrals corresponding to σ_0, α, β, and $\beta+\gamma+\delta$ were considered by Davis and, to within a numerical factor, are designated by the symbols I_1, I_7, I_6, and I_5, respectively.

Although (13c), (13d), and (13e) suffice to determine δ, as well as β and γ, an independent calculation was made to obtain an explicit expression for δ. This was done in the following way. If the magnetic field is taken to lie along the direction of the third axis, when the current-field relation is expressed in the form (1), the third component of current, I_3, does not contain a field-dependent term of the type $E_2H_3^2$. On the other hand, suppose that the crystal is kept fixed and the coordinate axes are rotated about the first axis through an infinitesimal angle ω so that the transformation of the wave number vector is

$$\begin{aligned}k_1'&=k_1,\\ k_2'&=k_2+\omega k_3,\\ k_3'&=-\omega k_3+k_3,\end{aligned} \tag{14}$$

in which the primed variables refer to the new coordinate axes. If the magnetic field is directed along the new 3-axis there is a term in I_3' of the type $E_2'H_3'^2$, the coefficient of which is $-\delta\omega$. Thus,

$$-\delta\omega=\frac{e^4}{4\pi^3\hbar^6c^2}\int\frac{\partial\epsilon}{\partial k_3}\frac{\partial f_0}{\partial\epsilon}\tau\Omega_3'\left[\tau\Omega_3'\left(\tau\frac{\partial\epsilon}{\partial k_2'}\right)\right]dV', \tag{15}$$

in which all functions are expressed in terms of the primed variables. The functions may be expressed in terms of the unprimed variables, however, by use of the relation

$$g(k_1'k_2'k_3')=g(k_1k_2k_3)+\omega\left(k_3\frac{\partial g}{\partial k_2}-k_2\frac{\partial g}{\partial k_3}\right). \tag{16}$$

The contribution to (15) from the terms of the type (16) that are independent of ω vanish whereas the term linear in ω gives a direct expression for δ.

In the following we shall assume that ϵ is an isotropic function of the form,

$$\epsilon=(\hbar^2k^2)/2m, \tag{17}$$

and that the collision frequency may be taken in the form

$$\tau(k)=\tau_0(k)+\tau_1(k)Y. \tag{18}$$

Here τ_0 and τ_1 are functions of the scalar value of k which have a constant ratio and Y is the fourth-order spherical harmonic having cubic symmetry

$$\begin{aligned}Y&=P_4(\cos\theta)+(\cos^4\varphi/168)P_4^4(\cos\theta)\\ &=x^4+y^4+z^4-3(x^2y^2+y^2z^2+z^2x^2)\end{aligned} \tag{19}$$

in which x, y, and z are the Cartesian coordinates of points on a unit sphere and θ and φ are the usual polar coordinates of the radius vector.

The parameters (13a) to (13e) have the values

$$\sigma_0=-\frac{e^2}{4\pi^3\hbar^2}\frac{4\pi}{3}\left(\frac{\hbar^2}{m}\right)^2\int k^2\tau_0\frac{\partial f_0}{\partial\epsilon}k^2dk, \tag{20a}$$

$$\alpha=\frac{e^3}{4\pi^3\hbar^4c}\frac{4\pi}{3}\left(\frac{\hbar^2}{m}\right)^3\int k^2\tau_0^2\frac{\partial f_0}{\partial\epsilon}k^2dk, \tag{20b}$$

$$\beta=[1+(\tau_1/\tau_0)^2(532/231)]I, \tag{20c}$$

$$\gamma=-[1+(\tau_1/\tau_0)^2(212/231)]I, \tag{20d}$$

$$\delta=-(\tau_1/\tau_0)^2(240/231)I, \tag{20e}$$

in which

$$I=\frac{e^4}{4\pi^3\hbar^6c^2}\frac{4\pi}{3}\left(\frac{\hbar^2}{m}\right)^4\int k_2\tau_0^3\frac{\partial f_0}{\partial\epsilon}k^2dk. \tag{21}$$

The value of the coefficient of (τ_1/τ_0) in β is four times smaller than the value given by Davis in the expression for his integral I_6. Since we have derived the foregoing expression for δ in two independent ways, as outlined previously, the foregoing value will be assumed to be the correct one.

If we assume that f_0 is the Maxwell-Boltzmann distribution function and that τ_0 varies inversely as the first power of the velocity, corresponding to a constant mean free path, the foregoing constants have the following values

$$\sigma_0 = ne\mu, \tag{22a}$$

$$\alpha = -ne(3\pi\mu^2)/(8c), \tag{22b}$$

$$I = ne(9\pi\mu^3)/(16c^2), \tag{22c}$$

where μ, the mobility, is

$$\mu = (8e\lambda)/(3\pi m\bar{V}) \tag{23}$$

in which λ is the mean free path and

$$\bar{V} = 4(kT/2\pi m)^{\frac{1}{2}}. \tag{24}$$

The coefficients ϵ', λ', and η' in (3) can readily be expressed in terms of integrals of the type (13). In the isotropic approximation these reduce to

$$\epsilon' = \lambda' = \eta' = -(9\pi\mu^2\alpha)/(8c^2)$$

in which α is given by (22b).

The writer is indebted to Professor Estermann (see accompanying paper) and to members of the Bell Telephone Laboratories, in particular Drs. Shockley, Pearson, and Suhl, for discussions of the topic presented here. These investigators have carried out extensive experimental and theoretical work bearing on this subject which will be published[6] in the near future.

[6] See, for example, W. Shockley, Phys. Rev. 78, 172 (1950).

PHYSICAL REVIEW VOLUME 79, NUMBER 2 JULY 15, 1950

Effect of Pressure on the Low Frequency Dielectric Constant of Ionic Crystals*

SUMNER MAYBURG
Department of Physics, University of Chicago, Chicago, Illinois
(Received February 24, 1950)

Data on the pressure dependence of the dielectric constant ϵ of MgO, LiF, NaCl, KCl and KBr at 1000 c.p.s. and room temperature are given as a function of hydrostatic pressure from 0 to 8000 bars. The dielectric constants are found to decrease with an initial slope $(\partial \ln\epsilon/\partial p)_T$ ranging from -0.32×10^{-6} bar^{-1} in the case of MgO to -1.17×10^{-6} bar^{-1} in the case of KBr. Present lattice theories are only capable of explaining these data if the inner field decreases with increasing pressure.

I. INTRODUCTION

MANY measurements have been made on the effect of hydrostatic pressures on the dielectric constant of gases and liquids, and these are reviewed in a recent article by Bridgman.[1] Previous measurements on solids have been concerned primarily with the effect of pressure on the Curie temperature of rochelle salt,[2] and of barium titanate.[3] This report presents data on a very simple class of solid dielectrics, ionic crystals, for which there is sufficient knowledge to allow a prediction concerning the pressure dependence of the low frequency dielectric constant. To the extent that this prediction is verifiable by experiment, the validity of present lattice theories can be tested.

There are large changes in the densities of gases and liquids at high pressures, and the dielectric constant is found to increase, as might be expected from the fact that the number of dipoles per unit volume increases. The density changes in ionic crystals are comparatively small, at most about 5 percent for pressures up to 10,000 bars. The dielectric properties of these solids could be influenced more by the changes in polarizabilities and inner fields under high pressures than by the changes in density. In fact, Mueller[4] has calculated the effect of pressure on the optical dielectric constant of some ionic crystals from strain optical data,[5] and, assuming the Lorentz form for the inner field, has shown that the polarizabilities of the ions decrease with increasing pressure. He finds the relative change of the

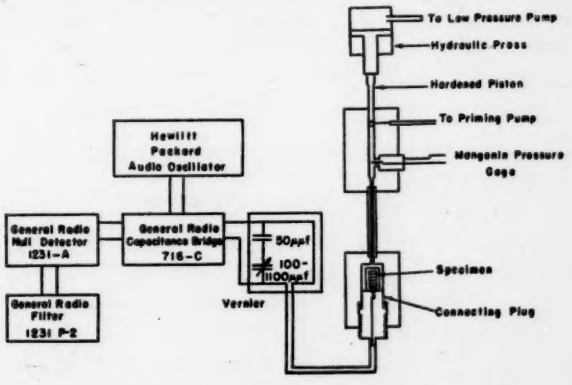

FIG. 1. Experimental set-up. Schematic diagram of high pressure system and electrical apparatus.

* The experiment was carried out in the High Pressure Laboratory of the Institute for the Study of Metals and was supported in part by funds made available under contract N-6ori-20-XX between the ONR and the University of Chicago.

[1] P. W. Bridgman, Rev. Mod. Phys. 18, 69 (1946).
[2] D. Bancroft, Phys. Rev. 53, 587 (1938).
[3] W. J. Merz, Phys. Rev. 78, 341 (1950).
[4] H. Mueller, Phys. Rev. 47, 947 (1935).
[5] F. Pockels, *Lehrbuch der Kristalloptik* (Teuber, Leipzig, 1906), p. 480.

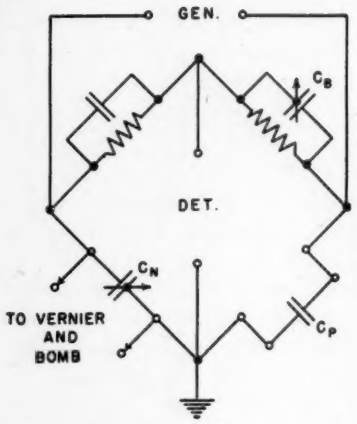

FIG. 2. Schering bridge used in substitution method. Condenser C_N measures the unknown capacity and condenser C_B compensates for changes in the resistance of the unknown.

polarizability to be about one-half the relative change in density. Thus, for the polarizability of the electrons of the ions, which seemingly should be rather insensitive to pressure, the relative changes with increasing pressure are of the same order of magnitude as are the relative changes in density.

At optical frequencies the dielectric constant arises wholly from the polarizabilities of the ions, but at frequencies lower than the characteristic frequency of the lattice, there is also a polarization caused by the displacement of the lattice of positive ions with respect to the lattice of negative ions. Bretscher[6] has found that the change in dielectric constant with temperature is largely caused by the change in the polarizability of the lattice, and he suggests that the change in lattice polarization also plays an important role in the change in the dielectric constant with pressure. The lattice polarization may reasonably be expected to change markedly with pressure, because its magnitude is large or small depending on whether the restoring force for the displacement is weak or strong. Since the effect of pressure is usually to increase these restoring forces, an increase in pressure should reduce the lattice polarization. If the relative change in the lattice polarization is large compared to the relative change in density, the low frequency dielectric constant should decrease. The research described below was undertaken to ascertain whether the low frequency dielectric constant of ionic crystals does indeed decrease at high pressures.

II. EXPERIMENTAL METHOD

(A) Electrical Measurements

Since the low frequency dielectric constant of ionic crystals is relatively constant through the low frequency range into the infra-red, measurements are made only at 1000 c.p.s. The change in the dielectric constant with pressure is determined by measuring the change of capacity of a parallel plate condenser with a capacitance bridge and auxiliary apparatus, shown schematically in Fig. 1. The measurements of capacity are made by a substitution method in the manner illustrated by Fig. 2.

[6] E. Bretscher, Trans. Faraday Soc. **30**, 684 (1934).

In order to measure changes of capacity as small as 0.01 $\mu\mu$f, a capacity vernier was constructed from a small fixed condenser in series with a large variable condenser. The vernier is shown in Fig. 1.

The bridge condenser is used as the capacity standard for these measurements. It was checked against another condenser of the same model and found to be within the manufacturer's specification, which states that measurements of small capacities by substitution methods have an error of ± 0.1 $\mu\mu$f. The variable condenser in the vernier was calibrated against the bridge condenser. The capacity range of the bridge condenser used for this calibration is 3.0 $\mu\mu$f. There is very little scatter, even though the points are taken at the smallest intervals possible (every 0.2 $\mu\mu$f) on the scale of the bridge condenser. Since the scatter of the calibration points is small, the error in the capacities measured by the variable vernier condenser is at most the error of 3.0 $\mu\mu$f of the bridge condenser which is ± 0.1 $\mu\mu$f or ± 3 percent.

Capacity changes observed on the vernier condenser must be corrected for changes in the dissipation factor of the sample in order to obtain the true capacity change of the sample when it is exposed to the high pressure. This correction was found to be negligible for all the measurements reported here.

Connections are made with cable which has a capacitance of 13.5 $\mu\mu$f per foot and a temperature coefficient which is less than 2×10^{-4}/°C. It is estimated, taking into account the temperature coefficients of other parts of the system and the magnitudes of the capacities involved, that a fluctuation in ambient tem-

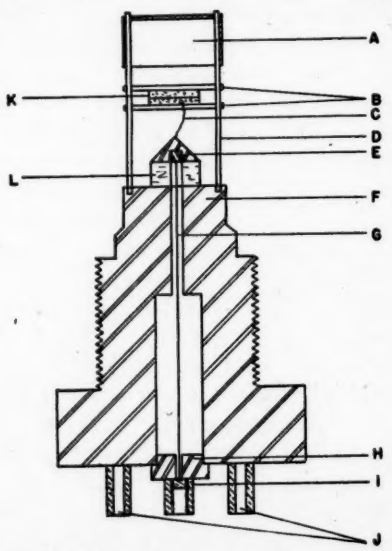

FIG. 3. Sample holder and plug for high pressure bomb. A. Pill box container for sodium. B. Sample supports and electrical grounds. C. 3 mil manganin wire. D. Supporting pins. E. Hardened steel cone with optical flat base and threaded hole. F. Hardened steel plug with top surface optically flat. G. 8-mil piano wire. H. Insulating bushing. I. High electrode. Threaded tube with threaded anchor soldered to piano wire. J. Ground electrodes. K. Slabs of dielectric. L. Sapphire washer with both faces optically flat.

TABLE I. Experimental data to be used in calculations.

	D.c. dielectric constant[a]	Optical dielectric constant[a]	Lattice constant[a]	Volume changes under high pressure at room temperature[b] $\frac{-\Delta V}{V_i}=ap-bp^2$		Thermal expansion[d]	Change of d.c. dielectric constant with temperature[d]	Change of refractive index with density[e]
	ϵ	ϵ_0	L (A)	a $\times 10^7$ bars	b $\times 10^{12}$ (bars)^2	$\left(\frac{\partial \ln V}{\partial T}\right)_p$ $\times 10^4$(°C)	$\left(\frac{\partial \ln \epsilon}{\partial T}\right)_p$ $\times 10^4$(°C)	$\frac{dn}{d \ln \rho}$
LiF	9.27	1.92	2.07	15.20	5.5	1.05	37.5	0.1
NaCl	5.62	2.25	2.81	43.1	49.6[c]	1.20	34.0	0.24
KCl	4.68	2.13	3.14	56.8	72.4[c]	0.96	30.3	0.23
KBr	4.78	2.33	3.29	67.0	105.3			0.35
MgO	9.8	2.95		5.95	1.0			

[a] Values for the first three columns were obtained from summaries of experimental values by K. Hojendahl, K. Danske Vidensk Selskab, **16**, No. 2 (1938).
[b] Volume changes under pressure were measured by Bridgman and Slater and are tabulated by F. Birch *et al.*, Geological Society of America, Special Papers No. 86, *Handbook of Physical Constants* (1942), p. 52.
[c] Values of a and b for NaCl and KCl are taken from the elastic constant measurements of D. Lazarus, Phys. Rev. **76**, 545 (1949).
[d] $(\partial \ln V/\partial T)_p$ and $(\partial \ln \epsilon/\partial T)_p$ are taken from a A. Eucken and A. Buchner, Zeits. f. physik. Chemie **B27**, 321 (1934).
[e] $dn/d \ln \rho$, is taken from E. Burstein and P. L. Smith, Phys. Rev. **74**, 229 (1948).

perature of 1°C will produce an error of 10^{-2} $\mu\mu$f. A pressure run lasts at most three hours. The temperature was always measured after a run and found to be within a half-degree of the temperature before the run. Therefore, the effects of room temperature fluctuations are insignificant.

(B) High Pressure Apparatus

The system for generating high pressures is similar to those previously described[7] and is shown schematically in Fig. 1. The pressure fluid is normal hexane. Pressures are measured by use of a manganin resistance gauge whose pressure coefficient of resistance $(\partial \ln R/\partial p)_T$ is 2.48×10^{-6} bar^{-1}, as determined by using the freezing point of mercury at 0°C.[8]

The main high pressure problem in this experiment was to make a packing for the electrical lead into the high pressure bomb. Most of the high pressure packings which are satisfactory for measuring resistances or for carrying currents into a high pressure chamber are unsatisfactory for our purpose, either because the capacity changes too much as a function of pressure, or because the capacity at zero pressure shifts after an application of high pressure. The type of electrical load which has proven most satisfactory for pressures up to 8000 bars is that shown in Fig. 3. The packing is similar to the type used extensively in the laboratory of Michels, but differs from it in that an Al_2O_3 crystal is used as the insulating washer instead of fused silica. The Al_2O_3 is less apt to fail under the high pressures, provided it is well annealed, and is polished to remove all sharp corners from which rupture may start. The washer is $\frac{5}{8}''$ in diameter, $\frac{1}{4}''$ thick and has a $\frac{1}{16}''$ diameter hole. The c-axis of the crystal is parallel to the axis of the hole so that the cylindrical geometry is preserved when pressure is applied. Both faces of the washer and all steel in contact with it are optically flat to $\frac{1}{4}$ of a wave-length of visible light, causing the surfaces to stick without the aid of adhesives. Nevertheless, a thin layer of a thermoplastic wax was used between the flat surfaces in order that a sudden release of pressure would not separate the washer from the steel parts and thus cause a leak.

In spite of all these precautions in the construction of the packing, long exposure to pressures higher than 8000 bars caused deterioration of the packing washer around the small hole in the washer. For this reason measurements on dielectric constants were restricted to pressures less than 8000 bars. The variation of the capacity of the electrical lead with sapphire packing is 0.15 $\mu\mu$f in 8000 bars, and its zero pressure capacity changes at most 0.01 $\mu\mu$f during a pressure cycle.

(C) Preparation of Samples

The samples are prepared in the form of parallel plate condensers by cleaving thin slabs from large

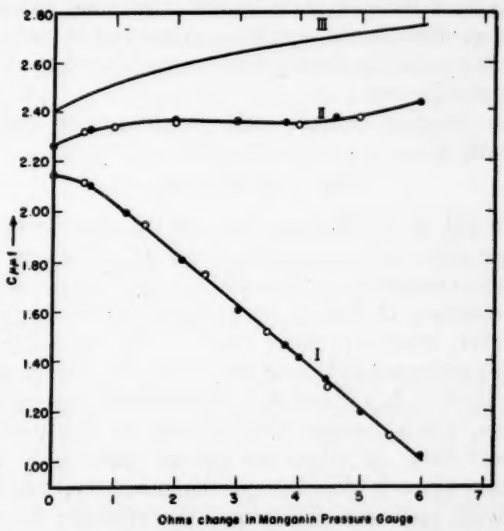

FIG. 4. Capacity measurements for a sample of NaCl. Curve *I* is change of capacity of plug and sample. Curve *II* is change of capacity of plug alone. Curve *III* is correction curve for the sample capacity required because the fringing capacity changes with pressure.

[7] P. W. Bridgman, *Physics of High Pressures* (Macmillan Company, Inc., New York, 1931), Chapter 2.
[8] D. Lazarus, Phys. Rev. **76**, 547 (1949).

single crystals. The slabs are usually about 2 cm² in area and 1 mm thick. All the ionic crystals studied here are cubic and since the dielectric constant is the same in all directions in a cubic crystal, no attempt has been made to orient the crystals. It is likely, however, that the faces of the cleaved slabs are (100) planes, since these are the planes in the crystals which are most readily cleaved.

Platinum electrodes are sputtered onto the crystals in vacuum. This technique gives good adhesion to the crystal surface because the glow discharge, which accompanies the sputtering, cleans the crystal surface before the platinum deposits. Such surfaces were found to be superior to various silver and platinum paints and to evaporated aluminum, all of which deteriorated when exposed to the high pressure.

The actual geometry in which the condensers of the dielectric are used is shown in Fig. 3. Two slabs are held by brass plates which act both as supports and as electrical ground connections. The other connection is a 0.003″ insulated manganin wire, one end of which is soldered to the electrical lead at the top of the cone, while the other end is placed between the two slabs of the sample. The pill box at the top of the specimen holder contains sodium to keep the system dry.

(D) Measurements

The plug with the sample in place is mounted in the high pressure bomb, the bomb is filled with hexane and the capacity of the system is determined as a function of pressure. Next, the manganin lead wire is unsoldered, disconnecting the sample, and the procedure is repeated to ascertain the variation of the lead capacity with pressure. In order to find the variation in capacity of the sample itself, the second set of pressure measurements are subtracted from the first, and, since no guard rings are used on the samples, a correction is made for the fringing of the electric field around the edges of the slabs of dielectric.

The fringing capacity ΔC_f is determined experimentally since

$$\Delta C_f = \Delta M/(K_1 - 1),$$

where ΔM is the difference between the capacity of the sample when it is measured immersed in hexane and when it is measured immersed in air and K_1 is the dielectric constant of hexane at one atmosphere pressure. However, when a pressure run is made, the sample is always immersed in hexane and so the effective fringing capacity is $K\Delta C_f$ where K is the dielectric constant of hexane, which changes with pressure as measured by Chang.[9] Now, ΔC_f does not change appreciably with pressure since it depends on the geometry, which is relatively constant. Therefore, the effective fringing capacity varies with pressure as the dielectric constant of hexane.

Figure 4 shows a typical set of measurements for a sample of NaCl with a total initial capacity of 18.5 $\mu\mu$f. Curve *I* is the change of capacity of the lead and the sample; Curve *II* is the change of capacity of the lead alone, and Curve *III* is the change in the fringing capacity of the sample in the sample holder. Curve *III* is computed using the fact that for this sample $\Delta M = 0.77$ $\mu\mu$f. Note that in these curves the capacity origin is unimportant since the thing of interest is the change of capacity from its zero pressure value. The circles on Curves *I* and *II* represent readings taken with decreasing pressure, while the dots represent readings taken with increasing pressure. The circles serve as a check to determine whether the platinum electrode is worked off the surface of the crystal by the pressure cycle. To obtain the change in capacity ΔC of the sample, Curves *II* and *III* are subtracted from Curve *I*; and to give the relative change in capacity of the sample, ΔC is divided by the initial capacity C_i.

The relative change in dielectric constant $\Delta\epsilon/\epsilon_i$ follows directly from the relative change in capacity of the sample $\Delta C/C_i$, providing a correction is made for the effect of pressure on the geometry of the sample. This correction is easily made. Capacity is proportional to a length and the appropriate length here is the dimension of the crystal. Thus, $C \sim \epsilon l$ and $\Delta\epsilon/\epsilon_i = \Delta C/C_i - \Delta l/l_i$, neglecting second order terms. The quantity $\Delta l/l_i = \Delta V/(3V_i)$ is obtained from the volume measurements of Bridgman or others (Table I).

III. RESULTS

Figure 5 shows the results of the measurements for $\Delta\epsilon/\epsilon_i$. The origin of each curve is displaced in order to fit all curves of the same graph. For LiF and NaCl two sets of measurements on the same sample were made.

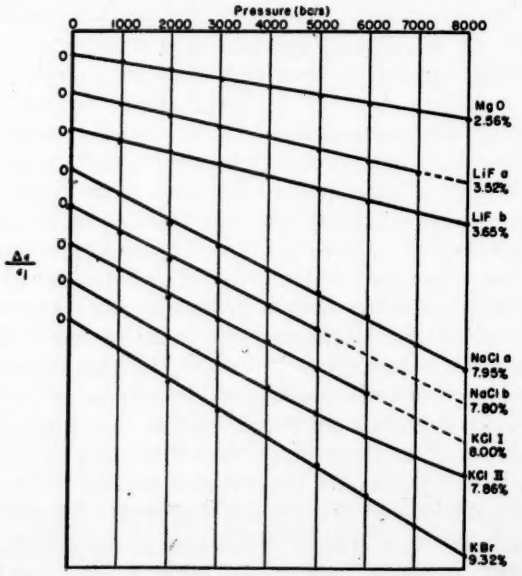

FIG. 5. The pressure dependence of the 1000 c.p.s. dielectric constant at room temperature. The origin of each curve is vertically displaced so that all curves fit on the same graph. The dashed line indicates an extrapolation. The total relative change is given at 8000 bars for all curves.

[9] Z. T. Chang, Chin. J. Phys. 1 (No. 2), 1 (1934).

For KCl two measurements, each one on a different sample, were made. It is rather difficult to evaluate any spurious error associated with the high pressure problem. For this reason more than one run was made for several samples. The difference between two runs on the same sample gives a qualitative idea of the reproducilibity of the data.

The dielectric constant of all materials decreases with increasing pressure. For the hard materials LiF and MgO the dielectric constant is linear with pressure. For the softer materials, NaCl, KCl and KBr, there may be a slight tendency for the dielectric constant to decrease more slowly at the higher pressures. This tendency for most of the runs borders on the edge of the experimental error; but for KCl *II*, where the sample capacity is large enough so that its capacity change is very large compared to the corrections, the dielectric constant does decrease more slowly with increasing pressure.

The most significant quantity obtained from these measurements is the initial slope $(\partial \ln\epsilon/\partial p)_T$. The values of $-(\partial \ln\epsilon/\partial p)_T$ are listed in Table II. The error in each value is ± 3 percent as a result of the estimated error in capacity measurements. The over-all error is listed with the average value of $-(\partial \ln\epsilon/\partial p)_T$. From these values of $(\partial \ln\epsilon/\partial p)_T$ it is possible to calculate the volume electrostrictive coefficient. The electrostriction is found to be so small that it can have no influence on the results of the measurements.

It may be of interest to see whether ϵ could be described as depending only on the volume and implicitly through it on the temperature and pressure. The validity of such an assumption would be tested by the extent to which we should have

$$\left(\frac{\partial \ln\epsilon}{\partial T}\right)_P \Big/ \left(\frac{\partial \ln V}{\partial T}\right)_P = \left(\frac{\partial \ln\epsilon}{\partial p}\right)_T \Big/ \left(\frac{\partial \ln V}{\partial p}\right)_T.$$

In Table III this relation is tested for LiF, NaCl, and KCl. The agreement is poor, indicating that even for these simple materials the dielectric constant cannot be considered to be a function of the volume alone.

TABLE II.* Values of $-(\partial \ln\epsilon/\partial p)_T$ at room temperature and atmospheric pressure.

Substance	Room temp. (°C)	$-(\partial \ln\epsilon/\partial p)_T \times 10^5$ bars	Average $-(\partial \ln\epsilon/\partial p)_T \times 10^5$ bars
MgO	30	0.320	0.320±0.019
LiF *a*	28	0.440	0.448±0.028
LiF *b*	29	0.456	
NaCl *a*	25	0.994	0.98±0.06
NaCl *b*	30	0.975	
KCl *I*	29	1.00	1.05±0.08
KCl *II*	28	1.10	
KBr	26	1.17	1.17±0.09

* The alkali halides and the magnesium oxide used in these measurements were obtained from the Harshaw Chemical Company and the Norton Company, respectively.

TABLE III.* The dependence of ϵ on the volume.

	$(\partial \ln\epsilon/\partial T)_P \alpha^{-1}$	$-(\partial \ln\epsilon/\partial p)_T a^{-1}$
LiF	3.57	2.95
NaCl	2.84	2.30
KCl	3.15	1.86

* Values of $(\partial \ln\epsilon/\partial T)_P$, the thermal expansion coefficient α, and the compressibility, a, are given in Table I.

IV. COMPARISON WITH THEORY

Many writers have considered the dielectric properties of ionic crystals.[10] In particular, Mott and Littleton[11] present a point of view which is useful in discussing the measurements reported here. This theory is an extension of the ideas of Heckmann,[12] and is in many ways similar to the discussion of Hojendahl.[13]

Mott and Littleton derive the equation

$$\frac{\epsilon-1}{4\pi} = \frac{8\pi\beta\beta_0(\gamma-1)/3+(\beta+\beta_0)}{1-4\pi(\beta+\beta_0)/3+16\pi^2\beta\beta_0(1-\gamma^2)/9}, \quad (1)$$

where ϵ is the dielectric constant, β_0 is the polarizability of the electrons of the ions per unit volume, β is the polarizability of the lattice per unit volume and γ is called here the constant of the inner field. The quantity γ has the value unity when the inner field can be described by the Lorentz field, which is the case in the NaCl type structure if there is no overlap between adjacent ions; it is defined by an equation of the type

$$F = E + 4\pi\gamma P/3, \quad (2)$$

where F is the effective polarizing field, E is the electric field in the medium and P is the total polarization per unit volume. The paper of Mott and Littleton should be consulted to see the particular manner in which they introduce γ.

At optical frequencies when the lattice polarizability vanishes, Eq. (1) can be written in the familiar Lorentz-Lorenz form

$$(\epsilon_0-1)/(\epsilon_0+2) = 4\pi\beta_0/3, \quad (3)$$

[10] For general discussions see N. Born and M. Goeppert-Mayer, Handb. d. Phys. **24/2**, 759 (1933) and N. F. Mott and R. W. Gurney, *Electronic Processes in Ionic Crystals* (Oxford University Press, London, 1940), Chapter 1. For discussions concerning the optical dielectric constant see: K. Fajans and G. Joos, Zeits. f. Physik **23**, 1 (1924). K. F. Herzfeld and K. L. Wolf, Ann. d. Physik (4) **78**, 35 and 195 (1925). H. Mueller, Phys. Rev. **47**, 947 (1935). W. Shockley, Phys. Rev. **70**, 105 (1946). For discussions concerning the low frequency dielectric constant see: G. Heckmann, Zeits. f. Krist. **61**, 250 (1925). A. Eucken and A. Buchner, Zeits. f. physik. Chemie (13) **27**, 321 (1934). N. F. Mott and M. J. Littleton, Trans. Faraday Soc. **34**, 485 (1938). K. Hojendahl, K. Danske Vidensk Selskab. **16**, No. 2 (1938). S. Roberts, Phys. Rev. **76**, 1215 (1949). For discussions of the infra-red eigenfrequency see: M. Born and E. Brody, Zeits. f. Physik **11**, 327 (1922). R. B. Barnes, Zeits. f. Physik **75**, 732 (1932). J. A. Wasastjerna, Soc. Sc. Fennica. Com. Phys. Mat. **8**, No. 20 (1935). R. H. Lyddane and K. F. Herzfeld, Phys. Rev. **54**, 846 (1938).

[11] N. F. Mott and M. J. Littleton, Trans. Faraday Soc. **34**, 485 (1938).

[12] G. Heckmann, Zeits. f. Krist. **61**, 250 (1925).

[13] K. Hojendahl, K. Danske Vidensk. Selskab **16**, No. 2 (1938).

TABLE IV.* Calculated data on γ and $(\partial\gamma/\ln\rho)_T$.

	γ	$(\partial\gamma/\partial\ln\rho)_T$	$\frac{\Delta\epsilon\gamma}{\Delta\epsilon}$	γ_H	$(\partial\gamma_H/\partial\ln\rho)_T$	$\frac{\Delta\epsilon\gamma_H}{\Delta\epsilon}$
LiF	0.25	−0.5±1.0	0.1	0.73	−0.5±0.3	0.4
NaCl	−0.08	−0.4±1.3	0.1	0.47	−1.0±0.5	0.5
KCl	−0.05	−3.0±1.0	0.6	0.46	−1.8±0.4	0.8
KBr	−0.04	−2.2±0.7	0.5	0.42	−1.7±0.5	0.8

* γ and $(\partial\gamma/\partial\ln\rho)_T$ are calculated from the theory of Mott and Littleton; γ_H and $(\partial\gamma_H/\partial\ln\rho)_T$ from the theory of Hojendahl. Data for the calculation are given in Tables I and II. The part of the total change of ϵ which is attributed to the change of the inner field is listed in the third and sixth columns.

TABLE V.* The relative discrepancy between ν calculated by means of Eqs. (10) and (12) and the measured eigenfrequency ν_M.

	$(\nu_M-\nu)/\nu_M$
LiF	0.05
NaCl	0.09
NaBr	0.07
NaI	0.07
KCl	0.09
KBr	0.07
KI	0.11

* Data for the calculation are taken from summaries of experimental data by Hojendahl (reference 12) except for the compressibilities which are taken from F. Birch, Geological Society of America, Special Papers No. 86, 52, (1942).

where ϵ_0 is the square of the optical refractive index. Equation (3) is used to determine values of β_0. At frequencies below the characteristic frequency of the lattice the lattice polarizability per unit volume exists and is defined as

$$\beta=N(Ze)^2/R, \tag{4}$$

where Ze is the ionic charge, N is the number of ion pairs per unit volume, and R times the relative displacement of the positive ions with respect to the negative ions is the repulsive overlap force resisting this displacement. If the values of β_0 and β, as given by Eqs. (3) and (4), are substituted into Eq. (1), one finds the relation

$$\frac{\epsilon-1}{\epsilon+2}=\frac{(\epsilon_0+2)/(\epsilon_0-1)+3R/4\pi N(Ze)^2-2(1-\gamma)}{(\epsilon_0+2)/(\epsilon_0-1)[3R/4\pi N(Ze)^2]-(1-\gamma)^2}. \tag{5}$$

For many ionic crystals, Mott and Littleton have calculated R for the cases $\gamma=0$ and $\gamma=1$. They compare these values of R with R as calculated from the Born-Mayer potential between nearest neighbors, and find that the agreement is far better for the case $\gamma=0$ than it is for $\gamma=1$.

Mott and Littleton also re-derive a relation given by Heckmann[12] connecting the infra-red eigenfrequency, ν, with the dielectric constants and γ. This equation is

$$\epsilon-\epsilon_0=(Ne^2/\pi M\nu^2)[1+\tfrac{1}{3}\gamma(\epsilon_0-1)]^2, \tag{6}$$

where M is the reduced mass of a positive and a negative ion. If in Eq. (6) $\gamma=0$, the familiar equation of Born[14] is obtained.[15] From Eq. (6) Mott and Littleton compute γ for several ionic crystals from the measured dielectric constants and eigenfrequencies. These values of γ are also much closer to zero than to unity. Mott and Littleton attribute this decrease of γ from the Lorentz value of one to the interpenetration of nearest neighbor ions.[16]

The pressure dependence of all quantities entering Eq. (5) except γ has been measured, or can be estimated independently of the dielectric constant. By using Eq. (5) to calculate the change in γ with pressure from the change in the dielectric constant with pressure, the theory can be checked in a qualitative way as follows. According to the picture of Mott and Littleton, γ is less than unity because of the overlap of neighboring ions; the effect of high pressures is to reduce the inter-ionic distance and increase the overlap; therefore, γ should decrease with increasing pressure.

(A) The Repulsive Force Constant at High Pressure

Before the change of γ with pressure can be calculated from Eq. (5), it is necessary to know the change in the repulsive force constant R with pressure in addition to the pressure dependence of ϵ, ϵ_0, and N. Since R cannot be measured directly, it must be related to the elastic constants or to the compressibilities because the pressure dependence of these quantities have been measured.

Equation (6), which relates γ to the dielectric constants and to the eigenfrequency ν is not used to calculate the change in γ with pressure because the pressure variation of ν has not been measured. Furthermore, there seems to be no precise way by which ν can be related to the elastic properties independently of γ and of the dielectric constant.

For a lattice under zero external pressure, the repulsive force constant R has been related to the compressibility x and the interionic distance, L, by Hojendahl.[17] An obvious extension of Hojendahl's calculation for the case of a lattice under external pressure p, yields the relation

$$R=6L/x-8pL \tag{7}$$

for the NaCl type lattice. This result was obtained with the assumption that the overlap interaction energy acts only between nearest neighbors and is a function only of the distance between the ions. Furthermore, it is assumed that the lattice is at the absolute zero of tem-

[14] M. Born and M. Goeppert-Mayer, Handb. d. Phys. **24/2**, 646 (1933).

[15] In Eq. (10), ν corresponds to the characteristic transverse frequency of long wave-length. Since the low frequency dielectric constant ϵ is usually measured in a parallel plate condenser, one might wonder if the dielectric constant should be related to the characteristic frequency of longitudinal polarization waves. This point is discussed by R. H. Lyddane and K. F. Herzfeld, Phys. Rev. **54**, 861 (1938), and they show that ν is properly the transverse frequency.

[16] Mott and Littleton, reference 11, or Mott and Gurney, reference 10, p. 16.

[17] K. Hojendahl, K. Danske Vidensk. Selskab, **16** (No. 2), 110 (1938).

perature. If values of the lattice constant and compressibility at high pressures are substituted in Eq. (7), it is found that R increases with pressure. Hence by Eq. (4) the lattice polarizability decreases with increasing pressure.

(B) The Calculation of γ and $(\partial\gamma/\partial \ln\rho)_T$

When the values of $N=L^{-3}/2$ and R for the NaCl type structure are substituted into Eq. (5), we have

$$(1-\gamma)=\frac{\epsilon+2}{\epsilon-1}\left\{1\pm\left[\left(\frac{\epsilon-1}{\epsilon+2}\right)\left(\frac{\epsilon_0+2}{\epsilon_0-1}\right)-1\right]^{\frac{1}{2}}\times\left[\left(\frac{\epsilon-1}{\epsilon+2}\right)\frac{9L^4(1-4px/3)}{\pi(Ze)^2x}-1\right]^{\frac{1}{2}}\right\}. \quad (8)$$

Table IV gives the values of γ at zero pressure calculated from Eq. (8) by using the negative root. The positive root is rejected because when the eigenfrequency ν is calculated by elimination of γ from Eqs. (6) and (8) the negative root alone yields values of ν which are physically plausible. In Table V are listed the percentage discrepancies between valances of ν calculated in this way and the eigenfrequency ν_M measured by Barnes and Czerny.[18] This comparison, in addition to indicating the proper sign in Eq. (12), may serve to give some additional justification to the use of γ, a quantity whose physical meaning is somewhat ambiguous.

From Table IV it is seen that γ is nearer to zero than to the Lorentz value of unity, which Mott and Littleton concluded using the Born-Mayer repulsion to calculate the repulsive force. In the case of MgO, an imaginary value of γ is obtained from Eq. (8). This result may arise from the assumption of central forces in the calculation of the repulsive force constant for MgO or the neglect of next nearest neighbor interactions.

For comparison with the values of γ calculated from the theory of Mott and Littleton, the values of γ calculated by the theory of Hojendahl[19] are listed in Table IV where they are denoted by γ_H. The values of γ_H, as well as the values of γ, are less than unity at zero pressure. There is very poor correlation between the degree of ionicity in the crystals and the values of the γ's as calculated from the theories. For example, since the value of γ is nearer to unity in LiF than in NaCl, there should be less overlap in LiF than in NaCl, and hence LiF should be more ionic than NaCl. However, NaCl is known to be more ionic than LiF. As Hojendahl has remarked, part of the cause of the anomalously large value of the constant of the inner field calculated for lithium salts is that the theory has neglected the overlap between negative ions, and in lithium salts this effect is important.

The constant of the inner field, as used by Hojendahl, is really only an adjustable parameter, while Mott and Littleton try to give it some physical significance in their theory. For this reason, and because the theory of Mott and Littleton reduces to the accepted Lorentz-Lorenz relation, Eq. (3), for the optical dielectric constant while the theory of Hojendahl does not, we have given the preference in this paper to the theory of Mott and Littleton.

Since in both theories the inner field is less than the Lorentz value at zero pressure, one might expect the inner field to decrease further from the Lorentz value of one at high pressure. In Table IV are listed values of the change of γ with density, which are obtained by differentiation of Eq. (8), and also values which are obtained by differentiation of Hojendahl's Eq. (75),[20] in which x is replaced by $x(1-(4/3)px)^{-1}$. The calculated change of γ with respect to the density is negative in all cases.

(C) Discussion

The values of $(\partial\gamma/\partial \ln\rho)_T$ indicate that γ decreases more rapidly in materials of high compressibility than in those of low compressibility. However, it is dangerous to attach too much significance to the numerical values of this coefficient since these values are very sensitive to the quantity b which is determined from volume measurements at high pressures through the equation

$$-\Delta V/V_i=ap-bp^2, \quad (9)$$

where ΔV is the change in volume, V_i is the initial volume, and a and b are constants to fit the data. Of course, b can also be related to data on the pressure dependence of the elastic constants. We believe that the values of b which are obtained from the elastic constant measurements of Lazarus[8] by a single differentiation of the data, are more reliable than those obtained from volume measurements by two differentiations of the data. Unfortunately, elastic constant measurements have been made only on NaCl and KCl. For other salts the only values of b available are from volume measurements (see Table I).

Since $(\partial\gamma/\partial \ln\rho)_T$ is very sensitive to the value of b used in the calculation, one should inquire whether the errors in b are sufficiently large to cause uncertainty in the sign of $(\partial\gamma/\partial \ln\rho)_T$. The errors in the values of $(\partial\gamma/\partial \ln\rho)_T$ are calculated from an assumed error in b of 5 percent and from the error in $(\partial \ln\epsilon/\partial p)_T$ listed in Table II. The precision of b appears better than 5 percent. However, the main uncertainty comes rather from the assumption that the volume at the high pressures can be represented by the two parameter equation, Eq. (9). In fact, Bridgman's recent measurements[21] at very high pressures indicate that b itself is a function of pressure.

The errors in $(\partial\gamma/\partial \ln\rho)_T$ listed in Table IV indicate that no definite conclusion can be made concerning the

[18] R. B. Barnes, Zeits. f. Physik 75, 732 (1932).

[19] Reference 17, p. 116. Hojendahl uses the symbol β_K instead of γ_H used here.

[20] Reference 17, p. 112.

[21] F. Birch, Geological Society of America, Special Papers, No. 86, 52 (1942).

sign of this coefficient for LiF and NaCl, as calculated from the theory of Mott and Littleton. In all the other cases its sign is well established as negative, and the calculations indicate that the contribution to the decrease of the low frequency dielectric constant from the decrease of the inner field is large. This is shown by the values of $\Delta\epsilon\gamma/\Delta\epsilon$ listed in the third and sixth columns of Table IV.

V. CONCLUSION

The low frequency dielectric constant of ionic crystals was measured at high pressures and found to decrease with increasing pressure. The existing lattice theories explain this decrease as arising not only from the decrease in the lattice polarizability produced by the increase of the repulsive forces but also because the increasing overlap of adjacent ions at high pressures reduces the internal field.

In contradistinction to liquids and gases, the change in density of ionic crystals plays a minor role compared to the change in overlap in affecting the low frequency dielectric constant.

The author wishes to thank his sponsor, Professor A. W. Lawson, for his interest and helpful suggestions throughout the course of the work; Dr. J. B. Garrison for many interesting discussions; Mr. K. Lindholm and Mr. N. D. Nachtrieb for construction of the high pressure apparatus; Mr. J. Getsholtz for optical polishing; Mr. F. Bruce and Mr. T. Y. Tang for assistance in taking data, and the staff of the Institute for the Study of Metals, where this research was carried out, for their generous cooperation at all times. In addition, the author wishes to thank Mr. W. H. Henson of the Norton Company for the gift of the MgO crystals, and Miss Flora E. Riddle of the Pipestone Indian School, Pipestone, Minnesota, for the gift of some pipestone which is used as a high pressure packing.

PHYSICAL REVIEW VOLUME 79, NUMBER 2 JULY 15, 1950

A Simplified Method of Computing the Cohesive Energies of Monovalent Metals

T. S. KUHN* AND J. H. VAN VLECK
Harvard University, Cambridge, Massachusetts

(Received March 2, 1950)

A method is developed which, within the limits of the spherical cell approximation first presented by Wigner and Seitz, permits the evaluation of the cohesive energy, lattice constant, and compressibility of a monovalent metallic solid without the explicit computation of a central field for the atom. It is shown that empirical values of the first few s and p levels of the free atom can supply the relevant information usually obtained through the computation of a central field, so that a considerable simplification is possible. The method is applied to the calculation of the usual solid state parameters for the alkali metals, Na, K, and Rb. The results for Na compare very favorably with experiment as well as with those gained by previous workers. The K and Rb computations agree decidedly less well with experiment, but the values for K are appreciably better than those previously computed utilizing an explicit central field. The errors shown by the K and Rb computations are believed to be the inevitable consequence of any theory derived by replacing the effect of the core electrons by an equivalent central field rather than a result of any peculiarities inherent in the present approach.

I. Introduction: In the well-known s-sphere approximation developed by Wigner and Seitz[1] for the computation of the physical parameters of metallic lattices the ground-state energy of the solid is the lowest eigen-energy, ϵ_0, of the equation

$$\frac{d^2U^{(l)}}{dr^2}+\left[\epsilon-V(r)-\frac{l(l+1)}{r^2}\right]U^{(l)}=0, \tag{1}$$

solved with $l=0$ subject to the boundary conditions that $U^{(0)}$ be zero at the origin and that

$$\left[r\frac{dU^{(0)}}{dr}\right]_{r=r_s}=U^{(0)}(r_s). \tag{2}$$

In these equations the radius, r, is measured in Bohr units and the energy, ϵ_0, in Rydberg units. The quantity r_s is the radius of the s-sphere and is related to the lattice parameter, d, of a body-centered cubic lattice like that of the alkali metals by the equation

$$d=(8\pi/3)^{\frac{1}{3}}r_s. \tag{3}$$

The potential $V(r)$ is taken to be identical with that of the free atom, so that (1) is just the radial wave equation of the free atom.

In addition to its ground-state energy the solid possesses a mean Fermi energy which, at absolute zero, is given by

$$\epsilon_F=\frac{9\pi}{10}\left(\frac{3}{2\pi}\right)^{\frac{4}{3}}\frac{\alpha}{r_s^2}=\frac{2.21\alpha}{r_s^2}, \tag{4}$$

where α is a constant which Bardeen[1] has shown is

* Junior Fellow, Society of Fellows.

[1] E. Wigner and F. Seitz, Phys. Rev. **43**, 804 (1933); **46**, 509 (1934); F. Seitz, Phys. Rev. **47**, 400 (1935). This outline of the method follows the development presented by J. Bardeen, J. Chem. Phys. **6**, 367 (1938).

given by

$$\alpha=\frac{r_s[U^{(0)}(r_s)]^2}{3\int_0^{r_s}[U^{(0)}]^2dr}\left[\frac{r}{U^{(1)}}\frac{dU^{(1)}}{dr}-1\right]_{r=r_s}. \quad (5)$$

Here $U^{(1)}(r)$ is that solution of (1) with $l=1$ which goes to zero at the origin.

The total binding energy of the solid is given by

$$\epsilon_B=\epsilon_0+\epsilon_F+\epsilon_C, \quad (6)$$

where ϵ_C is a small correction[2] term introduced to allow for effects of electronic interactions and of deviations of the solid state potential function from that of the free atom. This correction energy may be approximated by

$$\epsilon_C=\frac{0.284}{r_s}-\frac{0.576}{r_s+5.1}. \quad (7)$$

The value of r_s for which ϵ_B takes its minimum value is related to the lattice constant of the metal at absolute zero by (3). The value of this minimum binding energy less the first ionization potential of the free atom is the cohesive energy of the metal at absolute zero. The compressibility of the metal can be computed from the formula

$$\frac{1}{\kappa}=\frac{3.87\cdot10^{12}}{r_s}\frac{d^2\epsilon_B}{dr_s^2}\ \text{cm}^2/\text{dyne}. \quad (8)$$

These three parameters exhaust the important physical information to be gained without more knowledge of the zone structure of the metal than is available in the s-sphere approximation.

The problem of computing the above parameters is now reduced to that of integrating Eq. (1) for $l=0$ and $l=1$. The solutions produced must all be zero at the origin and in the case $l=0$ must satisfy the additional condition (2) at the cell boundary. For $l=1$ the desired solutions are completely determined (except in amplitude) by the boundary condition at the origin and the condition that the energy appearing in the wave equation be ϵ_0, the eigen-energy of the solution $U^{(0)}$. Such solutions have been carried out by Wigner and Seitz[1] for Na, by Seitz[1] for Li, by Bardeen[1] for Na and Li, and by Gorin[3] for K. All of these authors utilized central fields of the Prokofjew or of the Hartree type and carried through graphical or numerical integrations of (1). All but Gorin obtained reasonably good agreement with experiment.

Such numerical solutions of the wave equation are entirely practicable, but the required integrations are lengthy and are completely dependent upon the even more tedious computation of a potential function. The function matching method developed here succeeds in avoiding many of these complexities. For it is noted that values of the physical parameters of metallic solids depend primarily upon the behavior of the solid state wave functions outside the atomic core, and that in this region the family of wave functions which are zero at the origin is completely determined by the value of its logarithmic derivative. This logarithmic derivative is, in turn, a single-valued function of the energy parameter in the wave equation and can, with the aid of laboratory values of the first few energy levels of the free atom, be approximated without an explicit knowledge of $V(r)$. The procedure, of course, assumes the existence of some such "best central field" for the atom, but it avoids the difficulties inherent in the calculations of and with such a field.

II. Outline of the Function Matching Method: The functions $U^{(l)}(r)$ may be considered to form a one-parameter family (parameter ϵ_0) of those solutions of (1) which are zero at the origin. In terms of these a new function $\phi_R{}^{(l)}(\epsilon_0)$ may be defined as the logarithmic derivative of $U^{(l)}(r)$ at $r=R$, i.e., by

$$\phi_R{}^{(l)}(\epsilon_0)=\left[\frac{1}{U^{(l)}}\frac{dU^{(l)}}{dr}\right]_{r=R}. \quad (9)$$

It can now be shown quite generally that, for sufficiently small values of R, $\phi_R{}^{(l)}(\epsilon_0)$ is a smooth, non-oscillating function of ϵ_0. For since the function $V(r)$ must be expressible in Rydberg units in the form $-2Z/r+g(r)$, where $g(r)$ is an analytic function with a zero at the origin, it follows straightforwardly that the logarithmic derivative can always be expressed in the form

$$\phi_R{}^{(l)}(\epsilon_0)=\frac{1}{R}+\sum_{k=0}^{\infty}a_k{}^{(l)}(\epsilon_0)R^k, \quad (10)$$

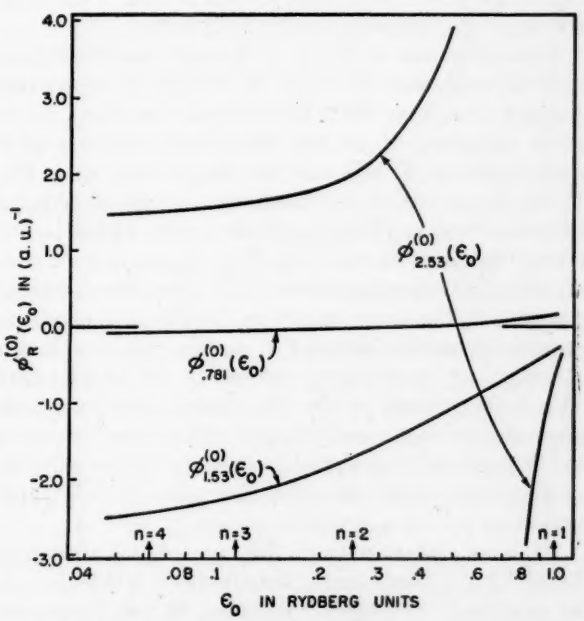

FIG. 1. Logarithmic derivative of hydrogenic wave functions as a function of energy for various sphere radii.

[2] These corrections are discussed completely in the references above and in E. Wigner, Phys. Rev. 46, 1002 (1934); Trans. Faraday Soc. 34, 678 (1938).

[3] E. Gorin, Physik. Zeits. Sowjetunion 9, 328 (1936).

TABLE I. Matching radius and hydrogenic deviations for computations on Na, K, and Rb.

	Na(s and p)	K(s)	K(p)	Rb(s and p)
R	2.00	2.53	3.12	3.12
$Z_{eff}-1$	0.11[a]	0.08[b]	0.02[b]	0.05[c]

[a] W. Prokofjew, Zeits. f. Physik 58, 255 (1929).
[b] D. R. Hartree, Proc. Roy. Soc. A143, 506 (1934).
[c] D. R. Hartree, Proc. Roy. Soc. A151, 96 (1935).

in which the coefficients $a_k^{(l)}$ are polynomial functions of the energy parameter ϵ_0. Further, the degree of these polynomial functions increases quite slowly with k; $a_0^{(l)}$ is independent of ϵ_0, $a_1^{(l)}$ and $a_2^{(l)}$ are linear functions of ϵ_0, and, generally, $a_{2k-1}^{(l)}$ and $a_{2k}^{(l)}$ are polynomials of degree k in ϵ_0. Thus, for all physically significant values of ϵ_0 and for sufficiently small values of R, $\phi_R^{(l)}(\epsilon_0)$ will be constant since terms beyond $a_0^{(l)}$ may be discarded. With R somewhat larger, so that the coefficients through $a_3^{(l)}$ must be kept, $\phi_R^{(l)}(\epsilon_0)$ will show a linear dependence on ϵ_0, etc. The increase of the complexity of the behavior of $\phi_R^{(l)}(\epsilon_0)$ is slow, and the function will be seen to be essentially simple for reasonably large values of R.

An example of this behavior is shown in Fig. 1, where $\phi_R^{(0)}(\epsilon_0)$ is plotted as a function of energy for values of $|\epsilon_0| \leq 1$ *Ry.* and for $R=0.781$, 1.53, and 2.53 a.u. These curves are derived by integrating (1) with a hydrogenic potential, $V=-2/r$, in which case exact solutions, with zeros at the origin, are given by Whittaker's[4] function $M_{n,\frac{1}{2}}(2r/n)$ with $n=1/(-\epsilon_0)^{\frac{1}{2}}$. It will be noted that on a scale which places the radius of the first Bohr orbit at unity, the logarithmic derivative is almost constant for $R=0.753$, well behaved for $R=1.53$, and shows an infinite discontinuity for $R=2.53$. It is believed that curves computed with other atomic potential functions will show qualitatively similar behavior.

This behavior is made physically reasonable by remembering that for small R, $|V(R)| \gg |\epsilon_0|$ so that changes in ϵ_0 have little effect on the solutions of the wave equation, or on the logarithmic derivatives of these solutions. This is confirmed quantitatively in Fig. 1, for if $\epsilon_0=-1$ is the minimum energy of physical interest, then $\epsilon_0=V(R)=-1$ for $R=2$, which is precisely the range in which $\phi_R^{(0)}(\epsilon_0)$ ceases to behave in an essentially simple manner. When heavier atoms are considered, the same reasoning justifies our expecting essentially smooth behavior of $\phi_R^{(l)}(\epsilon_0)$ for all values of R within or immediately outside of the atomic core. This is illustrated by the Na s-state wave functions, computed with a non-hydrogenic Prokofjew potential, by Wigner and Seitz[1] which show no appreciable dependence on ϵ_0 for values of the radius $r \leq 2.3$ atomic units.

At large distances from the core of the atom (say for all $r \geq R'$), the potential function, $V(r)$, must exhibit an essentially hydrogenic behavior. In this hydrogenic region the general solution of (1) is given by an arbitrary linear combination of Whittaker's[5] two well-known solutions of the confluent hypergeometric equation, $W_{n,l+\frac{1}{2}}(2r/n)$ and $W_{-n,l+\frac{1}{2}}(-2r/n)$, where again $n=1/(-\epsilon_0)^{\frac{1}{2}}$. The first of these solutions, $W_{n,l+\frac{1}{2}}(2r/n)$ is known to go to zero as $r\to\infty$, so that if the atomic term levels of the free atom are given by the set $\epsilon_k(k=1, 2, 3, \ldots)$, then throughout the region $r \geq R'$ the functions $W_{n_k,l+\frac{1}{2}}(2r/n)$ computed with $n_k=1/(-\epsilon_k)^{\frac{1}{2}}$ are the radial wave functions of the valence electron of the free atom. It follows that whenever $\epsilon_0=\epsilon_k$, the function $U^{(l)}(r)$ must be identical (except in amplitude) with the function $W_{n_k,l+\frac{1}{2}}(2r/n)$ throughout the region $r \geq R$, for whenever $\epsilon_0=\epsilon_k$ the functions $U^{(l)}(r)$ are the exact radial wave functions of the free atom. This leads immediately to the conclusion that whenever $\epsilon_0=\epsilon_k$, the logarithmic derivative of the functions $W_{n_k,l+\frac{1}{2}}(2r/n)$, evaluated at $R(\geq R')$, must be exactly equal to $\phi_R^{(l)}(\epsilon_k)$.

To this point the development is exact. The next step, however, requires a crucial assumption whose justification will be postponed to the next section. Assume that there is some radius R which is small enough so that $\phi_R^{(l)}(\epsilon_0)$ is an essentially well-behaved function of ϵ_0 and large enough so that $V(r)$ is essentially hydrogenic for all $r \geq R$. Then values of the logarithmic derivative of the well-known functions $W_{n_k,l+\frac{1}{2}}(2r/n)$ computed at $r=R$ and for $n_k=1/(-\epsilon_k)^{\frac{1}{2}}$ will yield a discrete set of points lying on the smooth curve $\phi_R^{(l)}(\epsilon_0)$, and a simple polynomial function passing through these points will serve to represent $\phi_R^{(l)}(\epsilon_0)$ throughout the range of ϵ_0 of physical interest. For any atom satisfying the above assumption, it is thus possible, knowing the values of ϵ_k, to produce a close approximation to $\phi_R^{(l)}(\epsilon_0)$ without a knowledge of the central field of the atom. Further, once this function is given it is possible, for all $r \geq R$ and for any ϵ_0, to compute the solutions, $U^{(l)}(r)$, which satisfy (1) and are zero at the origin. This follows since, in the hydrogenic region, $U^{(l)}(r)$ must be some linear combination of the two known functions $W_{n,l+\frac{1}{2}}(2r/n)$ and $W_{-n,l+\frac{1}{2}}(-2r/n)$, and this linear combination is completely determined (except in amplitude) by its logarithmic derivative $\phi_R^{(l)}(\epsilon_0)$, which is now known.

Finally, if $R \leq r_s$ all the solid state parameters discussed in Section I may be computed utilizing the wave function derived by the procedure above. The only exception is presented by the quantity α, whose definition includes the term

$$\int_0^{r_s} [U^{(0)}(r)]^2 dr.$$

However, since the integrand is negligible for values of r inside the core, reasonably accurate values of α are computed by extrapolating values of the integrand into

[4] E. T. Whittaker and G. N. Watson, *Modern Analysis* (Cambridge University Press, London), fourth edition, §16.1.

[5] Reference 4, §16.12.

TABLE II. The functions $\phi_R^{(0)}$ and $\phi_R^{(1)}$ for Na, K, and Rb: data and results.

Element	ms	$-\epsilon_k$	Source	R	$\phi_R^{(0)}(\epsilon_0)$	mp	$-\epsilon_k$	Source	R	$\phi_R^{(1)}(\epsilon_0)$
Na	3	0.3778	a	2.000	$-0.1820\epsilon_0^2$ $+0.9252\epsilon_0$ $+0.8704$	3	0.22232	b	2.000	$-0.6088\epsilon_0^2$ $+0.8568\epsilon_0$ $+1.7348$
	4	0.1432				4	0.10197			
	5	0.07518				5	0.05844			
	6	0.04628				6	0.03786			
K	4	0.3191	a	2.531	$0.8313\epsilon_0$ $+1.0687$	4	0.200522	c	3.125	$-1.0092\epsilon_0^2$ $+1.7112\epsilon_0$ $+1.3340$
	5	0.1274				5	0.093884			
	6	0.06886				6	0.054741			
						7	0.035893			
Rb	5	0.3071	a	3.125	$1.7706\epsilon_0$ $+0.2943$	5	0.191121	d	3.125	$0.7342\epsilon_0^2$ $-0.3658\epsilon_0$ $+0.5078$
	6	0.1236				6	0.090511			
	7	0.06725				7	0.053187			

[a] R. F. Bacher and S. Goudsmit, *Atomic Energy Levels* (McGraw Hill Book Company, New York, 1932).
[b] C. E. Moore, *A Multiplet Table of Astrophysical Interest* (Princeton, New Jersey, 1945, published by the observatory). Corrections for vacuum wavelengths were taken from the *International Critical Tables*.
[c] C. E. Moore, *Atomic Energy Levels* (National Bureau of Standards, Circular 467, Washington, D. C., 1949), Vol. I.
[d] H. R. Kratz, Phys. Rev. **75**, 1846 (1949).

the core from the hydrogenic region in which it is accurately known.

The argument above may be conveniently summarized as follows. For a given value of ϵ_0, the solutions $U^{(l)}(r)$ of the wave equation which is zero at the origin must be identical (in the hydrogenic region $r \geq R$) with some linear combination of Whittaker's two well-known functions. The particular linear combination desired is completely determined by the function $\phi_R^{(l)}(\epsilon_0)$, which is just the logarithmic derivative of the correct solution, $U^{(l)}(r)$, computed at R. If the hydrogenic region extends near enough the core so that $\phi_R^{(l)}(\epsilon_0)$ is a well-behaved function of ϵ_0, then the behavior of $\phi_R^{(l)}(\epsilon_0)$ (and hence of the wave functions in the hydrogenic region) is completely determined by the first few values of $\phi_R^{(l)}(\epsilon_k)$, where the ϵ_k are the atomic term levels. Finally, with the term levels given, these values of $\phi_R^{(l)}(\epsilon_k)$can be computed from the first of Whittaker's functions, $W_{n_k, l+\frac{1}{2}}(2r/n)$.

III. The Choice of a Matching Radius R: There is of course no single radius R beyond which the potential function of a complex atom is rigorously hydrogenic. In practice therefore it is necessary to choose the largest matching radius R such that the points $\phi_R^{(l)}(\epsilon_k)$ lie on a curve which may be described by a simple polynomial. If the field is nearly enough hydrogenic at the largest R, the function matching approach may always be applied, for examination of Fig. 1 clearly disposes of the danger that it should be possible to pass a smooth curve through the points $\phi_R^{(l)}(\epsilon_k)$ under circumstances in which the function $\phi_R^{(l)}(\epsilon_0)$ was itself oscillatory or otherwise irregular.

The computations discussed in the next section show clearly that the points $\phi_R^{(l)}(\epsilon_k)$ can be accurately fitted by a simple curve at distances, R, well outside the atomic core. It will now be indicated that the deviations of the potential from hydrogenic behavior at these distances may be expected to have negligible effect upon the results of computation, for the deviations themselves are small, and the errors they introduce are, to a first approximation, mutually compensating.

TABLE III. Ground state energy and α as a function of sphere radius for Na, K, and Rb.

z_s	Na $-\epsilon_0$	Na α	K $-\epsilon_0$	K α	Rb $-\epsilon_0$	Rb α
4.0	0.1440					
4.5	0.6150		-0.0826			
5.0	0.6644	0.962	0.4686		0.3986	
5.5	0.6235	0.980	0.5281	0.745	0.5040	
6.0	0.5666	1.013	0.5070	0.909	0.4933	0.132
6.5	0.5125		0.4679	1.122	0.4584	0.427
7.0			0.4280		0.4202	0.781
7.5			0.3942		0.3866	

If the actual potential function of the atom is written in the standard form $V(r) = -2Z_{eff}/r$, then the value of $Z_{eff}-1$ at R is just the fractional deviation of the potential from hydrogenic behavior at the matching radius. Table I lists the matching radii used for the s and p computations for Na, K, and Rb and the corresponding values of $Z_{eff}-1$ derived from standard Hartree and Prokofjew fields for these atoms. It is observed that the deviations from hydrogenic behavior are comparatively small and that the worst deviation is found to occur for† Na, the only one of the elements for which the over-all computation yields excellent results.

It is not at once apparent that the "small" deviations listed in Table I will have a negligible effect on the computation of the solid-state parameters, but both theory and practice show this to be the case. For example, a repetition of the Na ground-state computation at $R=2.53$ (an increase of 25 percent in matching radius which reduced $Z_{eff}-1$ from 0.11 to 0.03) changed the value of the ground-state energy by less than 1.5 percent throughout its range. This behavior, which was duplicated again and again during the computations, indicates both that the procedure is insensitive to changes in R, as it should be, and that a ten percent deviation from hydrogenic behavior at the matching

† The Prokofjew field for Na would be expected to yield a larger value of $Z_{eff}-1$ than a Hartree field for the same element, since the former allows for the polarization of the core by the valence electron and the latter does not. However, an estimate of the polarization effect indicates that the Hartree deviation would be at least 0.05, so that the deviation for Na is at least as great as that for the other elements.

TABLE IV. Lattice constant, cohesive energy, and compressibility for Na.

	Experiment[a]	Wigner-Seitz[b]	Bardeen[b]	Kuhn and VV
d(A°)	4.25	4.74	4.53	4.14
Cohesive energy (K cal./mole)	26	23.2	23	25.9
$\kappa \cdot 10^{12}$ (cm²/dyne)	12.3		12.0	13

[a] Except where otherwise noted experimental values are taken from J. Bardeen, J. Chem. Phys. 6, 372 (1938).
[b] See reference 1.

radius does not produce errors of equivalent magnitude in the end products of computation.

That the error in the final product of the computation must be smaller than the deviations from hydrogenic behavior can also be discovered by a rigorous quantitative investigation of a closely analogous problem. Consider the potential $V(r)$ to be strictly hydrogenic ($V(r)=-2/r$) for all $r \geq R'$ and to be given in the region $r \leq R'$ by $-2/r+g(r)$. Then for continuity of potential and field it is necessary that $g(R')=g'(R')=0$. Further, let the functions $U^{(l)}(r)$ be the exact solutions of (1) which are zero at the origin, and define an additional set of functions $W^{(l)}(r)$ which are exact solutions of the hydrogenic form of (1) and which are identical with the functions $U^{(l)}(r)$ for all $r \geq R'$. With these assumptions and definitions the errors due to matching in the non-hydrogenic region may be made explicit.

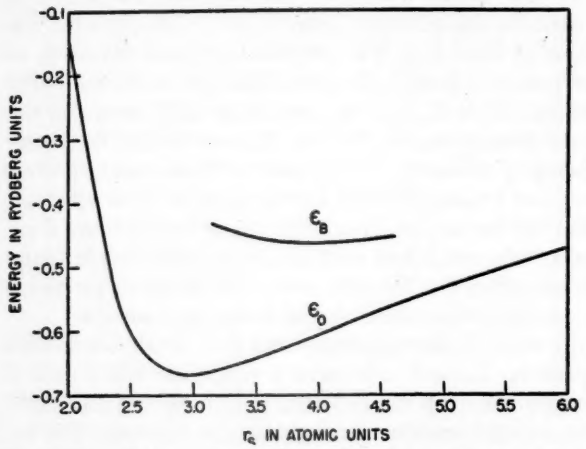

FIG. 2. Ground state and total energy *vs.* sphere radius for sodium.

For suppose that the matching process is carried out at a radius R ($<R'$) and that ξ ($\equiv R'-R$) is a small quantity. The deviation from hydrogenic behavior of the potential function at the matching radius is then $0(\xi^2)$ and straightforward comparison of the two series expansions about R' shows that the difference between the correct wave functions $U^{(l)}$ and the hydrogenic wave functions $W^{(l)}$ used in computation is only $0(\xi^4)$. The difference between the correct logarithmic derivative $U^{(l)\prime}/U^{(l)}$ and the logarithmic derivative $\phi_R{}^{(l)}$ ($=W^{(l)\prime}/W^{(l)}$) computed with the hydrogenic wave functions is larger, being $0(\xi^3)$. But it can again be shown by the comparison of the appropriate series that when this "wrong" $\phi_R{}^{(l)}$ is used to select an appropriate "wrong" wave function $W^{(l)}$, the two errors are compensatory so that the net error is again $0(\xi^4)$. It follows that if the potential function $V(r)$ shows a small fractional deviation, δ, from hydrogenic behavior at the matching radius, then the total error in the final computation may be expected to be of order δ^2, which will normally be negligible.

IV. Computations and Results: Practical application of the method described in Section II requires an accurate knowledge of the values of the functions $W_{\pm n,\, l+\frac{1}{2}}(2r/n)$ over a wide variety of values of r and n. Since interest is not restricted to integral and half-integral values of n, the existing computations of the confluent hypergeometric function prove inadequate, and it is necessary either to compute Whittaker's functions over the range of r and n of physical interest or to develop a new form for the general solution of the hydrogenic wave equation.

The second alternative has proved the more practical, for it was possible, following a lead provided by Wannier and Jastrow,[6] to produce two independent solutions of the wave equation, $\bar{W}^{(l,\,n)}(r)$ and $\tilde{W}^{(l,\,n)}(r)$, which are related to the standard forms by the formulas

$$M_{n,\, l+\frac{1}{2}}(2r/n)=\Gamma(2l+2)n^{-l-1}\bar{W}^{(l,\,n)}(r) \tag{11a}$$

$$W_{n,\, l+\frac{1}{2}}(2r/n)=\Gamma(n+l+1)n^{-l-1} \times\{\cos(n-l-1)\pi\bar{W}^{(l,\,n)}(r) +\sin(n-l-1)\pi\tilde{W}^{(l,\,n)}(r)\}. \tag{11b}$$

The particular advantage of this choice of solutions is that both $\bar{W}^{(l,\,n)}(r)$ and $\tilde{W}^{(l,\,n)}(r)$ may be computed from the series form

$$\bar{W}^{(l,\,n)}(r)=\sum_{k=0}^{\infty} n^{-2k}\bar{W}^{(l)}(r);$$
$$\tilde{W}^{(l,\,n)}(r)=\sum_{k=0}^{\infty} n^{-2k}\tilde{W}^{(l)}(r); \tag{12}$$

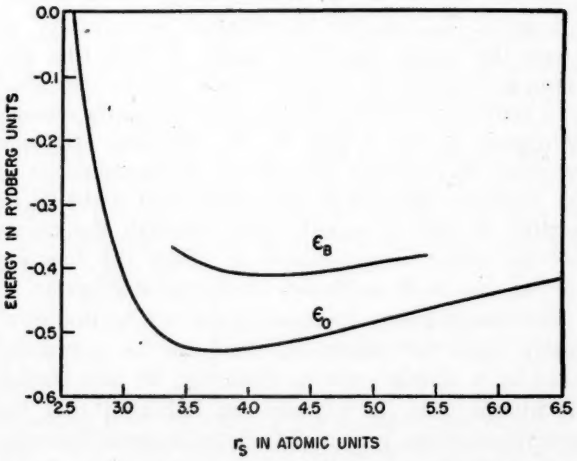

FIG. 3. Ground state and total energy *vs.* sphere radius for potassium (complete computation).

[6] G. H. Wannier, Phys. Rev. 64, 358 (1943). R. Jastrow, Phys. Rev. 73, 60 (1948).

TABLE V. Lattice constant, cohesive energy, and compressibility for K.

	Experiment[a]	Gorin[b] Uncorrected	Gorin[b] Corrected	Kuhn and VV Complete	Kuhn and VV Plane wave
d(A°)	5.27	5.8	5.8	4.51	5.01
Cohesive energy (K cal./mole)	22.6[c]	6	14.5	27.9	24.2
$\kappa \cdot 10^{12}$ (cm²/dyne)	23.9			27	30

[a] See reference a, Table IV.
[b] See reference 3.
[c] F. Seitz, *The Modern Theory of Solids* (McGraw Hill Book Company, New York, 1940), p. 356. Bardeen quotes an earlier measurement in reference a, Table IV.

in which the coefficients $\bar{W}_k^{(l)}$ and $\tilde{W}_k^{(l)}$ are expressible in terms of Bessel functions of the first and second kind. The series (12) shows quite rapid convergence, so that if the coefficients are computed as functions of r, the complete wave functions can be rapidly determined for any value of n by a simple summation. It is really the versatility and manipulability of this form of the general solution of the hydrogenic wave equation which gives the present method its speed and simplicity. In fact, once the values of the coefficients have been tabulated, the computation of a set of curves like those in any one of the figures which follow is little more than a day's work. A complete analytic and numerical account of these solutions is presented elsewhere.[7]

One further remark may be of interest before the presentation of the results of the computations. It has been previously noted that for a suitably chosen value of R the points $\phi_R^{(l)}(\epsilon_k)$ must lie on a smooth curve, and it actually turns out during computation that the possibility of finding such a smooth curve is a very sensitive check on the consistency of a set of experimentally determined energy levels, ϵ_k. This was particularly true of the p-level computation, during which an error of a few tenths of an inverse centimeter in any one of the first four term levels made it impossible to fit a smooth curve to the computed points $\phi_R^{(1)}(\epsilon_k)$.

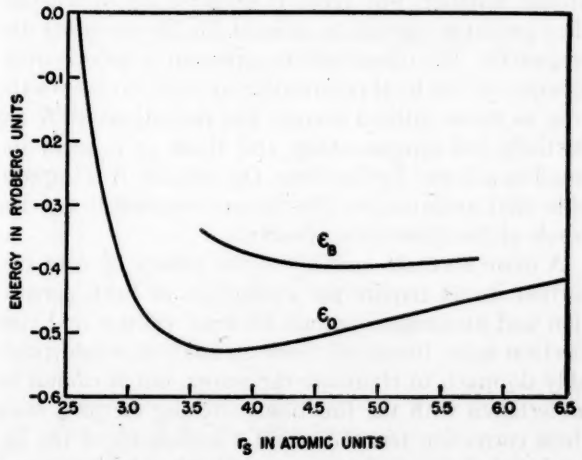

FIG. 4. Ground state and total energy *vs.* sphere radius for potassium (plane wave computation).

[7] T. S. Kuhn, Quarterly of Applied Math. (to be published).

TABLE VI. Lattice constant, cohesive energy, and compressibility for Rb.

	Experiment[a]	Kuhn and VV Plane wave
d(A°)	5.60	5.20
Cohesive energy (K cal./mole)	18.9	24.2
$\kappa \cdot 10^{12}$ (cm²/dyne)	31.9	26

[a] See reference a, Table IV.

This critical dependence of the products of computation on the precise values of the energy levels employed necessitated a thorough review of the data available on the p-levels of the alkali metals, and the authors are greatly indebted to Dr. Charlotte E. Moore of the Bureau of Standards for her invaluable assistance in locating the most accurate sources of this experimental information.

Table II below lists, for the elements Na, K, and Rb, the experimental energy levels used in the computations as well as the polynomial forms, $\phi_R^{(l)}(\epsilon_0)$, derived from these. In each case one more energy level of the atom is tabulated than was required to determine completely the corresponding polynomial. The extra energy level (normally the algebraically highest) was used to check the polynomial form and agreement was

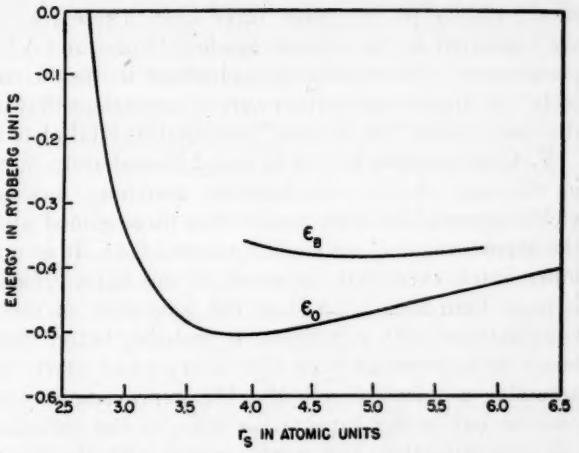

FIG. 5. Ground state and total energy *vs.* sphere radius for rubidium (plane wave computation).

in all cases better than 0.1 percent. Table III gives the values, computed by the function matching method outlined above, of ϵ_0 and of α for various values of a new variable, $z_s = (8r_s)^{\frac{1}{2}}$.

In the range of values of r_s which are of greatest physical interest the functions $\epsilon_0(r_s)$ and $\alpha(r_s)$ are almost linear, so that it proved possible, by graphical interpolation, to compute values of these functions for intermediate values of r_s with an accuracy of better than 0.1 percent. Values computed in this manner were used with Eqs. (3), (4), (6)–(8) in the preparation of Figs. 2–5 and of Tables IV–VI. These tables present together the computed and experimental values of the three solid

TABLE VII. Estimate of fractional error due to dipole effects at the matching radius

	Na(s and p)	K(s)	K(p)	Rb(s and p)
$\eta/2R^3$	0.080	0.163	0.086	<0.264

TABLE VIII. Estimate of fractional error due to dipole effects at the sphere radius.

	Na	K complete	K plane wave	Rb
$\eta/2r_s^3$	0.011	0.037	0.026	<0.070

state parameters described in Section I. The results of previous computation are also tabulated for comparison.

Tables V and VI require further explanation. In the first of these Gorin's "uncorrected" results are the end products of a straightforward numerical integration of the wave equation utilizing a Hartree field; his improved or "corrected" results were gained from these by an essentially heuristic device, with little quantitative basis, designed to allow for increased "correlation effects" in the solid. Kuhn and Van Vleck's "complete" computation is the one described above. Because it appeared that much of the error in this result entered during the computation of α from Eq. (5), a second, approximate, computation of the binding energy was undertaken with $\alpha=1$, the value which would obtain in the plane wave case. These results are tabulated in the column headed "Kuhn and VV: plane wave." The values of α obtained in the "complete" rubidium computation were so anomalous that in this case only the "plane wave" computation is tabulated.

V. Conclusions: It will be noted immediately that, in the case of Na, the function matching method yields appreciably better results than those gained with the introduction of an explicit central field. It is not immediately clear that the extent of this improvement is more than fortuitous, since the agreement of these computations with experiment is probably better than ought to be expected from any theory which starts by assuming a spherical cell. But the improvement does confirm our earlier expectation that, in the spherical cell approximation, any results gained with the introduction of an explicit central field may be improved by the function matching method, since the latter bypasses the theoretical and practical difficulties inherent in explicit computation of a central field.

This conclusion is also supported in a general way by the computations for K and Rb. Both of these display marked deviations from experiment, but both are, almost uniformly, in better agreement with experiment than Gorin's computation with a Hartree potential. It is probable that the function matching method shares in the difficulties noted by those previous workers who have attempted a Wigner-Seitz computation for the heavier elements, but within the limits imposed by the uniform assumption that there is *some* best central field for atomic and solid state problems, the method developed above exhibits marked theoretical and practical advantages.

In an attempt to isolate the source of the error in our K and Rb computations, inconclusive attempts have been made to discover some approximation within the procedure which can be shown to break down more and more as the atomic number increases. Table I above, which lists the fractional deviation of the explicit fields from hydrogenic behavior at the matching radius, represents one such attempt. A similar estimate of this deviation at the sphere radius, r_s, (where the error introduced would not be self-compensating) gave even more negative results, for (except in the case of Na) the deviations were less than 0.2 percent, and neither at the matching radius nor at the sphere radius did the discrepancies show any marked increase with atomic number. The possibility that the error enters in fitting a smooth curve to the points $\phi_R^{(l)}(\epsilon_k)$ also seems barred, for again little increase in the difficulty of finding a fit was observed as the mass number increased.

It seems more probable that the existing errors are due to a distortion of the core by the valence electrons. To a first approximation such distortions may be treated as a simple polarization of the core, and this polarization effect does not appear in self-consistent fields like those used (except in the case of Na) for the computation of Table I. The contribution of this polarization to the potential function can, however, be estimated, for it may be expressed as a series whose leading (dipole) term is just η/r^4 Rydbergs, where η is the polarizability of the atom.

The constant η has been estimated by one of us[8] from the known quantum defects of non-penetrating orbits. With these values the fractional deviation due to polarization ($\eta/2r^3$) can be computed at the matching radius, R, and at the sphere radius, r_s. The results of such a computation are given in Tables VII and VIII below.

The estimates in Tables VII and VIII indicate clearly that the polarization effects do increase with atomic number, but there is question as to whether they are large enough to account for the observed discrepancies. The dipole effects represent a serious overestimate of the total polarization at radii so close to the core as those utilized above. The deviations at R are partially self-compensating, and those at r_s seem too small to account for the error. On balance, it is improbable that polarization effects are responsible for the whole of the gross error observed.

A more accurate account of the effects of core distortion would require the evaluation of Fock correlation and exchange integrals between valence and core electron wave functions. Such an analysis would probably do much to eliminate the errors, but it cannot be undertaken with the function matching method, since these correction terms demand a knowledge of the behavior of the wave functions within the atomic core.

[8] J. H. Van Vleck, *Theory of Electric and Magnetic Susceptibilities* (Clarendon Press, Oxford, 1932), p. 215 ff.

Letters to the Editor

PUBLICATION of brief reports of important discoveries in physics may be secured by addressing them to this department. The closing date for this department is five weeks prior to the date of issue. No proof will be sent to the authors. The Board of Editors does not hold itself responsible for the opinions expressed by the correspondents. Communications should not exceed 600 words in length.

On Charge Independence and High Energy Scattering*

ROBERT JASTROW
Institute for Advanced Study, Princeton, New Jersey
May 15, 1950

THE Berkeley experiments on $p-p$ scattering at 345 Mev indicate a roughly isotropic cross section between 20° and 90° with a mean magnitude of approximately 4 millibarns/steradian. This is in strong contrast with the results to be expected from a central attractive potential determined by the low energy scattering,[1] from which one obtains at 345 Mev a cross section which arises from 0.2 mb at 90°, to 12 mb at 0°. A qualitative difference is also to be noted between the $p-p$ scattering and the strongly anisotropic high energy $n-p$ scattering.[2]

We wish to show that a charge-independent static[3] potential is not excluded by these results. We assume for this purpose an interaction consisting of a strong short-range repulsion surrounded by an attractive well.[4] The combination is fitted to the low energy scattering. The attractive field is perhaps to be associated with the π-meson and the short-range repulsive field with a heavier particle.

Considering first $p-p$ scattering at high energies, the repulsive core has the following effect: at energies comparable with or greater than the depth of the surrounding well the effect of the core will dominate in the S state and the sign of the ^1S phase shift will change in this energy region from positive to negative. The D state will, at energies of a few hundred Mev, still be affected only by the outer or attractive region of the potential and the D phase shift will be positive. The difference in sign between the ^1S and ^1D phases causes the $S-D$ interference term in the differential cross section to be positive at 90° and negative at 0°, thereby reducing the anisotropy obtained without the core.

The following potential is used, in which for convenience of calculation the core is represented by a hard sphere and the attraction by an exponential well:

$$V=\infty,\ r<a,$$
$$V=V_0[(\alpha+\beta\sigma_1\cdot\sigma_2)\exp[-(r-a)/R]+\gamma S_{12}\exp(-r/R_{\text{tensor}})];\quad r>a \quad (1)$$
$$a=0.6\times10^{-13}\text{ cm},\quad R=0.4\times10^{-13}\text{ cm},\quad R_{\text{tensor}}=1.0\times10^{-13}\text{ cm},$$
$$V_0=100\text{ Mev},\quad \alpha=2.18,\quad \beta=-0.52,\quad \gamma=0.65.$$

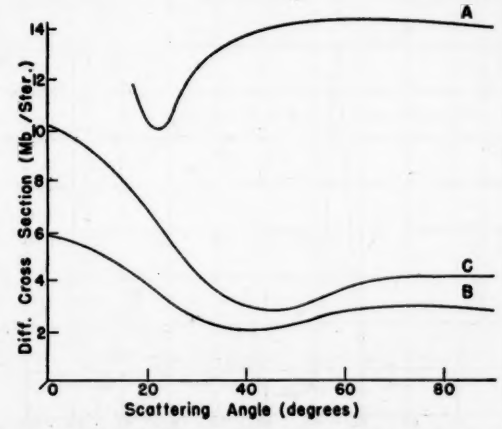

FIG. 1. $P-P$ scattering calculated from the potential (1) at A: 32 Mev; B: 250 Mev; C: 345 Mev. Curve A includes the effect of the Coulomb field, while curves B and C refer to nuclear scattering only.

The strength of the tensor forces in (1) is of the order of that required by the deuteron constants. The scattering at 345 Mev is computed exactly for the central forces and in Born approximation for the tensor forces, neglecting central-tensor interference. The resultant cross section is shown in curve C of Fig. 1, as well as the cross sections computed under the same conditions at 32 and 250 Mev (curves A and B). In curve C the scattering at 20° is 75 percent greater than the mean magnitude of the cross section between 30° and 90°, in contradiction with the experimental distribution. By using a more complicated potential the forward scattering may be substantially reduced. However, in view of the neglect of possible non-static forces an emphasis on precision of fit is perhaps unwarranted in comparison with the importance of simplicity in the interaction.

In treating the $n-p$ scattering we assume that in the charge-antisymmetric states (^3S, ^1P, ^3D, ^1F, $\cdots$) one has the interaction of Christian and Hart.[2] These states do not enter into the $p-p$ scattering, which is, therefore, unchanged by this assumption. In this way we can estimate the contribution from triplet states of even L by using the results of Christian and Hart. The singlet contribution is one-fourth of the corresponding $p-p$ cross section as given in Fig. 1. The result is: $\sigma_{np}(90°)=0.8$ mb; $\sigma_{np}(180°)=9.7$ mb. The effect of the core does not destroy the anisotropy of the $n-p$ cross section.

It is seen thus that the introduction of a short-range repulsive force permits one to reconcile the qualitative aspects of the $n-p$ and $p-p$ scattering results with the preservation of charge independence. The arbitrary nature of the particular form of interaction employed should, however, be emphasized, as well as the fact that this result may be obtained from other types of interactions.

The influence of the core on nuclear saturation may be expected to be appreciable because of the zero-point energy arising from the exclusion of each nucleon from the interiors of the other nucleons in a nucleus. This problem is under investigation.

A more detailed account of the work is in preparation.

* This research was supported by an AEC grant to the Institute for Advanced Study.

[1] R. S. Christian and H. P. Noyes, Phys. Rev. 79, 85 (1950).
[2] R. S. Christian and E. W. Hart, Phys. Rev. 77, 441 (1950).
[3] A simple velocity dependence, the spin-orbit interaction, has been investigated by K. M. Case and A. Pais, Phys. Rev. 79, 185 (1950), who conclude that it may be possible by means of this interaction to represent the $n-p$ and $p-p$ scattering qualitatively on a charge-independent basis. See also Blanchard, Avery, and Sachs, Phys. Rev. 78, 292 (1950).
[4] A similar type of interaction has been considered by N. M. Kroll in connection with $p-p$ scattering, and we are indebted to him for interesting and useful criticism. P. O. Olsson has examined the possibility of introducing a repulsion into the $n-p$ potential, as have also G. Parzen and L. Schiff, Phys. Rev. 74, 1564 (1948).

Gamma-Ray Measurements with NaI(Tl) Crystals*

R. HOFSTADTER AND J. A. MCINTYRE
Palmer Physical Laboratory, Princeton University, Princeton, New Jersey
May 29, 1950

IT has recently been shown[1] by an example with Co^{60} gamma-rays that relatively sharp lines appear in the pulse-height distributions of NaI(Tl) scintillations. These lines, giving directly the full finergy of the gamma-rays, have been interpreted in terms of a photoelectric component (in iodine of NaI) as well as a component arising from capture of all scattered and recoil products of the original gamma-ray in the NaI(Tl) crystal. This method can be used to measure gamma-ray energies (as well as intensities) and proves to be sensitive since the energies are given by sharp

maxima of pulse distributions. At higher energies, where $E>2mc^2$, the pair production process becomes important. The purpose of this letter is to extend the method of measurement to the energy range where "pair lines" are observed.[2]

Figure 1 shows the results obtained with Na^{24} (1.38 and 2.76 Mev) when the gamma-source (~1 mC) is collimated so that a narrow (1° divergence) bundle of rays travels through the middle of the NaI(Tl) crystal. Figure 2 shows a similar spectrum for a weak source in an uncollimated arrangement. About two hours of running time were required to obtain the data of Fig. 1 and about one hour for those of Fig. 2. Calibration data in Fig. 1 show the two Co^{60} "photoelectric" peaks at 1.17 and 1.33 Mev. The observed peaks in Na^{24} have been classified as to origin as indicated in Fig. 1. A tabulation of the corresponding pulse heights is given in Table I.

The constancy of the ratio in column 4 shows that the pulse heights are proportional to energy and supports the assignment given in Fig. 1. The shape of the peaks is also consistent with this assignment, for the photoelectric and pair peaks should be symmetrical and sharp while the Compton distributions are broad, unsymmetrical, and have an edge on the high energy side. The pair peak for the 1.38-Mev line which should occur at 0.36 Mev is too weak to be observed.

TABLE I. Pulse height *vs.* energy relation.

1 Peak	2 Pulse height (volts)	3 Energy (Mev)	4 Ratio pulse height/energy
I (Na^{24})	34.5[a]	—	—
II (Na^{24})	43.5±0.5	1.38	3.15
III (Na^{24})	55.0±0.5	1.74	3.15
IV (Na^{24})	75.0[a]	—	—
V (Na^{24})	88.0±0.5	2.76	3.18
VI (Co^{60})	37.0±0.5	1.17	3.16
VII (Co^{60})	42.5±0.5	1.33	3.19

[a] These values do not give the positions of the Compton edges but are shifted by the photo-multiplier statistics to slightly lower values.

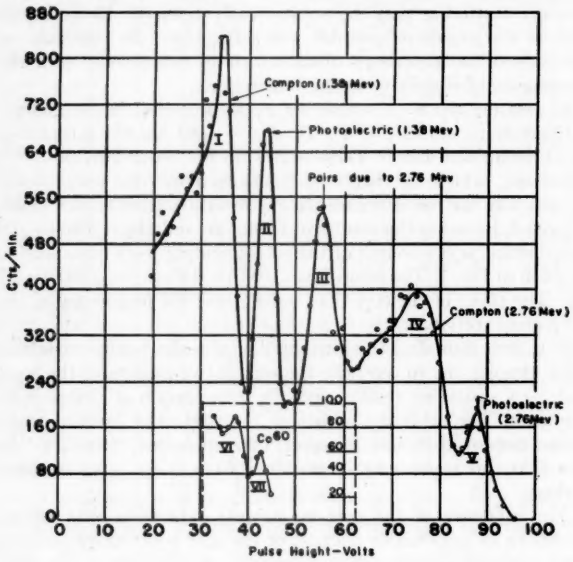

FIG. 1. Na^{24} collimated.

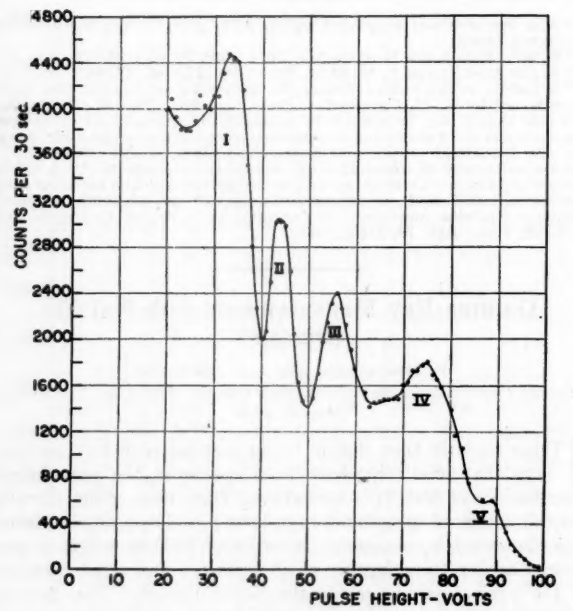

FIG. 2. Na^{24} uncollimated.

The general method made clear by Figs. 1 and 2 is based on determining gamma-ray energies by looking for associated triads consisting of two sharp lines separated by a broad peaked Compton distribution. The energy relations between these members of the triad are: highest energy peak[3] "photo-line" (E_{ph}), lowest energy peak "pair line" ($E_{pair}=E_{ph}-1.02$ Mev), and in between the Compton peak (E_c) near $E_{ph}-0.25$ Mev. At reasonably high energies E_{pair} and E_c predominate. At low energies E_c and E_{ph} predominate.

These results are not in agreement with those recently reported by Johannsen[4] with Na^{24} and NaI(Tl), since Johannsen did not observe pair lines. We have observed less resolution, apparently like Johannsen's, by using a large crystal.[1]

By using a two-crystal arrangement in coincidence[5] the two Compton lines appear at 34.5 and 77.5 volts (Fig. 3). The presence of the third "pair line" at 54 volts is caused by one of the two annihilation quanta being captured in the detector gate crystal. The appearance of the pair line suggests a modification of our two-crystal spectrometer at high energies. If the two annihilation quanta are captured in two separate crystals on opposite sides of the center crystal (struck by the gamma-rays), a coincidence

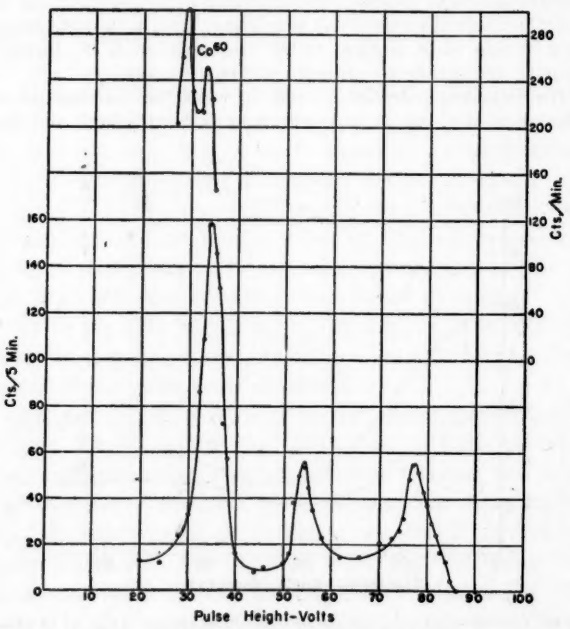

FIG. 3. Na^{24} two-crystal coincidence method.

between these signals can be used as a gate to eliminate completely all lines except pair lines.

The results given in Table I show that NaI(Tl) gives a linear response of pulse height *vs.* energy for electrons up to and including 2.76 Mev.

* This work received partial support from the U. S. Army Signal Corps and the joint program of the ONR and AEC.
[1] J. A. McIntyre and R. Hofstadter, Phys. Rev. **78**, 617 (1950).
[2] In a recent private communication Dr. R. W. Pringle has also reported observing pair lines.
[3] The "photo-line" probably has the full energy of the gamma-ray since the x-ray emitted by iodine is probably degraded and absorbed in the crystal.
[4] S. A. E. Johannsen, Nature **165**, 396 (1950).
[5] R. Hofstadter and J. A. McIntyre, Phys. Rev. **78**, 619 (1950).

Some Characteristics of the 11-Day Neodymium (147)

C. E. MANDEVILLE AND E. SHAPIRO
Bartol Research Foundation of The Franklin Institute, Swarthmore, Pennsylvania*
June 7, 1950

THE radiations of the 11-day neodymium (147) have been previously investigated[1-3] and the results obtained have been varied in character. In order to reinvestigate this activity, a quantity of exceptionally pure Nd_2O_3 prepared in ion exchange columns at the Institute for Atomic Research, Iowa State College, was irradiated by slow neutrons in the Oak Ridge pile.

Absorption curves in aluminum gave evidence of two beta-ray spectra having end points at 0.17 and 0.78 Mev. The intensity ratio is 1:2.

When the gamma-rays of Nd^{147} were absorbed in lead, components at 35 kev and 0.58 Mev were resolved. The gamma-rays were also absorbed in aluminum, and the half-value thickness of the softer component was found to be 0.33 cm, again indicating a quantum energy[4] of 35 kev. In order to ascertain more positively the nature of the soft quanta emitted in the decay of Nd^{147}, critical absorption measurements were carried out using as absorbers solutions of KI, $BaCl_2$, and $LaCl_3$. The absorption in barium and iodine was pronounced as compared with that in lanthanum, an indication that the soft quantum is the *K*-line of promethium. These critical absorption measurements are considered evidence that internal conversion takes place in the de-excitation of $*Pm^{147}$.

The beta-gamma-coincidence rate of Nd^{147} was measured as a function of aluminum absorber thickness before the beta-ray counter as shown in Fig. 1. The shape of the curve substantiates the previous conclusion that the beta-ray spectrum is complex. Since the gamma-ray counter of the beta-gamma-coincidence counting arrangement had been calibrated by the beta-gamma-coincidence rate of Sc^{46}, the curve of Fig. 1 could also be interpreted as showing that the inner beta-ray group at 0.17 Mev is coincident with the 0.58-Mev gamma-ray and that the harder beta-ray spectrum is coincident, on the average, with about 0.10 Mev of unconverted gamma-radiation.

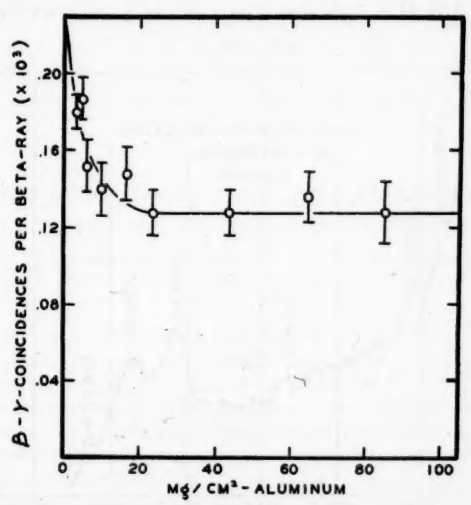

FIG. 1. The beta-gamma-coincidence rate of Nd^{147} as a function of the surface density of aluminum placed before the beta-ray counter. From this curve, it is concluded that both beta-ray spectra are coupled with unconverted quantum radiation.

A search for beta-beta-coincidences yielded no effect. The combined wall thickness and air path of each beta-ray counter was about 6 mg/cm². Soft conversion electrons having a range shorter than this amount would not have been detected. Since the beta-gamma-coincidence data do indicate quanta in coincidence with the harder beta-ray spectrum, and since the x-rays of promethium are very intense, it is concluded that each beta-ray of Nd^{147} is followed by one or more heavily converted gamma-rays in cascade, each one of which has an energy of 0.1 Mev or less. The absence of beta-beta-coincidences does show that the gamma-ray at 0.58 Mev is not appreciably converted.

No gamma-gamma-coincidences were detected in Nd^{147}. Whether this can be explained by excessive internal conversion of the soft cascade gamma-rays or by the low quantum efficiency of the counters for soft gamma-rays is not certain.

* Assisted by the joint program of the ONR and AEC.
[1] Marinsky, Glendenin, and Coryell, J. Am. Chem. Soc. **69**, 2781 (1947).
[2] C. O. Muehlhause, Plutonium Project Report CO-3750, 48 (January, 1947), quoted by G. T. Seaborg and I. Perlman, Rev. Mod. Phys. **20**, 585 (1948).
[3] Cork, Shreffler, and Fowler, Phys. Rev. **74**, 240 (1948).
[4] In a previous report C. E. Mandeville, Phys. Rev. **78**, 319 (1950), it was incorrectly stated that the x-rays are fourteen times more intense than the gamma-ray at 0.58 Mev. This estimate was based on the erroneous assumption that the quantum efficiency of the counter was linear with energy even at very low energies. The absorption data were obtained with the use of a counter equipped with a copper cathode so that a high quantum efficiency is developed in the x-ray region owing to the sharp rise in the value of the photoelectric absorption coefficient. The intensity of the x-rays relative to the other quantum radiations is thus exaggerated.

Properties of Single Crystals of Nickel Ferrite

J. K. GALT, B. T. MATTHIAS, AND J. P. REMEIKA
Bell Telephone Laboratories, Murray Hill, New Jersey
May 25, 1950

WE have succeeded in growing single crystals of nickel ferrite ($NiFe_2O_4$) and in determining several of their properties by measurements on small samples.

We find that NiO and Fe_2O_3 and $NiFe_2O_4$ dissolve in borax, and that at sufficiently high concentrations a precipitate forms. The data of Snoek[1] indicate that $NiFe_2O_4$ is in equilibrium with this system of compounds above about 1250°C, and we have therefore worked above this temperature. Our crystals are prepared as follows. A mixture of 16 to 17 g of borax glass (sodium tetra-borate fused and ground), 6.4 g Fe_2O_3, and 3.0 g NiO is heated in a platinum crucible to 1330°C and held there for 10 to 12 hr. It is then cooled at about 2°/hr. for 25 to 40 hr., and the furnace is then turned off completely. Crystals up to 2 mm on a side are found in the charge, although some are not structurally solid. Chemical analysis of the crystals confirms the formula $NiFe_2O_4$. The Ni and Fe proportions are within 0.1 percent of the values given by this formula, and impurity content is less than 0.5 percent.

We have measured the dielectric constant of these crystals using a capacitance bridge.[2] We find that $\epsilon=19$ at -185 to 195°C. Because of the high conductivity of the material, this value is only accurate to ± 20 percent and above this temperature satisfactory measurements were impossible. We also measured ϵ in a polycrystalline (ceramic) sample of nickel ferrite at -185 to -195°C and found $\epsilon=21$.

Saturation magnetization has been measured on a small crystal to an accuracy of about 10 percent by comparison with the deflection due to a small sample of iron in a hysteresis loop tracer[3]

and found to be 265 c.g.s. units. This is in agreement with the data of Guillaud and Roux[4] and in fair agreement with the value calculated using the picture developed by Néel.[5]

We have also measured the first-order crystalline magnetic anisotropy constant, K_1. This was done by measuring from hysteresis loops of a small crystal of known volume the difference in magnetization energies $\int HdM$ when the sample was magnetized along the (100) and the (111) directions. A spherical sample was used, so that the demagnetizing field was the same in all directions. The sample diameter was 0.10 cm. The value of K_1 obtained in this way is less accurate than that obtained from ferromagnetic resonance measurements,[6] but it is probably good to within 10 percent. We find that $K_1=-6.2\times10^4$ ergs/cc at room temperature and $K_1=-8.7\times10^4$ ergs/cc at -190°C.

Finally, measurements of complex initial permeability $(\mu'-j\mu'')$ have been made on two extremely small circular rings of square cross section cut so that the plane of the rings was the (111) crystal plane. Their dimensions were approximately as follows: outside diameters 0.1 cm, inside diameters 0.025 cm, thickness 0.04 cm. Measurements were obtained by making each ring the core of a solenoid and measuring the impedance of the solenoids on a radiofrequency Maxwell-type inductance bridge. A plot of the data obtained on the first ring is shown in Fig. 1. The second

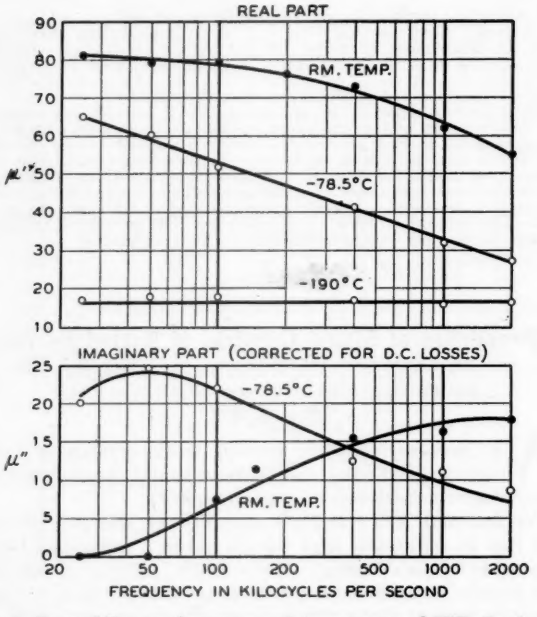

FIG. 1. Permeability *vs.* frequency and temperature of $NiFe_2O_4$ ring in (111) plane.

ring gave similar results. No measurable losses occurred at -190°C, so μ'' is not given for that temperature. The resistance as measured was corrected for the resistance of the solenoid wire before μ'' was calculated. The inductance due to the loop formed by the lead to the bridge terminals was also corrected for as well as possible before μ' was calculated from the measured inductance. It is felt, however, that this latter correction may have been inadequate by enough to reduce all values of μ' by about 10. This would have no effect on the relative values of μ', which we feel are more accurate than this, but it makes it possible to account for the value of μ' at -190°C in terms of the rotation of magnetization against crystal anisotropy.

It seems quite clear from Fig. 1 that a relaxation phenomenon is occurring, and since the permeabilities at temperatures above -190°C are much higher than those to be expected from the rotation of magnetization against crystalline anisotropy, the relaxation must be connected with domain wall motion. The sharp temperature dependence of the relaxation time suggests that the mechanism involves an activation energy, but we do not at present know the nature of the mechanism.

The authors wish to express their gratitude to W. L. Bond, C. D. Owens, and H. G. Hopper for technical assistance, and to Dr. C. Kittel for helpful discussions.

[1] J. L. Snoek, Physica **3**, 463 (1936), Fig. 7.
[2] W. D. Voelker, Bell Lab. Record **20**, 133 (1942).
[3] The hysteresis loop tracer used for this measurement was of the same general design as that of Wiegand and Hansen, Trans. A.I.E.E. **66**, 119 (1947). The samples used were of the order of 1 mg in weight.
[4] C. Guillaud and M. Roux, Comptes Rendus **229**, 1133 (1949).
[5] L. Néel, Ann. de physique **3**, 137 (1948).
[6] Yager, Galt, Merritt, Wood, and Matthias, Phys. Rev. **79**, 214 (1950). See also a paper to be published later.

Gamma-Rays from Po–Be Neutron Source and the Excited State of C^{12}

P. R. BELL AND W. H. JORDAN
Oak Ridge National Laboratory, Oak Ridge, Tennessee
May 25, 1950

A NUMBER of gamma-rays have been reported from the $Be^9(\alpha,n)C^{12}$ reaction produced by the α-particles from polonium.[1–3] The recent report by Terrell shows only one gamma-ray at 4.3 Mev in the range 2 to 10 Mev. His measurements were made by a magnetic pair spectrometer. The gamma-ray[4] comes from the excited state of C^{12}. Our measurement of this gamma-ray gives the value 4.44 ± 0.03 Mev and agrees well in energy with that reported by Bradford and Bennett[5] at 4.44 or 4.46 Mev. Their value was obtained by measuring the neutrons produced by monoenergetic alpha-particles.

We have used a scintillation spectrometer with a sodium iodide, thallium phosphor to measure the gamma-rays from a 5-curie Po–Be source. The crystal was shielded from the source neutrons by paraffin and boron. The energy calibration was accomplished by using the 2.62-Mev gamma-ray of ThC″ from natural thorium and the 0.661-Mev gamma-ray of Cs^{137}.

Figure 1 shows the pulse distribution in the energy range from zero to 4.6 Mev. In NaI, pair production and photoelectric peaks are quite prominent. The three peaks at 3.44, 3.94, and 4.42 Mev are due to a single gamma-ray of 4.44 ± 0.03 Mev. The peak of pulses at 4.42 Mev is produced by photoelectric effect with capture of the x-rays emitted from the iodine atom in which it occurs and by pair formation where both members of the pair are stopped and the annihilation radiation from the positron is completely absorbed, giving the full energy of the gamma-ray. The peak at 3.44 Mev is produced by stopping a pair with complete

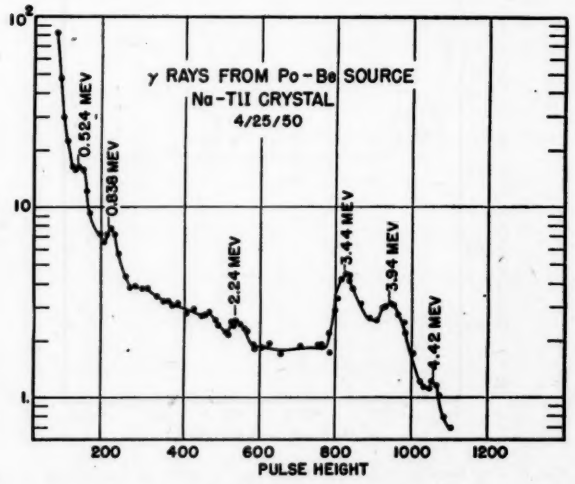

FIG. 1. Pulse distribution produced in the scintillation spectrometer by the gamma-rays of a Po-Be neutron source.

escape of the annihilation radiation; the intermediate peak is due to escape of only one annihilation photon. The continuum of Compton electrons of lower energy than these peaks has riding on it a number of other peaks. The weak peak at 2.24±0.04 Mev seems to be a photoelectric peak due to the capture gamma-ray of hydrogen in the paraffin. The peak at 0.83 Mev is that produced by the nuclear gamma-ray of polonium, while the peak at 0.52 Mev is that due to the excited state of Li^7 at 0.478 Mev. This radiation is produced by neutron capture in the boron shield.

Figure 2 shows the high energy section of the spectrum from 4.4 to 8.4 Mev. Integral counting shows that there is no significant number of pulses above this energy. The upper branch of this curve having a peak at about 6.4 Mev (gamma-ray energy 7.4 Mev) was obtained when a portion of the boron shield was

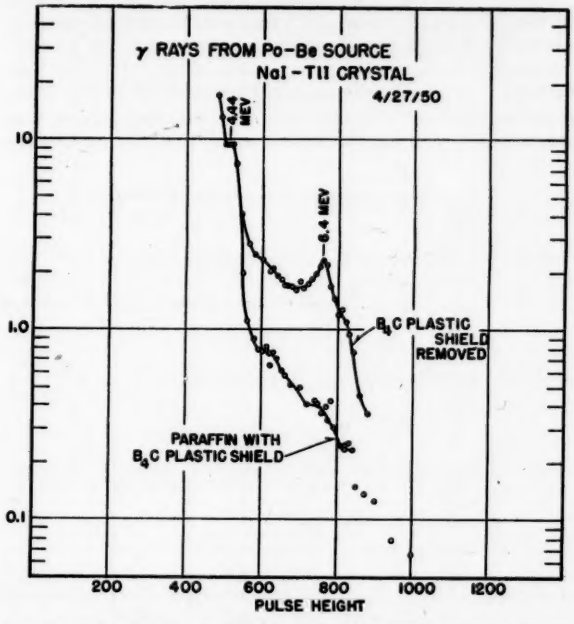

FIG. 2. Pulse distribution produced by a Po–Be neutron source between 4 and 8 Mev.

removed allowing the neutrons to strike the iron magnetic shield of the photo-multiplier. The small bulge in the shielded curve at about this same energy may well be due to neutrons escaping the paraffin and boron and reaching the iron.

[1] W. Bothe, Zeits. f. Physik **100**, 273 (1936).
[2] B. S. Dzelepov, Comptes Rendus, U.S.S.R. **23**, No. 1, 24 (1939).
[3] J. Terrell, Phys. Rev. **79**, 239 (1950).
[4] W. F. Hornyak and T. Lauritsen, Rev. Mod. Phys. **20**, 191 (1948).
[5] C. E. Bradford and W. E. Bennett, Phys. Rev. **78**, 302 (1950).

Variation of the Decay Time of the Fluorescence of Anthracene and Stilbene with Temperature

J. O. ELLIOT, S. H. LIEBSON, AND C. F. RAVILIOUS
Electricity Division, Naval Research Laboratory, Washington, D. C.
May 22, 1950

SINCE many of the early discrepancies of fluorescence decay time measurements of scintillating crystals were resolved when the phosphor temperature was taken into account, it became of interest to investigate the fluorescence decay time for a given phosphor over a wide range of temperatures. Kelley and Goodrich[1] published measurements of the decay time of anthracene in the temperature range 78 to 308°K; they found a linear variation of the decay time in this temperature range and extrapolated their linear curve finding a zero time intercept at 0°K. A report of preliminary data from this laboratory[2] gave the results of measurements of the decay time of anthracene at 290, 80, and 4°K; these

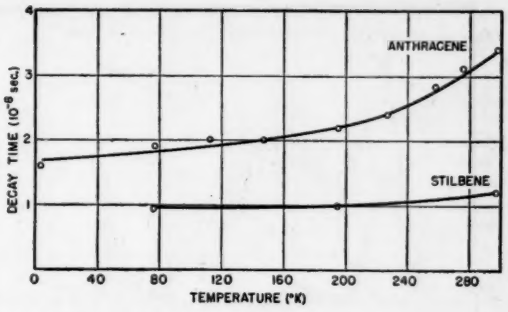

FIG. 1. Variation of the decay time of fluorescence with temperature.

results were in substantial agreement with those of Kelley and Goodrich at the two higher temperatures.

In order to extend the knowledge of the variation of the fluorescence decay time with temperature, a series of measurements have been made on an anthracene single crystal in the temperature range 4 to 298°K and on a stilbene single crystal in the range 78 to 298°K. The phosphor was mounted on the end of a quartz bar eight inches from the photo-cathode of a 931-A photo-multiplier; the phosphor was placed in the desired temperature bath while the photo-multiplier was operated at room temperature. A 10-μC Ra source was used for excitation, and the output of photo-multiplier was fed into a shorted coaxial line apparatus[3] to measure the decay time.

The results of these measurements are shown in Fig. 1, and they indicate within the limits of experimental error (±10 percent) that the decay time approaches a constant value at low temperatures. In the case of stilbene, measurements taken at widely spaced temperature points show its decay time to be almost a constant from dry ice temperature to room temperature. It should be noticed that variation of the stilbene light output with temperature is also approximately constant.[4] A suitable explanation for the variation of apparent time of decay with temperature can be made in terms of additional metastable states in the crystal. However, without further spectroscopic information such conclusions may not be warranted.

[1] G. G. Kelley and M. Goodrich, Phys. Rev. **77**, 138 (1950).
[2] S. H. Liebson and J. O. Elliot, Phys. Rev. **78**, 65 (1950).
[3] Elliot, Liebson, Myers, and Ravilious, Rev. Sci. Inst. (to be published).
[4] S. H. Liebson and J. W. Keller, Jr., Phys. Rev. **78**, 305 (1950).

The Low Energy Neutron Spectrum from $Li^7(d,n)Be^8$

W. D. WHITEHEAD
Bartol Research Foundation of The Franklin Institute, Swarthmore, Pennsylvania*
June 2, 1950

THE neutron spectrum from the $Li^7(d,n)Be^8$ reaction has been investigated by several observers, but the presence of the Li^6 isotope made it infeasible to interpret the low energy portion of the spectrum unambiguously. Staub and Stevens[1] observed the spectra in a cloud chamber using both recoil protons and recoil α-particles to determine the energy of the neutrons. With both gases they found a plateau which they attributed to the continuous distribution of neutrons from $Li^7+d \rightarrow He^4+He^5$, $He^5 \rightarrow He^4+n$, and an increase in intensity at about 1.5 Mev, but with the helium they also observed a group at 5.5 Mev which was not present in the proton spectra. Richards[2] made the first investigation of the spectra using photographic plates but he used such large energy intervals that the resolution was poor in the low energy region. Green and Gibson[3] have investigated carefully the high energy portion of the spectra at several angles using photographic plates and have determined the shape of several of the groups more accurately than did previous investigators.

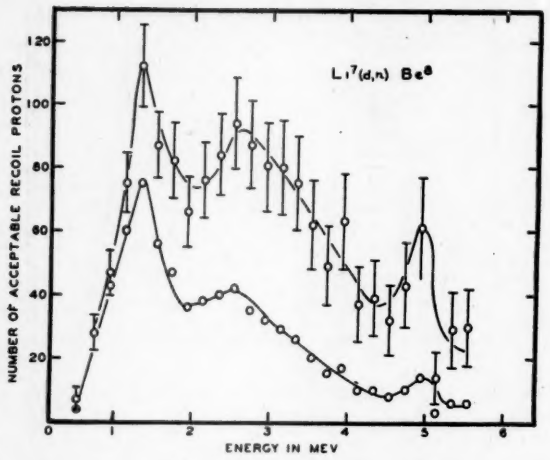

FIG. 1. Low energy neutrons from the disintegration of Li^7 by deuterons. The curve on which the probable errors have been indicated has been corrected for variation with energy of $n-p$ scattering cross section and acceptance probability.

A 100-kev thick target of Li_2SO_4, in which the Li was[4] 99.8 percent Li^7, was bombarded with 1.1-Mev deuterons from the Bartol Van de Graaff generator, and Ilford C_2 plates 10 cm from the target at 0° to the beam were irradiated with the reaction neutrons for approximately 5 μa hr. The recoil protons with ranges less than 210μ and an acceptance angle of 15° were counted. The angle between the direction of the beam and the recoil proton in the horizontal plane of the plate were recorded and the energies corrected according to the relation $E^2=E_n^2\cos^2\theta$. Seven hundred tracks were measured and these are plotted in 0.2-Mev intervals in Fig. 1.

Besides the continuum of neutrons from $Li^7+d\rightarrow He^4+He^5$, $He^5\rightarrow He^4+n$ there are two groups of neutrons which must arise from the reaction $Li^7+d\rightarrow Be^8+n$, at 1.36 and 4.9 Mev and give levels in Be^8 at 14.7 and 11.1 Mev; neutrons from carbon would give a group at approximately 0.8 Mev. The general shape of the curve agrees with that of Staub and Stevens, both curves having a peak at approximately 1.5 and 5 Mev besides the continuum.

* Assisted by the joint program of the ONR and AEC.
[1] H. Staub and W. E. Stephens, Phys. Rev. **55**, 845 (1939).
[2] H. T. Richards, Phys. Rev. **59**, 796 (1941).
[3] L. L. Green and W. M. Gibson, Proc. Phys. Soc. London **62**, 407 (1949).
[4] Furnished by Y-12 Plant, Oak Ridge, Tennessee.

A Measurement of the Positive π-μ-Decay Lifetime*

O. CHAMBERLAIN, R. F. MOZLEY, J. STEINBERGER, AND C. WIEGAND
Radiation Laboratory, Department of Physics, University of California, Berkeley, California
June 5, 1950

THE lifetime of π-mesons was first measured by Richardson[1] and later by Martinelli and Panofsky.[2] The method was the same in both cases: the fraction of π-mesons surviving various times of flight was measured by placing photographic detectors at various path lengths from a target in which π-mesons were produced.

In the experiment reported here we have observed the decay of π-mesons through the light emitted by a *trans*-stilbene crystal in which the decay events occur. The mesons were produced in a paraffin target which was placed in the x-ray beam of the 340-Mev synchrotron. The mesons of interest here passed through the first crystal and came to rest in the second crystal. There were three bursts of light from the second crystal when (1) the meson came to rest, (2) the (positive) π-meson decayed to a μ-meson which also came to rest in the crystal, and (3) the μ-meson decayed to a positron which escaped from the crystal. Photo-multiplier tubes were used to detect the light from the stilbene crystals.

As outlined in Fig. 1, a coincidence between the two detectors was used to start the sweep (10^{-8} sec./mm) of an oscilloscope and to initiate a delayed gate circuit (gate open from 0.5 to 2.5 μsec.). The output of the second detector was delayed 0.5×10^{-6} sec., amplified in a fast distributed amplifier, and fed to the vertical deflection plates of the oscilloscope. The oscilloscope traces, which were recorded photographically on a continuously moving film,

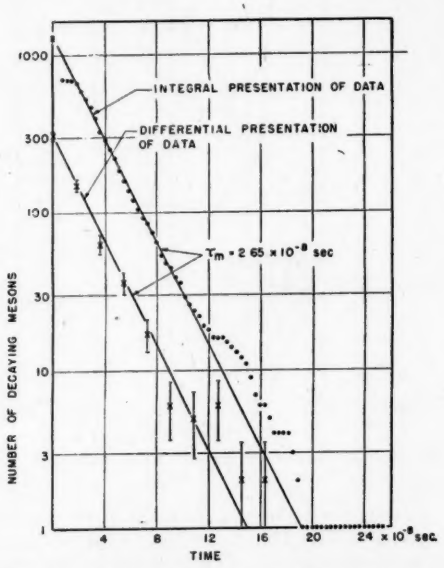

FIG. 2. Decay rate of the positive π-meson. The zero-time point on the integral curve represents all marked traces minus accidental traces. The zero-time point on the differential curve represents those traces with pulse separation between 2.17 and 3.98×10^{-8} sec., the next point those between 3.98 and 5.79×10^{-8} sec., etc.

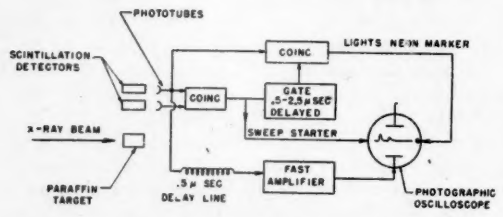

FIG. 1. Block diagram of apparatus.

showed in every case the pulse which initiated the sweep. If the responsible particle was a π^+-meson which stopped in the crystal, and if the meson lived at least 2×10^{-8} sec. before decaying to a μ-meson, then two pulses were seen on the trace. Measurement of the separation of these two pulses determined the life span of that meson. On some traces a third pulse was seen due to the μ-meson decay, although in most instances the sweep was finished before the μ-meson decayed. The purpose of the 0.5- to 2.5-μsec. delayed gate was to detect electronically the μ-meson decay. When a pulse fell within this gate time a neon bulb at the edge of the oscilloscope face flashed.

We consider only those pulses marked by a neon bulb flash. By so doing, we use a group of pulses constituted as follows. Five percent are background due to accidental coincidences of extraneous pulses with the delayed gate; three percent are μ-mesons formed by π-mesons which decayed in flight; 92 percent (1302 in number) are π^+-mesons stopped in the crystal. A total of 554 traces showed two distinct pulses whose separations could be measured with certainty.

In the differential interpretation of these data we ignore part of the information and consider only those 554 mesons which lived longer than 2.18×10^{-8} sec., so the time of their decay is accurately known. The information used is that shown in the differential decay curve of Fig. 2, where the curve is displaced toward the left to separate the two curves. The alternative integral interpretation takes account of the fact that the number of mesons decaying before 2.18×10^{-8} sec. (748) is also known, and so their mean life can be estimated. The integral decay curve of Fig. 2 shows the number of mesons decaying after time t *vs.* t.

The greater statistical accuracy obtainable with the integral interpretation is offset by the limited accuracy with which the total number of mesons stopped can be determined.

The mean life (with the calculated standard deviation) is:

$$\tau=(2.65\pm0.12)\times10^{-8}\ sec.\ \text{(differential interpretation)},$$
$$\tau=(2.59\pm0.12)\times10^{-8}\ sec.\ \text{(integral interpretation)}.$$

The previously reported values are

$$\tau=\left(1.11\pm\frac{0.45}{0.35}\right)\times10^{-8}\ \text{sec. (Richardson)},$$

$$\tau=\left(1.97\pm\frac{0.21}{0.25}\right)\times10^{-8}\ \text{sec. (Martinelli and Panofsky)}.$$

While this note was in preparation a third measurement has been reported by Kraushaar, Thomas, and Henri.[3] Using a method somewhat similar to ours they find that

$$\tau=(1.65\pm0.33)\times10^{-8}\ \text{sec.}$$

We wish to thank Professors E. McMillan and E. Segrè for their encouragement.

* This work was supported by the AEC.

[1] J. Richardson, Phys. Rev. **74**, 1720 (1948).
[2] E. A. Martinelli and W. K. H. Panofsky, Phys. Rev. **77**, 465 (1950).
[3] Kraushaar, Thomas, and Henri, Phys. Rev. **78**, 486 (1950).

The Coherent Neutron Scattering Cross Sections of Nickel and Its Isotopes

W. C. Koehler, E. O. Wollan, and C. G. Shull
Oak Ridge National Laboratory, Oak Ridge, Tennessee
May 26, 1950

THE coherent scattering cross section of normal nickel has been found from neutron diffraction measurements to be 13.5 barns.[1] The total scattering cross section has been measured by the Columbia group to be 17.0 barns.[2] Since the three major isotopic constituents of nickel are even-even isotopes, it is reasonable to ascribe the difference between the total and coherent scattering cross sections to the isotope effect, and since this difference is large it might be expected that the scattering properties of the different isotopes would be widely different. Accordingly, samples of nickel oxide (NiO) enriched in Ni^{58}, Ni^{60}, and Ni^{62} were studied with the crystal spectrometer. The scattering cross sections of Ni^{58} and Ni^{60} had been previously measured in this laboratory,[1] but under less favorable conditions than existed for the present set of measurements.

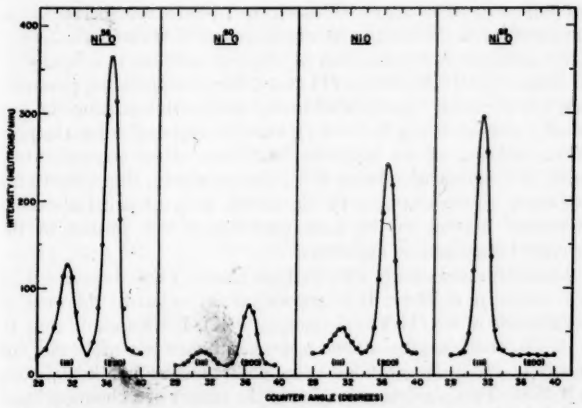

FIG. 1. Partial neutron diffraction patterns of isotopically enriched samples of NiO.

TABLE I. Scattering amplitudes and cross sections.

Isotope	Coherent scattering amplitude (10^{-12} cm)	σ (barns)	Contribution to normal nickel amplitude (10^{-12} cm)
Ni^{58}	1.48	27.6	1.00
Ni^{60}	0.28	0.97	0.073
Ni^{62}	−0.85	9.1	−0.032
Ni	1.03	13.3	−0
		Total	1.04

NiO is also of interest because of its magnetic properties. The neutron diffraction patterns of the various oxides all show, in addition to the nuclear peaks which vary from isotope to isotope, antiferromagnetic reflections which are identical in all samples within experimental error. Preliminary results of the magnetic scattering experiments have been given by Shull,[3] and a detailed report will be made at a later date.

In Fig. 1 are shown portions of the diffraction patterns obtained from the four oxide samples studied. These have all been normalized so that a direct comparison of the peak intensities can be made. The interpretation of the diffuse scattering is complicated by the fact that it is contributed to by isotopic diffuse scattering, multiple scattering, and scattering by the sample window, so that a direct comparison of the diffuse scattering in the patterns is not permissible. Since NiO has the rocksalt structure, a simple inspection of the diffraction pattern is sufficient to establish the phase of scattering of the nickel isotopes relative to that of oxygen. Clearly all scatter with positive phase except Ni^{62}, as evidenced by the very weak or absent (200) reflection in the pattern of $Ni^{62}O$.

The effective scattering amplitudes obtained from the isotopically enriched oxides were corrected for isotopic impurity and the resultant coherent scattering amplitudes and cross sections are given in Table I. In addition, the contribution of each of the isotopes to the normal nickel amplitude has been calculated, and the sum compared with the nickel amplitude as measured directly. The agreement between these two results is excellent.

As one sees, these three isotopes of nickel show marked differences in their scattering properties. In each case the scattering cross section differs widely from the potential scattering which has a value for Ni of about 4.4 barns,[4] and hence there must be a strong contribution from resonance effects. In the case of Ni^{58}, which has an unusually large cross section, a virtual resonance is indicated since only for $E>E_r$ does one get large cross sections due to constructive inteference between potential and resonance scattering. The small cross section for Ni^{60} most probably corresponds to a point near the minimum arising from destructive interference between potential and resonance scattering, and hence to a positive energy resonance. The relatively large negative scattering amplitude found for Ni^{62} must also correspond to a positive energy resonance. The only definitely known resonance for nickel that could account for either of these observed cross sections falls[5] at 3600 ev. For a resonance level at this energy to be responsible on the basis of the one level Breit-Wigner formula for either of the above observed thermal scattering amplitudes requires a neutron width of the order of 1000 ev.

[1] C. G. Shull and E. O. Wollan (unpublished work). Bernstein, Dial, Stanford, and Stephenson, Phys. Rev. **75**, 1302 (1949).
[2] Havens, Rainwater, Wu, and Dunning, Phys. Rev. **73**, 963 (1948).
[3] C. G. Shull, Phys. Rev. **78**, 638T (1950).
[4] Feshbach, Peaslee, and Weisskopf, Phys. Rev. **71**, 145 (1947).
[5] Ruderman, Havens, Taylor, and Rainwater, Phys. Rev. **75**, 1296 (1949).

Meissner Effect in Superconducting Alloys of Indium and Thallium

J. W. STOUT AND LESTER GUTTMAN
Institute for the Study of Metals, University of Chicago, Chicago, Illinois
May 29, 1950

THE magnetic properties associated with the superconductivity of solid solutions containing 5, 10, 15, and 20 atomic percent thallium in indium have been investigated. The samples were cylindrical rods, 0.6 cm diameter and 15 cm long, grown from the melt in a single crystal furnace. The etched surface of the crystals showed some twin markings, due presumably to slight deformation, and a very small volume or recrystallized material near these markings. The bulk of each specimen, however, was of a single crystallographic orientation. The composition of each sample was determined by chemical analysis of pieces cut from its ends. The 5 and 10 percent samples were uniform in composition within the accuracy of the analysis (0.2 percent of the thallium content). The 15 percent sample varied from 14.91 to 15.26 atom percent Tl and the 20 percent sample from 19.36 to 20.45. The samples were mounted in a helium cryostat in a longitudinal magnetic field uniform to 1.5 percent over the length of the specimens. The change in magnetic induction produced by interruption of the magnet current was measured by small coils wound around the equator of each sample and connected to a ballistic galvanometer.

We have found the behavior of these specimens to resemble much more that of pure metals than has been found previously[1] for alloys. In particular, most of the magnetic flux is expelled on decreasing the magnetic field below a critical value (Meissner effect). If the critical field is taken as that at which penetration begins for increasing field strength, then for all of the samples and for temperatures between 1.3 and 3.2°K the trapped flux remaining in zero applied field varied between 15 and 20 percent of that corresponding to complete penetration at the critical field. The initial penetration of flux into the sample upon isothermal application of a magnetic field occurred sharply for all samples. For the 5 and 10 percent specimens the penetration was complete within a two percent range of field strength, but occurred more gradually for the 15 and 20 percent samples. At the lowest temperature and for the 20 percent sample a field of nearly double that at which flux penetration began was needed before it was complete. The transition temperatures extrapolated to zero magnetic field strength agree fairly well with those determined from resistance measurements by Meissner, Franz, and Westerhoff.[2] Shoenberg[3] has shown that the compound Au_2Bi when properly prepared has superconducting properties resembling those of a pure metal and has suggested that the usual behavior of alloys is due to secondary causes, such as inhomogeneities. Our measurements support this idea but show further that the inhomogeneity on an atomic scale which is present in a disordered solid solution, and which drastically changes the resistance of the normal metal at low temperatures,[2] is apparently not responsible for the anomalous magnetic behavior that has previously been found in alloys.

[1] K. Mendelssohn, Rep. Prog. Phys. 10, 358 (1946). D. Shoenberg, *Superconductivity* (Cambridge University Press, London, 1938), Chapter VI.
[2] Meissner, Franz, and Westerhoff, Ann. d. Physik 13, 505 (1932).
[3] D. Shoenberg, Nature 142, 874 (1938).

Alternating Current Conduction in Ice

E. J. MURPHY
Bell Telephone Laboratories, Murray Hill, New Jersey
May 25, 1950

THE a.c. conductivity of any dielectric which exhibits anomalous dispersion due to a polarization of a single relaxation time increases monotonically with frequency and approaches a limit which we shall call σ_p. This quantity may be described as the *polarization conductivity* or *local conductivity* of the dielectric; it is a property of the polarizable structures which determine the dielectric constant.[1]

The writer has obtained data on the conductivity of ice which show that σ_p is given by

$$\sigma_p = 631 e^{-11500/RT}\ (\text{ohm}\cdot\text{cm})^{-1} \qquad (1)$$

in the interval (0, −35°C); R is the gas constant, T the absolute temperature. (The full expression, to be given later, has two terms.)

Pauling's theory of the residual entropy of ice, based on the assumption that each hydrogen nucleus has available at all temperatures two equivalent sites, is in good agreement with experiment.[2] Therefore we discuss Eq. (1) in terms of a model consistent with Pauling's model for ice, by assuming that the elementary polarizable structure in ice is a proton moving back and forth on the line between two adjacent oxygen atoms O_1 and O_2. We assume that the proton traverses a distance d and crosses an activation energy barrier of height w in moving from a site 0.99A from O_1 to a site 0.99A from O_2. An expression for σ_p can be derived for this model of the elementary polarization process by assuming that the probability that the proton has at least the energy w is given by an equilibrium calculation similar to that for the equilibrium between a solid and its vapor, and that while the proton has the energy w it is effectively moving as a gas particle in a one-dimensional box of length d with the average velocity of a Maxwell distribution. This motion is "biased" by the applied field E, and the resultant current is

$$i = ne[(2\pi mkT)^{\frac{1}{2}}/h]de^{-w/kT}(kT/2\pi m)^{\frac{1}{2}}2\sinh(Eed/2kT), \qquad (2)$$

where m is the mass of the proton, k is Boltzmann's constant, h is Planck's constant, e is the charge on the proton, and n is the number of protons per cc. If in Eq. (2) we take $\sinh x \cong x$ and change from e.s.u. to $(\text{ohm}\cdot\text{cm})^{-1}$ and from w in ergs per molecule to W in cal./mole, we obtain

$$\sigma_p = (9\times10^{11}h)^{-1}ne^2d^2\exp(-W/RT)(\text{ohm}\cdot\text{cm})^{-1}. \qquad (3)$$

From Eqs. (1) and (3) we have

$$ne^2d^2(9\times10^{11}h)^{-1} = 631\ (\text{ohm}\cdot\text{cm})^{-1} \qquad (4)$$

and taking $n = 2\times3.06\times10^{22}$, $e = 4.8\times10^{-10}$, $h = 6.55\times10^{-27}$, we get $d = 1.6\times10^{-8}$ cm. Pauling gives as the separation of the two equivalent sites of the hydrogen nucleus 0.78A. Taking d to be the average value of the projection in the field direction of randomly directed vectors 0.78A in length, we obtain 0.39×10^{-8} cm as the number with which the value $d = 1.6\times10^{-8}$ cm calculated above should agree.

The assumption in this model that the proton does not have vibrational energy when it is occupying its proper site 0.99A from an oxygen atom is a simplification based in part on the following consideration. There is an infra-red absorption for ice at $\lambda = 4.7\mu$ which is distinguished from the other bands by the fact that it does not appear in water vapor.[3] This suggests that it is associated with the presence of the hydrogen bond between H_2O molecules in ice. If we attribute it to vibration of the proton when it is bound in its proper site 0.99A from an O atom, the corresponding partition function should be represented in the model. But putting the frequency corresponding to $\lambda = 4.7\mu$ into the expression for the partition function of an harmonic oscillator gives approximately unity at temperatures below 0°C. Consequently, this vibrational frequency will not appear in the model. It is assumed also that vibrations normal to the path direction of the proton in the activated state can be neglected.

The activation energy (W) derived from (1) has the value 11.5 kcal./mole, or 0.50 ev. It is approximately equal to the heat of sublimation of ice (11.8 kcal./mole at 0°K). If we assume that W is due to the breaking of two hydrogen bonds per molecule, the energy of the hydrogen bond in ice comes out as 5.75 kcal./mole, or 0.25 ev. This is a determination of the energy of a chemical bond by means of radiofrequency measurements of dispersion: it agrees with the value 5.8±0.2 kcal./mole given by Fox and Martin as

the energy of the hydrogen bond derived from the heat of sublimation.[4,5]

[1] Murphy and Morgan, Bell Sys. Tech. J. 38, 502 (1939).
[2] Pauling, *Nature of the Chemical Bond* (Cornell University Press, Ithaca, New York, 1945), p. 301.
[3] Schaeffer and Matossi, *Das Utrarote Spektrum* (Verlag. Julius Springer, Berlin, 1930), p. 243.
[4] Fox and Martin, Trans. Faraday Soc. 36, 910 (1940).
[5] Bernal and Fowler, J. Chem. Phys. 1, 515 (1933).

An Attempt to Detect Thermal Energy Positrons*

LEON MADANSKY AND FRANCO RASETTI
Johns Hopkins University, Baltimore, Maryland
May 25, 1950

IT has been assumed that positrons diffuse through a solid during their lifetime.[1] It was considered worth investigating whether they would diffuse through and out of various materials. The number, n_s, of positrons of thermal energies diffusing out of a unit surface per unit time can be estimated as follows. The "average diffusion length" L is expressed by the formula $L=(\frac{1}{3}\lambda v\tau)^{\frac{1}{2}}$, where λ is the mean free path for elastic collisions, v the average thermal velocity, and τ the mean life. Assuming λ to be of the order of 10^{-8} cm, τ of the order[1] of 10^{-9} sec., the average diffusion length in a heavy metal would be of the order of $6\cdot10^{-6}$ cm. This means that the number of thermal positrons diffusing out of a metal should be of the order of the number of positrons stopped in a layer $6\cdot10^{-6}$ cm thick. This number may be compared with the number, n_f, of fast positrons emitted by the same material, assuming the radioactive atoms to be uniformly distributed. Fast positrons emerge from a layer of thickness equal to the range, or rather, in view of the continuous energy spectrum, of the order of the reciprocal of the absorption coefficient.

An experiment was attempted using as sources copper foils of initial activity of the order of 10 to 30 mC. The absorption coefficient of the positrons of Cu^{64} in copper may be taken[2] as 30 cm^3/g, hence fast positrons emerge from a layer 0.032 g/cm^2 or 0.0038 cm thick. Then the ratio n_s/n_f should be of the order of $5\cdot10^{-3}$.

In order to detect a small fraction of thermal energy positrons above the larger background of fast positrons, the following arrangement was used. The positron source was mounted at one end of an evacuated tube, containing, at a distance of 80 cm from the source, a thin aluminum foil kept at a negative potential and acting as positron collector. A pair of scintillation counters, placed opposite the collector and at 180° from each other, detected the positrons falling on the collector by means of coincidences between the two quanta of the annihilation radiation. The collector subtended approximately 5×10^{-5} of the total solid angle from the source, hence it absorbed less than that fraction of the fast positrons emerging from the copper foil. To increase the efficiency of collection of slow positrons, the tube was placed in an axial magnetic field of the order of 100 gauss. The tube, including a grid placed at 1 cm from the source, was at zero potential, and the source was either at +150 or −150 volts. Under these conditions with a positive source potential we expect the collector to capture most of the emerging thermal energy positrons, whereas none would reach the collector when the source is at a negative potential. From this calculation we might expect the effect of the thermal energy positrons, given by the difference in the numbers of counts with positive and negative source potentials, to be as much as 100 times greater than the fast positron background. Even allowing for a margin of error in the estimate of the mean life and mean free path, there should still be a considerable effect.

No difference in the number of counts exceeding the statistical error (about five percent) was observed. In order to avoid the possible unfavorable effect of the oxide layer on the copper surface, clean surfaces of various materials were used. A thin platinum foil heated at 1450°C in order to eliminate surface layers of adsorbed gases and other impurities gave negative results. No effect was observed with potassium evaporated in vacuum. Finally, assuming that positrons might diffuse in a liquid but not in a solid, we tried a thin, liquid layer of gallium evaporated in vacuum, and also obtained a negative result. No effect was observed with insulating layers of glass, mica, celluloid, and octoil.

In all these experiments the annihilation radiation from fast positrons reaching the collector was readily detectable, giving 20 to 100 counts per minute. The number of counts was almost doubled when the magnetic field was turned on, owing to partial focusing of the low energy portion of the positron spectrum. However, the effect was totally insensitive to the polarity of the source potential, showing that it was not due to positrons with energies of less than 150 ev.

In order to be certain that failure to observe the effect was not due to improper arrangement of the electric and magnetic fields, insufficiently good vacuum, or other imperfect experimental conditions, the identical arrangement was tested with electrons by coating the above-mentioned platinum foil with emitting oxides. With the filament at −150 volt, we immediately recorded large currents on the collector, even with much weaker magnetic fields than had been used in the previous experiments, showing the high efficiency of our focusing arrangement.

The conclusion is that thermal energy positrons do not appear to diffuse out of solids or liquids. Possible reasons are: (1) positrons do not diffuse through a crystal lattice, but are trapped in potential minima and annihilate before moving appreciable distances; (2) positrons diffuse through the lattice but are trapped at the surface; and (3) positronium is formed, and even if it should diffuse out of the material, it would not be detected in these experiments.

We wish to thank Dr. T. H. Berlin for stimulating discussions.

* This document is based on work performed for the AEC.
[1] DeBenedetti, Cowan, Konneker, and Primakoff, Phys. Rev. 77, 205 (1950).
[2] E. Bleuler and W. Zünti, Helv. Phys. Acta 19, 375 (1946).

Nuclear Magnetic Resonance in Metallic Hydrides

MARTIN A. GARSTENS
Electricity Division, Naval Research Laboratory, Washington, D. C.
May 29, 1950

THE method of nuclear magnetic resonance has been applied to the determination of the resonance absorption line widths at room temperature in some of the metal hydrides. The latter range in structure from true compounds to absorption mixtures, interstitial compounds, and solid solutions. It is frequently difficult to decide, in the cases of certain hydrides, which of these structures is present, especially since the same hydride may have different structures depending on the concentration of hydrogen present. Thus, palladium hydride is thought to exist as two immiscible solid solutions approaching a true compound as the concentration of hydrogen is increased.[1] As the concentration of hydrogen increases, tantalum is believed to go from a body-centered cubic phase to a hexagonal phase and back again to a body-centered cubic phase.[1] In some of these it is difficult to make out whether the hydrogen atoms or molecules wander freely through the metal lattice or cluster about certain fixed positions. A clue as to these possibilities is offered by observations of the nuclear magnetic absorption line widths due to proton resonance.

The experimental apparatus was similar to that of Bloembergen, Purcell, and Pound[2] except for the use of a twin T radio-frequency bridge. A phase-sensitive detector of about 1-cycle band width was used, since the resonance signals were too weak to be observed directly on an oscilloscope.

The spread between the maximum and minimum slopes of the absorption lines, as indicated on the output meter of the lock-in amplifier, was taken as a measure of the line width. The resonances

were observed as 28 Mc in a magnet which had a field inhomogeneity of about one gauss over the volume occupied by most of the samples.

Of the various metallic hydrides which were available to us, the line width data of titanium and tantalum are most significant.[3] The titanium hydride was available with hydrogen concentrations of 157, 72, and 38 atomic percent.[4] The absorption line measured was 12 gauss wide, within 10 percent accuracy and was independent of hydrogen concentration to this accuracy. This is quite a broad line and indicates on the one hand that line narrowing, due to internal motion of the hydrogen, is not a strong effect and that the hydrogen atoms present are sufficiently close, probably in molecular form, to allow the strong interaction necessary to produce a broad line. The lattice is thus a rigid one, the hydrogen molecules remaining in relatively fixed positions. The fact that changes in concentration do not affect the line widths shows further that the molecules settle into these fixed positions even when they are few in number and that any phase changes due to changes in concentration do not affect materially the relative distances of the interacting protons.

In contrast to this is the case of tantalum hydride which for all concentrations tried (66.9, 40.8, 24.5, and 11 percent) has a very narrow line width of less than one gauss. In this case the width was determined by the inhomogeneity of the magnetic field over the samples. Thus, rapid internal motion is indicated. According to the theory proposed by Bloembergen, Purcell, and Pound,[2] such motion in the case of liquids will produce a narrowing in the absorption line. Similarly, in the case of certain solids narrowing due to internal motion is known to occur.[5] To determine more precisely the kind of internal motion producing this narrowing it will be necessary to measure temperature effects on the line widths. The results of such measurements will be submitted in a more detailed report in the near future.[3]

The remaining hydrides examined are known to be true compounds which absorb hydrogen in a fundamentally different way. They are of lesser interest and are merely recorded here with their absorption line widths:

Calcium hydride	9.9 gauss
Lithium aluminum hydride	8.7 gauss
Sodium hydride	6.3 gauss
Lithium boron hydride	6.0 gauss
Sodium boron hydride	6.0 gauss.

[1] C. J. Smithels, *Gases and Metals* (Chapman and Hall, Ltd., London, 1937); F. Ephraim, *Inorganic Chemistry* (Oliver and Boyd, Ltd., Edinburgh, 1943).
[2] Bloembergen, Purcell, and Pound, Phys. Rev. **73**, 679 (1948).
[3] In the same class as titanium and tantalum, to be investigated, are the hydrides of palladium, zirconium, vanadium, thorium, and cerium. Line widths and measurements of relaxation times down to low temperatures on these hydrides will be reported on in the near future.
[4] The atomic percent is defined as the ratio of the number of atoms of hydrogen to that of the metal.
[5] Gutowsky, Kistiakowsky, Pake, and Purcell, J. Chem. Phys. **17**, 972 (1949).

Internal Conversion of the Gamma-Rays from Rh^{106}

FRANZ METZGER*
Massachusetts Institute of Technology,† Cambridge, Massachusetts
May 29, 1950

THE cascade gamma-rays emitted in about 17 percent[1] of the disintegrations of Rh^{106} exhibit very pronounced angular and polarization correlations.[2,3] The coefficients of these correlations, however, do not fit any of the predictions[4] for the possible combinations of quadrupole transitions and the existence of a strong $\cos^4$-term eliminates pure dipole radiation. Moreover, an investigation of the interference effects in the case of mixed dipole and quadrupole radiations[5] was not able to explain the experimental data. Therefore, if one accepted the disintegration scheme proposed by Peacock,[1] he was compeled to attribute at least one of the two gamma-rays to transitions of multipole orders higher than quadrupole.[5]

For electric octupole radiation, which is the least converted of the higher multipole radiations, the tables of Rose *et al.*[6] give K conversion coefficients of $(13.4\pm1.5)\times10^{-3}$ and $(4.5\pm0.4)\times10^{-3}$ for the gamma-ray energies of 0.51 ± 0.02 Mev and 0.73 ± 0.02 Mev, respectively.[1] As these conversion coefficients are of an order of magnitude which can be determined experimentally even in the presence of an intense beta-ray spectrum, we investigated the electron spectrum[7] of Rh^{106} with a thin lens spectrometer.

For the evaluation of our data we used the value of 18 percent given by Peacock[1] for the abundance of the 2.3-Mev partial beta-ray spectrum. We assumed that 17 percent of all disintegrations give rise to the gamma-ray cascade. The remaining one percent was attributed to the 1.25-Mev transition, although the position of this line in the disintegration scheme has not been determined beyond doubt. The experimental values for the K conversion coefficients (N_e/N_γ) obtained under these assumptions, are compared in Table I with the theoretical values[6] for electric quadrupole and electric octupole transitions.

TABLE I. Internal conversion of Pd^{106} gamma-rays.

E(Mev)	Exp. value $\alpha_K\times10^3$	Theoretical values: El. quadrupole $\alpha_K\times10^3$	Theoretical values: El. octupole $\alpha_K\times10^3$
0.51	5.4 ± 1.5	4.90	13.4
0.73[a]	<2.5	1.95	4.5

[a] Owing to the small conversion we can only give an upper limit for the conversion coefficient of this line. The resolution of the spectrometer was three percent.

The error indicated takes care of the uncertainty in the knowledge of the abundance of the partial beta-ray spectrum (18 ± 2 percent).

From Table I it is evident that neither of the two main transitions in Pd^{106} can be of a multipole order higher than quadrupole. Thus the results of our conversion measurements sharply contradict the conclusions drawn from the correlation experiments. In order to explain both results, we must assume that the disintegration scheme used so far[1] does not represent the actual situation in detail. These conclusions are in line with an observation of Goldhaber, der Mateosian, and Katcoff[8] that there is present to two to three percent a hard gamma-ray with an energy above the photo-threshold of deuterium, and also with a recent statement of Spiers[9] that it might be necessary to assume a more complicated decay scheme in order to explain the correlation data.

The author wishes to express his gratitude to Professor Deutsch for his interest and to the authorities of the Massachusetts Institute of Technology for the hospitality granted to him.

* Now at the University of Illinois, Urbana, Illinois.
† This work was assisted by the joint program of the ONR and AEC.
[1] W. C. Peacock, Phys. Rev. **72**, 1049 (1947).
[2] E. L. Brady and M. Deutsch, Phys. Rev. **74**, 1541 (1948).
[3] M. Deutsch and F. Metzger, Phys. Rev. **74**, 1542 (1948).
[4] D. R. Hamilton, Phys. Rev. **58**, 122 (1940).
[5] D. J. Ling and D. L. Falkoff, Phys. Rev. **76**, 431, 1639 (1949).
[6] Rose, Goertzel, Spinrad, Harr, and Strong, Phys. Rev. **76**, 104 (1949).
[7] The radioactive material was obtained from Oak Ridge.
[8] M. Goldhaber (private communication).
[9] J. A. Spiers, Phys. Rev. **78**, 75 (1950).

On the Isotope Effect in Superconductors

JULES DE LAUNAY
Naval Research Laboratory, Washington, D. C.
June 5, 1950

THE occurrence of the diamagnetic currents and their stability in the presence of the thermal vibrations of the lattice above the absolute zero of temperature is a primary phenomenon which is difficult to explain in developing an atomistic theory of super-

conductivity. Assuming, however, the existence of such currents and their stability at very low temperatures, it is natural to suppose that superconductivity cannot exist above a certain critical temperature T_c at which certain higher modes of the lattice become dominant in the lattice energy density spectrum. It was with this in mind that Dolecek and de Launay[1] sought to display a pattern for superconducting elements by plotting the critical temperature T_c against the Debye characteristic temperature, Θ_D.

For an element, the lattice spectra of the various isotopes at a given temperature will differ because of the different atomic weights, A. Thus the spectra will be similar, for the various isotopes of the element, at different temperatures. These spectra will be similar when the wave-length bearing the greatest energy density is the same for the various isotopes. Thus, this dominant wave-length can be used to identify the spectra and to determine the variation of T_c with A.

To determine how the dominant wave-length depends on temperature, in Debye's model of a solid, we have only to compare Debye's formula for the energy of a lattice with Planck's formula for the energy of blackbody radiation. The calculation of the dominant wave-length λ for blackbody radiation from Planck's formula leads to Wien's displacement law: $\lambda T = hc/4.965k$, where c is the velocity of light, h is Planck's constant, and k is Boltzmann's constant. The same method of analysis applied to Debye's formula also leads to Wien's displacement law where c, in the Debye case, is the velocity of sound. This relationship probably holds even for real lattices in the region of the T^3 law of specific heats.

The velocity of sound, c, besides being a function of the elastic constants and atomic volume, varies as $A^{-\frac{1}{6}}$. The elastic constants, atomic volume, and the required critical lattice spectrum characterized by the dominant wave-length λ, will not vary among the isotopes of a given element since they depend essentially on electron-ion configuration. Consequently, for the isotopes of the same element:

$$A^{\frac{1}{6}}T_c = \text{constant}. \tag{1}$$

If T_c is plotted as ordinate and A as abscissa, then in the short range over which A can be varied physically, Eq. (1) will be represented by a straight line of slope $(-T_c/2A)$. For Pb, Sn, and Hg, this slope should be about -0.0175, -0.0156, -0.0103 °K/atmos. wt., respectively.

Recently, Maxwell[2] and Reynolds, Serin, Wright, and Nesbitt[3] have observed a shift in the temperature T_c with change in A for the isotopes of mercury. The second of these two papers presents the data of both in a plot of T_c *versus* A. The result is a straight line of slope -0.009. This result is not only in agreement with Eq. (1) in sign but is also in reasonable numerical agreement.

Referring, finally, to a T_c *versus* Θ_D plot,[1] the isotope effect of any one of the superconducting elements would be represented by a straight line through the origin and the representative point of the element. Since T_c/Θ_D is roughly constant for the set of elements Al, Cd, Ga, Hf, Ti, Zn, and Zr, it would appear that this group of elements has similar electron-ion properties insofar as the dominant wave-length λ is involved.

[1] J. de Launay and R. L. Dolecek, Phys. Rev. **72**, 141 (1947).
[2] E. Maxwell, Phys. Rev. **78**, 477 (1950).
[3] Reynolds, Serin, Wright, and Nesbitt, Phys. Rev. **78**, 487 (1950).

Photo-Alpha-Reactions in Light Nuclei*

T. A. Welton
University of Pennsylvania, Philadelphia, Pennsylvania
June 5, 1950

A RATHER direct test of the alpha-particle picture of nuclear structure should be afforded by the study of reactions in which gamma-rays eject alpha-particles from nuclei such as C^{12}, O^{16}, and Ne^{20}. We consider the oxygen reaction, which seems to be essentially simpler. For gamma-rays between 7.2 and 12.1 Mev, alpha-emission will occur without competition, and a study of the angular distribution and energy dependence of the reaction is of interest. Millar and Cameron[1] have reported observing this reaction, while Hänni, Telegdi, and Zünti[2] and Wäffler and Younis[3] have observed the disintegration of C^{12} into three alphas. In this work we more or less follow the calculation of Telegdi and Verde[4] on the C^{12} cross section.

We assume, in the sense of the resonating group picture, that the O^{16} nucleus is composed of four pre-formed alpha-particles, each strongly bound but interacting relatively weakly with its neighbors. We further assume that a gamma-ray of energy above 7.2 Mev can excite this structure to a state in its continuum, in which one alpha emerges. For lack of better knowledge we take the ground state wave function to describe an alpha-particle bound, in an S state, to a cluster of three alpha's. The order of magnitude of the final answer is probably not particularly sensitive to the details of this wave function, except for a parameter specifying the approximate range of radii within which the single alpha is likely to be found. We assume an exponential distribution of the form $e^{-r/R}$, and leave R as an adjustable parameter.

For the final state we assume a Coulomb distorted plane wave for the wave function in the relative coordinates. That is, we neglect the effect of the nuclear forces on the wave functions of the continuum states. Because of the exact coincidence of the charge center and mass center in our assumed picture, the transition cannot be electric dipole. Because of the fact that the ground state is spherically symmetric, no magnetic dipole matrix element exists. The transition will then be pure electric quadrupole, so that only the D component of the final wave function will be involved in the calculation of the matrix element. This circumstance makes more plausible the neglect of nuclear forces in the final wave function.

These assumptions lead directly to a formula for the differential cross section:

$$\sigma(\theta)d\Omega = 0.88(R/r_0)''(4+\eta^2)(1+\eta^2)e^{2\eta^{-4}} \times (e^{2\pi\eta}-1)^{-1}\sin^2\theta\cos^2\theta d\Omega \text{ (barns)},$$

where R = length parameter previously introduced, r_0 = classical electron radius, ϵ = γ-ray energy in Mev, ϵ_0 = threshold energy = 7.2 Mev, and $\eta = 3.26(\epsilon-\epsilon_0)^{-\frac{1}{2}}$.

The energy dependence should be moderately reliable near the threshold, and the angular dependence follows in a very simple manner from the fact that a quadrupole transition is involved. The extremely sensitive dependence on R means that no prediction of the magnitude of the cross section will be reliable, but it may well be that R can be determined nicely from the results of the experiments. The somewhat unusual angular distribution which we have obtained seems to be peculiar to the alpha-particle model, since in a nuclear picture without alpha-particle structure, a sizable electric dipole cross section must also be expected, with a resulting drastic change in angular distribution.

* This work supported in part by the ONR.
[1] C. H. Millar and A. G. W. Cameron, Phys. Rev. **78**, 78 (1950).
[2] Hänni, Telegdi, and Zünti, Helv. Phys. Acta **21**, 203 (1948).
[3] Wäffler and Younis, Helv. Phys. Acta **22**, 414 (1949).
[4] Telegdi and Verde, Helv. Phys. Acta **22**, 380 (1949).

Equivalence Theorems for Meson-Nucleon Couplings

Edward J. Kelly
Department of Physics, Massachusetts Institute of Technology, Cambridge, Massachusetts
June 6, 1950

THE degree to which the scalar (pseudoscalar) and vector (pseudovector) couplings of the meson and nucleon fields are equivalent in scalar (pseudoscalar) meson theory has been discussed several times in the literature. Pointing out the incompleteness of earlier treatments[1,2] (which stressed only the equiva-

lence of the couplings in first order), Case,[3] in a paper of the above title, set the problem up generally in order to find the exact criteria of equivalence.

The Lagrangian (in Case's notation)

$$\mathcal{L}=-\hbar c\bar{\psi}[\gamma_\nu(\partial\psi/\partial x_\nu)+\kappa_0\psi]+ie\bar{\psi}\gamma_\nu\tfrac{1}{2}(1-\tau_3)\psi A_\nu -[(D_\nu^*\varphi^*)(D_\nu\varphi)+\kappa^2\varphi^*\varphi]-(R\varphi^*+R^*\varphi) -[\Gamma_\nu(D_\nu^*\varphi^*)+\Gamma_\nu^*(D_\nu\varphi)] \quad (1)$$

describes a charged scalar (pseudoscalar) meson field with both types of coupling to the nucleon field, both fields being coupled to an external potential A_ν. The interaction Hamiltonian is derived from $\mathcal{L}$ and the derivative is removed from the meson field variables by the rearrangement;[1]

$$\Gamma_\nu\frac{\partial\varphi^*}{\partial x_\nu}+\Gamma_\nu^*\frac{\partial\varphi}{\partial x_\nu}=\frac{\partial}{\partial x_\nu}(\Gamma_\nu\varphi^2+\Gamma_\nu^*\varphi)-\frac{\partial\Gamma_\nu}{\partial x_\nu}\varphi^*-\frac{\partial\Gamma_\nu^*}{\partial x_\nu}\varphi, \quad (2)$$

where $\partial\Gamma_\nu/\partial x_\nu$ can be evaluated from the Dirac field equations. Case then removes the divergence expression by a sequence of canonical transformations,[3] evaluating the transformed Hamiltonian to the second order in the meson-nucleon coupling constants.

We wish to point out only that the same rearrangement (2) can be performed directly in the Lagrangian, where the divergence expression can be dropped immediately, as it does not contribute to the equations of motion. This method has the advantages that, (1) no further canonical transformations are required beyond that needed to enter the interaction representation, and (2) there is no need to approximate the resulting Hamiltonian, the criteria of equivalence being obtained exactly. From the new Lagrangian

$$\mathcal{L}'=-\hbar c\bar{\psi}[\gamma_\nu(\partial\psi/\partial x_\nu)+\kappa_0\psi]+ie\bar{\psi}\gamma_\nu\tfrac{1}{2}(1-\tau_3)\psi A_\nu -[(D_\nu^*\varphi^*)(D_\nu\varphi)+\kappa^2\varphi^*\varphi]-(R\varphi^*+R^*\varphi) -(ie/\hbar c)(\Gamma_\nu\varphi^*-\Gamma_\nu^*\varphi)A_\nu+(ig/\kappa)[(\partial\bar{\psi}/\partial x_\nu)\gamma_\nu\gamma_5' \times(\tau_+\varphi^*+\tau_-\varphi)\psi+\bar{\psi}\gamma_\nu\gamma_5'(\tau_+\varphi^*+\tau_-\varphi)(\partial\psi/\partial x_\nu)], \quad (3)$$

we find the same field equations as before and the momenta

$$\pi\equiv-\frac{\partial\mathcal{L}'}{\partial(\partial\psi/\partial x_\nu)}n_\nu=\hbar c\bar{\psi}\gamma_\nu n_\nu-\frac{ig}{\kappa}\bar{\psi}\gamma_\nu n_\nu\psi_5'(\tau_+\varphi^*+\tau_-\varphi),$$

$$\bar{\pi}\equiv-\frac{\partial\mathcal{L}'}{\partial(\partial\bar{\psi}/\partial x_\nu)}n_\nu=-\frac{ig}{\kappa}\gamma_\nu n_\nu\gamma_5'(\tau_+\varphi^*+\tau_-\varphi)\psi,$$

$$\chi\equiv-\frac{\partial\mathcal{L}'}{\partial(\partial\varphi/\partial x_\nu)}n_\nu=n_\nu(D_\nu^*\varphi^*),$$

$$\chi^*\equiv-\frac{\partial\mathcal{L}'}{\partial(\partial\varphi^*/\partial x_\nu)}n_\nu=n_\nu(D_\nu\varphi).$$

We then construct the interaction part of the total Hamiltonian

$$T_{\mu\nu}n_\mu n_\nu=-\mathcal{L}'+\pi\left(n_\nu\frac{\partial\psi}{\partial x_\nu}\right)+\bar{\pi}\left(n_\nu\frac{\partial\bar{\psi}}{\partial x_\nu}\right)+\chi\left(n_\nu\frac{\partial\varphi}{\partial x_\nu}\right)+\chi^*\left(n_\nu\frac{\partial\varphi^*}{\partial x_\nu}\right).$$

The result is more simply expressed in the interaction representation, which is characterized by the transformations

$$\pi\to\hbar c\bar{\psi}\gamma_\nu n_\nu,\quad \bar{\pi}\to 0,\quad \chi\to n_\nu\partial\varphi^*/\partial x_\nu,\quad \chi^*\to n_\nu\partial\varphi/\partial x_\nu.$$

In this representation the interaction Hamiltonian is

$$\mathcal{H}=-ie\bar{\psi}\gamma_\nu\tfrac{1}{2}(1-\tau_3)\psi A_\nu-\frac{ie}{\hbar c}\left(\frac{\partial\varphi^*}{\partial x_\nu}\varphi-\varphi^*\frac{\partial\varphi}{\partial x_\nu}\right)A_\nu +(e/\hbar c)^2\varphi^*\varphi A_\mu A_\nu(\delta_{\mu\nu}+n_\mu n_\nu)+[1+(\epsilon-1)\kappa_0 g/\kappa f] \times(R\varphi^*+R^*\varphi)+(fg/\kappa\hbar c)\bar{\psi}[(1+\tau_3)-\epsilon(1-\tau_3)]\psi\varphi^*\varphi +(g^2/\kappa^2\hbar c)\bar{\psi}\gamma_\nu\tau_3\psi[(\partial\varphi^*/\partial x_\nu)\varphi-\varphi^*(\partial\varphi/\partial x_\nu)] +(2ieg^2/\kappa^2\hbar^2c^2)\bar{\psi}\gamma_\mu\tau_3\psi\varphi^*\varphi A_\nu(\delta_{\mu\nu}+n_\mu n_\nu), \quad (4)$$

where $\epsilon=1$ (scalar theory), -1 (pseudoscalar theory).

This result agrees with that of Case to first order; the remaining terms are similar to his, differing only by a canonical change of representation. It is to be noted that in the interaction representation the vector coupling is represented by terms of no higher explicit order than the second, while in the representation used by Case, explicit terms of all orders presumably appear. In addition, our result shows that scalar theories can be so formulated that contact terms *never* appear. That contact terms play no role in vector theories also can be inferred from the fact that they are explicitly surface-dependent terms, and will therefore disappear along with other surface terms when the first-order coupling is removed from the Hamiltonian by means of the Schwinger transformation.[4]

The author wishes to thank Dr. M. L. Goldberger for much helpful advice.

[1] E. C. Nelson, Phys. Rev. **60**, 830 (1941).
[2] F. J. Dyson, Phys. Rev. **73**, 929 (1948); K. J. Le Couteur and L. Rosenfeld, Phil. Mag. **40**, 151 (1949).
[3] K. M. Case, Phys. Rev. **76**, 14 (1949).
[4] P. T. Matthews, Phys. Rev. **76**, 1657 (1949).

The Radioactivity of Hf^{181}

MARTIN DEUTSCH
Laboratory for Nuclear Science and Engineering, Massachusetts Institute of Technology, Cambridge, Massachusetts*
AND
ARNE HEDGRAN
Nobel Institute of Physics, Stockholm, Sweden
June 1, 1950

A CONSIDERABLE number of investigations of the decay of Hf^{181} have been described in the literature. Most of these have been interpreted to support a disintegration scheme of the general type first proposed by Wiedenbeck and Chu[1] with minor modifications such as the scheme recently shown by Cork *et al.*[2] We have investigated some features of this decay by means of magnetic and scintillation spectrometers and coincidence techniques. The main new result is that most of the 345-kev gamma-radiation does not belong to the 45-day Hf^{181}. Delayed coincidence measurements in which the succeeding radiation was focused by a magnetic lens spectrometer showed that less than 10 percent of the conversion electrons of the 345-kev transition follow the 20-μsec. period while all of the electrons from the 132- and 481-kev transitions follow it. A similar result is obtained when the delayed radiation spectrum is studied by means of a NaI—TlI scintillation spectrometer. Because of our limited experience with the instrument it has not yet been possible to determine whether any 345-kev radiation at all appears with the decay of the metastable state, but it could only be a small part of the total.

While the conversion electrons of the 481-kev transition show "prompt" coincidences with electrons, presumably conversion electrons of the 132-kev transition, those due to the 345-kev component show a much smaller "prompt" coincidence rate. The situation concerning the 135-kev radiation is less clear since it was not resolved from the 132-kev radiation in the coincidence experiments. However, the relative heights of the K and L conversion peaks in the "prompt" and delayed coincidence spectra favors the idea that both of these gamma-rays follow the 20-μsec. period. We have also found a small "prompt" coincidence rate for the continuous spectrum. This rate was so small (about one-tenth of that for the 481-kev line) that one cannot rule out effects of impurities.

We are thus forced to the conclusion that the 345-kev transition either proceeds from a long-lived state in Ta^{181} or that it is not related to the beta-decay of Hf^{181} at all. To test the latter view the gamma-radiations of two samples of neutron irradiated hafnium differing in age by about 18 months were compared in the scintillation spectrometer. The relative abundance of the 345-kev radiation was much greater in the older sample, proving that this gamma-ray follows a longer period than Hf^{181}. Its behavior in chemical separations showed that it belongs almost certainly to a hafnium or zirconium activity. The fact that Cork *et al.*[2] find K, L, and M conversion lines due to a 342-kev transition converted in lutecium rather than tantalum favors the conclusion that the longer period is an electron-capture activity of hafnium, perhaps Hf^{176}.

On the basis of a single electron line ascribed somewhat arbitrarily to K conversion of a 344.5-kev gamma-ray in Ta^{181} Cork *et al.*[2] still favor the decay scheme of Wiedenbeck and Chu.[1] If such a gamma-ray does exist in the decay of Hf^{181}, its intensity must be much less than that of the 135-kev radiation. Thus our results seem to rule out the decay scheme of Wiedenbeck and Chu.[1] A more detailed description of the experiments will be published if further investigations permit us to reach some positive conclusions concerning the true scheme.

Samples of irradiated hafnium were obtained from the Isotopes Division of the AEC. The experiments with the magnetic spectrometers of the Nobel Institute were made possible by the generous hospitality of the Swedish Academy of Sciences.

* The work at Cambridge was supported in part by the joint program of the AEC and ONR.
[1] M. Wiedenbeck and K. Chu, Phys. Rev. **75**, 226 (1949).
[2] Cork, Stoddard, Rutledge, Branyan, and LeBlanc, Phys. Rev. **78**, 299 (1950).

On the Identification of the Predominant Photo-Nuclear Disintegrations in Nitrogen and Oxygen*

E. R. Gaerttner and M. L. Yeater
General Electric Company, Schenectady, New York
May 26, 1950

CLOUD-CHAMBER data already reported[1] have shown that the most probable photo-nuclear disintegrations in nitrogen and oxygen, with x-rays from a betatron operating at 100 Mev, are those for which one charged particle is emitted; these appear as "flags" in the cloud chamber. From the analysis described below, we find that about 66 percent of the nitrogen flags also involve the emission of a neutron. Experimental evidence indicates that these flags are mostly from the reaction $N^{14}(\gamma,np)C^{12}$. The remainder appear to be a mixture of (γ,p) and (γ,α) disintegrations, which are not separable with our present technique. In oxygen there are relatively few flags with associated neutrons. About 84 percent of the flags in oxygen are attributed to (γ,p) or (γ,α) disintegrations.

The following method is used to distinguish between cases in which a charged particle alone is emitted and those in which a neutron is also emitted. The flags are classified according to the direction of the resultant momentum as indicated by the projected angle between flag members and by their orientation with respect to the x-ray beam, as observed in the plane of the cloud chamber. The cases which clearly reveal neutron emission are those for which both members of the flag lie on the same side of the path of the incident proton,[2] and those for which the members lie on opposite sides but have a resultant momentum in the backward hemisphere (opposing the x-ray beam). The remaining cases, for which the resultant momentum is in the forward hemisphere, include flag disintegrations in which a neutron is emitted and those in which a charged particle alone is emitted. The net forward momentum of the latter comes only from the incident photon. The approximate number of flags with neutrons is obtained by adding the side-directed cases to twice the number with resultant momentum backward.[3] The excess of forward over backward disintegrations is attributed to (γ,p) and (γ,α) reactions.

In oxygen, most of the flags have a resultant forward momentum, with flag angles near 180°. Among the 234 flags analyzed in this way, 212 are forward, 6 to the side, and 16 to the rear. Hence about 84 percent represent the emission of a charged particle without an accompanying neutron. The only probable reactions[4] for these flags are (γ,p) or (γ,α).

For nitrogen, the average flag angle is about 145°. In a measured group of 198 flags, 112 are forward, 41 to the side, and 45 to the rear. About 66 percent, therefore, appear to be accompanied by neutrons. These are attributed to the reaction $N^{14}(\gamma,n)C^{12}$; other possible reactions[5] yielding neutrons are ruled out by the following evidence.

(1) The reaction $N^{14}(\gamma,n\alpha)B^9$ is ruled out by the instability of the residual B^9 nucleus (the event is expected to appear as a "star").

(2) The reaction $N^{14}(\gamma, He^3n)B^{10}$ is improbable owing to its relatively high threshold. A photon energy of about 40 Mev would be required to produce the observed disintegrations by this reaction. Our measurements of the flag yield as a function of x-ray energy indicate that most of the observed flags are formed below 40 Mev.

(3) The relative yields of photo-nuclear reactions with radioactive products have been studied by Perlman and Friedlander.[6] The only activity which they find for nitrogen is that of N^{13} from the (γ,n) reaction. Consequently the flags in nitrogen do not involve the reaction $(\gamma,p2n)$.

In addition to our study of nitrogen and oxygen, a preliminary analysis of photo-nuclear disintegrations in carbon has been made. As in oxygen, relatively few of the flags indicate neutron emission. For carbon, the (γ,p) reaction appears predominant among those yielding flags.

It is a pleasure to acknowledge the cooperation of the betatron staff. A relatively high pulsed x-ray intensity from the betatron has been an important factor in our current research.

* The cloud-chamber equipment used for this work was developed under contract with the ONR.
[1] E. R. Gaerttner and M. L. Yeater, Phys. Rev. **77**, 570, 714 (1950).
[2] If the residual nucleus from a (γ,p) disintegration were left in an excited state, the momentum of the secondary photon could give a small random deflection to the recoiling nucleus. Our measurements of the average angle and energy of the emitted particles show this to be a weak effect.
[3] This procedure is based on the assumption that there is the same probability for forward and backward neutron emission. A rough check on this has been made by a stereoscopic examination of 26 flags, in nitrogen, which have forward momentum and for which the fast member lies in the horizontal plane. In 11 of these cases the recoil is moving upward or downward, indicating the presence of a neutron from the disintegration.
[4] Some (γ,α) disintegrations in oxygen, produced by x-rays from a 24-Mev betatron, have been observed in emulsions by C. H. Millar and A. G. W. Cameron, Phys. Rev. **78**, 78 (1950).
[5] The chance that stray neutrons produce the flags has been ruled out by the observation that a negligible portion of the flag disintegrations originates outside of the path of the x-ray beam in the cloud chamber; whereas stray neutrons occur throughout the chamber, as we found by a study of proton recoils in hydrogen.
[6] M. L. Perlman and G. Friedlander, Phys. Rev. **74**, 442 (1948).

U^{235} in Thucholite

J. B. Orr
R. F. D. No. 3, Great Barrington, Massachusetts
May 22, 1950

FURTHER work on the isotope ratio of U^{235} to U^{238} in the mineral thucholite does not substantiate the preliminary results given in a previous letter.[1]

Additional thucholite collected at the Besner Mine, Henvey, Ontario was separated into two lots consisting of 12.03 g with a high count and 26.07 g with a low count. The high count sample yielded 33.4 percent loss on ashing and 25.2 percent U on extraction with C_2H_4O. The low count sample yielded 19.1 percent C and 5.6 percent U. Both of the above samples of U, and U extracted from uraninite from the Ruggles Mine, Grafton New Hampshire were examined for impurities spectrographically. These consisted of traces of Fe, Al, Ca, and Ba. Five hundred milligrams

Table I. Comparison of slow neutron fission counts from thucholite U and uraninite U.

Sample	Bias	Counts/min.
Ruggles No. 1	6.0	7.90±0.35
High count thucholite No. 1	6.0	8.30±0.32
Low count thucholite No. 1	6.0	7.68±0.35
Ruggles No. 2	6.5	7.86±0.35
High count thucholite No. 2	6.5	7.23±0.32
Low count thucholite No. 2	6.5	7.57±0.27

each of the U samples were converted to uranyl nitrate, dissolved in alcohol, and mixed with a one percent solution of lacquer and thinner. Six Al foils 17 cm in diameter weighing 4.9 mg/cm² were coated and baked to a thickness of 1 mg/cm² of U_3O_8.

The foils were placed in an argon-filled ionization chamber and counts were made of fission particles from slow neutrons from a 50-mg Ra–Be neutron source embedded in paraffin above the foil. The fission counts so obtained are shown in Table I.

It is readily seen that any real difference in the U^{235} isotope composition of the two sources of U must be less than six percent.

[1] J. B. Orr, Phys. Rev. 76, 155 (1949).

Masses of Si^{28}, Si^{29}, Mn^{55}, Fe^{56}, Ni^{58}, Pd^{110}, Cd^{110}, Cd^{112}, Cd^{116}, and Sn^{116}

HENRY E. DUCKWORTH AND RICHARD S. PRESTON
Scott Laboratory, Wesleyan University, Middleton, Connecticut*
May 1, 1950

MASS spectrographic mass measurements made in this laboratory have been extended to include Si^{28}, Si^{29}, Fe^{56}, Ni^{58}, Pd^{110}, Cd^{110}, Cd^{112}, Cd^{116}, and Sn^{116}. From the mass of Fe^{56} that of Mn^{55} can be deduced by using disintegration data.

Si^{28} and Fe^{56}.—A spark between two metal electrodes, slightly contaminated with iron as a result of earlier sparking against stainless steel, has been used as source when photographing the $Fe^{56}-Si^{28}-Co-C_2H_4$ quadruplet occurring at mass number 28. Measurements of the $C_2H_4-Si^{28}$ spacing on six photographs showed this packing fraction difference[1] to be 19.45±0.06. Meanwhile, from five photographs, the $CO-Si^{28}$ packing fraction difference was found to be 6.45±0.03. Assuming the packing fractions[2] of C_2H_4 and CO to be 14.37±0.015 and 1.38±0.007, respectively, that of Si^{28} is computed to be, first, −5.08±0.06 and, second, −5.07±0.04. Mattauch and Flammersfeld[3] and Alburger and Hafner[4] both list the value −5.20±0.04.

From eight photographs of the $CO-Fe^{56}$ doublet, $\Delta f=9.80\pm0.02$, while from seven photographs of the $C_2H_4-Fe^{56}$ doublet, $\Delta f=22.93\pm0.07$. The packing fraction of Fe^{56} computed from these is, first, −8.42±0.03 and, second, −8.56±0.08. A third value for Fe^{56} can be got by combining with the above Si^{28} value a previously reported[5] packing fraction difference for the $Si^{28}-Fe^{56}$ doublet of $\Delta f=3.32\pm0.02$. This gives for Fe^{56} $f=-8.39\pm0.05$.

Ni^{58} and Si^{29}.—A spark between stainless steel and zirconium gave a good triplet at mass 29 consisting of $Ni^{58}-COH-C_2H_5$. From five photographs, the $COH-Ni^{58}$ packing fraction difference was found to be 12.09±0.04. From eleven photographs of the $C_2H_5-Ni^{58}$ pair, $\Delta f=24.73\pm0.04$. Assuming packing fractions for COH and C_2H_5 of 4.132±0.016 and 16.67±0.018, respectively, that of Ni^{58} is computed to be, first, −7.96±0.05 and, second, −8.06±0.05. This value is to be compared with −8.5±0.35, −6.97±0.07, and −8.29±0.07 obtained by Aston,[6] Okuda *et al.*,[7] and Shaw,[8] respectively.

The mean value for Ni^{58}, −8.01±0.05, may be combined with a packing fraction difference of 3.07±0.02 reported earlier[5] for the $Si^{29}-Ni^{58}$ doublet to get for Si^{29} $f=-4.94\pm0.05$. Mattauch and Flammersfeld, and Alburger and Hafner both list the value −5.02±0.04.

Cd^{112}, Cd^{116}, Sn^{116}.—With a spark sometimes between a stainless steel and a cadmium electrode, and at other times between a stainless steel and a tin electrode the $Cd^{112}-Fe^{56}$, $Cd^{116}-Ni^{58}$, and $Sn^{116}-Ni^{58}$ doublets were photographed at mass numbers 56 and 58. The packing fraction differences were, respectively, 3.06±0.02 (five photographs), 3.01±0.02 (seven photographs), and 2.66 ±0.01 (nine photographs). These values, when combined with the above values for Fe^{56} and Ni^{58}, give for Cd^{112}, $f=-5.36\pm0.04$; for Cd^{116}, $f=-5.00\pm0.06$; and for Sn^{116}, $f=-5.35\pm0.05$.

On many photographs it was possible to measure the $Cd^{110}-Mn^{55}$ and $Cd^{114}-Fe^{57}$ packing fraction differences. These were found to be 2.53±0.03 (seven photographs) and 2.88±0.03 (seven photo graphs).

Mn^{55}, Pd^{110}, Cd^{110}.—Accurate Q-values are available for the $Mn^{55}(d,p)Mn^{56}$ reaction. Martin[9] has found 4.76±0.11 Mev, while Whitehead and Heydenburg[10] have obtained 5.01 Mev. Using $Q=4.95$ Mev with 2.86 and 0.84 Mev for the energies of the beta- and gamma-rays from Mn^{56}, leading to the ground state of Fe^{56}, as listed by Mattauch and Flammersfeld, the $Mn^{55}-Fe^{56}$ packing fraction difference is calculated to be 0.32±0.03. This with the above value for Fe^{56}, gives for Mn^{55} $f=-8.10\pm0.05$. This value can be combined with the Δf's for the $Pd^{110}-Mn^{55}$ ($\Delta f=2.70$ ±0.05, previously reported[11]) and $Cd^{110}-Mn^{55}$ doublets to give for Pd^{110}, $f=-5.40\pm0.07$ and for Cd^{110}, $f=-5.57\pm0.06$.

Table I is a summary of the new mass values.

TABLE I. Summary of new mass values.

Nuclide	Packing fraction	Mass
Si^{28}	−5.07±0.03	27.99581±0.00008
Si^{29}	−4.94±0.05	28.98567±0.00014
Mn^{55}	−8.10±0.05	54.95545±0.00027
Fe^{56}	−8.42±0.03	55.95285±0.00016
Ni^{58}	−8.01±0.05	57.95354±0.00029
Pd^{110}	−5.40±0.07	109.94060±0.00077
Cd^{110}	−5.57±0.06	109.93873±0.00066
Cd^{112}	−5.36±0.04	111.93997±0.00045
Cd^{116}	−5.00±0.06	115.94200±0.00070
Sn^{116}	−5.35±0.05	115.93794±0.00058

The authors were assisted in some of these experiments by Mr. Clifford Gieselbreth, Mr. Howard A. Johnson, and Mr. Richard F. Woodcock. They are grateful for the use of the Astronomy Department's comparator.

* This letter is based on work done at Wesleyan University under contract with the AEC.

[1] The factor $\times10^{-4}$ will be understood and not written in expressing the numerical value of the packing fraction.

[2] K. T. Bainbridge, Isotopic Weights of the Fundamental Isotopes, Preliminary Report No. 1, National Research Council (June, 1948).

[3] J. Mattauch and A. Flammersfeld, "Isotopic report—1948," Verlag. d. Zeits. f. Natur., Tübingen, Germany (1949).

[4] D. E. Alburger and E. M. Hafner, "The properties of atomic nuclei—III. Nuclear energy levels, $Z=11$–20," Brookhaven National Laboratory (July 1, 1949).

[5] Duckworth, Johnson, Preston, and Woodcock, Phys. Rev. **78**, 386 (1950).

[6] F. W. Aston, *Mass Spectra and Isotopes* (Edward Arnold and Company, London, England, 1942), p. 151.

[7] Okuda, Ogata, Kuroda, Sima, and Shindo, Phys. Rev. **59**, 104 (1941).

[8] A. E. Shaw, Phys. Rev. **75**, 1011 (1949).

[9] A. B. Martin, Phys. Rev. **72**, 378 (1947).

[10] W. D. Whitehead and N. P. Heydenburg, Phys. Rev. **78**, 338 (1950).

[11] Duckworth, Woodcock, and Preston, Phys. Rev. **78**, 479 (1950).

The Electrons in Cosmic Rays*

C. L. CRITCHFIELD, E. P. NEY, AND SOPHIE OLEKSA
University of Minnesota, Minneapolis, Minnesota
June 6, 1950

A SEARCH for primary electrons in cosmic rays was made by Hulsizer and Rossi,[1] who investigated the bursts produced in a lead-shielded ionization chamber at balloon altitudes. They obtained a value for the burst-producing radiation of 0.0082 particle cm^{-2} $sec.^{-1}$ $sterad.^{-1}$. Assuming a primary flux of 0.2 particle cm^{-2} $sec.^{-1}$ $sterad.^{-1}$, this sets an upper limit on the electron and photons of four percent of the primary flux. Our cloud-chamber data indicate that electrons cannot constitute more than 0.2 percent of the primaries and probably represent an even smaller fraction than this.

We have examined 1625 random expansion cloud-chamber pictures taken at 20 g/cm² atmospheric depth. All of the experiments were made with at least two ¼-in. lead plates in the cloud chamber so that a 1-Bev electron shower is easily discernible. This energy was chosen for study because it is just below the electron cut-off at our geomagnetic latitude of 55°N. The cloud-chamber sensitive time was 0.2 sec., and the geometric factor of the lead detectors was 39.0 sterad. cm². Eight electron showers of

1 Bev or greater unaccompanied by ionizing penetrating particles have been observed. Six other showers were accompanied by ionizing penetrating particles and were therefore believed to be of secondary origin. If the eight unaccompanied showers were due to primary electrons, the number of primaries necessary to account for them would be 0.0004 cm^{-2} $sec.^{-1}$. $sterad.^{-1}$. In this estimate we have taken multiplication in the 20 g/cm^2 of air into account. The above figure together with the previously assumed proton flux gives an upper limit for the number of electrons of 0.2 percent of the primary intensity. If one assumes that air showers are generated by primary electrons with an integral number spectrum[2]

$$N(>E)=CE^{-1.8},$$

one finds that the constant C which fits our data is at least 600 times too small to agree with the value of the same constant as determined from air shower experiments. It seems unlikely then that air showers are generated by primary electrons.

Because roughly half of the showers contained penetrating particles, we investigated the assumption that all the electrons observed are due to the decay of neutral mesons produced by the primary protons. We have used Chew's semi-empirical formula for the production of charged mesons[3] to make the calculations. The result of the theory is that the observations fix the ratio λ/H, where H is the fraction of the energy which goes into the *neutral* mesons, and λ is the mean free path for energy loss by the protons. Since one cannot determine accurately the energy of an electron shower, we used the estimated upper limit of 2 Bev. The ratio λ/H then becomes 2400 g/cm^2. A possible pair of values would be $\lambda=120$ g/cm^2 with one-twentieth of the energy absorbed in making neutral mesons. The calculations will be described in a later publication.

Assuming that all the primaries of energy greater than 15 Bev can contribute neutral mesons to this energy range, the total production cross section σ is $\sigma=1.8\times10^{-26}$ cm^2. This is to be compared with the geometric cross section for air which is 39×10^{-26} cm^2.

* This research was performed under the partial support of the joint program of the ONR and AEC. It was also materially assisted by the University of Minnesota Technical Research Fund subscribed to by General Mills, Inc., the Minneapolis Star Journal and Tribune Company, the Minneapolis Honeywell Regulator Company, the Minnesota Mining and Manufacturing Company, and the Northern States Power Company.

[1] R. Hulsizer, Phys. Rev. **76**, 164 (1949); also, Proceedings of the Echo Lake Cosmic-Ray Symposium, p. 218.
[2] W. Heisenberg, *Cosmic Radiation* (Dover Publications, New York, 1946), p. 39.
[3] G. Chew, Phys. Rev. **73**, 1128 (1948).

The Half-Life of Sodium 24

A. K. Solomon
Biophysical Laboratory, Harvard Medical School, Boston, Massachusetts*
May 26, 1950

In the course of biological experiments using Na^{24} as a tracer, half-life values appreciably longer than 14.8 hr., as given by Van Voorhis,[1] were obtained consistently. As a consequence the half-life has been redetermined on samples of radioactive sodium procured from the Isotopes Division of the AEC at Oak Ridge, Tennessee.

The material, after receipt from Oak Ridge, was purified by the use of ion exchangers. First, the material was absorbed on a Dowex 50 column and then eluted with 0.15N HCl, according to the method of Cohn and Kohn.[2] This procedure effects a quantitative separation between sodium and potassium, and may, therefore, be expected to separate the sodium from all other cationic contaminants. However, sodium purified in this fashion still contained about 0.15 percent of a long-lived impurity. The eluate from the Dowex 50 column was, therefore, further purified by passage through a column containing the anion absorption resin, Amberlite 1R-4B. A sample so purified was followed for a period of 13 half-lives, from 103,000 to 17 counts per min., with no departure from a logarithmic dependence of activity on time. All samples were purified by the same method.

Table I. Na^{24} half-lives.

Experiment number	Half-life
1	14.95
2	15.06
3	15.06
4	15.03
5	15.04
6	14.98
7	15.12
	Average 15.04±0.06

Samples were counted on a windowless proportional counter developed by Robinson.[3] Since proportional counters have no deadtime correction, counts were made up to rates of 100,000 counts per min. No departure from linear behavior has been observed up to this rate. The low background of the counter, 3 to 4 counts per min., permitted accurate counting at low activities. The disintegration constant was determined by fitting the data using the method of least squares. The average half-life is 15.04 hr. with a standard deviation of 0.06 hr. Results of individual runs are given in Table I.

The author wishes to express his thanks to Dr. C. V. Robinson for his assistance and counsel and to Miss E. White for making the counts.

* This work has been supported in part by the AEC.
[1] S. N. Van Voorhis, Phys. Rev. **49**, 889 (1936).
[2] W. E. Cohn and H. W. Kohn, J. Am. Chem. Soc. **70**, 1986 (1948).
[3] C. V. Robinson, Science (to be published).

The Genetic Relationship in Ag^{110}

John Miskel
Department of Chemistry, Brookhaven National Laboratory, Upton, Long Island, New York*
May 29, 1950

Recent studies[1] of the radiations emitted by Ag^{110} have indicated that the 270-day activity is caused by a level isomeric with the 24-sec. ground state. This genetic relationship has been confirmed by the separation of a short-lived activity from a sample of Ag^{110} obtained from Oak Ridge.

The separation was effected by collection of activity on copper electrodes immersed in an ether solution of silver tetraphenylporphin.[2] Two copper electrodes separated by about 3 mm were immersed in the solution and a potential difference of 600 volts was applied. After about 3 min., one of the electrodes was removed, washed with ether, and then counted with an end-window G-M tube. The G-M tube was connected to an Autoscaler and a Brush recording oscillograph. The sample was followed to constant background (3 to 4 min. after separation). Figure 1 shows a plot *vs.* t of the logarithm of the total number of counts observed between $t=t$ and $t=\infty$ (3 min.), minus the number of counts due to the constant background in this time interval. The background, which accounted for about 80 percent of the total counting rate at $t=0$, was due principally to the 270-day activity. Repeated experiments gave half-lives between 21 and 30 sec. A typical curve is shown in Fig. 1. The time between the removal of the electrode from the active solution and the start of counting was about 12 sec.

Separation occurred at both the anode and cathode with about equal efficiency although the background was generally lower on the anode. Separation was also obtained when a copper electrode was immersed in the solution with no potential applied, but the separation was not as clean. No separation was observed when an uncharged platinum electrode was introduced.

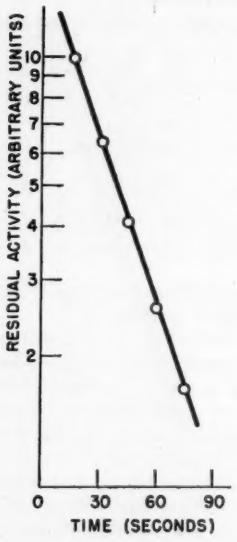

FIG. 1. Decay curve for short-lived Ag^{110} activity between $t=t$ and $t=\infty$ *vs.* t. $T_{\frac{1}{2}}=23$ sec.

The complexity of the Ag^{110} decay makes a determination of the separation factor difficult. A direct comparison of the ratio of the counting rates (observed with a 3.5-mg/cm² counter window) of the separated 24-sec. activity and the 270-day activity in solution gave an efficiency of about 25 percent using Siegbahn's estimate of three percent for the intensity of the 24-sec. branch.

It is probable that the silver tetraphenylporphin can be used for preparing high specific activity samples by a Szilard-Chalmer's process.

* Research carried out under the auspices of the AEC.
[1] K. Siegbahn, Phys. Rev. **77**, 233 (1950). M. Goldhaber and A. Sunyar private communication).
[2] We are indebted to Professor G. D. Dorough of Washington University for supplying the tetraphenylporphin used in the preparation of the silver compound.

A 5.7×10^{-9}-Sec. Isomeric State in $_{77}Ir^{191}$

F. K. McGowan
Oak Ridge National Laboratory, Oak Ridge, Tennessee*
June 7, 1950

An excited state in Ir^{191} with a half-life $(5.7\pm0.5)\times10^{-9}$ sec. has been observed with a delayed coincidence scintillation spectrometer. In Fig. 1 the number of delayed coincidences is plotted as a function of delay time obtained with a source of Os^{191} (32 hr.). The solid portion of the curve for delay time $T\geq2.5\times10^{-8}$ sec. represents the decay of the short-lived isomeric state which has been produced by the β^--decay of Os^{191}. Both the end point of the β^--spectrum announcing the formation of the isomeric state and the energy of the radiation emitted in the decay of the metastable have been determined.

The delayed coincidence scintillation spectrometer consists of the usual delayed coincidence unit[1] employing anthracene with Type 5819 multiplier tubes as detectors. In addition, a small portion of the signal from either detector is fed to a linear amplifier equipped with a differential pulse-height selector. This analyzer selects all pulses with amplitudes lying between E and $E+\Delta E$. The output pulses of the analyzer and the fast delayed coincidence pulses are fed into a relatively slow coincidence circuit. In this way only those pulses from the analyzer are selected that give rise to a delayed coincidence. When the detector feeding the analyzer channel is used to detect the radiation announcing the formation of the isomeric state, a measurement of the spectrum of the radiation preceding the metastable state is obtained. Similarly, when the detector is used to detect the delayed radiation, a measurement of its spectrum is obtained.

Curve (1) in Fig. 2 is the spectrum of the radiation resulting from the decay of the short-lived isomer in Ir^{191} obtained by counting delayed coincidences in a small height interval against pulse height. The internal conversion electron peak corresponds to 52 kev. The scale of pulse height was calibrated in energy units using internal conversion electron lines of γ-rays whose energies are well known from magnetic spectrometer measurements. Curve (2) shows the internal conversion electron lines at 65 and 122 kev of the 132-kev transition from the decay of the 22-μsec. metastable state of Ta^{181*} which announces the formation[2] of the 1.1×10^{-8}-sec. metastable state of Ta^{181*}. In addition, L internal conversion electrons of the 85- and 80-kev transitions following the β^--decay of Tm^{170} and Ho^{166}, respectively, were used for calibration.

Measurements of the radiation of other isomeric transitions with similar energy and lifetime have shown that the amount of internal conversion in the L shell is comparable to that in the K shell. Since only one internal conversion line appears in the spectrum of the decay of Ir^{191*}, the peak probably corresponds to L shell internal conversion. The energy of the transition is then (65 ± 5) kev which is less than the K shell electron binding energy (76 kev).

The spectrum of the radiation announcing the formation of the metastable state (not shown) appears to be a single beta-ray distribution whose maximum energy determined from a Kurie plot is 1.05 ± 0.03 Mev.

The decay curve of Fig. 1 was obtained with the analyzer gate accepting only small pulses corresponding to the 65-kev transition while the other channel was excited by the high energy β^--rays which gave rise to large pulses. Since the form of delayed coincidence resolution curves for originally simultaneous events depends essentially upon the distribution in amplitude of the original pulses, it is conceivable that the 65-kev transition is not metastable with respect to the β^--ray event. In order to rule out this possible instrumental effect on the resolution curve obtained with a coincidence system using amplifiers of finite rise time, a number of other sources were tested; namely, the 1.84-Mev β^--decay of Ho^{166} followed by a 80-kev internally converted

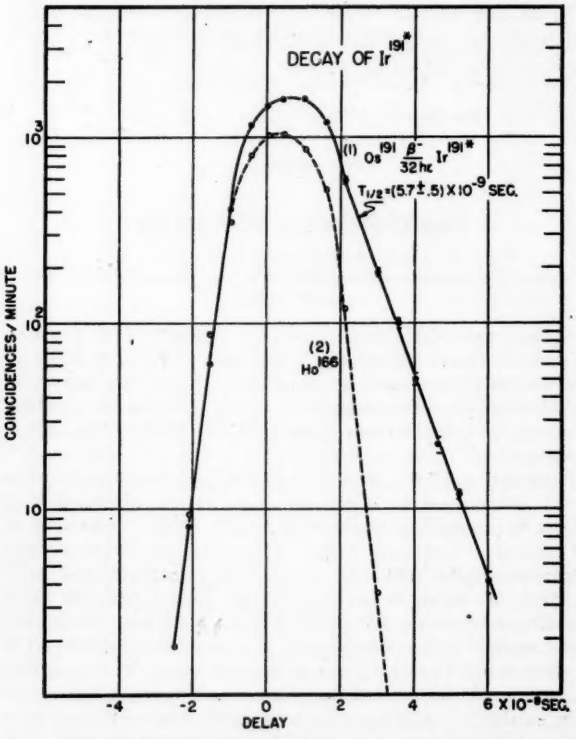

FIG. 1. Delayed coincidences as a function of delay time.

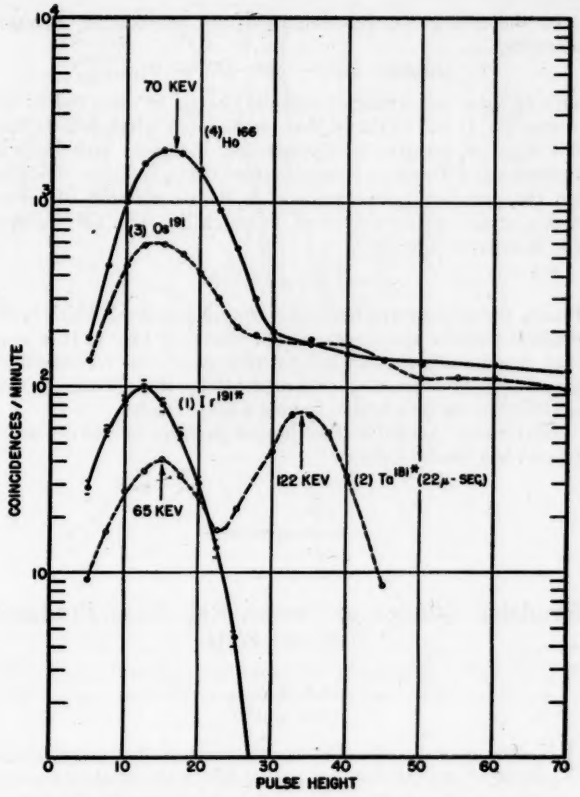

FIG. 2. Coincidence counting rate in a small pulse-height interval as a function of pulse height. Pulse-height interval was 2.5 pulse-height divisions.

γ-ray, the 900-kev β^--decay of Tm^{170} followed by a 85-kev internally converted γ-ray, and the 1.076-Mev β^--decay of Re^{186} followed by a 138-kev internally converted γ-ray. Curve (2) in Fig. 1 shows a typical resolution curve obtained with Ho^{166}. In each case the resolution curve obtained with the analyzer accepting only the low energy internally converted γ-ray was symmetrical with the leading and trailing edge being roughly exponential over three decades corresponding to a half-period 2×10^{-9} sec. In Fig. 2, curves (3) and (4), which are the low energy portion of the spectra of the simultaneous events from Os^{191} and Ho^{166}, respectively, show clearly the similarity of the two distributions in amplitude of the original pulses from the scintillation detector.

* This document is based on work performed for the Atomic Energy Project at Oak Ridge National Laboratory.

[1] F. K. McGowan, Phys. Rev. **76**, 1730 (1949).
[2] W. C. Barber, Phys. Rev. **78**, 641 (1950).

Superconducting Bismuth Alloys*

JOSEPH M. REYNOLDS† AND C. T. LANE
Sloane Physics Laboratory, Yale University,‡
New Haven, Connecticut

May 29, 1950

THE metal bismuth, noted for its anomalous electric and magnetic properties, is not known to be a superconductor down to about 0.05°K. It is, however, a curious fact that this substance when alloyed with other non-superconducting elements very often results in a superconductor.

The earliest discovered case[1] of the above is Au_2Bi. Subsequently the alloys[2-4] $NiBi_3$, $RhBi_2$, $RhBi_4$, and NaBi, all falling into the same category, have been reported. The experimental data on the above class of alloys are somewhat meager but, on the other hand, for binary alloys wherein one or both components is a superconductor the literature is very extensive. For the latter class the following properties are observed: (1) broad temperature transitions in zero field, often a degree or more, (2) large initial slopes of the magnetic threshold curves, (3) severe hysteresis in magnetic properties, and (4) incomplete Meissner effect. Pure elemental superconductors of the "soft" variety (e.g., Sn or Hg) have just the opposite behavior to that listed and are often, therefore, classed as "ideal."

Mendelssohn[5] has advanced a very plausible hypothesis to account for this "alloy" behavior and, on the basis of this, Shoenberg[6] in 1938 suggested that if an alloy of uniform composition throughout its volume could be prepared, it might be expected to show the characteristics of an ideal superconductor. The best chance of producing such an alloy would be to use "intermetallic compounds," i.e., those with the ingredients in stoichiometric proportions. Shoenberg investigated the stoichiometric alloy Au_2Bi and did indeed find a lessening of the alloy anomalies, although his results were not entirely conclusive, owing perhaps to impurities in his sample.

We have recently investigated two such alloys, (NaBi) previously reported[4] as superconducting, and (KBi_2) which, to our knowledge, has not previously been known to be a superconductor. For measurement we employed Webber's a.c. induction method[7]

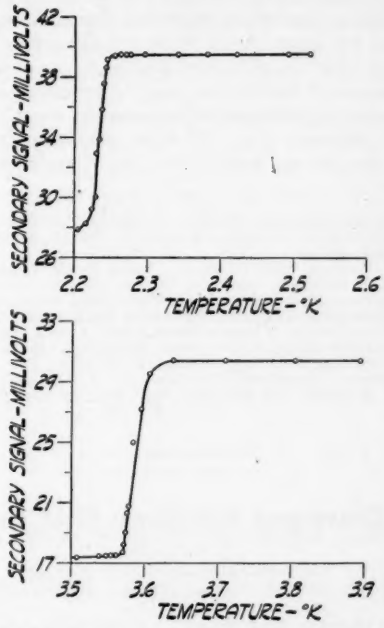

FIG. 1. The "zero field" transitions into superconductivity for NaBi (upper curve) and KBi_2. Mond (1949) vapor pressure tables are used.

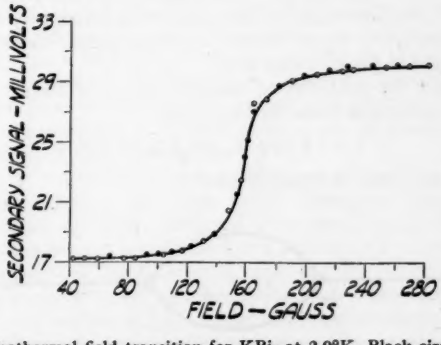

FIG. 2. Isothermal field transition for KBi_2 at 2.0°K. Black circles for increasing field and white circles for decreasing field.

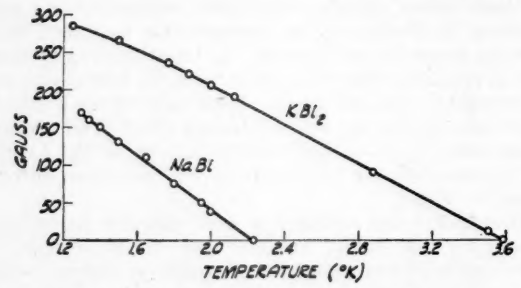

FIG. 3. Critical threshold curves for the two alloys.

which is particularly useful for "zero field" transition studies. The alloys were prepared from spectroscopically pure Bi, Na, and K by synthesis.

Figure 1 shows the very sharp zero field transitions; approximately 0.05°K for NaBi and 0.07°K for KBi_2. Figure 2 shows an isothermal magnetic transition for KBi_2 at 2.0°K. An almost complete lack of hysteresis is evident. Figure 2 is typical of 16 curves for both NaBi and KBi_2 at a whole series of temperatures between about 1.2°K and the normal transition temperatures.

Figure 3 shows the threshold curves for the two alloys these being evolved from data such as Fig. 2 by taking the saturation value of field as the critical threshold. The initial slopes are approximately 180 gauss/°K for NaBi and 130 gauss/°K for KBi_2. Such values would be considered small even for pure elementary superconductors of the soft variety. The measuring method used by us does not necessarily reveal information about the completeness of the Meissner effect, but in all other respects the results seem to give strong support to the Mendelssohn-Shoenberg hypothesis.

* Part of a dissertation presented by Joseph M. Reynolds to the Faculty of the Graduate School of Yale University in candidacy for the degree of Doctor of Philosophy.
† Now at Louisiana State University, Baton Rouge, Louisiana.
‡ Assisted by the ONR.
[1] de Haas, van Aubel, and Voogd, Leiden Comm. 197a (1929).
[2] N. E. Alekseyevsky, J. Phys. U.S.S.R. **9**, 350 (1945).
[3] N. E. Alekseyevsky, J. Exper. Theor. Phys. U.S.S.R. **18**, 101 (1948).
[4] N. E. Alekseyevsky, J. Exper. Theor. Phys. U.S.S.R. **19**, 671 (1949).
[5] K. Mendelssohn, Proc. Roy. Soc. **A152**, 34 (1935).
[6] D. Shoenberg, Nature **142**, 874 (1938).
[7] Webber, Reynolds, and McGuire, Phys. Rev. **76**, 293 (1949).

A Convergent Non-Linear Field Theory

J. C. WARD
Clarendon Laboratory, Oxford, England
April 24, 1950

NON-LINEAR field theories of the interaction of similar particles have been proposed by several authors, but only recently has it become possible to discuss whether or not they give rise to divergencies. It is interesting to note that a very simple theory of the interaction of scalar particles, which may be made convergent solely by the device of mass renormalization, can be constructed in the following way.

Consider the field theory, taken as a neutral theory for convenience, derivable from the Lagrangian

$$L=-\tfrac{1}{2}\{(\partial\phi/\partial x_\mu)^2+K^2\phi^2\}+\lambda\phi^3,$$

where λ is a small interaction constant.

FIG. 1. Feynman diagram for $E=2$, $n=2$.

In the interaction representation the Schrödinger equation becomes

$$ihc\delta\Psi(\sigma)/\delta\sigma(x)=\{\lambda\phi^3-\tfrac{1}{2}\delta K^2\phi^2\}\Psi(\sigma)$$

with δK^2 the logarithmically infinite change in mass due to the interaction. It will be shown that the S-matrix which follows from this equation contains no divergencies. Using the techniques of Feynman and Dyson, it is easy to show that a sufficient condition for the primitive convergence of a matrix element connected with a graph having n vertices, at which the term $\lambda\phi^3$ operates, and E external lines is

$$E+n\geqslant 5.$$

Hence, the only divergence arises from $E=2$, $n=2$ which is the simplest possible self-energy graph, shown in Fig. 1. It is clear that, whever this appears as part of a graph, the corresponding logarithmic divergence will be canceled by the self-energy term $-\tfrac{1}{2}\delta K^2\phi^2$ in the interaction, leaving a finite result.

Mixtures of charged and uncharged particles can, of course, be treated in a similar fashion.

Emulsion Studies of Cosmic-Ray Stars Produced in Metal Foils*

IAN BARBOUR AND LAWRENCE GREENE†
Kalamazoo College, Kalamazoo, Michigan
June 6, 1950

IN this investigation cosmic-ray induced disintegrations of nuclei of several elements are studied with metal foils placed between nuclear emulsions, in order to determine the dependence on atomic weight of the star-production cross section, and to observe the configurations typical of various target nuclei. It also appears probable that analysis of the cross section, multiplicity, and angular distribution of groups of minimum-ionization particles, shown to include predominantly mesons,[1] especially in comparison between heavy and very light nuclei, will throw light on whether meson production is mainly multiple or plural (simultaneous or successive nucleon-nucleon interactions). Our experimental method is described here and some preliminary cross-section results are given.

Perkins[2] and Harding[3] have poured emulsions with alternated layers of pure gelatin to compare star production in gelatin and emulsion, finding a ratio consistent with a geometrical cross section. In another possible method, comparing loaded with unloaded emulsions, very good statistics are required if the differences are to be reliable. Inclusion of small particles of metals within the emulsion is also possible, but quantities in excess of about one-half percent by volume interfere with subsequent scanning.[4]

In this experiment, foils of various metals were "sandwiched" between pairs of Ilford G-5 emulsions placed face-to-face, so that after development tracks could be observed in the emulsions and those originating in disintegrations of foil nuclei could be projected back to common centers outside the emulsion. Several difficulties revealed by preliminary experiments required special attention. If the two emulsion surfaces are too far apart during exposure, prongs from a given star in the foil may be separated from each other by considerable distances when they enter the emulsion, thus making it difficult to associate all those track segments attributable to one common disintegration. Thus, if the two emulsion surfaces are 75μ apart and the distribution of prongs from a disintegration in the foil is isotropic, eight percent of the tracks would enter the emulsion at a distance from the star center greater than 470μ, which at a scanning magnification of 200× is the diameter of our field of view and hence the maximum distance of definite identification. To insure a maximum emulsion separation of 75μ, it is *not* sufficient merely to use a thin foil, for it was

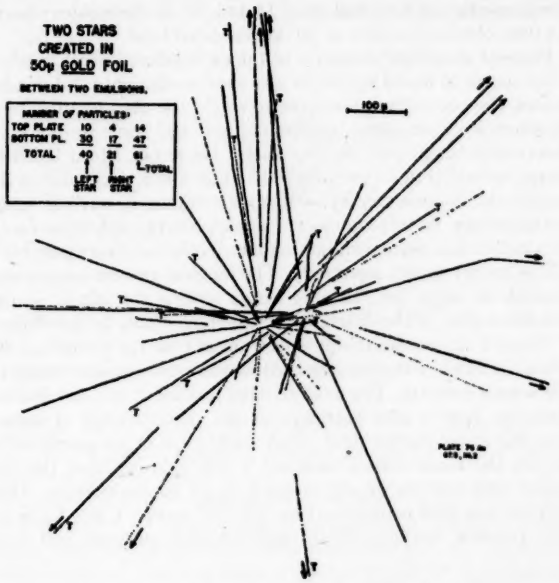

FIG. 1. Microprojection of tracks from two neighboring stars caused by the disintegration of gold nuclei. All the tracks can be seen to radiate from two points between the emulsions; the central portion of each track, representing the portion of the trajectory within the foil, is not observable. Tracks marked "T" were in the top plate, others in the bottom plate; arrows indicate tracks continuing beyond this field of view in the emulsion.

found that a new metal foil, even under moderate pressure, will not lie completely flat during exposure. It was found necessary to heat each foil to its annealing temperature to render it malleable, and then subject it to high pressure between two very flat steel surfaces. Finally the flattened foil is placed between 10μ sheets of cellulose acetate (or better, coated with a very thin layer of plastic) to prevent the interaction of the metal atoms with those of the emulsion. Clamped between pairs of nuclear plates, foils of Au, Pt, Ni, Cu, Sn, and Al were flown together in a flight of 6 hr. at 93,000 ft.[5]

After removal of the foils and development of the emulsions, the corresponding plates were placed face-to-face, the original alignment being reconstructed by x-ray dots[6] at the ends of the plates and by exact alignment of through tracks, and the edges were cemented, so that the pair of emulsions could be scanned together and observed with a magnification of 450×. Figure 1 is a microprojection of tracks from the disintegration of two gold nuclei which happened to be quite near each other. The weight and area of each foil were accurately measured, so that it was possible to calculate from the number of stars observed the cross section for star production per target nucleus. The correction for tracks missed outside the field of view was computed after determining the original emulsion separation by geometrical consideration of through tracks; a small correction for star tracks which never leave the foil must also be applied. Figure 2 shows values found for relative cross sections *per target nucleus* for the production of stars of various sizes in four materials. The data on very small stars (3, 4, and even 5 prongs) in the foils must be considered less reliable, because of the possibility that tracks, from a 4-prong star, for instance, could be so oriented in the two emulsions that the scanner might overlook their association with a common origin. The values for the emulsion stars are greater than anticipated, though the variety of elements present and uncertainty as to density and shrinkage factor make an exact interpretation difficult. Analysis of the complete data indicates a maximum at about 8 prongs per star for Au, and 6 for Sn, whereas for Cu and emulsion it occurs for smaller values. As an insert in Fig. 1 the integral cross section for stars of more than 4, 8, 6, and 10 prongs have been plotted on a log-log graph against the atomic weight, A, of the target nucleus. Approximate linearity indicates a dependence

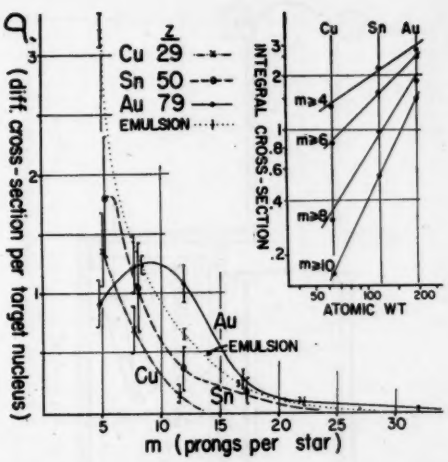

FIG. 2. Differential cross section (number of stars of m prongs observed per target nucleus $\times 10^{-25}$) *vs.* number of prongs (m) for four target materials. Insert at upper right shows a log-log plot of integral cross section (for stars of more than 4, 6, 8, and 10 prongs) *vs.* the atomic weight of the target foil.

of the form $\sigma_r = kA^s$, where for values of r (the minimum number of prongs considered) of 10, 8, 6, and 4, the corresponding values of the exponent, s, are 2.0, 1.5, 1.0, and 0.7. Estimating the extrapolation to include stars of 2 or 3 prongs, the total cross section for stars of all sizes is quite close to an $A^{\frac{1}{2}}$ law. This data refers to all observed star tracks and therefore includes, for each star, particles from both initial nucleon-nucleon collision processes and from subsequent "evaporation." A separate analysis of the groups of energetic particles ("meson showers"), their angular distribution and cross section as a function of the atomic weight, together with completion of the data on other metal foils, is in progress.

* This work has been aided by a Cottrell Grant from the Research Corporation.
† Now at Ohio State University, Columbus, Ohio.
[1] Camerini, Fowler, Lock, and Muirhead, Phil. Mag. **41**, 413 (1950).
[2] D. H. Perkins, *Cosmic Radiation* (Butterworth's Ltd., London, 1949).
[3] J. B. Harding, Nature **163**, 440 (1949).
[4] As a check on the present experiment, we are exposing such a suspension of Pb powder prepared by E. Hones of Duke University.
[5] Arranged through the kindness of the ONR and the General Mills Company.
[6] I. Barbour, Phys. Rev. **78**, 518 (1950).

Mesons Produced in Proton-Proton Collisions*

VINCENT Z. PETERSON
Radiation Laboratory, University of California, Berkeley, California
June 5, 1950

A FUNDAMENTAL problem in the study of mesons is that of their production in the collisions of protons with free protons, since the analysis is unhindered by considerations of the internal dynamics of complexed nuclei. Such an experiment can be performed by using a subtraction technique[1] employing C and CH_2, or a pure hydrogen target can be used to study the production directly. We have chosen to construct a liquid hydrogen target and have studied the meson energy distribution at various angles with respect to an incident beam of 345-Mev protons from the Berkeley 184-inch cyclotron.

Since the threshold for meson production in proton-proton collisions is very high (292 Mev in the laboratory system), the maximum kinetic energy available to the meson in the center-of-mass system is only about 25 Mev (for 345-Mev protons incident). Such a meson will have a velocity only slightly greater than the center-of-mass velocity, and hence the meson flux may be expected to be emitted in a predominantly forward direction in the laboratory system. Furthermore, the upper limit of meson energy decreases rapidly with angle, from 74 Mev at 0° to 7 Mev at 90°.

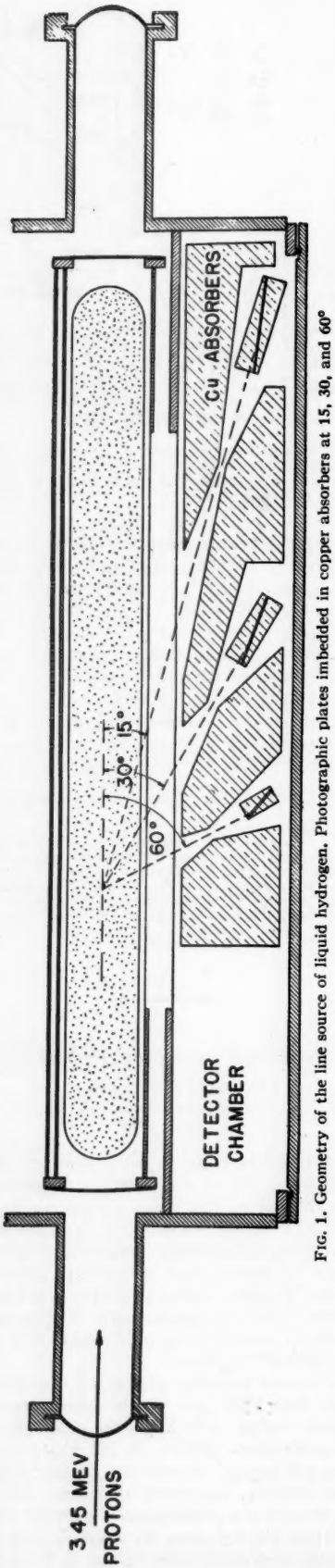

FIG. 1. Geometry of the line source of liquid hydrogen. Photographic plates imbedded in copper absorbers at 15, 30, and 60°

Consequently we have looked at 15 and 30° to the incident beam; the data obtained to date at 30° are reported here.

Figure 1 shows the geometry of the earlier experiments in which a line source of liquid hydrogen was used to eliminate end-window effects. Copper collimators serve to shield the photographic plate detectors from excessive background and also serve to define the observation angle and effective target thickness. Ilford C-2 100μ plates imbedded in copper absorbers at an angle to the meson flux sample the volume density of mesons stopping at various ranges in the copper. In this manner a complete energy spectrum can be obtained in one plate, eliminating many relative errors possible in taking energy points separately. The incident proton beam passes through an argon ion chamber before strking the target, so that absolute values of the differential cross section may be determined.

Figure 2 shows the energy spectrum of positive mesons at 30°, based on 115 π–μ-decays observed in one plate exposed using the line source gometry. The most striking feature of this distribution, apparent despite poor statistics, is the concentration of mesons near the upper energy limit. This sharp peak is not predicted by any of the usual meson theories[2] if one assumes that the final proton and neutron do not interact (Born approximation). However, as was first pointed out by Barkas[3] and by Chew,[4] it is not only possible but also likely that the final nucleons will either

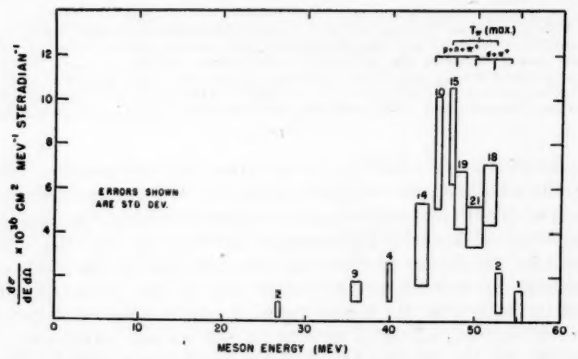

FIG. 2. Energy spectrum of positive π-mesons from 335-Mev protons on liquid hydrogen. Observation angle 30°±3°.

interact strongly or may even unite to form a real deuteron. In the latter case the reaction becomes a two-body problem, and one would expect a "line" of mesons of a single energy situated about 4 Mev (at 30° observation angle) beyond the continuous spectrum. It is not possible to confirm or deny the existence of such a line on the basis of the data of Fig. 2, owing to poor statistics and insufficient energy resolution. However, the calculated limits and line positions are shown for the range of angles included.

Since the exclusion principle limits the possible states of the initial proton-proton system, proof of the existence of deuterons in this reaction would impose definite restrictions on the type of meson-nucleon interactions which could be assumed. Therefore, it is of interest go try to improve both statistics and energy resolution in an effort to resolve the line, if it exists, from the continuous distribution. The magnitude of the peak cross section and the lack of negative mesons in the line-source experiments have encouraged us to use a thin-walled (0.002 in.) aluminum cylinder of 1½-in. diameter as a "point" source of liquid hydrogen in order to improve the angular resolution. In addition the use of a bending magnet to sort the positive mesons from elastically scattered protons has improved the meson-to-background ratio in the plates by a factor of about 500, with subsequent improved counting rate. Recent data based on 315 π–μ-decays obtained in this manner confirm the shape of the peak shown in Fig. 1 but still give no definite indication of fine structure. The estimated energy resolution for this run, however, was only about ±4 Mev. Further improvements in the energy resolution of the detection arrangement are being made. The best resolution will be determined by the energy spread of the

incident proton beam, which is estimated to have a total spread of less than 4 Mev.

Miss Dora Sherman and Mr. Edwin Iloff have assisted in scanning the plates.

* This work was sponsored by the AEC.
[1] Cartwright, Richman, Whitehead, and Wilcox, Phys. Rev. **78**, 823 (1950).
[2] K. Brueckner (private communication).
[3] W. Barkas, Phys. Rev. **75**, 1109 (1949).
[4] G. Chew (private communication).

The Beta-Spectrum of Sn^{125}

RAYMOND W. HAYWARD
Department of Physics, University of California, Berkeley, California
May 29, 1950

THE beta-spectrum of the 9.9-day tin activity has been examined in a magnetic lens spectrometer similar to the one described by Siegbahn.[1]

Ketelle, Nelson, and Boyd[2] identified this tin activity as Sn^{125} by irradiating tin samples electromagnetically enriched in Sn^{124} with a high flux of slow neutrons. They were able to milk chemically the 2.7-yr. Sb^{125} activity from the activated tin sample on successive occasions.

A sample of the 9.9-day tin made by fission of thorium by deuterons and chemically separated with 50μg of carrier was furnished by Dr. A. S. Newton. A source was prepared by mounting the sample on a Nylon film supported by a Lucite ring so that the mass of the source was about 0.4 mg/cm^2. A beta-spectrum was obtained and a Fermi plot of the data is shown in Fig. 1. Forgetting for the moment the low energy component, there is the characteristic non-linearity associated with the type of forbidden spectrum in which a spin change of two units and a parity change occur in the transition. In this type of transition it is theoretically appropriate to modify the conventional Fermi plot by dividing the ordinate by a factor $(p^2+q^2)^{\frac{1}{2}}$ where p and q are the momenta of the electron and the neutrino, respectively. When this is done, we obtain the modified Fermi plot shown in Fig. 2 where the linearity indicates the correctness in assuming the interaction to be of the first-forbidden type. The end-point energy from this modified Fermi plot is 2.37±0.02 Mev which is slightly higher than that obtained by Ketelle *et al.* The $f\tau_{\frac{1}{2}}$-value of 3.7×10^8 is in experimental agreement with the other known beta-spectra exhibiting this type of forbidden shape.[3]

The low energy beta-component accounts for about five percent of the total intensity and has an upper energy limit of 0.40±0.01 Mev. From the preceding facts the presence of a gamma-ray of about 2 Mev energy and five percent intensity would be suspected. Efforts to find this gamma-ray by observation of the Compton electrons from a copper radiator surrounding a source of Sn^{125} in the spectrometer proved negative, but this could have been due to insufficient activity and the low branching ratio. However, absorption measurements in lead by Newton and McDonell[4] indicate the possible presence of a gamma-ray of about 1.5 Mev which could be the 2-Mev gamma-ray since absorption measurements in this energy range are inherently inaccurate when the intensity is low.

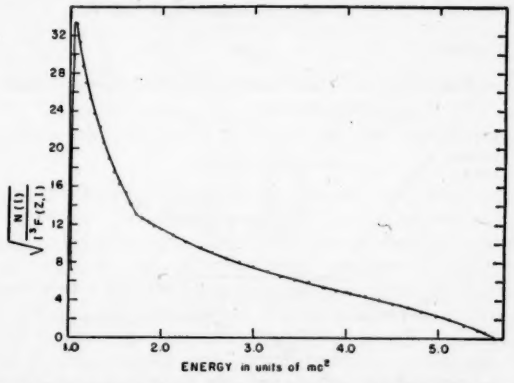

FIG. 1. A conventional Fermi plot of the Sn^{125} beta-spectrum in which only the density of final states for the beta-particle and the neutrino and the perturbation by the Coulomb field of the nucleus on the beta-particle are taken into account.

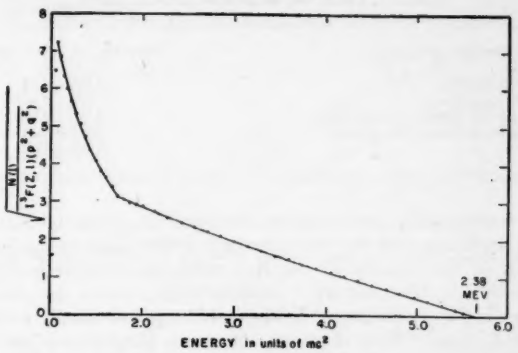

FIG. 2. A modified Fermi plot of the Sn^{125} beta-spectrum in which an additional factor $(p^2+q^2)^{\frac{1}{2}}$ is included, taking into account the dependence of the nuclear matrix elements on the momenta of the beta-particle and the neutrino.

[1] K. Siegbahn, Phil. Mag. **37**, 181 (1946).
[2] Ketelle, Nelson, and Boyd, Bul. Phys. Rev. **79**, 242 (1950).
[3] L. M. Langer and H. C. Price, Jr., Phys. Rev. **76**, 641 (1949).
[4] A. S. Newton and W. R. McDonell (unpublished work).

Electronic Mobility in Germanium*

V. A. JOHNSON AND K. LARK-HOROVITZ
Purdue University, Lafayette, Indiana
May 25, 1950

SOME time agao we analyzed the resistivity behavior[1] of a large number of germanium samples, prepared by adding varying amounts of various elements to high purity germanium. We found that it is possible to account for the observed resistivity from near the melting point down to very low temperatures as the sum of a lattice resistivity ρ_L due to scattering of carriers by lattice ions and an impurity resistivity ρ_I due to the Rutherford scattering of carriers by impurity ions.[2] The mobility associated with ρ_L is characteristic of the germanium lattice and so should be the same, at a given temperature, for all N-type germanium samples.

In our original analysis we used the classical expression for the Hall coefficient, $R=-3\pi/(8ne)$, where R is given in cm^3/coulomb, e in coulombs, and the electron density n in cm^{-3}. Hence the mobility was calculated from $b_L=8|R|/(3\pi\rho_L)$. Such computations yielded a room temperature electron mobility of 1450±300 cm^2/volt-sec. The samples in this group were polycrystalline and of low resistivity material (0.005 to 0.5 ohm-cm). More recently, measurements[3] have been made on samples of very high purity, usually single crystals. Analysis of the data for such samples usually has led to mobility values far higher than those previously obtained. In addition, Pearson, Haynes, and Shockley[4] have found that the mobility measured from drift velocities is constant, the same from sample to sample, but having a value considerably higher than that calculated by the use of $b=8|R|/(3\pi\rho)$.

In the hope of explaining these mobility discrepancies we have re-examined[5] the classical Hall coefficient expression and found that the numerical coefficient should be replaced by a variable quantity whose value is dependent upon the fraction of the total resistivity due to impurity scattering. This modification arises because the classical expression is based on the assumption that the mean free path of a conduction electron is independent of its kinetic energy; such is the case for lattice scattering except at very

TABLE I. Electronic mobilities in Ge at 300°K.

Nature of samples	Mobility in cm²/volt-sec.
Polycrystalline	3200±750
Single crystals	3370±550
Resistivity above 1.0 ohm-cm	3330±230
Resistivity below 0.1 ohm-cm	3250±790
All	3270±700

low temperatures, but impurity scattering is primarily Rutherford scattering with the mean free path proportional to the fourth power of the velocity. If the Hall coefficient is represented by $R=-r/(ne)$, the quantity r depends upon ρ_I/ρ in the manner shown in Fig. 1 of reference 5. The mobility is now calculated from $b_L=|R|/(r\rho_L)$. Table I shows the room temperature electron mobility, associated with lattice scattering, as obtained in the manner just described. The measure of error for the averages in Table I is given by the standard deviations of the respective data. The large deviations are due primarily to the uncertainty in the determination of the probe separations used in the resistivity measurements. In conclusion, it should be noted that, (1) the average mobility calculated in the manner described is in agreement with the "drift" and "conductivity" mobilities measured by Pearson *et al.*, (2) there is no significant difference in mobility between polycrystalline and single crystal samples, and (3) there is no significant difference in mobility between high and low resistivity samples.

* Work assisted in part by Signal Corps contract.

[1] K. Lark-Horovitz and V. A. Johnson, Phys. Rev. **69**, 258 (1946); K. Lark-Horovitz, Contractor's Final Report, NDRC14-585 (November, 1945), pp. 36–41.

[2] E. Conwell and V. F. Weisskopf, Phys. Rev. **69**, 258 (1946); **77**, 388 (1950).

[3] G. L. Pearson, Phys. Rev. **76**, 179 (1949); R. E. Davis and K. Lark-Horovitz, Progress Report of Purdue University Department of Physics to Signal Corps (August 1, 1948), p. 77; R. Bray, Progress Report (August 1, 1948), p. 86; C. S. Hung and J. R. Gliessman, Progress Report (December 1, 1949), p. 36.

[4] Pearson, Haynes, and Shockley, Phys. Rev. **78**, 295 (1950).

[5] V. A. Johnson and K. Lark-Horovitz, Phys. Rev. **79**, 176 (1950).

Spectrometer and Coincidence Studies on Np^{238}

M. S. FREEDMAN, A. H. JAFFEY, AND F. WAGNER, JR.
Argonne National Laboratory, Chicago, Illinois
May 1, 1950

THE Np^{238} used in these experiments was prepared by pile irradiation of Np^{237}, and subsequently separated from other activities and foreign salts. Spectrometer samples (~0.03 mg/cm²) were mounted on conducting LC-600 films. An anthracene scintillation detector was used, and the double-lens spectrometer resolution was three percent.

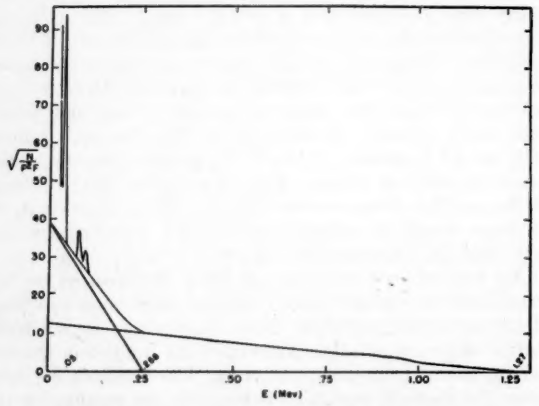

FIG. 1. Kurie plot of Np^{238} beta-spectrum. The Kurie plot of the low energy beta-component ($E_0=0.258$ Mev) can be seen at the left.

TABLE I. Radiations of Np^{238}.

Radiation	Energy[a] (Mev)	Binding energy of conversion electron (Mev)	Gamma-energy (Mev)	Abundance of conv. electron (rel. to weak β) (percent)	Conv. coef.[b] (percent)
β	0.258			100	
β	1.272			89	
Conv. elec.	0.913	0.124(*K*)	1.04	0.6	1.2
Conv. elec.	0.859	0.124(*K*)	0.98	0.6	1.2
Conv. elec.	0.0979	0.0048(*M*)	0.1028	2.2	4.7
Conv. elec.	0.0802	0.0222(*L*)	0.1029	3.5	7.5
Conv. elec.	0.0419	0.0048(*M*)	0.0467	6.0	12
Conv. elec.	0.0374	0.0048(*M*)	0.0422	27	27
Conv. elec.	0.0247	0.0222(*L*)	0.0469	37	74
Conv. elec.	0.0208	0.0222(*L*)	0.0430	71	71
Numerous conversion lines below 20 kev are also observed.					
Photo-electron	1.010	0.020(*L*)	1.030		
Photo-electron	0.966	0.020(*L*)	0.986		
Photo-electron	0.914	0.116(*K*)	1.030[c]		
Photo-electron	0.867	0.116(*K*)	0.983[c]		

[a] Calibration based on *K* conversion line of Au^{198}.
[b] According to decay scheme of Fig. 2.
[c] Gamma-energy taken from these values.

Table I summarizes the radiations observed. Photo-electron peak shift corrections were negligible for the 3.7-mg/cm² uranium radiator.[1] We estimate the 1.030 gamma to have 1.02 times the intensity of the 0.983 gamma. *L* and *M* binding energies for plutonium were obtained from a Moseley law extrapolation from the heavy element region. The Kurie plot, calculated with a relativistic Coulomb function, and by neglecting shielding, appears in Fig. 1. The transitions are seen to be both of the allowed shape, though the higher energy beta is empirically second forbidden ($ft=2.26\times10^8$). The lower beta is empirically allowed ($ft=1.03\times10^6$). The relative beta-intensities are consistent with these *ft*-values and with the relative beta-energies. For similarly high *Z* (79) the linear shape has been observed even for second-forbidden transitions.[2]

Gammas of low energy were sought with 30-mg/cm² uranium radiators and 5-mg/cm² gold radiators without success. By using a spiral baffle in the spectrometer together with an intense (100μC) beta-source, positrons were looked for, and an upper limit on the ratio of $\beta^+/\beta^-=0.001$ in the energy range above 50 kev was established. No x-ray or conversion line corresponding to *K*-capture was observed, contrary to predictions.[3] Using proportional counters, coincidences were found between (1) soft beta and *L* x-rays, (2) hard beta and *L* x-rays, (3) *L* x-rays and *L* x-rays, (4) soft beta and hard gamma, and (5) *L* x-rays and hard gamma. Measurements by D. Engelkemeir of this laboratory with anthracene scintillation counters showed coincidences between the hard beta and a quantum radiation of about 100 kev. A more precise half-life value, 2.10±0.01 days, was determined.

A tenatative decay scheme is suggested in Fig. 2.

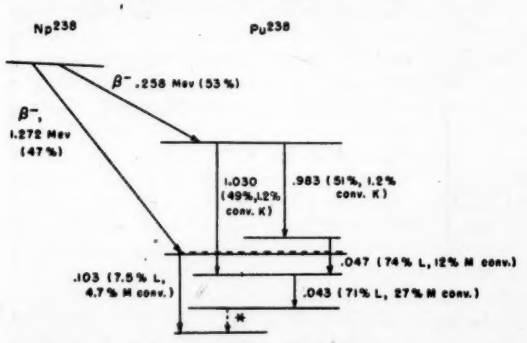

FIG. 2. Suggested decay scheme for Np^{238}. The transition marked * may be a 44-kev gamma whose conversion lines are unresolved from those of the 43-kev gamma; a 13-kev gamma if the dotted level is identical with that about it; or a 60-kev gamma (unlikely) if the dotted level is identical with that immediately below it.

We are indebted to Mary Novick, Robert Keyes, Jerome Lerner, and Jack May for assistance in various phases of these experiments. A final report on this work will be submitted to this Journal.

[1] Hornyak, Lauritsen, and Rasmussen, Phys. Rev. **76**, 731 (1949).
[2] D. Saxon, Phys. Rev. **73**, 811 (1948).
[3] Perlman, Ghiorso, and Seaborg, Phys. Rev. **77**, 26 (1950).

A 1.0-Mev Energy Level in C^{13}

ISADORE B. BERLMAN
Physics Department, Washington University, St. Louis, Missouri*
May 23, 1950

THERE has been some discussion recently in the literature[1-3] as to whether C^{13} has a 1.0-Mev energy level as obtained from the reaction $C^{12}(dp)C^{13}$. A carbon target[4] was bombarded by 10-Mev deuterons from the Washington University cyclotron. The recoil particles were recorded in Ilford E-1 nuclear emulsion plates which were placed at various angles to the cyclotron beam. At 90° there was a homogeneous group of particles which was attributed to the reaction $C^{12}(dp)C^{13}$. There were no recoil particles from the reaction in which C^{13} would be left in the 1.0-Mev excited state. However at 115° and 155° there were two prominent groups of proton tracks, the first of which was analyzed as being due to the above reaction where C^{13} was left in the ground state, and the second as being due to the reaction where C^{13} was left in the 1.0-Mev excited state. These results indicate that there is an angular dependence for the second group of tracks.

To prove that there was no oxygen in the carbon target as a contaminant which would be producing these proton groups due to the ground state of O^{17} and the well-known 0.88-Mev level, a second target composed of Li_2O was bombarded with 10-Mev deuterons and the recoil particles were recorded at 90° to the beam. In this case there were two homogeneous proton groups from the reactions $O^{16}(dp)O^{17}$ and $O^{16}(dp)O^{17*}$. If oxygen were a contaminant of the carbon targets causing the observed groups at 115 and 155° one would also expect the two groups of particles at 90°.

The reason that Buechner[1] and Heydenburg[2] did not find the 1.0-Mev level in C^{13} may be the fact that they used lower bombarding energies.

I wish to thank Dr. R. N. Varney for his constant interest, encouragement, and assistance.

* Assisted by the joint program of the ONR and AEC.
[1] Buechner, Strait, Sperduto, and Malm, Phys. Rev. **76**, 1543 (1949).
[2] Heydenburg, Inglis, Whitehead, and Hafner, Phys. Rev. **75**, 1147 (1949).
[3] K. Boyer, Phys. Rev. **78**, 345 (1950).
[4] To be published in greater detail later.

Gamma-Gamma-Correlation Experiments*

J. R. BEYSTER AND M. L. WIEDENBECK
Department of Physics, University of Michigan, Ann Arbor, Michigan
May 31, 1950

THE correlation of successive gamma-rays has been reported previously for a number of radioactive substances.[1] We have also investigated the gamma-gamma-correlation for several of these activities and for a few other isotopes. The apparatus consisted of two scintillation gamma-counters with 931-A photomultipliers and stilbene crystals. Figure 1, curve A, shows the observed function for Co^{60} and Fig. 2 that of Rh^{106}. These are essentially in agreement with the observations of Deutsch and Brady. The significance of the function for Co^{60} has been discussed by Brady and Deutsch[1] and by Segrè and Helmholtz.[2] The explanation of the Rh^{106} data is still a matter for speculation.

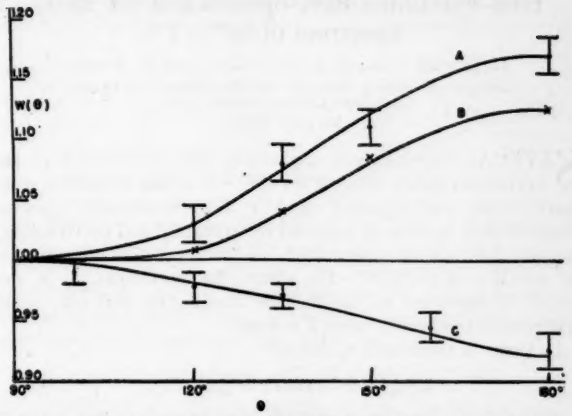

FIG. 1. Gamma-gamma-correlation functions of Co^{60} (curve A), Cs^{134} (curve B), and Ag^{110} (curve C).

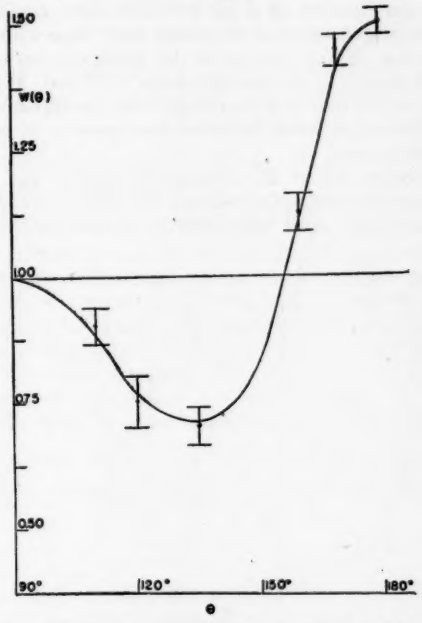

FIG. 2. Gamma-gamma-correlation function of Rh^{106}.

Figure 1, curve B, is the observed function for Cs^{134}. It will be recalled that Cs^{134} has essentially three gamma-rays in cascade, the upper gamma occurring about 25 percent of the time.[3] It is possible to explain the experimental data with the assumptions that the two lower transitions are quadrupole between states possessing angular momenta $J=4$, 2, and 0, and that the upper transition is quadrupole with $J=4$, 5, or 6 for the uppermost state. The polarization correlation experiments[4] and the measurements of the total absolute conversion coefficient[5] for Cs^{134} indicate that one of the lower transitions may be magnetic quadrupole.

Curve C is the observed correlation function for Ag^{110}. An interpretation of this function is difficult because of the large number of gamma-rays present in the structure.[6]

We have also observed that the correlation function for Na^{24} is the same as that of Co^{60}, and have found some evidence of gamma-gamma-correlation in Hf^{181} and Tb^{160}.

* This research was supported in part by the AEC.
[1] E. L. Brady and M. Deutsch, Phys. Rev. **74**, 1541 (1948).
[2] E. Segrè and A. C. Helmholtz, Rev. Mod. Phys. **21**, 293 (1949).
[3] L. G. Elliott and R. E. Bell, Phys. Rev. **72**, 979 (1947). K. Siegbahn and M. Deutsch, Phys. Rev. **73**, 410 (1948).
[4] A. Williams and M. L. Wiedenbeck, Phys. Rev. **78**, 822 (1950).
[5] M. L. Wiedenbeck and K. V. Chu, Phys. Rev. **72**, 1171 (1947).
[6] Kai Siegbahn, Phys. Rev. **77**, 233 (1950).

First-Forbidden Beta-Spectra and the Beta-Spectrum of $Sr^{90}-Y^{90}$

L. JACKSON LASLETT, E. N. JENSEN, AND A. PASKIN
Institute for Atomic Research and Department of Physics, Iowa State College, Ames, Iowa*
May 25, 1950

SEVERAL investigations supporting the applicability of the correction factor $(W_0-W)^2+(W^2-1)$ to first-forbidden beta-spectra have been reported[1] recently. The theoretically expected shape of such spectra, as reported by Marshak[2] and by Greuling,[3] suggests that a more precise form for this correction factor would be $a=(W_0-W)^2+\Lambda(W^2-1)$, where the coefficient Λ is not strictly independent of the electron momentum and may differ appreciably from unity when Z is large.

In terms of Greuling's notation,[3]

$$\Lambda=[(S_1+2)/(2S_0+2)][F_1/F_0];$$

a plot[4] of Λ as a function of electron momentum is shown in Fig. 1, for $Z=40$ and $Z=60$. Although the introduction of the coefficient Λ may result in no more than a very small modification of the spectral form expected for a first-forbidden beta-transition when Z is in the neighborhood of 40, recent work[5] here with Pr^{142} has indicated that the introduction of this coefficient can result in a noticeable change in the spectral shape of $Z=60$. This note is submitted at this time with the thought that the application of the modified correction factor indicated here may be of interest to other investigators.

In a previous letter[6] the beta-spectra of Sr^{90} and Y^{90} were reported as of the first-forbidden form discussed above. An indication of the rather small improvement obtained in this case by including the coefficient Λ in a comparison of the experimental data with theory is afforded by the following weighted r.m.s. relative differences between the theoretical curves and the individual counting rates observed in the Y^{90} spectrum (for the interval $2.079\leqslant W\leqslant 5.256$): with $\Lambda=1$, r.m.s. deviation = 1.5 percent; with Λ from Fig. 1, r.m.s. deviation = 0.8 percent; and from statistical counting error, expected r.m.s. deviation = 0.6 percent.

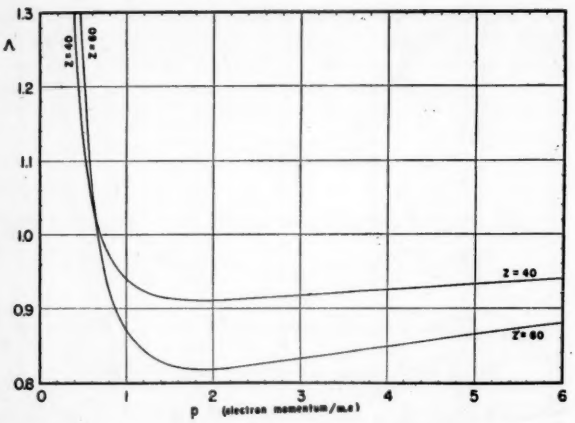

FIG. 1. Graph of the coefficient Λ, which appears in the correction factor $a=(W_0-W)^2+\Lambda(W^2-1)$.

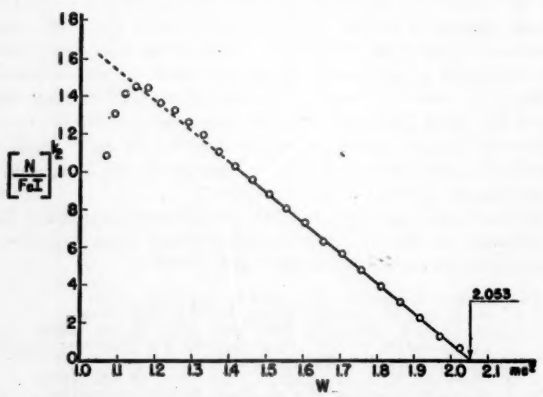

FIG. 2. Modified Kurie plot, $(N/FaI)^{\frac{1}{2}}$ *vs.* W, for a separated Sr^{90} source.

A more adequate separated source of Sr^{90} was obtained[7] since our first work on this activity was performed and a modified Kurie plot of the more recent data is shown in Fig. 2 to supplement the results previously reported.[6] Upper limits of 2.24 and 0.54 Mev (kinetic energy) are obtained for the Y^{90} and Sr^{90} beta-spectra, respectively.

The *ft*-values were calculated with the more precise correction factor a included with the Fermi function in the integral expression for f. Values of 1.7×10^9 and 2.0×10^9 were obtained for Sr^{90} (19.9 yr.[8]) and Y^{90} (62 hr.), respectively.

* Contribution No. 104. The work was performed at the Ames Laboratory of the AEC.

[1] L. M. Langer and H. C. Price, Jr., Phys. Rev. **75**, 1109 (1949), **76**, 641 (1949); C. L. Peacock and A. C. G. Mitchell, Phys. Rev. **75**, 1272 (1949); E. N. Jensen and L. J. Laslett, Phys. Rev. **75**, 1949 (1949); Braden, Slack, and Shull, Phys. Rev. **75**, 1964 (1949); Slack, Braden, and Shull, Phys. Rev. **75**, 1965 (1949); C. S. Wu and L. Feldman, Phys. Rev. **76**, 696 (1949); D. Saxon and J. Richards, Phys. Rev. **76**, 982 (1949); L. M. Langer, Phys. Rev. **77**, 50 (1950); and H. M. Agnew, Phys. Rev. **77**, 655 (1950).

[2] R. E. Marshak, Phys. Rev. **61**, 431 (1942).

[3] E. Greuling, Phys. Rev. **61**, 568 (1942).

[4] The values of F_0 were computed by means of a series expression for the logarithm of the modulus of the gamma-function appearing as a factor in F_0 and were in agreement with those given in a preliminary coarse-mesh table subsequently obtained from the Computation Laboratory of the National Bureau of Standards through the kindness of Dr. Fano. The computation of F_1/F_0 was based on the use of a similar series to represent F_1.

[5] Jensen, Laslett, and Zaffarano (manuscript in preparation).

[6] E. N. Jensen and L. J. Laslett, Phys. Rev. **75**, 1949 (1949).

[7] We are indebted to Dr. A. F. Voigt and Mr. E. Dewell in the Radiochemistry Section of this Laboratory for their assistance in performing this separation.

[8] R. Powers and A. F. Voigt (private communication).

The Effect of Nuclear Structure on the Elastic Scattering of Fast Electrons

L. R. B. ELTON
University College, London, England
May 22, 1950

THE cross section for the scattering of electrons by atomic nuclei has been investigated at energies for which the nuclei can no longer be treated as point charges. Three nuclear models were used: (A) point charge, (B) uniform spherical charge distribution of radius R, (C) uniform spherical shell charge distribution of radius R. The radius R is taken to be[1] $R=e^2A^{\frac{1}{3}}/2mc^2$, in the usual notation.

Preliminary calculations, based on Born's approximation, showed that significant deviations from the cross sections using a point nucleus should occur for a light element, such as Al, at about 30 Mev, and for a heavy element, such as Au, at about 15 Mev. For Al, Born's approximation is valid,[2] but for Au it is not. Hence an exact calculation without any approximation was carried out for Au and 20-Mev electrons by calculating the phases for the lower order partial cross sections, using models (B) and (C). It was found that only the zero-order phases $(\eta_0-\eta_{-2})$ were significantly different for model (A) and for models (B) and (C). The calculations for model (A) by Bartlett and Watson[3] (these were done for Hg, but are sufficiently accurate also for Au) were then modified accordingly in the zero-order phases. The ratio $R_{B,C}=I_{B,C}(\theta)/I_A(\theta)$ of the differential cross section for an extended nucleus to that of a point nucleus is given in Table I, where the values for Al are calculated by Born's approximation and those for Au are calculated exactly. The energy has been adjusted to 16.5 Mev, so that comparison can be made with the experimental results,[4] R_{exp}. Because of the electrostatic repulsion of the charges inside the nucleus, the charge density is likely to increase with the radius, and so the true distribution is likely to be somewhere

TABLE I. Ratio of the differential cross section for an extended nucleus to that for a point nucleus for 16.5-Mev electrons being scattered by Al and Au nuclei.

	$\theta=$	30°			90°			150°		
Z		R_B	R_C	R_{exp}	R_B	R_C	R_{exp}	R_B	R_C	R_{exp}
Al	13	1.00	0.99	0.97	0.97	0.95	0.75	0.89	0.84	0.94
Au	79	0.99	0.97	0.88	0.45	0.30	0.45	0.29	0.19	0.38

between models (B) and (C). R_{exp} would therefore be expected to lie between R_B and R_C. It is seen that in view of the preliminary nature of the experimental results agreement is quite satisfactory.

A full account of this investigation will be published in the *Proceedings of the Physical Society*.

The author wishes to thank Professor H. S. W. Massey for his suggestion of this problem and general guidance of the work.

[1] J. A. Wheeler, Rev. Mod. Phys. **21**, 133 (1949).
[2] W. A. McKinley, Jr. and H. Feshbach, Phys. Rev. **74**, 1759 (1948).
[3] J. H. Bartlett and R. E. Watson, Proc. Am. Acad. Arts Sci. **74**, 53 (1940).
[4] Lyman, Hanson, and Scott, Phys. Rev. **79**, 228 (1950).

Stopping Power of K-Electrons

H. A. BETHE, L. M. BROWN, AND M. C. WALSKE
Cornell University, Ithaca, New York
May 25, 1950

AN expression for the contribution B_K of the K-electrons to the stopping number has been given by Livingston and Bethe[1] in the form

$$B_K(\theta,\eta)=A(\theta)\ln\eta+B(\theta)-C_K(\theta,\eta), \quad [\eta=(mv^2/2Z_{eff}^2Ry)\gg 1]. \tag{1}$$

Here θ is the ratio of the observed ionization potential to the "ideal ionization potential" Z_{eff}^2Ry, m is the electronic mass, and v is the velocity of the incident particle; $A(\theta)$, $B(\theta)$, and $C_K(\theta,\eta)$ can be computed directly by using the excitation and ionization probabilities of the K-shell.[1,2] The coefficient of the $\log\eta$ term is described in reference 1 as "the total oscillator strength of all optical transitions from the K-shell into the continuous spectrum (and to the unoccupied discrete levels)," and the formula has been applied, with this interpretation of $A(\theta)$, to higher atomic shells.[3] It is the purpose of this letter to show that this coefficient, $A(\theta)$, is actually $1+f$ where $2f$ is the above-mentioned total oscillator strength.

The Born approximation expression for the stopping number (per K-electron) is

$$B=\sum_n{}'\int_{q_{min(n)}}^{q_{max}}(dq/q)\varphi_n(q), \tag{2}$$

with $\varphi_n(q)=(E_n-E_1)|(e^{iqz})_{1n}|^2/q^2$, E_n being the energy of the nth atomic state and q^2 being the square of the momentum loss of the incident particle divided by $2m$ (both E_n and q^2 measured in units of Z_{eff}^2Ry). Energy-momentum considerations give $q_{max}=(4\eta)^{\frac{1}{2}}$ and $q_{min}=(E_n-E_1)(4\eta)^{-\frac{1}{2}}$; Σ_n' indicates the summation over all unoccupied states. Letting q_1 be a small value of q, independent of n and η, and $q_0=q_{min}(n=\infty)=(4\eta)^{-\frac{1}{2}}$, we can write

$$B=\sum_{\text{all states}}\int_{q_0}^{q_{max}}\varphi_n(q)dq/q - \sum_{\text{occupied levels}}\left[\int_{q_0}^{q_1}\varphi_n(0)dq/q+\int_{q_1}^{\infty}\varphi_n(q)dq/q\right] - \sum_n{}'\int_{q_0}^{q_{min(n)}}\varphi_n(0)dq/q. \tag{3}$$

This expression is correct, except that in the second and last term $\varphi_n(q)$ has been replaced by $\varphi_n(0)$, neglecting higher terms in q^2 because q_0, q_1, and $q_{min(n)}$ are all small for large η. In the third term, the upper limit q_{max} has been replaced by ∞ because, for occupied states, $\varphi_n(q)$ decreases as q^{-14} with increasing q.

To evaluate the first term, we change the order of summation and integration and use the well-known rule[2] that $\Sigma\,\varphi_n(q)=1$; then we obtain simply $\ln(q_{max}/q_0)=\ln 4\eta$. Since q_0 and q_1 are both independent of n, we obtain for the second term

$$-(1-f)\ln(q_1/q_0)=-\tfrac{1}{2}(1-f)\ln 4\eta-(1-f)\ln q_1$$

where $f=\Sigma'\varphi_n(0)$ is the total oscillator strength per electron for transitions going to unoccupied states. Since q_1 is independent of η and since the third integral converges at $q=\infty$, it yields a result independent of η. The last term gives

$$-\Sigma'\,\varphi_n(0)\ln(q_{min}/q_0)=-\Sigma'\,\varphi_n(0)\ln(E_n/E_1)$$

which is also independent of η. The η-dependent part of B arises therefore from the first and second terms alone and is:

$$\ln\eta-\tfrac{1}{2}(1-f)\ln\eta=\tfrac{1}{2}(1+f)\ln\eta. \tag{4}$$

It is not possible to calculate $B(\theta)$ by this general method, but if we write Eq. (1) in the form

$$B_K(\theta,\eta)=(1+f)\ln(2mv^2/\lambda Z_{eff}^2Ry)-C_K(\theta,\eta), \tag{5}$$

a Born approximation calculation[2] using hydrogenic wave functions gives the results displayed in Table I. The first line of Table I refers to the complete hydrogen atom, the other lines to the K-shells of heavier atoms, θ increasing with Z. It is remarkable that λ is so very nearly constant; note that this makes the "effective ionization potential" close to Z_{eff}^2Ry, not to the observed ionization potential. It may also be useful to note that f is very nearly inversely proportional to θ^3 (last column of Table I).

TABLE I. Calculated results for hydrogenic wave functions.

	λ	f	$\theta^3 f$
Hydrogen	1.1018	1	——
$\theta=0.7$	0.9542	0.813	0.398
0.75	0.9392	0.722	0.406
0.8	0.9295	0.646	0.413
0.9	0.9207	0.525	0.425

[1] M. S. Livingston and H. A. Bethe, Rev. Mod. Phys. **9**, 264 (1937).
[2] L. M. Brown, Phys. Rev. **79**, 297 (1950).
[3] J. O. Hirschfelder and J. L. Magee, Phys. Rev. **73**, 207 (1948).
[4] H. A. Bethe, Ann. d. Physik **5**, 325 (1930).

Decay of Au^{199}

R. D. HILL
Physics Department, University of Illinois, Urbana, Illinois*
May 29, 1950

AN estimate[1] given for the capture cross section of Au^{198} for slow neutrons was based on the intensity of a 159-kev transition from Au^{199}. A decay scheme for Au^{199} devised by Beach, Peacock, and Wilkinson[2] was used and a value of 3.5×10^4 barns was obtained for the cross section.

The radiations from a Au^{199} source[3] separated from Pt^{199} have since been studied and the complete identity of the spectra from Au^{199} produced by both methods has been shown. Further analysis of the Au^{199} electron conversion spectrum is given in Table I. Other lines present in the spectrum are due to the conversion of mercury K x-rays (~70 kev) and L x-rays (~10 kev). If a 230-kev γ-ray is present, as claimed by Beach *et al.*,[3] it can be estimated from the absence of its K conversion line that its intensity is less than 15 percent of the 158.5-kev transition.

The N_K/N_L ratio of 0.37 for the 158.5-kev transition suggests a 2^3-pole electric transition, for which according to Hebb and Nelson the theoretical value is 0.4. However, the N_{L111}/N_{L1} ratio for electric 2^3, according to Goodrich and Drell,[4] is of the order of 20, whereas the experimental value is $0.55\pm<0.1$. Nor will a combination of 2^2 magnetic and 2^3 electric transitions assist in bringing these values into closer accord with theory. A similar conflict for

TABLE I. Electron conversion lines from Au^{199}.

Line	γ_1-L	γ_1-M	γ_1-N	γ_2-K	γ_2-L_1	γ_2-L_{111}	γ_2-M	γ_2-N	γ_3-K	γ_3-L_1	γ_3-L_{111}
Energy (kev)	35.7	47.5	50.0	78.5	144.5	146.5	156	158	125.5	193.8	196.2
Intensity (arb.)	——	——	——	4.0	7.0	3.9	1.6	1.2	3.7	0.7	

$\gamma_1=50\pm1$ kev, $\gamma_2=158.5\pm0.3$ kev, $\gamma_3=208.5\pm0.3$ kev

a 155±4-kev transition in Hg^{199} has been observed by Hole[5] who studied the decay of 43-min. Hg^{199m}. This 155-kev transition, for which Hole measured a N_K/N_L ratio of <0.43 and a $(K+L)$ conversion coefficient of 0.20, is undoubtedly the same as the 158.5-kev transition from Au^{199}. The theoretical value of the $(K+L)$ conversion coefficient for a 2^3 electric transition is 2.7. It would appear therefore that the 158.5-kev transition is probably of lower multipole order than 3.

The experimental N_K/N_L ratio for the 208.5-kev transition is of the order 5, which might indicate a 30 to 70 percent mixture of 2^1 magnetic and 2^2 electric transitions. Theoretical values of the K conversion coefficients for 2^1 magnetic and 2^2 electric transitions are 0.94 and 0.16, respectively.

From the above experimental and estimated conversion coefficients it can be calculated that the branching ratio of 158.5-kev to 208.5-kev transitions is approximately 2:1, and the slow neutron-capture cross section of Au^{198} is accordingly reduced to 1.6×10^4 barns. From the fact that the 158.5-kev transition and not the 208.5-kev transition was observed in the decay of Hg^{199m}, it is to be inferred that the 158.5-kev transition probably follows the 50-kev transition, which arises from the same level as does the 208.5-kev transition. Coincidence experiments are in progress.

* This work was supported in part by the joint program of the AEC and ONR.

[1] R. D. Hill and J. W. Mihelich, Phys. Rev. **79**, 275 (1950).
[2] Beach, Peacock, and Wilkinson, Phys. Rev. **76**, 1585 (1949).
[3] This material was obtained from the Isotopes Division, Oak Ridge, Tennessee. The chemical separation of the gold was performed by M. Glaubman.
[4] Private communication.
[5] N. Hole, Arkiv. f. Mat. Ast. o Fysik **36A**, No. 9 (1948).

PHYSICAL REVIEW VOLUME 79, NUMBER 2 JULY 15, 1950

Proceedings of the American Physical Society

MINUTES OF THE MEETING OF THE SOUTHEASTERN SECTION AT LOUISIANA STATE UNIVERSITY APRIL 7–8, 1950

THE sixteenth annual meeting of the Southeastern Section of the American Physical Society was held at Louisiana State University, Baton Rouge, Louisiana on April 7–8, 1950. Approximately 250 members and guests were in attendance. The Section was honored by the presence of a number of visitors from the states west of its boundary.

The program consisted of thirty-one ten-minute contributed papers and five papers by invited speakers. The abstracts of the contributed papers are printed below; the invited papers were:

A Medium Resolution Lens Spectrometer for Beta-Ray Energies from 1 Kev to 4.5 Mev. S. K. HAYNES AND D. A. THOMAS, *Vanderbilt University* (given by Dr. Haynes).

Proportional and Scintillation Counters. C. J. BORKOWSKI, *Oak Ridge National Laboratory.*

Recent Research in Low Temperature Physics, CHARLES F. SQUIRE, *The Rice Institute.*

The Cosmic Abundances of Nuclear Species. HARRISON S. BROWN, *Institute for Nuclear Studies, The University of Chicago.*

The Role of Physics in Biology. ROBERT T. NIESET, *The Tulane University of Louisiana.*

The officers of the Section elected for 1950–51 are Eric Rodgers, *Chairman*; Alvin H. Nielsen, *Vice-Chairman*; Dixon Callihan, *Secretary*; Robert T. Lagemann, *Treasurer*; Paul Shearin, Member of the Executive Committee; Walter Gordy, Member of the Executive Committee for one year of the unexpired term of the late Clyde Crawley. The 1951 meeting will be held at the University of Chattanooga, Chattanooga, Tennessee.

DIXON CALLIHAN, *Secretary*
Southeastern Section
American Physical Society
Oak Ridge, Tennessee

ABSTRACTS

1. Radiofrequency Positive Ion Source. F. J. RINK, *Oak Ridge National Laboratory.* (*Introduced by John I. Hopkins.*)—A radiofrequency positive ion source will be described which is, at present, the source of positive ions in a 300-kev accelerator. The discharge is excited by the radiofrequency field of a coil which comprises the resonant circuit of a 120-Mc per sec. oscillator. An axial magnetic field supplied by Helmholtz coils materially improves efficiency for ion production. The ions are extracted through a pumping canal (2.5 mm in diameter and 16 mm long) by means of simple electrodes assisted by an axial magnetic field of about 210 gauss. A study of this source has been made, as regards beam current for gas consumed, relative abundance of various masses, energy spreads, etc. The results of this study will be presented along with details of the construction of the source.

2. Neutrons from the Bombardment of Li^6 by Deuterons.* WARD WHALING AND J. W. BUTLER, *The Rice Institute.*—The neutron energy spectrum of the following two reactions was determined from cloud chamber measurements of recoil proton tracks:

$$Li^6+H^2\rightarrow Be^7+n^1+3.30 \text{ Mev} \quad (1)$$

$$Li^6+H^2\rightarrow He^4+He^3+n^1+1.68 \text{ Mev}. \quad (2)$$

The measured neutrons were in the direction of the deuteron beam of mean energy 595 kev. Using only those tracks within

10° of the direction of the incident neutrons, about 1260 tracks were recorded. A group with its peak at 3.75 Mev and a half-width of 500 kev was attributed to reaction (1). The other group exhibited a continuum from 1500 kev down to the lowest energies measured, 500 kev, and was attributed to reaction (2).

* Assisted by the Research Corporation and by the joint program of the ONR and AEC.

3. Neutrons from the Disintegration of C^{13} by Deuterons. J. E. RICHARDSON, *The Rice Institute. (Sponsored by T. W. Bonner.)*—Energy levels in the N^{15} nucleus were observed by studying neutrons emitted when separated targets of C^{13} were bombarded by deuterons giving the reaction: $C^{13}+H^2\rightarrow(N^{15})^*\rightarrow N^{14}+n+Q$. There are three known groups of neutrons from this reaction with Q-values of 0.4,[1] 1.2,[2] and 5.2[2] Mev, respectively. By means of the Rice Institute Van de Graaff particle accelerator, the high energy neutron group was studied for deuteron energies ranging from 500 kev to 2.1 Mev. The neutrons were detected with a high pressure helium counter, and the discriminator was calibrated so that helium recoils resulting from the $C^{12}(d, n)N^{13}$ reaction and from the lower energy groups of the $C^{13}(d, n)N^{14}$ reaction were not counted. Broad resonances were found at 1 and 1.8 Mev. There are indications of a narrower resonance at 1.58 Mev. These correspond to excited states in the N^{15} nucleus of 17.00, 17.50, and 17.69 Mev.

[1] Bennett, Bonner, Hudspeth, Richards, and Watt, Phys. Rev. **59**, 781 (1941).
[2] T. W. Bonner and W. M. Brubaker, Phys. Rev. **50**, 308 (1936).

4. A Magnetic Lens Pair Production Gamma-Ray Spectrometer,* S. J. BAME, JR. AND L. M. BAGGETT, *The Rice Institute.*—A two-coil solenoidal-type beta-ray spectrometer has been constructed. The spectrometer is to be used in conjunction with a Van de Graaff generator using a magnetic analyzer, so the spectrometer has been shielded from stray magnetic fields by spacing iron rings along its tube.[1] A modification of the counting system has adapted the spectrometer to count electron-positron coincidences from pairs ejected by high energy gamma-rays from a radiator in the source position. The members of the pair are focused through the exit aperture and then pass through a magnetic deflection field which separates the electrons and positrons. Two banks of counters are arranged so that the opposite members of the pairs are deflected into opposite banks of counters so that coincidences between the two rows of counters may be counted. Another system of counting the pairs in coincidence which requires no separation magnet is under consideration. In this system, members of a pair falling upon multiple counters after being focused generally will fall upon different counters, permitting coincidence counting of the pair.

* Assisted by the joint program of the ONR and AEC.
[1] D. E. Alburger, Rev. Sci. Inst. **19**, 474 (1948).

5. Measurements from a Magnetic Lens Pair Spectrometer.* L. M. BAGGETT AND S. J. BAME JR., *The Rice Institute.*—In preparation for using the magnetic lens pair spectrometer for the measurement of high energy gamma-rays from nuclear reactions produced by the Rice Van de Graaff generator, the spectrometer is being calibrated and its properties studied by obtaining the spectra from various sources. The internal conversion line of the 0.663-Mev gamma-ray of Cs^{137} has been used to determine the calibration of the spectrometer for various settings of the resolving system, and to check the calculations of the separation field required to deflect the electrons into one bank of the double row Geiger counters after they have passed through the exit aperture. The line shape of the coincidences between pair members is being studied by using the 2.62-Mev gamma-ray from ThC″ and the 4.3-Mev gamma-ray from a polonium-beryllium source.

* Assisted by the joint program of the ONR and AEC.

6. Pair Spectrometer Investigation of High Energy Gamma-Rays.* JAMES TERRELL,† *The Rice Institute.*—High energy gamma-ray spectra are being investigated by means of a pair-production spectrometer. The present instrument is a redesign of an earlier spectrometer[1] found to have insufficient intensity; the general design is similar to that of Walker and McDaniel.[2] A uniform magnetic field produces 180° focusing of pairs ejected from a large radiator. These secondaries are counted by four counters on each side of the radiator; coincidences between counters on the two sides are measured as a function of magnetic field. Investigation of a MsThI source shows the expected single peak, corresponding to the 2.62-Mev gamma-ray from ThC″. Investigations are under way of other gamma-ray sources, in particular a polonium-beryllium source on loan from Los Alamos.

* This research is supported by the joint program of the AEC and ONR.
† AEC Predoctoral Fellow.
[1] N. J. Terrell, Phys. Rev. **73**, 647A (1948).
[2] R. L. Walker and B. D. McDaniel, Phys. Rev. **74**, 315 (1948).

7. An Empirical Method for Calculating Electron Orbits and Line Shapes for a Point Source of Electrons in a Thick-Lens Beta-Ray Spectrometer. J. F. PERKINS AND A. W. SOLBRIG, JR., *Vanderbilt University. (Introduced by S. K. Haynes.)*—Ring-focusing baffles have been designed for use with a thick-lens beta-ray spectrometer. By numerical integration of the field equations several trajectories of point-source electrons have been calculated. Empirical relations among trajectory parameters have been determined. In the instrumental arrangement considered the ring focus is in a relatively weak magnetic field, so that in the interesting portion of a trajectory the radial coordinate is a linear function of the axial coordinate. Because of this simplification it is possible to determine graphically which electron paths are blocked by a given baffle, and thus to calculate the instrumental line shape for a point source of monoenergetic electrons resulting from a given combination of baffles. There is a single optimum position for an inner baffle, but the position of an outer baffle is not so critical. The use of two or more outer baffles results in a line shape which is steeper on the high energy side, though this improvement over a single outer baffle is probably appreciable only when small sources are used.

8. Electron Energy Studies with the Anthracene Scintillation Spectrometer.* JOHN I. HOPKINS,† *Oak Ridge National Laboratory.*—It has been reported previously[1,2] that light pulses produced by electrons striking anthracene give pulse heights proportional to the energy of the impinging electrons. It has been observed that this proportionality exists even if some of the electrons pass through the crystal. However, when this happens, the shape of the pulse distribution becomes distorted because of the scattering of electrons by the crystal. The error in determining the energy of electrons by the pulse height differentiating method is not greater than one percent for the energy range 125 to 1900 kev. Response studies have been made for crystal thickness of 0.38, 1.29, and 2.50 cm. The pulse-height-energy curves can easily be reconciled to one and the same curve.

* This document is based on work performed for the AEC.
† On leave from Vanderbilt University, Nashville, Tennessee.
[1] Phys. Rev. **77**, 406 (1950).
[2] A. P. S. Meeting, Oak Ridge, Tennessee (March 16–18, 1950).

9. A Flat Response Proportional Counter for Fast Neutrons. G. S. HURST AND R. H. RITCHIE, *Oak Ridge National Laboratory. (Introduced by K. Z. Morgan.)*—Calculations indicate that a counting response characteristic which is essentially constant from 0.5 to 20 Mev neutron energy may be obtained by using a specially shaped hydrogenous radiator. If a uniform beam of neutrons is normally incident upon the radiator, the number of protons scattered out of the solid will be a function of neutron flux only. The emerging protons may be counted

directly in a proportional counter. Such an apparatus could be made very small in size, i.e., 3 to 4 cm on a side and could be operated in a relatively high gamma-field. It will be useful in the evaluation of neutron source strength.

10. Theory of Models of Acoustical Systems. W. C. WINELAND AND CLYDE B. CRAWLEY,* *Naval Ordnance Laboratory.*†—A theory of acoustical systems analogous to that which is well-known for electromagnetic systems[1] is developed. The transformation equations relating various acoustical quantities in the full-scale and model systems are presented, and several applications of these equations are discussed.

* Decreased October, 1949.
† This work was done while the second of the authors was on leave from the University of Kentucky.
[1] George Sinclair, Proc. I.R.E. 36, 1364 (1948).

11. Vibrations Produced by Water Flowing through a Constricted Elastic Tube. ELMER B. CARNES, *Vanderbilt University.*—Vibrations are sometimes produced in a fluid column flowing through an elastic tube containing a constriction. These vibrations are accompanied by periodic disturbances of the surrounding media which are often audible. Experiments have been performed to learn what factors determine the frequency of vibration in the case of water flow through rubber tubing; the constriction being formed by applying forces which tend to collapse the tube at a given cross section. The apparatus was designed so that the following could be controlled and measured: the rate of flow of water through the rubber tube; the applied force causing the constriction; the length of the tube from the constriction to the open end. The frequency of vibration was measured by means of a strobotac. Data show that the frequency varies inversely as the length of the rubber tube from the constriction to the open end, thus suggesting that standing waves are set up in the tube.

12. A Liquid Prism Photoelectric Raman Spectrograph. JOSEPH W. STRALEY AND MORITA CRYMES, *University of North Carolina.*—A Raman spectrograph utilizing a CS_2 prism has been in operation for several months at the University of North Carolina. Liquid prisms have not been utilized in spectroscopic instruments frequently in the past because of the high dependence of the index of refraction on temperature. This difficulty is largely overcome by a photoelectric instrument by virtue of the relatively short time required to secure a spectrogram. The depolarization factors of a number of liquids have been measured. These data together with data on the relative intensity of Stokes and anti-Stokes lines indicate that this instrument should be quite useful in a variety of applications.

13. Transmission and Reflection of Ultrasonic Waves from a Solid Plate in Water.* M. S. WEINSTEIN AND W. C. WINELAND, *Naval Ordnance Laboratory.*—The transmission of 1-Mc/sec. ultrasonic waves through a solid plate immersed in water is studied experimentally and compared with the theoretical analysis of Smyth and Lindsay.[1] The angle of incidence is varied continuously, for each of six aluminum plates of thickness from $\frac{1}{32}$ to $\frac{1}{2}$ in., over a range from normal incidence to angles greater than the critical angles for both dilatational and shear waves. Good agreement is found between experimental and theoretical results over the range studied. Reflection measurements made with the same plates and additional brass and steel plates, for the cases of water and air backing, indicate that the reflection is entirely specular over the range of thickness studied, and that, in general, the reflection obtained with air backing is greater than that with water backing.

* This is a portion of a thesis to be submitted by the first of the authors to the University of Maryland in partial fulfillment of the requirements for the degree of Master of Science.
[1] J. B. Smythe and R. B. Lindsay, J. Acous. Soc. Am. 16, 20 (1944).

14. The Infra-Red Absorption Spectrum of Tung Oil. F. M. MCGEHEE, JR.* AND E. SCOTT BARR, *University of Alabama.*—The infra-red absorption spectrum of tung oil has been measured from 1 to 15μ. Samples from various sources were found to give essentially identical spectra: a specially prepared sample furnished by the U. S. Department of Agriculture Tung Laboratory (Bogalusa, Louisiana) was measured carefully and taken as the working standard. In view of the importance of this oil as a drying oil, studies were made of spectral changes for various conditions of drying. It was found that such changes were observable at 2.31, 2.90, 3.31, 3.45, 3.50, 5.73, 10.05, and 10.33μ. The nature and degree of change seemed to be determined by the drying conditions. Drying under ultraviolet radiation produced different results from those following infra-red radiation. Drying under ultraviolet was more rapid than for ordinary light, and drying under ultraviolet was less rapid than under infra-red radiaion. It was found that when the film of oil was between two rocksalt plates, rather than directly exposed to the air, only slight spectral changes took place. Measurements were also made on solutions in carbon tetrachloride, and on a fraction of the oil produced by partial freezing. Spectra for these cases show some bands intensified.

* Now at the University of Virginia.

15. The Infra-Red Absorption Spectra of Some Vegetable Oil and Related Compounds. E. SCOTT BARR, *University of Alabama.*—The infra-red absorption spectra in the rocksalt region have been measured for a group of samples of peanut oil, consisting of one refined in 1942, and a group representing steps in the processing of a particular batch of crude oil. It was found that no great spectral changes take place during the processing or with ageing, except in the region of 2.3 and 3μ. The observed changes indicate that processing largely involves the removal of oxidation products, and that ageing does little more than reverse this process. Due to the complex nature of peanut oil, it was felt desirable to study some simpler related compounds. Spectra were therefore measured for: oleic acid, methyl oleate and caprate, and ethyl caprate, laurate, and myristate. Intercomparison of absorption bands for these materials should prove helpful in making oil band assignments. The samples mentioned above were supplied by the Regional Research Laboratory of the U. S. Department of Agriculture, at New Orleans, Louisiana. Some additional vegetable oils from other sources have been measured, and the work is still in progress.

16. Some New Measurements on the Infra-Red and Raman Spectra of SiF_4.* PATRICIA J. H. WOLTZ AND ERNEST A. JONES, *K-25 Laboratories, Carbide and Carbon Chemical Division;* AND ALVIN H. NIELSEN, *University of Tennessee.*—The infra-red spectrum of SiF_4[1] has been repeated from 2.19μ and extended to 25μ. Bands at 645, 838, 912, 1447, and 2332 cm^{-1} reported by Bailey, Hale, and Thompson are not observed in the present experiment, and are believed to be impurity bands. Also, the absorption region at 1200 cm^{-1} is considerably weaker than shown in their measurements. Present observations of all other bands previously reported by them show some structural details not exhibited by the earlier work. ν_4, not previously observed, but predicted at 420 cm^{-1} has been observed at 410 cm^{-1}. The structure is uncertain. A Raman line in liquid SiF_4 has been observed at 390 cm^{-1} which may doubtless be ascribed to ν_4. No evidence was found of the line at 463 cm^{-1} reported by Yost.[2] Records of all bands except the ones at 780 and 410 cm^{-1} have been made with a prism-grating instrument. Four new bands which

overlap intense absorption regions have been observed. All bands are resolved into PQR structure, and accurate band centers will be given.

* This document is based on work performed for the AEC by Carbide and Carbon Chemicals Division, at Oak Ridge, Tennessee.
[1] Bailey, Hale, and Thompson, Proc. Roy. Soc. London **A167**, 555 (1938).
[2] Yost, Proc. Ind. Acad. J. Sci. **8A**, 333 (1936).

17. Coriolis Perturbation in Methane. EMILY W. JONES AND JOSEPH W. STRALEY, *University of North Carolina.*—The infra-red spectrum of methane has been investigated in the 6.5μ region and a band with its center at 1523 cm^{-1} has been located. This band has been identified as due to the fundamental vibration ν_2. This "forbidden" band has been observed previously in germane and silane. It appears in the spectrum of these molecules because of a Coriolis perturbation with the neighboring frequency ν_4. From a rotational analysis of this band, the moments of inertia in the ground and the excited ν_2-states have been determined to be 5.6×10^{-40} g cm^2 and 5.4×10^{-40} g cm^2. It was not possible to compute these moments of inertia to more precision because of the heavy absorption of vapor in this region.

18. Probability Distributions of the Resultants of Two or More Vibrations.* C. F. KENT AND J. E. BOYD, *Georgia Institute of Technology.*—By use of the method of "random flights" outlined by Chandrasekhar,[1] probability distributions are derived for the resultants of two, three, four, and more vibrations of equal amplitude and random phase. The method of calculation is extended to cases involving functionally varied amplitudes, as well as random phases. When normalized relative to their mean intensities, the probability distribution curves for the resultants of relatively small numbers of vibrations (10 or more) of equal amplitude are closely similar to the Rayleigh[2] distribution for an immense number of vibrations. Two random-phased components with a Gaussian distribution of amplitude give a probability curve which is almost identical with the Rayleigh curve. Experimental frequency distributions of microwave radio signal strength, obtained in overland propagation measurements under changing atmospheric conditions, are also shown and compared with the theoretical probability distributions. The observed distributions of signal intensity are similar to the theoretical probability distributions for many vibrations.

* This work was supported in part by the Watson Laboratories, Air Materiel Command, Contract No. W28-099-ac-175.
[1] S. Chandrasekhar, Rev. Mod. Phys., **15**, 1 (1943).
[2] Lord Rayleigh, *Theory of Sound* (Dover Publications, New York, 1945).

19. Specific Ionization of Air by 10- to 45-kev Hydrogen Particles. ARTHUR E. LOCKENVITZ AND J. T. KOPECEK, *University of Texas.*—Hydrogen particles accelerated through a difference of potential of between 10,000 to 45,000 volts were admitted into an air ionization chamber through a pinhole having an area of the order of 10^{-5} sq. cm. The pressure in this chamber could be varied from about 0.01 mm Hg to about 5 cm Hg. The ionization caused by the hydrogen particles over a distance of the order of 1 mm in the chamber was measured as a function of the energy of the hydrogen particles, and as a function of the pressure in the chamber for particles of fixed energy. The ionization per unit path is approximately proportional to the energy of the incident particles. For fixed energy particles the ionization, when corrected for variation in pressure, showed a maximum for pressures of about 0.2 mm Hg regardless of the energy of the incident particles. The data are presented graphically. The ionization chamber consists of two plates 2×10 cm separated by 2 cm. The one plate is split into three sections and the middle section 1 mm long is used as a collector with the outer sections acting as guard plates.

20. The Production of High Currents Electrical Discharges over Long Paths. CRESSWELL HATCHETT AND JOHN W. FLOWERS, *University of Florida.*—In the laboratory the production of spark paths, similar to lightning in current magnitude and time duration, require sufficiently high voltage to strike the path and sufficient capacity to furnish the desired current. A 500-kv impulse generator of relatively low capacity has been employed to discharge a bank of capacitors, charged to 25 kv, over a path much greater than that corresponding to 25-kv breakdown. This is equivalent, in many respects, to multiplying the capacity of the lower voltage bank by the number of times the path initiation voltage is increased. This effectively increases the available capacitance for the production of high currents, provided the increased path impedance does not enter as a limiting factor. Where the impedance does enter, it becomes available for study.

21. The Recombination of Positive Ions and Electrons. RICHARD HANAU,* *University of Michigan.*—Steady-state low voltage thermionic arc and Geissler glow discharges in helium were used to investigate the recombination of positive ions and electrons. For the arc an electron beam from an equipotential, thermionic cathode passed vertically downward through a slit in the anode, was collimated, entered the viewing space, and was incident on a collector. For the glow a neon sign transformer was connected between the collimator slit and collector. For both discharges two large metal plates, externally connected but otherwise floating, were introduced into the field-free viewing space with their parallel surfaces vertical. Spectral line intensities were measured for various positions of these plates. Results indicate that the plates do not affect the recombination process. This can be explained if the recombination rate is a linear function of ionic concentration. The entire recombination process in discharge plasmas may be viewed as one which approximates the conventional quadratic law for low ionic concentrations, and a linear law for high concentrations. Photometric methods are apt to give a clearer picture of the true recombination process; electrical meshods frequently give results interpretable only by the quadratic law. Steady-state experiments are preferable, since afterglow measurements are often indecisive.

* Now at the University of Kentucky.

22. Ultrafiltration Experiments with Silver Membranes. W. C. SKINNER* AND F. G. SLACK, *Vanderbilt University.*—Porous silver membranes have been made by hydrochloric acid attack on thin sheets of silver-zinc alloy. With one atmosphere driving pressure liquid flow rates through these membranes are 30 to 35 ml/hr.-cm^2; even with very small driving pressures flow rates are high enough to permit filtration experiments. The mean pore diameter for a fictitious equivalent membrane with straight cylindrical pores is 900A. The effective filtration pore diameter has been determined by means of a series of gold hydrosols of graded particle size. Adsorption interference with this determination was suppressed by the procedure of satisfying the adsorption demand with a gold hydrosol of particle size an order of magnitude less than the pore diameter. The effective pore diameter for filtration was found to be 600A or less. There is some evidence, incomplete in nature, for an effective pore diameter for filtration on the order of 500A.

* Socony-Vacuum Fellow.

23. The Diamagnetism of Free Electrons. D. J. BESDIN, *The Rice Institute.*—The results of a theoretical calculation of the magnetic susceptibility of a system of about 2300 electrons, in a cylindrical container whose height is about 30 times its radius, are given for several values of the externally applied field H. The electron energies are obtained as a series in H, but only terms to H^2 are used. The electron wave functions

are required to vanish at the cylinder walls. The calculation is numerical and exact, avoiding the uncertainties of approximate methods of evaluating the partition function. The cases of $T=0$ and $E_0/kT\approx 100$ are treated, where E_0 is the maximum energy of the occupied electron states at $T=0$. At $T=0$, a periodic variation of susceptibility with H is obtained, but at the higher temperature this effect has largely disappeared. The results are reminiscent of the de Haas-van Alphen effect, and may have application of the problem of superconductivity.

24. The Oscillations of Magnetic Suspensions. K. MILLSAPS, *Alabama Polytechnic Institute.*—The oscillations of a magnetic suspension between two equal poles is formulated in terms of a non-linear ordinary differential equation of the second order that may be integrated in terms of elliptic integrals of the second kind. The case of unequal poles is treated by an analogous procedure involving a Legendre reduction. The further refinement of viscous damping is treated by the classical method of isoclines after the manner of Van der Pol. Some generalizations are made to the more complicated cases of suspensions by circular poles.

25. Lower Bounds on the Range of the Neutron-Proton Interaction. A. A. BROYLES AND B. KIVEL, *University of Florida.* (*Introduced by R. C. Williamson.*)—The experimental values of the binding energy $E_0=2.17$ Mev, and the quadrupole moment, $Q=2.73\times10^{-27}$ cm², have been used to determine a lower bound for the range of the neutron-proton interaction of 0.39 e^2/mc^2 entirely independent of the shape of the potential well. The assumption was made that the bound state of the deuteron is made up of only S and D wave functions and that the radial parts of these wave functions are real. For a given value of the maximum force range, r_0, the wave functions will yield a maximum value of Q if they are zero for values of r less than r_0. Thus, the exponentially decaying exterior functions may be used to compute the maximum value of Q. The magnetic moment of the deuteron also sets a lower bound for r_0 on the doubtful assumptions that the neutron and proton moments remain inteact in the deuteron and that relativistic effects are negligible.[1] The experimental value requires the percent D wave to be less than five percent which sets a lower bound of 0.61 e^2/mc^2 for r_0.

[1] J. Schwinger, Phys. Rev. **60**, 164A (1941).

26. Radiation from Short-Lived Tantalum Isomer. MAX GOODRICH* AND EDWARD C. CAMPBELL, *Oak Ridge National Laboratory.*—The previously reported[1] 0.33-sec. neutron-induced activity in tantalum has been investigated further with the aid of a scintillation spectrometer. Correlation of the size of the pulses so obtained with those due to a 7.5-kev x-ray source and with absorption data in several materials shows conclusively that the radiation detected consisted of photons of 8 to 11 kev energy and not conversion electrons, as was previously reported on the basis of absorption measurements alone. Critical absorption measurements indicate that the radiation is complex and that it probably consists of the L x-rays from tatalum. Since no pulses corresponding to energies above 25 kev are observed, the radiation is believed to be from a low energy isomeric transition in tantalum which is highly converted in the L shell.

* On leave from Physics Department, Lousiana State University.
[1] Edward C. Campbell and Wilfred M. Good, Phys. Rev. **76**, 195 (1949).

27. Long-Lived Cadmium Activities. J. M. CASSIDY AND P. R. BELL, *Oak Ridge National Laboratory.* (*Introduced by John I. Hopkins.*)—Some long-lived cadmium activities have been investigated with the scintillation spectrometer. Neutron bombardment of cadmium produces 43-day[1] and 330-day[2] activities as well as several shorter ones. The electrons from the 43-day activity have a maximum energy of 1.7 Mev, and the gamma-radiation is quite weak. The long-lived activity has a beta-ray of 0.55 Mev and many soft electrons presumably from the 88-kev gamma-ray of Ag^{109*} to which the K-capture transition goes. Only soft gamma-rays were found.

[1] Seren, Engelkemier, Sturm, Friedlander, and Turkel, Phys. Rev. **71**, 409 (1947).
[2] Bradt, Gugelot, Huber, Medicus, Preiswerk, Scherren, and Steffen, Helv. Phys. Acta, **20**, 153 (1947).

28. Single-Channel Differential Pulse-Height Analyzer. J. E. FRANCIS, JR., P. R. BELL, AND J. C. GUNDLACH, *Oak Ridge National Laboratory.* (*Introduced by E. C. Campbell.*)—A single-channel analyzer has been built for measuring the energy spectrum obtained from scintillation counters and proportional counters. The analyzer contains a non-overload feed-back amplifier followed by two pulse-height selectors, a memory circuit, and an anticoincidence circuit. The feed-back amplifier amplifies a segment of the pulse distribution. The "lower" pulse-height selector is biased to fire on very small pulses from the amplifier. The output of this pulse-height selector is used to turn on the memory circuit. This output is also differentiated to produce a pulse which marks the beginning and end of the pulse. The pulse marking the end is used to hold the memory circuit on and is also fed into the anticoincidence circuit. The "upper" pulse-height selector fires only if the output from the amplifier is above a certain value. The pulse from this selector is fed into the memory circuit. The memory circuit controls one input of the anti-coincidence circuit. If the upper selector fires, the memory circuit provides one input to the anticoincidence circuit until after the differentiated pulse from the lower selector has entered the anticoincidence circuit. When only the lower selector fires there is no coincidence; therefore, there is an output pulse.

29. The Phase Spectrum in Pulse Analysis. T. N. HATFIELD, FRED MORRIS, AND CHARLES HAGER, *University of Texas.*—The general methods employed in pulse analysis are based on energy measurements and therefore give only the amplitude spectrum of a pulse. In order to completely represent a pulse, it is necessary to obtain the phase spectrum. A method has been developed for doing this. A step-function is fed into the analyzer simultaneously with the pulse and the effects on the amplitude spectrum of the pulse allows the determination of the phase spectrum.

30. Observations of the Effect of Temperature on the Luminescence of an Alpha-Particle Excited Wurtzite Phosphor. J. R. JACQUES AND H. A JARRELL, *Clemson Agricultural College.*—An attempt is made to observe the variation in pulse-height distribution with temperature of a wurtzite phosphor excited by 5-Mev alpha-particles. The observations cover the temperature range -195 to 300°C. A means of producing the temperature variation and scintillation detection is discussed. The pulse-height distribution is observed to increase slightly from -195 to -100°C remain fairly constant from -100 to 195°C, and then to drop rapidly from 195°C to zero in the neighborhood of 300°C.

31. Dielectric Properties of Selenium. F. J. MORRIS, *University of Texas.*—The dielectric constants and losses of several samples of selenium have been measured at temperatures from -50 to 150°C, and at frequencies from 0 to 50 Mc. The temperature coefficient of the dielectric constant has been examined for two forms of selenium. The a.c. capacitance and losses are measured with commercial bridges. The d.c. capacitance and resistance are measured with a ballistic galvanometer. The d.c. resistance is also measured with a Wheatstone bridge. The results of these experiments and the methods of preparing the selenium are discussed.